Faculty of Science and Engineering
School of Earth and Planetary Sciences

Integration Frameworks for Merging Satellite Remote Sensing Observations with Hydrological Model Outputs

Mehdi Khaki

This thesis is presented for the Degree of
Doctor of Philosophy
of
Curtin University

June 2018

Declaration

To the best of my knowledge and belief this thesis contains no material previously published by any other person except where due acknowledgement has been made. This thesis contains no material which has been accepted for the award of any other degree or diploma in any university.

Mehdi Khaki

List of publications

This Ph.D. thesis is a collection of 8 first-author peer-reviewed articles in high impact journals (6 published; 2 revised; see list below and Table 1.1 on page 17). Other cross-sectoral contributions, which are indirectly connected to the thesis are also listed below. Copyright permissions/authorization of the journals are presented in Appendix A while Appendix B contains the signed declarations for author and co-author contributions regarding the published manuscripts adapted for the thesis.

1. **Khaki, M.**, Forootan, E., Kuhn, M., Awange, J., Longuevergne, L., Wada, Y., (2018a). Efficient Basin Scale Filtering of GRACE Satellite Products. Remote Sensing of Environment, 204:76-93, doi:10.1016/j.rse.2017.10.040.

2. **Khaki, M.**, Schumacher, M., J., Forootan, Kuhn, M., Awange, E., van Dijk, A.I.J.M., (2017a). Accounting for Spatial Correlation Errors in the Assimilation of GRACE into Hydrological Models through localization. Advances in Water Resources, 108:99-112, doi:10.1016/j.advwatres.2017.07.024.

3. **Khaki, M.**, Hoteit, I., Kuhn, M., Awange, J., Forootan, E., van Dijk, A.I.J.M., Schumacher, M., Pattiaratchi, C., (2017b). Assessing sequential data assimilation techniques for integrating GRACE data into a hydrological model. Advances in Water Resources, 107:301-316, doi:10.1016/j.advwatres.2017.07.001.

4. **Khaki, M.**, Forootan, E., Kuhn, M., Awange, J., Papa, F., Shum, C.K., (2018b). A Study of Bangladesh's Sub-surface Water Storages Using Satellite Products and Data Assimilation Scheme. Science of The Total Environment, 625:963-977, doi:10.1016/j.scitotenv.2017.12.289.

5. **Khaki, M.**, Forootan, E., Kuhn, M., Awange, J., van Dijk, A.I.J.M., Schumacher, M., Sharifi, M.A., (2018c). Determining Water Storage Depletion within Iran by Assimilating GRACE data into the W3RA Hydrological Model. Advances in Water Resources, 114:1-18, doi:10.1016/j.advwatres.2018.02.008.

6. **Khaki, M.**, Awange, J. (2018d). The Application of Remotely Sensed Products to Enhance Model-derived Water Storage Changes over South America. Science of The Total Environment, 647:1557-1572, doi:10.1016/j.scitotenv.2018.08.079.

7. **Khaki, M.**, Ait-El-Fquih, B., Hoteit, I., Forootan, E., Awange, J., Kuhn, M., (2017c). A Two-update Ensemble Kalman Filter for Land Hydrological Data Assimilation with an Uncertain Constraint. Journal of Hydrology, 555:447-462, doi:10.1016/j.jhydrol.2017.10.032.

8. **Khaki, M.**, Ait-El-Fquih, B., Hoteit, I., Forootan, E., Awange, J., Kuhn, M., (2018e). Unsupervised Ensemble Kalman Filtering with an Uncertain Constraint for Land Hydrological Data Assimilation. Journal of Hydrology, 564:175-190, doi:10.1016/j.jhydrol.2018.06.080.

Other cross-sectoral collaborations indirectly related to this thesis are

9. **Khaki, M.**, Hamilton, F., Forootan, E., Hoteit, I., Awange, J., Kuhn, M., (2018). Non-parametric Data Integration scheme for Land Hydrological Applications. Water Resources Research, 54:4946–4964, doi:10.1029/2018WR022854.

10. Anyah, R., Forootan, E., Awange, J., **Khaki, M.**, (2018). Understanding linkages between global climate indices and terrestrial water storage changes over Africa using GRACE products. Science of The Total Environment, 635:1405-1416, doi:10.1016/j.scitotenv.2018.04.159.

11. **Khaki, M.**, Hoteit, I., Kuhn, M., Forootan, E., Awange, J., (2018). Assessing Data Assimilation Frameworks for Using Multi-mission Satellite Products in a Hydrological Context. Science of The Total Environment, 647:1031-1043, doi:10.1016/j.scitotenv.2018.08.032.

12. **Khaki, M.**, Awange, J., Forootan, E., Kuhn, M., (2018). Understanding the association between climate variability and the Nile's water level fluctuations and water storage changes during 1992–2016. Science of The Total Environment, 645:1509-1521, doi:10.1016/j.scitotenv.2018.07.212.

13. **Khaki, M.**, Zerihun, A., Awange, J., Gibberd, M., (2018). Integrating satellite soil moisture estimates and hydrological model products over Australia. Manuscript in final stage of acceptance for publication in Australian Journal of Earth Sciences.

14. Forootan, E., **Khaki, M.**, Schumacher, M., Awange, J., Shum, C.K., Akinluyi, F., Ramillien, G., (2018). Monitoring Global Hydrological Droughts Using Multiple Drought Indices from Combined Satellite Products. Revised and resubmitted to Science of The Total Environment.

Abstract

Global water resources are under threat as a result of climate change and the increasing demands for freshwater. This is more problematic for countries that depend on soil moisture and groundwater for agricultural productivity such as Australia and many African and Asian countries. Therefore, it is essential to develop techniques for monitoring and predicting their changes. Land hydrological models have been widely used to study water storage changes in various regions. These models, however, contain uncertainties due to different factors, e.g., data limitations and simplification of hydro-meteorological processes. With a growing number of available datasets especially from satellite remote sensing, there is a great opportunity to increase our understanding of hydrological processes by integrating these data, that are samples of the real world, with hydrological models. Data assimilation is a procedure that constrains the dynamic of a model with available observations in order to improve its estimates. In the past few years, assimilation of terrestrial water storage (TWS) estimates obtained from the Gravity Recovery And Climate Experiment (GRACE) into a hydrological model has gained increasing interests. Integrating GRACE TWS into hydrological models constrains the summation of surface and sub-surface water storage changes, which can introduce missing water storage signals (e.g., anthropogenic) into the models. Importantly, the approach can be applied to improve model simulations over different areas, where there are limited ground-based measurements. GRACE TWS with global coverage can effectively be used to enhance model performance over such regions. GRACE data assimilation, however, is very challenging in terms of filtering the data prior to the assimilation, modeling its errors during the process, and efficiently merging it with models. Assimilating GRACE TWS into a hydrological model requires a strategy for dealing with its spatio-temporal resolutions and corresponding error covariances, as well as an extended review of the existing assimilation filtering techniques and their capabilities for incorporating GRACE observations into the system states. Moreover, the impacts of TWS updates, which can violate the dynamical balances between water fluxes and water storage changes within the model, should be accounted for during the assimilation.

In this thesis, a comprehensive data assimilation framework containing multiple stages is proposed and tested. The framework starts by applying a new filtering method, the Kernel Fourier Integration (KeFIn), to reduce GRACE errors including colored/correlated noise of high-frequency mass variations (i.e., stripes) and spatial leakage errors to prepare the observations for data assimilation. Tuning techniques are then applied to maximize the effect of GRACE observation by using its full error information. Furthermore, the impacts of the GRACE TWS different spatial and temporal resolutions are investigated during assimilation. Multiple sequential data assimila-

tion filtering techniques are examined regarding their performance from various perspectives, e.g., forecasting, state estimate improvement, uncertainties quantification, and stability during the process. Based on the examination of existing assimilation filtering techniques, a new constrained ensemble Kalman filter is introduced that satisfies the closure of the water balance equation after integrating water storage observations while taking the uncertainties in datasets into the account. The performance of the proposed framework at each stage is analyzed through various experiments (i.e., synthetic and real cases) over different spatial domains, e.g., Australia, Bangladesh, and globally distributed basins. Furthermore, multiple datasets including in-situ measurements of groundwater, soil moisture, and discharge measurements, different remotely sensed observations, and independent hydrological model outputs are used to examine the results.

Acknowledgements

First and foremost I offer my sincerest gratitude to my supervisor, Dr Ehsan Forootan (Cardiff University), who has guided me throughout my thesis with his patience and knowledge. You supported me greatly and were always willing to help me. Ehsan, I want to thank you not only for your excellent scientific cooperation but also for more than five years of valuable friendship.

I would like to express my deepest gratitude to my thesis advisors A/Prof Michael Kuhn and Prof Joseph L. Awange for their patience, motivation, enthusiasm, immense knowledge, and continuous support of my Ph.D. study and research. You have provided me extensive personal and professional guidance and taught me a great deal about both scientific research and life in general. My appreciation also goes to Prof Charitha Pattiaratchi (the University of Western Australia) for his guidance. I could not have imagined having a better advisor and mentor for my Ph.D. study.

Special thanks to Curtin International Postgraduate Research Scholarships (CIPRS)/ORD Scholarship provided by Curtin University, programme, which supported my Ph.D. work during the entire period.

I would also like to thank the experts who were involved in this project. Without their passionate participation and input, my researches could not have been successfully conducted.

I sincerely acknowledge all participants who took part in the studies that make up this thesis. Their guidance, help, idea, and feedback have been absolutely invaluable.

Finally, I must express my very profound gratitude to my family, especially to my beloved wife, Elahe, for providing me with unfailing support and continuous encouragement throughout my years of study and through the process of researching and writing this thesis. This accomplishment would not have been possible without them. Thank you.

Contents

Chapter 1

Data Assimilation: Improving monitoring of water storage changes

1.1 Terrestrial water storage

Hydrology and water resource analyses have become more important due to the impacts of climate change (e.g., Huntington, 2006; Adams and Peck, 2008; Piao et al., 2010; Coumou and Rahmstorf, 2012), as well as anthropogenic activities (e.g., Kang et al., 2004; Mohammadi-Ghaleni and Ebrahimi, 2011; Van Camp et al., 2012; Chenoweth et al., 2014; Qureshi et al., 2015). Accurate estimates of water storage changes over land areas can benefit our understanding of these effects on hydrological processes and correspondingly better water resources management. Terrestrial water storage (TWS), defined as the summation of all water stored above, on and below the Earth's surface, e.g., surface storages such as lakes and reservoirs, soil moisture, groundwater, canopy, and snow water, plays an important role in the environment, Earth's climate system, and correspondingly human life all around the world. Quantifying this major water resource is, therefore, essential for environmental assessments and provides information for water resources analyses.

It is also important to investigate TWS interactions with various water budget components including evapotranspiration $\mathbf{e}$, precipitation $\mathbf{p}$, and discharge $\mathbf{q}$ (van Dijk et al., 2014). Any change in any of these components, namely precipitation, evaporation, discharge, and changes in water storage $\Delta\mathbf{s}$ can affect other water budget components due to the existing interrelationship between them through the water balance equation; $\Delta\mathbf{s} = \mathbf{p} - \mathbf{e} - \mathbf{q}$ (e.g., Jung et al., 2010; Eicker et al., 2016). There are various tools such as in-situ measurements, land hydrological models, and satellite remote sensing products that can be used to study water storage changes and their connections to other water compartments.

1.1.1 Hydrological models

Land hydrological models offer important tools for modeling/simulating and predicting hydrological processes at regional (e.g., Chiew et al., 1993; Wooldridge and Kalma, 2001; Christiansen et al., 2007; Huang et al., 2016) and global (e.g., Döll et al., 2003; Huntington, 2006; Coumou and Rahmstorf, 2012; van Dijk et al., 2013) scales. With vast temporal and spatial coverages, hydrological models can provide valuable information at much higher spatio-temporal resolutions than ground-based measurements. The models are based on the water balance equation to describe the relationships between water budget components (Sokolov and Chapman, 1974). This guarantees a balance between water fluxes and water storages within a hydrological model. The model structure governs variations in the water state changes due to the incoming and outgoing hydrological water fluxes. Furthermore, considering that the models rely on the physical processes implemented in the model equations, they are able to provide information about various water components, e.g., groundwater, soil moisture, discharge, and snow water equivalent, which cannot be acquired from either satellite products or in-situ data. In the last few decades, hydrological models (of different kinds; Moradkhani and Sorooshian, 2008; Devi et al., 2015) have extensively been used to determine and monitor stored water and fluxes in different forms such as ice and snow, glaciers, aquifers, soils, and surface waters within landscapes (e.g., Chiew et al., 1993; Wooldridge and Kalma, 2001; Döll et al., 2003; Huntington, 2006; van Dijk, 2010a).

Models are still being developed to better simulate all available hydrological processes (e.g., groundwater recharge) and the inclusion of all interactions between water cycle components (e.g., evapotranspiration, precipitation, and discharge). Nevertheless, due to various sources of uncertainty, for example, imperfect modeling, data limitations on both temporal and spatial resolutions, their errors, as well as limited knowledge about empirical model parameters, the accuracy of model simulations can be degraded (Vrugt et al., 2013; van Dijk et al., 2011, 2014). Making the models more complex introduces ever increasing model parameters that cannot be well interpreted and makes computations more intensive. Alternatively, integrating additional accurate observations into models is an effective approach to overcome these limitations (e.g., McLaughlin, 2002; Zaitchik et al., 2008; van Dijk et al., 2014; Gharamti et al., 2016). Growing number of satellite observations with wide spatio-temporal coverages provide a unique opportunity to improve the models' performances.

1.1.2 Satellite remote sensing

Due to the fast emerging satellite platforms, especially in the last two decades, remote sensing observations with vast spatial and temporal coverage are gaining momentum for studying water resources around the world, especially over areas suffering from insufficient in-situ measurements. Remote sensing observations have been used in a number of studies to analyze Earth's hydrology

by monitoring various water components, e.g., TWS changes (e.g., Landerer and Swenson, 2012; Voss et al., 2013; Longuevergne et al., 2013; Awange et al., 2014a; Forootan et al., 2014a; Yao et al., 2016), soil moisture (e.g., Usowicz et al., 2014; Peng et al., 2015; Enenkel et al., 2016; Ray et al., 2017), precipitation (e.g., Tsonis et al., 1996; Kidd and Levizzani, 2011; Liechti et al., 2012; Awange et al., 2014b; Valdés-Pineda et al., 2016; Alazzy et al., 2017; Najmaddin et al., 2017), evapotranspiration (e.g., Caselles et al., 1992; Kustas and Norman, 1996; Wood et al., 2003; Glenn et al., 2007; Liou and Kar, 2014), water level height fluctuations (e.g., Birkett et al., 2002; Berry et al., 2005; Lee et al., 2009; Hwang et al., 2010; Becker et al., 2010; Khaki et al., 2014, 2015), and vegetation index (e.g., Batten, 1998; Carrasco-Benavides et al., 2010; Prashar and Jones, 2016; Xue and Su, 2017).

Amongst a variety of remotely sensed products, the Gravity Recovery And Climate Experiment (GRACE) satellite mission has a great potential for studying TWS changes. Since 2002, the GRACE satellite mission has been providing time-variable global gravity field solutions (Tapley et al., 2004). These variations are primarily caused by temporal changes in the gravity field due to changes in hydrology, ice masses of the cryosphere, or surface deformation, e.g., glacial isostatic adjustment (GIA). Within a temporal and spatial resolution of respectively one day to one month and a few hundred kilometers, GRACE products have proved to be very useful for various geophysical and hydrological studies (see, e.g., Kusche et al., 2012; Wouters et al., 2014). In particular, the so-called level 2 (L2) time-variable gravity fields have largely been used to quantify global (e.g., Rodell et al., 2004; Eicker et al., 2016; Kusche et al., 2016) and regional (e.g., Chen et al., 2009; Awange et al., 2014a; Munier et al., 2014) TWS changes. Several studies indicate that GRACE TWS can play an important role in better understanding surface and sub-surface physical processes related to water redistribution within the Earth's system (e.g., Huntington, 2006; Chen et al., 2007; Kusche et al., 2012; Forootan et al., 2014a; van Dijk et al., 2014; Wouters et al., 2014; Reager et al., 2015; Schumacher et al., 2016). A growing number of studies has also applied GRACE TWS to constrain the mass balance of hydrological models (e.g., Zaitchik et al., 2008; Thomas et al., 2014; van Dijk et al., 2014; Eicker et al., 2014; Tangdamrongsub et al., 2015; Reager et al., 2015; Tian et al., 2017; Schumacher et al., 2018). These studies show that GRACE TWS data has a great potential to correct for models errors. This, however, can be done more efficiently by using strong filtering strategies that lead to accurate integration.

1.2 Data integration

Data assimilation technique can be used to integrate available observations into models and has found increasing interests in recent decades with the availability of new data sources, such as those derived from satellite remote sensing observations (e.g., soil moisture remote sensing, satellite altimetry and GRACE TWS). Assimilation incorporates new observations of one or more variables

(according to their uncertainties) into a numerical (physical) model to increase consistency of model simulations of a certain variable with its changes in the 'real world' (Bertino et al., 2003; Hoteit et al., 2012). Many studies have implemented data assimilation in the fields of ocean and atmospheric sciences (e.g., Bennett, 2002; Hoteit et al., 2002; Kalnay, 2003; Schunk et al., 2004; Lahoz, 2007; Zhang et al., 2012; Hoteit et al., 2012). This technique has been used frequently in hydrological studies to increase the accuracy of model simulations of soil moisture (e.g., Reichle et al., 2002; Brocca et al., 2010; Renzullo et al., 2014; Kumar et al., 2014, 2015), evapotranspiration (e.g., Schuurmans et al., 2003; Pipunic et al., 2008; Irmak and Kamble, 2009), discharge (e.g., Vrugt et al., 2006; Komma et al., 2008; Neal et al., 2009; Lee et al., 2011; McMillan et al., 2013; Li et al., 2015), and surface water storage (e.g., Neal et al., 2009; Giustarini et al., 2011). There are a number of studies that use GRACE TWS to update hydrological model estimates (e.g., Zaitchik et al., 2008; van Dijk et al., 2014; Tangdamrongsub et al., 2015; Schumacher et al., 2016; Kumar et al., 2016; Girotto et al., 2016, 2017; Schumacher et al., 2018). Nevertheless, merging GRACE TWS data into the hydrological model estimates is associated with difficulties (e.g., accounting for its large correlated errors), which requires appropriate assimilation filtering techniques.

Data assimilation solutions are based on the Bayesian approach (Jazwinski, 1970; van Leeuwen and Evensen, 1996), which consists of updating a prior probability distribution of system states conditional on observations (the so-called posterior distribution; Bousserez and Henze, 2016). Bayes' rule basically computes the Probability Density Function (PDF) of the state, i.e., the model variable of the system that should be estimated, given the data. The updated distribution is then propagated with the model to the time of the next available observation to obtain the prior PDF. In reality, where a nonlinear or non-Gaussian system is present (as in hydrological models), the application of data assimilation becomes more complex because it is not possible to analytically derive the posterior (analysis) PDF of the state anymore (Hoteit et al., 2008; Vrugt et al., 2013). In such cases, the Bayesian estimation problem needs to be solved numerically, which generally can be done using variational or sequential filtering methods (Subramanian et al., 2012).

Variational methods look for the model trajectory that best fits the data by minimizing a chosen cost function that measures the misfit between the model state and the observations (Talagrand and Courtier, 1987). These methods require coding and executing an adjoint model, which is very demanding in terms of human and computational resources (Hoteit et al., 2005). Furthermore, the efficiency of variational methods might be limited to updating the estimation statistics during the data assimilation process (Courtier et al., 1994; Kalnay, 2003). In contrast, sequential techniques condition a prior PDF of the state with available observations to compute the posterior PDF based on Bayes' rule (Koch, 2007) in two steps; (1) a forecast step to propagate the state PDF using a dynamical model (forecasting) and (2) an analysis step to update the forecast PDF by assimilating observations. Monte Carlo methods are commonly used in the forecast step and Kalman (Ensemble Kalman filtering) or point-mass weight (Particle filtering) updates are applied in the analysis

step (Evensen, 2009; Hoteit et al., 2012). Sequential methods do not require an adjoint and are becoming increasingly popular because of their reasonable computational requirements (Hoteit et al., 2002; Bertino et al., 2003; Robert et al., 2006). There are various sequential filtering methods (e.g., ensemble Kalman filter and Particle filters) with different capabilities that can be used for the specific case of GRACE data assimilation.

1.3 Knowledge gaps and data merging challenges

Assimilation of satellite observations and in particular GRACE TWS into a land hydrological model can be challenging. There are various aspects that can affect the process such as the filtering method used as the core of sequential data assimilation techniques, which is important to efficiently update system states using new observations while considering their uncertainties. Furthermore, many remote sensing observations are subject to various sources of errors, e.g., spectral/spatial leakage errors in GRACE data (e.g., Swenson and Wahr, 2002; Seo and Wilson, 2005; Chen et al., 2007), which need to be dealt with before integrating data into a model as otherwise they can substantially degrade the whole process by incorporating inaccurate information into the system of interest. Moreover, anthropogenic impacts on water storage, which are reflected in GRACE TWS data should be investigated during data assimilation. In terms of model and data merging, data assimilation is very sensitive to the uncertainties associated with the model states and assimilated observations. In order to better undertake the process, one requires to fully use observations' error information and invests a considerable amount of efforts on applying tuning techniques during data assimilation to ensure to use the information as much as possible.

1.3.1 GRACE errors

GRACE L2 potential coefficients contain different types of errors. A part of these errors is related to colored/correlated noise due to the anisotropic spatial sampling of the mission, instrumental noise (K-band ranging system, GPS, and the accelerometer observations and star cameras), and temporal aliasing caused by the incomplete reduction of short-term mass variations by models (Forootan et al., 2013, 2014b; Dobslaw et al., 2016). These errors are manifested as north-south striping patterns in the spatial domain (e.g., gridded TWS products). Various smoothing techniques have been put forward to decrease the errors using the smoothing kernels such as the isotropic Gaussian in Jekeli (1981) or non-Gaussian Kernels (e.g., Swenson and Wahr, 2006; Kusche, 2007; Klees et al., 2008). The application of these spatial averaging filters, however, results in spatial interference of mass anomalies, i.e., spatial leakages, which causes signals attenuations. These errors do not allow for perfect separation of gravity anomalies by moving gravity anomalies from one region to another region, e.g., between land and oceans, and limit the detection

of small-scale hydrological signals (e.g., Chen et al., 2007; Baur et al., 2009).

A number of filtering methods have been proposed to mitigate spatial leakage effects. Some studies have estimated the leakages (leakage in and out) numerically using the averaging kernels (e.g., Swenson and Wahr, 2002; Han et al., 2005; Seo and Wilson, 2005; Baur et al., 2009; Longuevergne et al., 2010). There are other filtering methods that are based on scaling factors derived from synthetic data (e.g., Landerer and Swenson, 2012; Long et al., 2015). More recently, the use of inversion techniques for simultaneous signal separation and leakage reduction have also been investigated (e.g., Wouters et al., 2007; Frappart et al., 2011; Forootan et al., 2014b; Frappart et al., 2016). Nevertheless, these filtering methods have different drawbacks, e.g., the reliance on the hydrological model used to estimate the desired scale factors. The inversion techniques, on the other hand, require a prior information about mass changes within different storage compartments. The dependency of final signal separation results on these information has not been reported yet. The accuracy of GRACE TWS estimation is very important for hydrological data assimilation especially at the basin scale, where the sizes of the basins are small in comparison to the spatial resolution of GRACE (e.g., Yeh et al., 2006; Longuevergne et al., 2010). Therefore, better post-processing of GRACE data must be applied to improve consistencies between various types of products that are usually used for studying the water cycle (e.g., Eicker et al., 2016). This requires a powerful filtering method that can mitigate the measurement noise and the aliasing of unmodelled high-frequency mass variations, and also decrease the leakage errors. This problem has been addressed in this thesis and details can be found in Chapter 3 under Khaki et al. (2018a). Once these goals are achieved, GRACE observations can better be used for data assimilation.

1.3.2 Assimilation strategy

In order to efficiently assimilate GRACE data in a land hydrological model, a special focus should be undertaken to consider unique characteristics of the data such as the coarser spatio-temporal resolution compared to most of existing hydrological models. The coarse spatial resolution exists in both GRACE level 2 solutions provided in terms of spherical harmonics potential coefficients or mass concentration (mascon) solutions. Although mascon is provided on a finer spatial scale (e.g., 0.5°), the native resolution of the data is smaller (e.g., 3°; Watkins et al., 2015; Wiese, 2015). Different studies have tried to assimilate GRACE data in either basin scales (e.g., Zaitchik et al., 2008; Houborg et al., 2012; Li et al., 2012) or grid element scales (e.g., Eicker et al., 2014; Tangdamrongsub et al., 2015; Schumacher et al., 2016). Upscaling of the original established TWS with a limited spatial resolution to create a high spatial resolution data (e.g., 1°) with grid points that are not independent of each other increases spatial correlation significantly (see e.g., Schumacher et al., 2016). Accounting for these correlations is important especially in the context of data assimilation, where complete knowledge of the data error structure including uncertainties and existing correlations is necessary.

A successful assimilation filtering method should be able to account for these limitations in GRACE products (see, e.g., Schumacher et al., 2016). Data assimilation as an inverse problem uses the covariance information of model simulations and observations. GRACE correlated errors in the products yield covariance matrices that are badly conditioned or not invertible leading to inefficiency of the filtering process during data assimilation. Due to the lack of information (or to enhance computations), the decision of uncorrelated data (Gaussian error for observations) is often made to deal with this problem. Most of the previous studies assimilated GRACE TWS (e.g., grid-based or basin averaged) into models while assuming white noise (i.e., uncorrelated observations, e.g., in Zaitchik et al., 2008; Reichle et al., 2013; Tangdamrongsub et al., 2015; Kumar et al., 2016; Tian et al., 2017), which for basin averaged applications, might be justified to some extent as the spatial averaging of TWS observations adds up the non-Gaussian noise distributions and generates a mixture that is closer to Gaussian distribution according to the central limit theorem (Stone, 2004, Chapter 5). The uncorrelated observations' assumption, however, can be realistic only when observations' real spatial resolution (e.g., independent grid points of neighbors) is denser than models' (Berger and Forsythe, 2004; Stewart et al., 2008). For other cases such as using GRACE observations with coarser spatial resolution than most of the existing models for data assimilation, this assumption can lead to no improvement in the accuracy of final assimilation results (e.g., Liu and Rabier, 2003; Dando et al., 2007; Stewart et al., 2008). Eicker et al. (2014) studied the relationship of different GRACE spatial resolutions on the data assimilation process and reported that there is always a trade-off between employing GRACE data in a higher spatial resolution while keeping the GRACE error covariance matrices reasonably well conditioned. Girotto et al. (2016, 2017) have considered the fact that 1° GRACE error covariances are spatially highly correlated and to address this issue, they have used a spatial correlation length of 3° for the observation errors. Nonetheless, in these studies, GRACE error covariance for different spatial resolutions is hardly treated. A reliant data assimilation depends on rigorous modeling of the full error covariance matrix of the GRACE TWS estimates, as well as realistic error behavior for hydrological model simulations, which requires not only a robust strategy but also an appropriate filtering method. This is achieved in this thesis by tuning the GRACE data assimilation process in Chapter 4 according to Khaki et al. (2017a).

1.3.3 Data assimilation filters

As mentioned, different filtering methods have been proposed and developed in various fields for data assimilation objectives. Sequential methods, due to their large capability in dealing with high dimensional systems, have obtained more popularity, especially in hydrological applications. Two of the more common Sequential filtering techniques; the Particle filter (PF) and Ensemble Kalman filters (EnKF) have excessively been used in literature (see, e.g., Reichle et al., 2002; Moradkhani et al., 2005; Weerts et al., 2006; Zaitchik et al., 2008; Houborg et al., 2012; Morad-

khani et al., 2012; Eicker et al., 2014; Renzullo et al., 2014; Tangdamrongsub et al., 2015). However, a comprehensive comparison of the different sequential filtering techniques for assimilating GRACE TWS into hydrological models has not been fully explored. To determine the capability of an assimilation filter, there are various aspects that should be considered. In addition to improving the estimation of the system state and quantifying the associated uncertainties, a suitable data assimilation filtering technique is expected to keep the model dynamically stable during the assimilation process while incorporating GRACE data. Furthermore, as an important step in sequential techniques, effective sampling from the observation covariance is sometimes difficult (Whitaker and Hamill, 2002), which can be more critical for the case of GRACE error covariance matrix. There are various resampling techniques proposed for both PF (e.g., Multinomial and Systematic Resampling; Arulampalam et al., 2002) and EnKF (i.e., deterministic EnKFs; Sun et al., 2009; Hoteit et al., 2015) filters. An investigation is required to assess the performance of the common sequential filtering techniques for assimilating GRACE TWS into the hydrological model. A comprehensive examination of various sequential data assimilation techniques for GRACE TWS data assimilation undertaken in this thesis can be found in Chapter 5 according to Khaki et al. (2018b).

1.3.4 Preserving water balance of models after data assimilation

In addition to the importance of data assimilation filtering, the impacts of observations on the consistency between hydrological water fluxes, namely precipitation, evaporation, discharge, and water storage changes within a model should also be taken into an account. The application of data assimilation may violate the dynamical balances between water fluxes and water storage changes (Pan and Wood, 2006). In other words, models water storage states are in balance since model structure, e.g., its equations, governs variations in the water state changes due to the incoming and outgoing hydrological water fluxes. An assimilation of any water storages, as for instance soil moisture and/or terrestrial water storage (TWS), violates the existing balance because the assimilated state does not satisfy the water balance property, which results in mismatches between the estimated $\Delta\mathbf{s}$ and the flux deficit after each assimilation cycle. It is, therefore, essential to account for the water balance problem during assimilation, which allows for better interpretation of the updated water storage changes.

There are only few studies that account for water budget enforcement. Pan and Wood (2006) developed a constrained ensemble Kalman filter (CEnKF) based on the ensemble Kalman filter (EnKF; Evensen, 1994) to solve the disclosure of the water balance equation after implementing data assimilation over the southern Great Plains region of the United States. In addition to the use of CEnKF, Sahoo et al. (2011) and Pan et al. (2012) applied data merging algorithms to prepare the datasets from various sources (e.g., satellite and ground-based measurements) for data assimilation and to account for imbalance over various major river basins (see also Zhang et al., 2016). These studies, however, take advantage of perfect observations assumption in the closure

constraint, which does not account for uncertainties associated with water flux observations during the assimilation. This assumption leads to a strong constraint, which is unrealistic and can cause estimation errors and over-fitting issues (Tangdamrongsub et al., 2017). In order to enhance the estimation of model water storages (e.g., for $\Delta\mathbf{s}$), an effort is needed to involve flux observations errors in the assimilation procedure. This is done by introducing a new 2-step assimilation filter, weak constrained ensemble Kalman filter (WCEnKF) in this thesis (see details in Chapter 7 based on Khaki et al. (2017c)).

1.4 Thesis objectives

The primary objective of this thesis is to propose a unique powerful data assimilation framework to integrate GRACE TWS data into a hydrological model. This is done by introducing new filtering methods or developing existing approaches for the mentioned knowledge gaps in Section 1.3. The specific objectives of this research can be summarized as:

(i) Proposing a new GRACE post-processing, Kernel Fourier Integration (KeFIn), which is designed to reduce both types of GRACE errors including colored/correlated noise of high-frequency mass variations (i.e., stripes) and spatial leakage errors using a two-step algorithm. In the first step, the advantages of image processing techniques such as motion filters (e.g., Hichri et al., 2012; Zhang et al., 2009) are exploited to reduce the measurement noise and aliasing of unmodelled high-frequency mass variations. This attempt is designed to keep as much of the higher frequency information as possible. In the second step of the KeFIn filter, the leakage problem is mitigated using an anisotropic kernel to isolate the signals in the basin of interest. The main idea of this step is to combine the Fourier transform and basin kernel functions to increase the strength of the attenuated signals. It will be shown in the following that the KeFIn filter is suited to deal with basins of various shapes and sizes (Chapter 3, Khaki et al., 2018a).

(ii) Investigating the impacts of different spatio-temporal resolutions of GRACE TWS on the model states during assimilation. This is done by assimilation of GRACE TWS data at the grid resolutions of 1°, 2°, 3°, 4°, 5°, and at basin scale, as well as 5-day and monthly temporal scales. More importantly, a Local Analysis (LA) technique is employed for the first time to account for GRACE error correlation problem in the assimilation procedure. LA allows utilization of different GRACE TWS spatial resolutions by addressing instability in data assimilation that arises from the GRACE covariance matrices of the corresponding spatial resolutions (Chapter 4, Khaki et al., 2017a).

(iii) Assessing the performance of various sequential data assimilation techniques for integrating GRACE TWS into a land hydrological model. This includes diverse versions of the classical

ensemble Kalman filters (EnKF), both stochastic and deterministic variants, as well as Particle filters. These choices provide various opportunities for weighting observations and model simulations during the assimilation and also for investigating error distributions. The main goal is to find the best filtering technique for GRACE data assimilation (Chapter 5, Khaki et al., 2018b).

(iv) Investigating the capability of GRACE data assimilation for using a hydrological model to study water storage changes in different study regions. Based on the best-established tuning (cf. objective ii) and filtering (cf. objective iii) techniques, data assimilation is conducted over various areas (Bangladesh, Iran, and South America in addition to Australia) to monitor its effects on updating water storage simulations. This, further allows us to examine the use of proposed schemes in dealing with different hydrological processes in different areas (Chapter 6, Khaki et al., 2018b,d,e).

(v) Proposing a new two-update ensemble Kalman-based scheme that introduces uncertainty to the water budget balance enforcement equation. In the first update step of the proposed weak constrained ensemble Kalman filter (WCEnKF), water storages are corrected based on the observations as in the EnKF; the introduced water imbalance in this step is then reduced in the second update step by solving the water balance equation that adjusts the water fluxes ($\mathbf{p}$, $\mathbf{e}$, and $\mathbf{q}$) following a second EnKF correction. Two different strategies are considered for pseudo-observations error covariance. It is first assumed to be known while in the second scheme being solved along with system states using an unsupervised framework, i.e., Unsupervised WCEnKF (UWCEnKF) (Chapter 7, Khaki et al., 2017c, 2018c).

1.5 Research outline

The structure of this thesis is organized based on the published papers in the peer-reviewed journals, which are presented in different chapters and summarized in Table 1.1. The introduction (Chapter 1) is followed by six chapters covering the knowledge gaps and thesis objectives. Each of the following chapters, except for Chapter 8, contains a brief introduction and the paper(s) related to the corresponding objectives listed in Chapter 1.4. The last chapter (Chapter 8) concludes the thesis by binding the publications into a collective piece of work and also outlining future steps.

Table 1.1: List of publications in the peer-reviewed journals that are used to fulfil the thesis objectives. The chapter number contains each contribution and the target thesis objective is also indicated.

Paper	Journal	Chapter	Thesis objective
Khaki et al. (2018a)	Remote Sensing of Environment	3	(i)
Khaki et al. (2017a)	Advances in Water Resources	4	(ii)
Khaki et al. (2017b)	Advances in Water Resources	5	(iii)
Khaki et al. (2018b)	Science of The Total Environment	6	(iv)
Khaki et al. (2018c)	Advances in Water Resources	6	(iv)
Khaki et al. (2018d)	Science of The Total Environment	6	(iv)
Khaki et al. (2017c)	Journal of Hydrology	7	(v)
Khaki et al. (2018e)	Journal of Hydrology	7	(v)

Chapter 2

Data, model, and approach

2.1 Hydrological model

As the main part of this thesis, a hydrological model is used to allow for combining model and satellite observations through data assimilation framework. To this end, the World-Wide Water Resources Assessment system (W3RA), based on the Australian Water Resources Assessment - Landscape (AWRA-L) model (version 0.5) is used. The model has been applied in different continental and global studies (e.g., van Dijk et al., 2013, 2014; Beck et al., 2016; Schellekens et al., 2017). W3RA is a one-dimensional globally distributed system, which simulates water balance and landscape water stored in the vegetation and soil systems. More specifically, this model is a hybrid model that combines a grid-based and a lumped catchment model (van Dijk, 2010a). Although that different number of hydrological response units (HRUs) in each grid cell can be assumed, this version of the model contains 2 HRUs including tall, deep-rooted vegetation and short, shallow-rooted vegetation, where each HRU simulates the water balance of the topsoil, shallow soil and deep soil, and leaf biomass. Groundwater and surface water storages, on the other hand, are represented at grid resolution (see more details in van Dijk, 2010b). Meteorological forcing datasets are required to run the model. In this regard, minimum and maximum temperature, downwelling short-wave radiation, and precipitation products provided by Princeton University for the period of 2002 to 2013. This forcing availability limits the temporal scale of the data assimilation experiment to 2002–2013 even though assimilation observations, e.g., GRACE TWS cover a longer period.

In this thesis, daily W3RA estimates the top, shallow and deep root soil water, snow, vegetation, groundwater, and surface water storage are used for data. Regarding the surface water dynamics, this version of the model only represents the (temporary) storage of water in small river channels in the absence of river routing. This means that surface water storage changes in reservoir and lakes are not simulated by the model. Tregoning et al. (2012) also argued that the model merely accounts for surface water storage in the stream network. To address this issue, different scenarios including

removing the surface storage from TWS observations, adding the correct surface storages (from different resources) to W3RA surface water, and neglecting the assimilation effects on surface storage are considered in this thesis. Furthermore, W3RA does not consider anthropogenic effects (e.g., irrigation), thus, efforts are done to see how data assimilation can effectively improve this by incorporating satellite measurements, which contains the above effects (see, e.g., Schumacher et al., 2018), into the model simulations.

2.2 Assimilation observations

Various datasets are used for data assimilation in order to improve model simulations. The main used data is GRACE TWS between 2002 and 2013. In order to derive this product, the GRACE spherical harmonic coefficients up to degree and order 90 with their full error information are acquired from the ITSG-Grace2014 gravity field model (Mayer-Gürr et al., 2014). Traditionally, low degree coefficients are replaced with more accurate estimates, which includes degree 1 coefficients from Swenson et al. (2008) to account for the movement of the Earth's centre of mass and degree 2 and order 0 (C20) coefficients from Satellite Laser Ranging solutions (e.g., Chen et al., 2007). Furthermore, post glacial rebound is considered based on the estimated corrections by Geruo et al. (2013). Various filtering methods are also applied and tested to account for the colored/correlated noise in GRACE products (see details in Chapter 3). Note that in some applications presented in this thesis, filters other than the newly proposed KeFIn are used because of the fact that this filter has not been finalised or evaluated at the time of the respective studies. The L2 gravity fields are then converted to TWS fields at various spatial resolutions, e.g., 1°, 2°, 3°, 4°, 5°, and also a basin averaged scale following Wahr et al. (1998).

Satellite soil moisture products are also applied for data assimilation either along or separate from GRACE TWS. The soil moisture measurements are derived from the Advanced Microwave Scanning Radiometer for EOS (AMSR-E) for the period 2002–2011 and from European Space Agency (ESA) Soil Moisture Ocean Salinity (SMOS) Earth Explorer mission for the period 2011-2013. SMOS and AMSR-E are selected from ascending and descending passes subject to their higher agreement to in-situ measurements (see, e.g., De Jeu and Owe, 2003; Draper et al., 2009; Jackson and Bindlish, 2012; Su et al., 2013). AMSR-E and SMOS reflect soil content of the surface 0-2 cm and 0-5 cm, respectively. Accordingly, the satellite soil moisture products are mainly used to update model state variabilities rather than its absolute values. Cumulative distribution function (CDF) matching (Reichle and Koster, 2004; Drusch et al., 2005) is applied prior data assimilation to rescale observations and remove the bias between the model simulations and observations.

In addition, water fluxes observations of precipitation, evaporation, and discharge are used in the proposed 2-step data assimilation to control for water balance equation (see details in Chapter 7). These observations are acquired from different sources and merged for the period of 2002–

2013. Precipitation data are derived from the Tropical Rainfall Measuring Mission (TRMM-3B43; Huffman et al., 2007), NOAA CPC Morphing Technique (CMORPH; Joyce et al., 2004), the Global Precipitation Climatology Project (GPCP) Version 2.3 (Adler et al., 2003), Global Precipitation Climatology Centre (GPCC; Schneider et al., 2008), and CPC unified gauge dataset (Chen et al., 2002). Evaporation data are collected from MODIS Global Evapotranspiration Project (MOD16; Mu et al., 2007), Global Land Evaporation Amsterdam Model (GLEAM; Miralles et al., 2011), ERA-interim (Simmons et al., 2007), and Variable Infiltration Capacity (VIC) land surface model (Liang et al., 1994). Both precipitation and evaporation products are spatially rescaled into a $1^\circ \times 1^\circ$ with monthly scale. Regarding water discharge observations, data are provided from the Global Runoff Data Centre (GRDC), SIEREM (Systeme d'Informations Environnementales sur les Ressources en Eau et leur Modelisation), an environmental information system for water resources (Boyer et al., 2006), the United States Geological Survey (USGS), China Hydrology Data Project (Henck et al., 2010; Schmidt et al., 2011), the Australian Bureau of Meteorology under the Water Regulations (2008), the National River Flow Archive (NRFA), Department of Hydrology and Meteorology of Nepal, and the Hydrology and Geochemistry of the Amazon basin (HYBAM).

2.3 In-situ measurements

Independent in-situ measurements are used to validate the performance of data assimilation. These include in-situ groundwater and soil moisture measurement, provided from different sources. Well measurements from groundwater stations located in the Mississippi, St. Lawrence, and Murray-Darling basins are converted to storage anomalies using specific yield values acquired from the literature (e.g., Gutentag et al., 1984; Strassberg et al., 2007; Seoane et al., 2013). Soil moisture measurements are collected from the International Soil Moisture Network (ISMN) and the moisture-monitoring network. Efforts are made to extract the representative soil moisture sites (following De Lannoy et al., 2007) and use the corresponding soil moisture values for results evaluations (see also Famiglietti et al., 2008; Orlowsky and Seneviratne, 2014). Furthermore, different soil moisture layers from in-situ measurements are compared with corresponding soil moisture estimates from the model. For example, the model top layer is compared with in-situ measurements of 0-8 cm and 0-10 cm over the Murray-Darling and Mississippi basins, respectively. In-situ measurements of 0-30 cm (the Murray-Darling basin) and 0-50 cm (the Mississippi basin) are used to evaluate summations of the model top, shallow, and a small portion of deep-root soil layers. Finally, summations of the model's soil layers are compared to 0-90 cm (the Murray-Darling basin) and 0-100 cm (the Mississippi basin) soil moisture measurements.

2.4 Auxiliary datasets

In addition to above datasets, different products are used for various objectives such as studying the climate impact, producing synthetic data, and quantifying surface water storage. These data are listed below based on their application in this thesis.

1. Monthly $1^\circ \times 1^\circ$ Mass Concentration blocks (mascons) data (http://grace.jpl.nasa.gov) provided by Jet Propulsion Laboratory (JPL) are used to investigate the performance of the proposed KeFIn filter (Chapter 3). The data represents liquid water equivalent thickness post-processed using a Coastline Resolution Improvement (CRI) filter to separate the land and ocean portions of mass (Wiese, 2015; Watkins et al., 2015).

2. Synthetic experiments are used to further assess the performance of the KeFIn filter (Chapter 3) as well as data assimilation (Chapter 6). To this end, the Global Land Data Assimilation System (GLDAS) NOAH (Rodell et al., 2004) over 2003–2013 is used to generate synthetic monthly ($1^\circ \times 1^\circ$) TWS data, i.e., the summation of soil moisture, snow, and the canopy water storage. Following, the TWS fields are then converted to potential spherical harmonic coefficients (Wang et al., 2006) to test the KeFIn filter against other existing methods. Additionally, the WaterGAP Global Hydrology Model (WGHM; more details on Döll et al., 2003; Müller et al., 2014) TWS estimates with and without water abstractions are used to investigate the effectiveness of data assimilation for distributing corrections, based on the observations, between water compartments such as groundwater and soil moisture (see details on application of data assimilation within Iran in Chapter 6).

3. Multiple datasets are used to estimate surface water storage over different domains. This includes surface water storage data provided by Getirana et al. (2017) over South America and satellite-derived surface water data over Bangladesh provided by Papa et al. (2015). Moreover, satellite radar altimetry data of Jason-1 and -2, and Envisat are used to extend surface water storage over Bangladesh. The altimetry data are also used to derive surface water storage over Lake Urmia. Jason-1 and-2 covering 2002–2013 data are obtained from the Physical Oceanography Distributed Active Archive Center (PO.DAAC) and AVISO, respectively. Additionally, Envisat RA2 products for the period of 2002–2012 are obtained from European Space Agency (ESA). Before using these products for surface water storage estimation, altimeter ranges are corrected for atmospheric (Benada, 1997) and geophysical impacts (Birkett, 1995). Besides, the ExtR retracking method (Khaki et al., 2014, 2015) is applied on waveforms to improve range measurements.

4. In order to study the impacts of climate variabilities on water storage estimated by data assimilation, various datasets are used. In addition to precipitation data (cf. Section 2.2), Version 4 gridded daily Normalized Difference Vegetation Index (NDVI) derived from the

NOAA Climate Data Record (CDR), as well as monthly average temperature data from Climatic Research Unit (CRU; Harris, 2008) are obtained between 2002 and 2013.

2.5 Approach summary

This section summarizes the implemented approach and connection between the different contributions (Chapters 3–7). As mentioned, the study begins by presenting a new GRACE TWS filtering approach, the KeFIn filter, to reduce the measurement noise as well as the leakage errors (Chapter 3). This step is essential due to the great impact of GRACE data for studying TWS changes globally. More importantly, the main assimilation observation that is used in this thesis is GRACE TWS. This highlights the importance of applying an efficient method to improve the data products prior to the application of data assimilation. It will be shown that the application of the KeFIn filtering method successfully decreases the observation errors while accounting for the existing limitations in other filtering methods, e.g., the high sensitivity of them to prior models in the scale factor approaches. Once the observations are improved using the proposed KeFIn filter, they are used for data assimilation. Nevertheless, another step is required to investigate the impact of GRACE TWS on system states. In other words, the unique characteristics of GRACE data in terms of coarse temporal and spatial resolution compared to the hydrological model, make the assimilation process challenging. To this end, while investigating the effects of various spatial (1° to 5° grids, and basin scale) and temporal (5-day and monthly) scales of GRACE observations on the assimilation process, this thesis applies the local analysis (LA) method to maximize the contribution of GRACE TWS (Chapter 4). It is found that applying LA can effectively stabilize the assimilation process when using full GRACE error covariance matrix and further improve the results compared to the case where either no LA is applied or observations are assumed to be uncorrelated. Based on these, LA is applied for all GRACE TWS data assimilations presented here.

The next step is to evaluate the performance of different data assimilation filtering methods for incorporating GRACE TWS into model estimates. This data assimilation filtering assessment is done in Chapter 5, which contains the examination of various sequential data assimilation techniques for merging GRACE TWS into a hydrological model. The applied filters are the standard EnKF and its multiple deterministic variants, as well as Particle filter with two different resampling schemes. The applied methods include the standard EnKF and its deterministic variants, e.g., the Square Root Analysis (SQRA) scheme following Evensen (2004), the Ensemble Transform Kalman Filter (ETKF, Bishop et al., 2001), the Deterministic EnKF (DEnKF, Sakov and Oke, 2008), the Ensemble Square-Root Filter (EnSRF, Whitaker and Hamill, 2002), and the Ensemble Optimal Interpolation (EnOI, Evensen, 2003). Additionally, two nonlinear Particle filters based on two different resampling strategies: (i) Multinomial Resampling and (ii) Systematic Resampling techniques (Arulampalam et al., 2002) are tested. These methods are frequently used in the

community of data assimilation and offer less computational burden than previously used smoothing filtering methods such as the Ensemble Kalman Smoother (EnKS, see, e.g., Zaitchik et al., 2008; Houborg et al., 2012). As it will be presented, two extensions of the deterministic EnKF, the Square Root Analysis (SQRA) scheme and the Ensemble Square Root Filter (EnSRF), obtain the best results, thus, are used for the applications studies (Chapter 6).

In the applications studies, data assimilation using the best case scenarios from above is applied over Bangladesh, Iran, and South America. These studies are carried out to investigate (i) the capability of data assimilation for improving model simulation over different areas, and (ii) to study water storage changes in different compartments, e.g., groundwater and soil moisture. Furthermore, different statistical analyses, e.g., empirical mode decomposition (EMD, Chen et al., 2007), Canonical Correlation Analysis (CCA, see, e.g., Chang et al., 2013), and principal component analysis (PCA, Lorenz, 1956) are done to investigate the connection between these changes and climate variabilities to further assess the performance of data assimilation. Finally, the impact of data assimilation on the water balance equation in hydrology is investigated (Chapter 7). The WCEnKF filtering method and its extension UWCEnKF are proposed to retrieve the broken balance between water components after each data assimilation step. It will be shown that the proposed 2-step filtering mechanism effectively reduces imbalance error while improving estimates, especially compared to the general EnKF.

Chapter 3

GRACE error filtering

This chapter is covered by the following publication:

- **Khaki, M.**, Forootan, E., Kuhn, M., Awange, J., Longuevergne, L., Wada, Y., (2018a). Efficient Basin Scale Filtering of GRACE Satellite Products. Remote Sensing of Environment, 204:76-93, doi:10.1016/j.rse.2017.10.040.

This contribution illustrates a newly proposed GRACE data filtering technique, Kernel Fourier Integration (KeFIn) filter, to address the thesis objective (i) in Section 1.4. The filter is designed to smooth out GRACE measurement noises, e.g., colored/correlated noises and then reduces leakage effects. The KeFIn filter's performance is compared with commonly used filters using synthetic data over 43 globally distributed river basins and water flux observations through the water balance equations, as well as in-situ measurements. Results show considerable improvements in GRACE TWS filtered by the KeFIn filter in the experiments, i.e., more leakage error reductions in 34 out of the 43 tested river basins and larger agreement to in-situ measurements. For the remaining 9 basins, most of the applied filters including the KeFIn filter perform relatively close, which can be due to higher leakage errors in observations and correspondingly difficult for filters to retrieve the signals. The KeFIn filtering method successfully mitigates the existing problems with other leakage filtering methods, e.g., the high sensitivity of them to prior models in the scale factor approaches. The filter is also more flexible to different basins with various shapes and sizes. It is worth mentioning that efforts are made to use the full potential of other applied methods to better assess the KeFIn filter. Nevertheless, it can be expected that fully tuned filters, e.g., using different models for scale factor approaches, perform better compared to the configurations used in this study. By improving the GRACE-derived TWS, the proposed filter can positively affect the GRACE data assimilation, especially in small-scale basins. This covers the first knowledge gap outlined in Section 1.3.

Remote Sensing of Environment 204 (2018) 76–93

Contents lists available at ScienceDirect

Remote Sensing of Environment

journal homepage: www.elsevier.com/locate/rse

Efficient basin scale filtering of GRACE satellite products

M. Khaki[a,*], E. Forootan[b], M. Kuhn[a], J. Awange[a], L. Longuevergne[c], Y. Wada[d,e,f,g]

[a] Department of Spatial Sciences, Curtin University, Perth, Australia
[b] School of Earth and Ocean Sciences, Cardiff University, Cardiff, UK
[c] CNRS Gosciences Rennes, Universit de Rennes 1, Rennes, France
[d] Department of Physical Geography, Faculty of Geosciences, Utrecht University, Utrecht, The Netherlands
[e] NASA Goddard Institute for Space Studies, 2880 Broadway, New York, NY 10025, USA
[f] Center for Climate Systems Research, Columbia University, 2880 Broadway, New York, NY 10025, USA
[g] International Institute for Applied Systems Analysis, Laxenburg, Austria

ARTICLE INFO

Keywords:
GRACE filter
River basin
Leakage reduction
Hydrology
Hydrological fluxes

ABSTRACT

The Gravity Recovery And Climate Experiment (GRACE) satellite mission provides time-variable gravity fields that are commonly used to study regional and global terrestrial total water storage (TWS) changes. These estimates are superimposed by different error sources such as the north–south stripes in the spatial domain and spectral/spatial leakage errors, which should be reduced before use in hydrological applications. Although different filtering methods have been developed to mitigate these errors, their performances are known to vary between regions. In this study, a Kernel Fourier Integration (KeFIn) filter is proposed, which can significantly decrease leakage errors over (small) river basins through a two-step post-processing algorithm. The first step mitigates the measurement noise and the aliasing of unmodelled high-frequency mass variations, and the second step contains an efficient kernel to decrease the leakage errors. To evaluate its performance, the KeFIn filter is compared with commonly used filters based on (i) basin/gridded scaling factors and (ii) ordinary basin averaging kernels. Two test scenarios are considered that include synthetic data with properties similar to GRACE TWS estimates within 43 globally distributed river basins of various sizes and application of the filters on real GRACE data. The KeFIn filter is assessed against water flux observations through the water balance equations as well as in-situ measurements. Results of both tests indicate a remarkable improvement after applying the KeFIn filter with leakage errors reduced in 34 out of the 43 assessed river basins and an average improvement of about 23.38% in leakage error reduction compared to other filters applied in this study.

1. Introduction

Since 2002, the Gravity Recovery And Climate Experiment (GRACE) satellite mission has been providing time-variable global gravity field solutions (Tapley et al., 2004). These variations are primarily caused by temporal changes in the gravity field due to changes in hydrology, ice masses of the cryosphere, or surface deformation, e.g., glacial isostatic adjustment (GIA). Within a temporal and spatial resolution of respectively one day to one month and a few hundred kilometers, GRACE products have proved to be very useful for various geophysical and hydrological studies (see, e.g., Kusche et al., 2012; Wouters et al., 2014, for applications). In particular, the so-called level 2 (L2) time-variable gravity fields are widely used to quantify global (e.g., Eicker et al., 2016; Kusche et al., 2016; Rodell et al., 2004) and regional (e.g., Awange et al., 2014; Chen et al., 2009; Khaki et al., 2017a,b; Munier et al., 2014) terrestrial total water storage (TWS) changes, i.e., the sum of changes in surface and sub-surface water storage compartments. GRACE products are also applied to estimate changes of the terrestrial water cycle (e.g., Eicker et al., 2016; Ogawa et al., 2011) or to validate the water cycle in atmospheric reanalyses (e.g., Forootan et al., 2017; Kusche et al., 2016; Springer et al., 2014). Combined with information observed from other monitoring techniques (e.g., GPS and satellite altimetry) or simulations by land surface models, L2 products are applied to estimate surface (e.g., lakes and rivers) and sub-surface(e.g., soil moisture and groundwater) storage changes at (river) basin scales (e.g., Famiglietti and Rodell, 2013; Forootan et al., 2014; Longuevergne et al., 2010; Syed et al., 2005).

GRACE L2 products are provided in terms of potential spherical harmonic coefficients, e.g., up to degree and order 60 or 90, which mainly represent the large- to medium-scale (e.g., few hundred km) time-variable gravity changes. However, the L2 potential coefficients contain different types of errors. A part of these errors is related to

* Corresponding author.
E-mail address: Mehdi.Khaki@postgrad.curtin.edu.au (M. Khaki).

http://dx.doi.org/10.1016/j.rse.2017.10.040
Received 25 March 2017; Received in revised form 11 October 2017; Accepted 22 October 2017
Available online 07 November 2017
0034-4257/

colored/correlated noise due to the anisotropic spatial sampling of the mission, instrumental noise (K-band ranging system, GPS, and the accelerometer observations and star cameras), and temporal aliasing caused by the incomplete reduction of short-term mass variations by models (Dobslaw et al., 2016; Forootan et al., 2013, 2014a). These errors are manifested as north–south striping patterns in the spatial domain (e.g., gridded TWS products). The application of smoothing techniques with the primary aim of removing the stripes can lead to spatial leakages. The spatial averaging introduced by the smoothing kernels such as the Gaussian Kernel in Jekeli (1981) or non-Gaussian Kernels in Kusche (2007), results in spatial interference of mass anomalies. These leakage errors do not allow for perfect separation of gravity anomalies, e.g., between land and oceans, and limit the detection of small-scale hydrological signals. The accuracy of GRACE TWS estimation is very important for hydrological applications especially at the basin scale, e.g., to interpret redistribution of water storage or to indicate drought and flood patterns (e.g., Awange et al., 2016; Longuevergne et al., 2010; Yeh et al., 2006). Therefore, better post-processing of GRACE data must be applied to improve consistencies between various types of products that are usually used for studying the water cycle (e.g., Eicker et al., 2016).

Different filtering methods have been proposed to reduce north–-south striping errors, such as the isotropic Gaussian filter (Jekeli, 1981) and anisotropic filters (e.g., Klees et al., 2008; Kusche, 2007; Swenson and Wahr, 2006). A comprehensive review on filtering techniques has been done e.g., by Frappart et al. (2016). The isotropic Gaussian filter Jekeli (1981) is a degree-dependent filter in the spectral domain and bell-shaped filter in the spatial domain. Anisotropic filters, on the other hand, are introduced to deal with the correlated errors between the coefficients of L2 products (e.g., different marginal shapes in the north–south and the east–west directions). In general, filtering techniques that spatially smooth the L2 signal contents (e.g., Kusche et al., 2009; Wahr et al., 2006) down-weight L2's higher degree and order potential coefficients. Although these filters reduce noises, their main problem is that they also attenuate the signals. In addition, the application of filtering moves gravity anomalies from one region to another region. Generally speaking, after applying a smoothing kernel some parts of the signals inside an area of interest leak out from it or alternatively signals from outside leak into the area of interest (e.g., Baur et al., 2009; Chen et al., 2007). These issues become more critical for basin-scale studies, especially where the sizes of the basins are small in comparison to the spatial resolution of GRACE (e.g., Longuevergne et al., 2010; Yeh et al., 2006).

Several methods have been put forward to mitigate spatial leakage effects in TWS estimations from L2 products. These methods can largely be categorised into the following three groups (i) those that numerically estimate the leakages (leakage in and out) using the averaging kernels (e.g., Baur et al., 2009; Longuevergne et al., 2010; Seo and Wilson, 2005), (ii) those that are based on scaling factors derived from synthetic data (e.g., Landerer and Swenson, 2012; Long et al., 2015), and (iii) those that use inversion for simultaneous signal separation and leakage reduction (e.g., Forootan et al., 2014; Frappart et al., 2011, 2016; Wouters and Schrama, 2007). From the first group, Swenson and Wahr (2002) developed an isotropic kernel using a Lagrange multiplier filter to best balance signal and leakage errors over a basin of interest. A non-isotropic Gaussian filter proposed by Han et al. (2005) to improve spatial resolution during the filtering process also belongs to this group. In another effort, Harig and Simons (2015) used Slepian-function analysis to decrease leakage effects in Antarctica by maximizing signal energy concentration within the area of interest. The second category uses synthetic data, e.g., from land surface models (LSMs) or hydrological fluxes to derive scaling factors that can be multiplied by GRACE filtered products to recover the lost signals. In this approach, efforts are focused on the application of the same filtering techniques to the synthetic data (that is close enough to the signal contents of GRACE products). Basin-averaged or gridded scale factors are usually estimated as the solution of a least squares adjustment that compares data before and after application of the filter. Landerer and Swenson (2012) estimated gridded scaling factors for GRACE TWS anomalies to restore the signals lost after applying a regular smoothing filter (a Gaussian smoothing kernel). A similar study that uses a different spatial scale (basin averages) has been performed by Long et al. (2015) who estimated scale factors using a global hydrological model over the Yangtze River Basin in China. A possible drawback of this approach is its dependency on the reliability of the hydrological model used to estimate the desired scale factors. The inversion techniques in (iii) also require a prior information about mass changes within different storage compartments. The dependency of final signal separation results on these information has not been reported yet.

To address the above problems arising from the application of filtering methods, the present study proposes a new filtering method, Kernel Fourier Integration (KeFIn), which is designed to reduce both types of above-mentioned errors using a two-step algorithm. In the first step, the advantages of image processing techniques such as motion filters (e.g., Hichri et al., 2012; Zhang et al., 2009) are exploited to reduce the measurement noise and aliasing of unmodelled high-frequency mass variations. This attempt is designed to keep as much of the higher frequency information as possible. It should be mentioned here that, although the proposed KeFIn filter has less effect on high-frequency signals compared to the existing methods, some signal inferences still exist mainly due to the truncation of degree and order in L2 products. In the second step of the KeFIn filter, the leakage problem is mitigated using an anisotropic kernel to isolate the signals in the basin of interest. The main idea of this step is to combine the Fourier transform and basin kernel functions to increase the strength of the attenuated signals. It will be shown in the following that the KeFIn filter is suited to deal with basins of various shapes and sizes.

The primary objectives of this study is developing a filter for (i) dealing with colored/correlated noise of high-frequency mass variations (i.e., stripes); and (ii) reducing basin scale spatial leakage errors for hydrological applications. These objectives are addressed by introducing novel methodologies discussed in Sections 3.1.1 and 3.1.2, respectively. The performance of the introduced filtering method (KeFIn) in terms of leakage reduction is compared with commonly used methods that deal with leakage problem from the basin averaging kernel and the model-based scaling factor groups. For this purpose, both real and synthetic data sets are employed. The purpose of using synthetic data is to provide a more accurate evaluation of the newly proposed method in comparison to existing methods (e.g., Chen et al., 2009; Seo and Wilson, 2005). Therefore, we generate synthetic data in 43 globally distributed basins and use them to examine the performance of the proposed KeFIn and other commonly used filters. These filters are further assessed using water flux observations in the context of the water balance equation (see Eq. (1) in Section 2.3), as well as by comparisons with in-situ measurements.

2. Data

2.1. GRACE

Monthly GRACE L2 products along with their full error information are computed at the Technical University of Graz known as the ITSG-Grace2014 gravity field models (Mayer-Gürr et al., 2014). We use these products and their full covariance errors up to degree and order 60 covering the period 2002–2013 (https://www.tugraz.at/institute/ifg/downloads/gravity-field-models/itsg-grace2014). Degree 1 coefficients are replaced with those estimated by Swenson et al. (2008) to account for the movement of the Earth's center of mass. Degree 2 and order 0 (C20) coefficients are replaced by those from Satellite Laser Ranging solutions owing to unquantified large uncertainties in this term (e.g., Chen et al., 2007). We also account for the post-glacial rebound by incorporating the corrections provided by Geruo et al. (2013). The L2

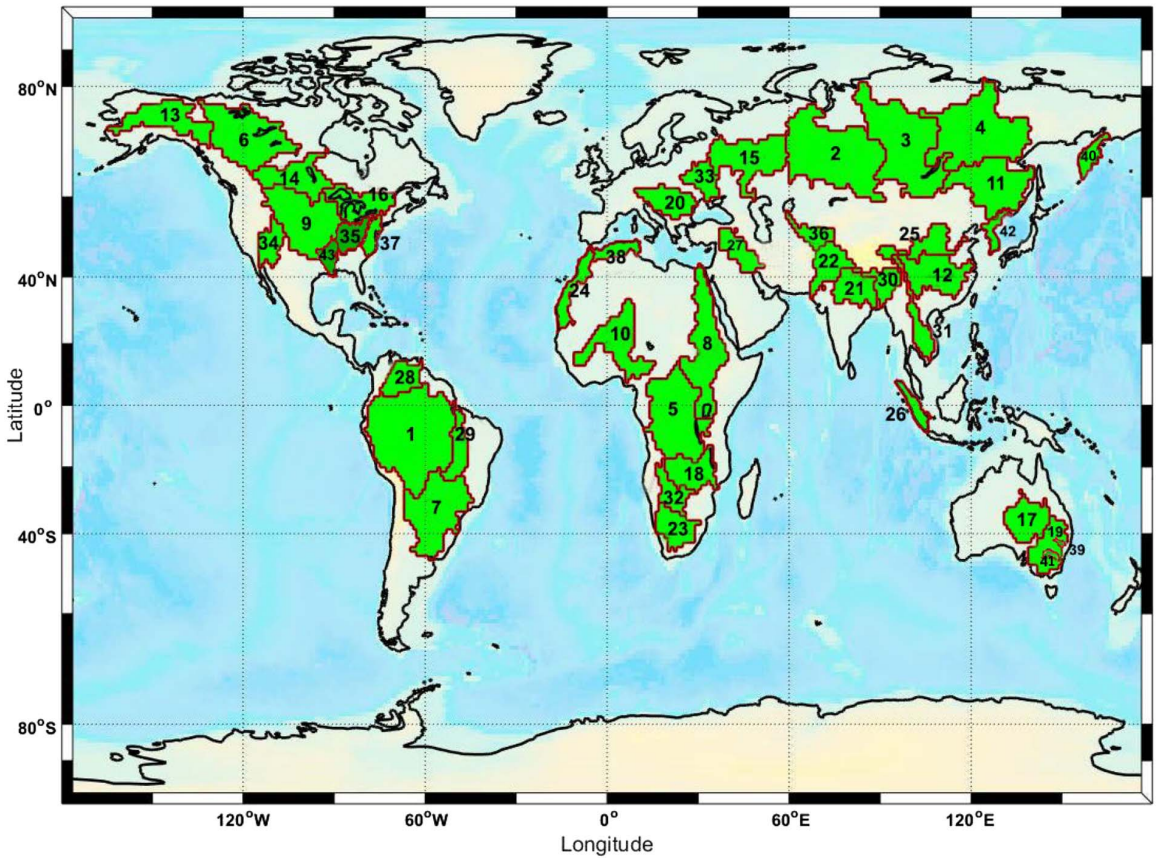

Fig. 1. Shapes, sizes and locations of the world's 43 major river basins (red borders and green areas) used in this study. (For interpretation of the references to color in this figure legend, the reader is referred to the web version of this article.)

gravity fields are then converted to $1^\circ \times 1^\circ$ TWS fields following the approach of Wahr et al. (1998). To evaluate the filtering techniques, no smoothing filter is applied at this stage on GRACE L2 products.

2.2. Synthetic data

In order to assess the efficiency of different filtering methods considered in this study, they are applied on synthetic data whose advantage is the possibility to unambiguously estimate leakage errors since the applied post-processing techniques must replicate the synthetic input data. For this purpose, the world's 43 major river basins with diverse sizes and shapes located at different places around the Earth are chosen (see Fig. 1). A large number of significantly different basins helps us to properly investigate the efficiency and reliability of the newly proposed KeFIn filter.

For synthetic TWS data, a summation of monthly ($1^\circ \times 1^\circ$) soil moisture, snow, and the canopy water storage from the Global Land Data Assimilation System (GLDAS) NOAH (Rodell et al., 2004) over 2003–2013 is used (http://giovanni.sci.gsfc.nasa.gov/). Following Wang et al. (2006), the TWS fields are converted to potential spherical harmonic coefficients up to degree and order 120. Only those coefficients that are up to degree and order 60 are used to generate similar spectral content as the real GRACE L2 products. These data are perturbed by north–south striping errors using the full covariance matrix of ITSG-Grace2014 products. Using the Cholesky decomposition method, the monthly covariance matrices are split into their upper triangular and their conjugate transpose matrices. By multiplying each of the upper triangular matrices with a column of the unit random matrix, the GRACE-type realizations of monthly errors are generated (see, e.g., Forootan and Kusche, 2012; Kusche et al., 2016). GLDAS TWS outputs are also used to compute model-derived scale factors using forward modelling following Long et al. (2015). These hydrological data sets have also been used to estimate gridded gain factors following Landerer and Swenson (2012). Results of these filters will be compared to the KeFIn filtering approach (see Section 4.1).

2.3. Auxiliary data sets

Recently developed Mass Concentration blocks (mascons) data (http://grace.jpl.nasa.gov) provided by Jet Propulsion Laboratory (JPL) are used to analyze their correlation to our estimation from L2 products as shown in Appendix A. The monthly JPL RL05 M Mascon solution is post-processed liquid water equivalent thickness data using a Coastline Resolution Improvement (CRI) filter to separate the land and ocean portions of mass (Watkins et al., 2015; Wiese, 2015). We apply land-grid-scaling coefficients provided with the data to water equivalent thicknesses in $1^\circ \times 1^\circ$ spatial resolution. These filtered data are compared with the results of filters applied in this study.

In addition, the temporal derivative of filtered GRACE data, known as total (hydrological) water fluxes (TWF) is compared with measured precipitation (P), Evapotranspiration (ET), and surface water discharge (or runoff, R) through the water balance equation below:

$$dS/dt = TWF = P - ET - R, \quad (1)$$

where the dS/dt represents TWF derived from the ITSG-Grace2014 products following the procedure in Eicker et al. (2016). The assessment in Eq. (1) requires additional hydrological water flux measurements, which are not easily accessible globally. Eight river basins are selected to perform this assessment, i.e., the Amazon (South America), Mekong (Southeast Asia), Arkansas-White (North America), Ohio

(North America), Lachlan (Australia), Namoi (Australia), Lower Mississippi (North America), and Macquarie-Bogan (Australia) basins. We use water fluxes data from both satellite remotely sensed and ground-based data. P is obtained from the Tropical Rainfall Measuring Mission (TRMM 3B43-v7, Huffman et al., 2007, from http://pmm.nasa.gov/data-access/downloads/trmm), and ET from Moderate the Resolution Imaging Spectroradiometer (MODIS-MOD16; the University of Montana's Numerical Terradynamic Simulation group). In addition, in-situ water discharge data sets are provided from different sources including the Global Runoff Data Centre (GRDC), the United States Geological Survey (USGS), hydrological and biogeochemical alteration and material transfers in the Amazon Basin (HYBAM, from http://www.ore-hybam.org/) that publish originally collected data by Brazilian Water Agency (ANA, http://www.snirh.gov.br/hidroweb/), New South Wales (NSW) Government for the Upper Murray river basin (from http://waterinfo.nsw.gov.au/), and China Hydrology Data Project (Henck et al., 2010; Schmidt et al., 2011).

Each data set is associated with a level of uncertainty and varies for different basins due to the diverse climatological condition. A number of studies has investigated the validity of above observations over various basins, e.g., Cai et al. (2012), Yan et al. (2014), andAwange et al. (2016) for TRMM, as well as Velpuri et al. (2013), Ramoelo et al. (2014), and Miralles et al. (2016) for MODIS products. Precipitation errors highly depend on temporal and spatial resolution (Chen et al., 2008). Uncertainty in measuring precipitation over lands are smaller compared to oceans since satellite data are merged with in-situ stations that are distributed over the continents. The major source of uncertainty in MOD16 is the misclassification of landcover types from the MODIS land cover products, scaling from flux tower to landscape, and other algorithm limitations (Ramoelo et al., 2014). Evaluation of MODIS data in previous studies (e.g., Mu et al., 2011; Zhang et al., 2010) have shown a good agreement between the data and eddy flux tower observations. The consideration of associated errors to the observation for imbalance problem in water budget closure (using Eq. (1)) is beyond the scope of this study, and the post-processing is restricted to filtering out the highly noisy measurements.

2.4. In-situ measurements

Groundwater in-situ measurements are used to assess filters' results. To this end, we provide bore stations data sets over the Arkansas-White, Ohio, and Lower Mississippi basins within the Mississippi Basin from USGS and Lachlan, Namoi, and Macquarie-Bogan basins within the Murray-Darling Basin from New South Wales (NSW) Government. The distribution of groundwater in-situ stations is presented in Fig. 2. Monthly well measurements are acquired and time series of groundwater storage anomalies are generated. Generally, a specific yield is required to convert well-water levels to variations in groundwater storage (GWS) in terms of equivalent water heights (Rodell et al., 2007; Zaitchik et al., 2008). Following Strassberg et al. (2007), we use an average (0.15) of specific yields ranging from 0.1 to 0.3 (suggested by Gutentag et al., 1984) over the Arkansas-White, Ohio, and Lower Mississippi basins, and 0.13 specific yield from the range between 0.115 and 0.2 (suggested by the Australian Bureau of Meteorology (BOM) and Seoane et al., 2013) for the Lachlan, Namoi, and Macquarie-Bogan basins.

Furthermore, we use in-situ soil moisture (SM) measurements obtained from the moisture-monitoring network (http://www.oznet.org.au/), as well as International Soil Moisture Network (https://ismn.geo.tuwien.ac.at/). These data provide long-term records of measured volumetric soil moisture at various soil depths for distributed stations (cf. Fig. 2). For each station and each depth, soil moisture anomalies over the study period are calculated. Following Strassberg et al. (2009), data for stations with shallow measurements are upscaled using soil moisture data from deeper stations. We then calculate average soil moisture storage anomalies from all stations within a $1^\circ \times 1^\circ$ cell. The same averaging process is done for groundwater measurements. Afterwards, area-weighted anomaly of groundwater and soil moisture are used to achieve GWS + SM. We use these GWS + SM, following Strassberg et al. (2009) and Longuevergne et al. (2010), to evaluate the performance of different filters considered in this study. This method does not account for snow water equivalent, canopy, and surface water storages due to their small contribution in TWS over the Mississippi (less than 5%, e.g., Strassberg et al., 2007) and Murray-Darling (less than 6%, e.g., BOM and Burrell et al., 2015) basins. In addition to GWS + SM, we also compare the results with only GWS by computing their correlation coefficients (see details in Section 4.2).

3. Methods

In this section, first, details of the proposed KeFIn technique are discussed. Afterwards, the other implemented filters including four filters based on the basin averaging approach and two filters that use scale factors' are presented. These techniques are chosen due to their popularity in hydrological studies.

3.1. Kernel Fourier Integration (KeFIn) filter

3.1.1. The KeFIn method — first step

The KeFIn approach follows a straight forward image processing technique, which has been widely applied to geophysical images to enhance their visual interpretation and geological understanding (Zhang et al., 2005). The application of image enhancement methods is also beneficial for users that are less familiar with processing and filtering the standard GRACE L2 products. The KeFIn includes two processing steps: (1) designing a 2D destriping filter in the spectral domain, and (2), defining an efficient averaging kernel to estimate basin average TWS and at the same time decreasing the leakage-in and -out in the grid domain. A 2-D filter in the spectral domain (Hichri et al., 2012; Zhang et al., 2009) is defined as:

$$G(u, v) = F(u, v)\cdot H(u, v), \tag{2}$$

where $G(u,v)$ stands for a Fourier transform of the noisy TWS fields with u and v being spatial frequencies, F denotes a Fourier transform of the ideal (unperturbed) signal (here the 'signal part' or the 'true' TWS values), H is a Fourier transform of a 2-D smoothing kernel to suppress the 'noise' part of the observations, and the dot represents the matrix multiplication. Ideally, F can be estimated by applying an inverse filtering if G and H are known.

In general, however, the information on H does not exist, and its determination usually requires some trial-and-error procedures. Besides, noise in data sets can be amplified leading to the destruction of previous attempts made in reconstructing the TWSs. One solution for restoring F is to use the Wiener Filter (W_i) as $F = W_i \cdot G$, which allows to use an averaging kernel as H to estimate F. Here, a motion filter is used as an averaging kernel (H) to mitigate the south–north stripping problem with different smoothing lengths, which provides us a convolutive filter with different averaging. More detail on creating the kernel with various smoothing lengths can be found e.g., in Bhagat and Gour (2013) (see Eq.(5)). The impact of smoothing length on the final TWS estimations is presented in Section 4.1.

Thereafter, F can be estimated using H and the Wiener Filter process as:

$$F(u, v) = \frac{|H(u, v)|^2\cdot G(u, v)}{|H(u, v)|^2\cdot H(u, v) + K}, \tag{3}$$

where K is a signal to noise ratio (Le Roux et al., 2010). A suitable estimate for K can be derived as:

$$K = S_G/S_F, \tag{4}$$

where S_G is estimated from the power spectral density of the noisy observed signal (G), and S_F is derived from the power spectral density of

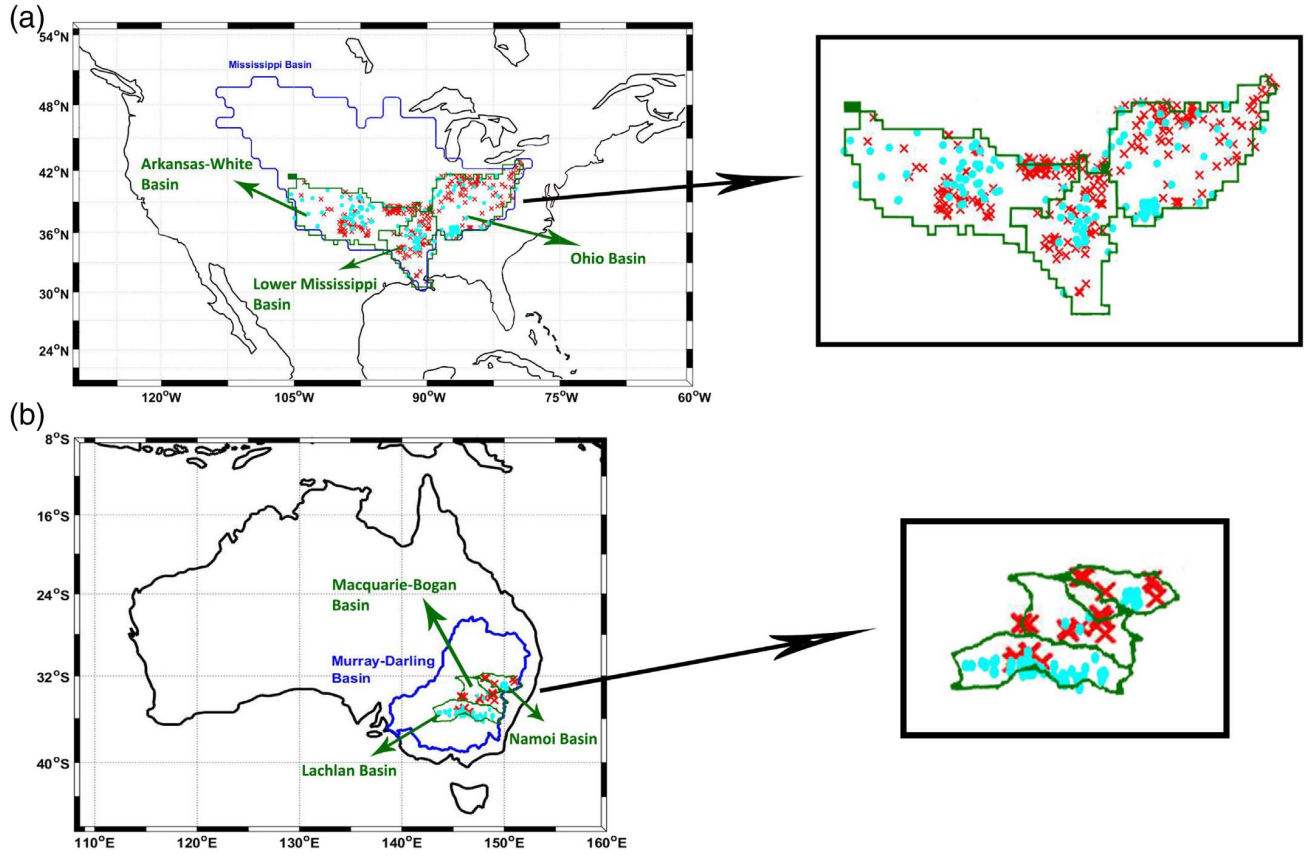

Fig. 2. Distribution of groundwater (red crosses) and soil moisture (cyan circles) stations over the six selected river basins of Arkansas-White, Lower Mississippi, Ohio, Macquarie-Bogan, Namoi, and Lachlan basins. (For interpretation of the references to color in this figure legend, the reader is referred to the web version of this article.)

the ideal (unperturbed) signal (F). The main difference between the new filter and an ordinary Gaussian filter at this stage is the inclusion of the parameter K, which makes Wiener filter more robust and better suited to reduce high-frequency spatial patterns that likely correspond to high magnitude striping patterns. Besides, it introduces a reasonable trade off that minimizes errors of the smoothing process. In order to calculate K in Eq. (4), S_G is derived from G. For S_F, where no information of ideal signal F exists, one can estimate the power spectral density of TWS estimated from a hydrological model and use the mean/median of the estimated powers of S_F (see details in Pitas, 1993). Alternatively one can derive S_F by trial-and-error from a range of values (here [0 10]) to control the smoothness of the output, e.g., when the signal is very strong relative to the noise, selecting $K \approx 0$ yields less smoothed signals. Different values of K and their impacts on the smoothness of TWS estimations are discussed in Section 4.1. Here, we also use average model TWS estimates from GLDAS NOAH during the study period to compare with the value of K obtained through trial-and-error. The proposed scheme retains most of the high-frequency (spatial) changes that are usually over-smoothed by an ordinary smoothing process (Sonka et al., 2001).

3.1.2. The KeFIn method — second step

In the second step of the KeFIn filter, we try to mitigate the problem that arose from the previous stage, i.e., leakage effects caused by spatial smoothing. In what follows, first, spatial averaging and the leakage problem are discussed, then a kernel is defined to reduce the leakage-in and leakage-out errors at the same time. Spatial averaging (Eq. (5)) is usually applied for improving surface mass anomalies within a specific area (Longuevergne et al., 2010; Swenson and Wahr, 2002; Vishwakarma et al., 2016),

$$F_R = \frac{1}{R}\int F\ h\ d\Omega, \tag{5}$$

where,

$$R = \int h\ d\Omega, \tag{6}$$

and F_R is the change in vertically integrated water storage averaged over the region of interest, shown by R, with the integrals done on a sphere. In both equations, h is a basin kernel with values 1 inside the basin and 0 outside of it as,

$$h(X) = \begin{cases} 1 & \text{if } X \in R \\ 0 & \text{if } X \in \Omega - R. \end{cases} \tag{7}$$

X refers to the positions on the surface of the Earth and Ω refers to the entire Earth's surface. Let us assume that $\overline{F}$ is derived after applying a filter (that contains smoothing) in step 1. The smoothing moves signals both inside and outside of the basin. In the following, we start by separating the signal F inside and outside the basin and investigate the effects of smoothing leading to $\overline{F}$.

The whole water storage changes can be written as a summation of water storage signals inside and outside the basin following Vishwakarma et al. (2016) represented by the terms Fh and $F(1-h)$, respectively, in Eq. (8) as,

$$\begin{aligned} F &= F\ h + F\ (1-h), \\ &= F_R + F_{1-R}. \end{aligned} \tag{8}$$

This is equal to Eq. (9) after applying the smoothing procedure from the first step, i.e.,

$$\overline{F} = \overline{F_l} + \overline{F_l}^*, \tag{9}$$

where $\overline{F_l}$ is the smoothed signals inside the basin (with leakage out effects) and $\overline{F_l}^*$ refers to the smoothed signals outside the basin (with leakage in effects). By multiplying both sides of Eq. (9) by h (Eq. (10)) and $(1-h)$ (Eq. (11)), we achieve the filtered water storage over the region R and outside of it $(1-R)$.

$$\overline{F}_R = \overline{F}_{l\,R} + E_{leakage\ in}, \tag{10}$$

$$\overline{F}_{1-R} = \overline{F}^*_{l\,1-R} + E_{leakage\ out}. \tag{11}$$

Considering that $\overline{F}_{l\,R}$ and $\overline{F}_{l\,1-R}$ are the attenuated signals of F_R and F_{1-R}, Longuevergne et al. (2010) showed that they are related using a scaling factor s. For signals inside the basin (the same approach can be used for signals outside the basin), it can be shown that,

$$F_R = s\,\overline{F}_{l\,R}, \tag{12}$$

$$s = \frac{\int h\ d\Omega}{\int h\ \bar{h}\ d\Omega}, \tag{13}$$

with $\bar{h}$ derived by smoothing h. Eq. (10), thus, can be rewritten as,

$$F_R = s\,(\overline{F}_R - E_{leakage\ in}). \tag{14}$$

To be able to estimate F_R, one needs to calculate the leakage error ($E_{leakage\ in}$) first. To this end, we developed a kernel to account for both leakage in and leakage out errors. The proposed method looks for stronger anomalies outside the basin (for leakage in) and inside the basin (for leakage out). The definition starts by creating a kernel expressed in terms of spherical harmonics as:

$$\begin{pmatrix} \upsilon^c_{lm} \\ \upsilon^s_{lm} \end{pmatrix} = \sum_{\theta}\sum_{\phi} \psi(\theta,\phi)\widetilde{P}_{lm}(\cos(\theta)) \begin{pmatrix} \cos(m\phi) \\ \sin(m\phi) \end{pmatrix} \sin(\theta). \tag{15}$$

In Eq. (15), $\widetilde{P}_{lm}$ are the normalized associated Legendre functions, υ^c_{lm}, υ^s_{lm} represent the spherical harmonic coefficients and the summation covers the entire surface of the Earth. The definition of the mask filter ψ is very important and different literatures have found various methods to implement this. For example, Seo and Wilson (2005) use a Gaussian filter to smooth mentioned kernel inside a basin (for B_1 and B_2 in their study). Swenson and Wahr (2003) applied Lagrange multiplier rather than a Gaussian filter. Here, we use a different definition and instead of simply having a value 1 inside a basin, the method tries to maximize signals concentrated in different regions while decreases their effects on the surrounding signals. For the leakage in effect, ψ contains values outside the basin with special focus on strong anomalies while for the leakage out effect, it considers values inside the basin again with a concentration on strong anomalies. Accordingly, the mask filter ψ is defined through the following procedure. Note that in the following, we consider $\overline{F}$ (the smoothed signal from step 1) as a 2D matrix and apply an image processing procedure (as follow) to extract strong signals.

A: The calculated $\overline{F}$ in the first part of the filtering process is used to create $\widetilde{F}$ as a measure of spatial variability of GRACE TWS.

$$\widetilde{F} = \left(\frac{(\overline{F} - \min(\overline{F}))}{(\max(\overline{F}) - \min(\overline{F}))}\right). \tag{16}$$

Then, the 2D intensity matrix (I),

$$I = \begin{cases} 1 & \text{if } \widetilde{F} > S_b \\ 0 & \text{if } \widetilde{F} < S_b, \end{cases} \tag{17}$$

can be used to identify strong anomalies using the normalized$\overline{F}$ (given by $\widetilde{F}$). The threshold S_b in Eq. (17) is chosen to be a value within [0 1]. Often the median of $\widetilde{F}$ can be a good choice for S_b. A smaller S_b yields a smoother intensity matrix that controls the mass anomalies being considered in the averaging, and which is less weighted. Different values of S_b are tested in this study and their results are reported in Section 4.1.

B: A high pass filter, e.g., Laplacian filter (Gonzalez and Woods, 1992, 2002) using Eq. (18), is applied to intensify strong anomalies (found in [A]) and reduce their effects on surrounding anomalies.

$$L = \frac{1}{\sin\theta}\frac{\partial}{\partial\theta}\left(\sin\theta\frac{\partial I}{\partial\theta}\right) + \frac{1}{\sin^2\theta}\frac{\partial^2 I}{\partial\phi^2}. \tag{18}$$

C: Convolving the filtered matrix L with a Gaussian filter (W in Eq. (19)), which can be applied with different averaging radii. Smoothing is applied because converting the basin kernel from spatial to spectral domain introduces short-wavelength errors due to the Gibbs effect and introduces artificial fluctuations around the high contrast edges (Zeng and Allred, 2009).

$$\overline{L} = \int W(\theta,\phi,\theta',\phi')\,L(\theta',\phi')\,d\Omega', \tag{19}$$

In Section 4.1, the impact of the smoothness on the final averaging values is assessed. It should be mentioned here that this step is not restricted to the application of a Gaussian filter, and one can use anisotropic filter such as the DDK smoothing filters proposed by Kusche et al. (2009). Nevertheless, in the following we only discuss the application of Gaussian smoothing for the sake of simplicity.

The mask filter ψ is then calculated by $\psi = 1 + \overline{L}$, which can be used in Eq. (15) to estimate υ^c_{lm} and υ^s_{lm}. Fig. 3 illustrates a schematic performance of the three steps above. The final form of the basin kernel (υ) is built as,

$$\upsilon(\theta,\phi) = \frac{1}{4\pi}\sum_{l=0}^{\infty}\sum_{m=0}^{l}\{\upsilon^c_{lm}\cos(m\phi) + \upsilon^s_{lm}\sin(m\phi)\}. \tag{20}$$

The created kernel is multiplied by the smoothed field from the first step to estimate F_N using,

$$F_N = \overline{F}\circ\upsilon, \tag{21}$$

where the operator $\circ$ performs a pixel-wise multiplication. Once F_N is computed, it is used rather than F to estimate leakage in and leakage out (Eqs. (22) and (23)). To estimate the leakage in, we only consider F_N outside the basin and apply smoothing to capture its effect inside. A similar process can be done to compute the effect of leakage out by only considering anomalies inside the basin. The smoothing in these procedures can be done by applying either the same smoothing procedure as the first step of the proposed filter or using a Gaussian filter, e.g.,

$$E_{leakage\ in} = \frac{h(\theta,\phi)}{4\pi}\int W(\theta,\phi,\theta',\phi')\,(1-h(\theta',\phi'))\,F_N(\theta',\phi')\,d\Omega', \tag{22}$$

$$E_{leakage\ out} = \frac{1-h(\theta,\phi)}{4\pi}\int W(\theta,\phi,\theta',\phi')\,h(\theta',\phi')\,F_N(\theta',\phi')\,d\Omega'. \tag{23}$$

The estimated $E_{leakage\ in}$ is used in Eq. (14) to obtain the averaged water storage over the region of interest. The example of the KeFIn filter performance in the second step is presented in Fig. 4. Synthetic signals are produced in the spatial domain (Fig. 4a) and are smoothed using an ordinary Gaussian filter (Fig. 4b). The application of the KeFIn with two different sets of parameters are shown in Fig. 4 c and d. The effects of the filter are clearly visible from the reduction of signals interferences caused by leakage. Implementing the filter with various Gaussian filter sizes (r) and different S_b (as in Eq. (17)) yields different results. Detailed results that indicate the filter's sensitivity to different parameters are presented in Section 4.1. Fig. 5 provides a flowchart that summarizes the filter process using the KeFIn algorithm.

3.2. Basin averaging kernel methods

Averaging using basin functions or basin kernels is a common

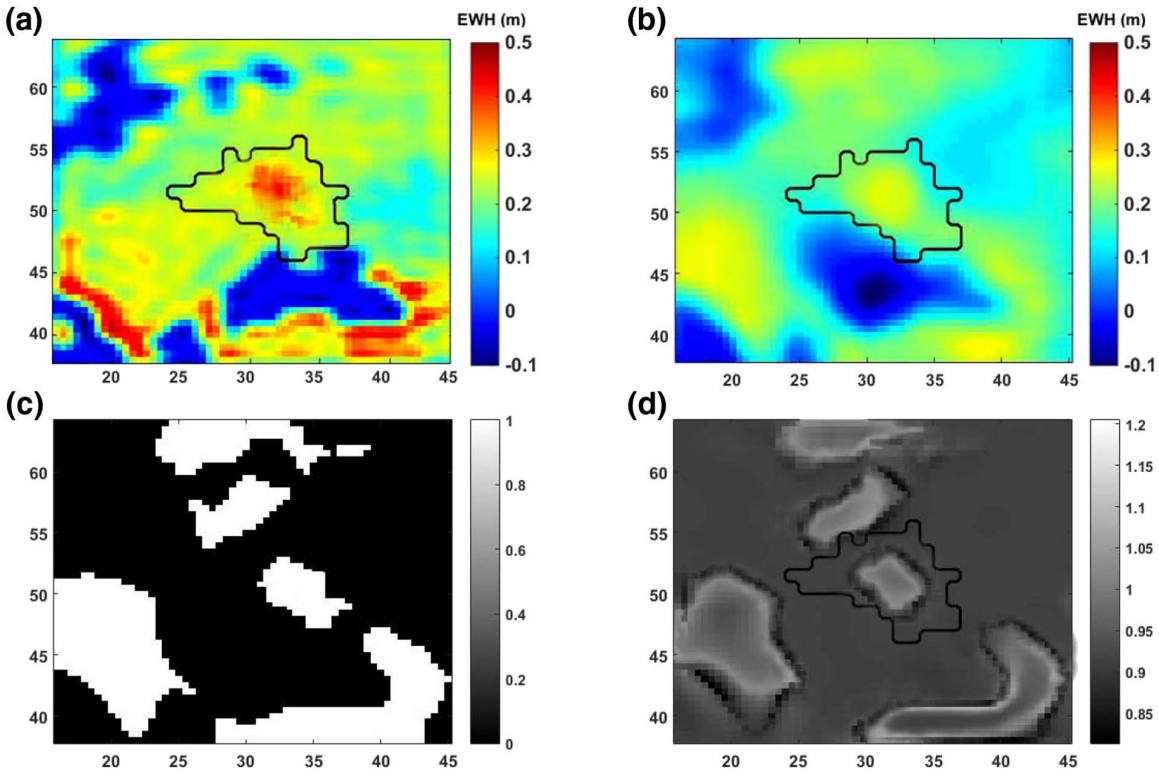

Fig. 3. A schematic view of the steps for preparing ψ in [A]–[C] described above. (a) shows the initial unperturbed signal, (b) represents the smoothed signal from the first step of the filter (applied with the motion length of 60), (c) is I in step [A] using $S_b = 0.5$, and (d) depicts the kernel ψ created by $r = 300$ km.

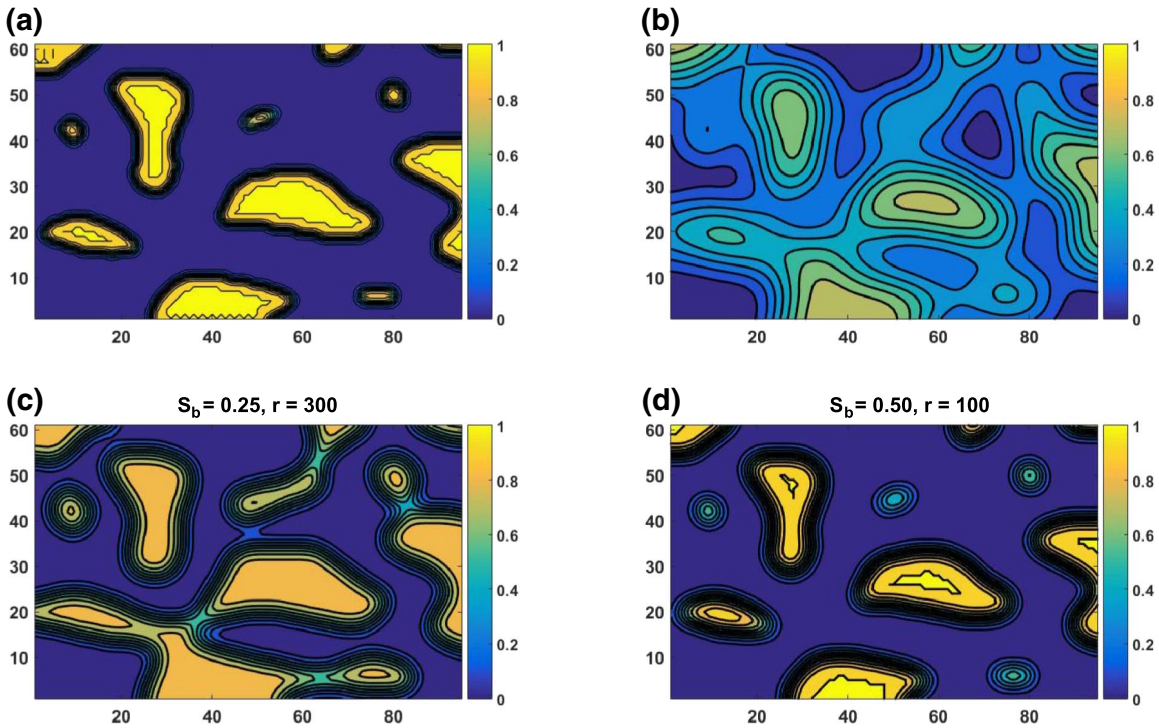

Fig. 4. Performance of the second step of the KeFIn filter based on synthetic data. (a) Initial TWS anomalies, (b) smoothed TWS using a Gaussian filter with the half-width radius of 500 km. (c) and (d) represent the performance of the KeFIn filter with different factors of S_b and r (half width radius in kilometer). In this figure, we show how the KeFIn filter tries to reproduce the signals in (a) based on the smoothed signal (b), which result in (c) and (d).

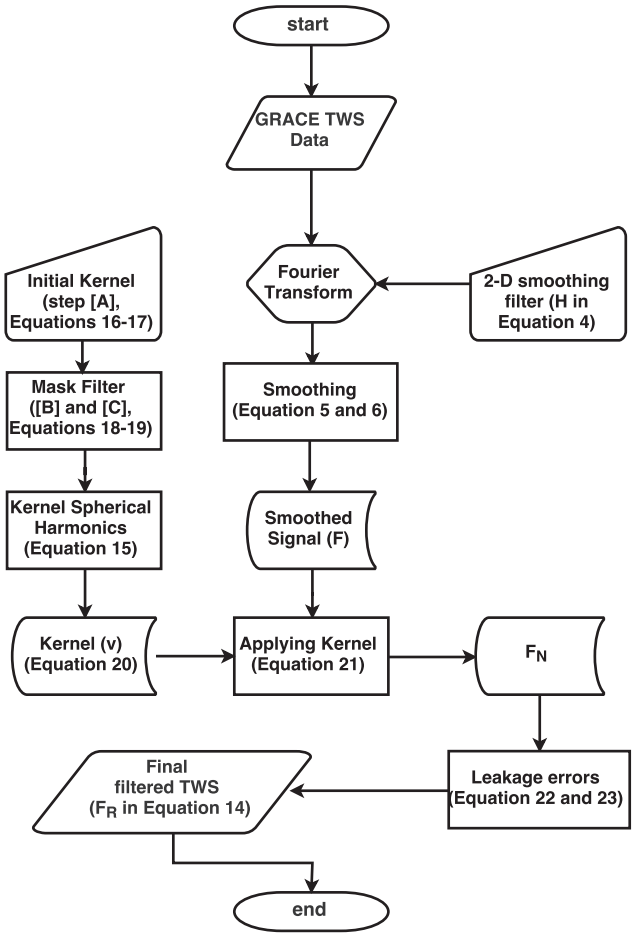

Fig. 5. Flowchart of the proposed KeFIn filtering process.

approach for estimating basin scale TWS (see e.g., Swenson and Wahr, 2002). The kernel h (cf. Eq. (7)) can be expanded in terms of spherical harmonic coefficients and subsequently combined with L2 potential coefficients to obtain basin averaged GRACE TWS estimates (see e.g., Swenson and Wahr, 2003, and more details in Section 3.1). Different kernel averaging methods will likely result in different signal attenuation and displaced mass anomalies based on the shape and size of the basins (Werth et al., 2009). Swenson and Wahr (2002) introduced the spatial averaging kernel for regional studies that try to minimize leakage errors coming from outside into the area of interest by isolating the signals inside the area (see also Swenson and Wahr, 2003). Their approach reduces short wavelength effects using a smooth averaging kernel with less power on short wavelengths using Lagrange multiplier rather than applying a Gaussian filter. For the Lagrange Multiplier method, we apply a smoothing radius of 300 km. Furthermore, we use a time-dynamic filter proposed by Seo and Wilson (2005). Here, we use filter number three (from four types of their filters), which can be directly applied to GRACE L2 products. This is a dynamic filter that scales spherical harmonic coefficients using the ratio of signal variance and signal plus noise variance that employs a least squares optimum approach. The method is based on the Lagrange Multiplier Method (Swenson and Wahr, 2003) while assuming that the root-mean-square (RMS) of the signal over the target basin is known from GLDAS model (for more details, see Seo and Wilson, 2005; Seo et al., 2006). Here, we use GLDAS NOAH for this purpose.

In a different approach, Han and Simons (2008) tried to maximize the ratio of the energy of the function within the target region (h) by constraining regional contributions to global spherical harmonics spectra based on Simons and Hager (1997). They argued that the resulted localized coefficients increase the signal-to-noise ratio. This method is also applied in the present study with the spectrum band-limited to spherical harmonic degree and order of 25.We also use a data-driven approach recently introduced by Vishwakarma et al. (2016), where leakage in and out are separately solved using a catchment mask and a filter kernel. A Gaussian filter of half width radius of 350 km (following Vishwakarma et al., 2016) is used to suppress the noise before implementing this approach in the present study. The data-driven filter is sensitive to basin sizes in a way that noise increases as the catchment size decrease (see Vishwakarma et al., 2016, for more details).

3.3. Scaling factor methods

Landerer and Swenson (2012) suggested the use of a scaling (gain) factor, which can be multiplied with filtered GRACE TWS estimates. In this study, monthly simulations of the GLDAS NOAH are used as synthetic input TWS (a summation of snow water equivalent, canopy water storage, soil layers, and surface water) to estimate scaling factors following Landerer and Swenson (2012) as in Eq. (24), where the goal is to find the scaling factor α by minimizing the quadratic sum of difference M between original ($\triangle S_T$) and filtered ($\triangle S_F$) GLDAS TWS fields, i.e.,

$$M = \sum (\triangle S_T - \alpha \triangle S_F)^2. \quad (24)$$

Following Landerer and Swenson (2012) and Long et al. (2015), synthetic TWS data is converted to spherical harmonics and truncated at degree and order 60. We then apply the destriping procedure after Swenson and Wahr (2006) and a 300 km Gaussian filter to smooth high-degree and order noises. The model-derived TWS estimates before

Table 1
A summary of the implemented GRACE leakage filtering methods, which are used in this study for comparison with the proposed KeFIn filter.

Study	Method	Case study	Evaluation method	Abbreviation*
Swenson and Wahr (2002)	Lagrange multiplier method	Mississippi River Basin	Using synthetic GRACE data	F_1
Han and Simons (2008)	Localization of Global Geopotential Fields	Java/Sunda trench	Using seismic model based data	F_2
Seo and Wilson (2005)	B_1, B_2, B_3, and B_4	Amazon, Mississippi, Lena, Huang He and Oranje Basins	Using synthetic GRACE data	F_3
Landerer and Swenson (2012)	Gridded gain factor	46 globally distributed basins	GLDAS data	F_4
Landerer and Swenson (2012)	Single gain factor	46 globally distributed basins	GLDAS data	F_5
Vishwakarma et al. (2016)	Data-driven approach	32 globally distributed basins	Closed-loop environment using monthly GLDAS fields	F_6
The present study	Kernel Fourier Integration (KeFIn)	43 globally distributed basins	Using synthetic data and soil moisture + groundwater data	*KeFIn*

* In the last column, the abbreviations are assigned to the filters we use in the present study.

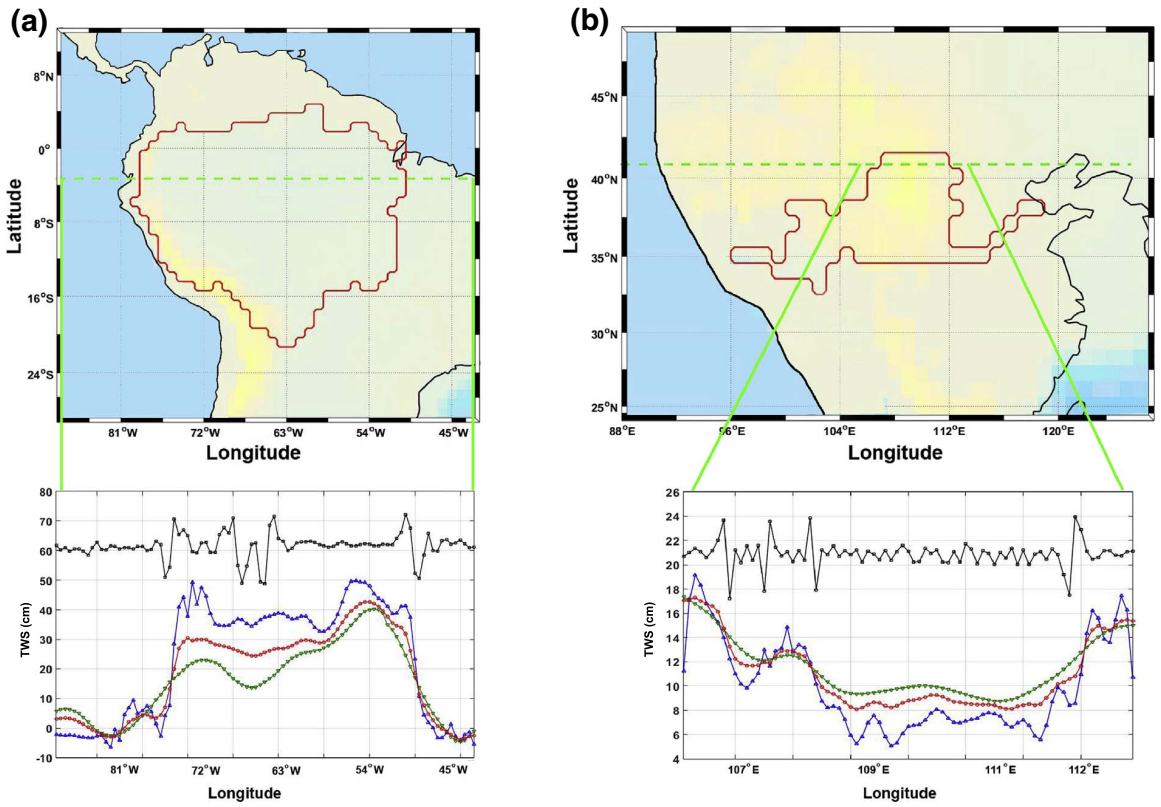

Fig. 6. Assessing the performance of two filtering techniques on synthetic GRACE-like TWS examples with realistic noise. (a) TWS is introduced in the Amazon River Basin, South America, and (b) TWS is introduced outside of the Huang He River Basin, China. The line plots indicate the TWS after application of Gaussian filter with 300 km radii (green) and the KeFIn filter (red), estimated using the motion length of 60, $S_b = 0.5$, and $r = 300$ km. Note that the line plot of kernel (black) is also shown in these figures, which are shifted for better visual demonstration. The initial synthetic TWS is represented by the blue lines. Units are in cm. (For interpretation of the references to color in this figure legend, the reader is referred to the web version of this article.)

($\triangle S_T$) and after ($\triangle S_F$) filtering are used to calculate scaling factors. In this study, two methods of scaling factors at grid points and basin scale are computed and used for comparison with the newly developed KeFIn and other filtering techniques. All filters used in this study are presented in Table 1.

3.3.1. *Application example of the proposed KeFIn filter*

First, the performance of the KeFIn filter with respect to both leakage-in and leakage-out errors is assessed, for which two tests are performed that correspond to each type of error (leakage-in and leakage-out). Setup (i), the signal is only introduced inside a basin and GRACE-like TWS noise is added as described in Section 2.2. A 300 km half width radius Gaussian filter (Jekeli, 1981) is then applied to smooth the introduced signals and noises, which causes signal leakage outside the basin. Setup (ii), TWS signals are introduced only outside a basin to assess the leakage-in effects. The KeFIn filter is applied to post-process both scenarios as shown in Fig. 6. In Fig. 6a bottom, the blue line represents the introduced synthetic TWS while the green lines show the signal after the application of a Gaussian filter. In Fig. 6a, the results correspond to a cross section at 3° S that passes the Amazon basin, South America, and in Fig. 6b, they correspond to a cross section at 41° N crossing the Huang He Basin, China. The results clearly indicate that the Gaussian filter attenuates the original signal and causes leakage-out and leakage-in effects shown in Fig. 6a and b, respectively. The smoothed signals of the KeFIn filter are shown by the red lines, which in both cases better follow the initial TWS (blue lines). It is worth mentioning that if there was no striping noise added to the signal, the red curve (KeFIn) would have closely reproduced the true signal (blue curve). Therefore, we avoid showing a close-loop or a noise free assessment of the KeFIn's performance.

Further, to better demonstrate how the proposed KeFIn filter operates, the results of its application over two basins with different shape and sizes (e.g. Colorado, USA, basin number 34 and Congo, Africa, basin number 5) out of the 43 basins in Fig. 1 are shown in Fig. 7. In this figure, each row of a and b corresponds to one specific basin, where the first column is the initial unperturbed signals (before applying the Gaussian filter), the second column represents the perturbed signals (after applying the Gaussian filter) using the synthetic data sets (see Section 2.2), and the third column contains the filtered signals. The Root-Mean-Square-Errors (RMSE) time series of the filters performances using the synthetic data over the basins is calculated and their averages are shown in Fig. 7c. This is done to compare the results of the KeFIn filter with other methods (F_1 to F_6 in Table 1). It is clearly visible in Fig. 7 that the KeFIn filter works properly in both basins. RMSE values over the Colorado Basin (Fig. 7c) suggest that the application of the KeFIn filter (i) successfully decreases leakage error, and (ii) improved results in relation to other filters. We find approximately 34% RMSE reduction compared to the unperturbed signals by implementing the KeFIn filter. By comparing RMSE values in the Congo basin, again, smaller errors are found for those associated with the KeFIn filter compared to the other six filters applied in this study. This indicates that the KeFIn filter successfully decreased leakage effects based on the GRACE-like artificial data, especially over smaller basins.

4. Results

In Section 4.1, various filtering techniques (cf. Table 1) are tested on the synthetic TWS data while in Section 4.2, the results from filtering

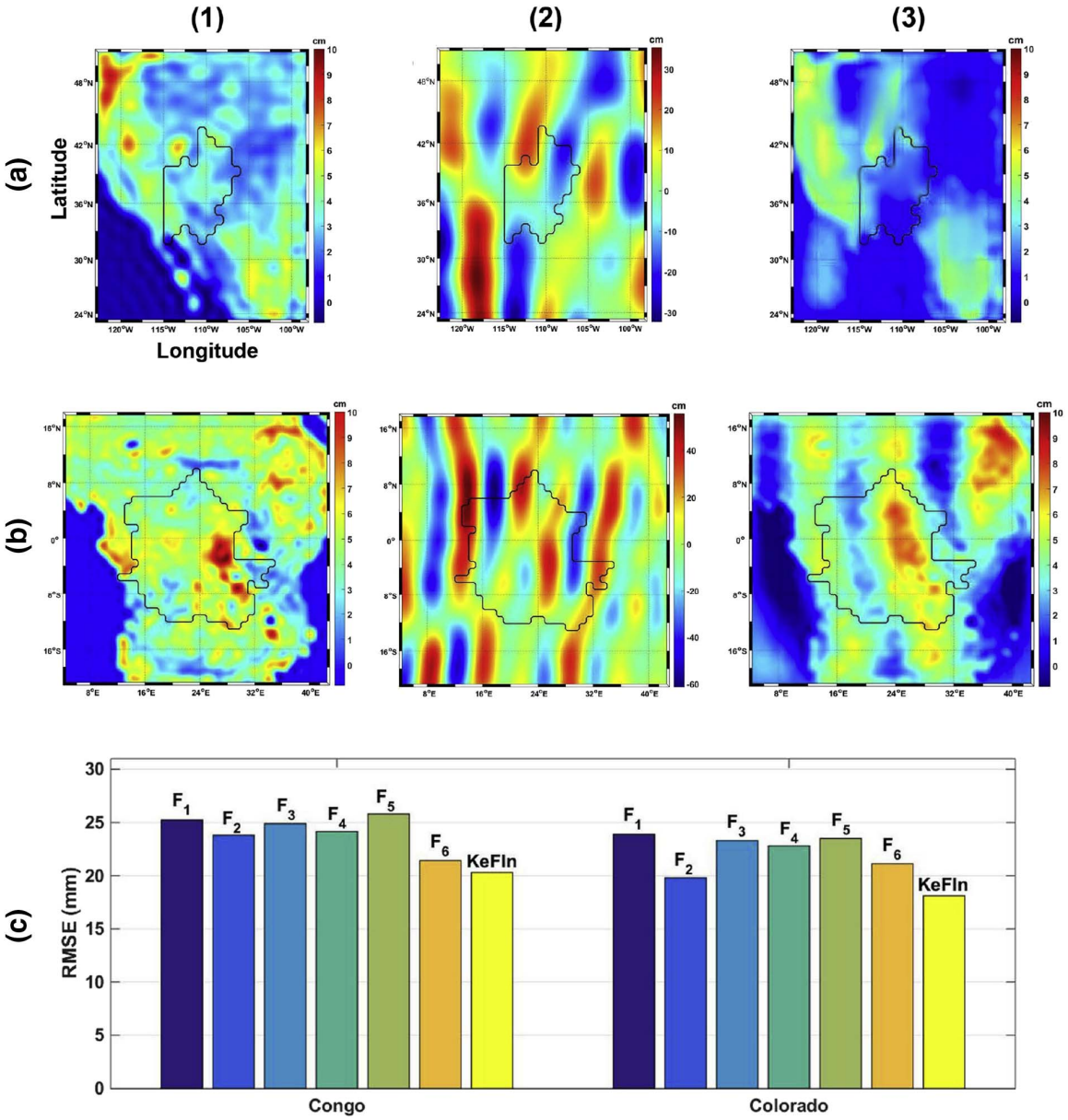

Fig. 7. The KeFIn filter operation over the Colorado (a) and Congo (b) basins using synthetic GRACE-like TWS signals and noise. In column (1), the unperturbed water storages are shown; in column (2), the corresponding perturbed water storages are shown, and the results of the KeFIn filtered TWS estimates are presented in column (3). Panel (c) shows the average RMSE results within both basins for the filters listed in Table 1.

the real GRACE data are assessed against direct observations of water fluxes through the water balance equation (Eq. (1)), as well as in-situ groundwater measurements.

4.1. Filter results based on synthetic data

There are two effective factors in each step of the proposed KeFIn filter, which potentially change the final filtering outcomes. The main aim here is to find out which choice yields an optimum performance of the filter in terms of leakage error reduction. Fig. 8a contains the results of applying the first step of KeFIn while considering different sizes for the motion filter (controlling the smoothing of north–south stripping error) and K to mitigate the signal attenuation. Each scenario (using Eqs. (3) and (4)) is applied separately to the basins and the average errors for all basins and are represented in Fig. 8a. From our investigations, using K from GLDAS provides the best results with ~14.76% higher leakage error reduction with different filter lengths. Considering K as a constant can lead to a promising result with the value of 1 with 58 mm average error. On the other hand, motion filters with bigger windows better decrease errors, where the optimum value in this study is derived from the 75° motion filter size. As mentioned, the first part of the filter deals with colored/correlated noise of high-frequency mass variations (i.e., stripes). In order to investigate the performance of this step of the filter, we compare its results with the widely used destriping algorithm by Swenson and Wahr (2006) and DDK smoothing filter following Kusche (2007) and Kusche et al. (2009). We apply these filters over all basins and illustrate the average results in Table 2. Note that we apply the KeFIn method with best cases of K and motion filter for the comparison presented in Table 2. Based on these results, the first step of the KeFIn filter performs comparable to other

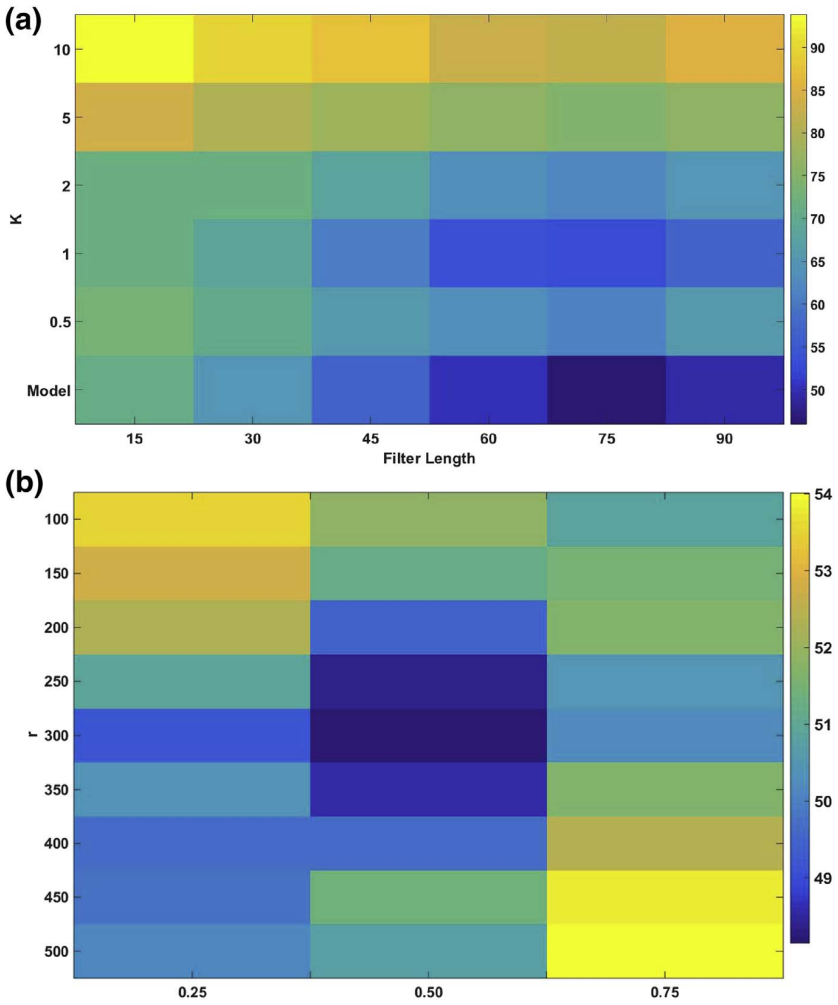

Fig. 8. Average error (mm) derived after applying the KeFIn filter with different values of K and the motion filter length (a) for the first step of the filter as well as different scenarios that contain S_b and r for the second step of the filter (b). (a) indicates that the filter length of larger than 30 km and K between 0 to 2 yield smaller errors, while (b) indicates S_b of 0.5 and $r = 300$ km yield the smallest errors.

Table 2
Average statistics derived after applying different filtering methods over the world's 43 major river basins using synthetic data (after removing seasonal effects) in comparison with the unperturbed synthetic data (F_0). Note that the first step of the KeFIn filter is used in this table.

	Gauss (250 km)	Gauss (350 km)	Gauss (500 km)	DDK1	DDK2	DDK3	KeFIn
RMSE (mm)	78.54	54.13	60.91	57.87	53.19	62.67	52.73
Correlation	0.73	0.81	0.78	0.83	0.80	0.76	0.81

filters in terms of RMSE reduction. The level of RMSE reduction, as well as correlation improvements for the KeFIn filter are larger in most of the cases, particularly compared to Gaussian with 250 km radii and DDK3.

In addition, we used the same experiment this time for the second part of the filter (cf. Eqs. (6) and (8)) while applying diverse values of S_b and selecting various smoothing radii (half-width radius, r) for the Gaussian filter. Using the best cases of K and motion filter length, we analyze the effects of different S_b and r on errors (Fig. 8b). In general, results indicate that a higher S_b needs lower r to derive better results. Nevertheless, applying the second part of the KeFIn filter with $S_b = 0.5$ and $r = 300$ km performed better in most of the cases.

For comparison, all the filters of F_1, F_2, F_3, F_4, F_5, and F_6 (cf. Table 1) as well as the KeFIn filter are then applied on the GRACE-like synthetic TWS fields. A summary of these results is presented in Table 3. For every basin, we estimate F_R (averaged signals inside the basin) and F_{1-R} (averaged signals outside the basin) using each filter and compare the results to initial unperturbed TWS values inside and outside the basins by calculating the RMSE and correlation coefficients. Note that for a better assessment, seasonal variations are removed from time series. The average results for the study period, i.e. 2002–2013, and for all the 43 basins (cf. Fig. 1) is given in Table 3. Note that detailed RMSE values for each individual basin can be found in Appendix A. From Table 3, it can be seen that higher correlations, both inside and outside the basin, can be found by applying the KeFIn filter. Estimated measures indicate that the KeFIn filter is more successful in recovering the spatial distribution of the synthetic TWS estimates. Overall, the KeFIn filter performs better both inside and outside the basins with an average of 73.6% TWS recovery from the perturbed synthetic data (cf. Table 3). Our results further indicate that the KeFIn filter works well over smaller river basins such as the Colorado, Ohio, Lachlan, and the Namoi basins, showing maximum ~81% TWS recovery from noisy data. We also found that in 35 out of the 43 basins, the proposed filter provides the lowest RMSE (cf. Appendix A). Nevertheless, in the other 8 cases, the KeFIn approach still demonstrates a promising performance in terms of RMSE reduction. Overall, Table 3 suggests that the proposed filter performs better in more than 80% of the basins.

Table 3
Average statistics derived after applying different filtering methods over the world's 43 major river basins using synthetic data in comparison with the unperturbed synthetic data (F_0). Averaged signals inside and outside of the basins are calculated using $C_R = \int F_0\, h\, d\Omega$ and $C_{1-R} = \int F_0\, (1-h)\, d\Omega$, respectively. Note that bold values in this table represent the largest correlation, the least RMSE, and the largest TWS improvement for each column.

Method	Inside the basin		Outside the basin		TWS improvement (%)	
	Correlation	RMSE (mm)	Correlation	RMSE (mm)	$(F_R-\bar{F}_R)/C_R$	$(F_{1-R}-\bar{F}_{1-R})/C_{1-R}$
F_1	0.77	32.02	0.68	49.52	19.25	11.32
F_2	0.83	28.71	0.77	44.08	21.14	13.81
F_3	0.79	31.03	0.72	47.84	20.13	12.44
F_4	0.88	29.12	0.87	37.26	22.67	19.53
F_5	0.82	30.86	0.84	39.95	19.09	18.20
F_6	0.85	28.17	0.83	41.30	21.18	16.79
KeFIn	**0.91**	**27.25**	**0.89**	**34.65**	**24.41**	**22.36**

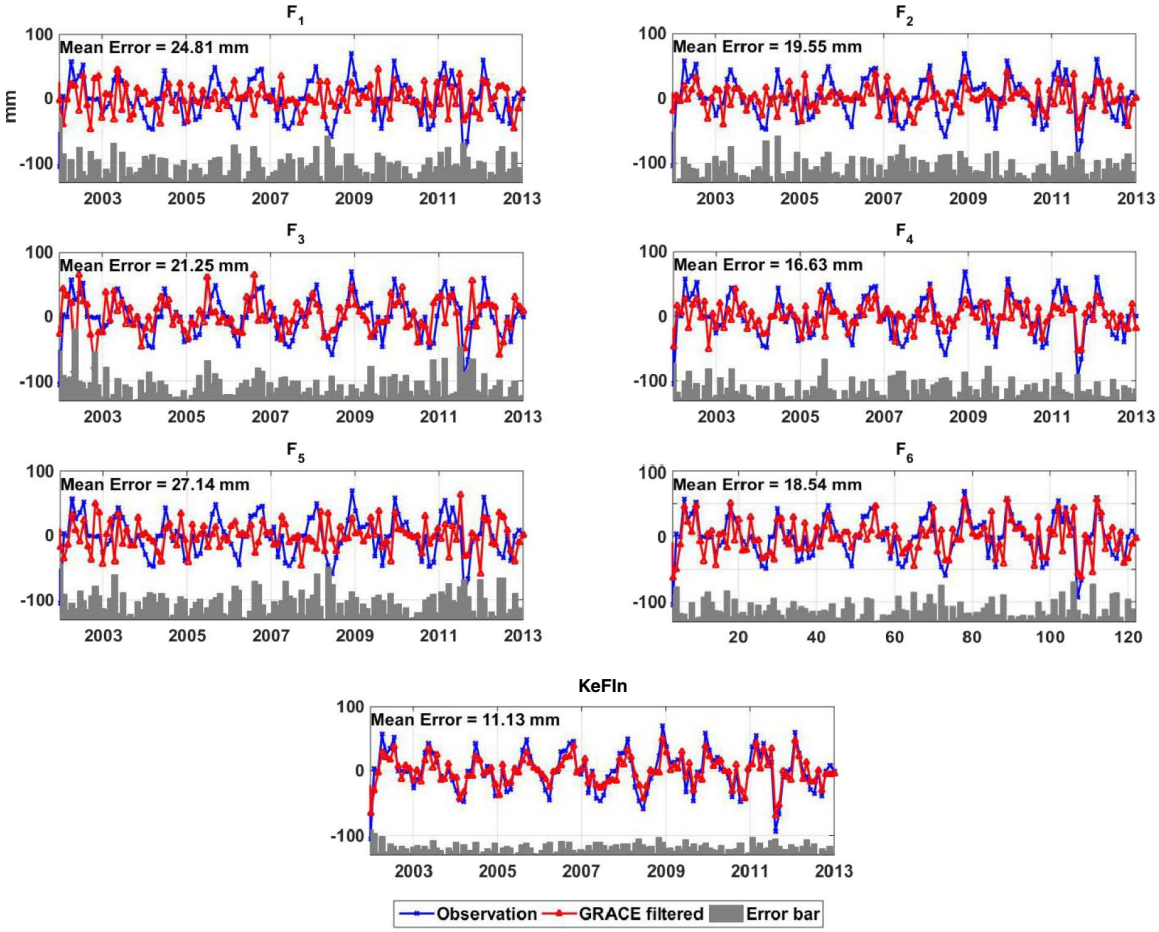

Fig. 9. Comparison between the derivative of filtered TWS (red) and TWF from observations (blue) within the Namoi Basin. Each sub-figure corresponds to one filter and also contains error bars that is computed as the absolute value of difference between GRACE derivatives and the observed TWF. (For interpretation of the references to color in this figure legend, the reader is referred to the web version of this article.)

4.2. Filter results based on GRACE data

4.2.1. Comparisons with hydrological total water flux

We further assess the performance of the filters, using independent data sets such as water fluxes. Therefore, TWS changes are evaluated through the water balance equation (cf. Eq. (1)) using TRMM 3B43-v7 precipitation, AVHRR data to account for evaporation products, and in-situ discharge data over the Amazon, Mekong, Arkansas-White (basins 1 and 31 in Fig. 1, respectively), Ohio, Lachlan, Namoi, Lower Mississippi, and Macquarie-Bogan basins (cf. Fig. 2).

To this end, we calculate TWF (from Eq. (1)) over each basin (see Section 2.3). Fig. 9, for example, shows the results of this comparison within the Namoi Basin. The figure also contains error bars for every filter representing the differences between the observed TWF and those derived by estimating the temporal derivative of filtered TWS change. It can be seen that the results of the KeFIn filter are much closer to the observed TWF with the smallest average error of 11.13 mm and overall 13% higher correlation in comparison with the other filters.

Average error estimates within different basins corresponding to each filter are illustrated in Fig. 10. Errors after applying the KeFIn filter are found to be the smallest in all the assessed basins. We find F_2, F_4, and to a lesser degree F_6 to be efficient in most of the cases, especially over the Ohio Basin. More details on results can be found in Table 4, in which correlations between the TWFs (estimated as

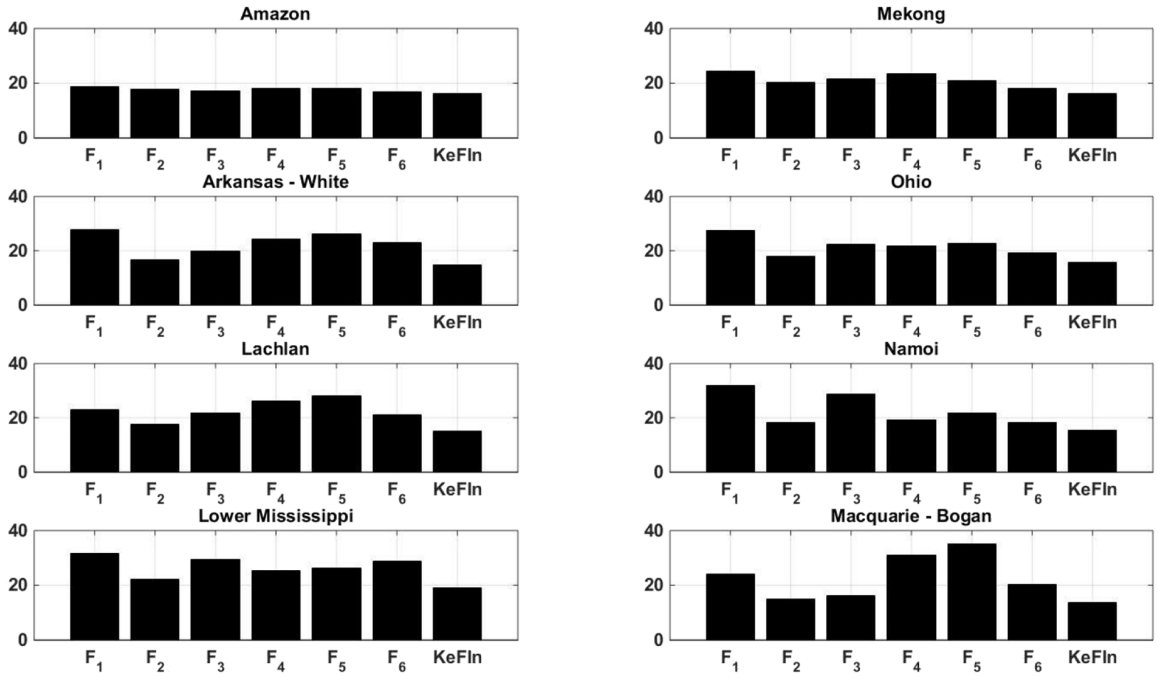

Fig. 10. The temporal average of errors defined as derivative of filtered TWS minus observed TWF. Each error bar is estimated after applying the F_1 to F_6 and KeFIn filters over 8 selected river basins (units are mm).

Table 4
Correlations between the TWFs as precipitation minus evaporation minus runoff, and the derivatives of TWS changes from each applied filter. The correlation coefficients have been computed at the 95% confidence level. The largest correlation in each row is displayed by the bold value.

Basin	F_1	F_2	F_3	F_4	F_5	F_6	*KeFIn*
Amazon	0.92	0.93	0.94	0.92	0.91	0.95	**0.95**
Mekong	0.85	0.92	0.88	0.88	0.89	0.91	**0.93**
Arkansas-White	0.78	0.82	0.81	0.75	0.73	0.75	**0.88**
Ohio	0.76	0.82	0.74	0.82	0.81	0.78	**0.85**
Lachlan	0.80	0.86	0.82	0.73	0.75	0.84	**0.89**
Namoi	0.72	0.87	0.78	0.80	0.82	0.81	**0.91**
Lower Mississippi	0.77	0.78	0.79	0.81	0.80	0.78	**0.84**
Macquarie-Bogan	0.79	0.85	0.81	0.78	0.74	0.69	**0.92**

precipitation minus evaporation minus runoff) and the derivatives of TWS changes that are filtered by all implemented filtering methods are represented. Maximum correlations are calculated for the proposed filter with 0.89 average correlation. A higher correlation is achieved from all the filters over the Amazon and Mekong basins, which can be due to their stronger signals compared to other basins. Results from F_2, F_3, and F_6 are found to have larger correlations to TWFs than those from F_1 and F_5.

4.2.2. Comparisons with groundwater and soil moisture

We further assess the results of the different filters against groundwater measurements as mentioned in Section 2.4. TWS estimates after implementing each filter and a summation of groundwater storage (GWS) and soil moisture contents (GWS + SM) are compared in the following basins: Arkansas-White, Ohio, Lachlan, Namoi, Lower Mississippi, and Macquarie-Bogan (cf. Fig. 2), where access to in-situ data is provided. For each basin and each filtering method, basin averaged values are compared with GWS + SM. For this purpose, absolute differences between the filtered results and in-situ measurements are illustrated in Fig. 11. Similar to the previous section, the minimum errors are found after using the KeFIn filter for these basins. It can be seen from the distribution of error points that the KeFIn results obtain errors with less magnitudes and variances. This indicates the smaller deviations of these results compared to in-situ measurements. Among the other filters, in general, smaller errors are found for F_2 and F_6. F_2 and F_5 depict less errors over the Ohio Basin and Lachlan Basin. In summary, the KeFIn filter and F_2 better decrease errors over these basins, respectively 38% and 22% (on average) better than the other filters. These show the higher capability of the two filters for reducing errors within smaller basins. For a better comparison, the average errors in Fig. 11 for all the basins are shown in Fig. 12.

Fig. 12 illustrates that the proposed KeFIn filter in all the cases has the minimum error (24.13 mm on average). Similar to the two basins discussed earlier in this section, using F_2, F_3 and to a lesser degree F_3 lead to a higher agreement with observations compared to the other methods (except the KeFIn filter). The results of these filters are much closer to those of the proposed filter in Arkansas-White and Macquarie-Bogan Basins. F_4 seems to have an approximately constant effect on different basins (37.58 mm on average) except for the Ohio Basin. The summary of comparisons between different filtered TWS and in-situ groundwater time series measurements are presented in Table 5. This is performed to show each filter's performance independent against direct observations without incorporating model estimates. Higher correlations are reported between the KeFIn filter results and in-situ data, which indicates 19.31%, 6.67%, 10.57%, 8.41%, 18.52%, and 6.33% improvements in comparison to F_1, F_2, F_3, F_4, F_5, and F_6, respectively. F_3, F_6, and F_4 results are also in good agreement with the in-situ groundwater data.

5. Discussion

Evaluation of the proposed KeFIn filter against common techniques (cf. Table 1) using different data sets suggests that this filter successfully removes striping and reduces leakage errors over basins of different shapes and sizes. Other filters show a different level of improvements within the world's major 43 basins (Figs. 9, 11, and 12). We find here that those filters based on the averaging kernel, especially F_2 (Han and Simons, 2008) and F_3 (Seo and Wilson, 2005), deal better with leakage errors over smaller basins compared to those based on scaling factor (F_4

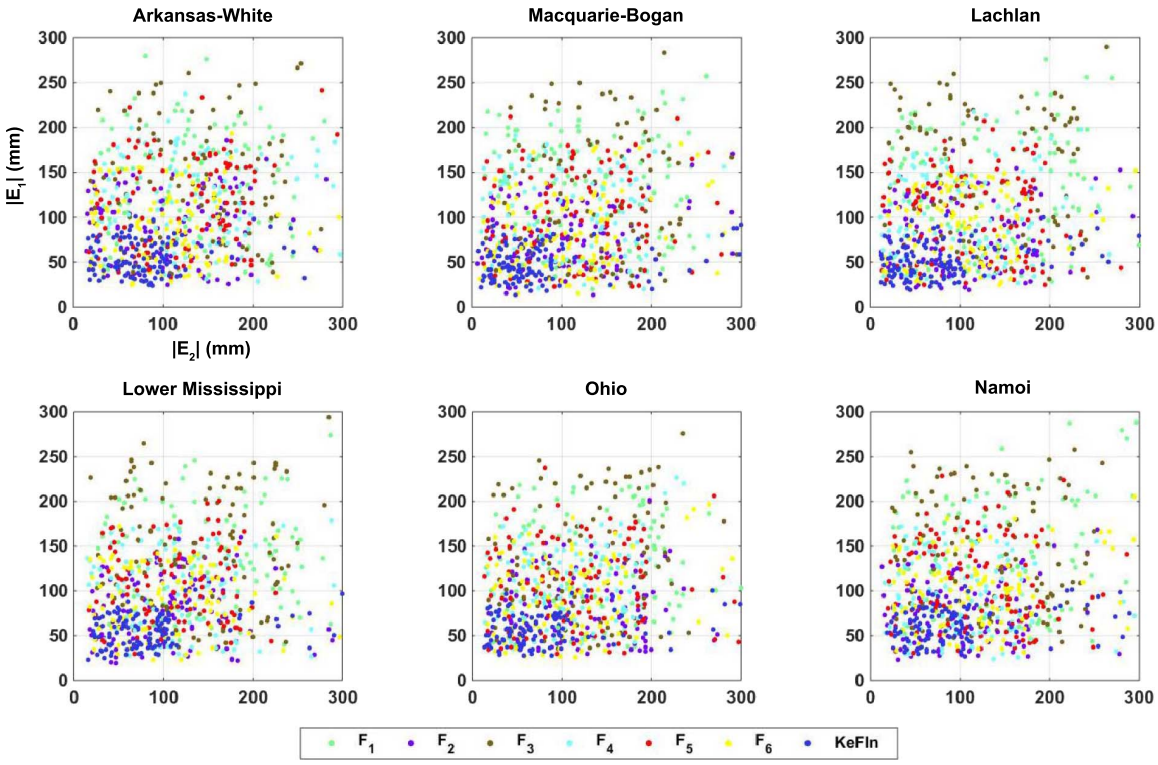

Fig. 11. Errors estimated at each epoch after applying the assessed filters F_1–F_6 and KeFIn on the Ohio (basin number 35, with blue circles) and Lachlan (basin number 41, with red triangles) basins. These values are calculated as differences between in-situ measurements (GWS + SM) and filtered TWS before (E_1) and after (E_2) removing seasonal effects. The average absolute error is indicated in each sub-figure and for each basin. (For interpretation of the references to color in this figure legend, the reader is referred to the web version of this article.)

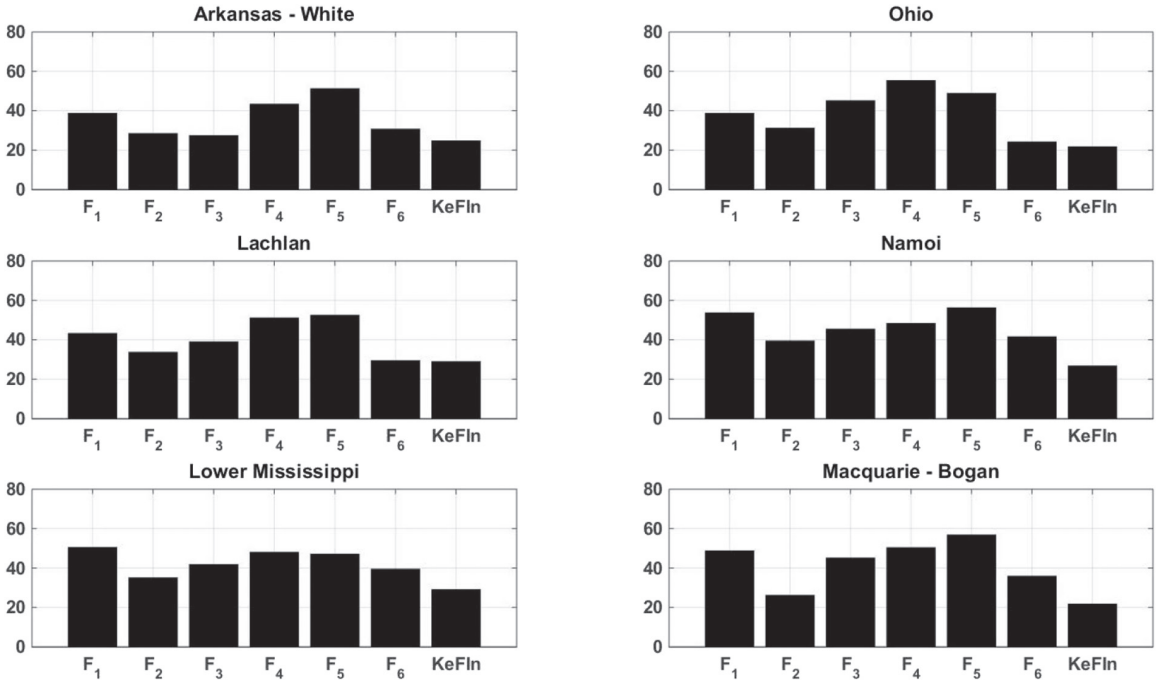

Fig. 12. Average differences between GRACE TWS and observed groundwater plus soil moisture content within 6 river basins. GRACE data are processed using 7 filtering techniques (F_1 to F_6 and KeFIn filters) over 6 selected river basins (units are mm).

Table 5
Correlations between the filtered results and in-situ measured groundwater time series. The largest correlation in each row is displayed by the bold value.

Basin	F_1	F_2	F_3	F_4	F_5	F_6	*KeFIn*
Arkansas-White	0.78	0.76	0.73	0.69	0.63	0.75	**0.81**
Ohio	0.76	0.82	0.73	0.63	0.69	0.84	**0.85**
Lachlan	0.69	0.71	0.75	0.67	0.68	0.78	**0.83**
Namoi	0.59	0.74	0.64	0.75	0.58	0.66	**0.80**
Lower Mississippi	0.54	0.78	0.73	0.66	0.67	0.72	**0.78**
Macquarie-Bogan	0.77	0.85	0.81	0.76	0.73	0.82	**0.88**

and F_5; Landerer and Swenson, 2012). Nevertheless, in general, F_2, F_6 (Vishwakarma et al., 2016), F_3, and F_4 perform better than F_1 and F_5 in most of the cases. The grid-based F_4 is found to better reduce leakage errors in comparison to the single gain factor F_5. Between basin average kernel methods, in general, F_6 and F_2 perform better compared to F_1. The results confirm that F_6 reduces leakage errors better than other basin average techniques when it is applied over larger basins as mentioned in Vishwakarma et al. (2016). This approach is, however, found to be sensitive to the basin size in a way that noise increases when the catchment size decreases.

Over smaller basins (e.g., Lachlan and Namoi basins), F_2 works significantly better than F_3 and F_4. This confirms the findings of Han and Simons (2008) that this filter is designed to address leakage errors over basins with a small area (cf. Table 4). In summary, our results indicate that the KeFIn filter and F_2 are likely better suited to deal with the leakage in small river basins. F_3, designed by Seo and Wilson (2005) and tested over the Mississippi Basin, shows reliable results over this basin with fewer similar performance in other basins. This likely indicates that filters must be extensively tested over different basins that are of different shapes and sizes with different magnitude and distribution of TWS signals.

We find that the proposed KeFIn filter reduces the leakage errors over ~82% of the basins with an area less than 1 million km^2, thus, we conclude it is suitable for leakage error reduction over basins with various sizes and shapes. Comparison with water flux observations indicates that in addition to the KeFIn filter, the recently developed F_6 and F_4 that use a hydrological model to recover GRACE smoothed signals (on a gridded basis), better approximate the derivatives of TWS changes than the other filters. Over the larger basins (e.g., Amazon and Mekong basins), the results of the F_1 and F_5 filters are found to be better than those in the smaller basins. Overall, more consistent leakage reduction within different basins is achieved by the KeFIn filter, F_2, F_6, and F_4 considering the results of Figs. 10and 12, as well as Table 3.

6. Conclusion

In this study, a new GRACE post-processing technique, the so-called KeFIn filtering method, is proposed and its performance in reducing GRACE TWS errors in higher spatial frequencies as well as leakage (in/out) errors is investigated. The KeFIn filtering method successfully mitigates the existing problems with other leakage filtering methods, e.g., the high sensitivity of them to prior models in the scale factor approaches. To demonstrate the benefit of using the KeFln filtering method, two different test scenarios are considered over the 43 river basins of different shapes and sizes. First, all the filtering methods are compared using generated synthetic data with properties similar to real GRACE TWS data within the 43 globally distributed river basins. In addition, we assessed the performance of the filters against water storage changes from water fluxes observation, as well as a summation of observed groundwater storage and soil moisture content over the selected basins. The results show that the KeFIn filter successfully (i) mitigates the amplitude damping caused by smoothing, and (ii) increases flexibility towards a variety of basins (shapes and sizes of basins as well as the magnitude of TWS). It is worth mentioning here that we do not claim that the KeFIn method is able to reduce all possible artificial features appearing in the two steps of the post-processing algorithm. Therefore, further investigations will be done to optimize parameters that are used to define the shape of the KeFIn filter.

Acknowledgments

We would like to thank Dr. Tim R. McVicar, the associate editor of Remote Sensing of Environment, and the three anonymous reviewers for their useful comments, which we used to improve this study. The authors acknowledge the efforts of providers of GLDAS, TRMM, and MODIS products, as well as GRACE ITSG-Grace2014 gravity field models. We would also like to thank USGS, GRDC, ANA, HYBAM and NSW for sharing ground-based data sets. M. Khaki is grateful for the research grant of Curtin International Postgraduate Research Scholarships (CIPRS)/ORD Scholarship provided by Curtin University (Australia). This work is a TIGeR publication.

Appendix A. Appendix

The following table shows the basin averaged RMSE values calculated by each filtering technique. The results in the table are temporally averaged (between 2002 and 2013), and indicate that the KeFIn filtering method works better compared to other filters in 35 out of the 43 basins, especially over smaller basins.

Table A1
Summary of RMSE (mm) estimated using the unperturbed basin averaged synthetic TWS and the perturbed TWS after using different filtering methods over the 43 river basins. Note that the basins are sorted according to their area and the least RMSE in each row is displayed by the bold value.

Basin	Area (million km^2)	F_1	F_2	F_3	F_4	F_5	F_6	*KeFIn*
1 (Amazon)	6.97	31.25	31.83	31.19	30.98	30.88	31.06	**30.69**
2 (Ob)	4.40	26.64	24.25	28.77	27.64	28.55	**22.93**	23.79
3 (Yenisey)	4.09	29.76	23.17	26.10	21.94	21.11	19.44	**17.63**
4 (Lena)	3.99	31.94	36.15	**27.56**	32.99	33.70	30.71	29.57
5 (Congo)	3.81	25.24	23.52	24.96	24.19	25.60	21.59	**20.47**
6 (Mackenzie)	2.88	24.60	29.23	31.42	26.63	28.56	23.86	**22.18**
7 (Parana)	2.64	37.97	31.83	38.18	30.27	32.71	26.97	**26.68**
8 (Nile)	2.48	34.17	34.01	33.86	34.15	33.45	37.36	**32.79**
9 (Mississippi)	2.35	42.93	38.52	37.51	38.22	43.37	39.83	**37.20**
10 (Niger)	2.11	34.56	33.01	29.34	34.93	33.38	27.84	**27.78**

11 (Amur)	1.85	52.03	49.35	**46.19**	50.33	50.24	47.73	48.52
12 (Yangtze)	1.81	39.90	36.93	38.56	40.20	41.81	36.68	**35.75**
13 (Yukon)	1.58	37.91	40.27	38.63	38.10	39.67	37.14	**36.69**
14 (Nelson)	1.43	31.50	24.22	30.43	22.99	26.21	24.12	**21.41**
15 (Volga)	1.38	30.00	34.84	31.33	32.01	33.71	**28.22**	28.93
16 (St. Lawrence)	1.27	39.53	39.97	33.82	36.02	37.68	34.14	**32.65**
17 (Lake Eyre)	1.12	24.10	26.49	24.94	17.51	29.60	19.45	**16.45**
18 (Zambezi)	1.12	29.54	28.10	31.67	34.98	33.10	29.05	**27.67**
19 (Murray Darling)	1.01	46.66	41.51	38.89	40.94	43.42	38.72	**37.84**
20 (Danube)	0.93	36.67	35.97	37.39	39.31	41.72	31.40	**29.20**
21 (Ganges, Brahmaputra)	0.92	28.92	**17.77**	33.88	26.03	25.19	29.75	28.25
22 (Indus)	0.91	41.31	33.39	36.57	**32.04**	34.04	35.50	33.69
23 (Orange)	0.90	18.71	14.96	21.82	13.01	16.08	11.67	**7.94**
24 (North West Coast)	0.80	16.85	17.97	18.81	22.10	17.58	19.39	**16.39**
25 (Huang He)	0.78	33.86	28.70	30.77	**23.09**	27.11	24.98	23.30
26 (Sumatra)	0.76	32.46	27.08	28.43	34.61	34.38	28.03	**26.19**
27 (Euphrates and Tigris)	0.74	35.91	22.20	19.75	22.00	24.36	19.08	**17.53**
28 (Orinoco)	0.73	42.57	35.90	34.65	38.94	35.99	32.69	**32.42**
29 (Tocantins)	0.71	25.32	**15.02**	16.05	18.99	20.29	22.72	20.65
30 (Ayeyarwady)	0.69	34.75	38.21	36.09	34.17	35.64	35.74	**33.97**
31 (Mekong)	0.68	34.46	35.78	32.27	33.06	36.82	38.03	**31.78**
32 (Kalahari Stampriet)	0.67	36.01	34.75	37.51	**32.32**	39.25	35.16	34.29
33 (Dnieper)	0.65	24.25	23.18	29.80	25.14	25.59	24.09	**22.84**
34 (Colorado)	0.63	23.12	19.32	23.05	22.95	23.87	21.79	**18.05**
35 (Ohio)	0.52	23.31	22.54	25.06	21.82	26.96	23.38	**20.46**
36 (Sirdaryo)	0.51	32.56	27.98	30.35	25.47	25.63	29.40	**24.74**
37 (Central East Coast)	0.49	40.21	42.51	37.21	38.64	39.23	41.20	**36.31**
38 (Western Mediterranean)	0.45	31.64	28.42	28.59	32.44	36.54	37.91	**27.06**
39 (Namoi)	0.43	21.80	12.80	14.33	17.09	25.31	19.53	**12.43**
40 (Kamchatka)	0.40	43.06	33.69	33.62	40.80	37.73	38.89	**32.90**
41 (Lachlan)	0.08	34.05	32.42	28.11	25.79	32.05	28.41	**24.46**
42 (Yalu)	0.03	13.07	12.33	11.40	12.76	18.40	14.73	**8.82**
43 (Lower Mississippi)	0.01	23.94	18.79	20.24	25.13	28.42	21.13	**18.49**

References

Awange, J., Forootan, E., Kuhn, M., Kusche, J., Heck, B., 2014. Water storage changes and climate variability within the Nile Basin between 2002 and 2011. Adv. Water Resour. 73, 1–15. http://dx.doi.org/10.1016/j.advwatres.2014.06.010.

Awange, J., Khandu, Schumacher, M., Forootan, E., Heck, B., 2016. Exploring hydro-meteorological drought patterns over the Greater Horn of Africa (1979-2014) using remote sensing and reanalysis products. Adv. Water Resour. (0309-1708) 94, 45–59. http://dx.doi.org/10.1016/j.advwatres.2016.04.005.

Baur, O., Kuhn, M., Featherstone, W.E., 2009. GRACE-derived ice-mass variations over Greenland by accounting for leakage effects. J. Geophys. Res. 114, B06407. http://dx.doi.org/10.1029/2008JB006239.

Bhagat, K.R., Gour, P., 2013. Novel approach to estimate motion blur kernel parameters and comparative study of restoration techniques. Int. J. Comput. Appl. 72 (17) 0975-8887.

Burrell, M., Moss, P., Petrovic, J., Ali, A., 2015. General Purpose Water Accounting Report 2014–2015: NSW Murray Catchment. NSW Department of Primary Industries, Sydney.

Cai, X., Wang, W., Zou, S., Xu, B., 2012. Evaluation of TRMM precipitation data over the Inland River Basins of Northwest China. In: International Symposium on Geomatics for Integrated Water Resource Management, Lanzhou. 2012. pp. 1–5. http://dx.doi.org/10.1109/GIWRM.2012.6349575.

Chen, J.L., Wilson, C.R., Famiglietti, J.S., Rodell, M., 2007. Attenuation effect on seasonal basin-scale water storage changes from GRACE time-variable gravity. J. Geod. 81 (4), 237–245. http://dx.doi.org/10.1007/s00190-006-0104-2.

Chen, M., Shi, W., Xie, P., Silva, V.B.S., Kousky, V.E., Wayne Higgins, R., Janowiak, J.E., 2008. Assessing objective techniques for gauge-based analyses of global daily precipitation. J. Geophys. Res. 113, D04110. http://dx.doi.org/10.1029/2007JD009132.

Chen, J.L., Wilson, C.R., Tapley, B.D., Yang, Z.L., Niu, Y., 2009. 2005 drought event in the Amazon River basin as measured by GRACE and estimated by climate models. J. Geophys. Res. 114, B05404. http://dx.doi.org/10.1029/2008JB006056.

Dobslaw, H., Bergmann-Wolf, I., Forootan, E., Dahle, C., Mayer-Guerr, T., Kusche, J., Flechtner, F., 2016. Modeling of present-day atmosphere and ocean non-tidal de-aliasing errors for future gravity mission simulations. J. Geod. 90 (5), 423–436. http://dx.doi.org/10.1007/s00190-015-0884-3.

Eicker, A., Forootan, E., Springer, A., Longuevergne, L., Kusche, J., 2016. Does GRACE see the terrestrial water cycle 'intensifying'? J. Geophys. Res. Atmos. 121, 733–745. http://dx.doi.org/10.1002/2015JD023808.

Famiglietti, J.S., Rodell, M., 2013. Water in the balance. Science 340 (6138), 1300–1301. http://dx.doi.org/10.1126/science.1236460.

Forootan, E., Kusche, J., 2012. Separation of global time-variable gravity signals into maximally independent components. J. Geod. 86, 477–497. http://dx.doi.org/10.1007/s00190-011-0532-5.

Forootan, E., Didova, O., Kusche, J., Löcher, A., 2013. Comparisons of atmospheric data and reduction methods for the analysis of satellite gravimetry observations. J. Geophys. Res. Solid Earth 118 (5), 2382–2396. http://dx.doi.org/10.1002/jgrb.50160.

Forootan, E., Didova, O., Schumacher, M., Kusche, J., Elsaka, B., 2014. Comparisons of atmospheric mass variations derived from ECMWF reanalysis and operational fields, over 2003 to 2011. J. Geod. 88, 503–514. http://dx.doi.org/10.1007/s00190-014-0696-x.

Forootan, E., Rietbroek, R., Kusche, J., Sharifi, M.A., Awange, J., Schmidt, M., Omondi, P., Famiglietti, J., 2014. Separation of large scale water storage patterns over Iran using GRACE, altimetry and hydrological data. J. Remote Sensing Environ. 140, 580–595. http://dx.doi.org/10.1016/j.rse.2013.09.025.

Forootan, E., Safari, A., Mostafaie, A., Schumacher, M., Delavar, M., Awange, J., 2017. Large-scale total water storage and water flux changes over the arid and semi-arid parts of the Middle East from GRACE and reanalysis products. Surv. Geophys. http://dx.doi.org/10.1007/s10712-016-9403-1.

Frappart, F., Ramillien, G., Leblanc, M., Tweed, S.O., Bonnet, M.-P., Maisongrande, P., 2011. An independent Component Analysis approach for filtering continental hydrology in the GRACE gravity data. Remote Sens. Environ. 115 (1), 187–204. http://dx.doi.org/10.1016/j.rse.2010.08.017.

Frappart, F., Ramillien, G., Seoane, L., 2016. Monitoring Water Mass Redistributions on Land and Polar Ice Sheets using the GRACE Gravimetry from Space Mission. In: Baghdadi, N., Zribi, M. (Eds.), Land Surface Remote Sensing in Continental Hydrology. Elsevier, Amsterdam, Nederland, pp. 255–279. http://dx.doi.org/10.1016/B978-1-78548-104-8.50008-5.

Geruo, A., Wahr, j., Zhong, S., 2013. Computations of the viscoelastic response of a 3-D compressible Earth to surface loading: an application to Glacial Isostatic Adjustment in Antarctica and Canada. Geophys. J. Int. 192 (2), 557–572. http://dx.doi.org/10.1093/gji/ggs030.

Gonzalez, R., Woods, R., 1992. Digital Image Processing. 1992. Addison Wesley, pp. 414–428.

Gonzalez, R., Woods, R., 2002. Digital Image Processing, 2nd edition. 2002 Prentice Hall Chap 4 Sec 4.3, 4.4; Chap 5 Sec 5.1 5.3.

Gutentag, E.D., Heimes, F.J., Krothe, N.C., Luckey, R.R., Weeks, J.B., 1984. Geohydrology of the High Plains aquifer in parts of Colorado, Kansas, Nebraska, New Mexico, Oklahoma, South Dakota, Texas, and Wyoming. U.S. Geol. Surv. Prof. Pap. 1400-B 66 pp.
Han, S.C., Shum, C.K., Jekeli, C., Kuo, C.Y., Wilson, C.R., Seo, K.W., 2005. Non-isotropic filtering of grace temporal gravity for geophysical signal enhancement. Geophys. J. Int. 163, 18–25. http://dx.doi.org/10.1111/j.1365-246X.2005.02756.x.
Han, S.-C., Simons, F.J., 2008. Spatiospectral localization of global geopotential fields from the Gravity Recovery and Climate Experiment (GRACE) reveals the coseismic gravity change owing to the 2004 Sumatra-Andaman earthquake. J. Geophys. Res. 113, B01405. http://dx.doi.org/10.1029/2007JB004927.
Harig, C., Simons, F.J., 2015. Accelerated West Antarctic ice mass loss continues to outpace East Antarctic gains. Earth Planet. Sci. Lett. 415, 134–141. http://dx.doi.org/10.1016/j.epsl.2015.01.029.
Henck, A.H., Montgomery, D.R., Huntington, K.W., Liang, C., 2010. Monsoon control of effective discharge, Yunnan and Tibet. Geology 38, 975–978.
Hichri, S., Benzarti, F., Amiri, H., 2012. Robust noise filtering in image sequences. Int. J. Comput. Appl. (0975 8887) 50 (18).
Huffman, G.J., Adler, R.F., Bolvin, D.T., Gu, G., Nelkin, E.J., Bowman, K.P., Hong, Y., Stocker, E.F., Wolff, D.B., 2007. The TRMM multi-satellite precipitation analysis: quasi-global, multi-year, combined-sensor precipitation estimates at fine scale. Journal. Hydrometeorol. 8 (1), 38–55.
Jekeli, C., 1981. Alternative methods to smooth the Earth's gravity field. In: Technical Report. 327 Department of Geodesy and Science and Surveying, Ohio State University.
Khaki, M., Hoteit, I., Kuhn, M., Awange, J., Forootan, E., van Dijk, A.I.J.M., Schumacher, M., Pattiaratchi, C., 2017. Assessing sequential data assimilation techniques for integrating GRACE data into a hydrological model. Adv. Water Resour. (0309-1708) 107, 301–316. http://dx.doi.org/10.1016/j.advwatres.2017.07.001.
Khaki, M., Schumacher, M., Forootan, J., Kuhn, M., Awange, E., van Dijk, A.I.J.M., 2017. Accounting for spatial correlation errors in the assimilation of GRACE into hydrological models through localization. Adv. Water Resour.(0309-1708)http://dx.doi.org/10.1016/j.advwatres.2017.07.024. Available online 1 August 2017.
Klees, R., Revtova, E.A., Gunter, B.C., Ditmar, P., Oudman, E., Winsemius, H.C., 2008. The design of an optimal filter for monthly grace gravity models. Geophys. J. Int. 175 (2), 417–432. http://dx.doi.org/10.1111/j.1365-246X.2008.03922.x.
Kusche, J., 2007. Approximate decorrelation and non-isotropic smoothing of time variable GRACE-type gravity field models. J. Geod. 81, 733–749. http://dx.doi.org/10.1007/s00190-007-0143-3.
Kusche, J., Schmidt, R., Petrovic, S., Rietbroek, R., 2009. Decorrelated GRACE time-variable gravity solutions by GFZ, and their validation using a hydrological model. J. Geod. 83, 903–913. http://dx.doi.org/10.1007/s00190-009-0308-3.
Kusche, J., Klemann, V., Bosch, W., 2012. Mass distribution and mass transport in the Earth system. J. Geodyn. 59-60, 1–8. http://dx.doi.org/10.1016/j.jog.2012.03.003.
Kusche, J., Eicker, A., Forootan, E., Springer, A., Longuevergne, L., 2016. Mapping probabilities of extreme continental water storage changes from space gravimetry. Geophys. Res. Lett. 43, 8026–8034. http://dx.doi.org/10.1002/2016GL069538.
Landerer, F.W., Swenson, S.C., 2012. Accuracy of scaled GRACE terrestrial water storage estimates. Water Resour. Res. 48 (4), W04531. http://dx.doi.org/10.1029/2011WR011453.
Le Roux, J., Vincent, E., Mizuno, Y., Kameoka, H., Ono, N., 2010. Consistent Wiener filtering: generalized time-frequency masking respecting spectrogram consistency. In: 9th Int. Conf. on Latent Variable Analysis and Signal Separation (LVA/ICA), Saint-Malo, France, pp. 89–96.
Long, D., Yang, Y., Wada, Y., Hong, Y., Liang, W., Chen, Y., Yong, B., Hou, A., Wei, J., Chen, L., 2015. Deriving scaling factors using a global hydrological model to restore GRACE total water storage changes for China's Yangtze River Basin. Remote Sens. Environ. 168, 177–193. http://dx.doi.org/10.1016/j.rse.2015.07.003.
Longuevergne, L., Scanlon, B.R., Wilson, C.R., 2010. GRACE hydrological estimates for small basins: evaluating processing approaches on the High Plains Aquifer, USA. Water Resour. Res. 46 (11), W11517. http://dx.doi.org/10.1029/2009WR008564.
Mayer-Gürr, T., Zehentner, N., Klinger, B., Kvas, A., 2014. ITSG-GRACE 2014: a new GRACE gravity field release computed in Graz. In: GRACE Science Team Meeting (GSTM) Potsdam am: 29.09.2014.
Miralles, D.G., Jiménez, C., Jung, M., Michel, D., Ershadi, A., McCabe, M.F., Hirschi, M., Martens, B., Dolman, A.J., Fisher, J.B., Mu, Q., Seneviratne, S.I., Wood, E.F., Fernández-Prieto, D., 2016. The WACMOS-ET project — part 2: evaluation of global terrestrial evaporation data sets. Hydrol. Earth Syst. Sci. 20, 823–842. http://dx.doi.org/10.5194/hess-20-823-2016.
Mu, Q., Zhao, M., Running, S.W., 2011. Improvements to a MODIS global terrestrial evapotranspiration algorithm. Remote Sens. Environ. 115 (8), 1781–1800.
Munier, S., Aires, F., Schlaffe, S., Prigent, C., Papa, F., Maisongrande, P., Pan, M., 2014. Combining data sets of satellite-retrieved products for basin-scale water balance study: 2. In: evaluation on the Mississippi Basin and closure correction model Journal of Geophysical Research: Atmospheres. 119. pp. 12,100–12,116. http://dx.doi.org/10.1002/2014JD021953.
Ogawa, R., Chao, B.F., Heki, K., 2011. Acceleration signal in GRACE time-variable gravity in relation to interannual hydrological changes. Geophys. J. Int. 184 (2), 673–679.
Pitas, I., 1993. Digital Image Processing Algorithms. Prentice Hall ISBN 0131458140, 9780131458147.
Ramoelo, A., Majozi, N., Mathieu, R., Jovanovic, N., Nickless, A., Dzikiti, S., 2014. Validation of global evapotranspiration product (MOD16) using flux tower data in the African Savanna, South Africa. Remote Sens. 6, 7406–7423.
Rodell, M., Houser, P.R., Jambor, U., Gottschalck, J., Mitchell, K., Meng, C.J., Arsenault, K., Cosgrove, B., Radakovich, J., Bosilovich, M., Entin, J.K., Walker, J.P., Lohmann, D., Toll, D., 2004. The global land data assimilation system. Am. Meteorol. Soc. 85 (3), 381–394. http://dx.doi.org/10.1175/BAMS-85-3-381.
Rodell, M., Chen, J., Kato, H., Famiglietti, J.S., Nigro, J., Wilson, C.R., 2007. Estimating groundwater storage changes in the Mississippi River basin (USA) using GRACE. Hydrogeol. J. 15, 159–166.
Schmidt, A.H., Montgomery, D.R., Huntington, K.W., Liang, C., 2011. The Question of Communist Land Degradation. New Evidence from Local Erosion and Basin-Wide Sediment Yield in Southwest China and Southeast Tibet. Annals of the Association of American Geographers.
Seo, K.W., Wilson, C.R., 2005. Simulated estimation of hydrological loads from GRACE. J. Geod. 78, 442–456. http://dx.doi.org/10.1007/s00190-004-0410-5.
Seo, K.W., Wilson, C.R., Famiglietti, J.S., Chen, J.L., Rodell, M., 2006. Terrestrial water mass load changes from Gravity Recovery and Climate Experiment (GRACE). Water Resour. Res. 42, W05417. http://dx.doi.org/10.1029/2005WR004255.
Seoane, L., Ramillien, G., Frappart, F., Leblanc, M., 2013. Regional GRACE-based estimates of water mass variations over Australia: validation and interpretation. Hydrol. Earth Syst. Sci. 17, 4925–4939. http://dx.doi.org/10.5194/hess-17-4925-2013.
Simons, M., Hager, B.H., 1997. Localization of the gravity field and the signature of glacial rebound. Nature 390, 500–504.
Sonka, M., Hlavac, V., Boyle, R., 2001. Image Processing, Analysis, and Machine Vision, 2nd edition. University Press, Cambridge ISBN-10:049508252X.
Springer, A., Kusche, J., Hartung, K., Ohlwein, C., Longuevergne, L., 2014. New estimates of variations in water flux and storage over Europe based on regional (Re) analyses and multisensor observations. J. Hydrometeorol. 15 (6), 2397–2417.
Strassberg, G., Scanlon, B.R., Rodell, M., 2007. Comparison of seasonal terrestrial water storage variations from GRACE with groundwater level measurements from the High Plains Aquifer (USA). Geophys. Res. Lett. 34, L14402. http://dx.doi.org/10.1029/2007GL030139.
Strassberg, G., Scanlon, B.R., Chambers, D., 2009. Evaluation of groundwater storage monitoring with the GRACE satellite: case study High Plains Aquifer, central USA. Water Resour. Res. 45, W05410. http://dx.doi.org/10.1029/2008WR006892.
Swenson, S., Wahr, J., 2002. Methods for inferring regional surface-mass anomalies from Gravity Recovery and Climate Experiment (GRACE) measurements of time-variable gravity. J. Geophys. Res. B9 (2193), 107. http://dx.doi.org/10.1029/2001JB000576.
Swenson, S., Wahr, J., 2003. Estimated accuracies of regional water storage variations inferred from the Gravity Recovery and Climate Experiment (GRACE). J. Geophys. Res. 39 (8), 1223. http://dx.doi.org/10.1029/2002WR001808.
Swenson, S., Wahr, J., 2006. Post-processing removal of correlated errors in GRACE data. Geophys. Res. Lett. 33, L08402. http://dx.doi.org/10.1029/2005GL025285.
Swenson, S., Chambers, D., Wahr, J., 2008. Estimating geocenter variations from a combination of GRACE and ocean model output. J. Geophys. Res. 113, B08410. http://dx.doi.org/10.1029/2007JB005338.
Syed, T.H., Famigletti, J.S., Chen, J., Rodell, M., Seneviratne, S.I., Viterbo, P., Wilson, C.R., 2005. Total basin discharge for the Amazon and Mississippi River basins from GRACE and a land-atmosphere water balance. Geophys. Res. Lett. 32, L24404. http://dx.doi.org/10.1029/2005GL024851.
Tapley, B.D., Bettadpur, S., Ries, J.C., Thompson, P.F., Watkins, M.M., 2004. GRACE measurements of mass variability in the Earth system. Science 305 (5683), 503–505.
Velpuri, N.M., Senay, G.B., Singh, R.K., Bohms, S., Verdin, J.P., 2013. A comprehensive evaluation of two MODIS evapotranspiration products over the conterminous United States: using point and gridded FLUXNET and water balance ET. Remote Sens. Environ. (0034-4257) 139, 35–49. http://dx.doi.org/10.1016/j.rse.2013.07.013.
Vishwakarma, B., Devaraju, B., Sneeuw, N., 2016. Minimizing the effects of filtering on catchment scale GRACE solutions. Water Resour. Res. 52, 5868–5890. http://dx.doi.org/10.1002/2016WR018960.
Wahr, J., Molenaar, M., Bryan, F., 1998. Time variability of the Earth's gravity field. Hydrological and oceanic effects and their possible detection using GRACE. J. Geophys. Res. 103 (B12), 30,205–30,229. http://dx.doi.org/10.1029/98JB02844.
Wahr, J., Swenson, S., Velicogna, I., 2006. Accuracy of GRACE mass estimates. Geophys. Res. Lett. 33 (6), L06401. http://dx.doi.org/10.1029/2005GL025305.
Wang, J., Xu, K., Zhou, K., Lin, S., Hu, S., Guo, B., 2006. Spherical harmonics scaling. Vis. Comput. 22, 713. http://dx.doi.org/10.1007/s00371-006-0057-8.
Watkins, M.M., Wiese, D.N., Yuan, D.N., Boening, C., Landerer, F.W., 2015. Improved methods for observing Earth's time variable mass distribution with GRACE using spherical cap mascons. J. Geophys. Res. Solid Earth 120. http://dx.doi.org/10.1002/2014JB011547.
Werth, S., Güntner, A., Schmidt, R., Kusche, J., 2009. Evaluation of grace filter tools from a hydrological perspective. Geophys. J. Int. 179 (3), 1499–1515. http://dx.doi.org/10.1111/j.1365-246X.2009.04355.x.
Wiese, D.N., 2015. GRACE Monthly Global Water Mass Grids NETCDF RELEASE 5.0. Ver. 5.0 PO.DAAC, CA, USA. http://dx.doi.org/10.5067/TEMSC-OCL05.
Wouters, B., Schrama, E.J.O., 2007. Improved accuracy of GRACE gravity solutions through empirical orthogonal function filtering of spherical harmonics. Geophys. Res. Lett. 34, L23711. http://dx.doi.org/10.1029/2007GL032098.
Wouters, B., Bonin, J.A., Chambers, D.P., Riva, R.E.M., Sasgen, I., Wahr, J., 2014. GRACE, time-varying gravity, Earth system dynamics and climate change. Rep. Prog. Phys. 77 (11), 116801. http://dx.doi.org/10.1088/0034-4885/77/11/116801.
Yan, N., Wu, B., Chang, S., Bao, X., 2014. Evaluation of TRMM precipitation product for meteorological drought monitoring in Hai basin. IOP Conf. Ser.: Earth environ. Sci. 17 (012093). http://iopscience.iop.org/1755-1315/17/1/012093.
Yeh, P.J.F., Swenson, S.C., Famiglietti, J.S., Rodell, M., 2006. Remote sensing of ground water storage changes in Illinois using the Gravity Recovery and Climate Experiment (GRACE). Water Resour. Res. 42, W12203. http://dx.doi.org/10.1029/2006WR005374.
Zaitchik, B.F., Rodell, M., Reichle, R.H., 2008. Assimilation of GRACE terrestrial water storage data into a land surface model: results for the Mississippi River Basin. J. Hydrometeorol. 9 (3), 535–548. http://dx.doi.org/10.1175/2007JHM951.1.

Zeng, G., Allred, R.J., 2009. Partitioned image filtering for reduction of the Gibbs phenomenon. 37 (2), 96–100. http://dx.doi.org/10.2967/jnmt.108.061556.
Zhang, L., Hao, T., Wu, J., Wang, J., 2005. Application of image enhancement techniques to potential field data. Appl. Geophys. 2, 145. http://dx.doi.org/10.1007/s11770-005-0017-5.
Zhang, Z.Z., Chao, B.F., Lu, Y., Hsu, H.T., 2009. An effective filtering for GRACE time-variable gravity: fan filter. Geophys. Res. Lett. 36, L17311. http://dx.doi.org/10.1029/2009GL039459.
Zhang, K., Kimball, J.S., Nemani, R.R., Running, S.W., 2010. A continuous satellite-derived global record of land surface evapotranspiration from 1983–2006. Water Resour. Res. 46, W09522. http://dx.doi.org/10.1029/2009WR008800.

Chapter 4

Assimilation tuning

This chapter is covered by the following publication:

- **Khaki, M.**, Schumacher, M., J., Forootan, Kuhn, M., Awange, E., van Dijk, A.I.J.M., (2017a). Accounting for Spatial Correlation Errors in the Assimilation of GRACE into Hydrological Models through localization. Advances in Water Resources, 108:99-112, doi:10.1016/j.advwatres.2017.07.024.

This contribution covers the thesis objective (ii) outlined in Section 1.4 by presenting the idea of applying local analysis (LA) to maximize the contribution of GRACE TWS in hydrological data assimilation by using its full error information. This paper further investigates the effects of various spatial (1° to 5° grids, and basin scale) and temporal (5-day and monthly) scales of GRACE observations on the assimilation process. The analysis is carried out over Australia subject to the availability of in-situ measurements for validation. It is shown that assimilating GRACE TWS data on 3° grid resolution and the 5-day period obtain the best results. The average error values for the 5-day assimilation is $\sim$7% smaller than using a monthly assimilation window (see also Khaki et al., 2018f). Further groundwater and soil moisture assessment results support the capability of LA for improving assimilation results for all spatial scales. The proposed method provides a solution to the existing gap (Section 1.3) in the literature by addressing the limitations in GRACE TWS products during data assimilation. The results indicate that LA is able to stabilize the assimilation process when dealing with full GRACE error covariance matrix with a rank deficiency issue for spatial resolutions of 1° and 2° with a positive impact on final estimates of all grid resolutions. The proposed framework successfully (a) solves the mathematical problem of using correlated data for assimilation especially when the observation's spatial resolution is high (e.g., 1° gridded TWS), and (b) improves the assimilation results using GRACE TWS data for different spatial resolutions (1°–5° and basin scale). It is also found that optimum value for LA for using GRACE observation is the 5° localization halfwidth length, which is large enough to capture the observation error

information within a specific area while skipping less effective information, which can be related to GRACE noises.

Advances in Water Resources 108 (2017) 99–112

Contents lists available at ScienceDirect

Advances in Water Resources

journal homepage: www.elsevier.com/locate/advwatres

Accounting for spatial correlation errors in the assimilation of GRACE into hydrological models through localization

M. Khaki[a,*], M. Schumacher[b], E. Forootan[a,c], M. Kuhn[a], J.L. Awange[a], A.I.J.M. van Dijk[d]

[a] Department of Spatial Sciences, Curtin University, Perth, Australia
[b] School of Geographical Sciences, University of Bristol, Bristol, UK
[c] School of Earth and Ocean Sciences, Cardiff University, Cardiff, UK
[d] Fenner School of Environment and Society, the Australian National University, Canberra, Australia

ARTICLE INFO

Article history:
Received 23 December 2016
Revised 31 July 2017
Accepted 31 July 2017
Available online 1 August 2017

Keywords:
Data assimilation
GRACE
Localization
Hydrological model

ABSTRACT

Assimilation of terrestrial water storage (TWS) information from the Gravity Recovery And Climate Experiment (GRACE) satellite mission can provide significant improvements in hydrological modelling. However, the rather coarse spatial resolution of GRACE TWS and its spatially correlated errors pose considerable challenges for achieving realistic assimilation results. Consequently, successful data assimilation depends on rigorous modelling of the full error covariance matrix of the GRACE TWS estimates, as well as realistic error behavior for hydrological model simulations. In this study, we assess the application of local analysis (LA) to maximize the contribution of GRACE TWS in hydrological data assimilation. For this, we assimilate GRACE TWS into the World-Wide Water Resources Assessment system (W3RA) over the Australian continent while applying LA and accounting for existing spatial correlations using the full error covariance matrix. GRACE TWS data is applied with different spatial resolutions including 1° to 5° grids, as well as basin averages. The ensemble-based sequential filtering technique of the Square Root Analysis (SQRA) is applied to assimilate TWS data into W3RA. For each spatial scale, the performance of the data assimilation is assessed through comparison with independent in-situ ground water and soil moisture observations. Overall, the results demonstrate that LA is able to stabilize the inversion process (within the implementation of the SQRA filter) leading to less errors for all spatial scales considered with an average RMSE improvement of 54% (e.g., 52.23 mm down to 26.80 mm) for all the cases with respect to groundwater in-situ measurements. Validating the assimilated results with groundwater observations indicates that LA leads to 13% better (in terms of RMSE) assimilation results compared to the cases with Gaussian errors assumptions. This highlights the great potential of LA and the use of the full error covariance matrix of GRACE TWS estimates for improved data assimilation results.

1. Introduction

The Gravity Recovery And Climate Experiment (GRACE) satellite mission provides global time-variable gravity field solutions that have been used to obtain global terrestrial water storage (TWS) changes (Tapley et al., 2004). Several studies indicate that GRACE TWS can play an important role in better understanding surface and sub-surface physical processes related to water redistribution within the Earth system (e.g., Huntington, 2006; Chen et al., 2007; Kusche et al., 2012; Forootan et al., 2014; van Dijk et al., 2014; Wouters et al., 2014). A growing number of studies has also been applying GRACE TWS to constrain the mass balance of hydrological models (e.g., Zaitchik et al., 2008; Thomas et al., 2014; van Dijk et al., 2014; Eicker et al., 2014; Tangdamrongsub et al., 2015; Reager et al., 2015; Khaki et al., 2017). This combination is motivated by the fact that hydrological models use conceptual or physical knowledge (or both) to simulate hydrological processes at global (e.g., Huntington, 2006; Coumou and Rahmstorf, 2012) and regional (e.g., Zaitchik et al., 2008; Chen et al., 2013; Munier et al., 2014) scales. The accuracy of simulations might be limited due to imperfect models (i.e., lack of knowledge about the processes or simplified model equations) and uncertainties in input and forcing data (Vrugt et al., 2013). Data limitation (both on temporal and spatial scales) also plays a substantial role in land hydrological modelling, especially for closing the water balance that requires reliable information about all storage compartments from which that of groundwater is very challenging. In this regard, GRACE TWS estimates are of great importance since they can be used through data

* Corresponding author.
E-mail address: mehdi.Khaki@postgrad.curtin.edu.au (M. Khaki).

http://dx.doi.org/10.1016/j.advwatres.2017.07.024
0309-1708/

assimilation to constrain the vertical summation of water storages (including groundwater) in the models.

Data assimilation is a technique to incorporate observations into a dynamic model in order to improve its state estimation (Bertino et al., 2003; Hoteit et al., 2012). It has been widely applied in the fields of ocean and climate science (Bennett, 2002; Elbern and Schmidt, 2001; Garner et al., 1999; Kalnay, 2003; Lahoz et al., 2007; Schunk et al., 2004; Zhang et al., 2012). In hydrological studies, different in-situ measurements (e.g., river discharge and soil moisture) have been assimilated into models (Liu et al., 2012) to improve their estimates of different hydrological quantities (see, e.g., Crow and Wood, 2003; Seo et al., 2003; Vrugt et al., 2005; Weerts and El Serafy, 2006; Reichle et al., 2010).

The application of remotely sensed data in data assimilation for hydrological purposes has gathered interests in the past few years. This is especially due to the increased development and availability of satellite remote sensing systems such as Sentinel, Soil Moisture Active Passive (SMAP), GRACE, and satellite radar altimetry (e.g., Moradkhani et al., 2006; Clark et al., 2008; Houborg et al., 2012; van Dijk et al., 2014; Renzullo et al., 2014; Reager et al., 2015; Kumar et al., 2016). Data assimilation can improve various water compartments of hydrological models such as soil (e.g., Reichle et al., 2002; 2008; Brocca et al., 2010; Kumar et al., 2014; Renzullo et al., 2014), surface water (e.g., Alsdorf et al., 2007; Neal et al., 2009; Giustarini et al., 2011), and snow (e.g., Liu et al., 2013; Kumar et al., 2015) storages. A number of studies has also investigated the possibility of using GRACE data to improve hydrological models (e.g., Zaitchik et al., 2008; Houborg et al., 2012; Li et al., 2012; Eicker et al., 2014; van Dijk et al., 2014; Tangdamrongsub et al., 2015; Kumar et al., 2016; Schumacher et al., 2016).

GRACE data with a suitable coverage, both temporally and spatially, provide a unique opportunity to study water storages in lands on global and regional scales. The mission now provides 15 years of data with a global coverage, which provides the chance to study seasonal to decadal changes in TWS. Before using GRACE TWS in any assimilation framework, however, there are some important aspects which should be considered such as the temporal and spatial resolution mismatch between GRACE observations and model simulations, as well as existing spatial and temporal correlations in the time series of GRACE TWS and model simulations. Its spatial resolution is limited to a few hundred kilometers depending on the signal strength and the inversion technique applied to recover time-variable gravity fields (Schmidt et al., 2008). This coarse spatial resolution exists in both GRACE level 2 solutions provided in terms of spherical harmonics potential coefficients or mass concentration (mascon) solutions. Although mascon is provided on a finer spatial scale (e.g., 0.5°), the native resolution of the data is smaller (e.g., 3°; Watkins et al., 2015; Wiese, 2015). Different studies have tried to assimilate GRACE data in either basin scales (e.g., Zaitchik et al., 2008; Houborg et al., 2012; Li et al., 2012) or grid element scales (e.g., Eicker et al., 2014; Tangdamrongsub et al., 2015; Schumacher et al., 2016). GRACE level 2 products have been truncated (e.g., at degree and order 60–120). They also have been filtered (e.g., Swenson and Wahr, 2006; Kusche, 2007) resulting in low spatial resolutions. Upscaling of the original established TWS with a limited spatial resolution to create a high spatial resolution data (e.g., 1°) with grid points that are not independent of each other increases spatial correlation significantly (see e.g., Schumacher et al., 2016). Accounting for these correlations is important especially in the context of data assimilation, where complete knowledge of the data error structure including uncertainties and existing correlations is necessary.

Data assimilation as an inverse problem uses the covariance information of model simulations and observations. Significantly correlated errors yield covariance matrices that are bad conditioned or not invertible leading to inefficiency in filtering process during data assimilation. Due to the lack of information (or to enhance computations), the decision of uncorrelated data (Gaussian error for observations) is often made to deal with this problem, which can be realistic when observations are denser than models' grid, e.g., independent grid points of neighbours (Berger and Forsythe, 2004; Stewart et al., 2008). In contrast, when the spatial resolution of models is finer than the assimilated observations, it can lead to no improvement in the accuracy of final assimilation results (e.g., Liu and Rabier., 2003; Dando et al., 2007; Stewart et al., 2008). In this regard, it is necessary to precisely consider the full GRACE error covariance for different spatial resolutions in data assimilation applications especially where the model spatial scale is finer than GRACE TWS, and the existing correlations in the observations are problematic (see e.g., Schumacher et al., 2016).

Most of the previous studies assimilated GRACE TWS (e.g., grid-based or basin averaged) into models while assuming white noise (i.e., uncorrelated observations). This, for basin averaged applications, might be justified to some extent as the spatial averaging of TWS observations adds up the non-Gaussian noise distributions and generates a mixture that is closer to Gaussian distribution according to the central limit theorem (Stone, 2004, Chapter 5). In this regard, for example, Zaitchik et al. (2008) applied GRACE TWS on a sub-basin scale (sub-basins of the Mississippi River) and assumed a Gaussian error (with zero correlation) for GRACE TWS measurements. Reichle et al. (2013) investigated the effects of coarse-scale satellite observations (e.g., GRACE) and vertically integrated measurements (such as TWS) on model variables within the assimilation system. For a grid-based assimilation of GRACE-TWS in models, Eicker et al. (2014) studied the relationship of different GRACE spatial resolutions on the data assimilation process and reported that there is always a trade-off between employing GRACE data in a higher spatial resolution while keeping the GRACE error covariance matrices reasonably well conditioned. Girotto et al. (2016); 2017) have considered the fact that 1° GRACE error covariances are spatially highly correlated and to address this issue, they have used a spatial correlation length of 3° for the observation errors (see also Kumar et al., 2016; Khaki et al., 2017). Schumacher et al. (2016) indicated that both the characteristics of GRACE error correlation and spatial discretization of TWS observations are important on the performance of the data assimilation process. In another effort, van Dijk et al. (2014) proposed an alternative approach for estimating GRACE TWS errors in data assimilation. The triple collocation technique was used to merge model-derived storage in (sub-) surface compartments with TWS estimates from GRACE measurements (van Dijk et al., 2014). In the studies discussed above, GRACE error covariance for different spatial resolutions is hardly treated. For example, Eicker et al. (2014) considered error covariance of various spatial resolutions that were rescaled (e.g., rescaling 0.5°–5°) rather than solving for distinct spatial resolution individually (e.g., 0.5°, 1°, and 5°).

In the present study, we extend the works above by employing a Local Analysis (LA) technique. LA allows utilization of different GRACE TWS spatial resolutions by addressing instability in data assimilation that arises from the GRACE covariance matrices of the corresponding spatial resolutions. The contribution of this study is, therefore, twofold: (i) we mathematically assess the efficiency of the localization technique to use GRACE TWS with its full error information and with high spatial resolution in an assimilation framework; and (ii), we compare the performance of a localization technique to in-situ data in a real case study covering the entire Australian continent. These will assess the ability of local data assimilation in maximizing the contribution of GRACE TWS into a hydrological model by considering its full error covariance matrix. Here, we use the full variance-covariance of GRACE to establish the observation error covariance matrices for the grid resolutions of 1°, 2°, 3°, 4°, 5°, and a basin scale, and examine their effects on

data assimilation. More importantly, for the first time, we offer a solution to increase the performance of data assimilation in using GRACE data. A localization technique is applied to account for correlations in high spatial resolution observations, which can lead to a rank deficiency problem and correspondingly an instability in the data assimilation procedure. In terms of localization technique, Local Analysis (LA) of the filter (Evensen, 2003; Ott et al., 2004) is considered mainly due to its ability in dealing with correlations by spatially limiting the use of ensemble-based covariance information of high-dimensional systems to the limited local region (Ott et al., 2004). LA effects on each data assimilation scenario (i.e., using different spatial resolutions) are assessed to explore its ability for improving the results. In addition, the application of LA has the potential to minimize a large part of error sources in the ensemble filtering methods when a small number of ensembles is used (Houtekamer and Mitchell, 2001; Mitchell and Houtekamer, 2000).

GRACE TWS data is assimilated into the World-Wide Water Resources Assessment (W3RA, van Dijk, 2010) over Australia. The ensemble-based sequential technique of the Square Root Analysis (SQRA) filtering scheme represented by Evensen (2004) is used to assimilate GRACE TWS into W3RA. SQRA, which is a deterministic form of ensemble Kalman filtering, has considerable advantages in comparison to some existing methods in terms of the computational speed, simplicity, and its independency to an observation perturbation unlike traditional Kalman filtering methods (see detail in Section 3.1 and Khaki et al., 2017). In addition to implementing the LA, in order to further address possible problems that arise from ensemble size, sampling errors, and insufficient ensemble variance in ensemble-based techniques (Anderson et al., 2007; Oke et al., 2007), ensemble inflation is applied. This technique, which has frequently been used in previous works (e.g., Anderson and Anderson, 1999; Anderson et al., 2007; Ott et al., 2004), tries to increase the variance of ensembles around the ensemble mean by inflating prior ensembles (Anderson et al., 2007).

The remainder of this contribution is organized as follows: in Section 2, the GRACE TWS data, W3RA, and in-situ observations are introduced. The SQRA filtering scheme used for data assimilation, ensemble inflation, and the applied localization method are described in Subsection 3.1 and dummyTXdummy- details of an experiment set up are provided in Subsection 3.2. In Section 4, the results of data assimilation and their evaluation against the in-situ validation data are presented and discussed, and finally in Section 5, the study is concluded.

2. Datasets

2.1. GRACE

Monthly GRACE level 2 (L2) potential coefficients products along with their full error covariance information are obtained from the ITSG-Grace2014 gravity field model (Mayer-Gürr et al., 2014). The solution is computed up to degree and order (d/o) 90 resulting in approximately $\sim$300 km spatial resolution at the equator. The study period (February 2003 to December 2012) is limited by the availability of the climate data (see Section 2.2) to force the hydrological model.

Following Swenson et al. (2008), degree 1 coefficients (http://grace.jpl.nasa.gov/data/get-data/geocenter/) are replaced to account for the movement of the Earth's centre of mass. Degree 2 and order 0 (C_{20}) coefficients (http://grace.jpl.nasa.gov/data/get-data/oblateness/) are not well determined and are replaced by those from Cheng and Tapley (2004). Correlated noise in the TWS data products is reduced by applying de-striping and smoothing using a Gaussian averaging kernel with 300 km half radius following Swenson and Wahr (2006). This causes some degree of signal attenuation (Klees et al., 2008) and moving anomalies from one region to another (Chen et al., 2007). This leakage effect can lead to some degree of signal inference especially at the land-ocean boundary. In order to address this issue, following Swenson and Wahr (2002), we apply an isotropic kernel using a Lagrange multiplier filter to best balance signal and leakage errors over the entire Australia. This filter uses a basin averaging kernel method expanded in spherical harmonic coefficients and subsequently combined with L2 potential coefficients to improve the GRACE estimates (see details in Swenson and Wahr, 2002).

The filtered gravity fields, are then converted to TWS changes (following Wahr and Molenaar, 1998) over the entire Australia in both grid and basin scales. The amount of rainfall over Australia, especially over its northeast, western, and central parts, is low in comparison to other inhabited continents on Earth leading to prolonged drought in the interior regions (Forootan et al., 2016). This effect can be seen from the average precipitation (between February 2003 and December 2012) in Fig. 1. This map shows small amount of rainfall over most parts of Australia (e.g., the western and eastern parts). Therefore, an accurate estimation of water storages (e.g., using hydrological models) is necessary to manage water resources in this region. TWS changes from GRACE are gridded into the spatial grid resolutions of 1°, 2°, 3°, 4°, 5°, and also a basin scale for 12 major Australian drainage divisions and river basin (cf. Fig. 1). As a number of studies have used basin averaged GRACE TWS for data assimilation (e.g., Zaitchik et al., 2008; Houborg et al., 2012), we test the LA in both grid and basin scales. Accordingly, for each grid size as well as basin scale error covariance matrices are calculated using the full error information of the L2 potential coefficients for each month. Note that the errors in lower degree potential coefficients provided along with degree 1 coefficients and C_{20} are substituted into the GRACE covariance matrix. No correlation is considered between the GRACE covariance matrix and errors in the lower degree potential coefficients. This error information is then used to reach observation errors for data assimilation. To this end, following Schumacher et al. (2016), an error propagation is implemented to convert the full error information of the GRACE coefficients to TWS errors.

2.2. W3RA

In this study, we use the World-Wide Water Resources Assessment system (W3RA), which was developed in 2008 by the Commonwealth Scientific and Industrial Research Organisation (CSIRO) to monitor, represent and forecast Australia's terrestrial water cycles (http://www.wenfo.org/wald/data-software/). W3RA is a grid distributed biophysical model that simulates water stores and flows with significant information of water storages over Australia (van Dijk, 2010; Renzullo et al., 2014). Globally distributed $1° \times 1°$ minimum and maximum temperature, downwelling shortwave radiation, and precipitation from Princeton University (http://hydrology.princeton.edu) are used as meteorological forcing data (see detail in Sheffield et al., 2006). The model parameters include effective soil parameters, water holding capacity and soil evaporation, relating greenness and groundwater recession, and saturated area to catchment characteristics (van Dijk et al., 2013). Model state in this study includes the W3RA water storages in the top, shallow, and deep root soil layers, groundwater storage, and surface water storage in a one-dimensional system (vertical variability). Here, we use W3RA (with a daily scale) for the same temporal coverage of GRACE (e.g., February 2003 to December 2012) and the spatial resolution of $1° \times 1°$. More detailed information on W3RA can be found in van Dijk et al. (2013).

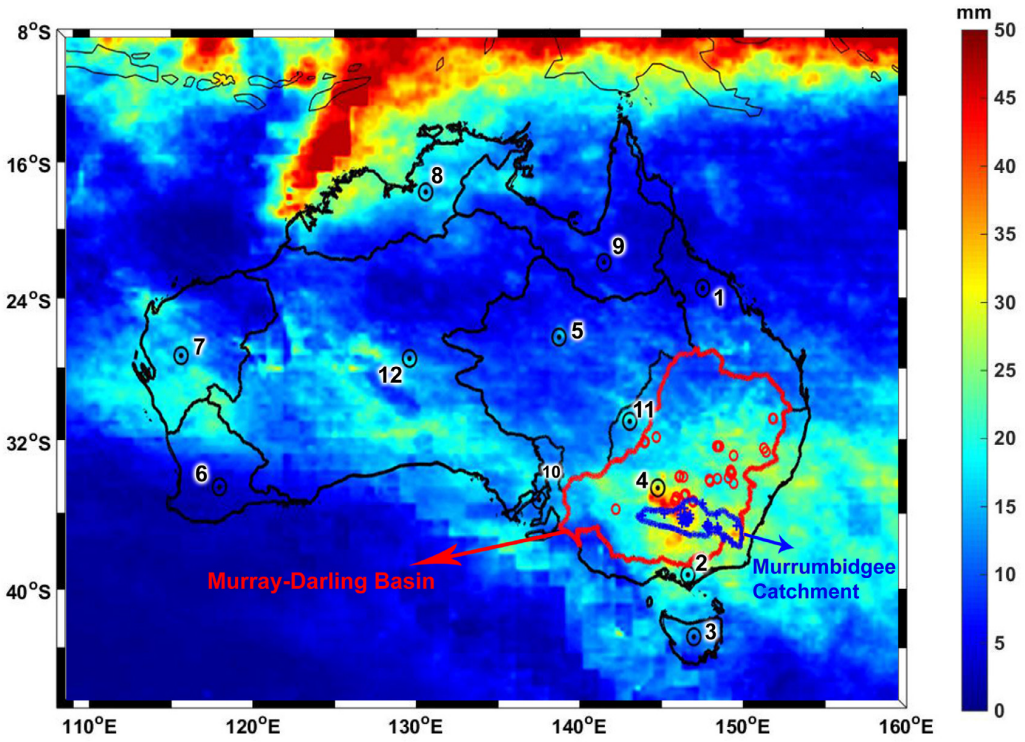

Fig. 1. Overview of the study area. The black polygons indicate the twelve river basins that are considered for spatial aggregation of GRACE data to basin scale. The red and blue polygons indicate the Murray-Darling Basin and Murrumbidgee Catchment, respectively. Data from in-situ groundwater stations (red circles) and data from the OzNet soil moisture network (blue circles) are used in these regions for independent validation of the data assimilation results. The underlaying map shows temporally averaged precipitation between 2003 and 2013 from TRMM-3B42 products (Huffman and Bolvin, 2012) on a $1° \times 1°$ grid. (For interpretation of the references to colour in this figure legend, the reader is referred to the web version of this article.)

2.3. Validation data

We use groundwater in-situ measurements over the Murray–Darling basin extracted from the New South Wales Government (NSW) groundwater archive (http://waterinfo.nsw.gov.au/pinneena/gw.shtml) to evaluate the performance of applied data assimilation. Although data assimilation is done over entire Australia, due to limited availability of in-situ stations, the existing in-situ measurements over the Murray-Darling basin are used for result assessment. Measurements with data gaps and those that did not exhibit seasonal variations are flagged as belonging to confined aquifers and are excluded (Houborg et al., 2012; Tangdamrongsub et al., 2015). Therefore, daily and monthly well measurements of 54 spatially distributed stations over the basin (cf. Fig. 1) are used and time series of groundwater storage anomalies are generated for each station. Selected well-water levels need to be converted to variations in groundwater (GW) storage in terms of equivalent water heights. This is usually done through the specification of yield estimates (e.g., Rodell et al., 2007; Zaitchik et al., 2008). However, such information does not exist in this study. Hence, following Tangdamrongsub et al. (2015), TWS variations from GRACE and soil moisture products from Global Land Data Assimilation System (GLDAS) NOAH (Rodell et al., 2004) are used to calculate the specific yield and scale the observed head water by modifying the magnitude of GW time series (Tregoning et al., 2012). As Tregoning et al. (2012) showed, the GW component can be extracted over Australia by removing the soil moisture component from GRACE TWS data. Other water compartments including biomass and surface water variations can be excluded due to their small contribution to regional scale mass variations within Australia. Through this approach, rather than assuming a constant specific yield everywhere (e.g., 0.1 by Tregoning et al., 2012), different yield values can be derived leading to a more realistic representation of groundwater systems in different areas.The calculated specific yields range between 0.08 and 0.16, falling within the 0.05–0.2 range suggested by the Australian Bureau of Meteorology (BOM) and Seoane et al. (2013), hence justifying the application of the method. The extracted yield factor is used at each in-situ location to scale the observed in-situ head time series (see also Rodell et al., 2007; Longuevergne et al., 2013). After removing temporal averages of in-situ groundwater time series, the anomaly time series are used in this study to assess W3RA estimates after the assimilation process.

Further result assessment is done using in-situ soil moisture measurements. These datasets are obtained from the moisture-monitoring network (http://www.oznet.org.au/) known as OzNet network and spotted in the Murrumbidgee catchment (Smith et al., 2012). OzNet network provides long-term records of measured volumetric soil moisture at various soil depths at 57 locations across the Murrumbidgee catchment area (cf. Fig. 1). The anomalies of in-situ soil moisture measurements are calculated and then averaged into daily scale. Following Renzullo et al. (2014), 0–8 cm data is used to evaluate the estimated model top-layer soil moisture and the 0–30 cm and 0–90 cm measurements are applied for the evaluation of the model shallow root-zone soil moisture estimation.

3. Data assimilation

3.1. Methods

3.1.1. Square root analysis (SQRA)

The solution of the data assimilation problem is based on Bayes' theorem (Jazwinski, 1970; van Leeuwen and Evensen, 1996), which

tries to improve the model state by updating the prior Probability Density Function (PDF) whenever new observations are introduced. The sequential data assimilation technique solves the Bayesian estimation problem numerically by providing a probabilistic framework and sequentially estimates the whole system using propagated information (ensembles) only forward in time (Jardak et al., 2007). There are various filtering methods in this framework, however, one of the mostly applied techniques is ensemble-based Kalman filter. In this study, we use the square root analysis (SQRA) scheme for the Ensemble Kalman Filter (EnKF), represented by Evensen (2004) as a data assimilation filtering method. SQRA is a deterministic form of ensemble-based Kalman filters and uses a statistical sample of state estimates (Sakov and Oke, 2008). The model state contains N different vectors (N is the number of ensembles), each with the same size of the model state variables. The forecast model state is represented by $X^f = [{X_1}^f \dots {X_N}^f]$, where ${X_i}^f$ ($i = 1 \dots N$) is the ith ensemble (hereafter 'f' stands for forecast and 'a' stands for analysis). The model state forecast error covariance of P^f is defined by:

$$P^f = \frac{1}{N-1}\sum_{i=1}^{N}({X_i}^f - \bar{X}^f)({X_i}^f - \bar{X}^f)^T = \frac{1}{N-1}A^f{A^f}^T, \quad (1)$$

where $\bar{X}^f$ is the ensemble mean and can be calculated using,

$$\bar{X}^f = \frac{1}{N}\sum_{i=1}^{N}(X_i). \quad (2)$$

Forecast ensemble of anomalies, $A^f = [{A_1}^f \dots {A_N}^f]$, is the deviation of model state ensembles from the ensemble mean,

$${A_i}^f = {X_i}^f - \bar{X}^f. \quad (3)$$

SQRA eliminates the need for the perturbation of measurements, which is essential in traditional EnKF (Burgers et al., 1998). Instead, SQRA uses unperturbed observations without imposing any additional approximations like uncorrelated measurement errors (Evensen, 2004) by introducing a new sampling scheme. Rather than updating each sample separately in the analysis step, SQRA updates all of them in two stages; firstly by updating the ensemble-mean using $\bar{X}^f$ (cf. Eq. (1)) as,

$$\bar{X}^a = \bar{X}^f + K(y - H\bar{X}^f), \quad i = 1 \dots N, \quad (4)$$

$$K = P^f(H)^T(HP^f(H)^T + R)^{-1}, \quad (5)$$

where $\bar{X}^a$ is the mean analysis state, K represent the Kalman gain, y and R are the observation vector and associated covariance matrix. The transition matrix from the state vector space to the observation space is shown by H. Next, SQRA computes the ensemble anomalies. In this regard, one needs to first calculate the ensemble version of the analysis error covariance matrix, which can be done using Eq. (6). Afterward, by inserting the forecast (P^f from Eq. (1)) and analysis (P^a from Eq. (6)) error covariances in Eq. (7) and solving for A^a, analysis ensemble of anomaly can be computed.

$$P^a = \frac{A^a(A^a)^T}{N-1} \quad (6)$$

$$P^a = (I - KH)P^f \quad (7)$$

After a few simplification steps (cf. Evensen, 2004), A^a can be obtained by,

$$A^a = A^f V\sqrt{I - \Sigma^T\Sigma\Theta^T}, \quad (8)$$

where Σ and V are calculated using singular value decomposition of A^f ($A^f = U\Sigma V^T$). Γ refers to the singular value decomposition and Θ is a random orthogonal matrix (e.g., the right singular vectors from a singular value decomposition of a random $N \times N$ matrix) for ensemble redistribution of the variance reduction (cf. Evensen, 2004; 2007; Khaki et al., 2017).

3.1.2. Filter tuning

Many studies have previously investigated the sensitivity of ensemble-based schemes on ensemble size (e.g., Houtekamer, 1995; Houtekamer and Mitchell, 1998; Keppenne, 2000; Mitchell et al., 2002; Keppenne and Rienecker, 2002). It has been proven that a large number of ensemble members in ensemble data assimilation systems causes computation time to significantly increase while using a small ensemble size can also be problematic, as it can lead to filter divergent or inaccurate estimation (Tippett et al., 2003). A successful ensemble-based filter needs to adequately span the model sub-space for a better approximation of probability distribution of the background errors (Ott et al., 2004). This, however, can be very challenging once a small ensemble number (considerably less than the model dimension) is used. To tackle this problem, we apply ensemble inflation, which uses a small coefficient to separately inflate prior ensemble deviation from the ensemble-mean and increases their variations (Anderson et al., 2007). Here, we use a constant factor ($S = 1.12$; Anderson, 2001) to inflate the ensemble perturbations as,

$$X'^f = S(X^f - \bar{X}^f) + \bar{X}^f, \quad (9)$$

with X'^f representing the new forecast state, which contains the inflated ensemble perturbation.

A further solution when dealing with a limited ensemble number is the application of localization techniques initially proposed by Houtekamer and Mitchell (2001). In this study, we use the Local Analysis (LA) scheme not only to address the issue of the small ensemble number, but also to investigate its effects in dealing with the GRACE error covariance for different spatial resolutions. LA works by restricting the information used for the covariance matrix computation to a spatially limited area and uses only measurements located within a certain distance from a grid point (Evensen, 2003; Khaki et al., 2017; Ott et al., 2004).

In using LA, at each horizontal grid point (m, n), with m and n representing geographic latitude and longitude directions, respectively, the selected measurements close to the grid point contribute to the SQRA filtering process. This means that only particular state variables close to the point (m, n) within an assumed distance and corresponding observations at the same locations are used in the assimilation process. To do this, a local system state vector, observations, and their covariance matrix need to be chosen at each grid point separately. Following Ott et al. (2004), a model state vector $X(r)$ (r is a two-dimensional vector with r_{mn}) is used to achieve the local forecast state vector X^f_{mn} in Eq. 9 using a linear operator M_{mn} by,

$${X'^f}_{mn} = M_{mn}X'^f(r). \quad (10)$$

At the specific grid point of (m_0, n_0), X'^f_{mn} contains the information of $X'^f(r_{m+m_0,n+n_0})$ with $-l \le m - m_0, n - n_0 \le l$ (l localization length) and limited to grid points close to (m_0, n_0) within a $(2l+1)$ by $(2l+1)$ patch (Ott et al., 2004).

Local state vectors and observations within the local region (y_{mn}) with covariance matrix R_{mn} can then be used in SQRA to locally estimate the model state for each grid point. In case of using a gridded GRACE TWS dataset in a finer spatial resolution (e.g., 1° and 2°), the calculated error covariances have rank deficiency mainly due to correlation errors (see more details in Section 4.1). This problem can cause instability in the data assimilation procedure. Applying LA, therefore, can be helpful since it numerically resolves the possible singularity in the filtering process during data assimilation. Ott et al. (2004) proved that LA yields a good approximate representation of the background covariance matrix using a

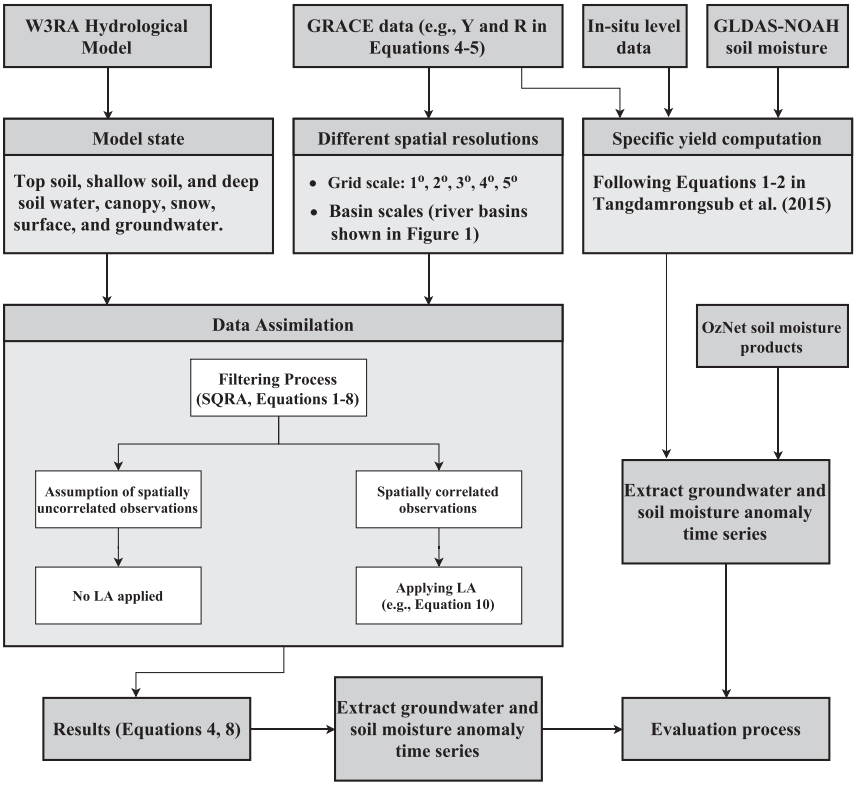

Fig. 2. A schematic illustration of the data assimilation approach implemented for this study and of the considered data sets.

small ensemble number with a rank much lower than the state dimension. LA localization can also be used in the vertical direction, where different water compartments (e.g., shallow and deep soil moisture, groundwater storage, and surface water storage) exist. This can be helpful to vertically decrease the influence of the layers on each other by limiting the filtering process to specific layers, especially when there is a high correlation between the observed components at different layers. Here, however, LA is applied only horizontally because the GRACE TWS observation at each grid point is assimilated to an aggregate of water compartments at the same point. Therefore, a vertical variability in system states is not reflected in the observation error covariance. Furthermore, we are more interested in monitoring the performance of the localization scheme on the GRACE covariance matrix rather than a state covariance matrix. Different trial localisation lengths (2°–10° for gridded TWSs) are applied in this study and their results are assessed against independent groundwater in-situ measurements (cf. Section 2.3) to find the best case (see details in Section 4.2).

3.2. Assimilating GRACE data

In order to address the rather low temporal resolution of GRACE (approximately 30 days), its monthly data and errors are interpolated to 5-day data following Tangdamrongsub et al. (2015), the spline interpolation between consecutive months is used to generate these time series, which allows the ensemble to gradually change between updates. Next, the mean water storage over the study area between 2003 and 2013 is calculated from the W3RA and is added to GRACE TWS changes time series in order to achieve the absolute values. The provided observations are assimilated into W3RA for the 5 different grid resolutions of 1°, 2°, 3°, 4°, and 5° and also in basin scales.

The $1^\circ \times 1^\circ$ spatial resolution of the model leads to a model state vector (X^f) with 794 elements within the Australian continent. Each of these elements contains different water compartments. This means that the state vectors for every grid point in our experiments are composed of the different water storages, including top soil, shallow soil, and deep soil water, canopy, snow, surface, and groundwater. The observations matrix (H) accumulates the state variables (the individual water storages) at each grid point to determine the simulated TWS in order to update them with the GRACE TWS during assimilation. In the update steps, the 5-day temporal average update increment (i.e., the difference between the simulated TWS and GRACE TWS) is applied.

Initial ensemble members are generated by perturbing the meteorological forcing fields following Renzullo et al. (2014). In this regard, the three most important forcing variables including precipitation, temperature, and radiation and their reported error characteristics (Sheffield et al., 2006) are used. To generate the perturbations, we assume a multiplicative error of 30% for precipitation, an additive error of $50 W m^{-2}$ for the shortwave radiation, and an additive error of $2^\circ C$ for temperature (Jones et al., 2007; Renzullo et al., 2014). Monte Carlo sampling of multivariate normal distributions with the errors representing the standard deviations without considering correlations (spatial and/or temporal) are used to produce an ensemble (according to Renzullo et al., 2014). Different ensemble sizes (30–120) and their spread are tested. The selected number of 72 members agrees with the suggestion by Oke et al. (2008) and shows promising performance and is used in this study. The perturbed meteorological forcing datasets, then, are integrated forward with the model for two years (January 2001 to January 2003). This provided a set of state vectors at the beginning of the study period, considered as the initial ensemble. A schematic illustration of the assimilation process steps is provided in Fig. 2.

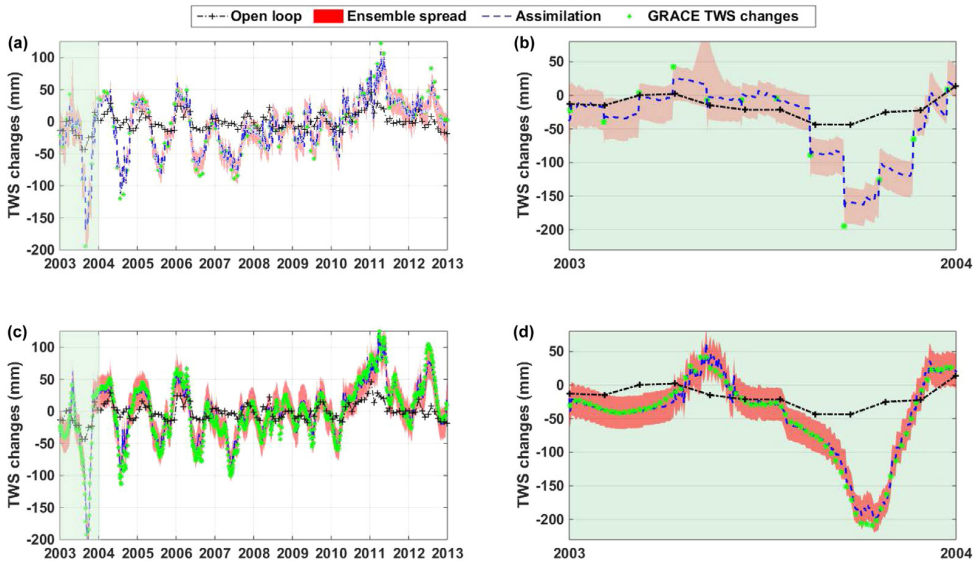

Fig. 3. Comparison between the assimilated time series using the 1° observations in a monthly (a) and 5-day temporal scale for an arbitrary point (c). (b) and (d) respectively magnified the green areas of (a) and (c) representing a zoom-in for one year. Ensemble spread represents the spread of the ensemble of updated TWS states. Note that we use LA to account for correlated errors in GRACE error covariance for this figure. (For interpretation of the references to colour in this figure legend, the reader is referred to the web version of this article.)

4. Results

In the following, we first analyze the effects of GRACE TWS spatial scaling on the error covariance matrix. Then, LA behavior in dealing with GRACE error covariance with different spatial resolutions is addressed. Afterwards, we evaluate the results of data assimilation using LA with respect to different resolutions against the in-situ groundwater and soil moisture products. These results are also compared with the data assimilation process without applying LA (with a consideration of zero correlation in GRACE data) to be able to better investigate its effects on the model estimations.

4.1. Scaling effect

In this section, we review the behavior of assimilating GRACE TWS data for different spatial resolutions into the W3RA model. To this end, GRACE TWS is assimilated with the following spatial resolutions, 1°, 2°, 3°, 4°, 5°, and a basin scale to monitor the effects of localization on the process. For each of the spatial resolution considered, 5-day GRACE TWS data (cf. Section 3.2) are assimilated into the model to address the coarser GRACE temporal scale in comparison to the model. As an example, in Fig. 3, we compare the assimilated time series using the $1° \times 1°$ observations for a monthly (Fig. 3a) and 5-day temporal scale over an arbitrary point (Fig. 3c) to show the effect of temporal rescaling. The denser temporal resolution in Fig. 3c eventuates in a much smoother time series. This is more obvious in Fig. 3b and d, which show only one year of the time series, respectively presented in Fig. 3a and c. Given daily time steps of W3RA, assimilating GRACE TWS data once a month (e.g., in the middle of the month) causes unnatural jumps at the assimilation steps (cf. Fig. 3b). Such a jump is much smaller in magnitude in Fig. 3d where a 5-day sampling interval is used. This leads to keeping the ensemble spread smoother without significant artefacts or temporal discontinuities. It should be mentioned that another solution for keeping ensemble spread smooth is the application of ensemble Kalman smoother (EnKS), which redistributes analysis increments evenly over all days of the month with the expense of more computational cost (see, e.g., Zaitchik et al., 2008; Houborg et al., 2012).

Table 1
The details of GRACE observations used in each grid resolution.

Spatial scale	Observation number	Rank	LA Rank*
1°	794	268	794
2°	220	211	220
3°	111	111	111
4°	67	67	67
5°	45	45	45
BasinScale	12	12	12

* Computed rank after the implementation of LA.

We can now assess the behaviour of LA on data assimilation when the full error covariance of GRACE is used for the different applied spatial scales. Fig. 4 shows the estimated correlation matrices for each grid resolution (following Eicker et al., 2014). This figure helps in understanding how different grid resolutions affect the corresponding observation covariance matrix. It can be seen that the spatial scaling influences the correlation between points. The correlation (off-diagonal elements) between grid points decreases for larger grid resolutions, with the least for the 5° gridded TWSs, which is significantly less than that of 1° grid resolution. This correlation is even smaller when the basin scale GRACE data is considered. To clarify how this affects the data assimilation procedure, Table 1 indicates the number of gridded observations in various grid resolutions and the estimated ranks of covariance matrices. We find that there is a close relationship between the grid resolution and covariance matrix rank (cf. Table 1). As mentioned earlier, rank deficiency problem in covariance matrices causes instability in the data assimilation procedure and inaccurate estimations. The application of LA, however, numerically addresses this issue. It can be seen that LA affects the estimated covariance matrix rank for each grid resolution. Details on the number of observations and the rank of the respective covariance matrices (cf. Table 1) demonstrates the LA effect on improving the process by solving the mathematical problem related to the rank deficiency especially in the cases of 1° and 2°.

Rank deficiency likely happens for error covariance matrices of GRACE TWS with grid resolutions that GRACE can resolve (e.g., 3°

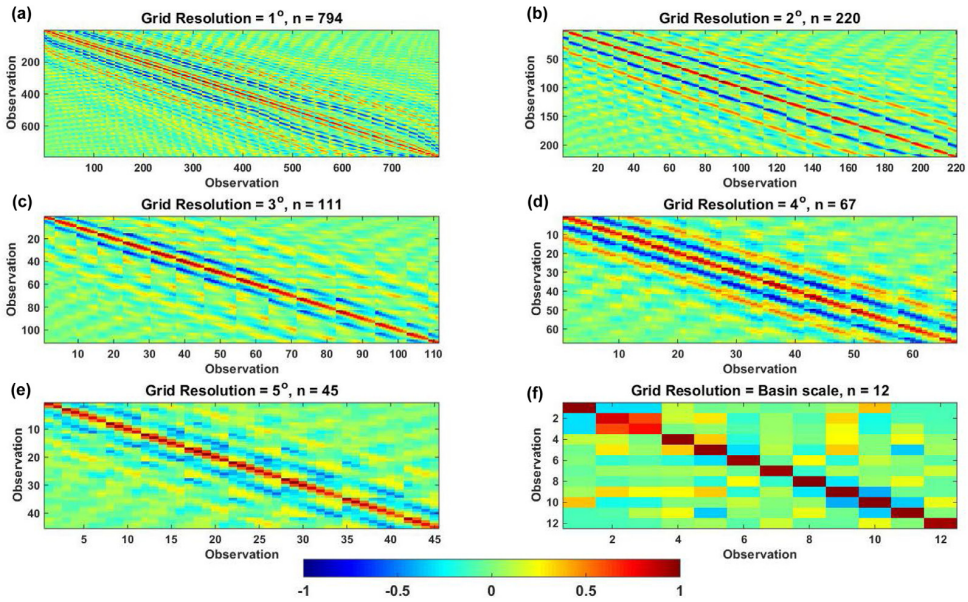

Fig. 4. Correlation matrices of the GRACE observations corresponding to various spatial aggregations. Here, no localization is applied. The variable n refers to the number of assimilated observations.

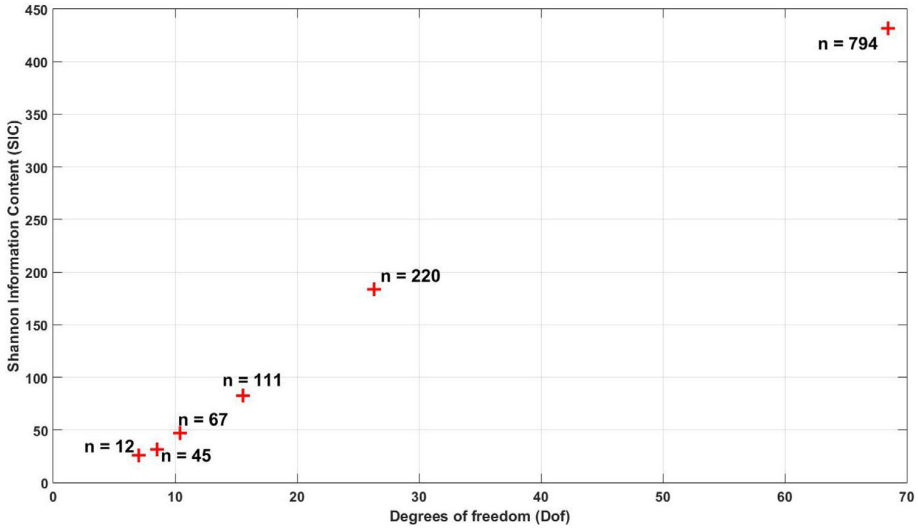

Fig. 5. Shannon Information Content (SIC) and Degrees of freedom (Dof) with respect to the number of assimilated GRACE observations (n).

or coarser). However, when using smaller grid resolutions, the matrix does not have a full rank leading to instabilities in the data assimilation procedure. Although applying GRACE data at lower spatial resolutions might be helpful in dealing with the covariance matrix, this will reduce the number of observations during data assimilation process (cf. Table 1) leading to some loss of signal in the observations. This might not be obvious considering the spatial correlation between grid points for higher resolution GRACE TWS. However, we show that using more observations and considering their full error covariance information in the assimilation process allows more information to be transferred with a higher number of observations into the system states. In this regard, we use the frequently employed indexes of Shannon Information Content (SIC or entropy reduction) and degrees of freedom (Dof) to measure information, which is transferred from observations into the system states (Rodgers, 2000) at the assimilation steps. SIC ($\frac{1}{2}ln(P^f/P^a)$) uses the information in the state probability density function (pdf) before and after assimilation to reflect a real-valued functional (Shannon and Weaver, 1949). Dof ($n - trace(P^a/P^f)$, with n number of observations) on the other hand, is a measure of the amount of information from observations that is used (Stewart et al., 2008). For each grid resolution, the indexes of SIC and Dof are measured (Fig. 5).

It can be seen in Fig. 5 that by decreasing the spatial resolution, some information contained within the observations is lost. Therefore, although increasing the scale size (reducing the resolution) might be helpful in dealing with GRACE error covariance, it is at the cost of losing part of the signal. This justifies the application of LA, which allows us to use information with a higher spatial resolution in datasets.

As outlined in Section 3.1.2, one important effect of LA is underestimating the influences of spatially distant grid points on each other. The distance in localization preserves the information in observations close to each other while at the same time making it

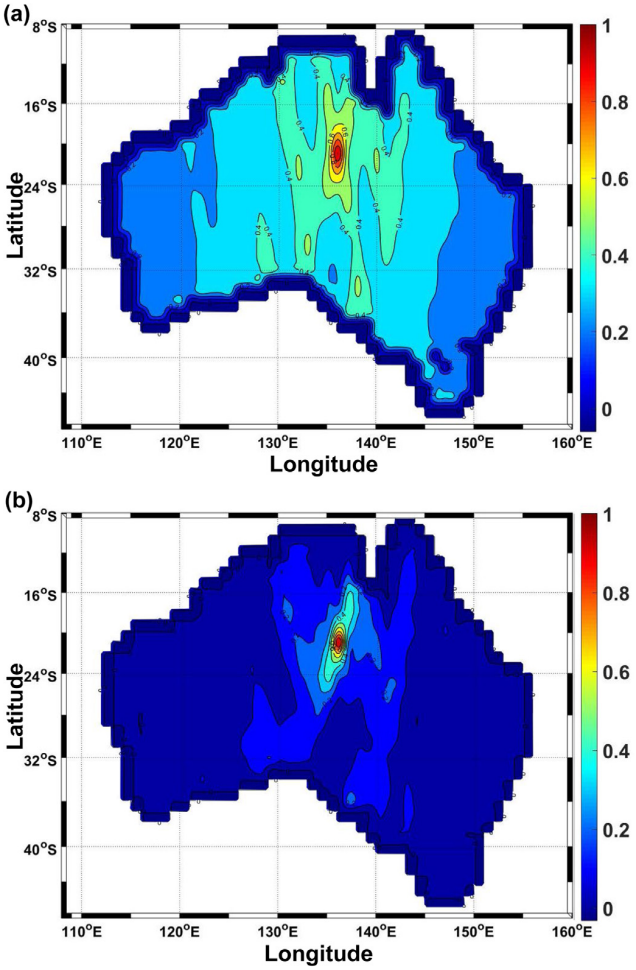

Fig. 6. 2-D representation of correlation coefficients between the TWS anomalies of the arbitrary point (136.6854°E and 23.9015°S) and the rest of the grid points. The temporal average of the correlation coefficients before and after assimilation using LA are shown in (a) and (b) respectively.

possible to use full error covariance information. To demonstrate this, we consider the correlation coefficient of the arbitrary point (at a location 136.6854°E and 23.9015°S) to the other grid points in Fig. 6. This point is chosen to be approximately in the middle of the study area for a better visual representation while similar results are achieved for all other grid points. We integrate the model and performed data assimilation using the 1° GRACE TWS (as the worst case among different applied resolutions) during the study period. The average correlation coefficients between the arbitrary point and the other grid points before and after assimilation using LA are then measured. Fig. 6b shows how LA successfully reduces the correlation coefficients for more distant grid elements but maintains the correlations in the close vicinity.

The important point to consider when using LA is the removal of some information from the data, which is not desirable. Thus, attention needs to be taken when choosing the localization length to preserve the adequate continuity of analysis on adjacent points (Zeng, 2014). LA length depends on the observation density and can be chosen arbitrarily. After testing different localization lengths, it is found that a small length (e.g., less than 5° for $1° \times 1°$ GRACE TWS) can result in large errors even though there would be no inverse problem in assimilation filter. We use groundwater in-situ measurements to assess the results of applying different localization lengths (2° to 10° for gridded TWSs). For every scenario (different grid resolutions), we interpolate assimilation time series at the location of the groundwater in-situ and calculate the root-mean-square error (RMSE). The average computed RMSE of each grid resolution for the applied lengths (Fig. 7) show that better results are obtained using the 5° localization halfwidth length compared to the other applied localization lengths.

A similar experiment is implemented to find efficient localization length for a basin scale spatial resolution. For each basin, we test different lengths mostly larger than those for grid scales (e.g., 5° to 15° with the best performance of 10° radii in average) and estimate TWS errors using the GRACE TWS data where in-situ measurements are not available for all basins. The localization length with the least error for each basin (Fig. 8) is used to assess the LA effects at the basin scale and also to compare corresponding results with grid scale resolutions.

4.2. Assessment with in-situ data

Post processed in-situ measurements of groundwater changes (cf. Section 2.3) over the Murray-Darling basin as well as OzNet soil moisture network in the Murrumbidgee catchment (see Fig. 1 for the location of the catchment) are used to evaluate the assimilation results. First, to compare the time series obtained from assimilation results with those of in-situ measurements, the GW results for each spatial resolution considered are spatially interpolated using the nearest neighbour (the closest four data values) to the location of the in-situ measurements. Afterward, the error time series are computed as the difference between the estimated GW and in-situ GW measurements. We then estimate average errors using these time series for each scenario of data assimilation.

The TWS time series of the assimilation process for the case of 3° is shown in Fig. 9a. Data assimilation with this spatial resolution results in a minimum GW error compared to the in-situ measurements. This figure also contains the open loop time series which refers to the estimations without implementation of any data assimilation and the assimilated observations. The absolute errors, i.e., the difference between the in-situ measurements and either the open loop or the assimilated estimates (for the best case of 3° spatial resolution) are presented in Fig. 9b. The assimilated time series fits well with the groundwater in-situ measurements (cf. Fig. 9a) and results in a higher correlation than the open loop time series (85% average). Note that in terms of representing the hydrology, sometimes the estimates do not really depict the signal of the in-situ measurements. In some instances, the error (for no assimilation) is as large as the signal itself. This could be due to the fact that W3RA only simulates the dynamics of unconfined aquifers, that is, groundwater that receives soil drainage and discharges into streams. In some cases, a deeper (confined) aquifer underneath can also affect groundwater measurements. Nevertheless, data assimilation causes the updated time series to reflect better the real fluctuations in groundwater storage in most of the cases as given by the in-situ measurements.

The average estimated error of all GW in-situ stations during the study period for each scenario illustrates the LA performances for the different spatial resolutions (Fig. 10). The least error is obtained from the 3° spatial resolution by comparing assimilation results of all scenarios. In addition, to be able to monitor the effectiveness of LA, data assimilation is also applied using GRACE-derived TWS and only diagonal elements of its error covariance matrix. Results without applying LA (represented in Fig. 10) refers to this case where correlations between grid points are neglected. This comparison is of interest because many of the previously presented studies in using GRACE for hydrological data assimilation have neglected the existing correlation in observations (see e.g.,

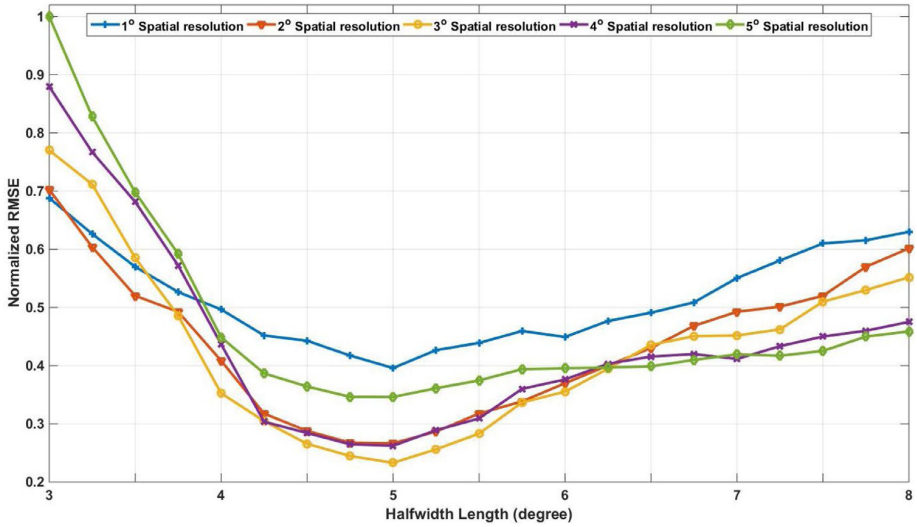

Fig. 7. Comparison between normalized RMSE of TWS anomalies for different localisation radii (degree) applied for each case of GRACE TWS spatial resolution used for assimilation. RMSEs are calculated in mm, however, for a better visual presentation, normalized values are presented.

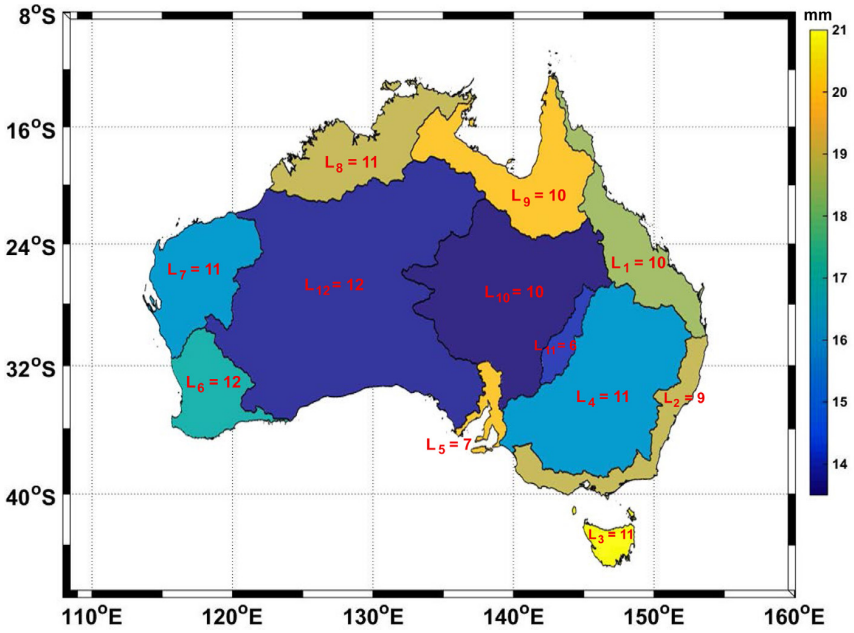

Fig. 8. The estimated optimized localisation radii (in degree and presented by L) and corresponding TWS errors with respect to the GRACE data for each basin.

Zaitchik et al., 2008; Houborg et al., 2012; Li et al., 2012; Tangdamrongsub et al., 2015; Sun et al., 2015; Kumar et al., 2016).

It can be seen that locally applying the GRACE observations effectively reduces errors for every grid resolution considered in comparison to the uncorrelated observation assumption. This, however, is more obvious for higher spatial resolution (e.g., 3° and higher) where a large difference between the assimilation results with and without the application of LA can be found. Although LA mathematically solves the inverse problem for using 1° gridded GRACE TWS data and associated error covariance (cf. Table 1) in the filtering process, this spatial resolution results in a larger error in comparison to the other scenarios. From Section 2.1, we know that truncating and smoothing procedures cause losing a part of GRACE data, especially in higher frequencies. Rescaling such a data into 1° spatial resolution results in an error in gridded GRACE TWS and correspondingly in the assimilation result (cf. Fig. 10). Fig. 10 shows that increasing the spatial resolution results in a better estimation when LA is not applied. This error reduction by using a higher spatial resolution is also true when LA is applied but only to the point of 3°. After this point, errors start increasing, which can be explained by fewer observations used leading to less information content to be transferred to model states. The application of LA, however, reduces the error for all spatial resolutions while in an absolute sense, the smallest errors are obtained for 3°. Interestingly, this spatial resolution is about the spatial resolution that GRACE can resolve.

More detailed results are proposed in Fig. 11 and Table 2 in terms of RMSE and correlation analysis. As mentioned before, first, assimilation time series are interpolated at the location of the groundwater in-situs and then, their anomalies are calculated. A

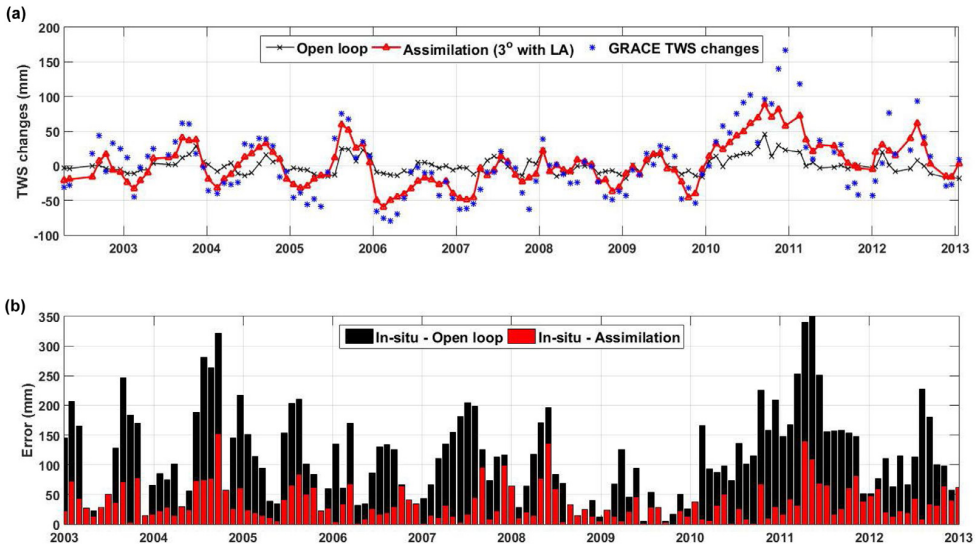

Fig. 9. (a) Comparison between the TWS time series of the assimilation process for the case of 3° spatial resolution (red), the GRACE observation (blue), with the open loop referring to the model estimation without applying data assimilation (black). (b) Absolute groundwater (GW) error bars before (black) and after (red) data assimilation process in comparison to the GW in-situ measurements. The time series shown in (a) and (b) are spatially averaged over the Murray-Darling Basin. (For interpretation of the references to colour in this figure legend, the reader is referred to the web version of this article.)

Table 2
A summary of the results belonging to each scenario of data assimilation. Improvements in groundwater are calculated using the estimated RMSE with and without applying data assimilation (open loop) in relation to groundwater in-situ measurements.

	Assimilation without LA		Assimilation with LA	
Spatial scale	RMSE (mm)	Improvement (%)	RMSE (mm)	Improvement (%)
1°	68.54	17.76	52.23	37.33
2°	51.09	38.70	35.11	57.87
3°	47.41	43.11	26.80	67.84
4°	43.18	48.19	32.35	61.18
5°	44.37	46.76	41.19	50.58
BasinScale	43.84	47.40	41.93	49.69

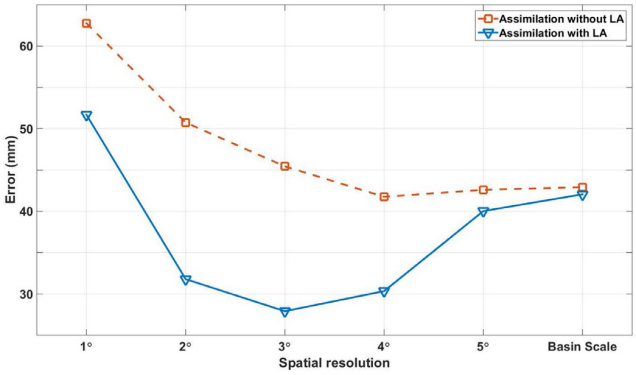

Fig. 10. Average estimated error in groundwater anomalies from assimilating GRACE data for different spatial scales with (blue) and without (red) implementation of LA. The results are spatial averages over all groundwater data points within the Murray-Darling Basin. (For interpretation of the references to colour in this figure legend, the reader is referred to the web version of this article.)

similar procedure is also applied to achieve assimilation time series over the soil moisture in-situ stations. Then for all stations, RMSE and correlation factor between assimilation results (for various scenarios) and in-situ measurements are calculated and their averages are used for assessment. Note that considering the difference between W3RA estimations (column water storage) and the OzNet measurements (volumetric soil moisture), only correlation analysis is assumed for assessing results against soil moisture in-situ data. The reason for this refers to the fact that converting model outputs (with unit 'mm') into volumetric units may introduce a bias (Renzullo et al., 2014). Estimated correlations between assimilation results and OzNet soil moisture (an average correlation for the total soil column; Fig. 11a) as well as groundwater in-situ level data (Fig. 11b) demonstrate the ability of LA in dealing with GRACE data. Also, both correlation analyses show that applying GRACE TWS with 3° leads to closer results to the in-situ measurements.

Based on the results in Table 2, all the results successfully improved the model estimation of water storage variation. Applying LA in data assimilation leads up to 24.73% (13% average) better estimations in comparison to the non-correlated assumption. This proves the importance of using local data assimilation for incorporating GRACE data into the hydrological model. We know from Eicker et al. (2014) that spatial upscaling of GRACE data to coarser resolutions (e.g., 5°) can significantly stabilize the assimilation process leading to more reliable results, however, LA can improve the results not only for these resolutions but also for smaller grid sizes (cf. Table 2).

It can be seen from Table 2 that using gridded TWS observation with 3° shows the best performance in terms of RMSE. Although there is no rank deficiency in using the full error covariance matrix for this grid resolution, local implementation of the assimilation process helps to improve the agreement with the in-situ

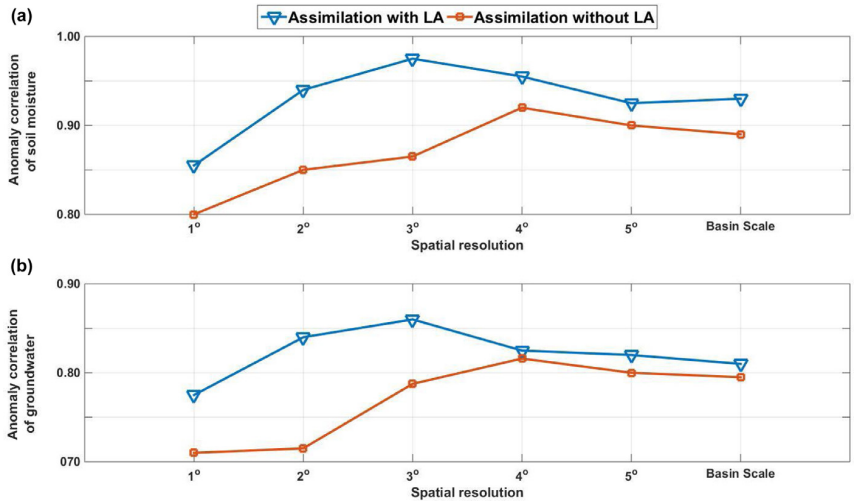

Fig. 11. Comparison between the correlation of assimilation results (using different spatial resolutions) with OzNet soil moisture anomalies spatially averaged over the Murrumbidgee Catchment (a) and with anomalies of groundwater in-situ level measurements spatially averaged over the Murray-Darling Basin (b). The correlation results in both cases of data assimilation using LA (blue) and without using LA (red) are shown. (For interpretation of the references to colour in this figure legend, the reader is referred to the web version of this article.)

measurements. The reason why LA does not have a similar impact on finer spatial resolutions, especially for a 1° resolution in comparison to 3°, could be due to the characteristic of GRACE L2 product as a degree limited data, e.g., truncated spherical harmonics sets. An interesting observation from Table 2 refers to the results of using GRACE TWS for a 2° spatial resolution. Considering Table 1, employing the 2° grid resolution causes a rank deficiency in covariance matrix leading to the unstable data assimilation. LA successfully solves this problem and significantly improves the results with a better performance (57.87% improvement). Fewer observations incorporated in the assimilation on a basin scale and for 5° resolution in comparison to the other spatial scales (e.g., 3°) leads to a weaker performance for these two cases.

5. Conclusion

The global time variable terrestrial water storage (TWS) data from the Gravity Recovery And Climate Experiment (GRACE) has provide an important opportunity for a hydrological model adjustment. In this study, we assessed the performance of local analysis (LA) method in accounting for the existing correlation in GRACE data and improving its effect on model states. To this end, we assimilated the GRACE-derived TWS changes into the World-Wide Water Resources Assessment system (W3RA) during 2003–2012 using Square Root Analysis (SQRA) filtering technique. LA was applied to (i) solve the mathematical problem of using correlated data for assimilation especially when the observation spatial resolution is high (e.g., 1° gridded TWS), and (ii) improve the assimilation results using GRACE TWS data for different spatial resolutions (1°–5° and a basin scale). The observations were applied for a 5-day temporal scale and for 5 different grid resolutions to monitor the impact of LA on each scenario. The results showed that implementing LA successfully reduced data assimilation errors for all the cases (54.08% on average). This improvement is larger for the cases with smaller grid sizes along with the higher error correlations. LA addressed the rank deficiency problem in using the full information from the error covariance matrix for a higher spatial resolution of GRACE TWS data (e.g., 1°). This, to the best of our knowledge, for the first time, allowed us to be able to apply GRACE TWS considering spatial error correlation information at finer spatial resolutions (e.g., 1° and 2°) for the hydrological data assimilation. LA also improved the assimilation results at all grid resolutions and basin scale especially in comparison to using non-correlated observations (13.76% average). This highlights the great potential of LA in different scenarios for improved data assimilation. The best performance with 67.84% improvement was found with the application of GRACE data in assimilation with 3° spatial resolution. Overall, the importance of the application of LA in hydrological data assimilation is: (1) stabilising the assimilation of GRACE TWS observation using its full error covariance for finer spatial resolutions (e.g., 1° and 2°), and (2) improving the results for all the spatial grid sizes without the assumption of white noise. This study offered a method to deal with the GRACE error covariance matrix during data assimilation, however, further assessment needs to be undertaken to examine other potential methods like inflation of the observation error variances and circulant approximation.

Acknowledgement

We would like to thank professor Harrie-Jan Hendricks-Franssen, the associate editor of Advances in Water Resources, and Dr. Manuela Girotto for their useful comments, which contributed to the improvement of this study. M. Khaki is grateful for the research grant of Curtin International Postgraduate Research Scholarships (CIPRS)/ORD Scholarship provided by Curtin University (Australia). This work is a TIGeR publication.

References

Alsdorf, D.E., Rodriguez, E., Lettenmaier, D.P., 2007. Measuring surface water from space. Rev. Geophys. 45, RG2002. http://dx.doi.org/10.1029/2006RG000197.

Anderson, J., 2001. An ensemble adjustment Kalman filter for data assimilation. Mon. Weather. Rev. 129, 28842903. http://dx.doi.org/10.1175/1520-0493(2001)129(2884:AEAKFF)2.0.CO;2.

Anderson, J.L., Anderson, S.L., 1999. A monte carlo implementation of the nonlinear filtering problem to produce ensemble assimilations and forecasts. Mon. Weather Rev 127, 27412758.

Anderson, M.C., Norman, J.M., Mecikalski, J.R., Otkin, J.A., Kustas, W.P., 2007. A climatological study of evapotranspiration and moisture stress across the continental united states based on thermal remote sensing: 1. model formulation. J. Geophys. Res. 112 (D10117). http://dx.doi.org/10.1029/2006JD007506.

Bennett, A.F., 2002. Inverse Modeling of the Ocean and Atmosphere. Cambridge University Press, New York, p. 234.

Berger, H., Forsythe, M., 2004. Satellite wind superobbing. Met Office Forecasting Research Technical Report 451.

Bertino, L., Evensen, G., Wackernagel, H., 2003. Sequential data assimilation techniques in oceanography. Int. Stat. Rev. 71 (2), 223–241.
Brocca, L., Melone, F., Moramarco, T., Wagner, W., Naeimi, V., Bartalis, Z., Hasenauer, S., 2010. Improving runoff prediction through the assimilation of the ASCAT soil moisture product. Hydrol. Earth Syst. Sci. 14 (18811893). http://dx.doi.org/10.5194/hess-14-1881-2010.
Burgers, G., van Leeuven, P.J., Evensen, G., 1998. Analysis scheme in the ensemble Kalman filter. Mon. Weather Rev. 126, 17191724.
Chen, J.L., Wilson, C.R., Famiglietti, J.S., Rodell, M., 2007. Attenuation effect on seasonal basin-scale water storage changes from GRACE time-variable gravity. J. Geod. 81 (4), 237245. http://dx.doi.org/10.1007/s00190-006-0104-2.
Chen, J.L., Wilson, C.R., Tapley, B.D., 2013. Contribution of ice sheet and mountain glacier melt to recent sea level rise. Nat. Geosci. 6, 549552. http://dx.doi.org/10.1038/ngeo1829.
Cheng, M.K., Tapley, B.D., 2004. Variations in the earth's oblateness during the past 28 years. J. Geophys. Res. Solid Earth 109, B09402. http://dx.doi.org/10.1029/2004JB003028.
Clark, M.P., Rupp, D.E., Woods, R.A., Zheng, X., Ibbitt, R.P., Slater, A.G., 2008. Data assimilative modeling investigation of gulf stream warm core ring interaction with continental shelf and slope circulation, hydrological data assimilation with the ensemble kalman filter: Use of streamflow observations to update states in a distributed hydrological model. Adv. Water Res. 31 (10), 1309–1324. ISSN 0309–1708 doi: 10.1016/j.advwatres.2008.06.005.
Coumou, D., Rahmstorf, S., 2012. A decade of weather extremes. Nat. Clim. Change 2 (7), 491–496.
Crow, W., Wood, E., 2003. The assimilation of remotely sensed soil brightness temperature imagery into a land surface model using ensemble filtering: a case study based on ESTAR measurements during SGP97. Adv. Water Res. 26, 137149.
Dando, M.L., Thorpe, A.J., Eyre, J.R., 2007. The optimal density of atmospheric sounder observations in the met office NWP system. Q. J. R. Meteorol. Soc. 133, 19331943.
van Dijk, A.I.J.M., Renzullo, L.J., Wada, Y., Tregoning, P., 2014. A global water cycle reanalysis (2003–2012) merging satellite gravimetry and altimetry observations with a hydrological multi-model ensemble. Hydrol Earth Syst. Sci. 18, 29552973. http://dx.doi.org/10.5194/hess-18-2955-2014.
van Dijk, A. I. J. M., 2010. The australian water resources assessment system: Technical report 3, landscape model (version 0.5) technical description. WIRADA/CSIRO Water fora Healthy Country Flagship, Canberra. [Available at https://publications.csiro.au/rpr/download?pid=csiro:EP102927&dsid=DS4]
van Dijk, A.I.J.M., Pea-Arancibia, J.L., Wood, E.F., Sheffield, J., Beck, H.E., 2013. Global analysis of seasonal streamflow predictability using an ensemble prediction system and observations from 6192 small catchments worldwide. Water Resour. Res. 49, 27292746. http://dx.doi.org/10.1002/wrcr.20251.
Eicker, A., Schumacher, M., Kusche, J., Dll, P., Mller-Schmied, H., 2014. Calibration/data assimilation approach for integrating GRACE data into the waterGAP global hydrology model (WGHM) using an ensemble Kalman filter: first results. SurvGeophys 35 (6), 12851309. http://dx.doi.org/10.1007/s10712-014-9309-8.
Elbern, H., Schmidt, H., 2001. Ozone episode analysis by fourdimensional variational chemistry data assimilation. J. Geophys. Resour. 106, 35693590.
Evensen, G., 2003. The ensemble Kalman filter: Theoretical formulation and practical inplementation. Ocean Dyn. 53, 343367. http://dx.doi.org/10.1007/s10236-003-0036-9.
Evensen, G., 2004. Sampling strategies and square root analysis schemes for the enKF. Ocean Dyn. 54 (6), 539–560.
Evensen, G., 2007. Data Assimilation: the Ensemble Kalman Filter. Springer, Berlin, p. 279.
Forootan, E., Khandu Awange, J., Schumacher, M., Anyah, R., van Dijk, A., Kusche, J., 2016. Quantifying the impacts of ENSO and IOD on rain gauge and remotely sensed precipitation products over australia. Remote Sens. Environ. 172, 50–66. http://dx.doi.org/10.1016/j.rse.2015.10.027.
Forootan, E., Rietbroek, R., Kusche, J., Sharifi, M.A., Awange, J., Schmidt, M., Omondi, P., Famiglietti, J., 2014. Separation of large scale water storage patterns over iran using GRACE, altimetry and hydrological data. J. Remote Sens. Environ. 140, 580–595. http://dx.doi.org/10.1016/j.rse.2013.09.025.
Garner, T.W., Wolf, R.A., Spiro, R.W., Thomsen, M.F., 1999. First attempt at assimilating data to constrain a magnetospheric model. J. Geophys. Res. 104 (A11), 2514525152. http://dx.doi.org/10.1029/1999JA900274.
Girotto, M., De Lannoy, G.J., Reichle, R.H., Rodell, M., 2016. Assimilation of gridded terrestrial water storage observations from GRACE into a land surface model. Water Resour. Res. 52 (5), 4164–4183.
Girotto, M., De Lannoy, G.J., Reichle, R.H., Rodell, M., Draper, C., Bhanja, S.N., Mukherjee, A., 2017. Benefits and pitfalls of GRACE data assimilation: a case study of terrestrial water storage depletion in india. Geophys. Res. Lett. 44, 4107–4115. http://dx.doi.org/10.1002/2017GL072994.
Giustarini, L., Matgen, P., Hostache, R., Montanari, M., Plaza, D., Pauwels, V.R.N., De Lannoy, G.J.M., De Keyser, R., Pfister, L., Hoffmann, L., Savenije, H.H.G., 2011. Assimilating SAR-derived water level data into a hydraulic model: a case study. hydrol. Earth Syst. Sci. 15, 23492365. http://dx.doi.org/10.5194/hess-15-2349-2011.
Hoteit, I., Luo, X., Pham, D.T., 2012. Particle Kalman filtering: a nonlinear Bayesian framework for ensemble Kalman filters. Mon. Weather Rev. 140 (2), 528–542.
Houborg, R., Rodell, M., Li, B., Reichle, R.H., Zaitchik, B.F., 2012. Drought indicators based on model-assimilated gravity recovery and climate experiment (GRACE) terrestrial water storage observations. Water Resour. Res. 48, W07525. http://dx.doi.org/10.1029/2011WR011291.
Houtekamer, P.L., 1995. The construction of optimal perturbations. Mon. Weather Rev. 123, 28882898.
Houtekamer, P.L., Mitchell, H.L., 1998. Data assimilation using an ensemble Kalman filter technique. Mon. Weather Rev. 126 (796), 811.
Houtekamer, P.L., Mitchell, H.L., 2001. A sequential ensemble Kalman filter for atmospheric data assimilation. Mon. Weather Rev. 129 (1), 123–137.
Huffman, G., Bolvin, D., 2012. TRMM and other data precipitation data set documentation. Mesoscale Atmospheric Processes Laboratory, NASA Goddard Space Flight Center and Science Systems and Applications, Inc.. Mesoscale Atmospheric Processes Laboratory, NASA Goddard Space Flight Center and Science Systems and Applications, Inc.
Huntington, T.G., 2006. Evidence for intensification of the global water cycle: review and synthesis. J. Hydrol. 319 (14), 8395.
Jardak, M., Navon, I.M., Zupanski, M., 2007. Comparison of sequential data assimilation methods for the KuramotoSivashinsky equation. Int. J. Numer. Methods Fluids 62 (4), 374402. http://dx.doi.org/10.1002/fld.2020.
Jazwinski, A.H., 1970. Stochastic Processes and Filtering Theory. Academic Press, New York, p. 376.
Jones, D.A., Wang, W., Fawcett, R., Grant, I., 2007. Climate data for the australian water availability project. In: Australian Water Availability Project Milestone Report. Bur. Met., Australia, p. 37.
Kalnay, E., 2003. Atmospheric Modelling, Data Assimilation and Predictability. Cambridge University Press. pp.xxii 341 ISBNs 0 52179179 0, 0 521 79629 6 doi: 10.1256/00359000360683511.
Keppenne, C.L., 2000. Data assimilation into a primitive-equation model with a parallel ensemble Kalman filter. Mon. Weather Rev. 128, 19711981.
Keppenne, C.L., Rienecker, M., 2002. Initial testing of a massively parallel ensemble Kalman filter with the poseidon isopycnal ocean general circulation model. Mon. Weather Rev. 130, 29512965.
Khaki, M., Hoteit, I., Kuhn, M., Awange, J., Forootan, E., van Dijk, A.I.J.M., Schumacher, M., Pattiaratchi, C., 2017. Assessing sequential data assimilation techniques for integrating GRACE data into a hydrological model. In: Advances in Water Resources, 107, p. 301-316. ISSN 0309–1708 doi: 10.1016/j.advwatres.2017.07.001.
Klees, R., Revtova, E.A., Gunter, B.C., Ditmar, P., Oudman, E., Winsemius, H.C., 2008. The design of an optimal filter for monthly GRACE gravity models. Geophys. J. Int. 175 (2), 417–432. http://dx.doi.org/10.1111/j.1365-246X.2008.03922.x.
Kumar, S., Zaitchik, B., Peters-Lidard, C., Rodell, M., Reichle, R., Li, B., Jasinski, M., Mocko, D., 2016. Assimilation of gridded GRACE terrestrial water storage estimates in the north american land data assimilation system. J. Hydrometeor. 17, 19511972. http://dx.doi.org/10.1175/JHM-D-15-0157.1.
Kumar, S.V., Peters-Lidard, C.D., Mocko, D., Reichle, R.H., Liu, Y., Arsenault, K.R., Xia, Y., Ek, M., Riggs, G., Livneh, B., Cosh, M., 2014. Assimilation of remotely sensed soil moisture and snow depth retrievals for drought estimation. J. Hydrometeorol. 15, 2446–2469. http://dx.doi.org/10.1175/JHM-D-13-0132.1.
Kumar, S.V., Peters-Lidard, C.D., Santanello, J.A., Reichle, R.H., Draper, C.S., Koster, R.D., Nearing, G., Jasinski, M.F., 2015. Evaluating the utility of satellite soil moisture retrievals over irrigated areas and the ability of land data assimilation methods to correct for unmodeled processes. Hydrol. Earth Syst. Sci. 19, 4463–4478. http://dx.doi.org/10.5194/hess-19-4463-2015.
Kusche, J., 2007. Approximate decorrelation and non-isotropic smoothing of time–variable GRACE-type gravity field models. J. Geod. 81, 733739.
Kusche, J., Klemann, V., Bosch, W., 2012. Mass distribution and mass transport in the earth system. J. Geodyn. 59-60, 1–8. http://dx.doi.org/10.1016/j.jog.2012.03.003.
Lahoz, W.A., Geer, A.J., Bekki, S., Bormann, N., Ceccherini, S., Elbern, H., Errera, Q., Eskes, H.J., Fonteyn, D., Jackson, D.R., Khattatov, B., 2007. The assimilation of envisat data (ASSET) project. Atmos. Chem. Phys. 7, 1773–1796.
van Leeuwen, P.J., Evensen, G., 1996. Data assimilation and inverse methods in terms of a probabilistic formulation. Mon. Weather Rev. 124, 28982913.
Li, B., Rodell, M., Zaitchik, B.F., Reichle, R.H., Koster, R.D., van Dam, T.M., 2012. Assimilation of GRACE terrestrial water storage into a land surface model: Evaluation and potential value for drought monitoring in western and central europe. J. Hydrol. http://dx.doi.org/10.1016/j.jhydrol.2012.04.035.
Liu, Y., Peters-Lidard, C.D., Kumar, S., Foster, J.L., Shaw, M., Tian, Y., Fall, G.M., 2013. Assimilating satellite-based snow depth and snow cover products for improving snow predictions in alaska. Adv. Water Res. 54, 208227. http://dx.doi.org/10.1016/j.advwatres.2013.02.005.
Liu, Y., Weerts, A.H., Clark, M., Hendricks Franssen, H.-J., Kumar, S., Moradkhani, H., Seo, D.-J., Schwanenberg, D., Smith, P., van Dijk, A.I.J.M., van Velzen, N., He, M., Lee, H., Noh, S.J., Rakovec, O., Restrepo, P., 2012. Advancing data assimilation in operational hydrologic forecasting: progresses, challenges, and emerging opportunities. Hydrol. Earth Syst. Sci. 16, 3863–3887. http://dx.doi.org/10.5194/hess-16-3863-2012.
Liu, Z.Q., Rabier., F., 2003. The potential of high-density observations for numerical weather prediction: a study with simulated observations. Q. J. R. Meteorol. Soc. 129, 30133035.
Longuevergne, L., Wilson, C.R., Scanlon, B.R., Crtaux, J.F., 2013. GRACE water storage estimates for the middle east and other regions with significant reservoir and lake storage. Hydrol. Earth Syst. Sci. 17, 48174830. http://dx.doi.org/10.5194/hess-17-4817-2013.
Mayer-Gürr, T., Zehentner, N., Klinger, B., Kvas, A., 2014. ITSG-grace2014: a new GRACE gravity field release computed in Graz. GRACE Science Team Meeting (GSTM). Potsdam am: 29.09.2014.
Mitchell, H.L., Houtekamer, P.L., 2000. An adaptive ensemble Kalman filter. Mon. Weather Rev. 128, 416433.

Mitchell, H.L., Houtekamer, P.L., Pellerin, G., 2002. Ensemble size, balance, and model-error representation in an ensemble Kalman filter. Mon. Weather Rev. 130, 27912808.
Moradkhani, H., Hsu, K., Hong, Y., Sorooshian, S., 2006. Investigating the impact of remotely sensed precipitation and hydrologic model uncertainties on the ensemble streamflow forecasting. Geophys. Res. Lett 33, L12107.
Munier, S., Aires, F., Schlaffe, S., Prigent, C., Papa, F., Maisongrande, P., Pan, M., 2014. Combining data sets of satellite-retrieved products for basin-scale water balance study: 2. evaluation on the mississippi basin and closure correction model. J. Geophys. Res. Atmos. 119 (12), 100–12,116. http://dx.doi.org/10.1002/2014JD021953.
Neal, J., Schumann, G., Bates, P., Buytaert, W., Matgen, P., Pappenberger, F., 2009. A data assimilation approach to discharge esti- mation from space. Hydrol. Process. 23, 36413649.
Oke, P.R., Brassington, G.B., Griffin, D.A., Schiller, A., 2008. The bluelink ocean data assimilation system (BODAS). Ocean Model. 21, 4670. http://dx.doi.org/10.1016/j.ocemod.2007.11.002.
Oke, P.R., Sakov, P., Corney, S.P., 2007. Impacts of localisation in the enKF and enOI: experiments with a small model. Ocean Dyn. 57, 3245.
Ott, E., Hunt, B.R., Szunyogh, I., Zimin, A.V., Kostelich, E.J., Corazza, M., Kalnay, E., Patil, D.J., Yorke, J.A., 2004. A local ensemble Kalman filter for atmospheric data assimilation. Tellus 56A, 415–428.
Reager, J.T., Thomas, A.C., Sproles, E.A., Rodell, M., Beaudoing, H.K., Li, B., Famiglietti, J.S., 2015. Assimilation of GRACE terrestrial water storage observations into a land surface model for the assessment of regional flood potential. Remote Sens. 7, 14663–14679.
Reichle, R.H., McLaughlin, D.B., Entekhabi, D., 2002. Hydrologic data assimilation with the ensemble Kalman filter. Mon. Weather Rev. 130, 103114. http://dx.doi.org/10.1175/1520-0493(2002)130⟨0103:HDAWTE⟩2.0.CO;2.
Reichle, R.H., Crow, W.T., Keppenne, C.L., 2008. An adaptive ensemble Kalman filter for soil moisture data assimilation. Water Resour. Res. 44, W03423. http://dx.doi.org/10.1029/2007WR006357.
Reichle, R.H., De Lannoy, G.J., Forman, B.A., Draper, C.S., Liu, Q., 2013. Connecting satellite observations with water cycle variables through land data assimilation: examples using the NASA GEOS-5 LDAS, in The Earths Hydrological Cycle. Springer, Netherlands, p. 577606. http://dx.doi.org/10.1007/978-94-017-8789-5_6.
Reichle, R.H., Kumar, S.V., Mahanama, S.P.P., Koster, R.D., Liu, Q., 2010. Assimilation of satellite-derived skin temperature observations into land surface models. J. Hydrometeorol. 11, 1103–1122. http://dx.doi.org/10.1175/2010JHM1262.1.
Renzullo, L.J., Van Dijk, A.I.J.M., Perraud, J.M., Collins, D., Henderson, B., Jin, H., Smith, A.B., McJannet, D.L., 2014. Continental satellite soil moisture data assimilation improves root-zone moisture analysis for water resources assessment. J. Hydrol. 519, 27472762. http://dx.doi.org/10.1016/j.jhydrol.2014.08.008.
Rodell, M., Chen, J., Kato, H., Famiglietti, J.S., Nigro, J., Wilson, C.R., 2007. Estimating groundwater storage changes in the mississippi river basin (USA) using GRACE. Hydrogeol. J. 15, 159166.
Rodell, M., Houser, P.R., Jambor, U., Gottschalick, J., Mitchell, K., 2004. The global land data assimilation system. Bull. Am. Meteorol. Soc. 85, 381394.
Rodgers, C.D., 2000. Inverse Methods for Atmopsheric Sounding: Theory and Practice. World Scientific, Singapore.
Sakov, P., Oke, P.R., 2008. A deterministic formulation of the ensemble kalman filter: an alternative to ensemble square root filters. Tellus 60A, 361371.
Schmidt, R., Petrovic, S., Gntner, A., Barthelmes, F., Wnsch, J., Kusche, J., 2008. Periodic components of water storage changes from GRACE and global hydrology models. J. Geophys. Res. 113, B08419. http://dx.doi.org/10.1029/2007JB005363.
Schumacher, M., Kusche, J., Dll, P., 2016. A systematic impact assessment of GRACE error correlation on data assimilation in hydrological models. J Geodesy http://dx.doi.org/10.1007/s00190-016-0892-y.
Schunk, R. W., Scherliess, L., Sojka, J. J., Thompson, D. C., 2004. USU global ionospheric data assimilation models, In: Huang H.-L. A. and Bloom H.J. Proceedings of the SPIE, atmospheric and environmental remote sensing data processing and utilization: an end-to-end system perspective, 5548, 327–336, doi:10.1117/12.562448.
Seo, D.J., Koren, V., Cajina, N., 2003. Real-time variational assimilation of hydrologic and hydrometeorological data into operational hydrologic forecasting. J. Hydrometeorol. 4, 627641.
Seoane, L., Ramillien, G., Frappart, F., Leblanc, M., 2013. Regional GRACE-based estimates of water mass variations over australia: validation and interpretation. Hydrol. Earth Syst. Sci. 17, 4925–4939. http://dx.doi.org/10.5194/hess-17-4925-2013.
Shannon, C.E., Weaver, W., 1949. The Mathematical Theory of Communication. University of Illinois Press, Urbana.
Sheffield, J., Goteti, G., Wood, E.F., 2006. Development of a 50-year high-resolution global dataset of meteorological forcings for land surfacemodeling. J. Clim. 19 (13), 30883111.
Smith, A.B., Walker, J.P., Western, A.W., Young, R.I., Ellett, K.M., Pipunic, R.C., Richter, H., 2012. The murrumbidgee soil moisture monitoring network data set. Water Resour. Res. 48 (7), 16. http://dx.doi.org/10.1029/2012WR011976.
Stewart, L.M., Dance, S.L., Nichols, N.K., 2008. Correlated observation errors in data assimilation. Int. J. Numer. Meth. Fluids 56, 15211527. http://dx.doi.org/10.1002/fld.1636.
Stone, J.V., 2004. Independent Component Analysis: A Tutorial Introduction. MIT Press, London.
Sun, Q., Xie, Z., Tian, X., 2015. GRACE terrestrial water storage data assimilation based on the ensemble four-dimensional variational method PODEn4DVar: method and validation. Sci. China Earth Sci. 58, 371. http://dx.doi.org/10.1007/s11430-014-4978-1.
Swenson, S., Chambers, D., Wahr, J., 2008. Estimating geocentervariations from a combination of GRACE and ocean model output. J. Geophys. Res. 113, B08410. http://dx.doi.org/10.1029/2007JB005338.
Swenson, S., Wahr, J., 2002. Methods for inferring regional surface-mass anomalies from gravity recovery and climate experiment (GRACE) measurements of time-variable gravity. J. Geophys. Res. 107 (B9), 2193. http://dx.doi.org/10.1029/2001JB000576.
Swenson, S., Wahr, J., 2006. Post-processing removal of correlated errors in GRACE data. Geophys. Res. Lett. 33, L08402. http://dx.doi.org/10.1029/2005GL025285.
Tangdamrongsub, N., Steele-Dunne, S.C., Gunter, B.C., Ditmar, P.G., Weerts, A.H., 2015. Data assimilation of GRACE terrestrial water storage estimates into a regional hydrological model of the rhine river basin. Hydrol. Earth Syst. Sci. 19, 2079–2100. http://dx.doi.org/10.5194/hess-19-2079-2015.
Tapley, B.D., Bettadpur, S., Watkins, M., Reigber, C., 2004. The gravity recovery and climate experiment: mission overview and early results. Geophys. Res. Lett. 31, L09607. http://dx.doi.org/10.1029/2004GL019920.
Thomas, A.C., Reager, J.T., Famiglietti, J.S., Rodell, M., 2014. A GRACE-based water storage deficit approach for hydrological drought characterization. Geophys. Res. Lett. 41, 15371545.
Tippett, M.K., Anderson, J.L., Bishop, C.H., Hamill, T.M., Whitaker, J.S., 2003. Ensemble square root filters. Mon. Weather. Rev. 131, 148590.
Tregoning, P., McClusky, S., van Dijk, A.I.J.M., Crosbie, R.S., Pea-Arancibia, J.L., 2012. Assessment of GRACE satellites for groundwater estimation in australia. National Water Commission 82.
Vrugt, J.A., ter Braak, C.J.F., Diks, C.G.H., Schoups, G., 2013. Advancing hydrologic data assimilation using particle Markov chain monte carlo simulation: theory, concepts and applications. Adv. Water Resour Anniversary Issue - 35 Years 51, 457–478. http://dx.doi.org/10.1016/j.advwatres.2012.04.002.
Vrugt, J.A., Diks, C.G., Gupta, H.V., Bouten, W., Verstraten, J.M., 2005. Improved treatment of uncertainty in hydrologic modeling: combining the strengths of global optimization and data assimilation. Water Resour. Res 41, W01017. http://dx.doi.org/10.1029/2004WR003059.
Wahr, J., Molenaar, M., 1998. Time variability of the earth's gravity field' hydrological and oceanic effects and their possible detection using GRACE. J. Geophys. Res. 103. B12, 30, 205-30, 229 doi: 10.1029/98JB02844.
Watkins, M.M., Wiese, D.N., Yuan, D.-N., Boening, C., Landerer, F.W., 2015. Improved methods for observing earths time variable mass distribution with GRACE using spherical cap mascons. J. Geophys. Res. Solid Earth 120. http://dx.doi.org/10.1002/2014JB011547.
Weerts, A.H., El Serafy, G.Y.H., 2006. Particle filtering and ensemble Kalman filtering for state updating with hydrological conceptual rainfall-runoff models. Water Resour. Res. 42, W09403. http://dx.doi.org/10.1029/2005WR004093.
Wiese, D. N., 2015. GRACE monthly global water mass grids NETCDF RELEASE 5.0. ver. 5.0. PO.DAAC, CA, USA. dataset accessed [YYYY-MM-DD] at 10.5067/TEMSC-OCL05.
Wouters, B., Bonin, J.A., Chambers, D.P., Riva, R.E.M., Sasgen, I., Wahr, J., 2014. GRACE, time-varying gravity, earth system dynamics and climate change. Rep. Prog. Phys. 77 (11), 116801. http://dx.doi.org/10.1088/0034-4885/77/11/116801.
Zaitchik, B.F., Rodell, M., Reichle, R.H., 2008. Assimilation of GRACE terrestrial water storage data into a land surface model: results for the mississippi river basin. J. Hydrometeorol 9 (3), 535548. http://dx.doi.org/10.1175/2007JHM951.1.
Zeng, Y., 2014. Efficient radar forward operator for operational data assimilation within the COSMO-model. In: KIT Scientific Publishing, p. 187. ISBN 3731501287, 9783731501282.
Zhang, Y., Bocquet, M., Mallet, V., Seigneur, C., Baklanov, A., 2012. Real-time air quality forecasting, part i: history, techniques, and current status. Atmos. Environ. 60, 632655.

Chapter 5

Sequential filtering methods

This chapter is covered by the following publications:

- **Khaki, M.**, Hoteit, I., Kuhn, M., Awange, J., Forootan, E., van Dijk, A.I.J.M., Schumacher, M., Pattiaratchi, C., (2017b). Assessing sequential data assimilation techniques for integrating GRACE data into a hydrological model. Advances in Water Resources, 107:301-316, doi:10.1016/j.advwatres.2017.07.001.

Different filtering schemes are more suited to different data assimilation applications. This part accounts for the knowledge gap referring to the absence of a comprehensive analysis to assess the performance of the common sequential filtering techniques for assimilating GRACE TWS into the hydrological model (Section 1.3). The paper above examines the performance of various sequential data assimilation techniques for merging GRACE TWS into a hydrological model and covers the thesis' objective (iii) outlined in Section 1.4. The applied filters are the standard EnKF and its multiple deterministic variants, as well as Particle filter with two different resampling schemes. The results of assimilations are evaluated by comparing their estimates against independent in-situ measurements within the Murray-Darling basin and measurements from the moisture-monitoring network in the Murrumbidgee catchment in New South Wales, Australia. Various aspects of the filters, e.g., the stability of ensemble members, ensemble distributions through skewness and kurtosis, and state covariance estimates at forecast and analysis steps are analyzed. Different performances are observed from the applied filters. Two extensions of the deterministic EnKF, the Square Root Analysis (SQRA) scheme and the Ensemble Square Root Filter (EnSRF), reach the best results, i.e., decreasing groundwater RMSE at both forecast and analysis steps and increasing soil moisture correlations to those of in-situ stations. Both methods also perform better in terms of successful ensembles spread and state covariance error reduction compared to the other implemented filters.

Advances in Water Resources 107 (2017) 301–316

Contents lists available at ScienceDirect

Advances in Water Resources

journal homepage: www.elsevier.com/locate/advwatres

Assessing sequential data assimilation techniques for integrating GRACE data into a hydrological model

M. Khaki[a,*], I. Hoteit[b], M. Kuhn[a], J. Awange[a], E. Forootan[a,c], A.I.J.M. van Dijk[d], M. Schumacher[e], C. Pattiaratchi[f]

[a] Western Australian Centre for Geodesy and The Institute for Geoscience Research, Curtin University, Perth, Australia
[b] Division of Physical Sciences and Engineering, King Abdullah University of Science and Technology, Thuwal, Saudi Arabia
[c] School of Earth and Ocean Sciences, Cardiff University, Cardiff, UK
[d] Fenner School of Environment and Society, The Australian National University, Canberra, Australia
[e] School of Geographical Sciences, University of Bristol, Bristol, UK
[f] The University of Western Australia, 35 Stirling Highway, Crawley 6009, Australia

ARTICLE INFO

Article history:
Received 7 December 2016
Revised 2 July 2017
Accepted 3 July 2017
Available online 6 July 2017

Keywords:
Data assimilation
GRACE
Hydrological modeling
Kalman filtering
Particle filtering

ABSTRACT

The time-variable terrestrial water storage (TWS) products from the Gravity Recovery And Climate Experiment (GRACE) have been increasingly used in recent years to improve the simulation of hydrological models by applying data assimilation techniques. In this study, for the first time, we assess the performance of the most popular data assimilation sequential techniques for integrating GRACE TWS into the World-Wide Water Resources Assessment (W3RA) model. We implement and test stochastic and deterministic ensemble-based Kalman filters (EnKF), as well as Particle filters (PF) using two different resampling approaches of Multinomial Resampling and Systematic Resampling. These choices provide various opportunities for weighting observations and model simulations during the assimilation and also accounting for error distributions. Particularly, the deterministic EnKF is tested to avoid perturbing observations before assimilation (that is the case in an ordinary EnKF). Gaussian-based random updates in the EnKF approaches likely do not fully represent the statistical properties of the model simulations and TWS observations. Therefore, the fully non-Gaussian PF is also applied to estimate more realistic updates. Monthly GRACE TWS are assimilated into W3RA covering the entire Australia. To evaluate the filters performances and analyze their impact on model simulations, their estimates are validated by independent in-situ measurements. Our results indicate that all implemented filters improve the estimation of water storage simulations of W3RA. The best results are obtained using two versions of deterministic EnKF, i.e. the Square Root Analysis (SQRA) scheme and the Ensemble Square Root Filter (EnSRF), respectively, improving the model groundwater estimations errors by 34% and 31% compared to a model run without assimilation. Applying the PF along with Systematic Resampling successfully decreases the model estimation error by 23%.

1. Introduction

Hydrological models offer important tools for simulating and predicting hydrological processes at global (e.g., Doll et al., 2003; Huntington, 2006; Coumou and Rahmstorf, 2012; van Dijk et al., 2013) and regional (e.g., Chiew et al., 1993; Wooldridge and Kalma, 2001; Christiansen et al., 2007; Huang et al., 2016) scales. Models are still being developed to simulate all available hydrological processes (e.g., groundwater recharge) and the inclusion of all interactions between water cycle components (e.g., evapotranspiration, precipitation, and runoff). Currently, the most important deficiencies in hydrological models are caused by a high level of uncertainties in imperfect modeling of complex water cycle processes, data deficiencies on both temporal and spatial resolutions (e.g., limited ground-based observations), uncertainties in input and forcing data, and uncertainties of (unknown) empirical model parameters (van Dijk et al., 2011, 2014; Vrugt et al., 2013). Since making models more complex introduces ever increasing model parameters that cannot be well interpreted and makes computations more expensive, a logical step to address these limitations is the assimilation of observations into models (e.g., McLaughlin, 2002; Zaitchik et al., 2008; van Dijk et al., 2014). Data assimilation techniques have found increasing interests with the availability of new data sources,

* Corresponding author.
E-mail address: mehdi.khaki@postgrad.curtin.edu.au (M. Khaki).

http://dx.doi.org/10.1016/j.advwatres.2017.07.001
0309-1708/

such as those derived from satellite remote sensing observations. For example, time-variable gravity fields from the Gravity Recovery And Climate Experiment (GRACE) mission (Tapley et al., 2004) can be converted to terrestrial water storage (TWS) fields, a fundamental parameter of the water cycle that might be used to reduce uncertainties in hydrological models.

Data assimilation is a procedure that constrains the dynamic of a model with available observations in order to improve its estimates (Bertino et al., 2003). The solution of the data assimilation problem is based on the Bayes' rule (Jazwinski, 1970; van Leeuwen and Evensen, 1996), which basically computes the Probability Density Function (PDF) of the state, i.e., the model variable of the system that should be estimated, given the data. The updated distribution is then propagated with the model to the time of the next available observation to obtain the prior PDF. In the case of a nonlinear or non-Gaussian system (as it is the case for hydrological models), it is not possible to analytically derive the posterior (analysis) PDF of the state (Hoteit et al., 2008; Vrugt et al., 2013). The Bayesian estimation problem, therefore, needs to be solved numerically, using either variational smoothing or sequential filtering methods (Subramanian et al., 2012).

Variational methods look for the model trajectory that best fits the data by minimizing a chosen cost function that measures the misfit between the model state and the observations (Talagrand and Courtier, 1987). These methods require coding and executing an adjoint model, which is very demanding in terms of human and computational resources (Hoteit et al., 2005). Furthermore, variational methods do not provide an efficient framework for updating the estimating statistics during the data assimilation process (Courtier et al., 1994; Kalnay, 2003). In contrast, sequential techniques process the data as they become available following two steps including a forecast step to propagate the distribution forward in time and an analysis step to update the distribution with the newly available observation. Monte Carlo methods are commonly used in the forecast step (based on ensembles or particles) and Kalman (ensemble Kalman filtering) or point-mass weight (Particle filtering) updates are applied in the analysis step (Evensen, 2009; Hoteit et al., 2012). Sequential methods do not require an adjoint and are becoming increasingly popular because of their reasonable computational requirements (Bertino et al., 2003; Hoteit et al., 2002; Robert et al., 2006).

The Particle filter (PF) is based on a point-mass (particle) representation of the system state's PDF. It forecasts the PDF by propagating the particles forward in time. At the analysis time, the state PDF is updated by assigning new weights to the particles based on incoming observations (Doucet et al., 2001; Hoteit et al., 2012; Pham, 2001). The fundamental problem of this technique is the degeneracy phenomenon of its particles, with only very few particles carrying most of the weights (Subramanian et al., 2012). Moreover, errors in the assimilated observations may propagate to the estimated distribution because the method was not designed to improve the structure of the model (Hoteit et al., 2008; Smith et al., 2008). This problem is addressed by the Ensemble Kalman filters (EnKFs), which assume a Gaussian forecast PDF at the analysis time, so a Kalman update-step is applied to the particles (Hoteit et al., 2015). This allows an efficient implementation of the Bayesian filtering approach for data assimilation into large systems using small ensembles (Hoteit et al., 2008; van Leeuwen and Evensen, 1996).

EnKFs can be classified into stochastic and deterministic filters, depending on whether the observations are perturbed with noise before assimilation, or not (Hoteit et al., 2015; Tippett et al., 2003). In the stochastic EnKF, each ensemble member is updated with perturbed observations, readily providing an analysis ensemble for the next filtering cycle. In contrast, a deterministic EnKF updates only the mean and the covariance of the ensembles exactly as in the Kalman Filter, and thus require a resampling step to generate a new analysis ensemble. The resampling step is not unique, and as such several deterministic EnKFs have been proposed (Hoteit et al., 2015; Sun et al., 2009).

Sequential filtering methods have been extensively applied and compared in oceanic and atmospheric applications (Altaf et al., 2014; Bennett, 2002; Elbern and Schmidt, 2001; Garner et al., 1999; Kalnay, 2003; Lahoz et al., 2007; Schunk et al., 2004; Zhang et al., 2012). In hydrological studies, data assimilation has been used to estimate different water compartments, such as soil moisture (e.g., Reichle et al., 2002; Brocca et al., 2010; Renzullo et al., 2014) and surface water storage (e.g., Alsdorf et al., 2007; Neal et al., 2009; Giustarini et al., 2011). However, the efficiency of various filtering methods in dealing with remotely sensed data in hydrology has not been fully investigated (McLaughlin, 2002; Schumacher et al., 2016).

Global terrestrial water storage data derived from the GRACE satellite mission can be now employed to improve the behavior of hydrological models (e.g., Zaitchik et al., 2008; Tangdamrongsub et al., 2015; Thomas et al., 2014; van Dijk et al., 2014; Eicker et al., 2014; Reager et al., 2015), providing unprecedented temporal and spatial coverage. For instance, Zaitchik et al. (2008) demonstrated the relevance of GRACE data in improving the estimation of groundwater variability over the four major sub-basins of the Mississippi through data assimilation into the Catchment Land Surface Model using an ensemble Kalman smoother. Houborg et al. (2012) investigated drought conditions in North America through GRACE data assimilation. The developed GRACE-based drought indicators in the USA led to an improved monitoring of soil moisture and groundwater conditions of deep layers. The impact of GRACE error correlation structure on the assimilation of GRACE data was very recently studied by Schumacher et al. (2016). Yet, to the best of our knowledge, however, a comparison with the application of different sequential filtering methods for assimilating GRACE TWS in models has not been fully explored.

In this study, we investigate the performance of the most common sequential filtering techniques for data assimilation using the hydrological model of the World-Wide Water Resources Assessment (W3RA; van Dijk, 2010) over Australia. The amount of rainfall in Australia, especially over its northern and eastern parts, is low in comparison to other inhabited continents on Earth leading to prolonged drought in the interior regions (Forootan et al., 2016). Hence, accurate estimation of water storages (e.g., using hydrological models) is necessary to manage water resources in this region. Here, different filters are used to assimilate GRACE TWS into W3RA to improve its estimates. Both stochastic and deterministic EnKFs are tested and their performances are compared against two standard Particle filters. We applied the standard EnKF and its deterministic variants, including, the Square Root Analysis (SQRA) scheme following Evensen (2004) and Schumacher et al. (2016), the Ensemble Transform Kalman Filter (ETKF, Bishop et al., 2001), the Deterministic EnKF (DEnKF, Sakov and Oke, 2008), and the Ensemble Square-Root Filter (EnSRF, Whitaker and Hamill, 2002). We also implement the static-ensemble variant of the EnKF, the Ensemble Optimal Interpolation (EnOI, Evensen, 2003), in an attempt to reduce the computational burden. To mitigate the deficiency that may arise from limited ensemble sizes and knowledge of model errors' statistics (Anderson et al., 2007; Oke et al., 2007), covariance inflation (e.g., Anderson and Anderson, 1999; Anderson et al., 2007; Ott et al., 2004) and localization techniques (e.g., Bergemann and Reich, 2010; Hamill and Snyder, 2002) are applied. The performance of these ensemble filters is assessed against two nonlinear Particle filters based on two different resampling strategies: (i) Multinomial Resampling and (ii) Systematic Resampling techniques (Arulampalam et al., 2002). The summary of applied filters in this study is presented in Table 1. The results of assimilations

Table 1
A summary of the applied filters for data assimilation.

Filter	Acronym	Type	Reference
Ensemble Kalman filter	EnKF	Stochastic ensemble Kalman filter	Evensen (1994)
Square Root Analysis	SQRA	Deterministic ensemble Kalman filter	Evensen (2004)
Ensemble Transform Kalman Filter	ETKF	Deterministic ensemble Kalman filter	Bishop et al. (2001)
Ensemble Square-Root Filter	EnSRF	Deterministic ensemble Kalman filter	Whitaker and Hamill (2002)
Ensemble Optimal Interpolation	EnOI	Deterministic ensemble Kalman filter	Evensen (2003)
Deterministic ensemble Kalman filter	DEnKF	Deterministic ensemble Kalman filter	Sakov and Oke (2008)
Particle filter, Multinomial Resampling	PFMR	Particle filter	Arulampalam et al. (2002)
Particle filter, Systematic Resampling	PFSR	Particle filter	Arulampalam et al. (2002)

are evaluated by comparing their estimates against independent groundwater in-situ measurements over the Murray–Darling Basin and measurements from the moisture-monitoring network in the Murrumbidgee catchment in New South Wales, Australia.

2. Model and datasets

2.1. W3RA

The World-Wide Water Resources Assessment (W3RA), based on the Australian Water Resources Assessment system (AWRA) model (version 0.5) is used in this study (http://www.wenfo.org/wald/data-software/). The model was first developed in 2008 by the Commonwealth Scientific and Industrial Research Organisation (CSIRO) to monitor, represent and forecast Australian terrestrial water cycles. The W3RA is a grid-distributed biophysical model that simulates landscape water stores in the vegetation and soil systems (van Dijk, 2010). The $1^\circ \times 1^\circ$ global daily fields of minimum and maximum temperature, downwelling short-wave radiation, and precipitation from Princeton University (http://hydrology.princeton.edu) are used for meteorological forcing data (Sheffield et al., 2006). This one-dimensional grid-based water balance model represents the water balance of the soil, groundwater and surface water stores in which each cell is modeled independently of its neighbors (van Dijk, 2010; Renzullo et al., 2014). The model state is composed of the $1^\circ \times 1^\circ$ W3RA model storages of the top, shallow root and deep root soil layers, groundwater storage, and surface water storage in a one-dimensional system (vertical variability). In this study, we use W3RA providing daily model states for the period of February 2002 to December 2012. More detailed information on the W3RA model can be found in van Dijk (2010).

2.2. GRACE-derived terrestrial water storage

Here, we use monthly GRACE level 2 (L2) products along with their full error information between February 2002 and December 2012 as provided by the ITSG-Grace2014 gravity field model (Mayer-Gurr et al., 2014). The GRACE monthly Stokes' coefficients are truncated at spherical harmonic degree and order 90, which resulting in approximately $\sim$300 by 300 km spatial resolution at the equator.

Following Swenson et al. (2008), degree 1 coefficients are replaced to account for movements of the Earth's center of mass (i.e., realized by a set of tracking stations on the surface of the Earth). Degree 2 and order 0 (C20) coefficients from GRACE are not well determined (e.g., Tapley et al., 2004; Tregoning et al., 2012) and are replaced by more reliable estimations of the Satellite Laser Ranging solutions (Cheng and Tapley, 2004). Correlated noise exists in L2 products due to anisotropic spatial sampling, instrumental noise (K-band ranging system and GPS), and temporal aliasing caused by the incomplete reduction of short-term mass variations (Forootan et al., 2014). These errors are reduced by smoothing based on a Gaussian averaging kernel with 300 km half radius and destriping following Swenson and Wahr (2006). However, the smoothing may cause signal attenuation (Klees et al., 2008) and can result in considerable spatial leakage, such as the apparent movement of masses from one region to another (Chen et al., 2007) especially over coastlines (see examples within Australia in e.g., Brown and Tregoning, 2010; Forootan et al., 2012). In order to address this issue, following Swenson and Wahr (2002), we apply an isotropic kernel using a Lagrange multiplier filter to best balance signal and leakage errors over the basin of interest.

An additional post-processing step is applied to convert the filtered L2 gravity fields (after removing the mean field of study period) to gridded TWS fields ($1^\circ \times 1^\circ$) following Wahr et al. (1998). The GRACE TWS data are gridded at the same spatial $1^\circ \times 1^\circ$ resolution of W3RA resulting in 794 grid points for Australia that covers an area of 7.692 million km^2 located between 10°S and 46°S latitude, and 110°E and 160°E longitude. GRACE data provide changes in TWS while W3RA produces absolute TWS. Accordingly, the mean TWS for the study period is taken from W3RA and is added to the GRACE TWS change time series in order to obtain absolute values in accordance with the model (Zaitchik et al., 2008). In addition, the monthly full error information of the Stokes' coefficients is used to construct an observation error covariance matrix for the GRACE TWS fields (Eicker et al., 2014; Schumacher et al., 2016).

2.3. In-situ data

For validating the assimilation results, we use in-situ groundwater level data that are collected over the Murray–Darling Basin. The independent in-situ measurements from the model and observations are provided by New South Wales Government (NSW) groundwater archive (http://waterinfo.nsw.gov.au/pinneena/gw.shtml). Monthly well measurements are acquired and time series of groundwater storage anomalies are generated. Measurements with data gaps and those without showing seasonal variations are flagged (we assume these belong to confined aquifers) and are thus excluded (Houborg et al., 2012; Tangdamrongsub et al., 2015). Selected bore-water levels are then converted to variations in groundwater (GW) storage. To this end, instead of using specific yield estimates (Rodell et al., 2007; Zaitchik et al., 2008) that is not available in the region, TWS variation from GRACE and GLDAS soil moisture are used to scale the observed head following Tangdamrongsub et al. (2015). Tregoning et al. (2012) show that this approach can be used to find a scaling factor over the Canning Basin and Murray Basin in Australia. The scaled in-situ groundwater level fluctuations are then used to assess the assimilation results.

In addition, in-situ measurements of the moisture-monitoring network (http://www.oznet.org.au/) in Murrumbidgee catchment (Smith et al., 2012) are used to evaluate the results. These data are known as the OzNet network, which provides long-term records of measuring volumetric soil moisture at various soil depths at 57 locations across the Murrumbidgee catchment area. Following Renzullo et al. (2014), we averaged the measurements into a daily scale and use 0–8 cm to evaluate the estimated model top-layer

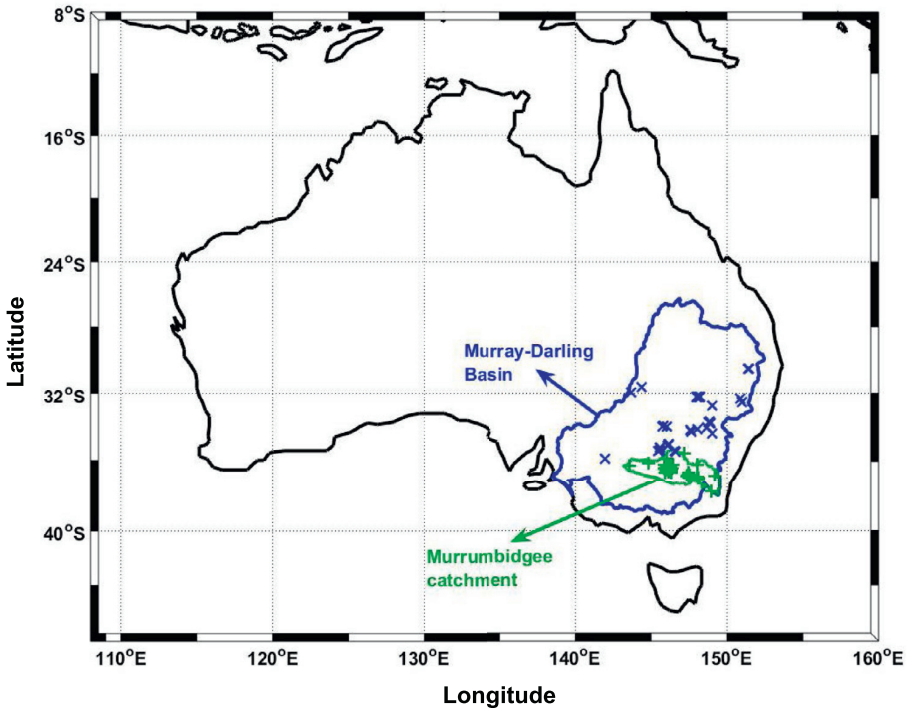

Fig. 1. The study area is represented by black solid line. The figure also contains the boundary of the Murray–Darling Basin and the locations of the groundwater bore stations (blue), and the outline of the Murrumbidgee catchment with the OzNet soil moisture network (green), which are used for results assessment. (For interpretation of the references to color in this figure legend, the reader is referred to the web version of this article.)

soil moisture and the 0–30 cm and 0–90 cm measurements for the evaluation of the model shallow root-zone soil moisture estimation. The distribution of the in-situ moisture network, as well as in-situ groundwater stations, are shown in Fig. 1.

3. Filtering methods and implementation

The Bayesian filtering procedures are selected here for data assimilation (Jazwinski, 1970; van Leeuwen and Evensen, 1996). The analytical process conditions a prior PDF of the state with available observations to compute the posterior PDF based on Bayes' rule (Koch, 2007) in two steps; (1) forecasting the state PDF using a dynamical model and (2) updating the forecast PDF by assimilating observations using Bayes' rule. In the case of a linear system with Gaussian noise, the popular KF provides the Bayesian filtering solution by computing the first two moments of the state PDF, which remains always Gaussian (van Leeuwen and Evensen, 1996). This two-step process is repeated whenever new observations become available. The basic KF equations are given by Kalman (1960) starting from an analysis of the state, X_t^a, and the associated error covariance, P_t^a, at a given time t. These can be summarized as:

(1) The forecast step consists of the evolution of the state estimate and its error covariance matrix with a linear dynamical model (M) to the assimilation step (the time of the next available observation),

$$X_{t+\Delta t}^f = MX_t^a + \eta, \tag{1}$$

$$P_{t+\Delta t}^f = MP_t^a M^T + Q, \tag{2}$$

where $X_{t+\Delta t}^f$ refers to the forecast state (X^f) at time $t+\Delta t$, with Δt represents the model time step, and T is the transpose index. In Eq. (1), η is the process noise, which is drawn from $N(0, Q)$ with covariance matrix Q, and $P_{t+\Delta t}^f$ (in Eq. (2)) denotes the forecast error covariance (P^f) at time $t+\Delta t$.

(2) The analysis step updates the forecast state using new incoming observations Y that are related to the state vector by the linear observation operator (H) as,

$$Y = HX + \epsilon, \tag{3}$$

where ϵ is the measurement noise. The analysis state (X^a) is then computed using

$$X^a = X^f + K(Y - HX^f), \tag{4}$$

$$P^a = (I - KH)P^f, \tag{5}$$

$$K = P^f H^T (HP^f H^T + R)^{-1}, \tag{6}$$

where K refers to the Kalman gain, R is the observation error covariance matrix, and I denotes the identity matrix.

The KF algorithm is not suited for high-dimensional or nonlinear systems (Pham, 2001). The ensemble Kalman filter provides an efficient alternative for the implementation of the KF with these systems by representing the first two-moments of the state using a sample of state vectors, called ensemble. The forecast state and covariance matrix in Eqs. (1) and (2) are then estimated as the sample mean and covariance of the ensembles members $X^i, i = 1, \ldots, N$:

$$\bar{X}^f = \frac{1}{N}\sum_{i=1}^{N} X^{f,i}, \tag{7}$$

$$P^f = \frac{1}{N-1}\sum_{i=1}^{N}(X^{f,i} - \bar{X}^f)(X^{f,i} - \bar{X}^f)^T = \frac{1}{N-1}A^f A^{fT}. \tag{8}$$

$\bar{X}^f$ is the forecast ensemble mean and A^f ($A^f = [A^{f,1}, \ldots, A^{f,N}]$) is the forecast ensemble of anomalies (perturbations; $A^{f,i} = X^{f,i} - \bar{X}$). When a new observation is available, the forecast ensemble is then updated with the data using Eq. (4), as in the KF. Several ensemble Kalman filters have been proposed, all sharing the same forecast step in which an available analysis ensemble ($[X^{a,1}, \ldots, X^{a,N}]$) is propagated forward with the model. The analysis step based on the KF, however, can be applied stochastically or deterministically.

3.1. Stochastic Ensemble Kalman Filter (EnKF)

The analysis step of the stochastic EnKF updates each ensemble member with a perturbed observation written as,

$$X^{a,i} = X^{f,i} + K(Y^i - HX^{f,i}), \quad i = 1, \ldots, N, \tag{9}$$

where $Y^i = Y + \varepsilon^i$, with ε^i a random error sampled from $N(0, R)$. The use of perturbed observations in the EnKF results in an analysis error covariance that matches that of the KF, in a statistical sense (Hoteit et al., 2012). The advantage of the stochastic update is that it readily provides a randomly sampled ensemble from the Gaussian-assumed state analysis PDF for the next forecast cycle (Hoteit et al., 2015). However, as illustrated by Whitaker and Hamill (2002), sampling error can be reflected in the EnKF background covariance matrix, especially for the small-size ensembles. This could be particularly pronounced when a large number of (independent) observations are assimilated (Nerger, 2004), as the observation covariance cannot be properly sampled with a small ensemble (Hoteit et al., 2015).

3.2. Deterministic ensemble Kalman filters

Instead of updating each forecast member separately, deterministic EnKFs (DEnKFs) update the forecast ensemble in two steps, first the ensemble-mean and then the ensemble perturbations (Tippett et al., 2003) are calculated so that the sample mean and covariance of the updated ensemble exactly match those of the Kalman filter in Eqs. (4) and (5).

Various methods have been proposed in order to update the ensemble perturbations. SQRA resamples the new ensemble perturbations (A^a) from the forecast ensemble perturbations (A^f) as,

$$A^a = A^f V \sqrt{I - \Sigma^T \Sigma \Theta^T}, \tag{10}$$

where Σ is computed by applying the following singular value decomposition (SVD),

$$U \Sigma V^T = SVD(\Lambda^{-\frac{1}{2}} Z^T HA), \tag{11}$$

$$Z \Lambda Z^T = (HP^f (H)^T + R)^{-1}, \tag{12}$$

where Θ in Eq. (10) being a random orthogonal matrix for redistribution of the variance among the ensemble members (see Evensen, 2004; 2007, for more details). This is very similar to the random rotation that has been introduced in the context of the Singular Evolutive Extended Kalman (SEEK) filter (Hoteit et al., 2002; Pham, 2001).

ETKF introduces a transformation matrix to directly compute the analysis ensemble perturbations from their forecast counterparts,

$$A^a = A^f . T, \tag{13}$$

where $T = U(I + \Lambda)^{-1/2}$, with U and Λ, respectively, being the orthogonal and diagonal matrices computed from an eigenvalue decomposition of $(HX^f)^T R^{-1} (HX^f)$.

DEnKF and EnSRF adopt a similar analysis step to the EnKF in the sense that they compute the analysis perturbations from the forecast perturbations by updating each ensemble perturbation with a Kalman-like update step. To match the KF covariance matrix by an ensemble of perturbations, DEnKF computes a first-order approximation of the Kalman gain (Sakov and Oke, 2008). This approximate gain $\tilde{K}$ is then used to compute the analysis perturbations as,

$$A^a = A^f - \frac{1}{2} KHA^f. \tag{14}$$

EnSRF exploits the serial formulation of the KF analysis step in which the observations are assimilated each at a time to compute the analysis perturbations that exactly match the KF covariance using the modified gain (αK) with,

$$\alpha = \left(1 + \sqrt{\frac{R}{HP^f H^T + R}}\right)^{-1}. \tag{15}$$

This requires the observations to be uncorrelated, which can always be satisfied by scaling the observations with the square-root inverse of the observational error covariance matrix (Hoteit et al., 2015).

Another form of ensemble Kalman filtering is the so-called Ensemble Optimal Interpolation (EnOI) scheme, which is basically the EnKF, but without an update of the ensemble anomalies. More precisely, EnOI only updates the forecast state with a Kalman gain computed from a preselected static ensemble. The main advantage of not updating the ensemble is of course to reduce the computational load, but it can also be beneficial to retain the spread of the ensemble and to enforce climatological smoothness in the update step. EnOI can be stochastic or deterministic (Hoteit et al., 2002). Here we only test the more standard stochastic variant (Evensen, 2003).

3.3. Particle filtering

Particle filtering is also a sequential Monte Carlo method that was originally proposed by Gordon et al. (1993) and has since been applied in numerous studies (Arulampalam et al., 2002; Doucet, 1998). The idea is to represent the state PDF by a set of weighted particles (Arulampalam et al., 2002), hence the name Particle filter (Doucet, 1998; Gordon et al., 1993), which is similar to the ensemble members in the EnKF but with non-uniform weights. The state PDF is then decomposed as,

$$P(X_t | Y_{1:t}) \approx \sum_{i=1}^{N} \omega_t^i \delta(X_t - X_t^i), \tag{16}$$

where $\{X_t^i; i = 1, \ldots, N\}$ are the particles at time t, observations between time 1 and t are denoted by $Y_{1:\,t}$, ω_t^i are the weights of the particles, and δ is the Dirac function. In the forecast step, the PF just integrates the particles forward with the model, exactly as the EnKF, and their weights remain the same. In the analysis step, only the weights, and not the particles, are updated with the incoming observation as,

$$\omega_t^i = \frac{P(y_t | X_{t|t-1}^i)}{\sum_j P(y_t | X_{t|t-1}^j)}. \tag{17}$$

The PF suffers from the degeneracy problem in which the weights of all particles become negligible except only for a very few, requiring a prohibitive number of particles to prevent particles collapse (Arulampalam et al., 2002). Degeneracy can be mitigated using the so-called resampling technique (Doucet et al., 2005), which resamples a new set of particles with uniform weights after every update step based on the analysis PDF. In this study, we consider two of the most common resampling techniques: the Particle filter with Multinomial Resampling (PFMR) and Particle filter with Systematic Resampling (PFSR), as proposed by Doucet et al. (2005).

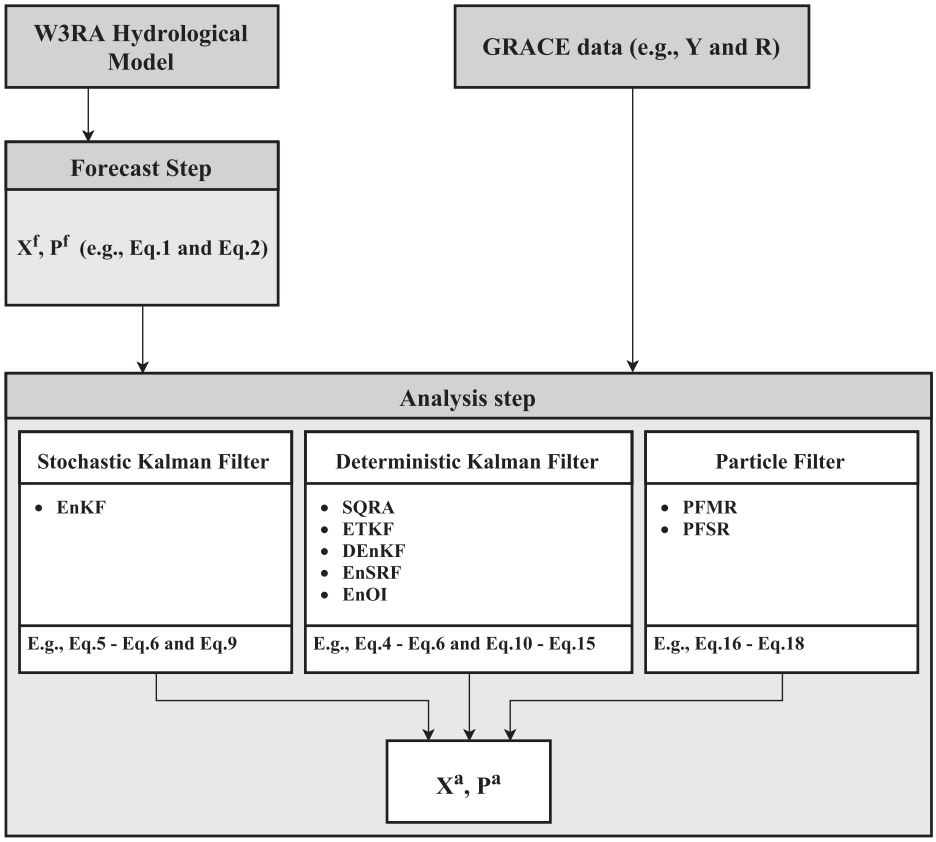

Fig. 2. A schematic illustration of the steps and filters applied for data assimilation in this study.

PFMR is the most straightforward resampling scheme, where N independent random numbers ($u \sim U(0, 1)$) are generated to select a particle from the old set. PFSR, which is also called universal sampling, draws only one random number $u_1 \sim U(0, 1/N)$ and the remaining $N-1$ numbers are then calculated from u_1 (Doucet et al., 2005) as,

$$U_i = u_1 + \frac{(i-1)}{N}, \quad i = 2, \ldots, N. \tag{18}$$

These are then used to select a new set of particles according to the multinomial distribution (Hol et al., 2006).

PF has been applied in few hydrological studies. Among them, Moradkhani et al. (2005) investigated the relevance of the PF for estimating the joint posterior distribution of the parameters and state. In another effort, Moradkhani et al. (2012) proposed a modified version of the PF, focusing on enhancing the sampling of the posterior with Markov chain Monte Carlo (MCMC) moves. Plaza et al. (2012) used the Sequential Importance Sampling with Resampling (SISR) Particle filter for soil moisture assimilation and focused on the consequent effect on baseflow generation. Existing studies focused on the different implementations of PF using various resampling techniques. However, a comparison between PFs performances with diverse resampling techniques and EnKFs has not been investigated yet in hydrology. Fig. 2 shows a summary of the steps and filters applied for data assimilation in this study.

3.4. Filter implementation

An experimental framework is developed in order to assess the relevance and efficiency of the filtering techniques presented in the previous section for assimilating GRACE data into the W3RA model. All filters are implemented under identical conditions, using the same spatial scales ($1^\circ \times 1^\circ$) for both the W3RA and the GRACE TWS, and daily temporal scales for the W3RA and monthly for the GRACE data. W3RA is integrated to simulate water storages over Australia using monthly sequential assimilation cycles of GRACE data applied at the middle of each month.

Several steps need to be undertaken before assimilating GRACE-derived TWS into the W3RA model. Initial ensemble members (particles) are first generated by perturbing the three most important forcing variables including precipitation, temperature, and radiation using their reported error characteristics (Sheffield et al., 2006). Monte Carlo sampling of multivariate normal distributions with the errors representing the standard deviations of the forcing sets are used to produce an ensemble (see details in Renzullo et al., 2014). Different ensemble sizes (30–120) and their spread are tested which the ensemble with 72 members (72–120 are suggested by Oke et al., 2008) shows promising performance and is used in this study. The model is integrated forward for two years (January 2001 to January 2003) using perturbed meteorological forcing datasets and provided a set of 72 different states at the beginning of 2003 (study period), considered as the initial ensemble (with 72 members). The same initial ensemble is used for all the filters.

We use two tuning techniques of ensemble inflation and localization in order to enhance the assimilation performance of all EnKFs. Ensemble inflation uses a small coefficient (i.e., 1.12 in our study; Anderson, 2001) to inflate prior ensemble deviation from the ensemble-mean to increase their variations and alleviate the inbreeding problem (Anderson et al., 2007). Another auxiliary technique that has been proved to be helpful when using limited ensemble size is localization, initially proposed by Houtekamer and

Mitchell (2001). We choose to use a Local Analysis (LA) scheme which works by restricting the impact of a given measurement in the update step to the points located within a certain distance from the measurement location (Evensen, 2003; Ott et al., 2004). Different localization lengths are applied to reach the best case (i.e., 5°). In terms of computational cost, all implemented filters are required more or less the same CPU (central processing unit) time (when implemented with the same number of members/particles), with the forecast step of the ensemble being the most demanding.

4. Results

In this section, we review and analyze the performance of all the selected filtering techniques based on various factors. The implemented filters include (stochastic) EnKF, ETKF, SQRA, DEnKF, EnSRF, EnOI and PF with Multinomial (PFMR) and Systematic (PFSR) Resampling. In addition to improving the estimation of the system state and quantifying the associated uncertainties, a suitable data assimilation technique is expected to keep the model system stable during the assimilation process after incorporating GRACE data. These are provided at coarse temporal and spatial scales in comparison to the W3RA model, leading to only one assimilation step every 30 model time-steps and providing information at about three times less than the model grid resolution. Our analysis is organized into two parts; we first examine the filters performance by comparing their estimates (analysis and forecasts) against the assimilated GRACE data over the whole study area as well as the independent in-situ measurements over the Murray–Darling River Basin as well as Murrumbidgee catchment. We also compare the filters estimates with the outputs of a model-free run (open-loop) that is integrated with the filters initial condition without assimilation to evaluate the impact of assimilating GRACE data on the model behavior. Next, the filters behaviors in terms of ensemble spread and the impact of assimilation on the forecast and analysis error covariances are investigated.

4.1. Assessment with GRACE and in-situ data

Spatial correlation maps with high correlations may suggest that the applied filtering method efficiently incorporates GRACE data into the model (Fig. 3). The correlation between the model TWS outputs without assimilation and the GRACE data range between 0.11 and 0.64, with the highest correlations in the northern region and the lowest in the southern region. All filters significantly improve the estimates correlations to the data after assimilation with some filters leading almost to the perfect correlation with the data (e.g., EnSRF). The model is not able to maintain this high correlation during the forecast and the 30-day assimilation window, with the correlations mainly decreasing in the center and southern regions. After monitoring the impact of observations on the model states throughout the study period, it is found that this effect is decreasing gradually (approximately 3–5 days to lose more than 10%) by comparing the correlation of the model states with and without assimilation. This mostly refers to the daily effects of the perturbed forcing sets on model estimations and may suggest that using the denser observation (temporally) could preserve assimilated information during the study. The level of improvement in correlations, however, is different for each filter. For instance, ETKF, SQRA, and PFSR lead to higher correlations with GRACE-derived TWS, suggesting that these methods better reflect the observations in the state estimates. Overall, EnKFs seem to perform better than PFs except only for DEnKF which shown no remarkable impact on the model behavior after assimilation of GRACE data.

Those methods with the highest correlations to GRACE data lead, as expected, also the least estimation errors (Fig. 4). The largest errors are found in the northern and southern parts of the domain (Fig. 4(a)), with some of the filters not able to improve remarkably the model behavior over these areas. TWS variations are generally higher in the northern part of the study area with larger amplitudes especially during monsoonal seasons (Awange et al., 2009; Seoane et al., 2013). The model seems unable to predict these amplitudes due to larger estimated errors even though it performs better in predicting their phases considering high correlations in this area. SQRA, EnSRF, and to some extent ETKF, significantly decrease the estimation error over the whole domain. This is very important because these filters are able to incorporate most of the GRACE signals into the model.

The Root-Mean-Squared Errors (RMSE) time series between the GRACE TWS and filters estimates are calculated (Fig. 5). In all cases, the analysis step decreases the RMSE with respect to the forecast. Nevertheless, the RMSE resulting from DEnKF, EnOI, and PFMR are significantly larger, indicating that these methods are not able to improve the model behavior after incorporating GRACE data as the rest of the filters do. Estimates by all filters have the largest error in some periods (e.g., July and October), which may be caused by uncertainties in forcing sets. The RMSEs from SQRA and EnSRF are smaller in comparison to the rest of the filters. The smaller average errors during the study period prove the more stable performance of SQRA and EnSRF. Results in Figs. 4 and 5 suggest that the deterministic SQRA, ETKF, EnSRF filters, and to less extent PFSR, are more efficient at assimilating GRACE data. This might be due to the fact that for the stochastic ensemble filters perturbations of the observations have to be generated that introduce an additional uncertainty source to the analysis step and might result in larger discrepancies to the assimilated observations compared to the deterministic filters. A summary of the filters' performance, including the coefficient of determination (R^2) and RMSE in comparison to the assimilated observations (shown in Table 2) indicates higher correlation (84% average) and smaller RMSEs (35% average improvement) in the analysis step for all the filters. The maximum improvements regarding the achieved RMSE are achieved by EnSRF and SQRA as 58.88% and 55.17%, respectively.

We investigate the performances of the filtering methods through comparison with the independent groundwater in-situ data over the Murray–Darling Basin (cf. Section 2.3). We use the 54 in-situ measurements over the Murray–Darling Basin for a grid comparison with the estimated GW (Fig. 6). The filters estimates are spatially interpolated to the nearest observation bore. For each filter, the average RMSEs (over all 54 in-situ data) of the forecast state (red) and analysis state (blue) are determined. As for the assimilated GRACE data (cf. Fig. 5), all the filters decrease the RMSE with respect to the in-situ data, with the largest errors resulting from DEnKF, EnOI, and PFMR. Furthermore, the average RMSEs are smaller in SQRA and EnSRF. The similar behavior of the filters in the analysis steps can be found in Fig. 6 as in Fig. 5. For some months (e.g., March and July), the larger errors can be seen in Fig. 6 which are not existed in Fig. 5. This can be associated to either an incompatibility between groundwater in-situ measurements and GRACE data or the absent water compartment terms such as the surface water storage in the model and in-situ data for the second assessment (Fig. 6).

The relationship between the estimated states and both GRACE data and in-situ measurements (Fig. 7) demonstrates the filters capability to dynamically propagate the information extracted from GRACE data into system variables. In agreement with the previous results, the best performances are obtained using SQRA, EnSRF, and ETKF (Figs. 6 and 7).

The R^2 coefficient and RMSE results are summarized in Table 3 as another measure of the filter performances. For each filter, 54 error time series are computed (i.e., for each individual well), and their averages are then used to calculate R^2 and RMSE. The results

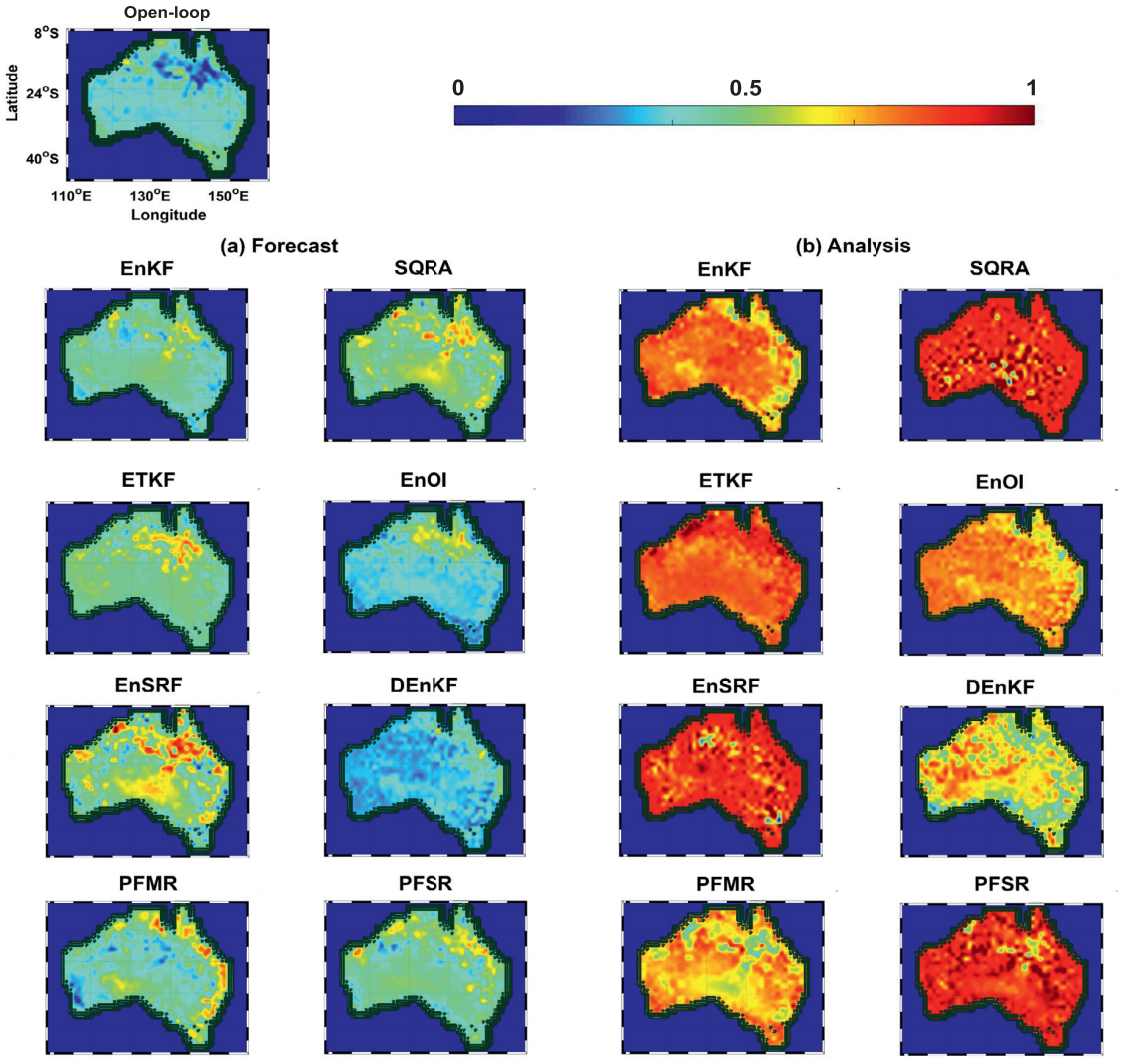

Fig. 3. Time average correlations between the assimilated GRACE TWS and different filters estimations at the (a) forecast and (b) analysis steps. Spatial correlation maps are generated at every assimilation step over the study period and their averages are presented.

Table 2
A summary of the statistics derived from the implemented methods using the assimilated GRACE data. The improvements in the analysis state RMSE estimates are calculated using the GRACE data in comparison to the model-free run.

Method	Forecast		Analysis		Improvement (%)
	RMSE (mm)	R^2	RMSE (mm)	R^2	
EnKF	26.5165	0.4354	16.5484	0.9084	39.59
SQRA	18.1156	0.4845	8.1208	0.9335	55.17
ETKF	21.8431	0.4456	14.8704	0.9123	41.92
EnOI	35.2105	0.3951	22.9304	0.7165	34.87
EnSRF	17.2950	0.4912	7.1105	0.9518	58.88
DEnKF	41.6417	0.3610	36.7408	0.6324	15.77
PFMR	37.6009	0.3851	30.2198	0.8137	19.63
PFSR	20.0344	0.4722	13.8711	0.9045	41.74

of all the filters summarized in Table 3 show improvements (by 35% average) in the analysis steps in all cases, similar to the assessment against GRACE data (cf. Table 2). SQRA and EnSRF lead to the highest correlations to the in-situ measurements of R^2, i.e., 0.75 and 0.72, respectively. These filters also provide the best estimates in terms of estimation error, while DEnKF and to a lesser degree EnOI have the highest RMSEs. The PFs, on the other hand, especially using the Systematic Resampling technique exhibit a reasonably good performance. In terms of the assessment results against GRACE data, deterministic filters provide the best performance (except for DEnKF), generally better than the stochastic EnKF. Over-

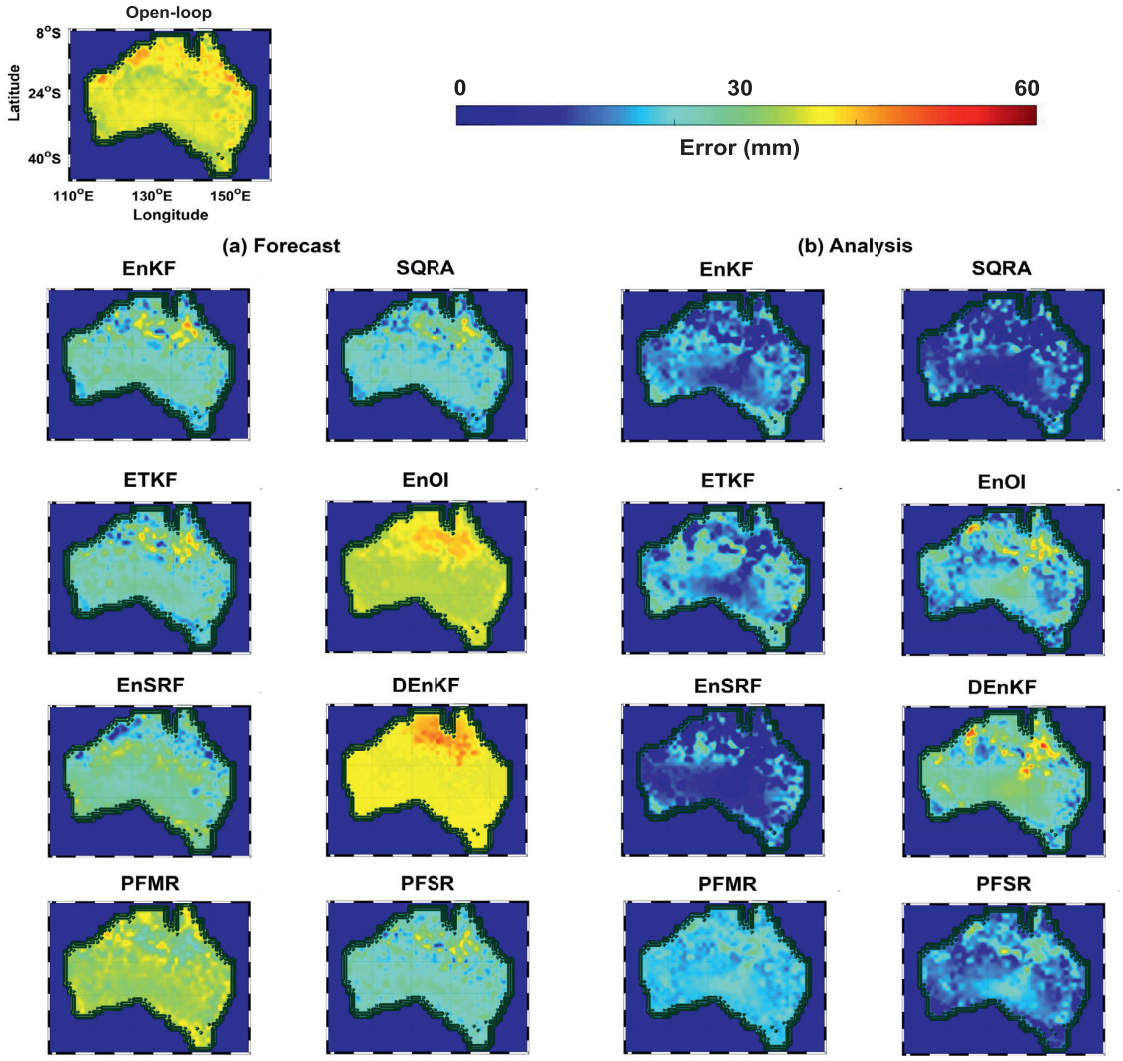

Fig. 4. Time average errors between the assimilated GRACE TWS and different filters estimations at the (a) forecast and (b) analysis steps (units are mm). The spatial distribution of the misfits between the filters solution and GRACE data is shown, which plots the time-averaged errors calculated at the forecast steps and the analysis steps.

Table 3
A summary of the statistics derived from implemented methods using the groundwater in-situ measurements. The improvements in the analysis state RMSE estimates are calculated using the in-situ measurements in comparison to the model-free run.

Method	Forecast		Analysis		Improvement (%)
	RMSE (mm)	R^2	RMSE (mm)	R^2	
EnKF	62.6521	0.2254	41.5469	0.6456	31.68
SQRA	56.3493	0.2834	32.1387	0.7546	42.96
ETKF	60.7741	0.2574	38.2156	0.6718	33.12
EnOI	89.5411	0.1756	61.0514	0.4675	23.82
EnSRF	58.5271	0.2378	33.7420	0.7225	42.35
DEnKF	112.9712	0.1454	84.3153	0.3385	10.36
PFMR	75.3744	0.1914	53.5445	0.5546	14.96
PFSR	61.0124	0.2246	35.4581	0.6840	37.88

all, SQRA and EnSRF seem to be the most efficient for assimilating GRACE data into W3RA.

The correlations between model estimations and OzNet data also indicate the superiority of the successful methods in previous assessments (Table 4). Note that considering the difference between W3RA estimations (i.e., column water storage measured in mm) and the OzNet measurements (i.e., volumetric soil moisture) and the fact that converting the model output into volumetric units may introduce bias (Renzullo et al., 2014), only correlation analysis is assumed here. After estimating correlations for each individual layer, we determine an average correlation for the total soil column (cf. Table 4). The higher correlations are found in anal-

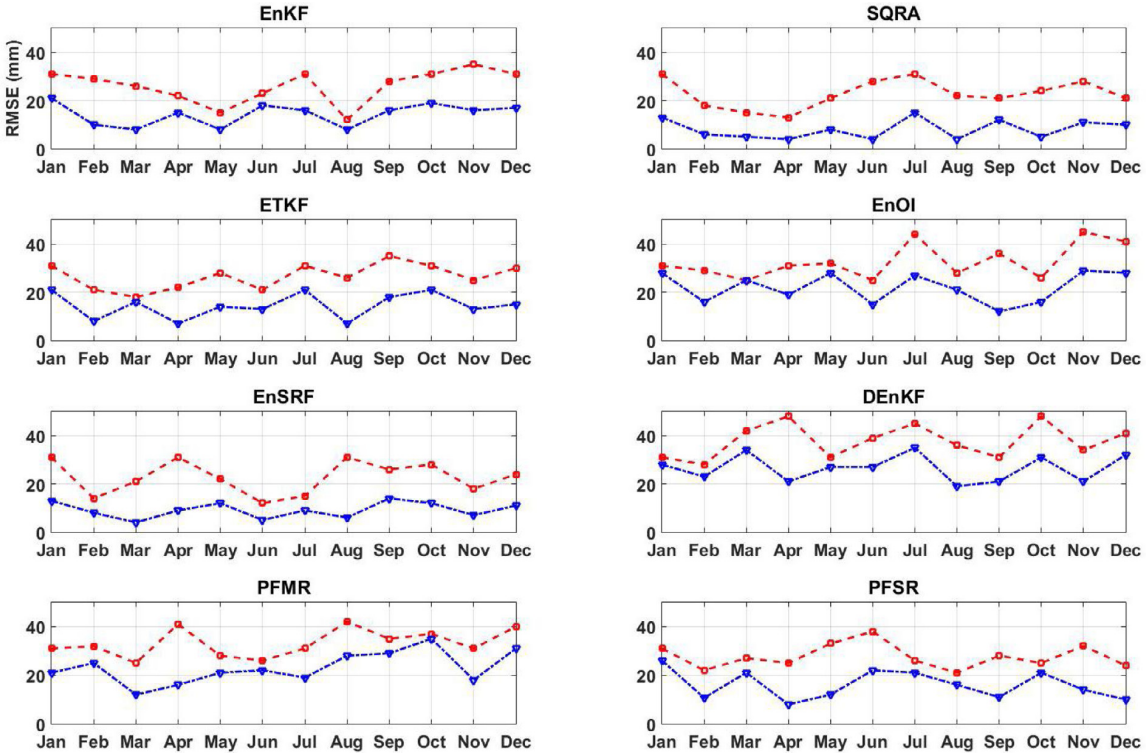

Fig. 5. RMSE time series between the assimilated GRACE TWS and the filters' forecasts and analyses which are calculated over all grid points at the forecast (red) and analysis (blue) steps and their averages at each month (during the study period) are shown here. (For interpretation of the references to color in this figure legend, the reader is referred to the web version of this article.)

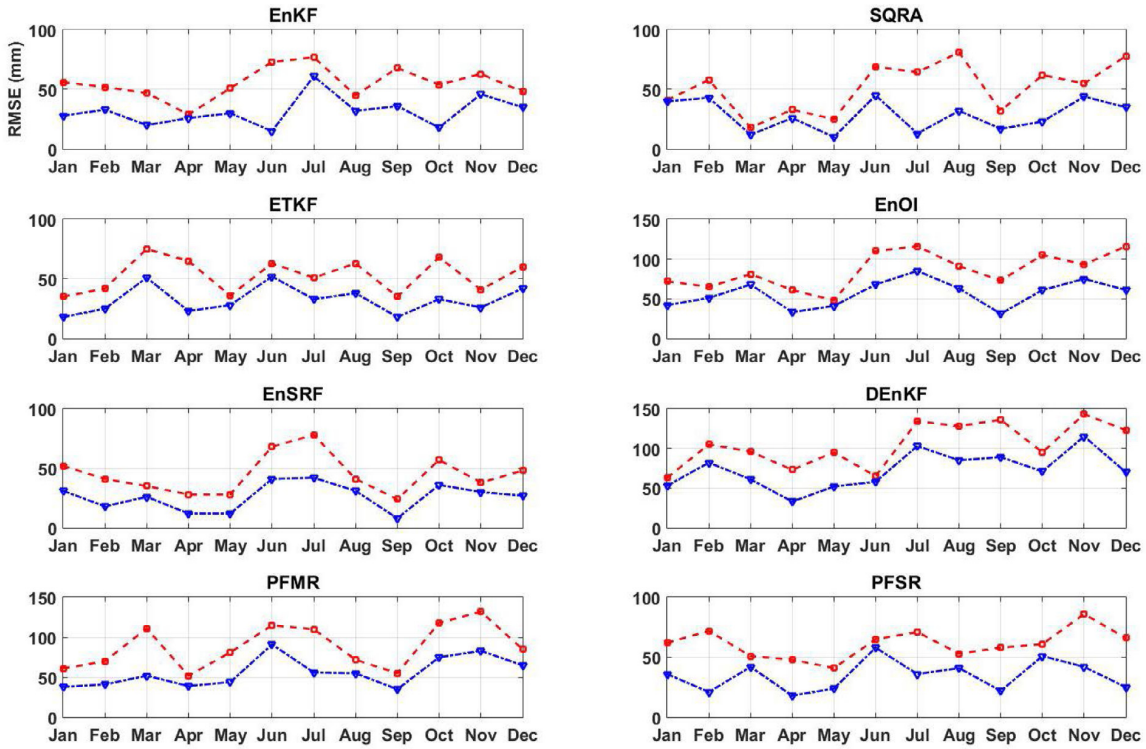

Fig. 6. Same as Fig. 5, but for the in-situ groundwater measurements and the filters estimates. (For interpretation of the references to color in this figure, the reader is referred to the web version of this article.)

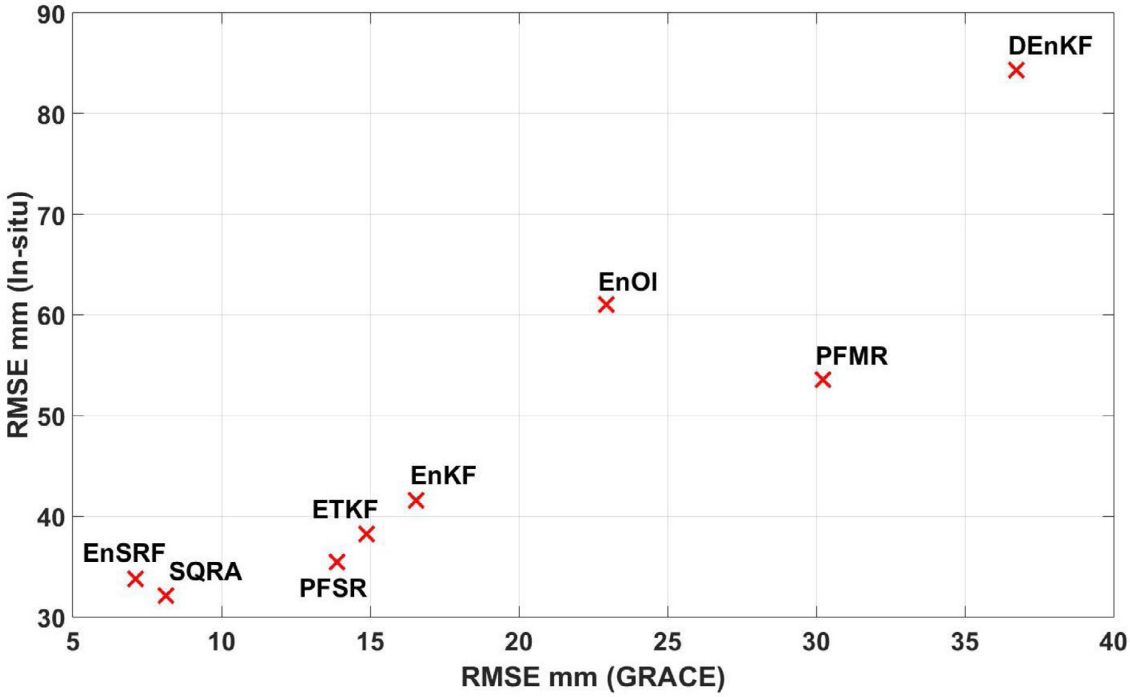

Fig. 7. Comparison between the computed average RMSEs of assimilation results from each applied filter using GRACE and the groundwater in-situ datasets. This figure presents the average of the best performances of the filters at the analysis steps from both assessments against GRACE and groundwater in-situs.

Table 4
A summary of the average correlations between state estimates derived from implemented methods and the soil moisture in-situ measurements. The improvements in the analysis state estimates are calculated using the in-situ measurements in comparison to the model-free run.

Method	Forecast	Analysis	Improvement (%)
EnKF	0.6248	0.7824	25.22
SQRA	0.6524	0.8216	35.93
ETKF	0.6412	0.8003	28.81
EnOI	0.5706	0.6940	21.63
EnSRF	0.6331	0.8431	38.17
DEnKF	0.4867	0.5754	18.22
PFMR	0.5574	0.6835	22.62
PFSR	0.6128	0.7568	32.50

ysis steps with the average of 74% in comparison to forecast steps (59%). The highest correlation to the OzNet soil moisture measurements belongs to EnSRF with R^2 0.84. SQRA also demonstrate a significant impact on model estimations with the 35% correlation improvement. The weakest performance with R^2 0.48 and 0.57 in forecast and analysis step respectively, is achieved from DEnKF. These results prove the capability of EnSRF and SQRA in improving non-assimilated model states through data assimilation.

4.2. Error analysis

Analyzing the filters sampled error covariance, particularly the ensemble spread is important to understand the filters behaviors and performances. The performance of ensemble-based filters relies on their ability to represent and propagate the error statistics, which of course depends on how the ensemble members are sampled and updated at the analysis steps (Sun et al., 2009). We assess the evolution of the ensemble spread and the error covariance matrix during the study period. An efficient filtering method should be able to preserve the variation of its ensemble to properly span the error sub-space. Error covariance matrices are analyzed in terms of estimated errors and correlations.

One important aspect of a filter performance refers to its ability to sample representative ensembles (or particles) at the analysis steps. Fig. 8 outlines how the different filtering techniques adjust the ensemble members during the assimilation procedure. The average TWS variations time series over Australia and their ensembles at the analysis steps are calculated for all filters (Fig. 8).

Several important points can be made from the evolution of ensembles in the assimilation period (Fig. 8). Firstly, most of the filters generate ensembles mean (red lines) close to the assimilated observations suggesting that the filters provide good estimates of the observed variables. However, one should also consider the distribution of the ensemble members. Those of EnKF, SQRA, ETKF, EnSRF, and PFSR are consistent over time, which suggests the robustness of these techniques over time. The ensemble members, especially those of the EnSRF and SQRA, are evenly distributed around the mean, implying a good coverage of the error sub-space. The ensembles distribution for DEnKF and EnOI, on the other hand, are different and exhibit an excessively large spread. In most of the cases, the range of the ensemble concentration in DEnKF and EnOI are either misplaced or overestimated. This would result in underestimating the forecast error and possibly inaccurate assimilation results. In the case of PF, the Systematic Resampling technique seems to be more robust; the PFMR ensembles and their variation (black dashed lines) span an unrealistically wide range space, even though the mean appears fairly close to the observations.

More information can be inferred about the filters ensemble distributions by evaluating the ensembles skewness and kurtosis. These indicate the departure of the ensembles distributions from a Gaussian distribution (with a skewness 0 and a kurtosis 3). Kurtosis quantifies the distribution shape (i.e., heavy-tailed or light-tailed, in comparison to a normal distribution) and skewness measures the distribution asymmetry. The average (forecast and anal-

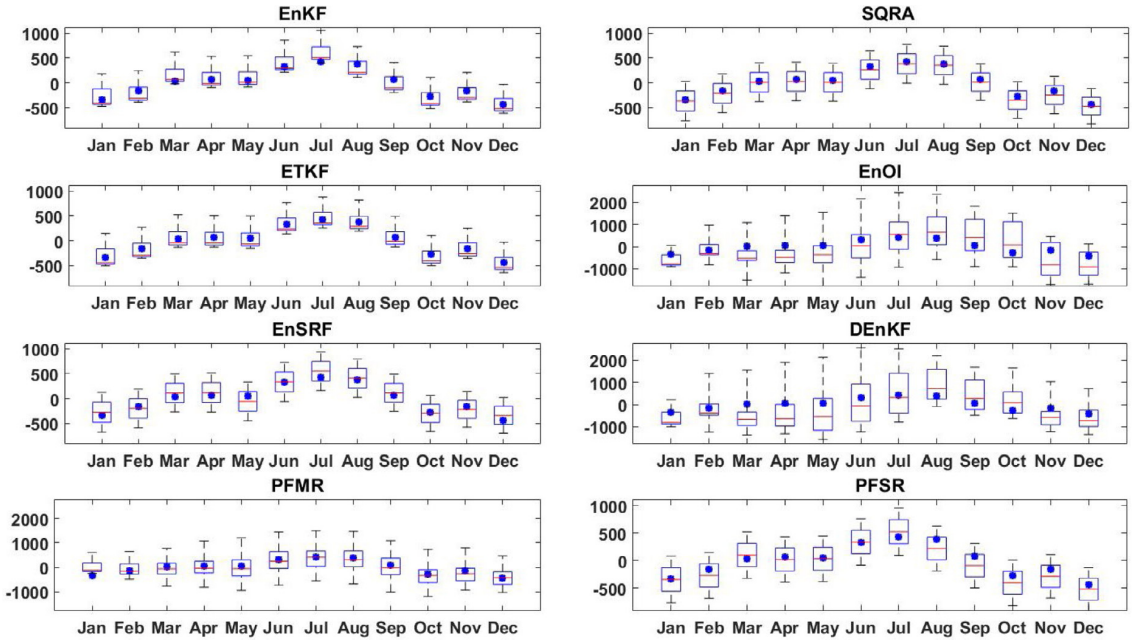

Fig. 8. The average TWS variation of ensembles during at the assimilation steps represent by black dashed lines for each filtering method (units are mm). The blue boxes are the ensemble concentrations and horizontal red lines show the median values of the ensembles at each analysis step. (For interpretation of the references to color in this figure legend, the reader is referred to the web version of this article.)

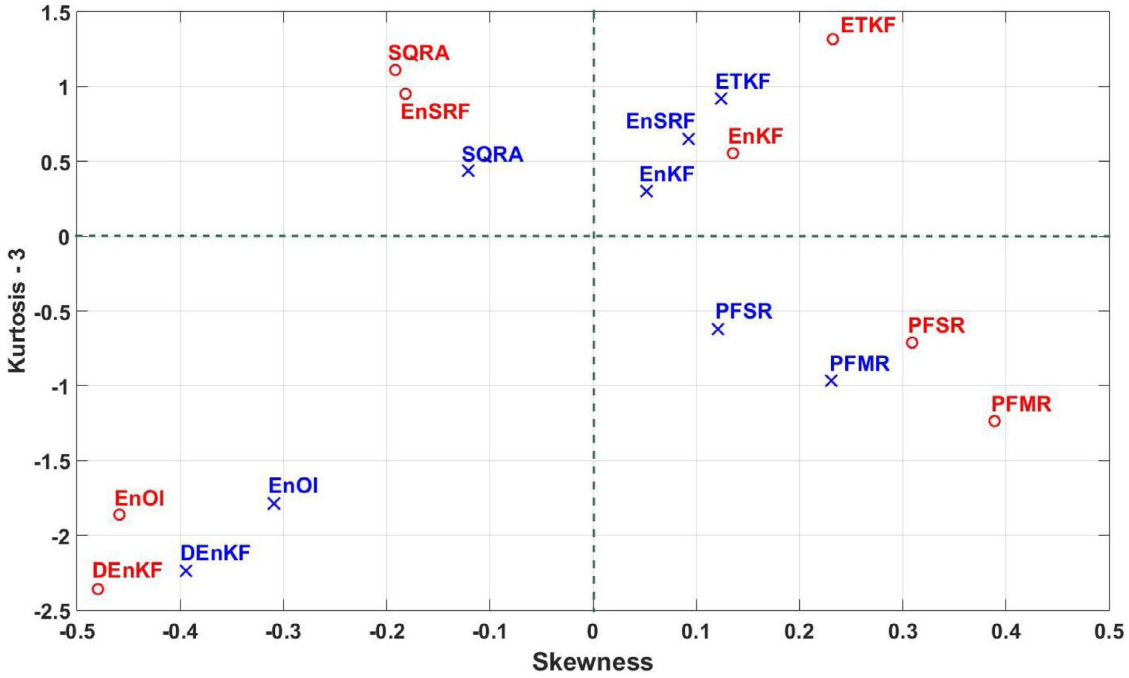

Fig. 9. Comparison between the average skewness and kurtosis of each filter for forecast (red circles) and analysis (blue crosses) steps. Note that a normal distribution has a kurtosis of 3 and uses as a reference so the excess kurtosis is usually presented by kurtosis-3. (For interpretation of the references to color in this figure legend, the reader is referred to the web version of this article.)

ysis) ensembles skewness and kurtosis of all filters (Fig. 9) show skewness and kurtosis are reduced after analysis steps for all filters, suggesting that the filters posterior become closer to Gaussian as assimilation proceeds. This is, however, more pronounced for skewness than for kurtosis, showing the filters higher impact on the ensembles distribution asymmetry. The stochastic EnKF ensemble is closer to a Gaussian distribution, which is related to the application of random noises to the observation (Hoteit et al., 2015). In contrast, the DEnKF and EnOI ensembles are not uniformly distributed, showing a remarkable departure from Gaussian distributions that is expected to introduce bias in the assimilation results.

As another evaluation of the filter performance, we further investigate how the model state error covariance changes over time for each filter. The forecast and analysis error covariance matrices

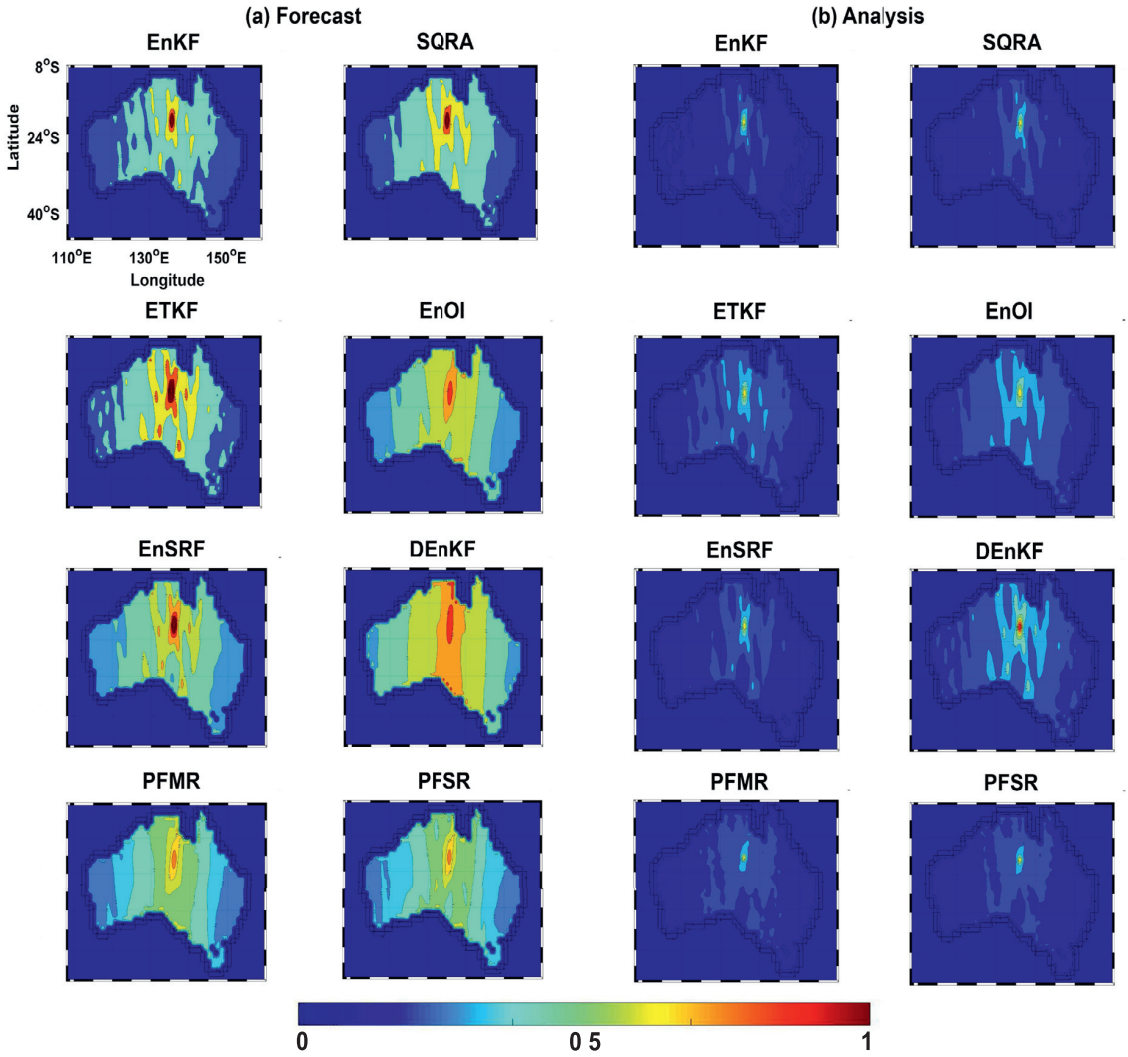

Fig. 10. 2-D representation of correlation coefficients of TWS estimated between the arbitrary point (136.6854°E and 23.9015°S) and the rest of the grid points from the covariance matrices. The temporal average of the computed correlation coefficients in forecast and analysis steps are presented.

Table 5
Effects of filtering methods on the model state covariance matrix as a percentage improvement.

	Method							
	EnKF	SQRA	ETKF	EnOI	EnSRF	DEnKF	PFMR	PFSR
Error reduction (%)								
Minimum	29	35	22	15	34	6	18	28
Maximum	47	52	44	38	55	20	35	48
Average	35	**44**	33	21	**47**	8	27	**38**

at the analysis step indicate how errors change over time, especially after assimilation. We perform two analyses to investigate the influence of the filtering methods on the forecast and analysis error statistics. First, the reductions of error (diagonal elements) in the analysis covariance matrices in comparison to the forecast covariance matrices are calculated at each assimilation step. Next, their minimum, maximum, and average are calculated. The results show how different methods can decrease the errors using GRACE data (Table 5). All the filters reduce errors, where the best performance resulting from SQRA, EnSRF, and, to a less degree, PFSR. Again, DEnKF and EnOI show the weakest effects on error covariance.

Further insights can be derived from the correlation between the estimated states on the grid points of the study area. For this, 794 grid-points over Australia are considered and the spatial correlation coefficients are computed between each of them and the rest of the points in the assimilation steps. In most of the cases (95%), data assimilation significantly decrease the correlation between grid points in the analysis error covariance matrices. As an example, an arbitrary point approximately in the middle of the study area (for a better visual representation) at the location

136.6854°E and 23.9015°S is chosen and its spatial correlation with the other grid points are plotted to show this effect. The average of spatial correlation map for all assimilation steps and for each filter is presented in Fig. 10. Similar results are achieved for the other grid points.

One can see from Fig. 10 that each filtering method affects the correlation between the specific point and the others differently where some filters like PFs show higher ability to decrease the correlations between errors. This can be related to the native of the algorithm of PF, which produces random particles that are consistent with model nonlinear dynamics. The results of the correlation analysis (cf. Fig. 10) are consistent with the other results, with DEnKF and EnOI showing the less ability to reduce errors, also having the least influence on the correlations. These results, along with the outcomes of the ensemble distribution analysis (cf. Figs. 8 and 9), demonstrate the effect of successful ensemble generation on estimated errors. The filters (e.g., EnKF, SQRA, and EnSRF) with the higher ability to sample representative ensembles lead to the less estimation errors as well as correlations in contrast to the other filters, especially DEnKF and EnOI.

Only a few filters show a good performance in both analyses. These filters, SQRA, and EnSRF, not only improve the model state estimates compared to GRACE data and the (groundwater level and soil moisture) in-situ measurements but also efficiently decrease the ensemble spread and spatial correlation errors. The resulting estimates of groundwater storage further exhibit less RMSE against independent groundwater level in-situ data.

5. Summary and conclusions

There is evidence that different filter types are more suited to different applications (Reichle et al., 2002). This study considered the implementation of different data assimilation filtering techniques based on the two most commonly applied algorithms, ensemble Kalman, and Particle filter, to assess their performances for assimilating GRACE data into the hydrological model of W3RA. GRACE-derived TWS over Australia was assimilated into the W3RA hydrological model using the various filters. Among the ensemble Kalman filters, we tested the stochastic and the deterministic schemes (EnSRF, ETKF, SQRA, DEnKF, and EnOI) along with two different resampling approaches of Particle filters (PFMR and PFSR). The effects of the filtering methods on the ensembles spread and the estimation error covariance matrices were investigated. The most promising results are obtained using SQRA, EnSRF, and EnKF, both in terms of ensemble generation as well as in dealing with the estimation error covariance matrices. The greatest error reduction with minimum error covariance is achieved by EnSRF (47% average) and SQRA (44% average). These two filters (along with EnKF) also show a good ability to sample representative ensembles with enough spread. The filters state estimates were evaluated against GRACE data, in-situ groundwater measurements, and in-situ soil moisture data. While improvements in the state estimations are observed for all implemented filters, the best results are obtained with, respectively, SQRA (75% correlation to the groundwater level in-situ measurements and 82% correlation to OzNet soil moisture network), EnSRF (42% error reduction), PFSR (37% error reduction) and slightly less successful ETKF (33% error reduction). In contrast, DEnKF was the least successful in dealing with error covariance matrices and suggested a larger error in the state estimates. SQRA and EnSRF, which efficiently dealt with the error covariances, provided the least RMSEs (32.14 mm and 33.74 mm) and maximum correlations to both groundwater level and soil moisture in-situ measurements. These two filters demonstrated a high capability in assimilating GRACE data. GRACE TWS fields are unique in term of resolution, both spatially (almost 3 times rougher than the model) and temporally (monthly). The weak spatial resolution also affects the observation error covariance structure by increasing the correlation between neighboring grid points when working with a fine (e.g., $1° \times 1°$) grid. Therefore assimilating such a dataset could be challenging requiring a filter that is robust to the system error covariances and also powerful in term of resampling representative ensembles after every assimilation step. However, a general conclusion on the preference of ensemble filters might not be possible from this study due to model-specific and application-specific characteristics. Thus, further research might be undertaken to investigate various aspects of filters in different hydrological applications and to explore other filters like new designed PFs that were not considered here.

Acknowledgement

M. Khaki is grateful for the research grant of Curtin International Postgraduate Research Scholarships (CIPRS)/ORD Scholarship provided by Curtin University (Australia). This work is a TIGeR publication.

References

Anderson, J., 2001. An ensemble adjustment Kalman filter for data assimilation. Mon. Weather Rev. 129, 2884–2903. http://dx.doi.org/10.1175/1520-0493(2001)129(2884:AEAKFF)2.0.CO;2.

Alsdorf, D.E., Rodriguez, E., Lettenmaier, D.P., 2007. Measuring surface water from space. Rev. Geophys. 45. RRG2002, 1–24, http://dx.doi.org/10.1029/2006RG000197.

Altaf, M.U., Butler, T., Mayo, T., Luo, X., Dawson, C., Heemink, A.W., Hoteit, I., 2014. A comparison of ensemble Kalman filters for storm surge assimilation. Mon. Weather Rev. 142 (8), 2899–2914.

Anderson, J., Anderson, S., 1999. A Monte Carlo implementation of the nonlinear filtering problem to produce ensemble assimilations and forecasts. Mon. Weather Rev. 127, 2741–2758.

Anderson, M.C., Norman, J.M., Mecikalski, J.R., Otkin, J.A., Kustas, W.P., 2007. A climatological study of evapotranspiration and moisture stress across the continental United States based on thermal remote sensing: 1. Model formulation. J. Geophys. Res. 112. D10117, 1–17, http://dx.doi.org/10.1029/2006JD007506.

Arulampalam, M.S., Maskell, S., Gordon, N., Clapp, T., 2002. A tutorial on particle filters for online nonlinear/non-Gaussian Baysian tracking. IEEE Trans. Signal Process. 50 (2), 174–188.

Awange, J., Sharifi, M., Baur, O., Keller, W., Featherstone, W., Kuhn, M., 2009. GRACE hydrological monitoring of australia: current limitations and future prospects. J. Spat. Sci. 54 (1), 23–35.

Bennett, A.F., 2002. Inverse Modeling of the Ocean and Atmosphere. Cambridge University Press, New York. 234

Bergemann, K., Reich, S., 2010. A mollified ensemble Kalman filter. Q. J. R. Meteorol. Soc. 136, 1636–1643. http://dx.doi.org/10.1002/qj.672.

Bertino, L., Evensen, G., Wackernagel, H., 2003. Sequential data assimilation techniques in oceanography. Int. Stat. Rev. 71 (2), 223–241. 2003.

Bishop, C.H., Etherton, B., Majumdar, S.J., 2001. Adaptive sampling with the ensemble transform Kalman filter, part I: theoretical aspect. Mon. Weather Rev. 129, 420–436.

Brocca, L., Melone, F., Moramarco, T., Wagner, W., Naeimi, V., Bartalis, Z., Hasenauer, S., 2010. Improving runoff prediction through the assimilation of the ASCAT soil moisture product. Hydrol. Earth Syst. Sci. 14, 1881–1893. http://dx.doi.org/10.5194/hess-14-1881-2010.

Brown, N.J., Tregoning, P., 2010. Quantifying GRACE data contamination effects on hydrological analysis in the Murray–Darling basin, Southeast Australia. Aust. J. Earth Sci. 57 (3), 329–335. http://dx.doi.org/10.1080/08120091003619241.

Chen, J.L., Wilson, C.R., Famiglietti, J.S., Rodell, M., 2007. Attenuation effect on seasonal basin-scale water storage changes from GRACE time-variable gravity. J. Geodesy 81 (4), 237–245. http://dx.doi.org/10.1007/s00190-006-0104-2.

Cheng, M.K., Tapley, B.D., 2004. Variations in the Earth's oblateness during the past 28 years. J. Geophys. Res. 109. B09402, 2156–2202, http://dx.doi.org/10.1029/2004JB003028.

Chiew, F.H.S., Stewardson, M.J., McMahon, T.A., 1993. Comparison of six rainfall-runoff modelling approaches. J. Hydrol. 147, 1–36.

Christiansen, L., Krogh, P.E., Bauer-Gottwein, P., Andersen, O.B., Leirio, S., Binning, P.J., Rosbjerg, D., 2007. Local to regional hydrological model calibration for the Okavango River Basin from in-situ and space borne gravity observations. In: Proceedings of Second Space for Hydrology Workshop, Geneva, Switzerland, pp. 12–14.

Coumou, D., Rahmstorf, S., 2012. A decade of weather extremes. Nat. Clim. Change 2 (7), 16.

Courtier, P., Thpaut, J.N., Hollingsworth, A., 1994. A strategy for operational implementation of 4DVAR using an incremental approach. Q. J. R. Meteor. Soc. 120, 1367–1387.

van Dijk, A. I. J. M., 2010. The Australian Water Resources Assessment System: Technical Report 3, Landscape Model (version 0.5) Technical Description, CSIRO: Water for a Healthy Country National Research Flagship.
van Dijk, A.I.J.M., Pea-Arancibia, J.L., Wood, E.F., Sheffield, J., Beck, H.E., 2013. Global analysis of seasonal streamflow predictability using an ensemble prediction system and observations from 6192 small catchments worldwide. Water Resour. Res. 49, 2729–2746. http://dx.doi.org/10.1002/wrcr.20251.
van Dijk, A.I.J.M., Renzullo, L.J., Rodell, M., 2011. Use of gravity recovery and climate experiment terrestrial water storage retrievals to evaluate model estimates by the Australian water resources assessment system. Water Resour. Res. 47, W11524. http://dx.doi.org/10.1029/2011WR010714.
van Dijk, A.I.J.M., Renzullo, L.J., Wada, Y., Tregoning, P., 2014. A global water cycle reanalysis (2003–2012) merging satellite gravimetry and altimetry observations with a hydrological multi-model ensemble. Hydrol. Earth Syst. Sci. 18, 2955–2973. http://dx.doi.org/10.5194/hess-18-2955-2014.
Doll, P., Kaspar, F., Lehner, B., 2003. A global hydrological model for deriving water availability indicators: model tuning and validation. J. Hydrol. 270, 105–134.
Doucet, A., 1998. On Sequential Simulation-based Methods for Bayesian Filtering. Technical report CUED/F-INFENG/TR 310. Department of Engineering, Cambridge University, Cambridge, UK..
Doucet, A., Cappe, O., Moulines, E., 2005. Comparison of resampling schemes for particle filtering. In: Proceedings of the Fourth International Symposium on Image and Signal Processing and Analysis (ISPA).
Doucet, A., Freitas, N., Gordon, N., 2001. Sequential Monte Carlo methods in practice. Springer-Verlag, New York.
Eicker, A., Schumacher, M., Kusche, J., Dll, P., Mller-Schmied, H., 2014. Calibration/data assimilation approach for integrating GRACE data into the waterGAP global hydrology model (WGHM) using an ensemble Kalman filter: first results. Surv. Geophys. 35 (6), 1285–1309. http://dx.doi.org/10.1007/s10712-014-9309-8.
Elbern, H., Schmidt, H., 2001. Ozone episode analysis by four dimensional variational chemistry data assimilation. J. Geophys. Res. 106, 3569–3590.
Evensen, G., 1994. Sequential data assimilation with a nonlinear quasi-geostrophic model using Monte Carlo methods to forecast error statistics. J. Geophys. Res. 99, 10143–10162. http://dx.doi.org/10.1029/94JC00572.
Evensen, G., 2003. The ensemble Kalman filter: theoretical formulation and practical inplementation. Ocean Dyn. 53, 343–367. http://dx.doi.org/10.1007/s10236-003-0036-9.
Evensen, G., 2004. Sampling strategies and square root analysis schemes for the enKF. Ocean Dyn. 54 (6), 539–560.
Evensen, G., 2007. Data Assimilation: The Ensemble Kalman Filter. Springer 279.
Evensen, G., 2009. Data Assimilation: The Ensemble Kalman Filter. second ed.. Springer, Berlin Heidelberg.
Forootan, E., Awange, J., Kusche, J., Heck, B., Eicker, A., 2012. Independent patterns of water mass anomalies over australia from satellite data and models. J. Remote Sens. Environ. 124, 427–443. http://dx.doi.org/10.1016/j.rse.2012.05.023.
Forootan, E., Didova, O., Schumacher, M., Kusche, J., Elsaka, B., 2014. Comparisons of atmospheric mass variations derived from ECMWF reanalysis and operational fields, over 2003 to 2011. J. Geodesy 88, 503–514. http://dx.doi.org/10.1007/s00190-014-0696-x.
Forootan, E., Khandu, Awange, J., Schumacher, M., Anyah, R., vanDijk, A., Kusche, J., 2016. Quantifying the impacts of ENSO and IOD on rain gauge and remotely sensed precipitation products over Australia. Remote Sens. Environ. 172, 50–66. http://dx.doi.org/10.1016/j.rse.2015.10.027.
Garner, T.W., Wolf, R.A., Spiro, R.W., Thomsen, M.F., 1999. First attempt at assimilating data to constrain a magnetospheric model. J. Geophys. Res. 104 (A11), 25145–25152. http://dx.doi.org/10.1029/1999JA900274.
Giustarini, L., Matgen, P., Hostache, R., Montanari, M., Plaza, D., Pauwels, V.R.N., DeLannoy, G.J.M., De Keyser, R., Pfister, L., Hoffmann, L., Savenije, H.H.G., 2011. Assimilating SAR-derived water level data into a hydraulic model: a case study. Hydrol. Earth Syst. Sci. 15, 23492365. http://dx.doi.org/10.5194/hess-15-2349-2011.
Gordon, N.J., Salmond, D.J., Smith, A.F.M., 1993. Novel approach to nonlinear/non-Gaussian Bayesian state estimation. IEE Proc. F 140, 107–113.
Hamill, T.M., Snyder, C., 2002. Using improved background-error covariances from an ensemble Kalman filter for adaptive observations. Mon. Weather Rev. 130, 1552–1572. http://dx.doi.org/10.1175/1520-0493(2002)130⟨1552:UIBECF⟩2.0.CO;2.
Hol, J.D., Schon, T.B., Gustafsson, F., 2006. On resampling algorithms for particle filters. In: Proceedings of the 2006 IEEE Nonlinear Statistical Signal Processing Workshop, Cambridge, UK, 2006, pp. 79–82. http://dx.doi.org/10.1109/NSSPW.2006.4378824.
Hoteit, I., Luo, X., Pham, D.T., 2012. Particle Kalman filtering: a nonlinear Bayesian framework for ensemble Kalman filters. Mon. Weather Rev. 140 (2), 528–542.
Hoteit, I., Pham, D.T., Blum, J., 2002. A simplified reduced order Kalman filtering and application to altimetric data assimilation in tropical pacific. J. Mar. Syst. 36, 101–127.
Hoteit, I., Pham, D.T., Gharamti, M.E., Luo, X., 2015. Mitigating observation perturbation sampling errors in the stochastic enKF. Mon. Weather Rev. 143 (7), 2918–2936.
Hoteit, I., Pham, D.T., Triantafyllou, G., Korres, G., 2008. A new approximate solution of the optimal nonlinear filter for data assimilation in meteorology and oceanography. Mon. Weather Rev. 136, 317–334.
Hoteit, I., Triantafyllou, G., Petihakis, G., 2005. Efficient data assimilation into a complex, 3-d physical-biogeochemical model using partially-local Kalman filters. Ann. Geophys. Eur. Geosci. Union 23 (10), 3171–3185.
Houborg, R., Rodell, M., Li, B., Reichle, R.H., Zaitchik, B.F., 2012. Drought indicators based on model-assimilated gravity recovery and climate experiment (GRACE) terrestrial water storage observations. Water Resour. Res. 48. W07525, 1–17, http://dx.doi.org/10.1029/2011WR011291.
Houtekamer, P.L., Mitchell, H.L., 2001. A sequential ensemble Kalman filter for atmospheric data assimilation. Mon. Weather Rev. 129 (1), 123–137.
Huang, S., Kumar, R., Flŋrke, M., Yang, T., Hundecha, Y., Kraft, P., Gao, C., Gelfan, A., Liersch, S., Lobanova, A., Strauch, M., Ogtrop, F.V., Reinhardt, J., Haberlandt, U., Krysanova, V., 2016. Evaluation of an ensemble of regional hydrological models in 12 large-scale river basins worldwide. Clim. Change. 141 (3), 381–397. http://dx.doi.org/10.1007/s10584-016-1841-8.
Huntington, T.G., 2006. Evidence for intensification of the global water cycle: review and synthesis. J. Hydrol. 319 (1–4), 83–95. http://dx.doi.org/10.1016/j.jhydrol.2005.07.003.
Jazwinski, A.H., 1970. Stochastic Processes and Filtering Theory. Academic Press, p. 376.
Kalman, R. E., 1960. A new approach to linear filtering and prediction problems. J. Basic Eng. Transactions of the ASME, 82 (Series D): 35-45.
Kalnay, E., 2003. Atmospheric Modelling, Data Assimilation and Predictability. Cambridge University Press. http://dx.doi.org/10.1256/00359000360683511. Xxii 341. ISBNs 0 521 79179 0, 0 521 79629 6
Klees, R., Revtova, E.A., Gunter, B.C., Ditmar, P., Oudman, E., Winsemius, H.C., 2008. The design of an optimal filter for monthly GRACE gravity models. Geophys. J. Int. 175 (2), 417–432. http://dx.doi.org/10.1111/j.1365-246X.2008.03922.x.
Koch, K.R., 2007. Introduction to Bayesian Statistics, second ed. Springer.
Lahoz, W.A., Geer, A.J., Bekki, S., Bormann, N., Ceccherini, S., Elbern, H., Errera, Q., Eskes, H.J., Fonteyn, D., Jackson, D.R., Khattatov, B., 2007. The assimilation of Envisat data (ASSET) project. Atmos. Chem. Phys. 7, 1773–1796.
van Leeuwen, P.J., Evensen, G., 1996. Data assimilation and inverse methods in terms of a probabilistic formulation. Mon. Weather Rev. 124, 2898–2913.
Mayer-Gurr, T., Zehentner, N., Klinger, B., Kvas, A., 2014. ITSG-Grace2014: a new GRACE gravity field release computed in Graz in: Proceedings of the 2014 GRACE Science Team Meeting (GSTM), Potsdam am: 29.09.2014.
McLaughlin, D., 2002. An integrate approach to hydrologic data assimilation: interpolation, smoothing, and filtering. Adv. Water Resour. 25, 1275–1286.
Moradkhani, H., DeChant, C.M., Sorooshian, S., 2012. Evolution of ensemble data assimilation for uncertainty quantification using the particle filter-Markov chain Monte Carlo method. Water Resour. Res. 48. W12520, 1–13.
Moradkhani, H., Hsu, K.L., Gupta, H., Sorooshian, S., 2005. Uncertainty assessment of hydrologic model states and parameters: sequential data assimilation using the particle filter. Water Resour. Res. 41. W05012, 1–17.
Neal, J., Schumann, G., Bates, P., Buytaert, W., Matgen, P., Pappenberger, F., 2009. A data assimilation approach to discharge estimation from space. Hydrol. Process. 23, 3641–3649.
Nerger, L., 2004. Parallel Filter Algorithms for Data Assimilation in Oceanography. Ph.D. thesis. University of Bremen.
Oke, P.R., Brassington, G.B., Griffin, D.A., Schiller, A., 2008. The bluelink ocean data assimilation system (BODAS). Ocean Model. 21, 46–70. http://dx.doi.org/10.1016/j.ocemod.2007.11.002.
Oke, P.R., Sakov, P., Corney, S.P., 2007. Impacts of localisation in the enKF and enOI: experiments with a small model. Ocean Dyn. 57, 32–45.
Ott, E., Hunt, B.R., Szunyogh, I., Zimin, A.V., Kostelich, E.J., Corazza, M., Kalnay, E., Patil, D.J., Yorke, J.A., 2004. A local ensemble Kalman filter for atmospheric data assimilation. Tellus 56A, 415–428.
Pham, D.T., 2001. Stochastic methods for sequential data assimilation in strongly nonlinear systems. Mon. Weather Rev. 129, 1194–1207.
Plaza, D.A., Keyser, R., Lannoy, G.J.M., Giustarini, L., Matgen, P., Pauwels, V.R.N., 2012. The importance of parameter resampling for soil moisture data assimilation into hydrologic models using the particle filter. Hydrol. Earth Syst. Sci. 16 (2), 375–390.
Reager, J.T., Thomas, A.C., Sproles, E.A., Rodell, M., Beaudoing, H.K., Li, B., Famiglietti, J.S., 2015. Assimilation of GRACE terrestrial water storage observations into a land surface model for the assessment of regional flood potential. Remote Sens. 2015 (7), 14663–14679.
Reichle, R.H., McLaughlin, D.B., Entekhabi, D., 2002. Hydrologic data assimilation with the ensemble Kalman filter. Mon. Weather Rev. 130, 103–114. http://dx.doi.org/10.1175/1520-0493(2002)130⟨0103:HDAWTE⟩2.0.CO;2.
Renzullo, L.J., VanDijk, A.I.J.M., Perraud, J.M., Collins, D., Henderson, B., Jin, H., Smith, A.B., McJannet, D.L., 2014. Continental satellite soil moisture data assimilation improves root-zone moisture analysis for water resources assessment. J. Hydrol. 519, 2747–2762. http://dx.doi.org/10.1016/j.jhydrol.2014.08.008.
Robert, C., Blayo, E., Verron, J., 2006. Comparison of reduced-order, sequential and variational data assimilation methods in the tropical pacific ocean. Ocean Dyn. 56 (624), 624–633. http://dx.doi.org/10.1007/s10236-006-0079-9.
Rodell, M., Chen, J., Kato, H., Famiglietti, J.S., Nigro, J., Wilson, C.R., 2007. Estimating groundwater storage changes in the mississippi river basin (USA) using GRACE. Hydrogeol. J. 15, 159–166.
Sakov, P., Oke, P.R., 2008. A deterministic formulation of the ensemble Kalman filter: an alternative to ensemble square root filters. Tellus 60A, 361–371.
Schumacher, M., Kusche, J., Dll, P., 2016. A systematic impact assessment of GRACE error correlation on data assimilation in hydrological models. J. Geodesy 90 (6), 537–559. http://dx.doi.org/10.1007/s00190-016-0892-y.
Schunk, R.W., Scherliess, L., Sojka, J.J., Thompson, D.C., Bloom, H.J., 2004. USU global ionospheric data assimilation models. In: Huang, H.-L. A. (Ed.), Proceeding of the 2004 SPIE on Atmospheric and Environmental Remote Sensing Data Pro-

cessing and Utilization: An End-to-End System Perspective, 5548, pp. 327–336. http://dx.doi.org/10.1117/12.562448.
Seoane, L., Ramillien, G., Frappart, F., Leblanc, M., 2013. Regional GRACE-based estimates of water mass variations over australia: validation and interpretation. Hydrol. Earth Syst. Sci. 17, 4925–4939. http://dx.doi.org/10.5194/hess-17-4925-2013.
Sheffield, J., Goteti, G., Wood, E.F., 2006. Development of a 50-year high-resolution global dataset of meteorological forcing for land surface modeling. J. Clim. 19 (13), 3088–3111.
Smith, A.B., Walker, J.P., Western, A.W., Young, R.I., Ellett, K.M., Pipunic, R.C., Richter, H., 2012. The Murrumbidgee soil moisture monitoring network data set. Water Resour. Res. 48 (7), 1–6. http://dx.doi.org/10.1029/2012WR011976.
Smith, P.J., Beven, K.J., Tawn, J.A., 2008. Detection of structural inadequacy in process-based hydrological models: a particle-filtering approach. Water Resour. Res. 44, W01410. http://dx.doi.org/10.1029/2006WR005205.
Subramanian, A.C., Hoteit, I., Cornuelle, B., Miller, A.J., Song, H., 2012. Linear versus nonlinear filtering with scale-selective corrections for balanced dynamics in a simple atmospheric model. Atmos.Sci. 69 (11), 3405–3419.
Sun, Y.A., Morris, A., Mohanty, S., 2009. Comparison of deterministic ensemble Kalman filters for assimilating hydrogeological data. Adv. Water Resour. 32 (2), 280–292. http://dx.doi.org/10.1016/j.advwatres.2008.11.006. ISSN 0309-1708
Swenson, S., Chambers, D., Wahr, J., 2008. Estimating geocenter variations from a combination of GRACE and ocean model output. J. Geophys. Res. 113, B08410. http://dx.doi.org/10.1029/2007JB005338.
Swenson, S., Wahr, J., 2002. Methods for inferring regional surface-mass anomalies from gravity recovery and climate experiment (GRACE) measurements of time-variable gravity. J. Geophys. Res. 107 (B9), 2193. http://dx.doi.org/10.1029/2001JB000576.
Swenson, S., Wahr, J., 2006. Post-processing removal of correlated errors in GRACE data. Geophys. Res. Lett. 33, L08402. http://dx.doi.org/10.1029/2005GL025285.
Talagrand, O., Courtier, P., 1987. Variational assimilation of meteorological observations with the adjoint vorticity equation – Part 1. Theory Q. J. R. Meteorol. Soc. 113, 1311–1328.
Tangdamrongsub, N., Steele-Dunne, S.C., Gunter, B.C., Ditmar, P.G., Weerts, A.H., 2015. Data assimilation of GRACE terrestrial water storage estimates into a regional hydrological model of the rhine river basin. Hydrol. Earth Syst. Sci. 19, 2079–2100. http://dx.doi.org/10.5194/hess-19-2079-2015.
Tapley, B.D., Bettadpur, S., Watkins, M., Reigber, C., 2004. The gravity recovery and climate experiment: mission overview and early results. Geophys. Res. Lett. 31, L09607. http://dx.doi.org/10.1029/2004GL019920.
Thomas, A.C., Reager, J.T., Famiglietti, J.S., Rodell, M., 2014. A GRACE-based water storage deficit approach for hydrological drought characterization. Geophys. Res. Lett. 41, 1537–1545.
Tippett, M.K., Anderson, J.L., Bishop, C.H., Hamill, T.M., Whitaker, J.S., 2003. Ensemble square root filters. Mon. Weather Rev. 131, 1485–1490.
Tregoning, P., Mc Clusky, S., van Dijk, A.I.J.M., Crosbie, R.S., Pea-Arancibia, J.L., 2012. Assessment of GRACE satellites for groundwater estimation in Australia. National Water Commission, Canberra, 82 pp, ISBN: 978-1-921853-54-8.
Vrugt, J.A., ter Braak, C.J.F., Diks, C.G.H., Schoups, G., 2013. Advancing hydrologic data assimilation using particle Markov chain monte carlo simulation: theory, concepts and applications. Adv. Water Resour. 51, 457–478. Anniversary Issue – 35 Years. http://dx.doi.org/10.1016/j.advwatres.2012.04.002.
Wahr, J., Molenaar, M., 1998. Time variability of the Earth's gravity field' hydrological and oceanic effects and their possible detection using GRACE. J. Geophys. Res. 103 (B12), 205–230. http://dx.doi.org/10.1029/98JB02844.
Whitaker, J.S., Hamill, T.M., 2002. Ensemble data assimilation without perturbed observations. Mon. Weather Rev. 130, 1913–1924.
Wooldridge, S.A., Kalma, J.D., 2001. Regional-scale hydrological modelling using multiple-parameter landscape zones and a quasi-distributed water balance model. Hydrol. Earth Syst. Sci. 5, 59–74.
Zaitchik, B.F., Rodell, M., Reichle, R.H., 2008. Assimilation of GRACE terrestrial water storage data into a land surface model: results for the mississippi river basin. J. Hydrometeorol 9 (3), 535–548. http://dx.doi.org/10.1175/2007JHM951.1.
Zhang, Y., Bocquet, M., Mallet, V., Seigneur, C., Baklanov, A., 2012. Real-time air quality forecasting, part I: history, techniques, and current status. Atmos. Environ. 60, 632–655.

Chapter 6

Data assimilation applications

This chapter is covered by the following publications:

- **Khaki, M.**, Forootan, E., Kuhn, M., Awange, J., Papa, F., Shum, C.K., (2018b). A Study of Bangladesh's Sub-surface Water Storages Using Satellite Products and Data Assimilation Scheme. Science of The Total Environment, 625:963-977, doi:10.1016/j.scitotenv.2017.12.289.

- **Khaki, M.**, Forootan, E., Kuhn, M., Awange, J., van Dijk, A.I.J.M., Schumacher, M., Sharifi, M.A., (2018c). Determining Water Storage Depletion within Iran by Assimilating GRACE data into the W3RA Hydrological Model. Advances in Water Resources, 114:1-18, doi:10.1016/j.advwatres.2018.02.008.

- **Khaki, M.**, Awange, J. (2018d). The Application of Remotely Sensed Products to Enhance Model-derived Water Storage Changes over South America. Revised and resubmitted to Science of The Total Environment.

The application of GRACE data assimilation is further investigated over Bangladesh, Iran, and various basins of South America. This is done to demonstrate the capability of GRACE data assimilation for using non-regional models to study water storage changes in various areas covering the thesis' objective (iv) in Section 1.4. Data assimilation, in addition to improving models performance, allows for separating GRACE TWS into different water compartments based on the physical processes implemented in the model equations. This makes it possible to separately analyze various water compartments, e.g., soil moisture and groundwater, using the improved estimates. The three contributions presented in this chapter discuss the results of GRACE data assimilation within the study areas above. Data assimilation is applied based on the best case scenarios achieved from the results of the previous studies (cf. Chapters 3–5). This includes using two best cases of the Square Root Analysis (SQRA) scheme following Evensen (2004) and the Ensemble Square-Root Filter (EnSRF, Whitaker and Hamill, 2002).

There are, however, differences between the application studies due to the unique characteristics of each region. Over Iran, considering that there are six major drainage divisions covering the whole country and correspondingly the experiment is separated for each division. This allows for a better analysis of drainage divisions to control how they act during assimilation and in terms of water storage changes. Besides, the relationship between sub-surface water storage changes and both climate (e.g., precipitation) and anthropogenic (e.g., farming) impacts are investigated. This is done due to a large impact of human water use on water resources in Iran. Similar to the case of Iran, South America is divided into 15 major basins. Nevertheless, due to the larger impact of climate variabilities, an analysis is applied on data assimilation results to explore the effects of climate indicators including rainfall and El Niño/Southern Oscillation (ENSO) on water storage changes. Moreover, soil moisture observations are assimilated along with GRACE TWS data over South America considering the importance of soil water content within the region. Different scenarios are tested to monitor the impact of this multi-observation data assimilation, which includes GRACE-only data assimilation, Soil moisture data assimilation, and Joint GRACE-soil moisture assimilation. Due to the great impact of surface water storage over South America and particularly Bangladesh, special focus is being invested on this water compartment during data assimilation. Various cases are considered to assess the performance of data assimilation in dealing with surface water storage. For this purpose, the surface storage are treated based on the following cases; (1) Removed surface storages from GRACE TWS, (2) Added surface storages to W3RA surface water, and (3) No surface storage correction applied. Accordingly, the best case scenarios (e.g., case (1)) is used over South America. Furthermore, using the improved estimates, connections between the model-derived sub-surface water storage changes and remotely sensed precipitations, as well as altimetry-derived river level variations, are investigated over Bangladesh.

In each domain, various assessments are considered using independent datasets to ensure the validity of results. It is found that data assimilation in every case successfully reduces mismatches between the ground-based measurements and assimilation estimates. Larger agreements are found between assimilated groundwater and soil moisture and those of in-situs than open-loop (model run without data assimilation) estimates. In Bangladesh, GRACE data assimilation along with the use of satellite radar altimetry lead to better understanding of sub-surface water storage changes. The approach shows a promising performance for estimating groundwater negative trends over most of Iran. The process further helps to improve our knowledge of groundwater and soil moisture spatio-temporal variations over South America's 15 main basins. The enhanced knowledge of water storage changes in each area, e.g., groundwater depletion in Iran and Bangladesh are important to better understand hydrological processes and can be used for water management and agriculture objectives.

Science of the Total Environment 625 (2018) 963–977

Contents lists available at ScienceDirect

Science of the Total Environment

journal homepage: www.elsevier.com/locate/scitotenv

A study of Bangladesh's sub-surface water storages using satellite products and data assimilation scheme

M. Khaki[a,*], E. Forootan[b], M. Kuhn[a], J. Awange[a], F. Papa[c,d], C.K. Shum[e,f]

[a] School of Earth and Planetary Sciences, Discipline of Spatial Sciences, Curtin University, Perth, Australia
[b] School of Earth and Ocean Sciences, Cardiff University, Cardiff, UK
[c] LEGOS, Université de Toulouse, IRD, CNES, CNRS, UPS, Toulouse 31400, France
[d] Indo-French Cell for Water Sciences (IFCWS), IRD-IISc-NIO-IITM Joint International Laboratory, Bangalore 560012, India
[e] Division of Geodetic Science, School of Earth Sciences, The Ohio State University, Columbus, OH, USA
[f] Institute of Geodesy and Geophysics, Chinese Academy of Sciences, Wuhan 430077, China

HIGHLIGHTS

- We assimilate GRACE data to improve a hydrological model estimations over Bangladesh.
- Square Root Analysis (SQRA) filter is used for data assimilation.
- We estimate sub-surface water storage changes within the country.
- Climate impacts on the water storages are investigated.
- Independent in-situ measurements are used to evaluate the results.

GRAPHICAL ABSTRACT

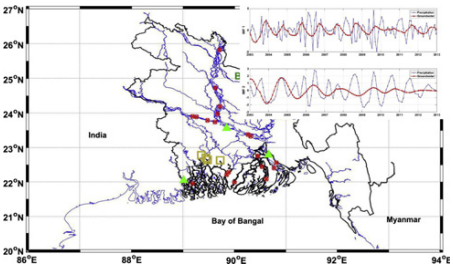

ARTICLE INFO

Article history:
Received 25 July 2017
Received in revised form 21 December 2017
Accepted 23 December 2017
Available online xxxx

Editor: R. Ludwig.

Keywords:
Bangladesh
Groundwater storage
Data assimilation
Hydrological modelling
GRACE

ABSTRACT

Climate change can significantly influence terrestrial water changes around the world particularly in places that have been proven to be more vulnerable such as Bangladesh. In the past few decades, climate impacts, together with those of excessive human water use have changed the country's water availability structure. In this study, we use multi-mission remotely sensed measurements along with a hydrological model to separately analyze groundwater and soil moisture variations for the period 2003–2013, and their interactions with rainfall in Bangladesh. To improve the model's estimates of water storages, terrestrial water storage (TWS) data obtained from the Gravity Recovery And Climate Experiment (GRACE) satellite mission are assimilated into the World-Wide Water Resources Assessment (W3RA) model using the ensemble-based sequential technique of the Square Root Analysis (SQRA) filter. We investigate the capability of the data assimilation approach to use a non-regional hydrological model for a regional case study. Based on these estimates, we investigate relationships between the model derived sub-surface water storage changes and remotely sensed precipitations, as well as altimetry-derived river level variations in Bangladesh by applying the empirical mode decomposition (EMD) method. A larger correlation is found between river level heights and rainfalls (78% on average) in comparison to groundwater storage variations and rainfalls (57% on average). The results indicate a significant decline in groundwater storage (~32% reduction) for Bangladesh between 2003 and 2013, which is equivalent to an average rate of 8.73 ± 2.45 mm/year.

1. Introduction

South Asia, and in particular Bangladesh, is amongst the most water vulnerable regions of the world exhibiting an increase in droughts and floods due to climate change (McCarthy et al., 2001).

* Corresponding author at: Department of Spatial Sciences, Curtin University, Perth, Australia.
E-mail address: Mehdi.Khaki@postgrad.curtin.edu.au (M. Khaki).

https://doi.org/10.1016/j.scitotenv.2017.12.289
0048-9697/

Groundwater is the main source of drinking and irrigation water (almost 90%) in the country (Islam et al., 2013). Any considerable change in climate will, therefore, affect Bangladesh's available water, which is stored in different forms including aquifers, soils, surface waters as rivers, lakes, man-made reservoirs, wetlands and seasonally inundated areas (Papa et al., 2015). Understanding the interaction between precipitation (mainly provided during the Monsoon season) and water storage changes is important to relate climate variability to hydrology. An in-depth understanding of this interaction can be more difficult in Bangladesh due to the changing behavior of monsoonal precipitation (Wang and Ding, 2006) as well as the lack of knowledge on their influence on the hydrology of the region (Shahid, 2010; Rafiuddin et al., 2010).

Groundwater accessibility has made Bangladesh an agro-based country with the main product being rice, making it one of the world's largest rice producer (Abdullah Aziz et al., 2015). The excessive groundwater usage during the last two decades has resulted in serious problems of both rapid falling of groundwater levels and the deterioration of its quality (Qureshi et al., 2015). Groundwater depletion has been reported by Shamsudduha et al. (2009) between 1985 and 2005 within different regions in Bangladesh such as north-central, northwestern, and southwestern parts of the country. This has also been shown by Shamsudduha et al. (2012) for the period of 2003 to 2007. Moreover, Sengupta et al. (2013) reported that groundwater in 63 (out of 64) districts of Bangladesh are seriously contaminated with arsenic, which is partly attributed to its depletion. A number of studies attribute the drop in groundwater level since 1972 to the rainfall decrease and increase in human water usage (see, e.g., Mainuddin, 2002; Ahmed, 2006; McBean et al., 2011; Dey et al., 2011; Adhikary et al., 2013). The Groundwater Monitoring Survey Report of Bangladesh Agricultural Development Corporation (BADC) and Institute of Water Modeling (IWM) showed a three-meter drop of groundwater levels in Dhaka (Sumon and Abul Kalam, 2014). Knappett et al. (2016) claimed that an excess extraction caused the groundwater level to decline more than 1 m near the Buriganga River, which passes in the southwest outskirts of Dhaka resulting in insufficient resources available for the rapidly growing population.

Soil water storage variation is another important factor that worsens the situation and affects agriculture. Furthermore, a considerable amount of surface water from rainfall is consumed by human and thus is not able to recharge the groundwater (e.g., Kanoua and Merkel, 2015; Qureshi et al., 2015; Alimuzzaman, 2017), which can aggravate the conditions mentioned above. Apart from efforts by these studies, a comprehensive study is missing to account for both groundwater and soil moisture variations and their connections to climate variability and change over the entire Bangladesh.

In this regard, hydrological models are important tools for simulating and predicting sub-surface water storages with high saptio-temporal resolutions (e.g., Wooldridge and Kalma, 2001; Döll et al., 2003; van Dijk et al., 2013). However, imperfect modeling of complex water cycle processes, data deficiencies on both temporal and spatial resolutions (e.g., limited ground-based observations), and uncertainties of (unknown) empirical model parameters, inputs and forcing data cause some degrees of deficiencies in them (Vrugt et al., 2013; van Dijk et al., 2011; van Dijk et al., 2014). These limitations are addressed through data assimilation, which is a technique that incorporates additional observations into a dynamic model to improve its state estimations (Bertino et al., 2003; Hoteit et al., 2012). The technique has been widely applied and validated in the fields of oceanography, climate, and hydrological science (Garner et al., 1999; Elbern and Schmidt, 2001; Bennett, 2002; Moradkhani et al., 2005; van Dijk et al., 2014; Reager et al., 2015). Several studies indicate that terrestrial water storage (TWS) derived from the Gravity Recovery And Climate Experiment (GRACE) can play a significant role in better understanding surface and sub-surface processes related to water redistribution within the Earth system (e.g., Huntington, 2006; Chen et al., 2007; Kusche et al., 2012; Forootan et al., 2014; van Dijk et al., 2014). In particular, Shamsudduha et al. (2012) showed a high capability of GRACE measurements for studying water storage variations in the Bengal Basin. A growing number of studies have also assimilated GRACE TWS in order to constrain the mass balance of hydrological models (e.g., Zaitchik et al., 2008; Thomas et al., 2014; van Dijk et al., 2014; Eicker et al., 2014; Tangdamrongsub et al., 2015; Reager et al., 2015; Khaki et al., 2017c; Schumacher et al., 2018).

The present study aims at assimilating GRACE TWS into the World-Wide Water Resources Assessment (W3RA) hydrological model (van Dijk, 2010) to analyze groundwater and soil moisture changes within Bangladesh. While the main focus is on groundwater and soil moisture, surface water as an important water source in Bangladesh is also studied since some surface water sources (e.g., lakes and rivers, except major ones) are not modeled in W3RA. Moreover, since GRACE TWS reflects the summation of all water compartments, for the first time, we use three different scenarios to account for surface water storage changes before data assimilation (see details in Section 3.1). The main reason for using the W3RA model to perform our investigations is to rely on the physical processes implemented in the model equations to consistently separate GRACE TWS (since both model and observation errors are considered) into different water compartments that includes groundwater and soil moisture. As hydrological models are usually better resolved than GRACE data during the assimilation procedure, observations are downscaled, and therefore, higher spatial resolution estimations of water storages will be available within the study region (see, e.g., Schumacher et al., 2016). Here, we use the ensemble-based sequential technique of the Square Root Analysis (SQRA) filtering scheme (Evensen, 2004) to assimilate GRACE TWS into W3RA. SQRA is preferred over the traditional ensemble Kalman filter since it offers a higher computational speed, simplicity, and independence of observation perturbations. Besides, Khaki et al. (2017a) showed that this method is highly capable of assimilating GRACE TWS data into a hydrological model.

After data assimilation, we investigate the connections between the estimated groundwater and soil moisture storages (from improved model) and both surface water level variations and rainfall from multi-mission satellite remote sensing data over Bangladesh. Satellite radar altimetry products of Jason-1 and -2, and Envisat are used in this study to provide 19 virtual river gauge stations for the period 2003 to 2013 distributed across Bangladesh. Since satellite altimetry was initially designed for ocean studies (Fu and Cazenave, 2001), its observations over inland water bodies must be carefully post processed (Birkett, 1998; Calmant et al., 2008; Khaki et al., 2015). Therefore, the Extrema Retracking (ExtR) technique, proposed by Khaki et al. (2014), is applied to retrack satellite waveform data to improve range estimations and consequently derive better water level estimations.

Further, we apply the statistical method of empirical mode decomposition (EMD, Chen et al., 2007) to explore connections between the groundwater and surface water from the model, rainfall data from the Tropical Rainfall Measuring Mission (TRMM), and retracked surface water heights. EMD is an efficient approach to extract cyclic/semi-cyclic components and is preferred over the classical techniques such as the Fourier analysis (Chen et al., 2007; Pietrafesa et al., 2016).

The remainder of this study is organized as follows: in Section 2, the study area, and datasets are presented. Section 3 provides a brief overview of the data assimilation filtering methods, the ExtR retracking method as well as the EMD approach. Results and discussion are presented in Section 4, and the study is concluded in Section 5.

2. Study area and data

2.1. Bangladesh

Bangladesh is located in the Bengal Basin, where the Ganges, Brahmaputra, and the Meghna rivers converge. The average temperature of the country ranges from 17 °C to 20.6 °C during winter and 26.9 °C to 31.1 °C during summer (Rajib et al., 2011). Thus, it is placed in the sub-tropical region with a humid, warm, and tropical climate, which is dominated by a subtropical monsoon originating over the Indian Ocean, which carry warm, moist, and unstable air (Ahmed, 2006; Khandu et al., 2017). An average drought frequency in the country is reported to be equivalent to 2.5 years (Adnan, 1993; Hossain, 1990) when rainfall, as the most important water supply, drops by almost 46% (Dey et al., 2011). The annual precipitation ranges from less than 1500 to ~5000 mm and varies over different parts of the country, e.g., 1276 mm and 1337 mm in the central and western regions, respectively (see, e.g., Hasan et al., 2013; Islam et al., 2014).

2.2. W3RA hydrological model

The globally distributed 1° × 1° World-Wide Water Resources Assessment (W3RA) model is used to simulate water storage over Bangladesh. W3RA is a daily grid distributed biophysical model developed in 2008 by the Commonwealth Scientific and Industrial Research Organisation (CSIRO). The model simulates water storage and flows to monitor, represent, and forecast terrestrial water storages (van Dijk, 2010; Renzullo et al., 2014). The meteorological forcing data sets for the model include minimum and maximum temperature, downwelling short-wave radiation, and precipitation from Princeton University (see detail in Sheffield et al., 2006). Effective soil parameters, including water holding capacity, and soil evaporation, related greenness and groundwater recession, and saturated area to catchment characteristics are the model parameters (van Dijk et al., 2013). The model states used in this study include the top, shallow, and deep root soil layers, groundwater storage, and surface water storage in a one-dimensional system (vertical variability). More detailed information on W3RA can be found in van Dijk et al. (2013).

2.3. Remotely sensed observations

2.3.1. GRACE

The GRACE level 2 (L2) monthly Stokes' coefficients up to degree and order 90 and their full error information (2003–2013) are obtained from the ITSG-Grace2014 gravity field model (Mayer-Gürr et al., 2014) and used in the data assimilation process. The monthly full error information of the Stokes' coefficients is used to construct an observation error covariance matrix for the GRACE TWS fields (Eicker et al., 2014; Schumacher et al., 2016). Note that different GRACE products from various centers can lead to different results depending on their data processing strategies (Shamsudduha et al., 2017). However, for the sake of data assimilation, in addition to GRACE observations, we also need full error information associated with the observations. Schumacher et al. (2016) and Khaki et al. (2017b) show that it is important to consider GRACE full error covariance matrix to conduct data assimilation experiments. A more comprehensive analysis of different GRACE products has already been performed in a recently published paper of Schumacher et al. (2018). Their results indicate that while using the full covariance matrix in the data assimilation procedure, differences between the GRACE products do not significantly change to affect the final results. Therefore, we only use ITSG-Grace2014 data for which we are sure that the full covariance field is well representative of the GRACE data's error structure.

Degree 1 of Stokes' coefficients are replaced with those estimated by Swenson et al. (2008) to account for the change in the Earth's center of mass. Degree 2 and order 0 (C20) coefficients are replaced by those from Satellite Laser Ranging solutions due to unquantified large uncertainties in this term (e.g., Cheng and Tapley, 2004; Chen et al., 2007). Colored/correlated noises in the L2 products are reduced using the DDK2 smoothing filter following Kusche et al. (2009). This smoothing causes some degree of signal attenuation (Klees et al., 2008) and moving anomalies from outside the region (e.g., Bay of Bengal) (Chen et al., 2007; Khaki et al., 2018). To mitigate this issue, following Swenson and Wahr (2002), we apply a Lagrange multiplier filter to decrease leakage errors over the entire Bangladesh. This filter uses a basin averaging kernel method expanded in terms of spherical harmonics and subsequently combined with L2 potential coefficients to improve the GRACE estimates (see details in Swenson and Wahr, 2002). The L2 gravity fields are then converted to 1° × 1° TWS fields following Wahr et al. (1998). Note that the GRACE data provide changes in TWS while W3RA produces absolute TWS. Accordingly, the mean TWS for the study period is taken from W3RA and is added to the GRACE TWS change time series to obtain absolute values and make them comparable with model outputs (Zaitchik et al., 2008).

2.3.2. Satellite radar altimetry

Satellite radar altimetry data of Jason-1 and -2, i.e., 20-Hz sensor geographic data records (SGDR), and Envisat, i.e., 18-Hz SGDR products are applied in this study. The data includes 260 cycles of Jason-1 covering 2002–2008, 166 cycles of Jason-2 covering 2008–2013, and 113 cycles of Envisat covering 2002–2012. Jason-2 is a follow-on mission of Jason-1 with a similar temporal resolution of ~9.915 days and the ground cross-track resolution of ~280 km (over the equator), with the same characteristics as Topex/Poseidon altimetry mission (Benada, 1997; Papa et al., 2010a). Jason-1 and-2 data are obtained from the Physical Oceanography Distributed Active Archive Center (PO.DAAC) and AVISO, respectively. Additionally, Envisat RA2 products with a 35 days repeat cycle (30 days for new orbit after October 2010) are derived from ESA (Table 1).

Altimeter ranges should be corrected for atmospheric impacts such as ionospheric, tropospheric, and electromagnetic effects (Benada, 1997). We apply geophysical correction, including solid earth tide, pole tide, and dry tropospheric (Birkett, 1995) to correct the ranges. The ExtR post-processing technique (Khaki et al., 2014) is applied on waveforms to retrack datasets and improve range measurements. The retracked altimetry data are then used to build virtual time series for 19 different points (Fig. 1) located on the satellite ground tracks and distributed throughout the study area. At each virtual point, several points belonging to the same satellite cycle are considered, and the median value of the retracked altimetry-based water levels is computed to address the hooking effect (Frappart et al., 2006). While a satellite is passing above a water body, its emitted signal is locked over a spatially limited part of the water, which can result in an error. The hooking effect, caused as result of off-nadir range measurements, leads to less accurate height estimations (Seyler et al., 2008; Boergens et al., 2016). Afterwards, time series of water level variations from Jason-1 and -2 are combined with those of Envisat products to produce monthly surface levels. Details of the datasets, model, and pass numbers of the altimetry missions used in this study are presented in Table 1.

2.3.3. Precipitation

We use precipitation data of the Tropical Rainfall Measuring Mission Project (TRMM-3B43 products; version 7, (TRMM), 2011; Huffman and Bolvin, 2012) to assess climate variability over

Table 1
A summary of the datasets used in this study.

Description	Platform	Detail	Data access
Terrestrial water storage (TWS)	GRACE	GRACE level 2 (L2)	https://www.tugraz.at/institute/ifg/downloads/gravity-_field-_models/itsg-_grace2014/
Altimetry-derived level height	Jason-1	Pass numbers 90 and 231	http://podaac.jpl.nasa.gov
	Jason-2	Pass numbers 90 and 231	http://avisoftp.cnes.fr/
	Envisat	Pass numbers 337, 438, 795, 896, and 982	http://envisat.esa.int/dataproducts/ra2-_mwr/
Precipitation	TRMM-3B42	Daily accumulated precipitation	http://disc2.gesdisc.eosdis.nasa.gov/data/TRMM_L3/TRMM_3B42_Daily.7
Hydrological model	W3RA	The Commonwealth Scientific and Industrial Research Organisation (CSIRO)	http://www.wenfo.org/wald/data-_software/
Surface water storage		Satellite-derived surface water storage in the Ganges–Brahmaputra River Basin	Papa et al. (2015)
In-situ measurements	BWDB	http://www.ffwc.gov.bd/	

Bangladesh. Incorporating more microwave sounding and imagery records as well as implementing better processing algorithms have caused a large improvement in this version of data (Huffman and Bolvin, 2012; Fleming and Awange, 2013). The data sets, validated by Khandu et al. (2017) over the study region showed promising performance. The gridded (0.25° × 0.25°) precipitation products (2003

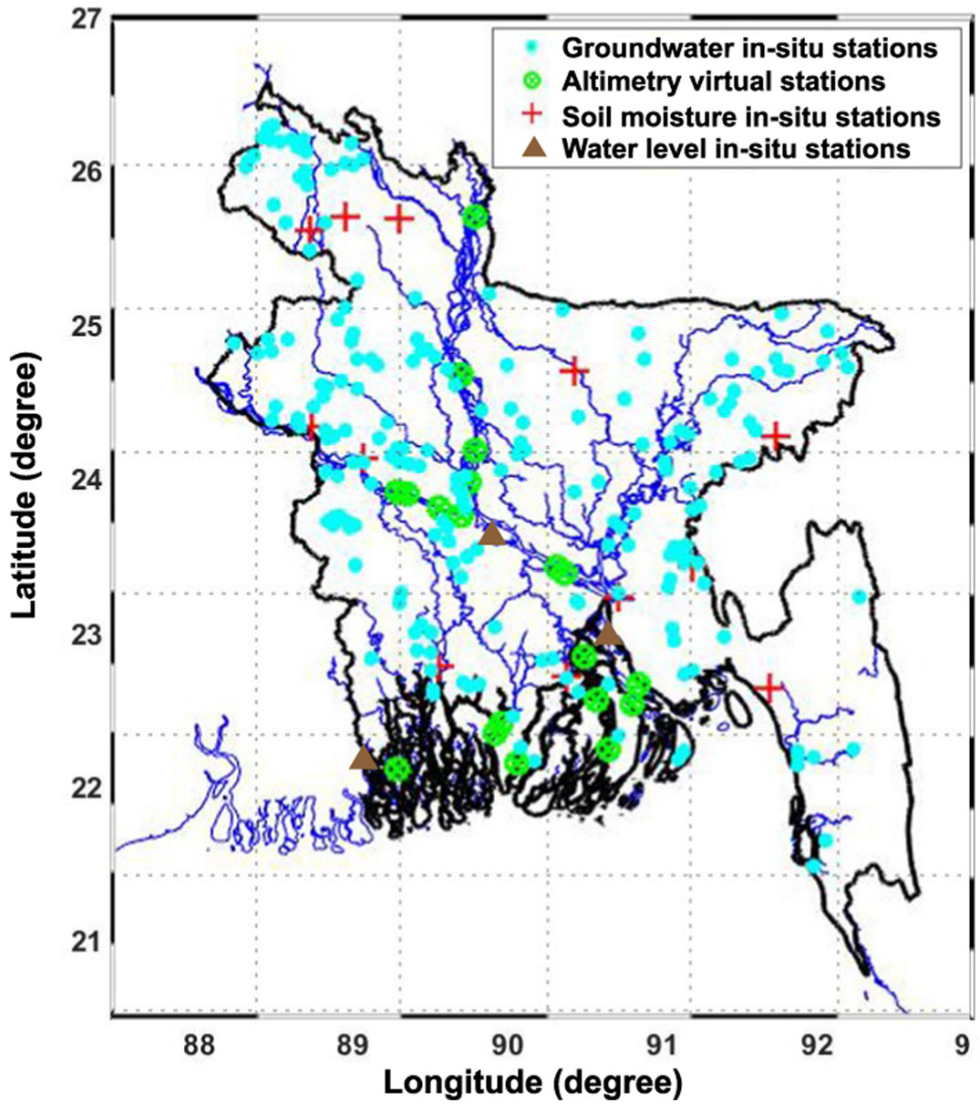

Fig. 1. The study area is represented by black solid line. The figure also contains the locations of virtual stations for satellite altimetry time series and various in-situ stations.

to 2013) are converted to 1° × 1° and used to investigate their connection to water storage changes.

2.4. Surface storage data

For the objective of data assimilation, considering that many surface water sources (in different forms, e.g., lakes and rivers except few major ones) are not modeled in W3RA, surface water storages should be removed from GRACE TWS data. To this end, we use satellite-derived surface water data in the Ganges–Brahmaputra River Basin (as the main source of surface water in Bangladesh) provided by Papa et al. (2015). The data is based on a multi-satellite approach that combines surface water extent from the Global Inundation Extent from Multi-Satellite (GIEMS, Papa et al., 2006; Papa et al., 2010a; Prigent et al., 2012) and level height variations of water bodies from Envisat radar altimetry to estimate surface water storage (Frappart et al., 2012) covering the period from 2003 to 2007. Since the study period is 2003 to 2013, canonical correlation analysis is applied to extend the data from 2007 to 2013. Satellite derived river height fluctuations of Section 2.3.2 that are distributed across the study area are used in the process of extending the surface water storage of Papa et al. (2015). More details on CCA are provided in Section 3.4.

2.5. In-situ measurements

To evaluate the performance of data assimilation, 198 groundwater stations and 12 soil moisture stations (see Fig. 1) are used. These data are provided by the Bangladesh Water Development Board (BWDB) and Institute of Water Modelling (IWM) in The Asian Development Bank (2011). Fig. 2 shows the sample products of different groundwater stations, as well as soil moisture variations measured at various depths. Specific yields ranging from 0.01 to 0.2 (Shamsudduha et al., 2011; BWDB, 1994) are used to convert well-water levels to variations in groundwater storage. Details of the datasets used in this study are outlined in Table 1.

3. Method

3.1. Data assimilation

3.1.1. Filtering method

The square root analysis (SQRA) scheme for the ensemble Kalman filter (EnKF), presented in Evensen (2004) is used to assimilate the GRACE TWS into W3RA. SQRA, which is a deterministic form of ensemble-based Kalman filters, uses a statistical sample of state estimates and unlike traditional Kalman filtering method, does not need an observation perturbation (Burgers et al., 1998; Sakov and Oke, 2008; Khaki et al., 2017a). Instead, by introducing a new sampling scheme, SQRA uses unperturbed observations without imposing any additional approximations like uncorrelated measurement errors (Evensen, 2004). The update stage in SQRA includes two steps starting with updating the ensemble-mean as,

$$\bar{X}^a = \bar{X}^f + K\left(y - H\bar{X}^f\right), \quad i = 1 \ldots N, \tag{1}$$

$$K = P^f(H)^T\left(HP^f(H)^T + R\right)^{-1}, \tag{2}$$

where 'f' stands for forecast, 'a' for analysis, and N is the ensemble number. In Eq. (1), $\bar{X}^a$ is the mean analysis state, K represent the Kalman gain, and y is the observation vector. The transition and observation covariance matrices are indicated by H and R, respectively. $\bar{X}^f$, which represents the forecast ensemble mean, and the model state forecast error covariance (P^f) are derived by,

$$\bar{X}^f = \frac{1}{N}\sum_{i=1}^{N}(X_i), \tag{3}$$

$$P^f = \frac{1}{N-1}\sum_{i=1}^{N}\left(X_i^f - \bar{X}^f\right)\left(X_i^f - \bar{X}^f\right)^T. \tag{4}$$

The model state contains N different vectors of the model state variables. Note that $A^f = [A_1^f \ldots A_N^f]$ is the ensemble of anomalies, the deviation of model state ensembles from the ensemble mean $\left(A_i^f = X_i^f - \bar{X}^f\right)$. In the second update step, SQRA computes the ensemble perturbations through.

$$A^a = A^f V\sqrt{I - \Sigma^T\Sigma\Theta^T}, \tag{5}$$

where Σ and V are result from singular value decomposition of A^f ($A^f = U\Sigma V^T$). Θ is a random orthogonal matrix (e.g., the right singular vectors from a singular value decomposition of a random $N \times N$ matrix) for ensemble redistribution of the variance reduction (cf. Evensen, 2004; Evensen, 2007; Khaki et al., 2017a).

3.1.2. Assimilation of GRACE data

To assimilate GRACE TWS into the model, we use a summation of model's vertical water compartments (e.g., soil moisture, groundwater, and surface water) at 13 grid points. This summation is then updated by the GRACE TWS at the same location at every assimilation step (whenever a new observation is available). Initial ensemble members are generated by perturbing the meteorological forcing fields following Renzullo et al. (2014). In this regard, the three most important forcing variables; precipitation, temperature, and radiation are perturbed using Monte Carlo sampling of multivariate normal distribution (with the errors representing the standard deviations) to produce an ensemble (with 72 members as suggested by Oke et al., 2008). The perturbed meteorological forcing datasets are then integrated forward with the model from 2000 to 2003 to provide a set of state vectors at the beginning of the study period.

Two widely used tuning techniques of ensemble inflation and localization are applied to enhance the assimilation performance especially when a limited ensemble size is assumed. Ensemble inflation uses a small coefficient (i.e., 1.12 in our study; Anderson, 2001) to inflate prior ensemble deviation from the ensemble-mean to increase their variations and alleviate the inbreeding problem (Anderson et al., 2007). For localization, the Local Analysis (LA) scheme (Evensen, 2003; Ott et al., 2004; Khaki et al., 2017b) is applied. LA restricts the impact of a given measurement in the update step to the points located within a certain distance (3° following Khaki et al., 2017b) from the measurement location. We also implement three different cases to deal with surface water storage during data assimilation.

- Case 1: Assimilating the GRACE TWS data after removing surface storages into the model states except for the surface water compartment.
- Case 2: Adding surface water storage to model surface water compartment and using the GRACE TWS to update the summations of all water compartments.
- Case 3: Assimilating the GRACE TWS to update the summations of all water compartments (including surface water compartment).

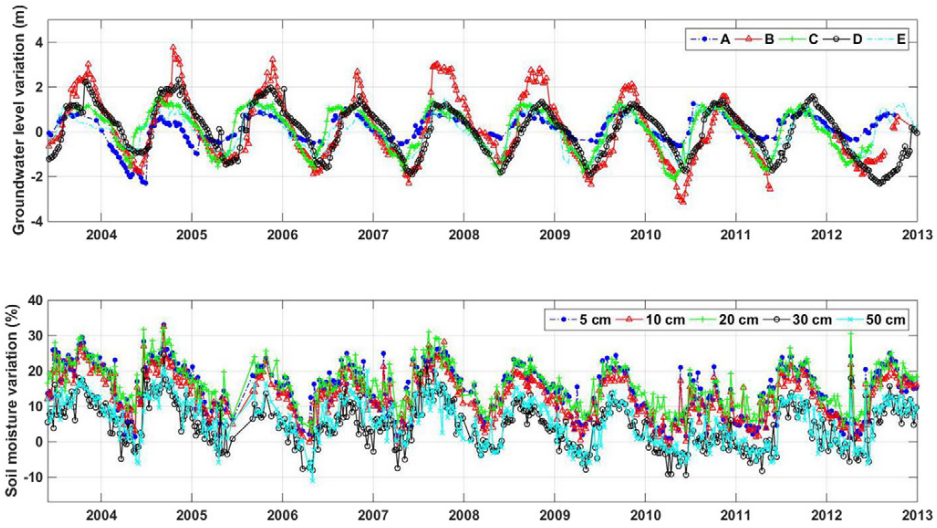

Fig. 2. (a): In-situ groundwater level variations of various stations (A: 21.790° latitude and 91.870° longitude, B: 24.450° latitude and 88.598° longitude, C: 26.190° latitude and 88.750° longitude, D: 25.590° latitude and 88.900° longitude, E: 22.110° latitude and 92.100° longitude). (b): Soil moisture variations at defferent depths belong to Rajshahi in-situ station (24.3670° latitude and 88.7000° longitude).

In Section 4.1, the results of all the case scenarios are compared with each other and evaluated against in-situ groundwater measurements.

3.2. Empirical mode decomposition(EMD)

The empirical mode decomposition (EMD) proposed by Chen et al. (2007) is used for analyzing multivariate datasets of this study. EMD establishes different frequencies and trends within time series, which are called Intrinsic Mode Functions (IMFs), by considering local oscillations (Flandrin et al., 2004; Rilling, 2003). The idea is that a signal is composed of fast oscillations superimposed by slow oscillations (Flandrin et al., 2004). Thus, EMD decomposes any complicated data set into a finite and often small number of IMFs hidden in the observations (Huang et al., 1998). We apply EMD on all available time series of this study to extract different frequencies and also to find local trends for a better understanding of their interrelationships.

3.3. Retracking scheme

In this study, we use the retracking method to improve altimetry estimations of river height variations. The retracking process is essential since complex waveform patterns are usually observed over rivers. To this end, Extrema Retracking (ExtR) post-processing technique (Khaki et al., 2014, 2015) is used. The ExtR is a three step filter that starts by applying a moving average filter to reduce the random noise of the waveforms. It then identifies extremum points of the filtered waveforms, and finally, extracts the main leading edge amongst the established extremum points. The method is applied to process different types of waveforms and improve level estimations as demonstrated in Khaki et al. (2014, 2015). The filter is employed here to retrack satellite radar altimetry data and then removing surface storage from TWS (see Section 3.4). Fig. 12 shows river level fluctuations for different parts of Bangladesh (Fig. 3a) and the entire area of the country (Fig. 3b).

3.4. Canonical correlation analysis(CCA)

Canonical correlation analysis (CCA) seeks to find the linear relationship between two sets of multidimensional variables x and y. The process extracts canonical coefficients u and v such that $X = x^T u$ and $Y = y^T v$ (X and Y are canonical variates) possess a maximum correlation coefficient (Chang et al., 2013) using the following function,

$$\begin{aligned} P &= \frac{E[XY]}{sqrt\left(E[X^2]E[Y^2]\right)} \\ &= \frac{E\left[u^T x y^T v\right]}{sqrt\left(E\left[u^T x x^T u\right] E\left[v^T y y^T v\right]\right)} \\ &= \frac{u^T C_{xy} v}{sqrt\left(u^T C_{xx} u v^T C_{yy} v\right]\right)}, \end{aligned} \tag{6}$$

where C_{xx} and C_{yy} are covariance matrices of x and y respectively and the objective in above function is to maximize the correlation P. Once the coefficients are calculated, they can be used to find the projection of x and y onto u and v as canonical variates with maximum correlation. Here, x contains the vectors of surface water storages from Papa et al. (2015) at each grid point and y includes river heights variations from satellite radar altimetry in a same temporal scale as the former data (2003 to 2007). After performing canonical correlation analysis, the computed canonical coefficient of u and v, and a new set of variables y (from 2007 to 2013) are used to estimate the canonical variate of x. The combination of surface water storages (x) using the extracted u from the first part has the maximum correlation to the altimetry-derived river heights variability. Hence, this coefficient vector can be used to transform river heights into surface waters at each grid point.

4. Results

4.1. Data assimilation

Before discussing groundwater and soil moisture variations within Bangladesh, the effect of data assimilation on terrestrial water storage time series and its capability to improve model simulations are investigated. Fig. 4 shows average TWS time series within Bangladesh before (model-free run) and after data assimilation. The figure also contains GRACE TWS time series. It can be seen that data

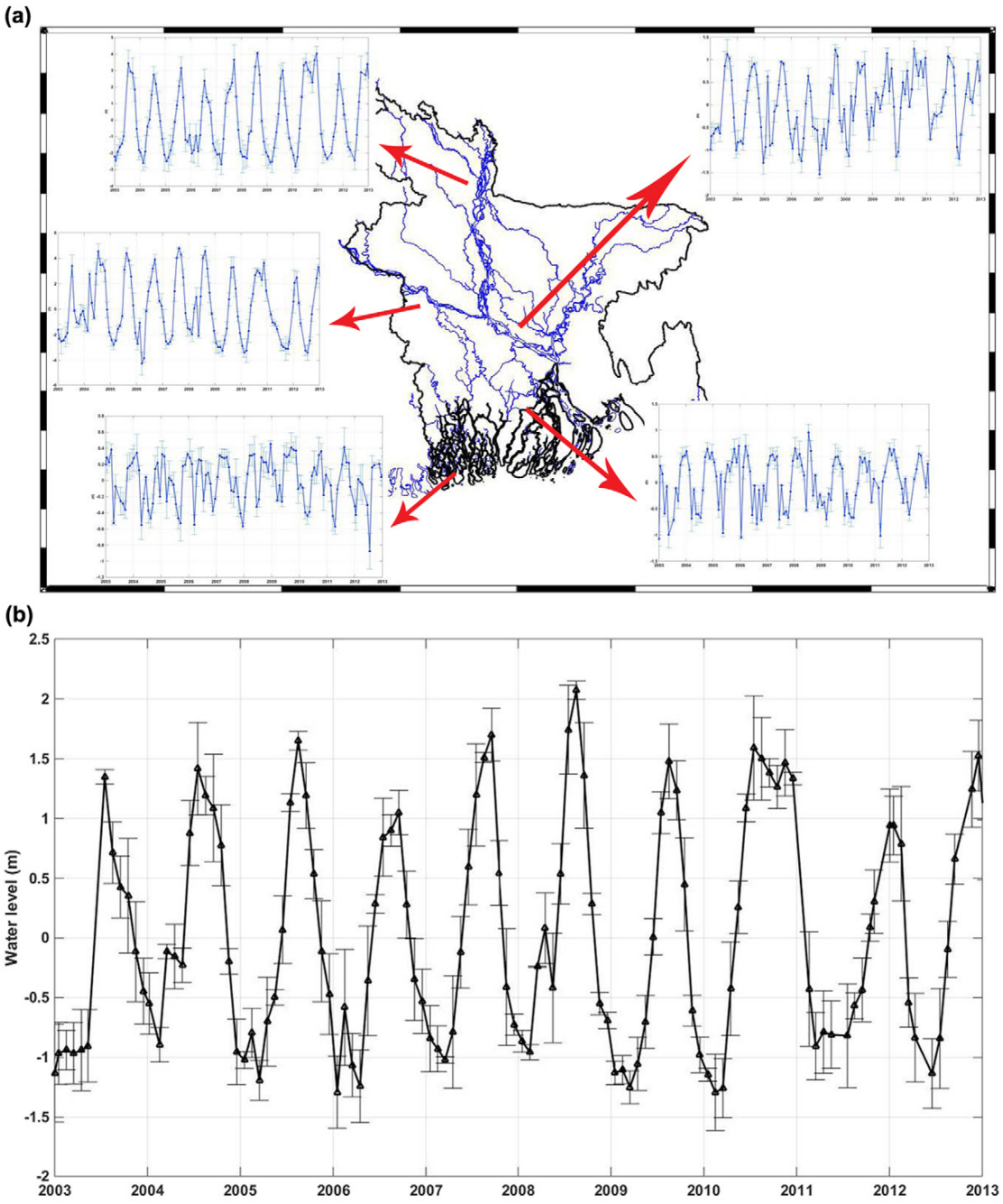

Fig. 3. Average river height variation time series from satellite radar altimetry for different parts (a) and for the entire area (b) of Bangladesh. The average error for each measurement is presented as error bars.

assimilation largely reduces misfits between model-free run and observations.

To assess whether data assimilation (e.g., in Fig. 4) can result in better water storage estimates, in-situ groundwater and soil moisture measurements are used for validation. Time series of groundwater and soil moisture anomalies are generated for each station. Groundwater and soil moisture results from all the three assimilation cases (cf. Section 3.1.2) are spatially interpolated using the nearest neighbour (the closest four data values) to the location of the in-situ measurements. This is also done for outputs of the WaterGAP Global Hydrology Model (WGHM; more details on Döll et al., 2003, Müller Schmied et al., 2014), as well as estimated storages by van Dijk et al. (2014), indicated here by W3, who merged GRACE observations with an ensemble of hydrological model outputs. The comparison between these products and data assimilation results allows us to better investigate any achieved improvements. For this purpose, the RMSE and correlations between in-situ and estimated time series are calculated.

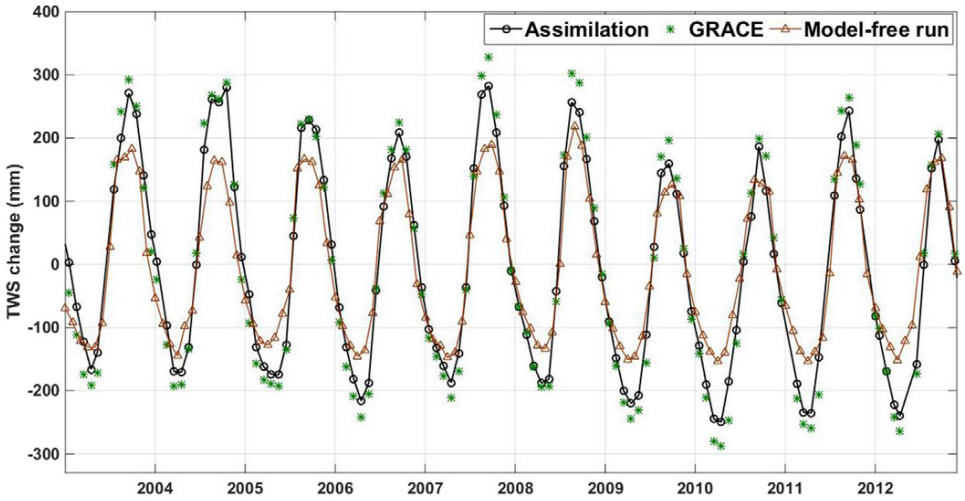

Fig. 4. Average TWS change time series from data assimilation (case 1), model-free run, and GRACE.

Table 2 summarizes the average RMSE and correlation for each of the three data assimilation case. From Table 2, it can be seen that the groundwater results are more correlated to in-situ measurements after the application of each assimilation case (0.81 on average), 0.39 larger than model simulations without applying data assimilation (model-free run). An average RMSE improvement of 51.16% (at 0.95 confidence level) in case 1 shows a significant influence of the data assimilation scheme, approximately 4.44% and 39.11% larger than cases 2 and 3, respectively. It is also evident from Table 2 that data assimilation results, especially cases 1 and 2 outperform groundwater estimates of WGHM. Note that the provided W3 does not include groundwater and therefore we use it for soil moisture comparison only. Table 2 emphasizes that model groundwater estimations can be successfully improved with respect to the in-situ measurements if they are fine tuned by GRACE data through the assimilation especially for cases 1 and 2.

Furthermore, correlation analysis is carried out between in-situ soil moisture measurements at various depths and data assimilation results from different scenarios, as well as soil moisture estimates of WGHM and W3 (Table 3). In-situ measurements at different depths are compared with different layers from data assimilation results. For this purpose, in-situ soil moisture time series of 0–10 cm, 0–30 cm, and 0–50 cm depths are compared to the model top, shallow, and deep soil moisture layers. While the model soil moisture of top layer corresponds to the thickness between 5 and 10 cm, the model shallow and deep-root soil layers broadly represent 10–21 cm and 3–6 m soil thicknesses (see also Renzullo et al., 2014; Tian et al., 2017). Here, we compare W3RA's top layer estimations with in-situ of 0–10 cm, top layer plus shallow-root simulations with in-situ of 0–20 cm, and summation of the top, shallow, and a portion of deep-root soil layers with 0–50 cm in-situ measurements. Note that WGHM and W3 outputs are provided at a single aggregated layer and correspondingly are compared with in-situ soil time series at the depth 0–50 cm. Table 3 shows that the highest correlation improvements, 18.31% (on average) for all layers and 25.25% for the deep layer. Case 2 also represents considerable improvements slightly smaller than case 1, still 11.57% larger than case 3, 6.97% larger than WGHM, and 9.25% larger than W3. Both Tables 2 and 3 demonstrate a high capability of data assimilation in improving model simulations of different compartments. These tables also indicate a better performance of the implemented data assimilation, specifically cases 1 and 2, compared to WGHM and W3.

To better analyze the differences between each assimilation case, we compare their RMSE during 2007. In 2007, a major flooding (following ENSO rains) occurred across South Asia affecting Bangladesh (Gaiha et al., 2010). This phenomenon can help us to monitor performances of each case in such an extreme situation and their ability to distribute observed TWS between all water compartments. Groundwater estimates from each case and in-situ measurements are used to calculate RMSE for each assimilation case (Fig. 5), where the least errors are estimated by cases 1 and 2. Assimilating the GRACE TWS without considering surface water storage within the area (case 3) causes larger errors especially in April and September. The largest error, however, is obtained for the

Table 2
Statistics of groundwater errors. For each case, the RMSE average and its range (±XX) at the 95% confidence interval is presented. Improvements in data assimilation results are calculated with respect to the groundwater storages from the model without implementing data assimilation.

			Improvement (%)	
Assimilation scenario	Correlation	RMSE (mm)	Correlation	RMSE
Case 1 [Removed surface storages from GRACE TWS]	0.86	35 ± 5.65	51.16	57.36
Case 2 [Added surface storages to W3RA surface water]	0.82	39 ± 5.18	48.78	52.92
Case 3 [No surface storage correction applied]	0.75	68 ± 7.72	44.02	18.25
WGHM	0.79	57 ± 5.37	46.83	30.89
Mode-free run	0.42	83 ± 9.29	–	–

Table 3
Average correlations improvements (at 95% confidence interval) between in-situ and soil moisture estimates with respect to model-free run.

Filter	0–10 cm	0–20 cm	0–50 cm
Case 1	10.42	19.27	25.25
Case 2	11.10	17.88	24.48
Case 3	5.25	8.34	12.91
WGHM	–	–	17.51
W3	–	–	15.23

model-free run. Hereafter, we use the result of data assimilation for case 1 since it performed slightly better than case 2 and significantly better than case 3 in terms of the RMSE (see Fig. 5).

The model's water storage variations computed by assimilating GRACE TWS data into W3RA are presented in Figs. 6 and 7. Temporal averages of soil moisture and groundwater storage variations for each grid point from data assimilation, WGHM, and W3 in the study area are displayed in Figs. 6 and 7, respectively. We find large correlations between assimilation results and WGHM (0.76 on average for soil moisture and 0.82 on average for groundwater) and W3 (0.71 on average for soil moisture) outputs. The results show more negative groundwater variations within different parts of Bangladesh than soil water storage variations (see Fig. 6). Both water compartments indicate larger signals (in terms of amplitude) in the central and northwestern parts of Bangladesh. Positive soil moisture variations are found in the center toward east and north within the study period, especially for the assimilation and WGHM maps. Larger groundwater variations are also captured in the same area. While assimilation results show negative groundwater changes over the central, eastern, and to a lesser degree southern parts, WGHM only indicates negative variations in the southern and eastern parts. Fig. 7 indicates that smaller water storage variations in the northwestern and northeastern parts of Bangladesh during 2003–2013.

The average time series of soil moisture and groundwater storages from data assimilation are shown in Fig. 8a and b, respectively. We estimate spatial averages for all the time series at grid points for this figure. Fig. 8a shows slight declines in the soil water storage after 2007, which can be related to variations of surface water storage in the same period. The correlation between the surface water storage and soil moisture time series (after removing seasonal effects) is found to be 0.92 (for a 95% confidence interval), 34% higher than the correlation between groundwater and soil moisture. This indicates that a stronger connection exists between

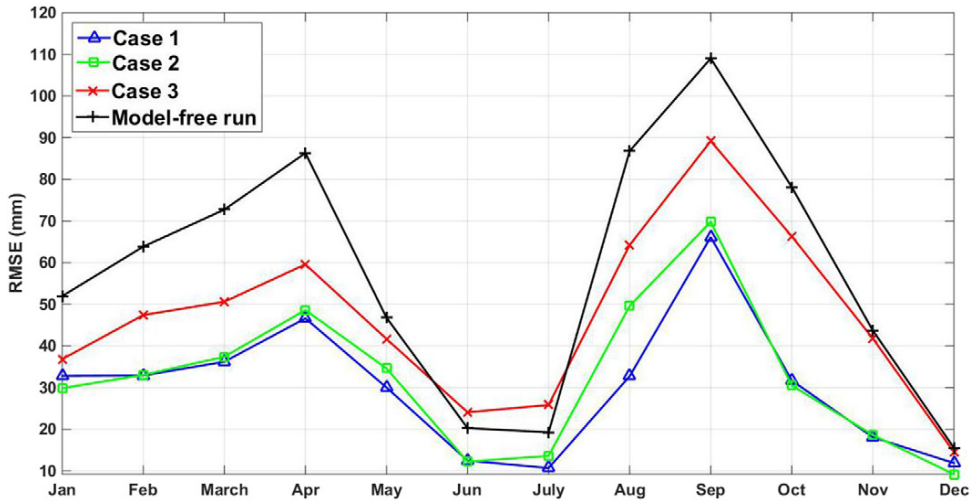

Fig. 5. Comparison between RMSE achieved from implementing each data assimilation scenario as well as model-free run during 2007. In case 1, surface storages is removed from GRACE TWS, in case 2, surface storages is added to W3RA surface water, and case 3 refers to the data assimilation with no surface storage correction.

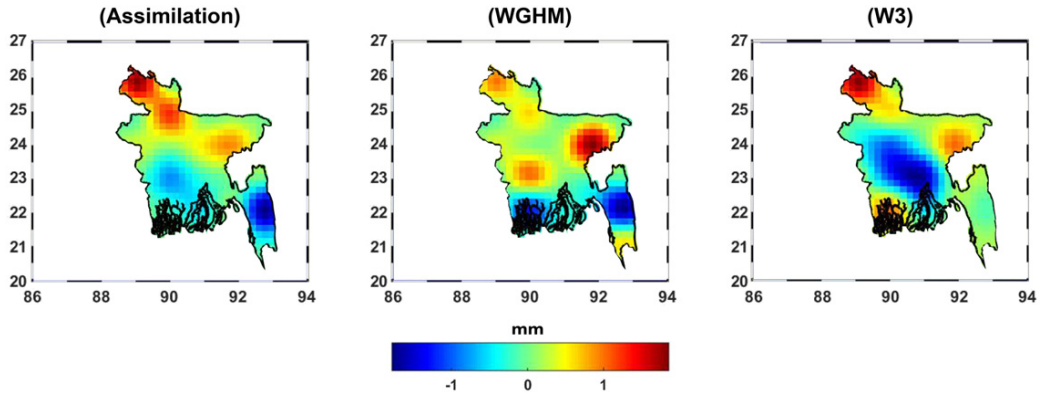

Fig. 6. Spatial distribution of average soil water storage variations from data assimilation, WGHM, and W3.

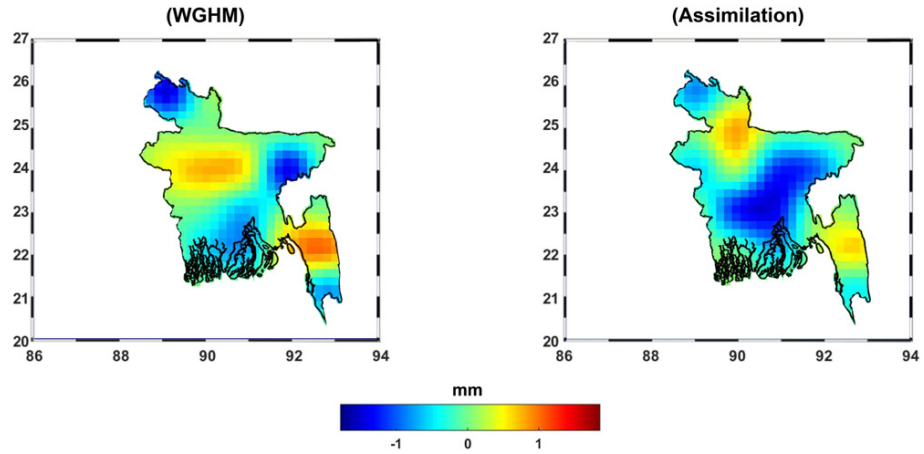

Fig. 7. Spatial distribution of average groundwater storage variations from data assimilation and WGHM.

the surface water storage and soil moisture over the area. Annual variations of groundwater storages, however, show a larger decline in comparison to soil moisture storage variations, especially between 2008 and 2012. A significant decrease in groundwater storage is seen in Fig. 8b with an average rate of 8.73 ± 2.45 mm/year, showing an overall ~46% reduction. The decline in water availability can be due to over-extraction of groundwater resources since such a decrease is not seen in precipitation (see Section 4.2 for more details).

4.2. Statistical analyses

First, the precipitation and TWS over Bangladesh is analyzed. To explore the climate variability and its relationship with water storages, precipitation will be compared to the data assimilation results. Principal component analysis (PCA Lorenz, 1956) is applied on GRACE TWS and precipitation time series at each grid point to explore their spatio-temporal variations. The first three most dominant empirical orthogonal functions (EOF1, EOF2, EOF3) for each variable are presented in Fig. 9. The spatial distribution of precipitation within Bangladesh indicates larger rainfall in south-eastern parts. TWS distribution in EOF2 follows the same pattern. Large water storages are captured by EOF3 in the northwest. More information can be extracted from precipitation and TWS time series. The first three principal components (PC1, PC2, and PC3) of each data set are shown in Fig. 10. Large precipitation impacts are found in 2003 and 2007. A negative anomaly in rainfall is found in 2010 and 2012, as well as in the period between 2005 and 2007 (PC1). TWS time series demonstrate declines between 2005 and 2007, and particularly after 2009 following a drop event (Mondol et al., 2017). Results, however, show an increase in 2007 in agreement with ENSO rainfall. The overall average of TWS variations during the study period is negative (~11.48 ± 3.19 mm/year) for the entire country. A similar trend, however, is not observed in precipitation even though there is a shorter period negative decline in 2005 and after 2010. Fig. 10 illustrates that although in some cases a variation in precipitation results in a changes in TWS, continuous TWS reduction

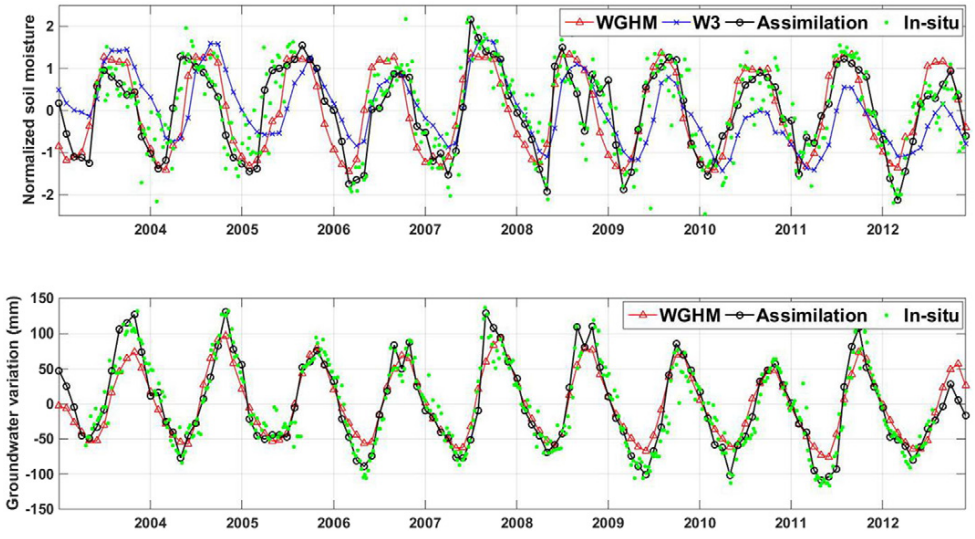

Fig. 8. Average soil moisture storage (a) and groundwater storage (b) time series from assimilation, WGHM, W3, and in-situ measurements.

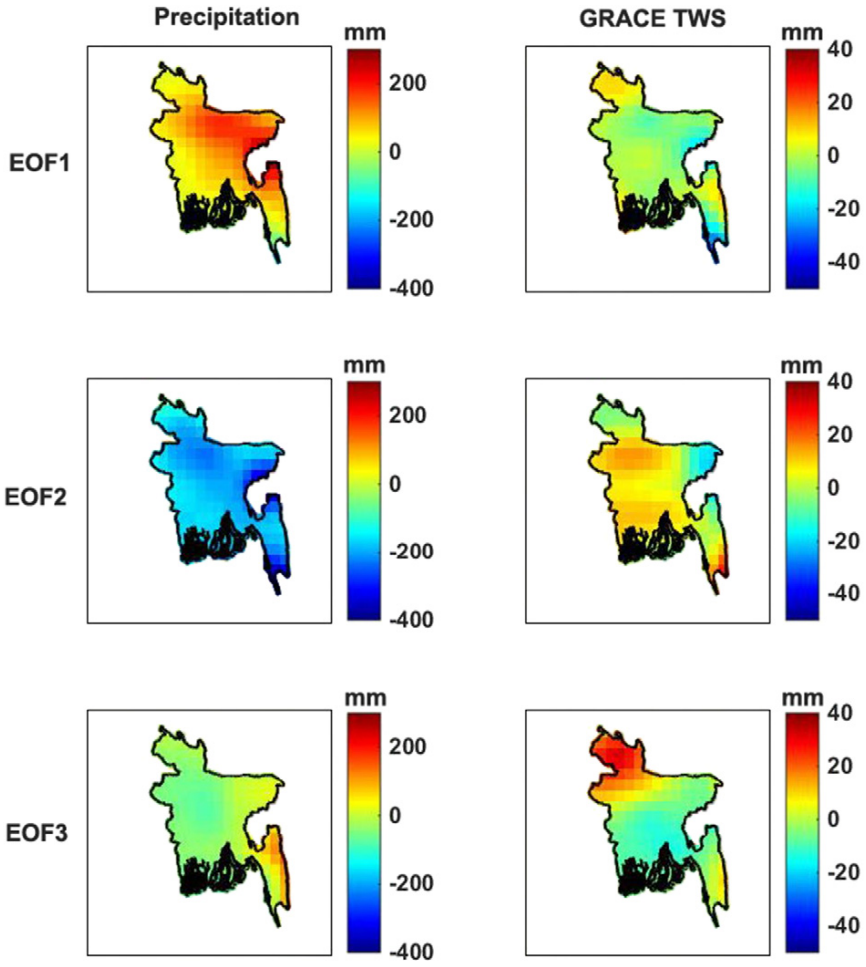

Fig. 9. Spatial distribution of of EOF1, EOF2, and EOF3 from applying PCA on precipitation and GRACE TWS.

possibly has different explanations that could become clear through the separation of the groundwater and surface water storages (cf. Section 3.4).

Details on surface and groundwater storage variations and their relationship to precipitation and rivers' level heights are presented in Table 4. For each grid point in the study area, we calculate water storage variation rates and depletions, and also a correlation coefficient between their time series and both precipitation and river height variations. Note that we use lag-correlation (cross correlation) to achieve the maximum correlation between each two time series. Table 4 illustrates that there is a water decline in both surface and groundwater storages at different rates. This can be inferred from the negative storage variation rates. An approximately 32% depletion in groundwater storage causes a significant decrease in TWS as shown in Fig. 10. This remarkable water reduction, unlike the rainfall pattern, is highly related to excessive groundwater usages, especially for irrigation. It can be concluded from Table 4, therefore, that groundwater storages are less correlated (16.5%) to river height variations and precipitation, respectively, in comparison to surface water storage. Consequently, variations in rainfalls and river heights are more reflected in surface storage variations.

To better analyze groundwater storage changes, we apply empirical mode decomposition (EMD) on time series in each grid point. EMD is used to extract Intrinsic Mode Functions (IMFs) of time series that are found to be most representative of the initial signals. The relationships between the groundwater IMFs and those of precipitation, TWS, and surface river fluctuations are shown in Fig. 11, which contains scatter bi-plots and the interpolated line representing the correspondence between two variables. The trend lines in the sub-figures show that the computed IMFs for the different variables are close to each other. The concentration of distributed points after applying EMD is more symmetric than for the initial time series especially for the groundwater and TWS, as well as the groundwater and water level variations. Table 5 contains the average correlation between the time series of groundwater and the variables of precipitation, TWS, and river height variation. The more symmetric distributed points in between the groundwater IMF and that of GRACE TWS shows the greater relationship between these two variables corresponding to a higher correlation presented in Table 5. The reason for this can be due to the use of GRACE TWS in data assimilation. A higher correlation is also obtained between the IMF of groundwater and those of river height. The least relationship is obtained for the groundwater IMF and precipitation, that implies the different pattern in variations of these two variables, which could be related to the non-climatic effects in the groundwater.

The extracted first two IMFs for the groundwater time series are illustrated in Fig. 12. In both subfigures, a decline in groundwater storages is observed. Such a trend, however, is more significant for

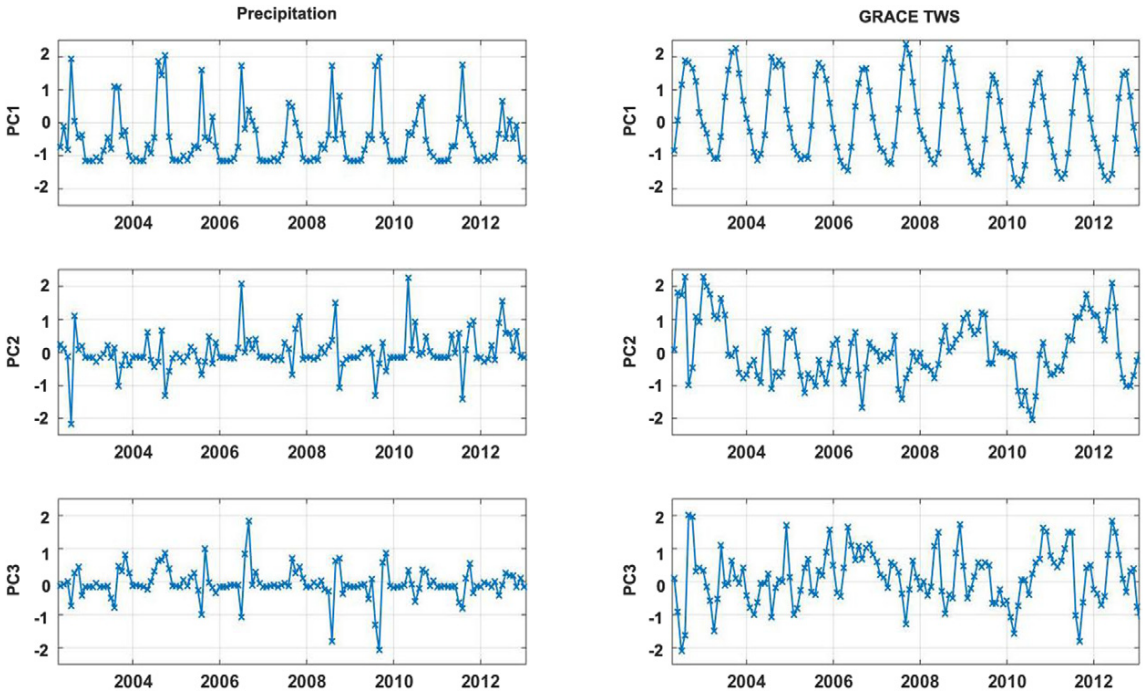

Fig. 10. The first three principal components from applying PCA on precipitation and GRACE TWS.

Table 4
Statistics of water storage variations.

		Depletion (%)			Correlation (95% confidence interval)	
Water storage	Variation rate (mm/year)	Min	Max	Mean	Precipitation	Water level height
Surface water	−1.54	0	38	11	0.74	0.81
Groundwater	−8.73	12	41	32	0.59	0.63

IMF 2. We also plot the first and second precipitation's IMFs for comparison. The precipitation's IMF 1 in Fig. 12, better indicates rainfall variation from Fig. 10. Two periods with larger rainfall can be seen for the years 2006 and 2009. A decrease in rainfall over Bangladesh is found from 2010 onwards, with smaller amplitudes during 2010 and 2012. This may impact the groundwater levels during similar temporal periods. There are several similar patterns in both time series (groundwater and precipitation) especially for IMF

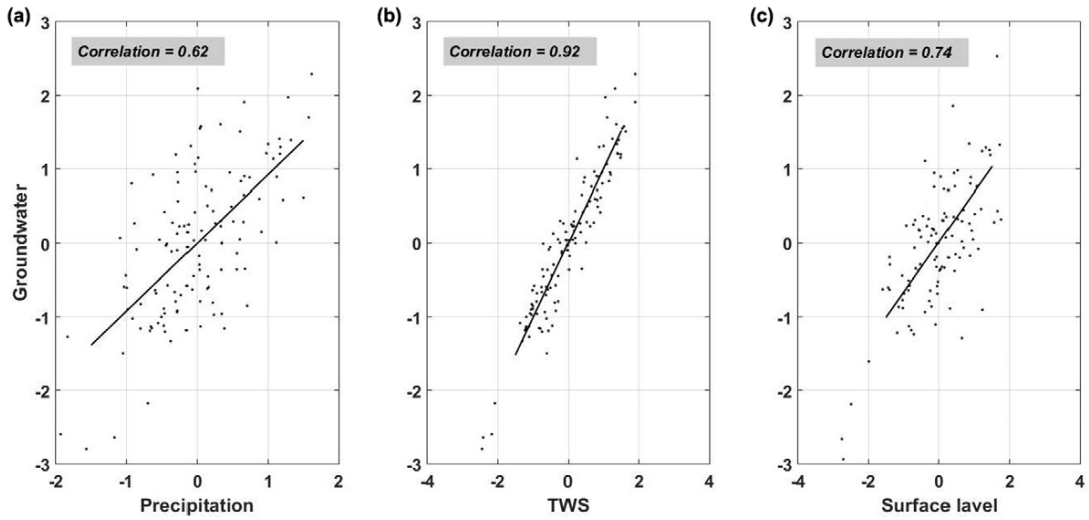

Fig. 11. Relationships between normalized Intrinsic Mode Functions (IMF) time series of groundwater and precipitation, TWS, and surface river height.

Table 5
Groundwater storage correlation to precipitation, TWS, and river level height variations.

	Precipitation	GRACE TWS	River level height
Before EMD	0.57	0.73	0.63
After EMD	0.71	0.88	0.77
Improvement(%)	12	15	14

1. Both groundwater and precipitation IMFs increase during 2006 and mid-2008 to mid-2009. Fig. 12b, presenting IMF 2 time series of assimilated groundwater, clearly shows the groundwater depletion despite having minimum changes in precipitations. This suggests that other factors (e.g., human impacts) affect groundwater storages in Bangladesh.

5. Conclusion

Terrestrial waters, as an essential factor for both human life and environment, can be affected by climate changes, especially over the South Asian areas. Bangladesh, in particular, is a highly vulnerable region in facing climate changes suffering from serious water issues, especially for irrigation. In this study, we analyze groundwater variations within Bangladesh using multi-mission satellite measurements, as well as by running a hydrological model during 2003 to 2013. The Gravity Recovery And Climate Experiment (GRACE) terrestrial water storage (TWS) data after removing surface water storages is assimilated into W3RA model using the ensemble-based sequential technique of the Square Root Analysis (SQRA) filter. This is done to improve the World-Wide Water Resources Assessment system (W3RA) simulations of groundwater, as well as soil water storages. We also apply the empirical mode decomposition (EMD) on water storages, precipitation, and altimetry-derived rivers level variations time series to explore the relationship between them in the area. The larger correlation is found between river level heights and rainfalls (78% average) in comparison to groundwater storage variations and rainfalls (57% average). The considerable difference between correlation coefficients indicates a different impact of rainfall on surface and groundwater variations, which could imply influences of groundwater depletion by population (especially for excessive irrigations) across the country. The results show an approximately 26%, groundwater depletion with a remarkable influence on the total water stored in the area. A significant decline in groundwater storage (~32% reduction over the study period) over the country is found by the assimilation results with an average rate of 8.73 mm/year. In the absence of any considerable decrease in precipitation over the region, a remarkable groundwater reduction is observed from the first and second Intrinsic Mode Functions (IMFs), which can be referred to human impacts. High spatio-temporal resolution remote sensing products along with the data assimilation methodology show a high capability for studying water storages in Bangladesh. Developing Earth observation missions dedicated to hydrology (GRACE follow-on and SWOT) can be very important to pursue and improve such modeling and assimilation studies.

Acknowledgments

We would like to thank Dr. Ashraf Dewan who provided in-situ groundwater and soil moisture measurements over Bangladesh used in this study. Authors are also grateful to BWDB (http://www.hydrology.bwdb.gov.bd/) for providing additional in-situ data used in this study. M. Khaki is grateful for the research grant of Curtin International Postgraduate Research Scholarships (CIPRS)/ORD Scholarship provided by Curtin University (Australia). This work is a TIGeR publication. This research is partially supported by the Belmont Forum/G8's coastal vulnerability program, via Australian Research Council, French ANR, German DFG, and US NSF (Grant No. ICER-1342644).

Appendix A. Supplementary data

Supplementary data to this article can be found online at https://doi.org/10.1016/j.scitotenv.2017.12.289.

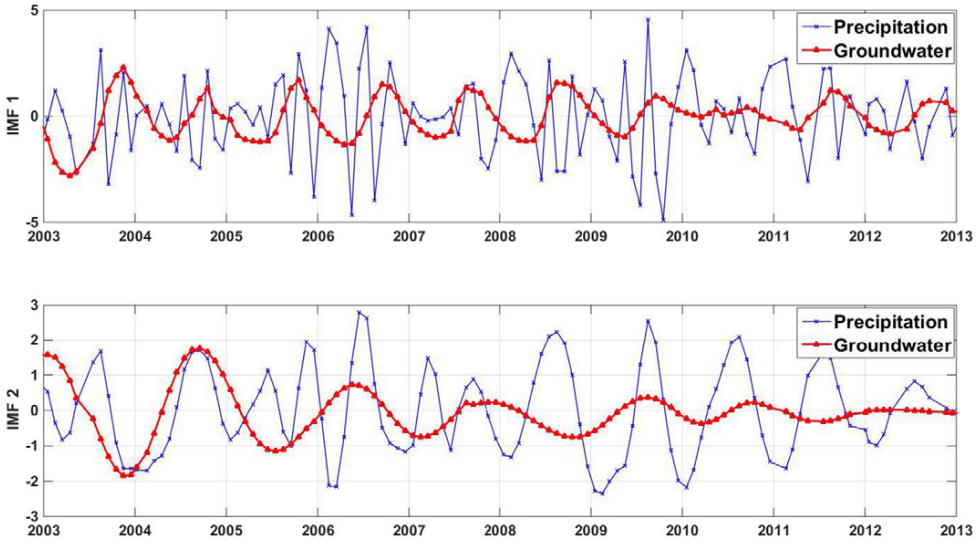

Fig. 12. The first and second extracted Intrinsic Mode Functions (IMF) time series of the groundwater storage (red) and precipitation (blue). (For interpretation of the references to color in this figure legend, the reader is referred to the web version of this article.)

References

Abdullah Aziz, M., Abul Kashem Majumder, M., Md., Shahjahan Kabir, Md., Ismail Hossain, Farhat Rahman, N.M., Rahman, F., Hosen, S., 2015. Groundwater depletion with expansion of irrigation in Barind tract: a case study of Rajshahi district of Bangladesh. Int. J. Geol. Agric. Environ. Sci. 3, 32–38.

ADB, Technical Assistance Consultant's Report, 2011. BANGLADESH: Khulnawater Supply Project (Financed by the Technical Assistance Special Fund), Institute of Water Modelling (IWM), Project Number: P42171-012. https://www.adb.org/sites/default/files/project_document/77210/42171_012_ban_tacr_01.pdf.

Adhikary, S.K., Das, S.K., Saha, G.C., Chaki, T., 2013. Groundwater Drought Assessment For Barind Irrigation Project in Northwestern Bangladesh, 20Th International Congress On Modelling and Simulation, Adelaide, Australia. www.mssanz.org.au/modsim2013.

Adnan, S., 1993. Living without Floods: Lessons from the Drought of 1992. Research and Advisory Services, Dhaka.

Ahmed, U.A., 2006. Bangladesh Climate Change Impacts and Vulnerability: A Synthesis. Climate Change Cell Department of Environment Component 4B. Comprehensive Disaster Management Programme, Bangladesh.

Alimuzzaman, U.A., 2017. Study of ground water recharge from rainfall in Dhaka City. International Journal of Science and Engineering Investigations 6 (6).ISSN: 2251-8843.

Anderson, J., 2001. An ensemble adjustment Kalman filter for data assimilation. Mon. Wea. Rev. 129, 2884–2903. https://doi.org/10.1175/1520-0493(2001)129<2884:AEAKFF>2.0.CO;2.

Anderson, M.C., Norman, J.M., Mecikalski, J.R., Otkin, J.A., Kustas, W.P., 2007. A climatological study of evapotranspiration and moisture stress across the continental United States based on thermal remote sensing: 1. Model formulation. J. Geophys. Res. 112, https://doi.org/10.1029/2006JD007506. (D10117).

Benada, J.R., 1997. PODAAC Merged GDR (TOPEX/POSEIDON) Generation B User's Handbook, Version 2.0. JPL D-11007. Jet Propulsion Laboratory, California Institute of Technology.

Bennett, A.F., 2002. Inverse Modeling of the Ocean and Atmosphere. Cambridge Univ. Press, New York. 234 pp.

Bertino, L., Evensen, G., Wackernagel, H., 2003. Sequential data assimilation techniques in oceanography. Int. Stat. Rev. 71 (2), 223–241. (Aug., 2003).

Birkett, C.M., 1995. The contribution of TOPEX/POSEIDON to the global monitoring of climatically sensitive lakes. J. Geophys. Res. 25, 179–25.

Birkett, C.M., 1998. Contribution of the TOPEX NASA radar altimeter to the global monitoring of large rivers and wetlands. Water Resour. Res. 34 (5), 1223–1239. https://doi.org/10.1029/98WR00124.

Boergens, E., Dettmering, D., Schwatke, C., Seitz, F., 2016. Treating the hooking effect in satellite altimetry data: a case study along the mekong river and its tributaries. Remote Sens. 8, 91. https://doi.org/10.3390/rs8020091.

Burgers, G., van Leeuven, P.J., Evensen, G., 1998. Analysis scheme in the ensemble Kalman filter. Mon. Wea. Rev. 126, 1719–1724.

BWDB (Bangladesh Water Development Board), 1994. Report on the Compilation of Aquifer Test Analysis Results, BWDB Water Supply Paper 534 Ground Water Circle II. BWDB, Dhaka.

Calmant, S., Seyler, F., Crétaux, J.F., 2008. Monitoring continental surface waters by satellite altimetry. Surv. Geophys. 29 (4-5), 247–269. https://doi.org/10.1007/s10712-008-9051-1.

Chang, B., Kruger, U., Kustra, R., Zhang, J., 2013. Canonical Correlation Analysis based on Hilbert-Schmidt Independence Criterion and Centered Kernel Target Alignment. Volume 28: Proceedings of the 30th International Conference on Machine Learning, 2, 28. pp. 316–324. http://jmlr.csail.mit.edu/proceedings/papers/v28/chang13.pdf.

Chen, J.L., Wilson, C.R., Famiglietti, J.S., Rodell, M., 2007. Attenuation effect on seasonal basin-scale water storage changes from GRACE time-variable gravity. J. Geod. 81 (4), 237–245. https://doi.org/10.1007/s00190-006-0104-2.

Cheng, M.K., Tapley, B.D., 2004. Variations in the Earth's oblateness during the past 28 years. J. Geophys. Res. Solid Earth 109, B09402. https://doi.org/10.1029/2004JB003028.

Dey, N.C., Alam, M.S., Sajjan, A.K., Bhuiyan, M.A., Ghose, L., Ibaraki, Y., Karim, F., 2011. Assessing environmental and health impact of drought in the northwest Bangladesh. J. Environ. Sci. Natural Resources 4 (2), 89–97. https://doi.org/10.3329/jesnr.v4i2.10141.

Döll, P., Kaspar, F., Lehner, B., 2003. A global hydrological model for deriving water availability indicators: model tuning and validation. J. Hydrol. 270, 105–134.

Eicker, A., Schumacher, M., Kusche, J., Döll, P., Müller-Schmied, H., 2014. Calibration/data assimilation approach for integrating GRACE data into the WaterGAP global hydrology model (WGHM) using an ensemble Kalman filter: first results. SurvGeophys 35 (6), 1285–1309. https://doi.org/10.1007/s10712-014-9309-8.

Elbern, H., Schmidt, H., 2001. Ozone episode analysis by four dimensional variational chemistry data assimilation. J. Geophys. Res. 106, 3569–3590.

Evensen, G., 2003. The ensemble Kalman filter: theoretical formulation and practical implementation. Ocean Dyn. 53, 343–367. https://doi.org/10.1007/s10236-003-0036-9.

Evensen, G., 2004. Sampling strategies and square root analysis schemes for the enKF. Ocean Dyn. 54 (6), 539–560.

Evensen, G., 2007. Data Assimilation: The Ensemble Kalman Filter. Springer.279 pp.

Flandrin, P., Gonçalvès, P., Rilling, G., 2004. Detrending and denoising with empirical mode decompositions. 12th European Signal Processing Conference, Vienna, 2004. pp. 1581–1584.

Fleming, K., Awange, J.L., 2013. Comparing the version 7 TRMM 3B43 monthly precipitation product with the TRMM 3B43 version 6/6a and Bureau of Meteorology Datasets for Australia. Aust. Meteorol. Oceanogr. J. 63 (3), 421–426.

Forootan, E., Rietbroek, R., Kusche, J., Sharifi, M.A., Awange, J., Schmidt, M., Omondi, P., Famiglietti, J., 2014. Separation of large scale water storage patterns over Iran using GRACE, altimetry and hydrological data. J. Remote Sens. Environ. 140, 580–595. https://doi.org/10.1016/j.rse.2013.09.025.

Frappart, F., Calmant, S., Cauhope, M., Seyler, F., Cazenave, A., 2006. Preliminary results of Envisat ra-2-derived water levels validation over the Amazon basin. Remote Sens. Environ. 100 (2), 252–264.

Frappart, F., Papa, F., Santos da Silva, J., Ramillien, G., Prigent, C., Seyler, F., Calmant, S., 2012. Surface freshwater storage and dynamics in the Amazon basin during the 2005 exceptional drought. Environ. Res. Lett. 7. https://doi.org/10.1088/1748-9326/7/4/044010. 044010, (7pp).

Fu, L.L., Cazenave, A., 2001. Satellite Altimetry and Earth sciences. A Handbook of Techniques and Applications. International Geophysics Series. 69. Academic, San Diego.

Gaiha, R., Hill, K., Thapa, G., 2010. Natural Disasters in South Asia. ASARC Working Papers, The Australian National University, Australia South Asia Research Centre. http://EconPapers.repec.org/RePEc:pas:asarcc:2010_06.

Garner, T.W., Wolf, R.A., Spiro, R.W., Thomsen, M.F., 1999. First attempt at assimilating data to constrain a magnetospheric model. J. Geophys. Res. 104 (A11), 25145–25152. https://doi.org/10.1029/1999JA900274.

Hasan, M.R., Mostafa, M.G., Matin, I., 2013. Effect of rainfall on groundwater level fluctuations in Chapai Nawabgonj district. Int. J. Eng. Res. Technol. (IJERT) 2 (4).ISSN: 2278-0181.

Hossain, M., 1990. Natural Calamities, Instability in Production and Food Policy in Bangladesh. The Bangladesh Development Studies (BDS). 18(1). Bangladesh Institute of Development Studies.,

Hoteit, I., Luo, X., Pham, D.T., 2012. Particle Kalman filtering: a nonlinear Bayesian framework for ensemble Kalman filters. Mon. Weather. Rev. 140 (2), 528–542.

Huang, N.E., Shen, Z., Long, S.R., Wu, M.C., Shih, H.H., et al. 1998. The empirical mode decomposition and the Hilbert spectrum for nonlinear and non-stationary time series analysis. Proc. R. Soc. Lond. A 454, 903–995.

Huffman, G., Bolvin, D., 2012. TRMM and Other Data Precipitation Data Set Documentation. Mesoscale Atmospheric Processes Laboratory, NASA Goddard Space Flight Center and Science Systems and Applications, Inc.

Huntington, T.G., 2006. Evidence for intensification of the global water cycle: review and synthesis. J. Hydrol. 319 (14), 83–95. https://doi.org/10.1016/j.jhydrol.2005.07.003.

Islam, M.N., Chowdhury, A., Islam, K.M., Rahaman, M.Z., 2014. Development of rainfall recharge model for natural groundwater recharge estimation in Godagari Upazila of Rajshahi district, Bangladesh. Am. J. Civil Eng. 2 (2), 48–52. https://doi.org/10.11648/j.ajce.20140202.16.

Islam, M.S., Alam, M.K., Rahman, M.A., 2013. Groundwater dynamics in Pabna district, Bangladesh. IOSR Journal Of Environmental Science, Toxicology And Food Technology (IOSR-JESTFT) 4 (2), 65–72. E-ISSN: 2319-2402,p- ISSN: 2319-2399. (May. - Jun. 2013).

Kanoua, W., Merkel, B.J., 2015. Groundwater recharge in Titas Upazila in Bangladesh. Arab J Geosci 8, 1361. https://doi.org/10.1007/s12517-014-1305-2.

Khaki, M., Ait-El-Fquih, B., Hoteit, I., Forootan, E., Awange, J., Kuhn, M., 2017c. A two-update ensemble Kalman filter for land hydrological data assimilation with an uncertain constraint. J. Hydrol. 555, 447–462.

Khaki, M., Forootan, E., Kuhn, M., Awange, J., Longuevergne, L., Wada, W., 2018. Efficient basin scale filtering of GRACE satellite products. Remote Sens. Environ. 204, 76–93. https://doi.org/10.1016/j.rse.2017.10.040. ISSN 0034-4257.

Khaki, M., Forootan, E., Sharifi, M.A., 2014. Satellite radar altimetry waveform retracking over the Caspian Sea. Int. J. Remote Sens. 35 (17), 6329–6356. https://doi.org/10.1080/01431161.2014.951741.

Khaki, M., Forootan, E., Sharifi, M.A., Awange, J., Kuhn, M., 2015. Improved gravity anomaly fields from retracked multimission satellite radar altimetry observations over the Persian Gulf and the Caspian Sea. Geophys. J. Int. 202 (3), 1522–1534. https://doi.org/10.1093/gji/ggv240.

Khaki, M., Hoteit, I., Kuhn, M., Awange, J., Forootan, E., van Dijk, A.I.J.M., Schumacher, M., Pattiaratchi, C., 2017a. Assessing sequential data assimilation techniques for integrating GRACE data into a hydrological model, Advances in Water Resources. 107 (2017), 301–316. https://doi.org/10.1016/j.advwatres.2017.07.001. ISSN 0309-1708.

Khaki, M., Schumacher, M., Forootan, J., Kuhn, M., Awange, E., van Dijk, A.I.J.M., 2017b. Accounting for spatial correlation errors in the assimilation of GRACE into hydrological models through localization. Adv. Water Resour. https://doi.org/10.1016/j.advwatres.2017.07.024. Available online 1 August 2017, ISSN 0309-1708.

Khandu, Awange, J.L., Kuhn, M., Anyah, R., Forootan, E., 2017. Changes and variability of precipitation and temperature in the Ganges-Brahmaputra-Meghna river basin based on global high-resolution reanalyses. Int. J. Climatol. 37, 2141–2159. https://doi.org/10.1002/joc.4842.

Klees, R., Revtova, E.A., Gunter, B.C., Ditmar, P., Oudman, E., Winsemius, H.C., 2008. The design of an optimal filter for monthly GRACE gravity models. Geophys. J. Int. 175 (2), 417–432. https://doi.org/10.1111/j.1365-246x.2008.03922.x.

Knappett, P.S.K., Mailloux, B.J., Choudhury, I., Khan, M.R., Michael, H.A., Barua, S., Mondal, D.R., Steckler, M.S., Akhter, S.H., Ahmed, K.M., Bostick, B., Harvey, C.F., Shamsudduha, M., Shuai, P., Mihajlov, I., Mozumder, R., van Geen, A., 2016. Vulnerability of low-arsenic aquifers to municipal pumping in Bangladesh. J. Hydrol. 539, 674–686.

Kusche, J., Klemann, V., Bosch, W., 2012. Mass distribution and mass transport in the Earth system. J. Geodyn. 59-60, 1–8. https://doi.org/10.1016/j.jog.2012.03.003.

Kusche, J., Schmidt, R., Petrovic, S., Rietbroek, R., 2009. Decorrelated GRACE time-variable gravity solutions by GFZ and their validation using a hydrological model. J. Geod. https://doi.org/10.1007/s00190-009-0308-3.
Lorenz, E., 1956. Empirical orthogonal function and statistical weather prediction. Technical Report Science Report No 1 Statistical Forecasting Project. MIT, Cambridge.
Mainuddin, M., 2002. Groundwater irrigation in Bangladesh: 'Tool for Poverty Alleviation' or 'Cause of Mass Poisoning'? Proceedings of the Symposium on Intensive Use of Groundwater: Challenges and Opportunities, Valencia, Spain. pp. 10–14.
Mayer-Gürr, T., Zehentner, N., Klinger, B., Kvas, A., 2014. ITSG-grace2014: a new GRACE gravity field release computed in Graz. GRACE Science Team Meeting (GSTM) Potsdam Am: 29.09.
McBean, E., deJong, A., Gharabaghi, B., 2011. Groundwater in Bangladesh: implications in a climate-changing world. Water Resour. Manag. 1 (3), 3–8.
McCarthy, J.J., Canziani, O.F., Leary, N.A., Dokken, D.J., White, K.S., et al. 2001. Climate change 2001: impacts, adaptation. and vulnerability. Inter-Governmental Panel on Climate Change (IPCC) Work Group II Input to the Third Assessment Report. Cambridge University Press, Cambridge.
Mondol, A.H., Ara, I., Das, S.C., 2017. Meteorological drought index mapping in Bangladesh using standardized precipitation index during 19812010. Adv. Meteorol. 2017, https://doi.org/10.1155/2017/4642060. 4642060.
Moradkhani, H., Hsu, K.L., Gupta, H., Sorooshian, S., 2005. Uncertainty assessment of hydrologic model states and parameters: sequential data assimilation using the particle filter. Water, Resour. Res. 41, W05012.
Müller Schmied, H., Eisner, S., Franz, D., Wattenbach, M., Portmann, F., Flörke, M., Döll, P., 2014. Sensitivity of simulated global-scale freshwater fluxes and storages to input data, hydrological model structure, human water use and calibration. Hydrol. Earth. Syst. Sci. 18, 3511–3538. https://doi.org/10.5194/hess-18-3511-2014.
Oke, P.R., Brassington, G.B., Griffin, D.A., Schiller, A., 2008. The bluelink ocean data assimilation system (BODAS). Ocean Model. 21, 46–70. https://doi.org/10.1016/j.ocemod.2007.11.002.
Ott, E., Hunt, B.R., Szunyogh, I., Zimin, A.V., Kostelich, E.J., Corazza, M., Kalnay, E., Patil, D.J., Yorke, J.A., 2004. A local ensemble Kalman Filter for atmospheric data assimilation. Tellus 56A, 415–428.
Papa, F., Durand, F., Rossow, W.B., Rahman, A., Bala, S.K., 2010a. Seasonal and interannual variations of the Ganges-Brahmaputra River discharge, 1993–2008 from satellite altimeters. J. Geophys. Res. 115, https://doi.org/10.1029/2009JC006075. C12013.
Papa, F., Frappart, F., Malbeteau, Y., Shamsudduha, M., Vuruputur, V., et al. 2015. Satellite-derived surface and sub-surface water storage in the Ganges-Brahmaputra River Basin. J. Hydrol. Regional Stud. 4 (Part A), 15–35. https://doi.org/10.1016/j.ejrh.2015.03.004. ISSN 2214-5818.
Papa, F., Prigent, C., Aires, F., Jimenez, C., Rossow, W.B., Matthews, E., 2010a. Interannual variability of surface water extent at global scale, 1993-2004. J. Geophys. Res. 115, https://doi.org/10.1029/2009JD012674. D12111.
Papa, F., Prigent, C., Durand, F., Rossow, W.B., 2006. Wetland dynamics using a suite of satellite observations: a case study of application and evaluation for the Indian Subcontinent. Geophys., Res. Lett. 33. https://doi.org/10.1029/2006GL025767.
Pietrafesa, L.J., Shaowu, B., Huang, N.E., Gayes, P., Yan, T., et al. 2016. Great Lakes water levels: decomposing time series for attribution. J. Climatol. Weather Forecasting 4, 153. https://doi.org/10.4172/2332-2594.1000153.
Prigent, C., Papa, F., Aires, F., Jimenez, C., Rossow, W.B., Matthews, E., 2012. Changes in land surface water dynamics since the 1990s and relation to population pressure. Geophys. Res. Lett. 39, https://doi.org/10.1029/2012GL051276. L08403.
Qureshi, A.S., Ahmad, Z.U., Krupnik, T.J., 2015. Moving from resource development to resource management: problems prospects and policy recommendations for sustainable groundwater management in Bangladesh. Water, Res. Manage. 29, 4269–4283.
Rafiuddin, M., Uyeda, H., Islam, M.N., 2010. Characteristics of monsoon precipitation systems in and around Bangladesh 30, 1042–1055. https://doi.org/10.1002/joc.1949.
Rajib, M.A., Mortuza, M.R., Selmi, S., Asif Khan Ankur, A.K., et al. 2011. Increase of heat index over Bangladesh: impact of climate change. World Acad. Sci. Eng. Technol. 5 (10), 340–343.
Reager, J.T., Thomas, A.C., Sproles, E.A., Rodell, M., Beaudoing, H.K., Li, B., Famiglietti, J.S., 2015. Assimilation of GRACE terrestrial water storage observations into a land surface model for the assessment of regional flood potential. Remote Sens. 2015 (7), 14663–14679.
Renzullo, L.J., Van Dijk, A.I.J.M., Perraud, J.M., Collins, D., Henderson, B., Jin, H., Smith, A.B., McJannet, D.L., 2014. Continental satellite soil moisture data assimilation improves root-zone moisture analysis for water resources assessment. J. Hydrol. 519, 2747–2762. https://doi.org/10.1016/j.jhydrol.2014.08.008.
Rilling, G., Flandrin, P., Goncalves, P., 2003. On Empirical Mode Decomposition and Its Algorithms. Proceedings IEEE-EURASIP Workshop on Nonlinear Signal and Image Processing NSIP-03, Grado I. pp. 3.
Sakov, P., Oke, P.R., 2008. A deterministic formulation of the ensemble Kalman filter: an alternative to ensemble square root filters. Tellus 60A, 361–371.
Schumacher, M., Forootan, E., van Dijk, A.I.J.M., Müller Schmied, H., Crosbie, R.S., Kusche, J., Döll, P., 2018. Improving drought simulations within the Murray-Darling Basin by combined calibration/assimilation of GRACE data into the waterGAP Global Hydrology Model. Remote Sens. Environ. 204, 212–228.
Schumacher, M., Kusche, J., Döll, P., 2016. A systematic impact assessment of GRACE error correlation on data assimilation in hydrological models. J. Geod. https://doi.org/10.1007/s00190-016-0892-y.
Sengupta, S., Kang, A., Jacob, N., 2013. Water Wealth A Briefing Paper on the State of Groundwater Management in Bangladesh. India Environment Portal. http://www.cseindia.org/userfiles/groundwater_management_bangladesh.pdf.
Seyler, F., Calmant, S., Santos da Silva, J., Filizola, N., Roux, E., Cochonneau, G., Vauchel, P., Bonnet, M.P., 2008. Monitoring water level in large trans-boundary ungauged basins with altimetry: the example of ENVISAT over the Amazon basin. J. Appl. Remote. Sens. 7150 (715017). https://doi.org/10.1117/12.813258.
Shahid, S., 2010. Rainfall variability and the trends of wet and dry periods in Bangladesh. Int. J. Climatol. 30, 2299–2313. https://doi.org/10.1002/joc.2053.
Shamsudduha, M., Chandler, R.E., Taylor, R.G., Ahmed, K.M., 2009. Recent trends in groundwater levels in a highly seasonal hydrological system: the Ganges-Brahmaputra-Meghna Delta. Hydrol. Earth Syst. Sci. 13, 2373–2385.
Shamsudduha, M., Taylor, R.G., Ahmed, K.M., Zahid, A., 2011. The impact of intensive groundwater abstraction on recharge to a shallow regional aquifer system: evidence from Bangladesh. Hydrogeol. J. 19, 901. https://doi.org/10.1007/s10040-011-0723-4.
Shamsudduha, M., Taylor, R.G., Jones, D., Longuevergne, L., Owor, M., Tindimugaya, C., 2017. Recent changes in terrestrial water storage in the Upper Nile Basin: an evaluation of commonly used gridded GRACE products. Hydrol. Earth Syst. Sci. 21, 4533–4549. https://doi.org/10.5194/hess-21-4533-2017.
Shamsudduha, M., Taylor, R.G., Longuevergne, L., 2012. Monitoring groundwater storage changes in the highly seasonal humid tropics: validation of GRACE measurements in the Bengal. Basin., Water Resour. Res. 48, W02508. https://doi.org/10.1029/2011WR010993.
Sheffield, J., Goteti, G., Wood, E.F., 2006. Development of a 50-year high-resolution global dataset of meteorological forcings for land surface modeling. J. Clim. 19 (13), 3088–3111.
Sumon, F.R., Abul Kalam, A.K.M., 2014. Rainwater Harvesting and the Scope of Enhancing Ground Water Table in Dhaka City. Dhaka Metropolitan Development Area and Its Planning Problems, Issues and Policies. Bangladesh Institute of Planners (BIP).
Swenson, S., Chambers, D., Wahr, J., 2008. Estimating geocenter variations from a combination of GRACE and ocean model output. J. Geophys. Res. 113, B08410. https://doi.org/10.1029/2007JB005338.
Swenson, S., Wahr, J., 2002. Methods for inferring regional surface-mass anomalies from Gravity Recovery and Climate Experiment (GRACE) measurements of time-variable gravity. J. Geophys. Res. 107 (B9), 2193. https://doi.org/10.1029/2001JB000576.
Tangdamrongsub, N., Steele-Dunne, S.C., Gunter, B.C., Ditmar, P.G., Weerts, A.H., 2015. Data assimilation of GRACE terrestrial water storage estimates into a regional hydrological model of the Rhine River basin. Hydrol., Earth Syst. Sci. 19, 2079–2100. https://doi.org/10.5194/hess-19-2079-2015.
Thomas, A.C., Reager, J.T., Famiglietti, J.S., Rodell, M., 2014. A GRACE-based water storage deficit approach for hydrological drought characterization. Geophys. Res. Lett. 41, 1537–1545.
Tian, S., Tregoning, P., Renzullo, L.J., van Dijk, A.I.J.M., Walker, J.P., Pauwels, V.R.N., Allgeyer, S., 2017. Improved water balance component estimates through joint assimilation of GRACE water storage and SMOS soil moisture retrievals. Water, Resour. Res. 53. https://doi.org/10.1002/2016WR019641.
Tropical Rainfall Measuring Mission (TRMM), 2011. TRMM (TMPA/3B43) Rainfall Estimate L3 1 Month 0.25 Degree X 0.25 Degree V7, Greenbelt, MD, Goddard Earth Sciences Data and Information Services Center (GES DISC), Accessed [Data Access Date]. URL https://disc.gsfc.nasa.gov/datacollection/TRMM_3B43_7.html.
van Dijk, A.I.J.M., 2010. The Australian Water Resources Assessment System: Technical Report 3 Landscape model (version 0.5). Technical Description. Water for a Healthy Country National Research Flagship.,
van Dijk, A.I.J.M., Pea-Arancibia, J.L., Wood, E.F., Sheffield, J., Beck, H.E., 2013. Global analysis of seasonal streamflow predictability using an ensemble prediction system and observations from 6192 small catchments worldwide. Water, Resour. Res. 49, 2729–2746. https://doi.org/10.1002/wrcr.20251.
van Dijk, A.I.J.M., Renzullo, L.J., Rodell, M., 2011. Use of Gravity Recovery and Climate Experiment terrestrial water storage retrievals to evaluate model estimates by the Australian water resources assessment system. Water, Resour. Res. 47, https://doi.org/10.1029/2011WR010714. W11524.
van Dijk, A.I.J.M., Renzullo, L.J., Wada, Y., Tregoning, P., 2014. A global water cycle reanalysis (2003–2012) merging satellite gravimetry and altimetry observations with a hydrological multi-model ensemble. Hydrol. Earth Syst. Sci. 18, 2955–2973. https://doi.org/10.5194/hess-18-2955-2014.
Vrugt, J.A., ter Braak, C.J.F., Diks, C.G.H., Schoups, G., 2013. Advancing hydrologic data assimilation using particle Markov chain Monte Carlo simulation: theory, concepts and applications, advances in water resources, anniversary issue – 35 years. 51, 457–478. https://doi.org/10.1016/j.advwatres.2012.04.002.
Wahr, J.M., Molenaar, M., Bryan, F., 1998. Time variability of the Earth's gravity field: hydrological and oceanic effects and their possible detection using GRACE. J. Geophys. Res. 108 (B12), 30205–30229. https://doi.org/10.1029/98JB02844.
Wang, B., Ding, Q., 2006. Changes in global monsoon precipitation over the past 56 years. Geophys. Res. Lett. 33, L06711. https://doi.org/10.1029/2005GL025347.
Wooldridge, S.A., Kalma, J.D., 2001. Regional-scale hydrological modelling using multiple-parameter landscape zones and a quasi-distributed water balance model. Hydrol. Earth Syst. Sci. 5, 59–74.
Zaitchik, B.F., Rodell, M., Reichle, R.H., 2008. Assimilation of GRACE terrestrial water storage data into a land surface model: results for the Mississippi River Basin. J. Hydrometeorol. 9 (3), 535–548. https://doi.org/10.1175/2007JHM951.1.

Advances in Water Resources 114 (2018) 1–18

Contents lists available at ScienceDirect

Advances in Water Resources

journal homepage: www.elsevier.com/locate/advwatres

Determining water storage depletion within Iran by assimilating GRACE data into the W3RA hydrological model

M. Khaki[a,*], E. Forootan[b], M. Kuhn[a], J. Awange[a], A.I.J.M. van Dijk[c], M. Schumacher[d], M.A. Sharifi[e,f]

[a] School of Earth and Planetary Sciences, Discipline of Spatial Sciences, Curtin University, Perth, Australia
[b] School of Earth and Ocean Sciences, Cardiff University, Cardiff, UK
[c] Fenner School of Environment and Society, The Australian National University, Canberra, Australia
[d] School of Geographical Sciences, University of Bristol, Bristol, UK
[e] Faculty of Surveying and Geospatial Engineering, College of Engineering, University of Tehran, Iran
[f] Research Institute of Geoinformation Technology (RIGT), College of Engineering, University of Tehran, Iran

ARTICLE INFO

Article history:
Received 19 June 2017
Revised 1 February 2018
Accepted 7 February 2018
Available online 8 February 2018

Keywords:
Iran
Groundwater storage
Data assimilation
Canonical correlation analysis
GRACE
W3RA Hydrological model
Water storage depletion

ABSTRACT

Groundwater depletion, due to both unsustainable water use and a decrease in precipitation, has been reported in many parts of Iran. In order to analyze these changes during the recent decade, in this study, we assimilate Terrestrial Water Storage (TWS) data from the Gravity Recovery And Climate Experiment (GRACE) into the World-Wide Water Resources Assessment (W3RA) model. This assimilation improves model derived water storage simulations by introducing missing trends and correcting the amplitude and phase of seasonal water storage variations. The Ensemble Square-Root Filter (EnSRF) technique is applied, which showed stable performance in propagating errors during the assimilation period (2002–2012). Our focus is on sub-surface water storage changes including groundwater and soil moisture variations within six major drainage divisions covering the whole Iran including its eastern part (East), Caspian Sea, Centre, Sarakhs, Persian Gulf and Oman Sea, and Lake Urmia. Results indicate an average of -8.9 mm/year groundwater reduction within Iran during the period 2002 to 2012. A similar decrease is also observed in soil moisture storage especially after 2005. We further apply the canonical correlation analysis (CCA) technique to relate sub-surface water storage changes to climate (e.g., precipitation) and anthropogenic (e.g., farming) impacts. Results indicate an average correlation of 0.81 between rainfall and groundwater variations and also a large impact of anthropogenic activities (mainly for irrigations) on Iran's water storage depletions.

1. Introduction

Water scarcity has become a serious issue in the Islamic Republic of Iran (abbreviated here as Iran) in recent years (e.g., Amery and Wolf, 2000; Madani, 2014; Michel, 2017; Trigo et al., 2010; Wolf and Newton, 2007). With the increased extraction of groundwater, its level has been reported to fall significantly (see, e.g., Afshar et al., 2016; Mohammadi-Ghaleni and Ebrahimi, 2011; Motagh et al., 2008; Sarraf et al., 2005; Van Camp et al., 2012). There have been studies that investigate surface and groundwater changes in Iran during the last decade (2003 onward) mainly using Terrestrial Water Storage (TWS) data from the Gravity Recovery And Climate Experiment (GRACE, Tapley et al., 2004). For example, Voss et al. (2013) reported ~143.6 km^3 reduction of freshwater from 2003 to 2009 over the north-central area of the Middle East, which largely covers the Tigris–Euphrates Basin. Forootan et al. (2014a) applied a statistical inversion to separate GRACE TWS using hydrological model outputs and altimetry data as a priori information, and found a decrease in water storage with an average linear rate of ~-15 mm/year between 2002 and 2011. A large negative trend (2003–2012) in TWS was observed by Joodaki et al. (2014) using GRACE TWS data over the western Iran and eastern Iraq.

Estimating sub-surface water storages is very important since they support the life in semi-arid areas like Iran. Fatolazadeh et al. (2016) used the wavelet approach to improve estimates of groundwater storage variations from GRACE and found a remarkable decrease in groundwater in 2008, 2010 and particularly in 2011. Forootan et al. (2017) compared changes in water storage and hydrological water fluxes in Iran using GRACE and climate re-

* Corresponding author.
E-mail address: Mehdi.Khaki@postgrad.curtin.edu.au (M. Khaki).

https://doi.org/10.1016/j.advwatres.2018.02.008
0309-1708/

analysis data. Their results indicated that the decline of TWS in the Urmia and Tigris-Euphrates basins are greater than the decrease in the monthly accumulated total water fluxes. Therefore, it was concluded that the anthropogenic contribution on surface and groundwater flow is significant, and results in the storage decline within Iran.

These studies have proved the effectiveness of GRACE to enhance the understanding of water storage changes within the country. However, they do not provide a full understanding of spatially distributed water resources changes in different water compartments in Iran. GRACE TWS measures the summation of all water masses in the surface and sub-surface compartment of the terrestrial water storage (vegetation, snow, surface waters, soil, groundwater, etc.). Therefore, GRACE TWS must be separated into different storage compartments, which has been achieved to date through a forward modeling or an inversion framework as is described in Forootan et al. (2014a) and the literature mentioned before.

To complement previous attempts, the aims of this study are to (i) update hydrological model simulations of sub-surface water storage changes (including water stored in the soil and groundwater storage) within Iran using GRACE data assimilation, and (ii) investigate climate and anthropogenic impacts on the estimated subsurface water storages in (i). This study is the first data assimilation attempt to integrate GRACE TWS into the World-Wide Water Resources Assessment (W3RA; vanDijk, 2010) hydrological model over Iran. This methodology has been implemented in studies to constrain the mass balance of hydrological models over different river basins (e.g., Eicker et al., 2014; Girotto et al., 2016; Reager et al., 2015; Schumacher et al., 2016; van Dijk et al., 2014; Zaitchik et al., 2008). The main rationale in following this approach is that one relies on the physical processes, implemented in the model equations, to separate GRACE TWS into water compartments (see similar arguments, e.g., in Bertino et al., 2003). Thus, by generating ensemble members for a model derived water storage simulation, we will compute a priori estimates of mass redistribution in the country. Then, by assimilating GRACE data, while considering their uncertainty, we update (correct) these model estimations. A similar concept has also been followed in studies in hydrology, climate, and oceanography (see, e.g., Bennett, 2002; Garner et al., 1999; Kalnay, 2003; Khaki et al., 2017a; 2017b; Lahoz et al., 2007; Schunk et al., 2004). In addition, by applying data assimilation, we will likely be able to reliably separate GRACE TWS data into different water compartments since both model and observation errors are considered. Considering that the spatial resolution of models is usually better than GRACE data, through the assimilation procedure, GRACE observations are downscaled, and therefore, higher resolution estimations of water storages will be available within the country (see also Khaki et al., 2018a; Schumacher et al., 2016).

Once improved model simulations are obtained, by assimilating GRACE TWS, relationships between the model-derived groundwater and soil moisture storages and climatic variables within Iran are investigated. To investigate the impacts of climate on the regional water storage estimates, precipitation from satellite remote sensing, temperature, and vegetation changes through the Normalized Difference Vegetation Index (NDVI) are used. Furthermore, anthropogenic effects are explored using the changes in water use for farming, industry, and human consumption. To this end, Canonical Correlation Analysis (CCA) is applied to provide an insight into the relations between model-derived water storages and both climatic and anthropogenic impacts by extracting spatio-temporal correlations between these inter-related data sets. For a better spatial analysis of water storage and to reduce the uncertainty of estimations, the study area is divided into six major areas: the eastern part of Iran (indicated by East), Caspian Sea, Centre, Sarakhs, Persian Gulf and Oman Sea, and Lake Urmia (Fig. 1).

The remainder of this study is structured as follows: Section 2 provides details on W3RA model, remotely sensed datasets, and in-situ measurements used. In Section 3, data assimilation filtering techniques, CCA algorithm, and the outline of our experimental setup are described. Results are presented and discussed in Section 4 including the data assimilation performance and analyzing the relationship between the model estimations, rainfall and NDVI through CCA. Finally, the study is concluded in Section 5.

2. Study area and data

2.1. Iran

Located in an arid and semi-arid region, Iran experiences strong regional differences in climate (Fig. 1). Subtropical conditions are dominant over the northern part, but 90% of the country has limited rainfall with extremely hot summers in the central and southern coastal regions (Golian et al., 2015). Much of the west to northwest of Iran is located in high plateaus and mountain ranges associated with strong temperature differences between winter and summer. By contrast, the centre to southern parts are warm (cf. Fig. 1) for most of the year with mild winters and hot summers. Annual rainfall, the main source of freshwater in Iran, varies from 50 mm in the deserts to 2275 mm in the northern part of the country (FAO, 0000). Only a fraction of the country receives enough rainfall for agriculture. A growing use of irrigation for agricultural productions (Ardakani, 2009) and the increasing population (from $\sim$55 million in 1990 to $\sim$80 million in 2015 Karamouzian and Haghdoost, 2015), make water availability an important issue across the country (Michel, 2017).

2.2. W3RA hydrological model

The present study uses the globally distributed World-Wide Water Resources Assessment system (W3RA) model, run at $1^\circ \times 1^\circ$. W3RA, based on the Australian Water Resources Assessment system (AWRA) model (version 0.5) developed in 2008 by the Commonwealth Scientific and Industrial Research Organization (CSIRO) is a daily grid-distributed biophysical model that simulates landscape water stored in the vegetation and soil systems (see details in vanDijk, 2010). The model represent and forecast terrestrial water cycles (Renzullo et al., 2014; vanDijk, 2010). W3RA does not consider anthropogenic effects (e.g., irrigation). Therefore, by assimilating GRACE TWS, which integrates both natural and anthropogenic signals (e.g., Schumacher et al., 2018), we hope to constrain the model's water storage simulations and introduce the missing variations. Meteorological forcing data that is used here are minimum and maximum temperature, down-welling short-wave radiation, and precipitation from the Princeton University (Sheffield et al., 2006). The model contains effective soil parameters, water holding capacity and soil evaporation, relating greenness and groundwater recession, and saturated area to catchment characteristics parameters (van Dijk et al., 2013). This one-dimensional grid-based water balance model represents the water balance of the soil, groundwater and surface water stores in which each cell is modeled independently of its neighbors (Renzullo et al., 2014; vanDijk, 2010). The model state, which is used for data assimilation (2002–2012), is composed of W3RA storages of the top, shallow root and deep root soil layers, and groundwater storage in an one-dimensional system (vertical variability).

2.2.1. Satellite-derived observations

We use monthly GRACE level 2 (L2) gravitational Stokes' coefficients truncated up to spherical harmonic degree and order 90

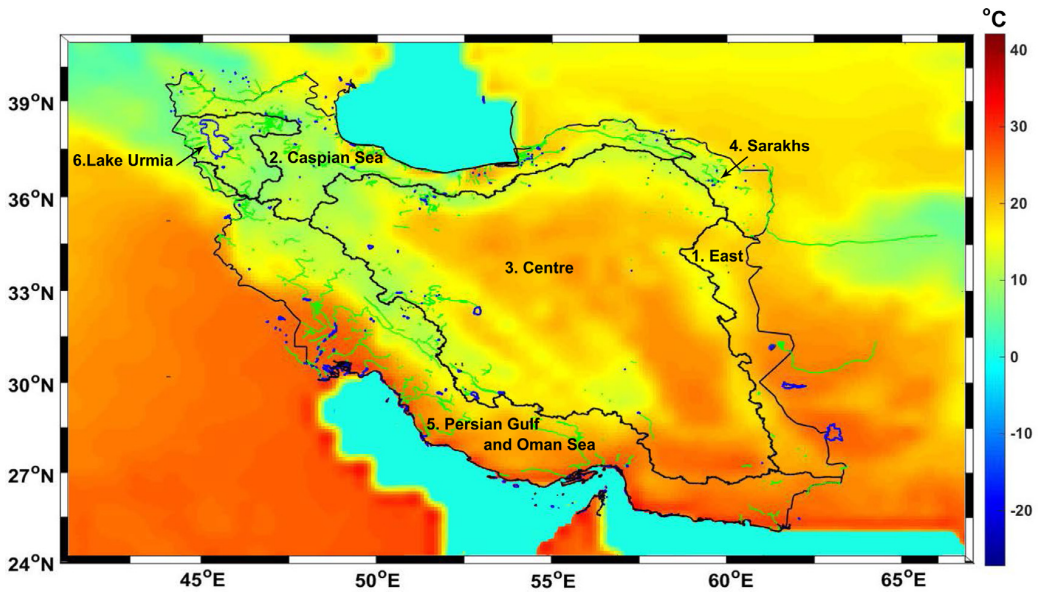

Fig. 1. The study area and its average temperature (Harris, 2008). The figure also contains the locations of 6 major catchments separated by black solid lines.

along with their full error information from 2002 to 2012 provided by the ITSG-Grace2016 gravity field model (Mayer-Gürr et al., 2014). The monthly full error information of the Stokes' coefficients is used to construct an observation error covariance matrix for the GRACE TWS fields to be used for data assimilation (Schumacher et al., 2016). Degree 1 of Stokes' coefficients are replaced with those estimated by Swenson et al. (2008) to account for the movement of the Earth's center of mass. Degree 2 and order 0 (C20) coefficients are replaced by those from Satellite Laser Ranging solutions due to unquantified large uncertainties in this term (e.g., Chen et al., 2007; Cheng and Tapley, 2004). Afterward, following Wahr et al. (1998), the L2 gravity fields is converted to gridded TWS fields with a $1^\circ \times 1^\circ$ spatial resolution.

Correlated noise in data due to anisotropic spatial sampling, instrumental noise (K-band ranging system and GPS), and temporal aliasing caused by the incomplete reduction of short-term mass variations (Forootan et al., 2014b) can be reduced by smoothing filters (e.g., Kusche et al., 2009). The application of smoothing, however, causes a spatial leakage problem that can be problematic given that strong water resources of Tigris River and the Persian Gulf Basin can affect GRACE signals, as leakage-in errors, over the northwest and south of Iran, respectively. To tackle these errors, we use a Kernel Fourier Integration (KeFIn) filter, proposed by Khaki et al. (2018b), which defines an efficient averaging kernel to improve GRACE TWS within Iran. The KeFIn filtering method accounts for signal attenuations and leakage effects caused by smoothing in a two step filtering scheme (see more details in Khaki et al., 2018b). Lastly, in order to reach absolute TWS estimates (similar to W3RA), the mean TWS for the study period is taken from W3RA and added to the GRACE TWS anomalies time series.

Furthermore, since W3RA does not simulate lake dynamics, one needs to account for the existing surface water storage over the Lake Urmia before assimilation of the GRACE TWS data. Water level height datasets from satellite radar altimetry of Jason-1 (260 cycles from 2002 to 2008) and Jason-2 (165 cycles from 2008 to 2012) are used to separate groundwater and surface water storage from GRACE TWS (more details in Section 3.1.2). We use the ExtR post-processing technique (Khaki et al., 2014; 2015) to retrack the data and improve water level measurements, which are erroneous within inland waters. Filtered surface heights are then used to create time series for virtual gauge stations over the Lake Urmia. These time series are subsequently used to remove the contribution of surface water storage changes from GRACE TWS data before implementing the proposed data assimilation (see also the procedure in Forootan et al., 2014a).

Satellite-derived precipitation data of TRMM-3B43 products (TRMM, 2011) from the Tropical Rainfall Measuring Mission Project (TRMM; version 7) is used to study rainfall variations. We convert the gridded precipitation products provided with a $0.25^\circ \times 0.25^\circ$ spatial scale to $1^\circ \times 1^\circ$ for the period between 2002 and 2012. In addition, we use Version 4 gridded daily Normalized Difference Vegetation Index (NDVI) derived from the NOAA Climate Data Record (CDR) between 2002 and 2012 to further investigate climatic impacts. This dataset is produced by the NASA Goddard Space Flight Center (GSFC) and the University of Maryland with a $0.05^\circ \times 0.05^\circ$ spatial resolution. The datasets are rescaled to a $1^\circ \times 1^\circ$ spatial resolution. A summary of the data sets and links to download the data are provided in Table 1.

2.2.2. Temperature

Monthly average temperature data for the temporal period of 2003 to 2012 is acquired from Climatic Research Unit (CRU; Harris, 2008), which is used in CCA as a climate indicator. This data is provided using more than 4000 weather stations distributed around the world. For the sake of consistency with other data sets, the collected $0.5^\circ \times 0.5^\circ$ spatial scale data is converted to $1^\circ \times 1^\circ$.

2.3. In-situ data

We use in-situ groundwater level data collected from 562 observation wells distributed over the six drainage divisions of East, Caspian Sea, Centre, Sarakhs, Persian Gulf and Oman Sea, and Lake Urmia water (cf. Figs. 1) to compare them with our results. Datasets are provided by the Iran Water Resources Management Company (IWRMC) and are categorized based on Iran's six largest provinces on a yearly temporal scale presenting groundwater storage changes for an entire aquifer (Forootan et al., 2014a). Fig. 2 shows an annual increase in groundwater extraction and the number of drilled wells for the entire country derived from IWRMC

Table 1
A summary of the datasets used in this study.

Description	Platform	Data access
Terrestrial water storage (TWS)	GRACE	https://www.tugraz.at/institute/ifg/downloads/gravity-field-models/itsg-grace2014/
Precipitation	TRMM-3B43	https://disc.gsfc.nasa.gov/datacollection/TRMM_3B43_7.html
Normalized Difference Vegetation Index (NDVI)	NASA-GSFC	ftp://eclipse.ncdc.noaa.gov/pub/cdr/avhrr-land/ndvi/
Hydrological model	W3RA	http://www.wenfo.org/wald/data-software/
Temperature	Harris (2008)	https://crudata.uea.ac.uk/cru/data/hrg/
Groundwater in-situ measurements	IWRMC	http://www.wrm.ir/
Average water consumption	IWRMC	http://www.wrm.ir/
Discharge data	IWRMC	http://www.wrm.ir/
Number of groundwater bore holes	IWRMC	http://www.wrm.ir/
Altimetry-derived level height	Jason-1	http://podaac.jpl.nasa.gov
Altimetry-derived level height	Jason-2	http://avisoftp.cnes.fr/

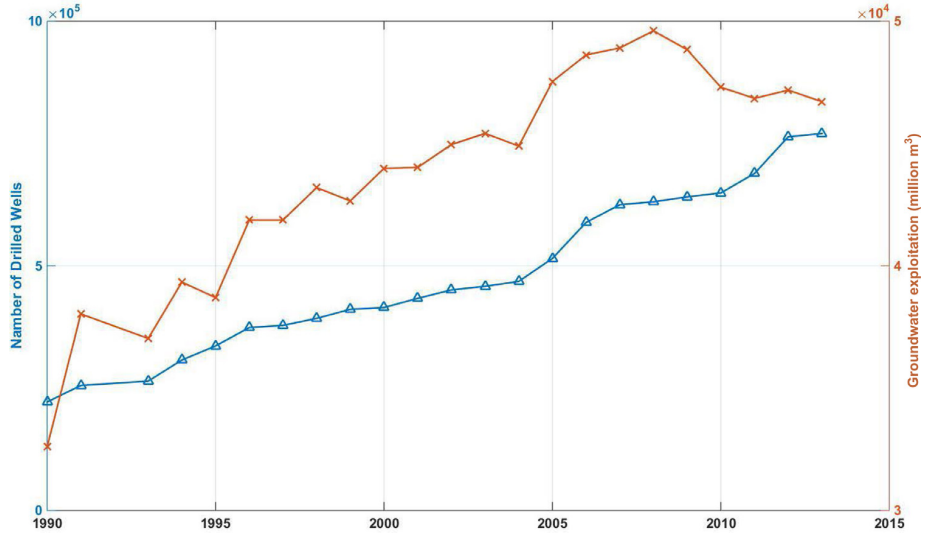

Fig. 2. Groundwater depletion and the number of drilled wells in Iran from IWRMC.

data sets. The IWRMC volumetric groundwater change measurements are converted to equivalent water height using the area of each aquifer. The area-averaged time series of groundwater changes for each aquifer is then generated and used for evaluating the results. The modified in-situ groundwater time series are compared separately to the average assimilation results for the same aquifer. River water discharge, the number of bore holes, and average water use for farming, industry, and urban use provided by IWRMC are also used in the CCA process (see Section 3.2). Details of all the applied datasets, as well as the model are presented in Table 1.

3. Method

3.1. Data assimilation

3.1.1. EnSRF filtering

In order to assimilate GRACE data into the W3RA model, we use the Ensemble Square-Root Filter (EnSRF) following Whitaker and Hamill (2002). EnSRF is an extended version of traditional Ensemble Kalman Filter (EnKF) that does not require the observations to be perturbed by introducing a new sampling scheme. Here, EnSRF is selected to avoid sampling errors that can be reflected in the background covariance matrix especially in using a limited number of ensembles (Whitaker and Hamill, 2002). Khaki et al. (2017a) showed that this method is highly capable of assimilating GRACE TWS data into a hydrological model amongst the most commonly used filters. EnSRF adopts a similar analysis step to the EnKF in the sense that the analysis perturbations are computed from the forecast perturbations by updating each ensemble perturbation with a Kalman-like update step. In the present study X consists of six different water storages including top soil, shallow soil, and deep soil water, vegetation, snow, and groundwater storages. Previous studies, e.g., Forootan et al. (2014a) and Tourian et al. (2015), have investigated the surface water variations, specifically, in the Lake Urmia Basin and the Caspian Sea as the major source of surface water storage changes in Iran. Therefore, here, we only focus on the estimation of sub-surface compartments including groundwater and soil moisture. The modified GRACE TWS data (see Section 2.2.1 for details) is then used to update the above water compartments excluding surface storage.

The forecast model state, the integrated model state by a dynamical model for N times (N is the ensemble number), is represented by $X^f = [{X_1}^f \cdots {X_N}^f]$, where ${X_i}^f$ $(i = 1 \cdots N)$ is the ith ensemble (hereafter 'f' refers to forecast and 'a' represents analysis). The corresponding model state forecast error covariance of P^f is defined by:

$$P^f = \frac{1}{N-1}\sum_{i=1}^{N}({X_i}^f - \bar{X}^f)({X_i}^f - \bar{X}^f)^T, \tag{1}$$

$$\bar{X}^f = \frac{1}{N}\sum_{i=1}^{N}(X_i). \tag{2}$$

The update stage in EnSRF contains two steps. First, it updates the ensemble-mean following,

$$\bar{X}^a = \bar{X}^f + K(y - H\bar{X}^f), \quad i = 1 \cdots N, \tag{3}$$

$$K = P^f(H)^T(HP^f(H)^T + R)^{-1}, \tag{4}$$

where K is the Kalman gain, y is the observation vector. The transition matrix and the observation covariance matrix are indicated by H and R, respectively. Next, EnSRF updates the forecast ensemble of anomalies $A^f = [{A_1}^f \cdots {A_N}^f]$ into the analysis ensemble deviation A^a. A^f as the deviation of model state ensembles from the ensemble mean is derived from,

$${A_i}^f = {X_i}^f - \bar{X}^f. \tag{5}$$

EnSRF exploits the serial formulation of the Kalman filter analysis step in which the observations are assimilated each at a time to compute the analysis perturbations that exactly match the Kalman filter covariance (Hoteit et al., 2008) using the modified gain ($\tilde{K}$) with,

$$A^a = (I - \tilde{K}H){A_i}^f, \tag{6}$$

$$\alpha = \left(1 + \sqrt{\frac{R}{HP^fH^T + R}}\right)^{-1}, \tag{7}$$

where I is an identity matrix. More details on EnSRF can be found in Whitaker and Hamill (2002) and Tippett et al. (2003).

3.1.2. Assimilating GRACE TWS into W3RA

Monthly gridded GRACE TWS data are assimilated into W3RA to update the model states, a summation of model vertical water compartments (here soil moisture, vegetation biomass, snow, and groundwater). Note that no parameter adjustment is considered here and the observations are only used to constrain the system states. The monthly increment (i.e., the difference between the monthly averaged GRACE TWS and simulated TWS) can be added to each day of the current month, which guarantees that the update of the monthly mean is identical to the monthly mean of the daily updates. In practice, the differences between the predictions and the updated states are added as offsets to the state vectors at the last day of each month to generate the ensembles for the next month assimilation step. We use Monte Carlo sampling of multivariate normal distributions with the errors representing the standard deviations of the forcing sets (precipitation, temperature, and radiation) to generate an initial ensemble (Renzullo et al., 2014). The perturbed meteorological forcing datasets, then, are integrated forward with the model from 2000 to 2002 providing 72 sets of state vectors (as suggested by Oke et al., 2008) at the beginning of the study period.

An application of small ensemble size is problematic in ensemble data assimilation systems, as it can lead to filter divergent or inaccurate estimation (Tippett et al., 2003). Therefore, we apply ensemble inflation that uses a small coefficient factor (here 1.12; AAnderson, 2001) to inflate prior ensemble deviation from the ensemble-mean and increases their variations (Anderson et al., 2007). Furthermore, the Local Analysis (LA) scheme (Evensen, 2003; Ott et al., 2004) is applied for localization. LA improves the assimilation procedure by restricting the observations used for the covariance matrix computation to a spatially limited area (Khaki et al., 2017c). As a result, only those measurements located within a certain distance from a grid point have an impact on the updated states (Evensen, 2003; Ott et al., 2004). Different localization lengths are tested and their results are assessed against in-situ groundwater measurements (Section 2.3) to reach the best case scenario (i.e., 5° half-width used in this study).

As mentioned, it is necessary to remove surface water storages from GRACE TWS data over Lake Urmia before data assimilation. For this purpose, following Forootan et al. (2014a) who undertook water analysis over the same area, we use satellite altimetry time series over the lake to derive surface water storage. The Global Land Data Assimilation System (GLDAS) outputs of total column soil moisture, snow water equivalent, and vegetation biomass water storage as well as water level variations from altimetry are used to estimate temporal and spatial patterns of surface water storage using Independent Component Analysis (ICA). The extracted patterns are then adjusted to GRACE TWS products using a least squares adjustment (LSA) procedure (see details in Forootan et al., 2014a). The GRACE data after removing surface water storage is used for the data assimilation process over Lake Urmia.

3.2. Canonical correlation analysis (CCA)

The present study applies Canonical Correlation Analysis (CCA) to find the linear connection of two sets of multidimensional variables of predictor (x_c) and criterion (y_c) values. CCA is selected here rather than simple correlation analysis due to its ability in establishing the relationships between multiple intercorrelated variables. CCA extracts canonical coefficients that represent common processes between two or more variables (Chang et al., 2013) using an eigenvector decomposition that yields linear weights, known as canonical coefficients, which describe maximum correlations between variables (see details in Steiger and Browne, 1984). The combination of variables with the first canonical coefficient for each set has the highest possible multiple correlations with the variables in the other set. CCA extracts canonical coefficients u and v such that $X_c = {x_c}^T u$ and $Y_c = {y_C}^T v$ (X_c and Y_c are canonical variates) possess a maximum correlation coefficient (Chang et al., 2013) using the following function,

$$\begin{aligned} R &= \frac{E[X_cY_c]}{sqrt(E[X_c^2]E[Y_c^2])} \\ &= \frac{E[u^Tx_c{y_c}^Tv]}{sqrt(E[u^Tx_c{x_c}^Tu]E[v^Ty_c{y_c}^Tv])} \\ &= \frac{u^TC_{x_c,y_c}v}{sqrt(u^TC_{x_c,x_c}uv^TC_{y_c,y_c}v])}, \end{aligned} \tag{8}$$

where C_{x_c,x_c} and C_{y_c,y_c} are covariance matrices of x_c and y_c, respectively and the objective in above function is to maximize the correlation R. We use an eigenvalue decomposition procedure to find the linear weights producing canonical coefficients, which imply maximum possible correlations (see details in Steiger and Browne, 1984). There are different canonical coefficients within each set leading to different uncorrelated coefficients. Nevertheless, the combination of variables with the first canonical coefficient for each set has the highest possible multiple correlations with the variables in the other set.

Two scenarios are considered for prediction: (i) the predictor (x_c) contains time series of both groundwater used for farming, industry, and human consumption from IWRMC and climate-related variables of precipitation, NDVI, and temperature (provided by Harris, 2008), and (ii) the predictor (x_c) includes only climate-related variables of precipitation, NDVI, and temperature. This is done to explore the impact of each scenario on water variations. The criterion (y_c) in both scenarios contains water storage (groundwater and soil moisture) and discharge (from IWRMC) variations. By applying CCA, we establish the best combinations between two sets of variables in two different cases. By comparing the results of these two scenarios, we can investigate how water use and climate variabilities impact water storage changes within Iran. Nevertheless, there are other effective components (e.g., large-scale ocean-atmosphere phenomenon, evaporation, and droughts) on the wa-

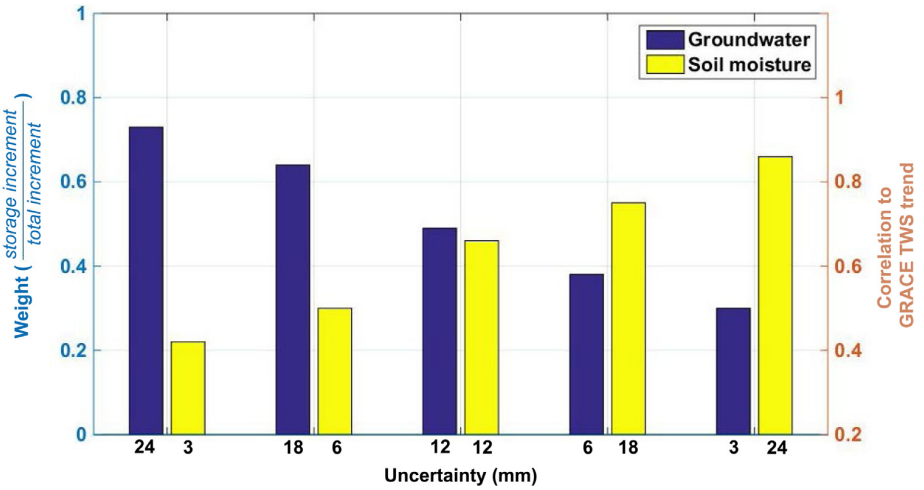

Fig. 3. Relationships between groundwater and soil moisture state variable uncertainties and corresponding weights during data assimilation.

ter storage, which is difficult to include all of them in the process. This CCA scheme, however, could provide an insight on the connection between the above components. Table 2 summarizes the experiments undertaken in this study. The corresponding research objectives and related sections that contain each experiment's results are also listed in the table.

4. Results and discussion

4.1. Simulated assimilation

In the following, we analyze the effect of various scenarios of observations on the assimilation. As mentioned earlier, GRACE TWS observations are used to update the sum of soil moisture, vegetation, snow, and groundwater compartments at each grid cell. Thus, it is important to investigate the distribution of the increments between these compartments, especially soil moisture and groundwater storage while the influence of the remaining storages (i.e., vegetation and snow) is negligible. In particular, we are interested in monitoring the impacts of trends in observations time series on different water components. Schumacher et al. (2018) showed that assimilating GRACE TWS data can improve model simulation of seasonality and trend of TWS, as well as individual water storage components. This point is important because the largest part of GRACE TWS trends caused by groundwater variations that originate from both natural and human-induced (e.g. water use) changes while soil moisture variations generally follow climate pattern. Simulation experiments are undertaken to monitor how observations' variations, and particularly their trends are reflected in soil moisture and groundwater estimates during assimilation.

To illustrate how GRACE data assimilation can improve model states, we perform a synthetic study, in which arbitrary errors (uncertainty with different magnitudes) are assigned to different model derived water storage states. We evaluate whether these states accurately receive increments from GRACE TWS. To this end, we introduce different uncertainties to model states and test how these are transferred to the assimilation forecast steps (cf. Eqs. (3) and (4)). Fig. 3 shows the relationship between selected uncertainties of water states and their corresponding weights in the (synthetic) assimilation. Based on this setup, six different scenarios are considered to explore the impact of weights as the ratio of the assigned increment derived for each storage state to the summation of all states. The results presented in Fig. 3 indicate an average influence of assimilating GRACE TWS data into W3RA over Iran between 2003 and 2013. In general, as theoretically expected, higher weight (i.e., larger increment) is assigned to a variable with a smaller uncertainty. In other words, by assimilating GRACE TWS, the model's water states with larger uncertainty receive larger increments, and this is reverse for states with smaller uncertainty. These results approve the recent results of Schumacher et al. (2018), who assimilate GRACE TWS data into WGHM model over Australia. Fig. 3 also shows that the average correlations between the individual estimated storage in each scenario and the assimilated GRACE TWS. The correlations are calculated after removing seasonal effects on time series to focus on trends. It can be seen that larger correlations to the GRACE TWS trends are obtained for a compartment with larger uncertainty and correspondingly with a larger increment. This means that the assimilation process transfers the observation trends into the more uncertain storage, which receives the larger corrections.

Another synthetic experiment is also implemented, where, different observation sets are assimilated into W3RA but this time without manipulating their uncertainties. The aim is to investigate whether the distribution of increments of different water states changes when the TWS observations change. Here, four different synthetic observation scenarios are considered, which include two versions of the WaterGAP Global Hydrology Model (WGHM; more details on Döll et al., 2003; Müller Schmied et al., 2014) TWS estimates with and without water abstractions, GRACE-derived TWS, and GRACE TWS minus WGHM soil moisture that roughly gives groundwater observations. The spatially averaged time series of the TWS observations (for the first three cases) over Iran are displayed in Fig. 4(a). The difference between the WGHM TWS observations with and without water use clearly show the anthropogenic impacts as a distinct negative trend in WGHM with water abstraction impact. A similar trend can also be seen in GRACE TWS. Assimilation of these observations can show how water storages, for example their trends, are distributed between soil moisture and groundwater estimates. Assimilating WGHM TWS without water use, which does not show any significant trends, might better estimate soil moisture. This is due to the fact that the main source of TWS's negative trends is groundwater exploitation, while soil moisture variations generally are related to climatic (e.g., precipitation) variations. Hence, comparing the soil moisture results of assimilating GRACE TWS and WGHM TWS with water use with those of WGHM TWS without water use can help to assess the performance of data assimilation in updating soil moisture. Furthermore, while the first three observation sets (i.e., WGHM with and with-

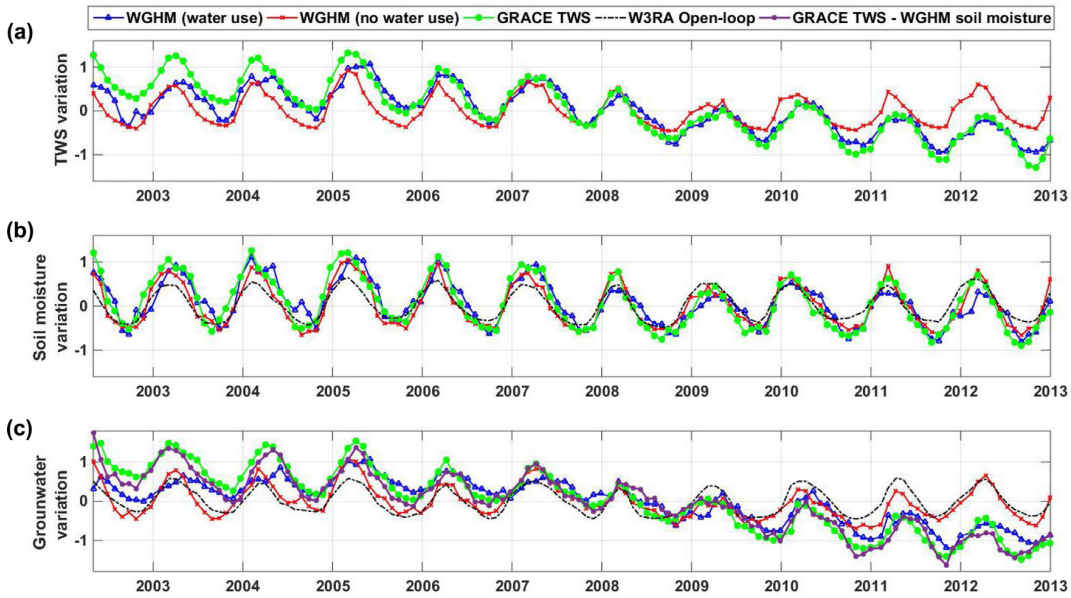

Fig. 4. (a) Simulated average TWS observations using WGHM with and without human use, and W3RA open-loop plus GRACE trend. Average soil moisture (b) and groundwater (c) estimates from data assimilation based on simulated observations in (a).

out water use and GRACE-derived TWS) are used to update the summation of all compartments, the last case (GRACE TWS minus WGHM soil moisture) is used to update only the groundwater simulations. The main rationale for updating only groundwater in the last experiment is to compare its results with the other scenarios, which can help to investigate how accurate groundwater corrections are applied from TWS increments in the other cases, where different compartments are available.

The results of the data assimilation variants are shown in Figs. 4(b) and (c) and updated groundwater estimates from assimilating GRACE TWS minus WGHM soil moisture is plotted in Fig. 4(c). The assimilation results for soil moisture (Fig. 4(b)) and groundwater (Fig. 4(c)) show that the negative TWS trends are largely reflected only in groundwater time series. The average correlation between the above TWS observations and corresponding groundwater estimates is 0.92, 42% (on average) larger than for the open-loop run, which indicates the suitability of data assimilation for constraining system states. For the entire area, there is a stronger agreement between the soil moisture from assimilation compared to the open-loop run, e.g., 22% (on average) for the GRACE TWS case and 28% (on average) for the WGHM TWS with water use case. Lower correlations are obtained for assimilating WGHM TWS without water use in comparison to other data assimilation scenarios (see also Fig. 4(b)). Furthermore, groundwater variations from the assimilated GRACE TWS are largely correlated to the groundwater estimates from assimilating only groundwater observations (GRACE TWS minus WGHM soil moisture). TWS observations of WGHM without water use have the least effect on groundwater variations.

It can be concluded from Fig. 4 that the data assimilation process successfully distributes TWS increments between soil moisture and groundwater storages. These results indicate that the largest part of increments during data assimilation is assigned to groundwater. The larger impact on groundwater, based on Fig. 3, suggests that the groundwater estimation of W3RA is more uncertain than its soil moisture and as a result it receive larger updates. This is even more clear in Fig. 5, where groundwater and soil moisture estimates by ensemble members between 2004 and 2008 are shown. This time period is selected because it includes an episode with strongly negative groundwater trend after 2005 (see also Fig. 4(c)), where ensemble spreads show a different pattern, e.g., larger spreads. The propagated groundwater ensemble members are more dispersed than those of soil moisture, which causes larger ensemble deviations from its mean and consequently larger uncertainty for the states (cf. Eqs. (1) and (2)). This can be due to the point that the W3RA model has a simplified simulation of groundwater dynamics for unconfined groundwater and does not simulate confined groundwater dynamics or anthropogenic groundwater extraction (Tregoning et al., 2012). The larger corrections applied to groundwater is also realistic considering the fact that a majority of water depletion in Iran occurs in groundwater due to large extractions for irrigation. The applied irrigation water is likely to locally increase total soil column water storage, which may contribute to a smaller decline in soil water content (Michel, 2017).

Even though the results indicate good performance of GRACE data assimilation, one might still expect artefacts from the TWS increments on the state estimates. The absence of groundwater abstractions and anthropogenic impacts in most hydrological models, especially where the rate of this extraction is high, can cause a misinterpretation of a negative TWS trend captured by GRACE in the system states. As shown by Girotto et al. (2017), the assimilation of GRACE TWS can successfully introduce the negative trends in the modeled TWS and groundwater, however, this can also introduce unrealistic decline in other components, e.g., soil moisture and evapotranspiration. This effect can be exacerbated when groundwater extraction is large and occurs over an extended period. The model dynamical range of groundwater may not be sufficient to accommodate the assimilated values (Li and Rodell, 2015; Zaitchik et al., 2008). Despite these, merging GRACE TWS data with high resolution models is the most efficient existing approach to analyze groundwater changes over wide areas, which in most cases results in an improvement in the estimates (Girotto et al., 2017; Li and Rodell, 2015). Here, we addressed this challenge by conducting a synthetic experiment, as well as by independently assessing groundwater and soil moisture from assimilation. However, more investigations are needed to be extended and the impacts of various data assimilation scenarios on each individual water compart-

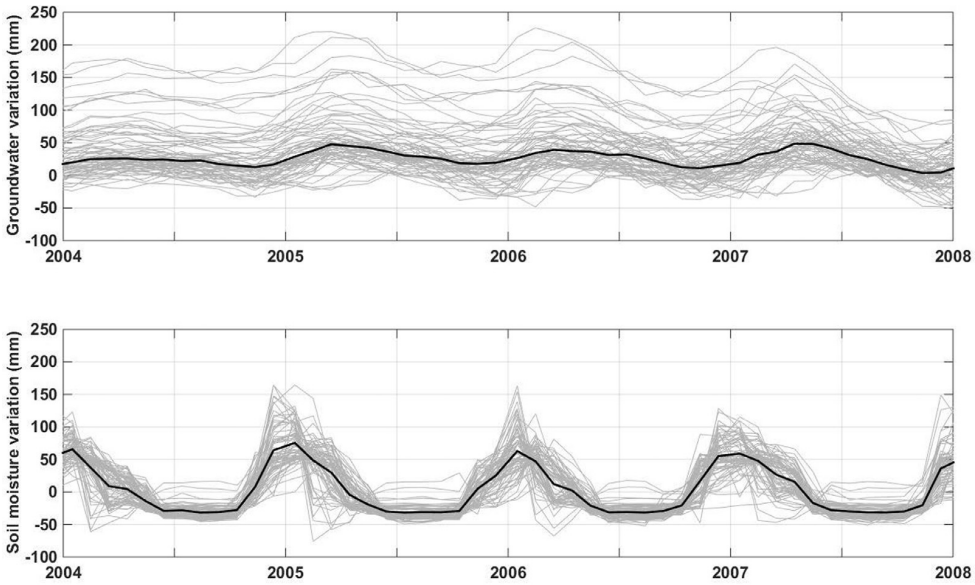

Fig. 5. Average groundwater and soil moisture ensemble spreads between 2004 and 2008 over Iran. Gray lines indicate ensemble members and the black solid line present ensemble mean. Larger ensemble propagation is evident compared to that of soil moisture that represents larger uncertainties in the former water storage compartment.

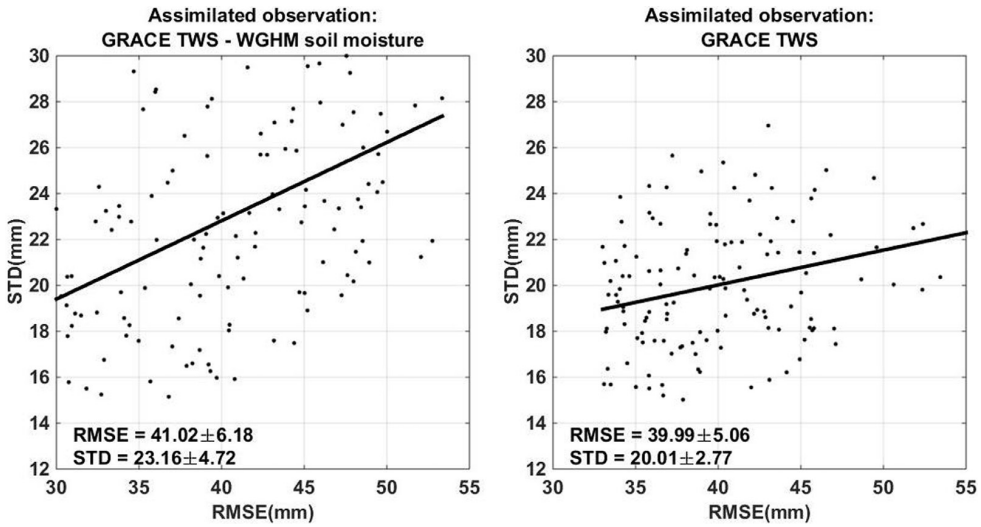

Fig. 6. Average groundwater RMSE and STD from assimilating GRACE TWS and GRACE TWS minus soil moisture.

ments need to be tested. These investigations are, however, out of the scope of this study.

4.2. Result evaluation

In this section, we assess the performance of data assimilation using in-situ groundwater measurements. To examine the validity of data assimilation results, in-situ groundwater measurements of the six major drainage regions in the area including the East, Caspian Sea, Centre, Sarakhs, Persian Gulf and Oman Sea, and Lake Urmia (cf. Fig. 1) are used. For each basin in Fig. 1, we calculate the spatial average time series of groundwater storages with and without data assimilation and compare them with the IWRMC in-situ and WGHM groundwater variation. We first analyze the performance of two assimilation cases of GRACE TWS and GRACE TWS minus WGHM soil moisture data assimilation experiments for improving groundwater estimates. Fig. 6 shows the average root-mean-square error (RMSE) and standard deviation (STD) calculated using groundwater from assimilation cases and in-situ measurements. Both cases perform comparably in terms of RMSE and STD with an average of 38% error reduction compared to open-loop. Nevertheless, assimilating GRACE TWS obtains the smaller RMSE than groundwater only data assimilation. This further confirms the effectiveness of the applied data assimilation for distribution TWS increments, especially for groundwater storage. Based on this assessment, hereafter only the results for GRACE TWS data assimilation are presented.

The results for groundwater examination from data assimilation, WGHM, and the open-loop run for each drainage division are illustrated in Fig. 7, which show that the strongest agreement between groundwater estimates and in-situ measurements occur in the assimilation results. In most of the cases, WGHM performs better than the open-loop. For a better assessment of data assimilation results, additional agreement statistics using RMSE and corre-

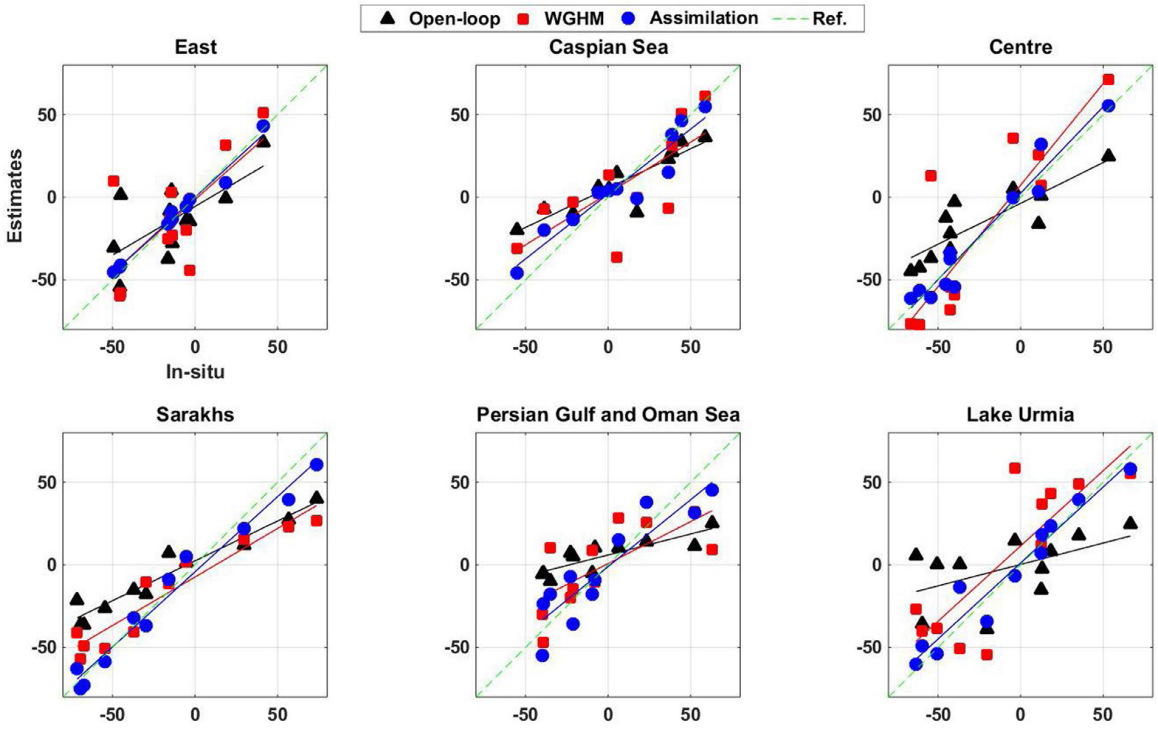

Fig. 7. Comparison between in-situ groundwater measurements and those estimated by open-loop run, data assimilation, and WGHM over different catchments (units are mm).

lation analysis are calculated and reported in Table 3. Significance at $p < 0.05$ was calculated using the Students t-test with consideration of temporal autocorrelation through effective sample size.

The computed time series for each region is compared to IWRMC data for the corresponding region in order to estimate the reported statistics in Table 3. Generally, the assimilation results are largely correlated with the in-situ data (0.85 on average) after data assimilation, with an improvement of 35% over open-loop results. The largest improvements in terms of correlation increase and RMSE reduction with respect to the in-situ measurements are achieved over Lake Urmia, Sarakhs, and to a lesser degree Persian Gulf and Oman Sea. Table 3 shows considerable groundwater decline in most of the regions especially within the Persian Gulf and Oman Sea and Lake Urmia (both mostly located in the western areas). The largest negative groundwater trend is exhibited for Lake Urmia while the lowest trend is found for the Caspian Sea division in the north, which could be attributed to a large amount of precipitation in the latter region.

We further examine the soil moisture estimates from data assimilation. In the absence of reliable in-situ soil moisture measurements over the study area, we use satellite-derived and independent model soil moisture products. Soil moisture observations from the Advanced Microwave Scanning Radiometer - Earth Observing System (AMSR-E) and Soil Moisture and Ocean Salinity (SMOS) are compared to the assimilated top layer soil moisture estimates. The motivation behind this comparison is based on the fact that SMOS and AMSR-E measurements are largely correlated, respectively, to surface 0–5 cm and 0–2 cm soil moisture content (Njoku, 2003). Fig. 8 shows the average time series of the above comparison within the study period. It can be seen that the assimilation top layer soil moisture is better matched (41% improvement in correlation) to the satellite measurements in comparison to the open-loop estimates. This shows a successful impact of GRACE TWS data assimilation on the model top layer.

Total soil moisture estimates from data assimilation, i.e., summation of soil moisture at top, shallow- and deep-root layers, are compared with soil moisture estimates of WGHM, the Global Land Data Assimilation System (GLDAS; Rodell et al., 2004), and soil moisture provided by van Dijk et al. (2014), who combined different data (e.g., GRACE) and model outputs (indicated here as W3). The results are displayed in Fig. 9. In all cases, data assimilation leads to a better agreement to other products with an average 25% improvement. The largest correlation, as well as the greatest improvement, are found for soil moisture after assimilation of WGHM. There is also a considerable correlation between the results and W3.

4.3. Water storage analysis

Based on the improved soil moisture and groundwater estimates, spatio-temporal variations of both compartments are analyzed in this section. The variation of groundwater storages within Iran before and after data assimilation are illustrated in Fig. 10. The blue graph in Fig. 10 represents the average groundwater variations of all grid points after data assimilation. This graph clearly shows a negative trend between 2002 and 2013 with an average −8.9 mm/year groundwater depletion for the entire country. However, such a trend is not present in the open-loop time series. GRACE TWS data assimilation constrains groundwater estimates and introduces this negative trend into the state as it exists in GRACE TWS observations (cf. Fig. 4). It is evident that the W3RA without data assimilation is not able to provide reliable long-term changes of groundwater, e.g., trend and multi-year variations. Therefore, data assimilation is vital for reliable interpretation of ground water beyond the annual cycle. However, without additional information the data assimilation results cannot differentiate between natural and anthropogenic causes. Apart from the trends, Fig. 10 also shows a multi-year cycle, e.g., positive trend between

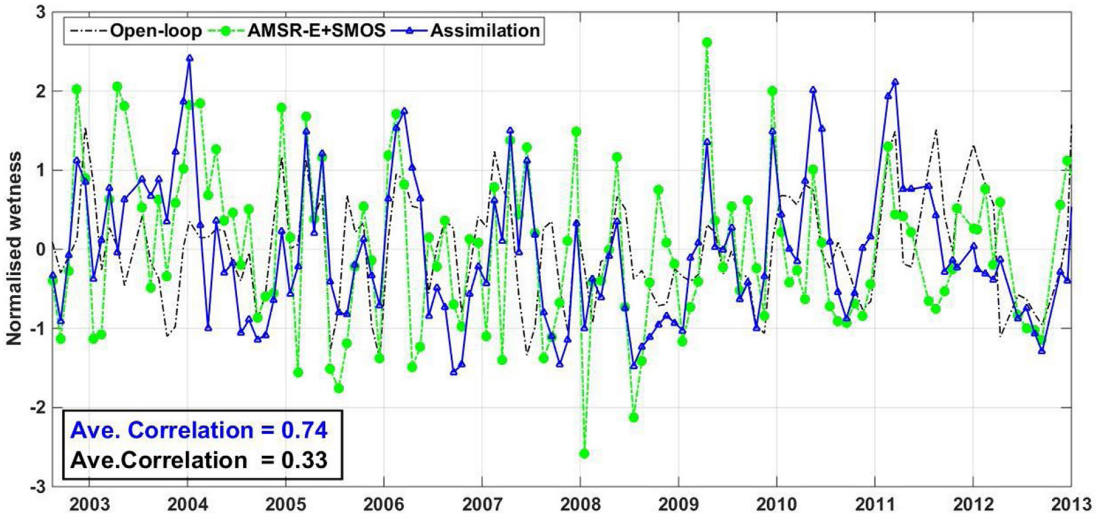

Fig. 8. Comparison between the average estimated top layer soil moisture with and without (open-loop) data assimilation and soil moisture observations from satellite remote sensing (AMSR−E+SMOS). Correlations between the satellite measurements and both open-loop and assimilation estimates are also repotted in the figure.

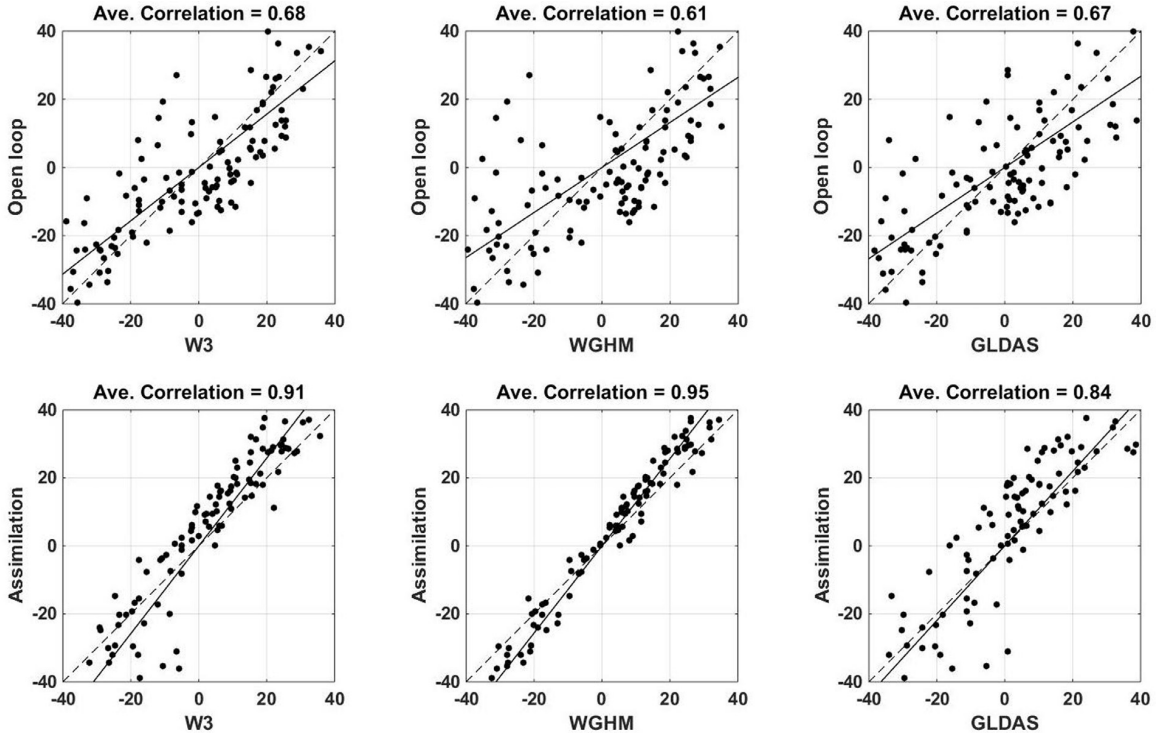

Fig. 9. Comparison between the average soil moisture estimates from open-loop and data assimilation, and soil moisture products of W3, WGHM, and GLDAS (units are mm).

2002 and 2005 and a stronger negative trend for the later years 2006 to 2013. Again, this trend is not visible in the open-loop simulations.

Furthermore, we separately analyze water compartments for each of Iran's major drainage regions. The soil moisture and groundwater average time series from W3RA before and after assimilating GRACE TWS for each of the divisions are shown in Fig. 11 and Fig. 12, respectively. Larger soil moisture variations (in terms of amplitude) exist for the data assimilation results compared to open-loop results in Fig. 11. In particular, this is evident for the Persian Gulf and Oman Sea and Caspian Sea. This could be due to a larger amount of annual precipitation over these areas. Declines in soil water content can be seen in Sarakhs, especially between 2005 and 2009, and Lake Urmia. In most of the regions, increases (e.g., large positive variations) are observed during 2004 and 2010. Overall, better agreements between open-loop and assimilation time series are found over East and Centre regions, where a semi-arid climate condition is dominant. GRACE data assimilation has the least impact on soil moisture estimates within these areas.

Fig. 12 depicts groundwater variations for each individual drainage division. Similar to soil moisture analysis (cf. Fig. 11), data

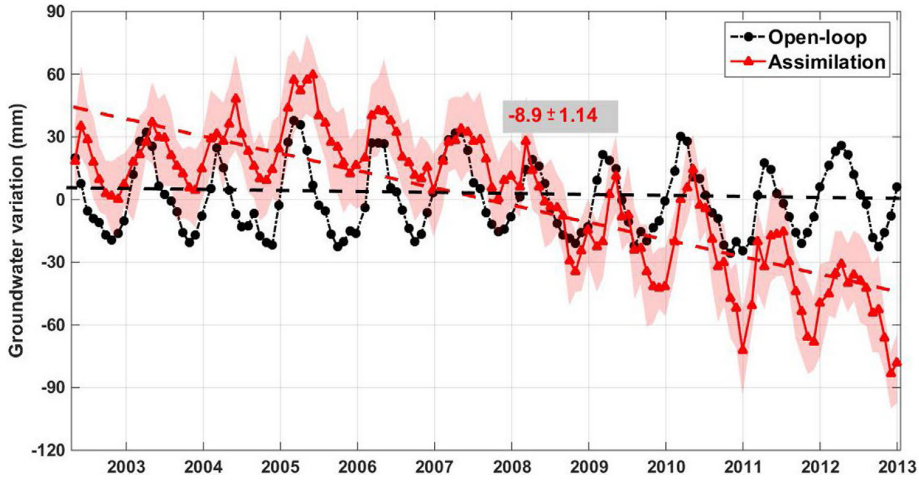

Fig. 10. Average groundwater variations within Iran from open-loop and data assimilation results and corresponding 95% confidence intervals (shaded blue). Trend lines for time series are also displayed by dashed lines. Note that the open-loop time series slop is not reported because no significant trend is observed. (For interpretation of the references to colour in this figure legend, the reader is referred to the web version of this article.)

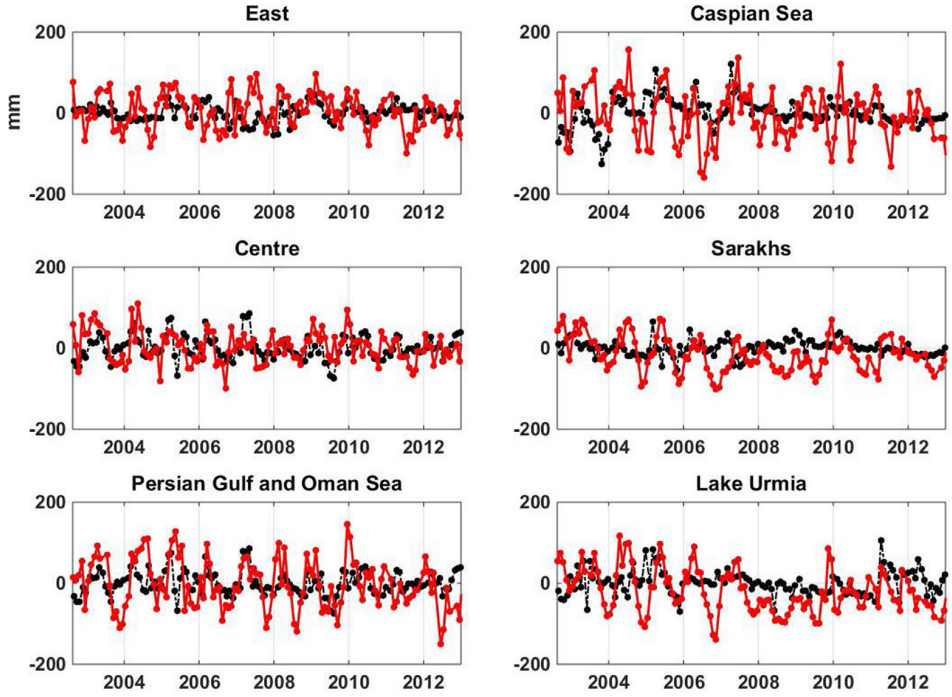

Fig. 11. Average time series of soil moisture variations over different catchments with (blue) and without (black) data assimilation. (For interpretation of the references to colour in this figure legend, the reader is referred to the web version of this article.)

Table 2
The undertaken experiments and corresponding research objectives. The result section associated to each experiment is also presented.

Experiment	Research objective	Result section
Simulated assimilation	To assess the impacts of GRACE observations on different water storage	Section 4.1
Evaluation procedure	To examine the validity of results against independent observations	Section 4.2
Water storage analysis	To analyze spatio-temporal variations of groundwater and soil moisture	Section 4.3
Climatic impacts using PCA	To investigate the impacts of climate indicators (e.g., precipitation) on water storage	Section 4.4
CCA	To establish the relations between water storages and human- as well as climate-related variables	Section 4.5

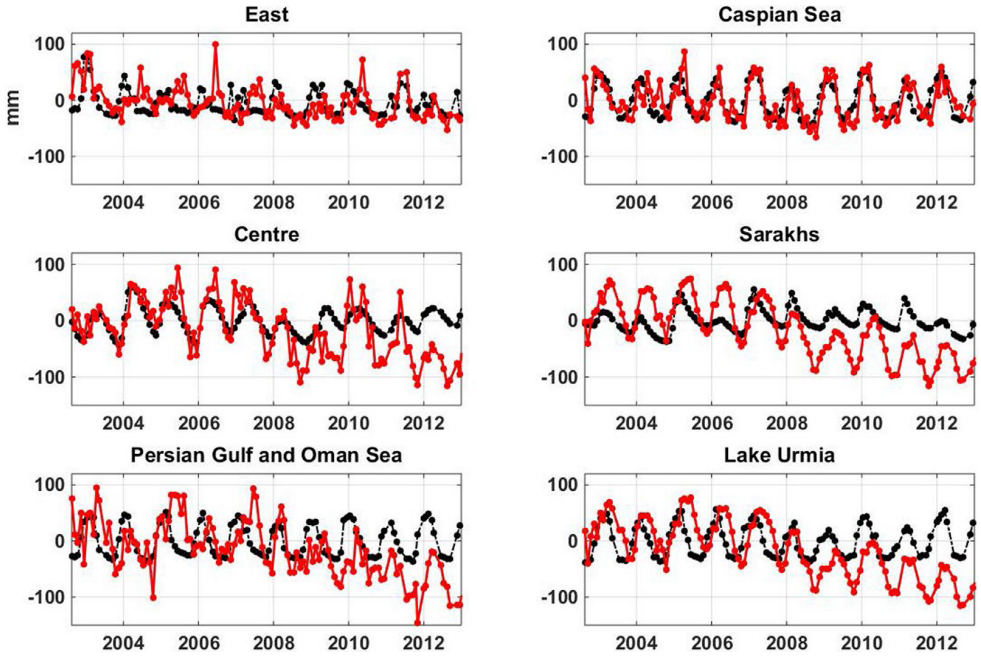

Fig. 12. Average time series of groundwater variations over different catchments with (blue) and without (black) data assimilation. The correlations of time series with the in-situ measurements, as well as the trends of assimilation results are reported in Table 2. (For interpretation of the references to colour in this figure legend, the reader is referred to the web version of this article.)

Table 3
Statistics of groundwater variations and its errors with respect to the in-situ observations. For each region the RMSE average and its range (±XX) at the 95% confidence interval is presented. Improvements in data assimilation results are calculated for each catchment in relation to the water storages from the model without implementing data assimilation.

Region	Groundwater trend (mm/year)	Assessment with In-situ				
		Open-loop		Assimilation		
		Correlation	RMSE (mm)	Correlation	RMSE (mm)	Improvement (%)
East	−3.8	0.57	60 ± 8.66	0.84	38 ± 4.64	36.29
Caspian Sea	−2.1	0.64	64 ± 9.19	0.73	46 ± 5.13	28.13
Centre	−6.7	0.63	55 ± 7.84	0.65	41 ± 5.01	26.55
Sarakhs	−5.4	0.61	52 ± 7.58	0.82	32 ± 4.26	38.64
Persian Gulf and Oman Sea	−9.3	0.56	79 ± 9.07	0.75	49 ± 5.17	37.81
Lake Urmia	−11.8	0.52	69 ± 8.28	0.81	40 ± 4.25	41.90

assimilation results demonstrate larger magnitudes than open-loop results. Except for the Caspian Sea, all the regions show a considerable decline in groundwater estimates during the study period. In particular, this is clear in Lake Urmia, Sarakhs, and Centre, especially after 2007. These trends are absent in the open-loop time series and derive from GRACE TWS after implementing data assimilation, which confirm the results shown in Fig. 10. Larger groundwater declines are found in regions over the western parts of the country (e.g., the Persian Gulf and Oman Sea and Lake Urmia). In most of the cases, groundwater rise is observed as a positive trend between 2004 and 2005. These increases are then followed by consistent declines despite some short-term increases such as during 2010. A large trend decline is observed after 2006 in Lake Urmia, Centre, Sarakhs, and to a lesser degree in Caspian Sea. For the Persian Gulf and Oman Sea, Sarakhs, and Center, the groundwater negative trend is remarkable after 2008. Despite a small negative trend in East for the study period, the groundwater variations have the smallest amplitudes in this region compared to other areas. Seasonal variations can clearly be seen in most of the regions while this pattern is dominant mostly in Caspian Sea. Fig. 12 and the reported negative trends in Table 3 show that groundwater depletion is a major issue in most parts of Iran resulting in a remarkable dryness across the country.

4.4. Climatic impacts

We further investigate the connection between climatic impacts and water storage variations. A comparison between groundwater and soil moisture variations and climate-related variables such as precipitation and NDVI can reveal such interactions these parameters. Fig. 13 shows maps of temporal average precipitation, soil moisture, and groundwater maps during the study period. The first row in Fig. 13 represent the average applied increment to soil moisture and groundwater storages, the second row indicates variations (average of time series at each grid point) of precipitation, soil moisture, and groundwater, and trends for each variable at each grid point are depicted in the third row.

Fig. 13 shows the spatial pattern of increments, i.e., the difference between assimilation results and open-loop estimates, applied to the system states. It can be seen that the largest increments are applied to groundwater storage as can be expected from Figs. 3 and 4. These corrections are mostly focused on the northwest to south and the eastern part of Iran. In soil moisture, the

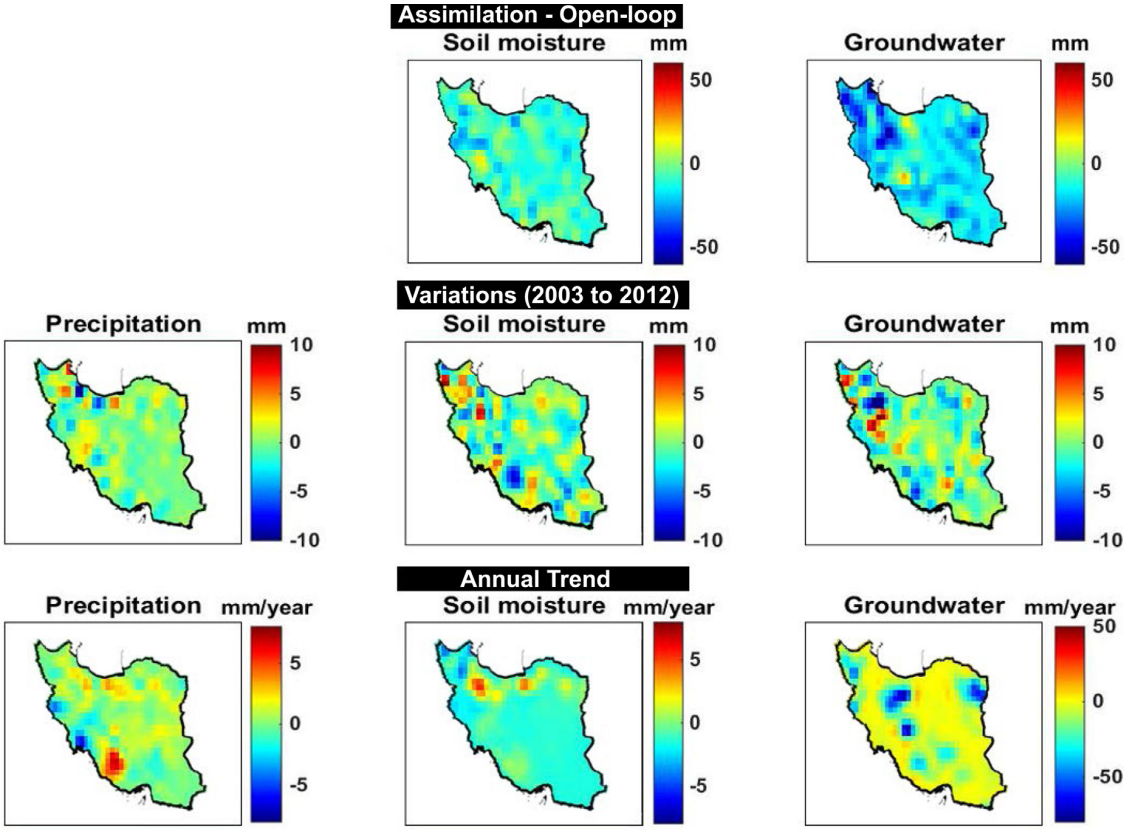

Fig. 13. First row: temporally averaged increments applied to soil moisture and groundwater storages. Second row: variation of precipitation, soil moisture, and groundwater (after data assimilation) estimated as the average of each time series at each grid point. Third row: gridded trend of time series precipitation, soil moisture, and groundwater (after data assimilation) time series.

increments can be found across the country, again, with larger concentrations in the western areas. The effect of data assimilation clearly can be seen by the increments illustrated in Fig. 13. The spatial pattern of precipitation, soil moisture, and groundwater variations in Fig. 13 show larger variations over the north toward northwest parts, where the Alborz mountain range cover a large portion of the areas. A similar pattern can also be seen in western parts, where the Zagros mountain range is located. Overall, the soil moisture map more closely reflects the precipitation patterns compared to groundwater variations, which can be attributed to impacts from water uses. Contrary to precipitation and soil moisture, negative groundwater variations are found over different regions, especially the north-western and southern parts. There are very limited variations in terms of amplitude changes for precipitation, soil moisture, and groundwater within the centre, eastern, and partially south-eastern parts of Iran. Trend maps (last row in Fig. 13) illustrate spatial patterns for each component. Both precipitation and soil moisture show increasing trends in the north and to a lesser degree in the south. Groundwater trends are generally negative in all regions, but more strongly in the west, where Lake Urmia is located. A significant groundwater depletion can be observed in the central parts extended to the north, where Tehran, Iran's capital city is located. Large groundwater extractions in Tehran during the study period can be the main reason for this while in other areas, an excessive irrigation is a potential candidate for the observed depletion. It can be seen that there is an agreement between the applied increment by data assimilation, especially for groundwater, and the negative observed trends. Again it can be concluded that without using assimilation, these negative trends are not captured.

To better quantify the spatio-temporal variations of water storage and climate variabilities, principal component analysis (PCA Lorenz, 1956) is applied on precipitation, NDVI, GRACE TWS, and groundwater time series. This allows us to monitor the relationship between the estimated groundwater and GRACE TWS, as well as their connection to climatic impacts through precipitation and NDVI. The first three extracted principal components (PC1, PC2, and PC3) of each component are plotted in Fig. 14. There is good agreement between the time series for all three cases, in particular for seasonal variations. All time series in PC1 show a clear annual variation. Negative trends, especially after 2009 are only captured by PC1 of GRACE TWS and groundwater. Stronger agreements between precipitation and NDVI PCs can be found. This can be attributed to vegetation growth response to rainfall and soil moisture. The assimilated groundwater storage variations largely follow the GRACE TWS variation patterns, both in terms of variability and trend, mainly due to the application of GRACE data assimilation. Both of these variables are strongly correlated with rainfall time series in PC2 and PC3 with an average correlation of 0.86. Various strong anomalies are occur in the time series, e.g., in 2005 and 2010. Increases in the time series occur in PC1 for all variables between 2004 and 2006 and during 2010 and 2012. PC2 shows similar rises in 2008 and 2010 followed by a strong decrease. PC3 shows an increase in 2009 and 2010 in the precipitation, GRACE TWS, and groundwater which explains the corresponding increase in water storages (cf. Figs. 10 and 12). Some negative anomalies

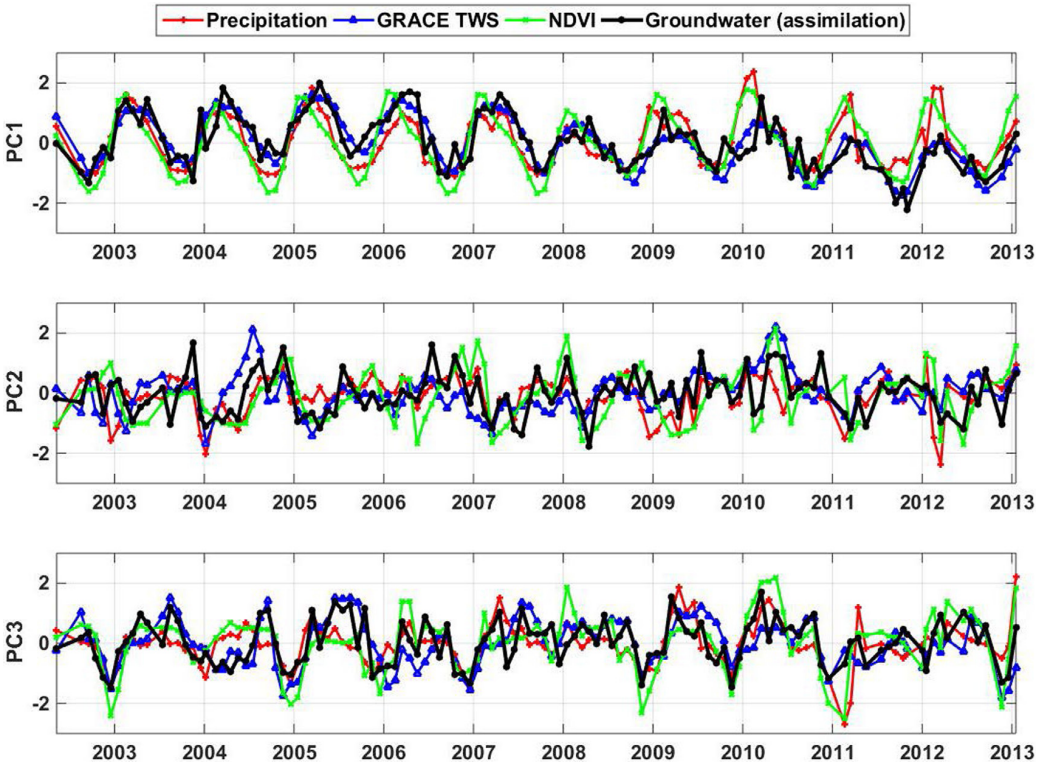

Fig. 14. The three first principal components of precipitation, GRACE TWS, NDVI, and groundwater.

are found in PC3 in 2003, 2005, and 2011 and also in 2006 and 2013. The other variables generally demonstrate the same variation pattern as precipitation, which shows a strong connection between water storage variations and climatic changes. Water storage variations in Iran, however, are also affected by non-climate factors (e.g., anthropogenic impacts), which are likely the cause of the observed negative trends in PC1 for GRACE TWS and groundwater.

The corresponding empirical orthogonal functions (EOF1, EOF2, and EOF3) extracted by applying PCA on precipitation, NDVI, GRACE TWS, and groundwater from data assimilation are shown in Fig. 15. Overall, the mode 1 represents a strong annual signal (as would be expected), mode 2 shows some deviations from the annual signal (e.g. inter-annual variations) in the same regions as for mode 1. Mode 3 to some extent shows inter-annual variations but importantly shows some extreme values. The spatial patterns of NDVI, GRACE TWS, and groundwater are largely correlated to rainfall pattern, especially in EOF1 and EOF2. Larger spatial variations exist over the northern and western parts of Iran, which seem to cause larger water storage and NDVI changes in the same areas. These are the parts with higher altitudes in which precipitation rates are generally high. GRACE TWS and groundwater EOF2 maps show strong positive signals over the north toward the northwest and partially in western areas. The rainfall EOF2 map, however, does not show a large signal over the north-western part but only over the northern and western parts, where the Alborz and Zagros mountain ranges are located. On the other hand, all variables show a negative signal in the south-eastern part. Positive signals over the eastern parts, with smaller amplitudes, compared to EOF1 and EOF2 for NDVI, GRACE TWS, and groundwater are displayed by EOF3 maps. Negative signals can be seen in EOF3 maps, especially for groundwater mostly over the northwestern areas, where Lake Urmia is located, as well as the northeast and Sarakh.

4.5. CCA results

We further implement CCA on the estimated water compartments (from the data assimilation) on the one hand, and human- as well as climate-related variables on the other hand in two different scenarios, i.e., (i) the predictor contains time series of both groundwater used (e.g., for farming and industry) and climate-related variables (precipitation, NDVI, and temperature), and (ii) the predictor includes only climate-related variables of precipitation, NDVI, and temperature (cf. Section 3.2). By this, we can establish the relations between water storages and other factors. CCA is applied to the spatially averaged time series of all variables to estimate canonical coefficients. Canonical loadings are used to interpret the CCA results, which measure the simple linear correlation between an observed variable and the estimated canonical variates (Dattalo, 2014). The interpretation is mostly based on examining the sign and the magnitude of the canonical coefficients assigned to each variable. Variables with larger coefficients contribute more to the variates and variables with opposite signs exhibit an inverse relationship with each other while those with the same sign exhibit a direct relationship. Detailed results of the CCA experiment for each scenario applied within Iran are presented in Table 4.

The table summarizes the contribution of each variable in CCA. Results indicate that scenario (i) leads to larger canonical correlation coefficients in comparison to scenario (ii). This means that variations in water storages are more correlated to variations of the combined human- and climate-related parameters. Note that CCA extract different sets of results (roots), thus, we only use the first root that is statistically significant (for a significant level of 0.05). It can be seen from Table 4 that the water use has strong negative correlations to water storage variations, especially groundwater, which has the largest loading. This means that water consumption for various uses (especially farming) is a very ef-

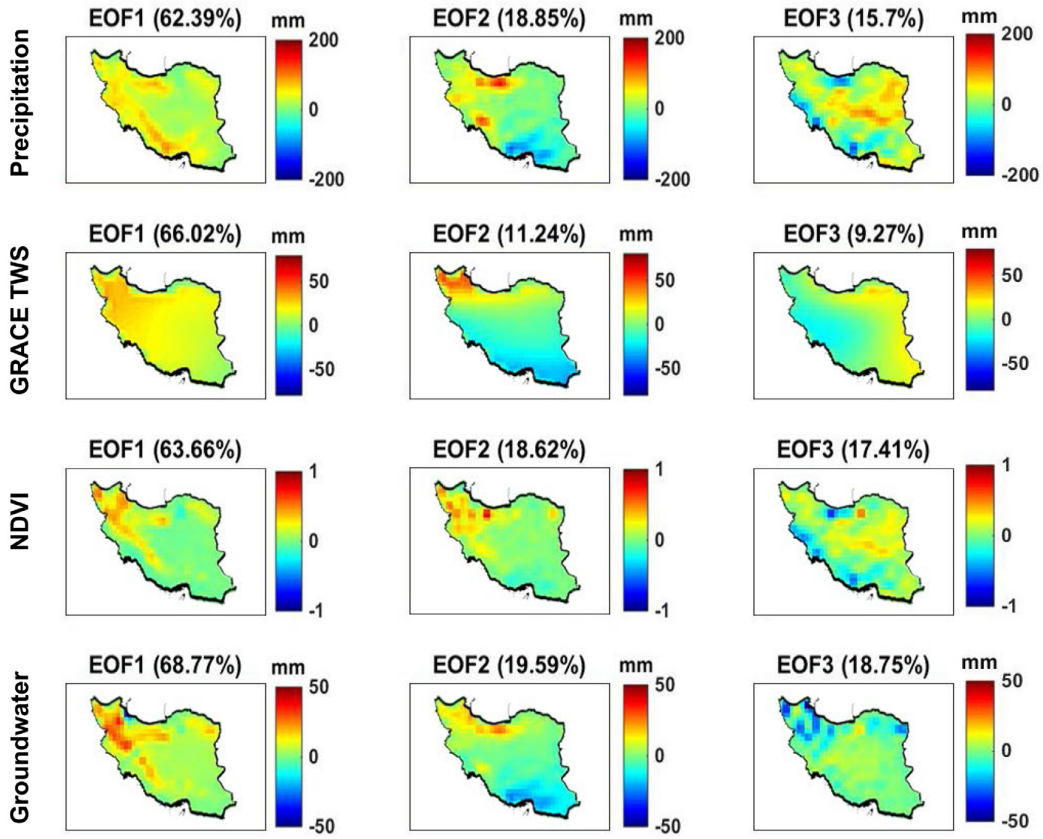

Fig. 15. The empirical orthogonal functions (EOF1, EOF2, and EOF3) extracted from precipitation, GRACE TWS, NDVI, and groundwater.

Table 4
Average canonical correlation coefficients and variable loadings for the data inputs in CCA for each scenario.

Canonical correlation coefficient			Scenario (i) Canonical coefficients 0.972	Scenario (ii) Canonical coefficients 0.841
Predictor variables		Precipitation	0.721	0.749
		NDVI	0.365	0.412
		Temperature	−0.591	−0.681
	Water use for:	# Farming	−0.938	–
		# Industry	−0.758	–
		# Drink (Urban use)	−0.820	–
		Number of bore holes	−0.893	–
Criterion variables		Groundwater	0.938	0.705
		Soil moisture	0.633	0.617
		Water discharge	0.174	0.249

fective factor within the country that causes the greatest impact on groundwater (with 0.938 canonical correlation). Among climate variables, precipitation, and to a lesser degree temperature have also a considerable influence on water storage variations. Not surprisingly, an increase (or decrease) in rainfall directly leads to increase (or decrease) in water storages as indicated by the same signs. Table 4 suggests that variations in groundwater use and climate parameters in both scenarios have minimum impact on water discharge. This may be due to the fact that surface waters compose a relatively small amount of water availability across Iran in comparison to other storages such as groundwater.

It can also be inferred from Table 4 that removing the water use from scenario (i) results in smaller canonical correlation in (ii), which means a smaller agreement between variables in scenario (ii) and water storage changes, even though this removal causes ~3% and 5% increase in loadings of precipitation and temperature, respectively. Comparing the results of both scenarios implies the large anthropogenic impact (more than climate-related factors) on water storages variations, which makes it essential to include this impact along with climatic effects while one studies sub-surface water storage variations in Iran. Fig. 16 depicts scatter bi-plots and the linear trend which represents the correspondence between two sets of variables using average canonical coefficients for each scenario. It can be seen that the distribution of the two datasets in scenario (i) has smaller deviations and is more symmetric (closer to the reference line than scenario (ii)), which leads to higher canonical correlation for the first scenario. Fig. 16 shows that incorporating the water use results in a better agreement between the criterion, i.e., water storage variations and predicant. This stresses the necessity of considering the water use and anthropogenic impacts (e.g., irrigation) on water storages analyzes, which cannot be happen without inclusion of GRACE TWS into the process.

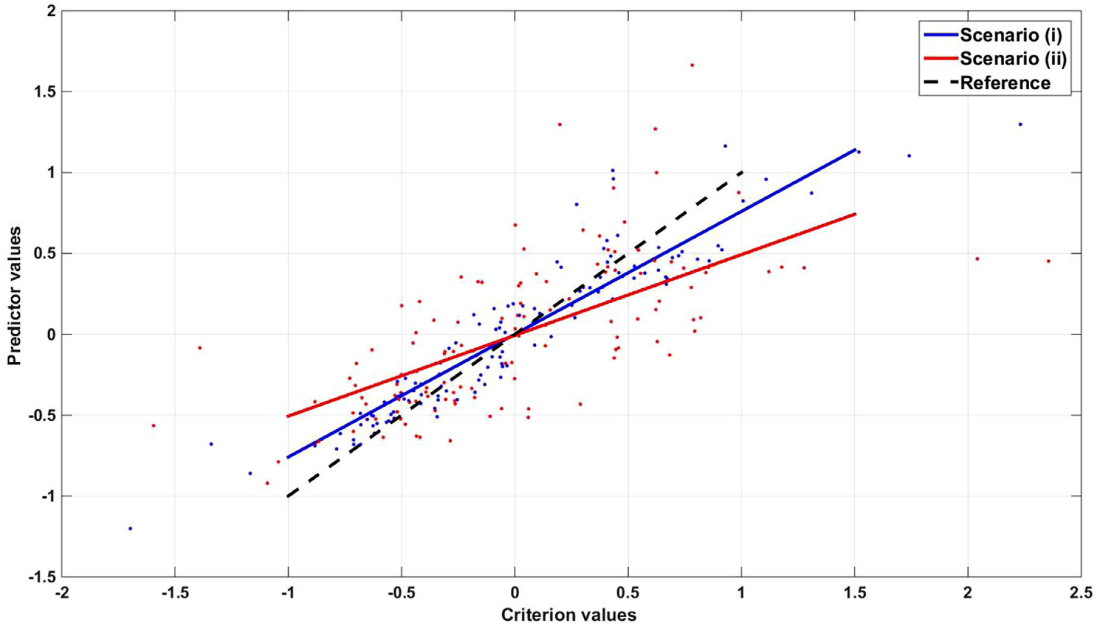

Fig. 16. Scatter bi-plots (circles) and the linear trend (solid lines) of average canonical coefficients from CCA for each scenario applied. The combination of the water storages and discharge data and their canonical coefficients are in the x-axis (as criterion variables), the y-axis represents the combination of the predictor variables. Black solid line represents the reference line.

5. Conclusions

Sub-surface water storages are a major source of freshwater in Iran. With increased population and irrigated land, water availability has become a serious issue across the country. In the present study we assimilate GRACE TWS into W3RA to separately analyze different water compartments including groundwater, soil moisture, and surface water storages. The six major drainage divisions in the area including the eastern part of Iran (East), Caspian Sea, Centre, Sarakhs, Persian Gulf and Oman Sea, and Lake Urmia are considered to better understand water availability in the different regions. An analysis is undertaken to examine the effects of GRACE data assimilation on different water storage compartments. It is found that the implemented process can effectively distribute the TWS increments between groundwater and soil moisture storages. Although the results show improvements in both groundwater and soil moisture, the data assimilation still may have introduced some artefacts into the simulated groundwater dynamics due to the massive effects of groundwater extraction within the country, which requires an independent extensive study and more comprehensive analysis.

It is found that the application of GRACE TWS data assimilation can significantly improve the performance of W3RA. Data assimilation successfully correct for the open-loop simulation variations, e.g., in terms of trends and multi-year variations, especially for groundwater storage. Based on the improved estimates, we find that groundwater trends in a large part of the country's central, western and southern areas are negative representing a significant water availability issue. An average −8.9 mm/year water storages decline is observed during 2002 to 2012 with a larger rate since 2005 suggesting that Iran is becoming considerably dryer. Larger water store depletions are found to occur in the Persian Gulf and Oman Sea and Lake Urmia with lesser effects on soil moisture in these regions. In the Caspian Sea region, however, due to a large amount of precipitation, smaller groundwater and soil moisture trends are observed. In the Persian Gulf and Oman Sea, −9.3 mm/year (on average) groundwater trend is found, which is the second largest negative trend after that of Lake Urmia.

Furthermore, PCA is applied to investigate the relationship between the estimated groundwater and GRACE TWS, as well as their connection to climatic impacts in various parts of Iran. Larger water storage spatial variations are observed over the northern and western parts of Iran with higher altitudes in which precipitation rates are generally high. Contrary to rainfall maps, strong positive GRACE TWS and groundwater signals are found over the north toward the northwest and partially in western areas. In terms of temporal variations, water storage variables generally demonstrate the same variation pattern as precipitation, however, they are also affected by non-climate factors (e.g., anthropogenic impacts), which are likely the cause of the observed negative trends in GRACE TWS and groundwater time series. Therefore, CCA is applied to explore the relationship between water storages estimated by data assimilation and climatic, as well as anthropogenic indicators. The application of CCA reveals strong correlation (0.89 in average) suggesting that the groundwater use has a major impact on water storage variations.

Acknowledgements

M. Khaki is grateful for the research grant of Curtin International Postgraduate Research Scholarships (CIPRS)/ORD Scholarship provided by Curtin University (Australia). This work is a TIGeR publication.

References

Afshar, A.A., Joodaki, G.R., Sharifi, M.A., 2016. Evaluation of groundwater resources in iran using GRACE gravity satellite data. JGST. 5 (4), 73–84. http://jgst.issge.ir/article-1-381-fa.html.

Amery, H.A., Wolf, A.T., 2000. Water in the Middle East: A Geography of Peace. University of Texas Press, Austin, Tex.

AAnderson, J., 2001. An ensemble adjustment kalman filter for data assimilation. Mon. Wea. Rev. 129, 28842903. https://doi.org/10.1175/1520-0493(2001)129(2884:AEAKFF)2.0.CO;2.

Anderson, M.C., Norman, J.M., Mecikalski, J.R., Otkin, J.A., Kustas, W.P., 2007. A climatological study of evapotranspiration and moisture stress across the continental united states based on thermal remote sensing: 1. model formulation. J. Geophys. Res. 112 (D10117). https://doi.org/10.1029/2006JD007506.

Ardakani, R., 2009. Overview of water management in iran. proceeding of regional center on urban water management. Tehran, Iran.

Bennett, A.F., 2002. Inverse Modeling of the Ocean and Atmosphere. Cambridge Univ. Press, New York. 234.

Bertino, L., Evensen, G., Wackernagel, H., 2003. Sequential data assimilation techniques in oceanography. Int. Stat. Rev. 71 (2), 223–241.

Chang, B., Kruger, U., Kustra, R., Zhang, J., 2013. Canonical correlation analysis based on hilbert-schmidt independence criterion and centered kernel target alignment. Volume 28: Proceedings of The 30th International Conference on Machine Learning 2 (28), 316–324. http://jmlr.csail.mit.edu/proceedings/papers/v28/chang13.pdf.

Chen, J.L., Wilson, C.R., Famiglietti, J.S., Rodell, M., 2007. Attenuation effect on seasonal basin-scale water storage changes from GRACE time-variable gravity. J. Geod. 81 (4), 237245. https://doi.org/10.1007/s00190-006-0104-2.

Cheng, M.K., Tapley, B.D., 2004. Variations in the earth's oblateness during the past 28 years. J. Geophys. Res. Solid Earth 109, B09402. https://doi.org/10.1029/2004JB003028.

Dattalo, P., 2014. A Demonstration of Canonical Correlation Analysis with Orthogonal Rotation to Facilitate Interpretation. In press, School of Social Work. Virginia Commonwealth University, Richmond, Virginia.

Döll, P., Kaspar, F., Lehner, B., 2003. A global hydrological model for deriving water availability indicators: model tuning and validation. J. Hydrol. 270, 105134.

Eicker, A., Schumacher, M., Kusche, J., Dll, P., Mller-Schmied, H., 2014. Calibration/data assimilation approach for integrating GRACE data into the waterGAP global hydrology model (WGHM) using an ensemble kalman filter: first results. Surv. Geophys. 35 (6), 12851309. https://doi.org/10.1007/s10712-014-9309-8.

Evensen, G., 2003. The ensemble kalman filter: theoretical formulation and practical inplementation. Ocean Dyn. 53, 343367. https://doi.org/10.1007/s10236-003-0036-9.

FAO, 2009. (Food and Agriculture Organization of the United Nations). FAO water report, 34.

Fatolazadeh, F., Voosoghi, B., Naeeni, M.R., 2016. Wavelet and gaussian approaches for estimation of groundwater variations using GRACE data. Groundwater 54, 7481. https://doi.org/10.1111/gwat.12325.

Forootan, E., Rietbroek, R., Kusche, J., Sharifi, M.A., Awange, J., Schmidt, M., Omondi, P., Famiglietti, J., 2014a. Separation of large scale water storage patterns over iran using GRACE, altimetry and hydrological data. J. Remote Sens. Environ. 140, 580–595. http://doi.org/10.1016/j.rse.2013.09.025.

Forootan, E., Didova, O., Schumacher, M., Kusche, J., Elsaka, B., 2014b. Comparisons of atmospheric mass variations derived from ECMWF reanalysis and operational fields, over 2003 to 2011. J. Geod. 88, 503–514. https://doi.org/10.1007/s00190-014-0696-x.

Forootan, E., Safari, A., Mostafaie, A., Schumacher, M., Delavar, M., Awange, J., 2017. Large-scale total water storage and water flux changes over the arid and semi-arid parts of the middle east from GRACE and reanalysis products. Surv. Geophys.. https://doi.org/10.1007/s10712-016-9403-1.

Garner, T.W., Wolf, R.A., Spiro, R.W., Thomsen, M.F., 1999. First attempt at assimilating data to constrain a magnetospheric model. J. Geophys. Res. 104 (A11), 2514525152. https://doi.org/10.1029/1999JA900274.

Girotto, M., De Lannoy, G.J., Reichle, R.H., Rodell, M., 2016. Assimilation of gridded terrestrial water storage observations from GRACE into a land surface model. Water Resour. Res. 52 (5), 4164–4183.

Girotto, M., De Lannoy, G. J., Reichle, R. H., Rodell, M., Draper, C., Bhanja, S. N., Mukherjee, A., 2017. Benefits and pitfalls of GRACE data assimilation: a case study of terrestrial water storage depletion in india. Geophys. Res. Lett.

Golian, S., Mazdiyasni, O., Agha Kouchak, A., 2015. Trends in meteorological and agricultural droughts in iran. Theor. Appl. Climatol. 119, 679688. https://doi.org/10.1007/s00704-014-1139-6.

Harris, I.C., 2008. Climatic Research Unit (CRU) Time-series Datasets of Variations in Climate with Variations in Other Phenomena. In: Jones, P.D. (Ed.), NCAS British Atmospheric Data Centre, date of citation, University of East Anglia Climatic Research Unit. http://catalogue.ceda.ac.uk/uuid/3f8944800cc48e1cbc29a5ee12d8542d.

Hoteit, I., Pham, D.T., Triantafyllou, G., Korres, G., 2008. A new approximate solution of the optimal nonlinear filter for data assimilation in meteorology and oceanography. Mon. Weather Rev. 136, 317–334.

Joodaki, G., Wahr, J., Swenson, S., 2014. Estimating the human contribution to groundwater depletion in the middle east, from GRACE data, land surface models, and well observations. Water Resour. Res. 50, 26792692. https://doi.org/10.1002/2013WR014633.

Kalnay, E., 2003. Atmospheric Modelling, Data Assimilation and Predictability. Cambridge University Press. Xxii 341, ISBNs 0 521 79179 0, 0 521 79629 6, https://doi.org/10.1256/003590003603683511.

Karamouzian, M., Haghdoost, A.K., 2015. Population Control Policies in Iran. In: The Lancet, Volume 385, Issue 9973, 2127 March 2015, Page 1071, ISSN, pp. 0140–6736. https://doi.org/10.1016/S0140-6736(15)60596-7.

Khaki, M., Forootan, E., Sharifi, M.A., 2014. Satellite radar altimetry waveform retracking over the caspian sea. Int. J. Remote Sens. 35 (17), 63296356. https://doi.org/10.1080/01431161.2014.951741.

Khaki, M., Forootan, E., Sharifi, M.A., Awange, J., Kuhn, M., 2015. Improved gravity anomaly fields from retracked multimission satellite radar altimetry observations over the persian gulf and the caspian sea. Geophys. J. Int. 202 (3), 1522–1534. https://doi.org/10.1093/gji/ggv240.

Khaki, M., Hoteit, I., Kuhn, M., Awange, J., Forootan, E., van Dijk, A.I.J.M., Schumacher, M., Pattiaratchi, C., 2017a. Assessing sequential data assimilation techniques for integrating GRACE data into a hydrological model. Adv. Water Resour. 107, 301–316. ISSN 0309–1708, https://doi.org/10.1016/j.advwatres.2017.07.001.

Khaki, M., Ait-El-Fquih, B., Hoteit, I., Forootan, E., Awange, J., Kuhn, M., 2017b. A two-update ensemble kalman filter for land hydrological data assimilation with an uncertain constraint. J. Hydrol.. 2017, ISSN 0022–1694, https://doi.org/10.1016/j.jhydrol.2017.10.032.

Khaki, M., Schumacher, M., Forootan, J., Kuhn, M., Awange, E., van Dijk, A.I.J.M., 2017c. Accounting for spatial correlation errors in the assimilation of GRACE into hydrological models through localization. Adv. Water Resour.. 2017, ISSN 0309–1708, https://doi.org/10.1016/j.advwatres.2017.07.024.

Khaki, M., Forootan, E., Kuhn, M., Awange, J., Longuevergne, L., Wada, W., 2018b. Efficient basin scale filtering of GRACE satellite products. Remote Sens. Environ. 204, 76–93. ISSN 0034–4257, https://doi.org/10.1016/j.rse.2017.10.040.

Khaki, M., Forootan, E., Kuhn, M., Awange, J., Papa, F., Shum, C.K., 2018a. A study of bangladesh's sub-surface water storages using satellite products and data assimilation scheme. Sci. Total Environ. 625, 963–977. 2018, ISSN 0048–9697, https://doi.org/10.1016/j.scitotenv.2017.12.289.

Kusche, J., Schmidt, R., Petrovic, S., Rietbroek, R., 2009. Decorrelated GRACE time-variable gravity solutions by GFZ and their validation using a hydrological model. J. Geod. https://doi.org/10.1007/s00190-009-0308-3.

Lahoz, W.A., Geer, A.J., Bekki, S., Bormann, N., Ceccherini, S., Elbern, H., Errera, Q., Eskes, H.J., Fonteyn, D., Jackson, D.R., Khattatov, B., 2007. The assimilation of envisat data (ASSET) project. Atmos. Chem. Phys. 7, 1773–1796.

Li, B., Rodell, M., 2015. Evaluation of a model-based groundwater drought indicator in the conterminous US. J. Hydrol. 526, 78–88.

Lorenz, E., 1956. Empirical Orthogonal Function and Statistical Weather Prediction. Technical Report Science Report No 1. Statistical Forecasting Project. MIT, Cambridge.

Madani, K., 2014. Water management in iran: what is causing the looming crisis? J. Environ. Stud. Sci. https://doi.org/10.1007/s13412-014-0182-z.

Mayer-Gürr, T., Zehentner, N., Klinger, B., Kvas, A., 2014. ITSG-Grace2014: A New GRACE Gravity Field Release Computed in Graz. GRACE Science Team Meeting (GSTM), Potsdam am: 29.09.2014.

Michel, D., 2017. Iran's Impending Water Crisis. In: Reed, D. (Ed.), Water, Security, and US Policy, p. 438. ISBN-10:1138051519.

Mohammadi-Ghaleni, M., Ebrahimi, K., 2011. Assessing Impact of Irrigation and Drainage Network on Surface and Groundwater Resources Case Study: Saveh Plain. In: Iran, ICID 21st International Congress on Irrigation and Drainage, p. 1523. 2011, Tehran, Iran.

Motagh, M., Walter, T.R., Sharifi, M.A., Fielding, E., Schenk, A., Anderssohn, J., et al., 2008. Land subsidence in iran caused by widespread water reservoir overexploitation. Geophys. Res. Lett. 35, L16403. https://doi.org/10.1029/2008GL033814.

Müller Schmied, H., Eisner, S., Franz, D., Wattenbach, M., Portmann, F., Flrke, M., Dll, P., 2014. Sensitivity of simulated global-scale freshwater fluxes and storages to input data, hydrological model structure, human water use and calibration. Hydrol. Earth. Syst. Sci. 18, 35113538. https://doi.org/10.5194/hess-18-3511-2014.

Njoku, E.G., et al., 2003. Soil moisture retreival from AMSR-e. IEEE Transactions on Geo-science and Remote Sensing 41 (2), 215–229.

Ott, E., Hunt, B.R., Szunyogh, I., Zimin, A.V., Kostelich, E.J., Corazza, M., Kalnay, E., Patil, D.J., Yorke, J.A., 2004. A local ensemble Kalman Filter for atmospheric data assimilation. Tellus 56A, 415–428.

Oke, P.R., Brassington, G.B., Griffin, D.A., Schiller, A., 2008. The bluelink ocean data assimilation system (BODAS). Ocean Modell. 21 (4670). https://doi.org/10.1016/j.ocemod.2007.11.002.

Reager, J.T., Thomas, A.C., Sproles, E.A., Rodell, M., Beaudoing, H.K., Li, B., Famiglietti, J.S., 2015. Assimilation of GRACE terrestrial water storage observations into a land surface model for the assessment of regional flood potential. Remote Sens. 7, 14663–14679.

Renzullo, L.J., Van Dijk, A.I.J.M., Perraud, J.M., Collins, D., Henderson, B., Jin, H., Smith, A.B., Mc Jannet, D.L., 2014. Continental satellite soil moisture data assimilation improves root-zone moisture analysis for water resources assessment. J. Hydrol. 519, 27472762. https://doi.org/10.1016/j.jhydrol.2014.08.008.

Rodell, M., Houser, P.R., Jambor, U., Gottschalck, J., Mitchell, K., Meng, C.J., Arsenault, K., Cosgrove, B., Radakovich, J., Bosilovich, M., Entin, J.K., Walker, J.P., Lohmann, D., Toll, D., 2004. The global land data assimilation system. Am. Meteorol. Soc. 85 (3), 381–394. https://doi.org/10.1175/BAMS-85-3-381.

Sarraf, M., Owaygen, M., Ruta, G., Croitoru, L., 2005. Islamic Republic of Iran: Cost Assessment of Environmental Degradation. Technical Report 32043-IR. Washington, D.C.: World Bank.

Schumacher, M., Forootan, E., van Dijk, A.I.J.M., Mller Schmied, H., Crosbie, R.S., Kusche, J., Dll, P., 2018. Improving drought simulations within the murray-darling basin by combined calibration/assimilation of GRACE data into the waterGAP global hydrology model. Remote Sens. Environ. 204, 212–228. 2018, ISSN 0034–4257, https://doi.org/10.1016/j.rse.2017.10.029.

Schumacher, M., Kusche, J., Dll, P., 2016. A systematic impact assessment of GRACE error correlation on data assimilation in hydrological models. J. Geod.. https://doi.org/10.1007/s00190-016-0892-y.

Schunk, R.W., Scherliess, L., Sojka, J.J., Thompson, D.C., 2004. USU Global Ionospheric Data Assimilation Models. In: Huang, H.L.A., Bloom, H.J. (Eds.), Atmospheric and Environmental Remote Sensing Data Processing and Utilization: an End-to-End

System Perspective. In: Proc. of SPIE, 5548, pp. 327–336. https://doi.org/10.1117/12.562448.
Sheffield, J., Goteti, G., Wood, E.F., 2006. Development of a 50-yearhigh-resolution global dataset of meteorological forcings for land surfacemodeling. J. Clim. 19 (13), 30883111.
Steiger, J.H., Browne, M.W., 1984. The comparison of interdependent correlations between optimal linear composites. Psychometrika 49, 1121.
Swenson, S., Chambers, D., Wahr, J., 2008. Estimating geocentervariations from a combination of GRACE and ocean model output. J. Geophys. Res. 113, B08410. https://doi.org/10.1029/2007JB005338.
Tapley, B.D., Bettadpur, S., Watkins, M., Reigber, C., 2004. The gravity recovery and climate experiment: mission overview and early results. Geophys. Res. Lett. 31, L09607. https://doi.org/10.1029/2004GL019920.
Tippett, M.K., Anderson, J.L., Bishop, C.H., Hamill, T.M., Whitaker, J.S., 2003. Ensemble square root filters. Mon. Weath. Rev. 131, 148590.
Tourian, M.J., Elmi, O., Chen, Q., Devaraju, B., Roohi, S., Sneeuw, N., 2015. A spaceborne multisensor approach to monitor the desiccation of lake urmia in iran. Remote Sens. Environ. 156, 349–360. ISSN 0034–4257, https://doi.org/10.1016/j.rse.2014.10.006.
Tregoning, P., Mc Clusky, S., van Dijk, A.I.J.M., Crosbie, R.S., Pea-Arancibia, J.L., 2012. Assessment of GRACE satellites for groundwater estimation in australia. Waterlines report, National Water Commission, Canberra.
Trigo, R.M., Gouveia, C.M., Barriopedro, D., 2010. The intense 20072009 drought in the fertile crescent: impact and associated atmospheric circulation. Agric. For. Meteorol. 150, 12451257.
Tropical Rainfall Measuring Mission (TRMM), 2011. TRMM (TMPA/3b43) rainfall estimate l3 1 month 0.25 degree x 0.25 degree v7, greenbelt, MD, goddard earth sciences data and information services center (GES DISC). Accessed [Data Access Date] https://disc.gsfc.nasa.gov/datacollection/TRMM_3B43_7.html.
Van Camp, M., Radfar, M., Martens, K., Walraevens, K., 2012. Analysis of the groundwater resource decline in an intramountain aquifer system in central iran. Geologica Belgica 15/3, 176180.
vanDijk, A.I.J.M., 2010. The Australian water resources assessment system. Technical report 3, landscape model (version 0.5) technical description, CSIRO: Water for a healthy country national research flagship.
van Dijk, A.I.J.M., Pea-Arancibia, J.L., Wood, E.F., Sheffield, J., Beck, H.E., 2013. Global analysis of seasonal streamflow predictability using an ensemble prediction system and observations from 6192 small catchments worldwide. Water Resour. Res. 49, 27292746. https://doi.org/10.1002/wrcr.20251.
van Dijk, A.I.J.M., Renzullo, L.J., Wada, Y., Tregoning, P., 2014. A global water cycle reanalysis 20032012 merging satellite gravimetry and altimetry observations with a hydrological multi-model ensemble. Hydrol. Earth Syst. Sci. 18, 29552973. https://doi.org/10.5194/hess-18-2955-2014.
Voss, K.A., Famiglietti, J.S., Lo, M.H., de Linage, C., Rodell, M., Swenson, S.C., 2013. Groundwater depletion in the middle east from GRACE with implications for transboundary water management in the tigris euphrates western iran region. Water Resour. Res. 49. https://doi.org/10.1002/wrcr.20078.
Wahr, J.M., Molenaar, M., Bryan, F., 1998. Time variability of the earth's gravity field: hydrological and oceanic effects and their possible detection using GRACE. J. Geophys. Res. 108 (B12), 3020530229. https://doi.org/10.1029/98JB02844.
Whitaker, J.S., Hamill, T.M., 2002. Ensemble data assimilation without perturbed observations. Mon. Wea. Rev. 130, 19131924.
Wolf, A.T., Newton, J.T., 2007. Case study transboundary dispute resolution: the tigris-euphrates basin. Transboundary Freshwater Dispute Database (TFDD), Oregon State University. http://www.transboundarywaters.orst.edu/.
Zaitchik, B.F., Rodell, M., Reichle, R.H., 2008. Assimilation of GRACE terrestrial water storage data into a land surface model: results for the mississippi river basin. J. Hydrometeorol. 9 (3), 535548. https://doi.org/10.1175/2007JHM951.1.

Science of the Total Environment 647 (2019) 1557–1572

Contents lists available at ScienceDirect

Science of the Total Environment

journal homepage: www.elsevier.com/locate/scitotenv

The application of multi-mission satellite data assimilation for studying water storage changes over South America

M. Khaki[a,b,*], J. Awange[a]

[a] School of Earth and Planetary Sciences, Spatial Sciences, Curtin University, Perth, Australia
[b] School of Engineering, University of Newcastle, Callaghan, New South Wales, Australia

HIGHLIGHTS

- We use a hydrological model to study sub-surface water storages within South America.
- GRACE and satellite soil moisture data are used to improve the model estimates.
- Ensemble Square-Root Filter (EnSRF) is used for data assimilation.
- Climate induced water storage changes are investigated using rainfall products.
- More accurate estimates of groundwater and soil moisture variations are achieved.

GRAPHICAL ABSTRACT

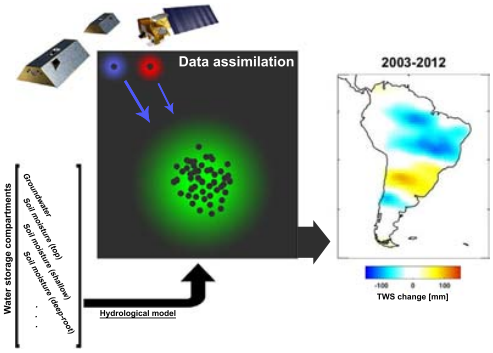

ARTICLE INFO

Article history:
Received 20 April 2018
Received in revised form 3 August 2018
Accepted 5 August 2018
Available online 8 August 2018

Editor: Ashantha Goonetilleke

Keywords:
South America
Satellite remote sensing
Data assimilation
Hydrological modeling
GRACE
Satellite soil moisture

ABSTRACT

Constant monitoring of total water storage (TWS; surface, groundwater, and soil moisture) is essential for water management and policy decisions, especially due to the impacts of climate change and anthropogenic factors. Moreover, for most countries in Africa, Asia, and South America that depend on soil moisture and groundwater for agricultural productivity, monitoring of climate change and anthropogenic impacts on TWS becomes crucial. Hydrological models are widely being used to monitor water storage changes in various regions around the world. Such models, however, comes with uncertainties mainly due to data limitations that warrant enhancement from remotely sensed satellite products. In this study over South America, remotely sensed TWS from the Gravity Recovery And Climate Experiment (GRACE) satellite mission is used to constrain the World-Wide Water Resources Assessment (W3RA) model estimates in order to improve their reliabilities. To this end, GRACE-derived TWS and soil moisture observations from the Advanced Microwave Scanning Radiometer - Earth Observing System (AMSR-E) and Soil Moisture and Ocean Salinity (SMOS) are assimilated into W3RA using the Ensemble Square-Root Filter (EnSRF) in order to separately analyze groundwater and soil moisture changes for the period 2002–2013. Following the assimilation analysis, Tropical Rainfall Measuring Mission (TRMM)'s rainfall data over 15 major basins of South America and El Niño/Southern Oscillation (ENSO) data are employed to demonstrate the advantages gained by the model from the assimilation of GRACE TWS and satellite soil moisture products in studying climatically induced TWS changes. From the results, it can be seen that assimilating these observations improves the performance of W3RA hydrological model. Significant improvements are also achieved as seen

* Corresponding author at: School of Earth and Planetary Sciences, Spatial Sciences, Curtin University, Perth, Australia.
E-mail address: Mehdi.Khaki@postgrad.curtin.edu.au (M. Khaki).

https://doi.org/10.1016/j.scitotenv.2018.08.079

from increased correlations between TWS products and both precipitation and ENSO over a majority of basins. The improved knowledge of sub-surface water storages, especially groundwater and soil moisture variations, can be largely helpful for agricultural productivity over South America.

1. Introduction

South America, with unique ecosystems and a high biodiversity, has extreme geographic variations and diverse patterns of weather and climate that include tropical, subtropical and extratropical features (Garreaud et al., 2008). The region is largely under the influence of large-scale ocean-atmosphere phenomena including mainly El Niño Southern Oscillation (ENSO) and the North Atlantic Oscillation (NAO), which affects climate and its phases associated with droughts, floods, and extreme weather events within different parts of the continent (Magrin et al., 2007; Tedeschi and Collins, 2016). Climate variability throughout South America can be categorized based on the distance from the equator and the altitude of the area. The Andes mountain ranges, running along South America's western side, plays an important role in tropical as well as subtropical latitudes by keeping dry conditions on the west and moist conditions on the east (Garreaud et al., 2008). These climate variabilities, e.g., due to the different climatic zones across the continent and/or large-scale ocean-atmosphere phenomena, have significant impacts on the continent's water storages (surface water, groundwater, soil moisture, and vegetation water). There are other important factors that largely threaten water resources such as excessive water use, especially for agricultural purposes (Grau and Aide, 2008; Magrin et al., 2014). Therefore, the study of South America's water storage changes in light of the climate change and anthropogenic impacts is necessary for any future water use planning.

To study South America's water storage changes at high spatio-temporal resolutions, hydrological models have come in handy (e.g., Betts et al., 1996; Koster and Suarez, 1999; Döll et al., 2003; van Dijk, 2010; De Paiva et al., 2013; Getirana et al., 2014), particularly over the regions with a few ground-based observations such as Venezuela, Ecuador, Chile, and Peru. The applications of these models are especially important for agriculture and sustainable water managements (e.g., Bharati et al., 2008; Yu et al., 2015; Kourgialas and Karatzas, 2015). However, in general, data limitations and other factors, e.g., imperfect modeling and uncertainties of model parameters can weaken performances of the models for simulation of hydrological processes (van Dijk et al., 2011; Vrugt et al., 2013). In this regards, data assimilation provides a unique opportunity to improve model reliabilities (Bertino et al., 2003). This approach integrates additional observations that have not been considered in those models into their dynamics to constrain its state estimates (Bertino et al., 2003; Hoteit et al., 2012).

Data assimilation has been used in different applications, e.g., atmospheric fields (Elbern and Schmidt, 2001; Schunk et al., 2004; Altaf et al., 2014), oceanic (Bennett, 2002; Lahoz et al., 2007) and magnetospheric (Garner et al., 1999) studies. The method has also been applied in hydrological contexts to increase models' performances for estimating various water compartments (e.g., Reichle, 2002; Alsdorf et al., 2007; de Goncalves et al., 2009; Renzullo et al., 2014; Dillon et al., 2016; Khaki et al., 2018a; Khaki et al., 2018b). The use of models to study hydrological variables over South America are reported, e.g., in the works of Yates (1997), Chou et al. (2002), Grimson et al. (2013), and Erfanian et al. (2017), who investigate the application of the models on hydrological resources, droughts, and water storage changes. In the works above, the limitations have been that the models have not incorporated remotely sensed hydrological products such as the Gravity Recovery And Climate Experiment (GRACE) with a large capability of estimating terrestrial water storage (TWS) changes.

The main objective of the present study is, therefore, to use multimission satellite data products to improve hydrological model estimates of sub-surface water storages over South America. For this purpose, GRACE-derived TWS and soil moisture observations from the Advanced Microwave Scanning Radiometer - Earth Observing System (AMSR-E) and Soil Moisture and Ocean Salinity (SMOS) are assimilated into the World-Wide Water Resources Assessment (W3RA) hydrological model (van Dijk, 2010). The model has been applied at different continental and global studies including South America (e.g., van Dijk et al., 2013; van Dijk et al., 2014; Beck et al., 2016; Schellekens et al., 2017). In terms of observations, several studies indicate that using GRACE TWS (e.g., Zaitchik et al., 2008; Houborg et al., 2012; Li et al., 2012; Eicker et al., 2014; Li et al., 2015; Reager et al., 2015; Li and Rodell, 2015; Kumar et al., 2016; Girotto et al., 2016; Khaki et al., 2017a; Khaki et al., 2017b; Girotto et al., 2017; Khaki et al., 2018c) and satellite soil moisture (e.g., Tian et al., 2008; Renzullo et al., 2014; Dumedah et al., 2015; Tian et al., 2017; Kolassa et al., 2017) for data assimilation can successfully constrain the hydrological models simulations. The present study aims at investigating the effectiveness of multi-satellite data assimilation for studying sub-surface water storage changes using a non-regional hydrological model. It should be pointed out that although similar studies by the authors have been undertaken for other regions and using different products (e.g., Khaki et al., 2017c; Khaki et al., 2018d), the main distinction and innovativeness between the current work over South America and those undertaken by the authors above, is that for the first time, both GRACE TWS and soil moisture products are employed in assimilation over the area. Furthermore, the contribution of climate variability on South America's water storage derived from assimilation using satellite precipitation products is also investigated.

Assimilation of GRACE TWS data allows users to consistently separate TWS (since both model and observation errors are considered) into different water compartments that include groundwater and soil moisture. This is due to the fact that the W3RA model relies on the physical processes implemented in the model equations. Besides, GRACE-derived TWS observations are spatially downscaled using this approach, and therefore, higher spatial resolution estimations of water storages will be available within the study region (see, e.g., Schumacher and Kusche, 2016). Moreover, the application of soil moisture observations in the assimilation can improve the performance of the process by separately updating model soil moisture estimates (e.g., Tian et al., 2017). For the purpose of data assimilation, here, we use the ensemble-based sequential technique of the Ensemble Square-Root Filter (EnSRF) filtering scheme (Whitaker and Hamill, 2002) to integrate GRACE TWS into W3RA. EnSRF, as shown in Khaki et al. (2017a), is preferred over the traditional ensemble Kalman filter (e.g., Evensen, 2003; Evensen, 2007; Eicker et al., 2014) due to its higher computational speed, simplicity, and independence of perturbed observations.

Following the assimilation step, in-situ measurements are used to assess the performance of the approach. Furthermore, the study investigates the use of the model to study climate induced water storage changes by comparing correlations between assimilated and non-assimilated results with climate variability indicators of the Tropical Rainfall Measuring Mission (TRMM) rainfall and ENSO

ocean-atmospheric couple indicator. For a better discussion, the study area is divided into 15 major basins selected (Fig. 1) based on their importance and large hydro-climatic effects, which also allow us to spatially have a better analysis. We also apply principal component analysis (PCA, Lorenz, 1956) on the TRMM rainfall data, groundwater, soil moisture results from model over each basin to better understand the spatial and temporal variations of water storages and their interactions with precipitation. Frappart et al. (2013) found that PCA modes can better represent spatiotemporal variations in time series compared to the full signals by separating dominant water mass change signals, especially over South America (see also Abelen et al., 2015).

In the remainder of this study, first, datasets and method are presented in Section 2. We then discuss the data assimilation filtering scheme in Subsection 2.5 and provide a detailed explanation of the experimental setup in Subsection 2.6. Results and discussions are provided in Section 3, and the study concluded in Section 4.

2. Materials and methods

2.1. W3RA hydrological model

Vertical water compartments (e.g., soil moisture, groundwater, and surface water) of the globally distributed $1^\circ \times 1^\circ$ World-Wide Water Resources Assessment system (W3RA; http://www.wenfo.org/wald/data-software/) model are used to simulate water storage over South America. The model was developed in 2008 by the Commonwealth Scientific and Industrial Research Organisation (CSIRO; Australia) to simulate water storages (van Dijk, 2010). In terms of forcing data, minimum and maximum temperature, downwelling short-wave radiation, and precipitation products provided by Princeton University (http://hydrology.princeton.edu) are used. Daily W3RA estimates of top, shallow, and deep root soil layers, groundwater storage, and surface water storage in a one-dimensional system (vertical variability) are used for data assimilation (see details in Subsection 2.6).

2.2. Remotely sensed observations (GRACE, soil moisture and TRMM products)

2.2.1. GRACE TWS

Monthly TWS observations at a $3^\circ \times 3^\circ$ spatial resolution (suggested by Khaki et al., 2017b for data assimilation objectives) derived from the GRACE level 2 (L2) monthly Stokes's coefficients (Wahr et al., 1998 following) up to degree and order 90 are used for the assimilation. L2 products along with their full error information are obtained from the ITSG-Grace2014 gravity field model (Mayer-Gürr et al., 2014) for the period between 2002 and 2013. Before converting L2 data into TWS, low degree coefficients of 1 and 2 (C20) are respectively replaced by those estimated by Swenson et al. (2008) and Satellite Laser Ranging solutions, respectively, to account for the change in the Earth's center of mass and large uncertainties (e.g., Cheng and Tapley, 2004; Chen et al., 2007). The DDK2 smoothing filter by Kusche et al. (2009) is applied to tackle colored/correlated noises in spherical harmonics. In order to reduce leakage effects, for every one of the 15 basins considered, an isotropic kernel using a Lagrange multiplier filter proposed by Swenson and Wahr (2002) is applied. This approach reduces short wavelength effects using Lagrange multiplier to minimize the leakage for a given value of satellite error. Here, the satellite error is selected based on the acquired GRACE full error covariance matrix. Khaki et al. (2018e) showed that this filtering technique can effectively reduce leakage errors, e.g., over Amazon basin. Finally, the mean TWS for the study period is taken from W3RA and added to the GRACE TWS change time series to obtain absolute values and make them comparable with model outputs (Zaitchik et al., 2008).

2.2.2. Satellite soil moisture

In addition, soil moisture observations from the Advanced Microwave Scanning Radiometer for EOS (AMSR-E), between 2002 and 2011, and ESA's Soil Moisture Ocean Salinity (SMOS) Earth Explorer mission, between 2011 and 2013, are used in the data assimilation to update model soil moisture variabilities. The AMSR-E measurements are correlated to the surface 0–2 cm soil moisture content (Njoku et al., 2003), while SMOS maps land soil moisture for the 0–5 cm depth. Level 3 CATDS (Centre Aval de Traitement des Donnees SMOS) products (Jacquette et al., 2010) are acquired. SMOS and AMSR-E are selected from ascending and descending passes, respectively, subject to their higher agreement to in-situ measurements (see, e.g., De Jeu and Owe, 2003; Draper et al., 2009; Jackson and Bindlish, 2012; Su et al., 2013). Both data products with a daily temporal resolution are spatially rescaled from $0.25^\circ \times 0.25^\circ$ to $1^\circ \times 1^\circ$ resolution using the nearest neighbor interpolation to match W3RA. Note that these soil moisture observations are used in different periods during the assimilation process, i.e., AMSR-E soil moisture is assimilated for the period 2002–2011 and SMOS soil moisture is assimilated for the period 2011–2013.

2.2.3. Precipitation

Furthermore, monthly precipitation data of the Tropical Rainfall Measuring Mission Project (TRMM-3B43 products; version 7, (TRMM), 2011; Huffman and Bolvin, 2012) are used to assess climate induced water storage changes. Due to the fact that ground validation over land is applied for TRMM-3B43 products, uncertainty in measured precipitation are smaller compared to those of the oceans. Several studies have implemented and validated these products over South America and proved their capabilities (see, e.g., Condom et al., 2011; Ceccherini et al., 2015; Cabrera et al., 2016). The rainfall data are provided on a $0.25^\circ \times 0.25^\circ$ gridded spatial resolution and to make them comparable to those of the model (cf. Section 2.1), they are converted to $1^\circ \times 1^\circ$ using the nearest neighbor interpolation for the period of 2002 to 2013.

2.3. Surface storage data

Although the focus of the present study is on sub-surface water storage compartments, in order to efficiently assimilate GRACE TWS data into W3RA, however, a special focus should be invested on surface water storage variations due to their large contribution in water storage changes over South America (Getirana et al., 2017). In particular, this is important because many surface water sources (in different forms, e.g., lakes and rivers, except for a few major ones) are not modeled in W3RA. To address this problem, the recently developed surface water storage data provided by Getirana et al. (2017) is used. The data is based on a coupled system compromising Noah land surface model (LSM) with multi-parameterization options (Noah-MP; Niu et al., 2011) and the Hydrological Modeling and Analysis Platform (HyMAP) river routing scheme (Getirana et al., 2012). Multiple meteorological forcings and precipitation datasets are used to generate an ensemble of 12 runs, and to establish reference product with associated uncertainties (see details in Getirana et al., 2017). The $1^\circ \times 1^\circ$ monthly gridded surface water data for the period of 2012 to 2013 are subtracted from GRACE TWS before data assimilation.

2.4. In-situ groundwater measurements

In order to evaluate the obtained data assimilation results, independent in-situ groundwater measurements over 34 stations obtained from Global Groundwater Network (GGMN; https://ggmn.un-igrac.org/) and propagated within the study area (see Fig. 1) are compared with estimated groundwater storage changes obtained from data assimilation. Groundwater level measurements should

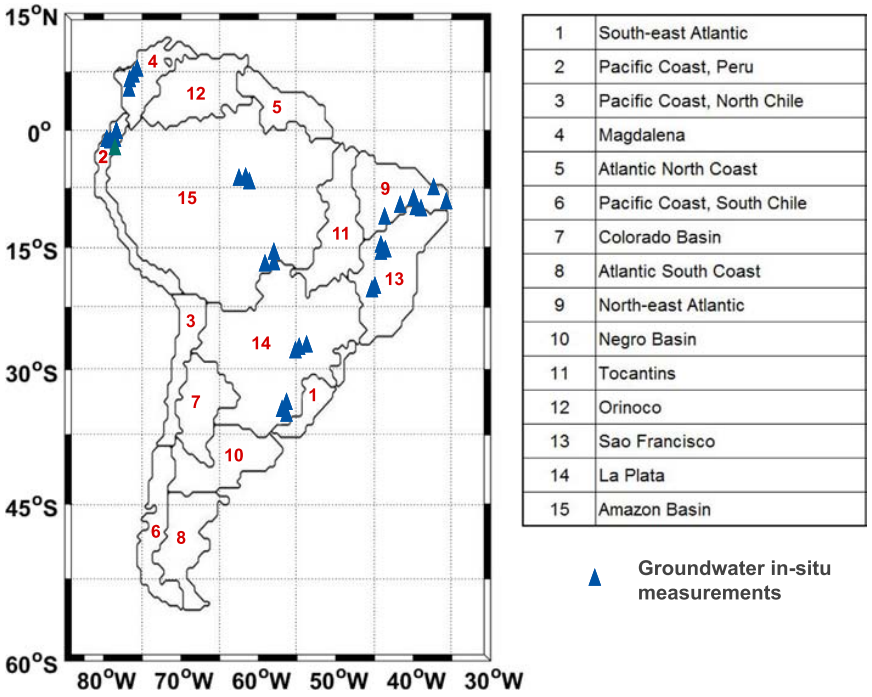

1	South-east Atlantic
2	Pacific Coast, Peru
3	Pacific Coast, North Chile
4	Magdalena
5	Atlantic North Coast
6	Pacific Coast, South Chile
7	Colorado Basin
8	Atlantic South Coast
9	North-east Atlantic
10	Negro Basin
11	Tocantins
12	Orinoco
13	Sao Francisco
14	La Plata
15	Amazon Basin

Fig. 1. Overview of the study area. The black polygons indicate the 15 river basins considered. These basins are selected according to HydroSHEDS (http://www.hydrosheds.org/) classification with small modifications to combine smaller basins and also for a better representation. The basins are sorted according to their areas. Data from in-situ groundwater stations (blue triangles) are used to provide independent validation of the assimilation results. (For interpretation of the references to color in this figure legend, the reader is referred to the web version of this article.)

be converted into groundwater (GW) storage, which requires specific yield values. In the absence of such information, following Tangdamrongsub et al. (2015), TWS variation from GRACE and Global Land Data Assimilation System (GLDAS, Rodell et al., 2004) soil moisture are used to calculate the specific yield and scale the observed head. The scaled in-situ groundwater level fluctuations are then used to assess the results. Afterwards, the assimilation results are spatially interpolated to the location of the in-situ measurements using the nearest neighbor (the closest four grid values). The Root-Mean-Squared Error (RMSE) and correlations between the in-situ and estimated groundwater storage measurements are then computed.

2.5. Data assimilation filtering method

The filtering technique of Ensemble Square-Root Filter (EnSRF) proposed by Whitaker and Hamill (2002) is used to assimilate GRACE TWS and soil moisture data into the W3RA model. The method is based on a traditional Ensemble Kalman Filter (EnKF) that poses a new sampling scheme. The filtering process starts with the forecast step, which includes integrating N (ensemble number) samples of model state X that contains top soil, shallow soil, and deep soil water, snow, vegetation, and groundwater by a dynamical model. The forecast state, thus, can be shown as,

$$X^f = \left[X_1{}^f \ldots X_N{}^f\right], X_i{}^f \; i = 1 \ldots N, \tag{1}$$

where 'f' stands for forecast ('a' in following represents analysis). The corresponding model state forecast error covariance of P^f and the mean state forecast $\bar{X}^f$ are defined by:

$$P^f = \frac{1}{N-1}\sum_{i=1}^{N}\left(X_i^f - \bar{X}^f\right)\left(X_i^f - \bar{X}^f\right)^T, \tag{2}$$

$$\bar{X}^f = \frac{1}{N}\sum_{i=1}^{N}(X_i). \tag{3}$$

The update stage in EnSRF contains two steps. First, it updates the ensemble-mean following,

$$\bar{X}^a = \bar{X}^f + K(y - H\bar{X}^f), \quad i = 1 \ldots N, \tag{4}$$

$$K = P^f(H)^T(HP^f(H)^T + R)^{-1}, \tag{5}$$

where K is the Kalman gain, y is the observation vector and transition matrix is indicated by H. R represents the observation covariance matrix. Data assimilation methods are largely sensitive to the observations uncertainties. Therefore, it is important to assign accurate error values to each observation used in data assimilation. Here, for GRACE observations, TWS error covariance matrix is constructed from Full error information about the GRACE Stokes' coefficients. There is no covariance error information available for satellite soil moisture observations, thus, we assume their error covariances to be uncorrelated and consider various uncertainties to monitor their impacts on data assimilation by comparing the results with independent measurements. This allows us to obtain optimum error values for soil moisture part of observation error covariance. Accordingly, **R** is assumed to be diagonal with an error standard deviation of 0.04 ($m^3\,m^{-3}$) for SMOS (suggested by Leroux et al., 2016) and 0.05 ($m^3\,m^{-3}$) for AMSR-E (suggested by De Jeu et al., 2008). In addition, for the observation error covariance in simultaneous data assimilation case, GRACE data and both SMOS and AMSR-E observations are assumed to be uncorrelated. It is worth mentioning that more study is still required to efficiently estimate the spatially varying observations uncertainties, which also account for error correlations. This can lead to different results and potentially improved

data assimilation. $\bar{X}^a$ in Eq. (4) is the analysis ensemble-mean. In the next step, i.e., the analysis step, the filter updates the forecast ensemble of anomalies,

$$A^f = \left[{A_1}^f \dots {A_N}^f\right], \tag{6}$$

$${A_i}^f = {X_i}^f - \bar{X}^f, \tag{7}$$

into the analysis ensemble deviation A^a in Eq. (8). EnSRF exploits the serial formulation of the Kalman filter analysis step in which the observations are assimilated each at a time to compute the analysis perturbations that exactly match the Kalman filter covariance (Hoteit et al., 2008) using the modified gain ($\tilde{K} = \alpha K$) with,

$$A^a = (I - \tilde{K}H){A_i}^f, \tag{8}$$

$$\alpha = \left(1 + \sqrt{\frac{R}{HP^fH^T + R}}\right)^{-1}, \tag{9}$$

where I is an identity matrix. This definition requires the observation errors to be uncorrelated, which can always be satisfied by scaling the observations with the square-root inverse of the observational error covariance matrix (Hoteit et al., 2015). This, however, is not the case here because there is no rank deficiency on observation error covariance. We assume that soil moisture observations are uncorrelated. Furthermore, the correlation between GRACE TWS on the one hand and soil moisture observations, on the other hand, is also assumed to be zero. The rank deficiency issue raised from GRACE TWS block in the covariance matrix is mitigated by applying GRACE TWS observations in a $3^\circ \times 3^\circ$ spatial resolution along with the implementation of Local Analysis (LA) (Evensen, 2003) scheme, which restricts the information used for the covariance matrix computation to a spatially limited area and uses only measurements located within a certain distance from a grid point (cf. Section 2.6, see also Khaki et al., 2017b). More details regarding the EnSRF algorithm and its performance in GRACE TWS data assimilation against other filters are described, e.g., in Whitaker and Hamill (2002) and Khaki et al. (2017a).

2.6. Experimental setup

As already mentioned, the state vector includes different water storages, i.e., soil moisture, vegetation, snow, and groundwater, simulated by W3RA. Previous studies have investigated the surface water variations over South America (e.g., De Paiva et al., 2013; Getirana et al., 2017), thus, we only focus on the estimation of subsurface compartments; groundwater and soil moisture. The modified GRACE TWS data (cf. Section 2.3) is then used to update the above water compartments excluding surface storage. The observation operator aggregates different water storages at each grid point (1688 points in total) to update with GRACE TWS and scales top-layer soil storage by the field capacity value to provide a relative wetness for updating with soil moisture products of AMSR-E and SMOS (Renzullo et al., 2014).

Considering the different temporal resolution of assimilation observations, e.g., monthly GRACE TWS and daily soil moisture measurements, both observation sets are temporally rescaled into a 5-day resolution for data assimilation. This is done to allow for a simultaneous data assimilation of GRACE TWS and satellite soil moisture measurements. Khaki et al. (2017b) showed that assimilating GRACE TWS in a 5-day temporal scale leads to a better improvement in state variables compared to daily and monthly scales. Therefore, in the analysis steps during the assimilation, the 5-day temporal average update increment (cf. Eq. (4)) is applied. In order to produce ensemble for EnSRF filtering, we use Monte Carlo sampling of multivariate normal distribution, with the errors representing the standard deviations to perturb three main forcing parameters; precipitation, temperature, and radiation (see details in Renzullo et al., 2014). Afterwards, by integrating perturbed meteorological forcing forward in time with the model from 2000 to 2002, 72 sets of state vectors (ensemble; as suggested by Oke et al., 2008) is created at the beginning of the study period.

While implementing data assimilation with a large number of ensemble members results in a heavy computational burden, using a small ensemble size can also be problematic, as it can lead to filter divergence or inaccurate estimation (Tippett et al., 2003). To address this issue, two filter tuning is applied including ensemble inflation and LA. Ensemble inflation helps ensemble members to adequately span the model sub-space by inflating prior ensemble deviation from the ensemble-mean and increases their variations (Anderson, 2001; Anderson et al., 2007). Various inflation factors ([1–1.8]) are tested and their impacts ensemble spreads are monitored to determine the best value (i.e., 1.12). Furthermore, LA (Evensen, 2003; Ott et al., 2004) is applied to both account for a limited ensemble number and also GRACE limited spatial resolution. Applying GRACE TWS data on a high spatial resolution (e.g., $1^\circ \times 1^\circ$) causes correlation errors, which degrades the performance of data assimilation (Khaki et al., 2017a,b). Khaki et al. (2017b) showed that LA can successfully mitigate this problem by restricting the impact of the measurements in the update step to variables located within a certain distance only, e.,g, 5°, which is applied in the present study.

2.7. Climate variability impacts

In order to investigate the model's enhancement for studying climate induced impacts, TRMM rainfall and ENSO data are employed. At each grid point, correlations between TWS with and without data assimilation for both rainfall (at the same point) and ENSO are calculated. Afterwards, improvements achieved by data assimilation with respect to no assimilation of TWS are explored. Furthermore, principal component analysis (PCA; Lorenz, 1956) is applied on the estimated groundwater and soil moisture storages (from assimilation), as well as on TRMM rainfall to better analyze the spatio-temporal changes of water storages and precipitation. This is done to examine the precipitation patterns within the area between 2002 and 2013 and to investigate their connections to water storage changes. Since precipitation is the major effective parameter on water storage recharge, the process helps to study the role of climate variability on water storage variations. A schematic illustration of the methodology steps is provided in Fig. 2.

3. Results and discussions

3.1. Data assimilation

In what follows, data assimilations results and their comparison with in-situ measurements are first discussed. First, we investigate the impacts of assimilated observations, e.g., GRACE TWS and satellite soil moisture on water storage estimates (cf. Section 3.1.1). Note that the results presented in this section are not used for validation and only show how the assimilation results differ from the open-loop (no data assimilation) results. Evaluation against independent measurements will also be discussed (cf. Section 3.1.2).

3.1.1. Observation impacts on state variables

The spatially averaged time series of TWS variations estimated by EnSRF over South America is presented in Fig. 3a, which shows that the application of data assimilation reduces misfits (Fig. 3b) between the results and GRACE TWS compared to the open-loop.

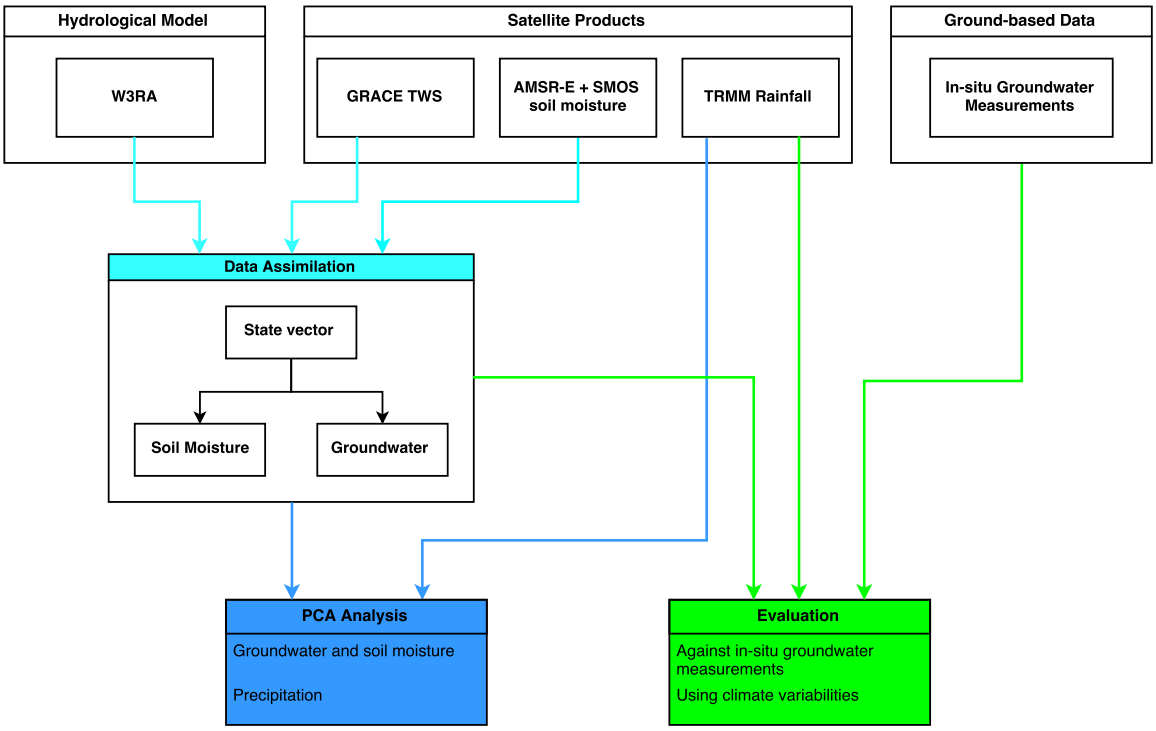

Fig. 2. Schematic illustration of the methodology steps including data used, assimilation scheme, and evaluation processes. In data assimilation process, W3RA is used for forecasting and GRACE TWS and satellite soil moisture measurements are used to update forecasts from the model. Once the groundwater and soil moisture are estimated from the assimilation process, their relationship with rainfall data is investigated using PCA analysis. The in-situ groundwater measurements as well as rainfall data are further used to assess the data assimilation estimates.

Furthermore, Fig. 3c shows the average time series of soil moisture variations from the model top layer open-loop and assimilation, as well as satellite remote sensing. Similar to Fig. 3b, Fig. 3d indicate that the data assimilation successfully decreases the differences between soil moisture estimates and the observations. The average discrepancy between the estimated (assimilated) TWS and those by GRACE is approximately 46%, and between soil moisture estimates and satellite (AMSR-E and SMOS) observations is 34% less than those of between open-loop and observations, which demonstrate that data assimilation successfully incorporates observations into the system states. The effects of data assimilation can better be seen where large anomalies exist such as 2005 and 2011. The large anomaly in Fig. 3a during 2011 could be related to the strong ENSO impact (see, e.g., Boening et al., 2012). It is clear that this strong anomaly captured by GRACE is successfully reflected into assimilation TWS contrary to that of open-loop.

For a better discussion, we also calculate the correlation between the soil moisture variations from satellites and estimations for each of the 15 basins (Fig. 3e). This is done on a basin scale due to the fact that basin averaged time series can be more representative of water storage changes in the area. In all the cases, regardless of the method, data assimilation resulted in higher correlations with the observations compared to the open-loop (un-assimilated model products). Assimilation of only one satellite products, e.g., GRACE TWS or soil moisture, increases the correlation values in Fig. 3e. As expected, GRACE TWS data assimilation has more effects on enhancing TWS correlations, however, it can be seen that even soil moisture only data assimilation in most of the cases causes higher TWS correlation than the open-loop results. It can also be seen that the correlation between joint data assimilation (GRACE TWS and satellite soil moisture) results in Fig. 3e are largely in agreement with the observed variables compared to GRACE-only data assimilation. This indicates that assimilation of soil moisture products along with GRACE TWS leads to more improvements. One main reason for this is that while GRACE TWS data assimilation is generally an effective approach for updating models TWS (e.g., Zaitchik et al., 2008; Reager et al., 2015; Khaki et al., 2018a; Khaki et al., 2018b), it can also introduce artifact effects to different storage such as by assigning wrong increments to either groundwater or soil moisture (Li et al., 2015; Girotto et al., 2017; Khaki et al., 2018c). Assimilation of soil moisture products can account for this problem by independently constraining soil moisture estimates. Fig. 3e shows that this joint assimilation leads to better estimations of soil moisture.

In addition, the average correlation improvement from jointly assimilating GRACE TWS and soil moisture in comparison to the open-loop is presented in Fig. 3f. Note that only the results of joint data assimilation are presented in the figure due to its better performance (cf. Fig. 3e). Fig. 3f demonstrates that higher correlations are achieved after data assimilation. For GRACE TWS, higher correlations are achieved within larger basins such as Amazon (number 15) and Tocantins (number 11). This suggests that GRACE TWS data assimilation has larger impacts on these basins. It can be seen that the minimum improvement happens for the Pacific Coast, North Chile basin (number 3), where GRACE TWS data are expected to have larger errors in comparison to other basins like the Amazon basin with small leakage errors (Wiese, 2015). Nevertheless, in general, the assimilation process increases the correlation between outputs and GRACE TWS.

3.1.2. *Evaluation results*

In order to examine the validity of the data assimilation, groundwater in-situ measurements from various stations are spatially averaged to the location of nearest model grid points and compared with their estimates. As mentioned (cf. Section 2.4), we calculate RMSE

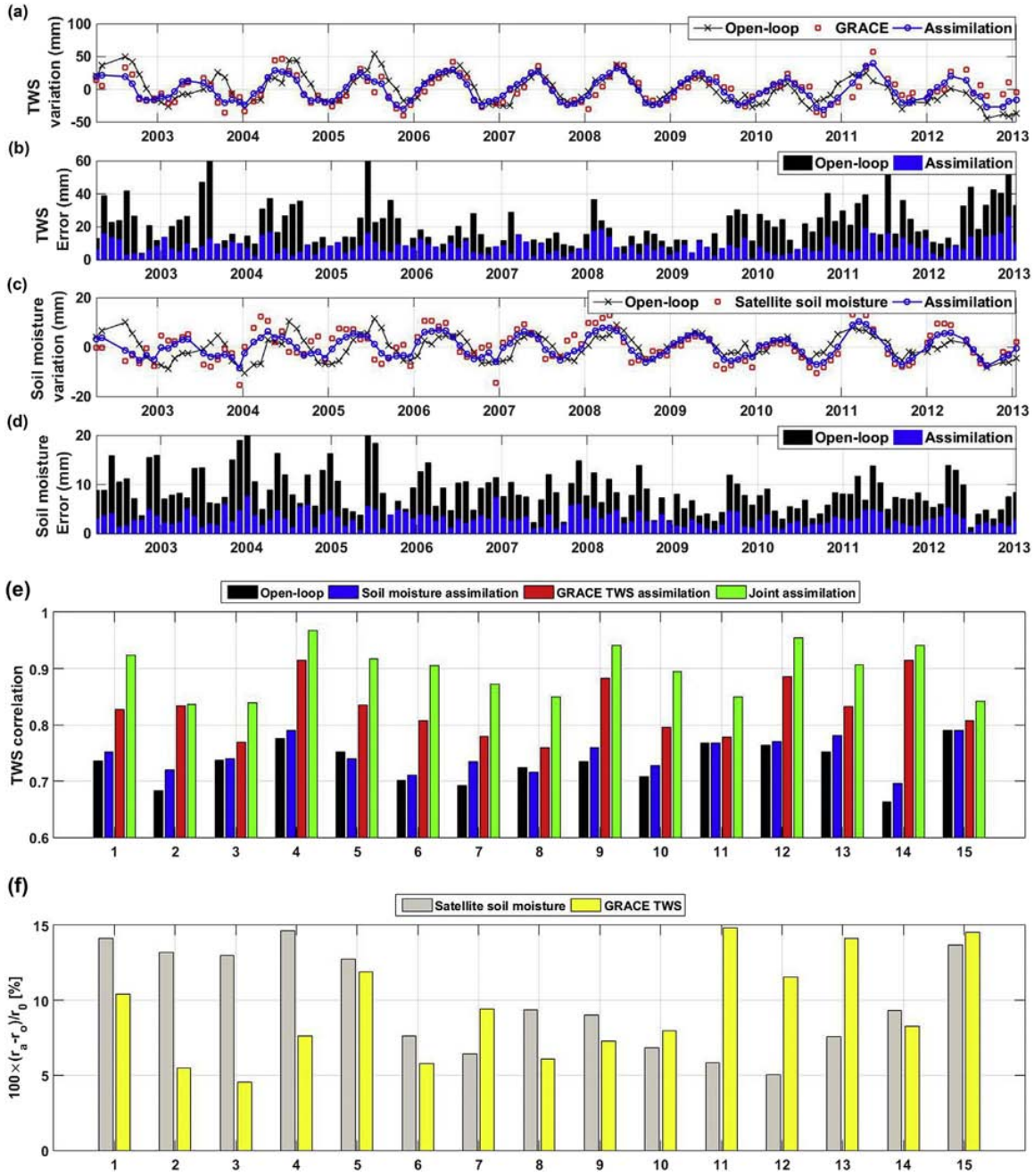

Fig. 3. (a) Comparison between the TWS time series from the assimilation process (blue), GRACE TWS (red), with the open-loop referring to the model estimation without applying data assimilation (black). (b) Absolute error bars before (black) and after (blue) data assimilation process in comparison to the GRACE TWS observations. (c) and (d) are similar to (a) and (b), respectively, but for soil moisture observations. (e) Average correlations between GRACE-derived TWS and TWS simulated by W3RA before assimilation, GRACE TWS only assimilation, soil moisture only assimilation, and joint data assimilation for each basin (cf. Fig. 1). (f) Correlation improvement between joint data assimilation results and GRACE TWS and soil moisture observation with respect to the open-loop results. (For interpretation of the references to color in this figure legend, the reader is referred to the web version of this article.)

and correlation for three tests including the open-loop, GRACE-only TWS data assimilation, and joint GRACE-soil moisture assimilation. Table 1 presents the average RMSE, corresponding RMSE reduction, and Nash-Sutcliffe coefficient (NSE) of the results before and after assimilation. In order to statistically assess the significance of the results, the Student's*t*-test is applied after considering the autocorrelation in time series. The estimated *t*-values and the distribution at 0.05 significant level are used to calculate p-values. Data assimilation results indicate significantly smaller RMSE and higher NSE in cases of GRACE TWS and joint data assimilation. Soil moisture only data assimilation has small positive impacts on NSE improvement (e.g., 3%) but with no significant RMSE improvement. An average improvement of 23.43% in RMSE and 14.08% in NSE (for all assimilation experiments) proves the capability of data assimilation to improve model simulations with respect to the reality. Nevertheless, the joint data assimilation indicates larger improvements in terms of RMSE

Table 1
Statistics of groundwater errors. For each case, the RMSE average and its range (±XX) at the 95% confidence interval is presented. Improvements in data assimilation results are calculated with respect to the groundwater storages from the model without implementing data assimilation.

Experiment scenario	NSE	RMSE (mm)	Improvement (%)	
			NSE	RMSE
Open-loop	0.63	69.26 ± 7.38	–	–
GRACE-only data assimilation	0.75	54.19 ± 5.79	16.01	21.76
Soil moisture data assimilation	0.65	66.48 ± 7.12	3.07	–
Joint GRACE-soil moisture assimilation	0.82	51.87 ± 5.16	23.17	25.11

reduction and NSE improvements than GRACE-only data assimilation. This shows that this method can better constrain different water storage compartments. It can be seen that soil moisture observations help in better controlling the distribution of increments between storages.

Furthermore, it is found that this joint data assimilation better reduces the forecast uncertainties. We calculate the average standard deviation (STD) of ensemble members before and after each data assimilation step for all assimilation cases. These ensemble uncertainties generally refer to forcing errors that grow by running the model forward in time. While all the cases, as expected, lead to a smaller STD (5.31% on average) in the analysis steps (after assimilating observations), the least uncertainty is achieved for the joint data assimilation (11.78% STD reduction). Note that the smaller ensemble STD can also lead to a weaker ensemble spread, however, this is not the case here. The achieved STD reduction means that the method can better propagate ensemble members by improving the spread of forecast ensemble members based on the observations and their associated uncertainties. These results show that data assimilation can improve our understanding of water storage changes. More importantly, monitoring groundwater using reliable information is crucial over South America, where only a few studies have focused on it (e.g., International Groundwater Resources Assessment Centre, 2004; Villar, 2016). Groundwater is a major water resource along with surface storages within the area providing almost 60% of freshwater use (Villar, 2016). This number is even higher for some countries such as Chile, Peru, Venezuela, Suriname and The Guyanas (Morris et al., 2003). The application of the proposed approach for studying groundwater variations can benefit many of these countries to better monitor groundwater using the enhanced estimates.

As previously mentioned, data assimilation, especially when using GRACE TWS data, can introduce artifacts to other variables. This can be the case not only for different variables in the state vector (e.g., groundwater and soil moisture) but also for non-assimilated variables such as water discharge. To monitor this effect, we compare model water discharge to streamflow in-situ measurements obtained from Hydrology and Geochemistry of the Amazon basin (HYBAM). The monthly in-situ discharge measurements, computed as the sum of the daily discharge, are spatially interpolated to the closest grid points and compared with the estimates at those grid points. Fig. 4a shows the average discharge time series over the Amazon basin before and after data assimilation, as well as from in-situ measurements. It can be seen that assimilation of GRACE TWS and soil moisture reduces the misfits between model and in-situ water discharge time series. Furthermore, Fig. 4b and c presents the average scatter plots of the discharge estimates from the open-loop and assimilation compared to the in-situ values. The average correlations between time series are also indicated in the plots, which show the larger agreement between the assimilation results and in-situ streamflow measurements. Data assimilation decreases the RMSE values from 6.47 cm to 2.88 cm and increases NSE from 0.47 to 0.71. Assimilation of GRACE TWS and soil moisture, thus, effectively reduces discharge error. This confirms the findings of Syed et al. (2005), who used GRACE TWS and additional model-derived fluxes observations to study water discharge over the Amazon basin. Undermining groundwater and moisture storage changes in their experiment, however, led to some degree of discrepancy between the estimated and observed discharge. In contrast, in this study, updating different water compartments including groundwater during the assimilation analysis results in a better agreement between the results and in-situ measurements. In general, Fig. 4 indicates that the joint assimilation process not only causes any artifact errors but also improve the discharge estimates (cf. Fig. 4).

To further investigate the effect of data assimilation, we compare the TWS estimates from the joint data assimilation and the open-loop run with precipitation over the Amazon Basin. The rationale behind this choice is due to the fact that various studies have reported different droughts (see, e.g., Chen et al., 2009; Frappart et al., 2013) over the basin and a successful data assimilation should be able to capture these phenomena. Fig. 5 shows the TWS variations over the basin from the above approaches, as well as precipitation. The average correlation between TWS estimates and precipitation is 0.89, ~17% larger than that of the open-loop run. It can be seen that the data assimilation time series better capture large anomalies such as in 2004 and 2009 reflected also in the precipitation time series. La Niña impact during 2011 (see also Boening et al., 2012) is better captured by the assimilation results. Furthermore, 2005 drought over the Amazon Basin (see, e.g., Chen et al., 2009) is reflected in both open-loop and assimilation results, while the later show a larger amplitude.

Table 2 contains the correlations between the open-loop run and joint data assimilation TWS results and precipitation. The table also reports the correlation improvements in the assimilation results with respect to those of the open-loop against both precipitation as well as ENSO (using Niño 3.4 indicator), as the dominant climate variability index over South America (Tourre et al., 2008; Xavier et al., 2010; Flantua et al., 2016) for each basin. It can be seen that significant improvements are achieved by assimilating remotely sensed TWS and soil moisture observations into W3RA hydrological model. Correlation with both precipitation and ENSO over a majority of the basins showcase these improvements. Note that only precipitation correlation improvements are statistically significant. An average correlation between rainfall and TWS anomalies within South America is found to be 0.89, ~11% larger than the open-loop results. This indicates that there is a larger agreement between the assimilation results and rainfall over the area than the case of the model simulations without data assimilation. The improvements in terms of correlations with ENSO are different for various basins. For example, larger correlations and corresponding improvements are estimated for Atlantic North Coast (basin 5), Pacific Coast, North Chile (basin 3), Negro (basin 10), Magdalena (basin 4), and Orinoco (basin 12) basins. The reason for this is due to the fact that ENSO effects on precipitation are larger over basins located within the north toward the northeast and the southeast parts of South America and partially over

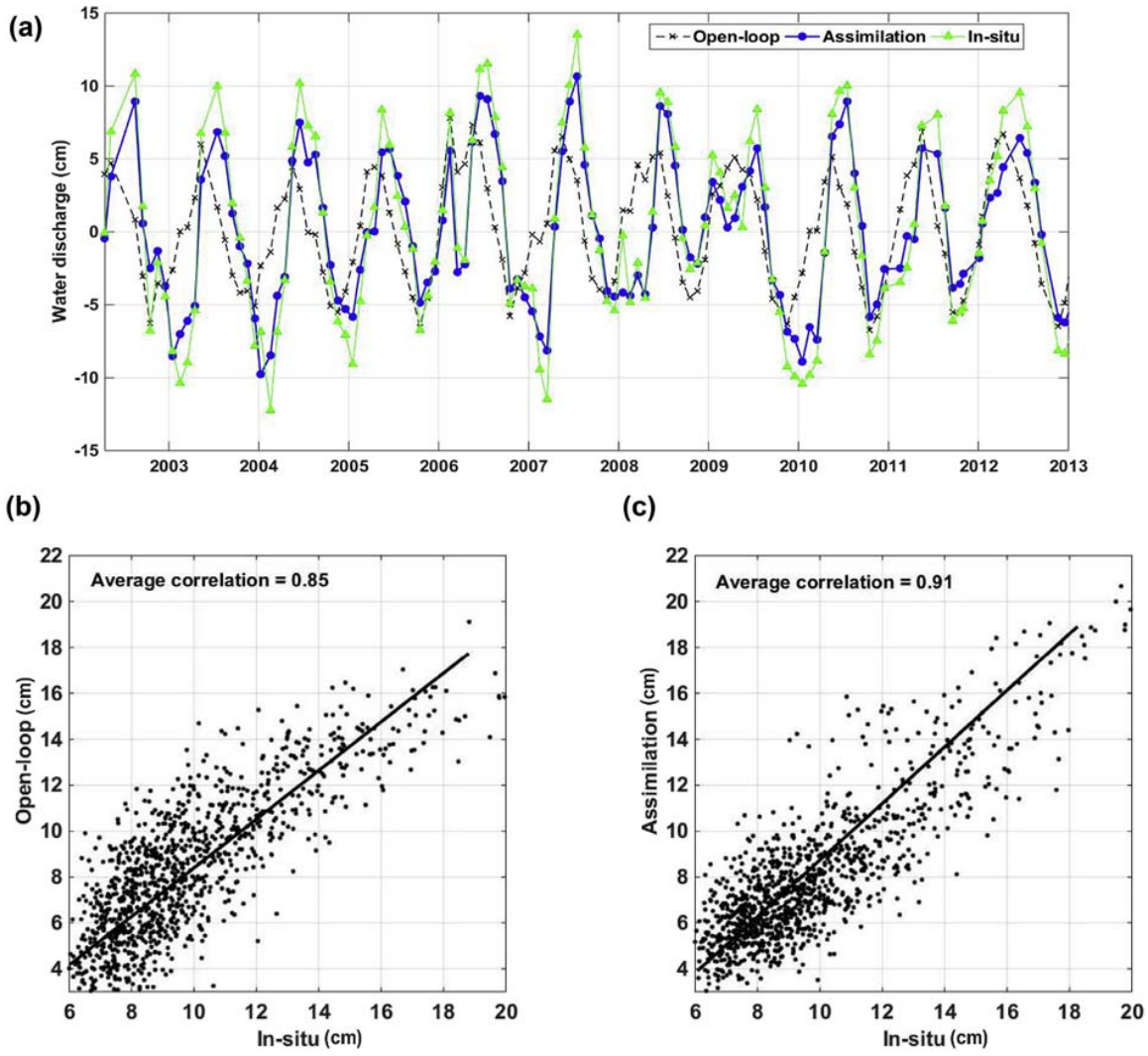

Fig. 4. (a) Average discharge time series before and after data assimilation, as well as from in-situ measurements. Scatter plots of average discharge from the open-loop and joint data assimilation with respect to in-situ measurements are presented in (b) and (c), respectively.

the Amazon basin (Flantua et al., 2016). These larger effects lead to a similar impact on water storage changes that is successfully captured by data assimilation results. In general, larger correlations between the estimated TWS and precipitation over larger basins, e.g., Amazon (basin 15), La Plata (basin 14), and Sao Francisco (basin 13) are also found. This could be due to the ability of GRACE to solve larger basins that better constrain system states during data assimilation.

3.2. Water storage changes and climatic impacts

Average monthly TWS variations over South America from joint data assimilation is shown in Fig. 6. Different time spans are used for the averaging period including 2003–2012(the entire study period) and 2005, 2009, 2010, 2011, and 2012 with remarkable extreme climate event that could potentially affect TWS anomalies. Larger water storage changes can be seen generally for basins located in the northern (e.g, Amazon basin) and southern (e.g., Orinoco and Negro basins) parts of South America. Fig. 6 suggests that more water content, and subsequently more TWS variations exist over these areas. This could be due to the abundance of precipitation over these regions (see, e.g., Sanso and Guenni, 1999; Marengo, 2009; Buytaert et al., 2013). On the other hand, basins located in the west and northwest parts, e.g., Magdalena, Pacific Coast-Peru, and Pacific Coast-north Chile basins experience smaller TWS anomalies. The negative water storage anomalies in the northern parts (e.g., Amazon basin) of South America are observed during 2005 and 2010, and also in the southern parts (e.g., Negro basin) during 2009, 2010, 2011, and 2012. These results are supported by the findings of Humphrey et al. (2016) who also demonstrated water storage deficits, e.g., over northern parts (2004–2005), majority parts of Amazon basin (2010), and the western parts of South America (2011). The impact of the 2012 drought, which can be attributed to the anomalous SST in the Atlantic Ocean (Pereira et al., 2014) can clearly be seen within the eastern and southern parts of South America (see also Sun et al., 2016). Furthermore, El Niño effect in 2009 (Tedeschi et al., 2013) and La Niña effect in 2011 (Boening et al., 2012) can be seen through large anomalies, e.g., in the north, northeast, and southern parts.

To better analyze spatio-temporal variations of sub-surface water storages within South America, PCA is applied to groundwater and soil moisture results. Fig. 7 shows the first three dominant modes.

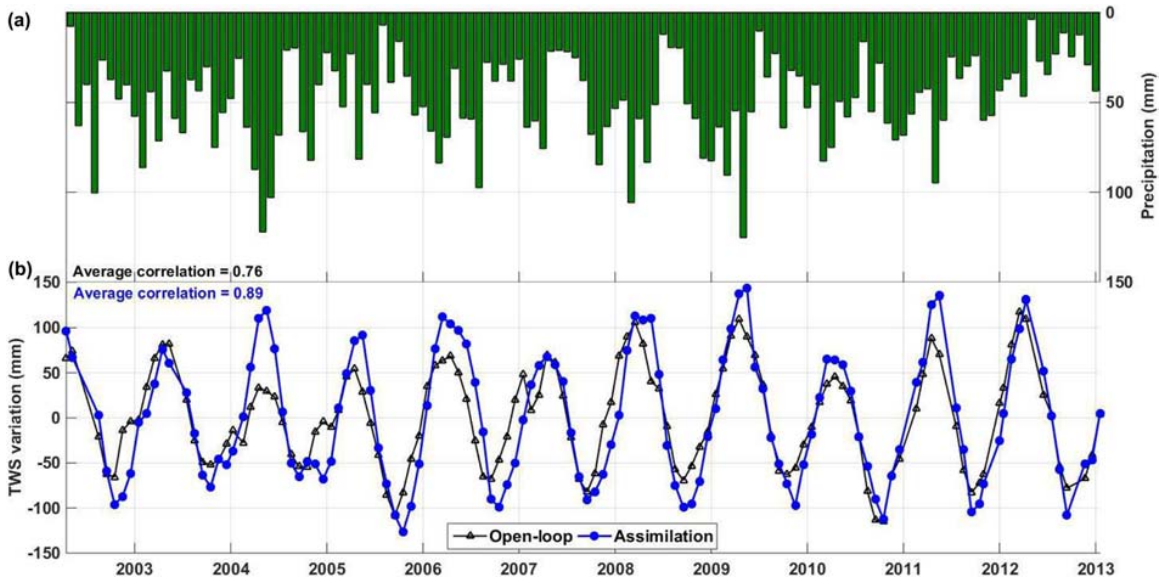

Fig. 5. Average precipitation (a) and TWS time series from the open-loop and joint data assimilation (b) over Amazon basin.

Furthermore, rainfall variations both spatially and temporally are investigated to explore their connections to water storage variations. Major water storages can be found from central to northern parts of South America, areas with rainfall patterns dominated by ENSO phenomena (Carrillo, 2010). This shows a larger amount of storages over the area mainly due to more rainfall. Considerable soil moisture content variations are found over North-east Atlantic (mode 2 and mode 3) and La Plata (mode 3). Larger groundwater variations can also be seen in Amazon and La Plata. To a lesser degree, the Orinoco and Atlantic North Coast basins contain large signal variations both for groundwater and soil moisture. It can also be seen that both groundwater and soil moisture variations modestly follow the same pattern except for mode 3, where negative variations exist in the soil moisture map over the south-eastern parts while the negative variations in groundwater map can be found over the central to northern parts. The positive anomalies over northern parts in soil moisture variations, as it will be shown, matches precipitation patterns in the same areas. This suggests that between the two water compartments, soil moisture variations follow precipitation more closely, whereas groundwater changes which can largely be affected by non-climatic factors, e.g., anthropogenic impacts. In general, based on these maps, more sub-surface water variabilities exist over the central toward northern and western parts of the continent compared to the south-western areas.

In terms of temporal variations, the first three extracted principal components (PC) of groundwater and soil moisture are also demonstrated in Fig. 7. The time series of both water storages largely depict annual effects dominant over the majority of South America's parts including its central to the north. These parts are also affected by the Strong influence of La Niña for 2010–2011, as well as El Niño effect in 2008–2009. Negative trends in groundwater are captured by PC2 over the northeast and central toward western parts before 2006, between 2007 and 2009, and also between 2010 and 2012. Such trends cannot be seen in soil moisture time series suggesting that non-climatic impacts such as the water used for power generation in Brazil (Sun et al., 2016) could possibly be responsible for the

Table 2
Average correlation between the open-loop and assimilation TWS and precipitation. Correlation improvements are calculated using the increase of correlation between TWS from data assimilation and both precipitation and ENSO with respect to open-loop TWS.

	Correlation to precipitation		Correlation improvements	
Basins	Open-loop	Assimilation	Precipitation	ENSO
(1) South-east Atlantic	0.88	0.90	2.27	3.33
(2) Pacific Coast, Peru	0.84	0.89	5.95	7.78
(3) Pacific Coast, North Chile	0.79	0.91	15.19	8.17
(4) Magdalena	0.87	0.92	5.75	7.23
(5) Atlantic North Coast	0.91	0.95	4.39	8.45
(6) Pacific Coast, South Chile	0.84	0.89	5.95	3.12
(7) Colorado Basin	0.78	0.91	16.67	1.72
(8) Atlantic South Coast	0.80	0.87	8.75	2.60
(9) North-east Atlantic	0.85	0.88	3.53	–
(10) Negro Basin	0.67	0.83	23.88	11.35
(11) Tocantins	0.69	0.89	28.98	4.54
(12) Orinoco	0.73	0.86	17.81	9.85
(13) Sao Francisco	0.92	0.92	–	3.06
(14) La Plata	0.75	0.94	25.33	5.17
(15) Amazon Basin	0.92	0.94	2.17	5.35

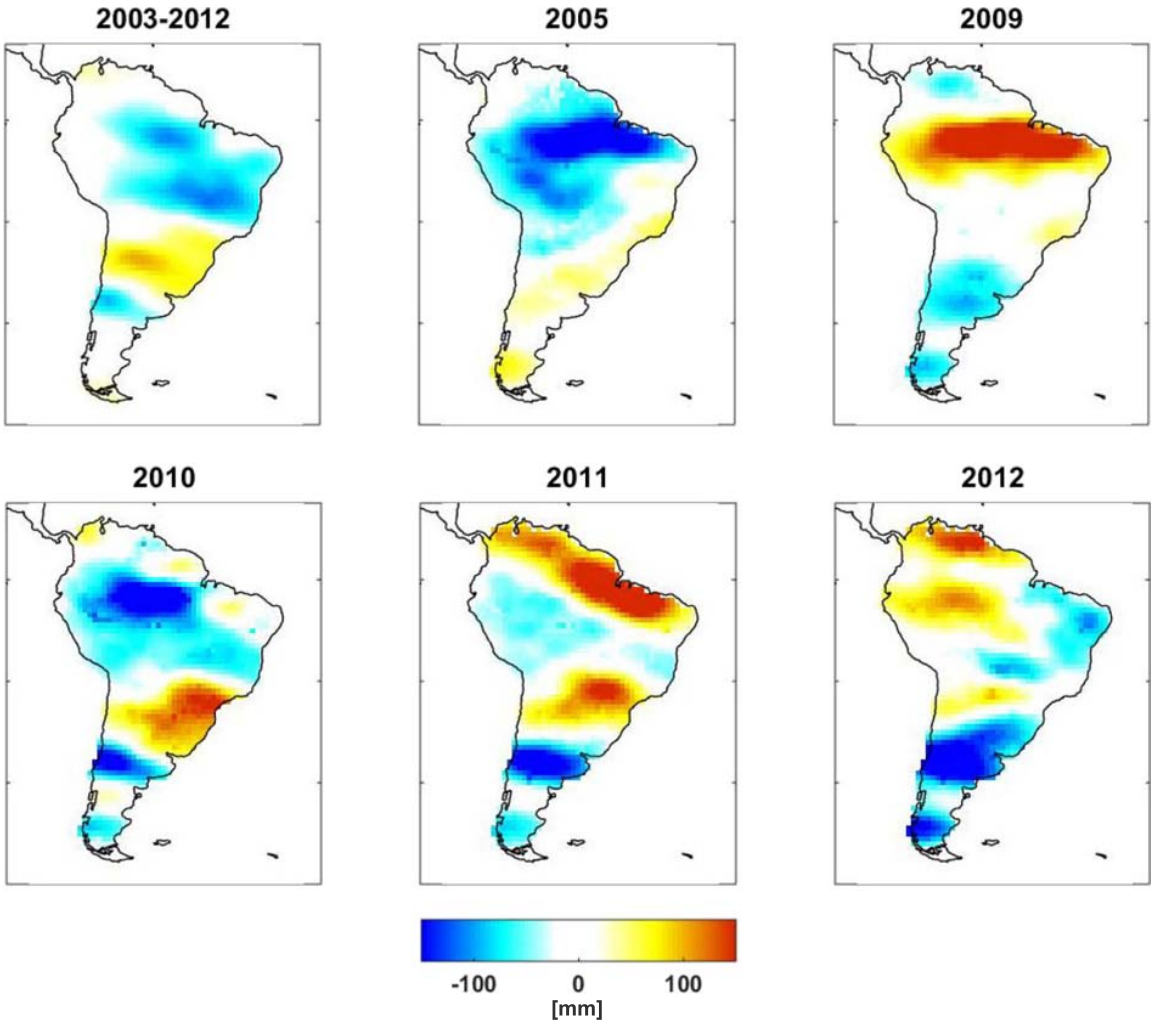

Fig. 6. Average monthly TWS variations from data assimilation for different time periods.

groundwater depletion. The negative soil moisture variations (mode 2) in the central part can be attributed to the multiple drought conditions, e.g., in the La Plata basin (2008–2009, Abelen et al., 2015). This soil moisture reduction was also reported by Escobar (2015) over the Amazon basin, which could be due to the anthropogenic impact on forest conservation. Dry events from 2012 to 2014 suggested

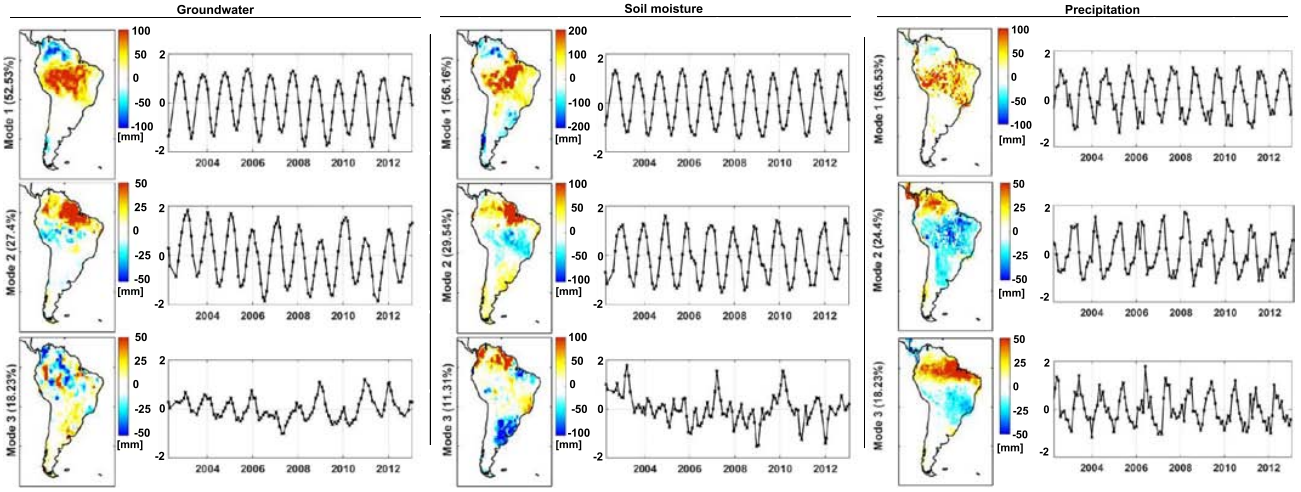

Fig. 7. Three first modes of spatial distribution and temporal variations from the application of PCA on groundwater, soil moisture, and precipitation.

by Humphrey et al. (2016) and Getirana (2016) can be seen in the northern and eastern parts of the South America, also reflected in groundwater and soil moisture time series (PC3 in Fig. 7). Considerable anomalies are found in 2006–2007 and 2010 from groundwater and soil moisture mostly over the northern and eastern parts, which could be attributed to extreme climatic events in the same periods. On the other hand, a negative anomaly is detected in 2004 by both water storages. The 2005 dry condition effects on soil moisture is captured by soil moisture's second mode, which confirms the same impacts presented in Fig. 6. The third mode of soil moisture time series depicts a negative anomaly for the period of 2002–2006 mostly over Negro basin, which, as will be shown, matches the third precipitation mode. El Niño effect in 2009 causes groundwater negative anomaly in both modes 2 and 3 (see also Fig. 6) affecting the central and eastern parts. Similar negative anomalies can also be seen in 2006 for groundwater, and in 2005 for soil moisture. A big part of these variations (e.g., over 2005, 2009–2012) can be related to climate variabilities while some of them, e.g., groundwater negative trends between 2003 and 2006 and also 2007 and 2009, can be due to non-climate factors such as human usage and irrigations.

A major rainfall pattern is found over the central toward northern parts of South America, especially Amazon basin, where most of groundwater and soil moisture variations are explored. While the spatiotemporal distributions of rainfall are highly matched to those of groundwater and soil moisture in the first mode, the precipitation second mode is more correlated to that of soil moisture. This, as expected, indicates that precipitation has larger influence on soil moisture variations while groundwater can be largely affected by other factors (e.g., water usages). Next, Atlantic North Coast, La Plata, and Negro basins indicate larger signals in contrast to south-western basins, e.g., Pacific Coast, South Chile and Atlantic South Coast. Similar to groundwater and soil moisture mode 1, rainfall time series in Fig. 7 also displays strong seasonal variations. In contrast to the negative anomalies in groundwater second mode time series, precipitation mode 2 does not show similar trends. However, both modes 2 and 3 indicate a rainfall decline after 2012 mostly affecting the eastern toward northern parts (see, e.g., Humphrey et al., 2016; Getirana, 2016). Similar to water storage time series, the La Niña effect can be observed for 2010–2011 (Boening et al., 2012). Large anomalies are also captured in 2005, 2006, and 2010, which considerably impacts water storages. El Niño effect in 2009 can also be seen in the second mode, which also affected groundwater and soil moisture variations within the central and south-eastern parts. A negative anomaly can be seen before 2004 in the mode 3, which can be related to a weak El Niño causing negative anomalies of precipitation during the wet season (Juarez et al., 2009). Sun et al. (2016) suggested that this period exhibits months drier than the normal seasonal cycle of TWS due to the rainfall rates lower than the average. These prolonged reductions in rainfall can explain similar negative anomalies that occurred in groundwater and soil moisture time series seen.

Average trends for groundwater and soil moisture from the open-loop run and joint assimilation are presented in Table 3 for the basins. To this end, the modified Mann–Kendall trend test (Yue and Wang, 2004) is applied on deseasonalized time series. Note that the autocorrelation analysis is also used to compute an effective sample size and to correct the Mann–Kendall statistic. The trends when the p-values fall below 0.05 are considered statistically significant. It is worth mentioning that in addition to groundwater and soil moisture, the basin averaged precipitation time series are also considered here to investigate the climatic impacts on water storage changes. It can be seen that the application of data assimilation in many cases causes changes in either amplitude of trends or their signs. For example, over the Orinoco, the signs of variations become negative after data assimilation while these remained the same for La Plata with different amplitudes. For some other basins like South-east Atlantic, the trend values are close before and after data assimilation, which could be due to the smaller impacts of data assimilation.

It is also evident that there are larger agreements between precipitation and soil moisture trends. This further indicates that soil moisture changes mostly rely on rainfall pattern within South America. The mismatch between precipitation and groundwater trend signs over most of the basins, e.g., Pacific Coast, South Chile, Orinoco, South-east Atlantic and Colorado, suggests that non-climatic factors mostly influence the groundwater changes. This, in all of the cases, leads to a groundwater depletion while precipitation shows neither negative nor statistically significant trends. Nevertheless, negative trends are found in precipitation, soil moisture, and also groundwater over La Plata, Atlantic North Coast, Atlantic South Coast, and North-East Atlantic. Even though one can conclude that a majority of groundwater depletion over these basins can be caused by the precipitation decline, human impacts can still be an effective factor whereas assessing their contributions require additional information.

From Table 3, negative groundwater trends can be seen in most of the basins. For example, Sao Francisco and North-east Atlantic basins show the largest groundwater depletion compared to the other basins. This can be attributed to the fact that these basins have been under an unprecedented water depletion as can be inferred from the studies of Getirana (2016) and Sun et al. (2016). Trend signs of soil moisture changes generally follow precipitation's. This, however, is different for some basins such as Pacific Coast, South Chile and Amazon. This mismatch over the Amazon basin can be explained by the fact that anthropogenic impacts on forest conservation results in soil

Table 3
Statistics of groundwater and soil moisture variation rates (mm/year) from the open-loop run and joint data assimilation. The statistically significant values at 95% confidence limit are demonstrated in bold.

	Open-loop		Assimilation		
Basins	Groundwater	Soil moisture	Groundwater	Soil moisture	Precipitation
(1) South-east Atlantic	**−0.37**	**−0.44**	**−0.57**	**+0.44**	**+0.09**
(2) Pacific Coast, Peru	**−0.10**	**−0.13**	**−1.09**	+0.12	+0.06
(3) Pacific Coast, North Chile	–	–	−0.03	−0.05	+0.13
(4) Magdalena	−0.02	**+0.16**	**+0.62**	+0.05	−0.01
(5) Atlantic North Coast	+0.02	+0.01	**−0.17**	**−0.23**	**−0.22**
(6) Pacific Coast, South Chile	–	-0.07	**−1.52**	**−0.76**	**+0.22**
(7) Colorado Basin	**−0.25**	**+0.20**	**−0.21**	**+0.23**	**+0.28**
(8) Atlantic South Coast	−0.06	–	**−0.57**	**−0.27**	**−0.12**
(9) North-east Atlantic	**+0.26**	+0.36	**−0.98**	**−0.47**	**−0.17**
(10) Negro Basin	−0.04	–	**−0.21**	–	–
(11) Tocantins	+0.02	+0.07	**+0.54**	+0.03	+0.02
(12) Orinoco	**+0.17**	**+0.35**	**−0.53**	+0.09	+0.01
(13) Sao Francisco	−0.07	−0.06	**−0.47**	**−0.24**	−0.03
(14) La Plata	**−0.89**	**+0.09**	**−1.09**	**−0.14**	**−0.10**
(15) Amazon Basin	+0.05	**+0.14**	+0.07	−0.02	+0.05

moisture decline (see, e.g., Escobar, 2015). Similar negative trends are observed for both groundwater and soil moisture over La Plata, and also groundwater over Orinoco (Ramirez et al., 2017), which can be attributed to deforestation and excessive water use that have also been reported, e.g., by Pereira et al. (2011) for La Plata and Ramirez et al. (2017) for Orinoco basins (see also Frappart et al., 2015). There are also discrepancies between soil moisture and groundwater trend signs, e.g., over La Plata and Pacific Coast, North Chile. While the rate of the changes are smaller over Pacific Coast North Chile, La Plata, which are located in the most populated areas of South America, they have larger negative groundwater trends that could possibly be due to increased agricultural and livestock water usage in the basin (see also Chen et al., 2010). For some of the basins (e.g., the Amazon basin), the trends are not significant, especially the soil moisture and precipitation changes (e.g., over the Tocantins). In general, the annual rate of groundwater anomaly is −0.24(mm/year) in South America, suggesting its depletion between 2002 and 2013. This could be due to climatic impacts (e.g., droughts, see, e.g., Bates et al., 2008; Chen et al., 2010; Treidel et al., 2011; Getirana, 2016; Sun et al., 2016) and/or exponential increase of agriculture and industrial activities (Bocanegra et al., 2010). This negative trend is very important due to its effects on South America's water and its use for agriculture. Groundwater is a major source of irrigation over most of the countries within South America such as major rice-growing regions of North Eastern Argentina, South Brazil and Uruguay (Herring, 2012). Besides, groundwater depletion can largely increase water quality challenges (e.g., Arsenic growth) as a potential issue over South America (see, e.g., Herring, 2012; Munoz et al., 2002; Perez-Carrera and Cirelli, 2009).

4. Conclusion

Multimission satellite datasets including Terrestrial water storages (TWS) from the Gravity Recovery And Climate Experiment (GRACE) satellite mission and soil moisture products from the Advanced Microwave Scanning Radiometer - Earth Observing System (AMSR-E) and Soil Moisture and Ocean Salinity (SMOS) are assimilated into the World-Wide Water Resources Assessment (W3RA) model using the Ensemble Square-Root Filter (EnSRF) to increase the model performance for estimating groundwater and soil moisture over South America. The application of joint data assimilation causes improvements in W3RA estimates against groundwater in-situ measurements. This effect could clearly be seen for TWS estimates and importantly for groundwater simulations, which emphasize the potentials of assimilating remotely sensed products to increase the reliability of the W3RA hydrological model. We further investigate the correlation between assimilation results and precipitation from the Tropical Rainfall Measuring Mission (TRMM), as well as El Niño/Southern Oscillation (ENSO). The results indicate that assimilation TWS are more correlated to the TRMM rainfall and ENSO data compared to open-loop TWS estimates. Both of these assessments demonstrate the capability of data assimilation for improving model simulations of water resources over South America. Based on the results, the new information of groundwater and soil moisture are more reliable, which can be used for water management and agriculture objectives. From the application of principal component analysis (PCA) on water storage variations within South America and its 15 major basins, more soil moisture and groundwater anomalies are found over central toward northern and western parts of South America. Based on the results, a negative trend for groundwater is observed over most parts of South America. Negative trends are found for groundwater and to a lesser degree for soil moisture variations over the majority of the studied basins. This study shows that application of data assimilation can successfully improve our understanding of water storage changes. Nevertheless, more investigations are still needed to fully assess the approach's performance, e.g., by applying new observations such as GRACE follow-on and Surface Water and Ocean Topography (SWOT), sensitivity analysis regarding data uncertainties, and the impacts of GRACE data assimilation on non-assimilated variables.

Acknowledgments

We would like to thank Dr. Augusto Getirana for providing the surface water storage data and also his review suggestions, which contributed to the improvement of this study. M. Khaki is grateful for the research grant of Curtin International Postgraduate Research Scholarships (CIPRS)/ORD Scholarship provided by Curtin University (Australia). J. Awange is grateful for the Brazilian Science Without Borders Program/CAPES Grant No. 88881.068057/2014-01. This work is a TIGeR publication.

References

Abelen, S., Seitz, F., Abarca-del Rio, R., Güntner, A., 2015. Droughts and floods in the la plata basin in soil moisture data and GRACE. Remote Sens. 7, 7324–7349. https://doi.org/10.3390/rs70607324.

Alsdorf, D.E., Rodriguez, E., Lettenmaier, D.P., 2007. Measuring surface water from space. Rev. Geophys. 45, RG2002. https://doi.org/10.1029/2006RG000197.

Altaf, M.U., Butler, T., Mayo, T., Luo, X., Dawson, C., Heemink, A.W., Hoteit, I., 2014. A comparison of ensemble Kalman filters for storm surge assimilation. Mon. Weather Rev. 142:8, 2899–2914.

Anderson, J., 2001. An ensemble adjustment Kalman filter for data assimilation. Mon. Wea. Rev. 129, 28842903. https://doi.org/10.1175/1520-0493(2001)129<2884:AEAKFF>2.0.CO;2.

Anderson, M.C., Norman, J.M., Mecikalski, J.R., Otkin, J.A., Kustas, W.P., 2007. A climatological study of evapotranspiration and moisture stress across the continental United States based on thermal remote sensing: 1. Model formulation. J. Geophys. Res. 112 (D10117). https://doi.org/10.1029/2006JD007506.

Bates, B.C., Kundzewicz, Z.W., Wu, S., Palutikof, J.P., 2008. Climate Change and Water, Chapter 3 Linking Climate Change and Water Resources: Impacts and Responses, IPCC Secretariat. , pp. 210. Geneva.

Beck, H.E., van Dijk, A.I.J.M., de Roo, A., Miralles, D.G., McVicar, T.R., Schellekens, J., Bruijnzeel, L.A., 2016. Global-scale regionalization of hydrologic model parameters. Water Resour. Res. 52, 3599–3622. https://doi.org/10.1002/2015WR018247.

Bennett, A.F., 2002. Inverse Modeling of the Ocean and Atmosphere. Cambridge Univ. Press, New York., pp. 234.

Bertino, L., Evensen, G., Wackernagel, H., 2003. Sequential data assimilation techniques in oceanography. Int. Stat. Rev. 71 (2), 223–241. Aug., 2003.

Betts, A.K., Ball, J.H., Beljaars, A.C.M., Miller, M.J., Viterbo, P.A., 1996. The land surface-atmosphere interaction: a review based on observational and global modeling perspectives. J. Geophys. Res. 101 (D3), 7209–7225.

Bharati, L., Rodgers, C., Erdenberger, T., Plotnikova, M., Shumilov, S., Vlek, P., Martin, N., 2008. Integration of economic and hydrologic models: exploring conjunctive irrigation water use strategies in the Volta Basin. Agric. Water Manag. 95 (8), 925–936. https://doi.org/10.1016/j.agwat.2008.03.009. 2008, ISSN 0378-3774.

Bocanegra, E., Silva, G.C., Custodio, E., Manzano, M., Montenegro, S., 2010. State of knowledge of coastal aquifer management in South America. Hydrogeol. J. 18 (1), 261–267. https://doi.org/10.1007/s10040-009-0520-5.

Boening, C., Willis, J.K., Landerer, F.W., Nerem, R.S., Fasullo, J., 2012. The 2011 la niña: so strong, the oceans fell. Geophys. Res. Lett. 39, L19602. https://doi.org/10.1029/2012GL053055.

Buytaert, W., Breuer, L., Buytaert, W., Breuer, L., et al. 2013. Water Resources in South America: Sources and Supply, Pollutants and Perspectives, Symposium on Understanding Freshwater Quality Problems in a Changing World / Joint Assembly of IAHS, IAPSO and IASPEI. INT ASSOC HYDROLOGICAL SCIENCES., pp. 106–113. ISSN: 0144-7815.

Cabrera, J., Yupanqui, R.T., Rau, P., 2016. Validation of TRMM daily precipitation data for extreme events analysis. The case of Piura watershed in Peru. Procedia Eng. 154, 154–157. https://doi.org/10.1016/j.proeng.2016.07.436. 2016. ISSN 1877-7058.

Carrillo, C.M., 2010. The Rainfall Over Tropical South America Generated by Multiple Scale Processes. Graduate Theses and Dissertations, pp. 11536. http://lib.dr.iastate.edu/etd/11536

Ceccherini, G., Ameztoy, I., Hernndez, C., Moreno, C., 2015. Highresolution precipitation datasets in South America and West Africa based on satellite-derived rainfall, enhanced vegetation index and digital elevation model. Remote Sensing 7, 6454–6488. https://doi.org/10.3390/rs70506454.

Chen, J.L., Wilson, C.R., Famiglietti, J.S., Rodell, M., 2007. Attenuation effect on seasonal basin-scale water storage changes from GRACE time-variable gravity. J. Geod. 81 (4), 237–245. https://doi.org/10.1007/s00190-006-0104-2.

Chen, J.L., Wilson, C.R., Tapley, B.D., Longuevergne, L., Yang, Z.L., Scanlon, B.R., 2010. Recent La Plata basin drought conditions observed by satellite gravimetry. J. Geophys. Res. 115, D22108. https://doi.org/10.1029/2010JD014689.

Chen, J.L., Wilson, C.R., Tapley, B.D., Yang, Z.L., Niu, G.Y., 2009. 2005 drought event in the Amazon River basin as measured by GRACE and estimated by climate models. J. Geophys. Res. 114, B05404. https://doi.org/10.1029/2008JB006056.

Cheng, M.K., Tapley, B.D., 2004. Variations in the Earth's oblateness during the past 28 years. J. Geophys. Res. Solid Earth 109, B09402. https://doi.org/10.1029/2004JB003028.
Chou, S.C., Tanajura, C.A.S., Xue, Y., Nobre, C.A., 2002. Validation of the coupled eta/SSib model over South America. J. Geophys. Res. 107 (D20), 8088. https://doi.org/10.1029/2000JD000270.
Condom, T., Rau, P., Espinoza, J.C., 2011. Correction of TRMM 3B43 monthly precipitation data over the mountainous areas of Peru during the period 1998–2007. Hydrol. Process. 25, 1924–1933. https://doi.org/10.1002/hyp.7949.
de Goncalves, L.G., Shuttleworth, W.J., Vila, D., Larroza, E., Bottino, M.J., Herdies, D.L., Aravequia, J.A., De Mattos, J.G., Toll, D.L., Rodell, M., Houser, P., 2009. The South American land data assimilation system (SALDAS) 5-yr retrospective atmospheric forcing datasets. J. Hydrometeor. 10, 999–1010. https://doi.org/10.1175/2009JHM1049.1.
De Jeu, R.A.M., Owe, M., 2003. Further validation of a new methodology for surface moisture and vegetation optical depth retrieval. Int. J. Remote Sens. 24, 4559–4578. https://doi.org/10.1080/0143116031000095934.
De Jeu, R.A.M., Wagner, W., Holmes, T.R.H., Dolman, A.J., van de Giesen, N.C., Friesen, J., 2008. Global soil moisture patterns observed by space borne microwave radiometers and scatterometers. Surv. Geophys. 29 (45), 399420. https://doi.org/10.1007/s10712-008-9044-0.
De Paiva, R.C.D.R.C.D., Buarque, D.C.D.C., Collischonn, W., Bonnet, M.P.M.P., Frappart, F., Calmant, S., Bulhes Mendes, C.A.C.A., 2013. Large-scale hydrologic and hydrodynamic modeling of the Amazon River basin. Water Resour. Res. 49, 1226–1243. https://doi.org/10.1002/wrcr.20067.
Dillon, M.E., Skabar, Y.G., Ruiz, J., Kalnay, E., Collini, E.A., Echevarra, P., Saucedo, M., Miyoshi, T., Kunii, M., 2016. Application of the WRF-LETKF data assimilation system over southern South America: sensitivity to model physics. Wea. Forecasting 31, 217–236. https://doi.org/10.1175/WAF-D-14-00157.1.
Döll, P., Kaspar, F., Lehner, B., 2003. A global hydrological model for deriving water availability indicators: model tuning and validation. J. Hydrol. 270, 105–134.
Draper, C.S., Mahfouf, J.F., Walker, J.P., 2009. An EKF assimilation of AMSR-e soil moisture into the ISBA land surface scheme. J. Geophys. Res. 114, D20104. https://doi.org/10.1029/2008JD011650.
Dumedah, G., Walker, J.P., Merlin, O., 2015. Root-zone soil moisture estimation from assimilation of downscaled soil moisture and ocean salinity data. Adv. Water Resour. 84, 14–22. https://doi.org/10.1016/j.advwatres.2015.07.021. ISSN 0309-1708.
Eicker, A., Schumacher, M., Kusche, J., Döll, P., Müller-Schmied, H., 2014. Calibration/data assimilation approach for integrating GRACE data into the waterGAP global hydrology model (WGHM) using an ensemble Kalman filter: first results. Surv Geophys 35 (6), 1285–1309. https://doi.org/10.1007/s10712-014-9309-8.
Elbern, H., Schmidt, H., 2001. Ozone episode analysis by fourdimensional variational chemistry data assimilation. J. Geophys. Res. 106, 3569–3590.
Erfanian, A., Wang, G., Fomenko, L., 2017. Unprecedented Drought Over Tropical South America in 2016: Significantly Under-Predicted by Tropical SST. Scientific Reports 7, Article number: 5811. https://doi.org/10.1038/s41598-017-05373-2.
Escobar, H., 2015. Drought triggers alarms in Brazils biggest metropolis. Science 2015 (347), 812-812.
Evensen, G., 2003. The ensemble Kalman filter: theoretical formulation and practical inplementation. Ocean Dyn. 53, 343–367. https://doi.org/10.1007/s10236-003-0036-9.
Evensen, G., 2007. Data assimilation: the ensemble Kalman filter. Springer 279.
Flantua, S.G.A., Hooghiemstra, H., Vuille, M., Behling, H., Carson, J.F., Gosling, W.D., Hoyos, I., Ledru, M.P., Montoya, E., Mayle, F., Maldonado, A., Rull, V., Tonello, M.S., Whitney, B.S., Gonzlez-Arango, C., 2016. Climate variability and human impact in South America during the last 2000 years: synthesis and perspectives from pollen records. Clim. Past 12, 483–523. https://doi.org/10.5194/cp-12-483-2016.
Frappart, F., Papa, F., Malbeteau, Y., León, J.G., Ramillien, G., Prigent, C., Seoane, L., Seyler, F., Calmant, S., 2015. Surface freshwater storage variations in the Orinoco floodplains using multi-satellite observations. Remote Sens. 7, 89–110.
Frappart, F., Seoane, L., Ramillien, G., 2013. Validation of GRACE-derived terrestrial water storage from a regional approach over South America. Remote Sens. Environ. 137, 69–83. Elsevier. 2013.
Garner, T.W., Wolf, R.A., Spiro, R.W., Thomsen, M.F., 1999. First attempt at assimilating data to constrain a magnetospheric model. J. Geophys. Res. 104 (A11), 25145–25152. https://doi.org/10.1029/1999JA900274.
Garreaud, R.D., Vuille, M., Compagnucci, R., Marengo, J., 2008. Present-day South American climate. Paleogeogr. Palaeoclimatol. Palaeoecol https://doi.org/10.1016/j.palaeo.2007.10.032.
Getirana, A., 2016. Extreme water deficit in Brazil detected from space. J. Hydrometeorol. 17, 591–599.
Getirana, A., Dutra, E., Guimberteau, M., Kam, J., Li, H., Decharme, B., Zhang, Z., Ducharne, A., Boone, A., Balsamo, G., Rodell, M., Toure, A.M., Xue, Y., Drapeau, G., Arsenault, K., Kumar, S.V., Leung, L.R., Peters-Lidard, C., Ronchail, J., Sheffield, J., 2014. Water balance in the Amazon basin from a land surface model ensemble. J. Hydrometeorol. 15, 2586–2614. https://doi.org/10.1175/JHM-D-14-0068.1.
Getirana, A., Kumar, S., Girotto, M., Rodell, M., 2017. Rivers and floodplains as key components of global terrestrial water storage variability. Geophys. Res. Lett. 44. https://doi.org/10.1002/2017GL074684.
Getirana, A.B., Yamazaki, D., Decharme, B., Papa, F., Mognard, N., 2012. The hydrological modeling and analysis platform (hyMAP): evaluation in the Amazon basin. J. Hydrometeorol. 13, 1641–1665. https://doi.org/10.1175/JHM-D-12-021.1.
Girotto, M., De Lannoy, G.J.M., Reichle, R.H., Rodell, M., 2016. Assimilation of gridded terrestrial water storage observations from GRACE into a land surface model. Water Resour. Res. 52, 4164–4183. https://doi.org/10.1002/2015WR018417.
Girotto, M., De Lannoy, G.J.M., Reichle, R.H., Rodell, M., Draper, C., Bhanja, S.N., Mukherjee, A., 2017. Benefits and pitfalls of GRACE data assimilation: a case study of terrestrial water storage depletion in India. Geophys. Res. Lett. 44, 4107–4115. https://doi.org/10.1002/2017GL072994.
Grau, H.R., Aide, M., 2008. Globalization and land-use transitions in Latin America. Ecol. Soc. 13 (2), 16. www.ecologyandsociety.org/vol13/iss2/art16/.
Grimson, R., Montroull, N., Saurral, R., Vasquez, P., Camilloni, I., 2013. Hydrological modelling of the Iber Wetlands in southeastern South America. J. Hydrol. 503, 47–54. https://doi.org/10.1016/j.jhydrol.2013.08.042. ISSN 0022-1694.
Herring, M., 2012. Agriculture and Biodiversity: Opportunities for a Better Marriage Rice Growers Association Annual Conference. NSW, One Tree.
Hoteit, I., Luo, X., Pham, D.T., 2012. Particle Kalman filtering: a nonlinear Bayesian framework for ensemble Kalman filters. Mon. Weather Rev. 140 (2), 528–542.
Hoteit, I., Pham, D.T., Gharamti, M.E., Luo, X., 2015. Mitigating observation perturbation ampling errors in the stochastic enKF. Mon. Weather Rev. 143 (7), 2918–2936.
Hoteit, I., Pham, D.T., Triantafyllou, G., Korres, G., 2008. A new approximate solution of the optimal nonlinear filter for data assimilation in meteorology and oceanography. Mon. Weather Rev. 136, 317–334.
Houborg, R., Rodell, M., Li, B., Reichle, R., Zaitchik, B.F., 2012. Drought indicators based on modelassimilated gravity recovery and climate experiment (GRACE) terrestrial water storage observations. Water Resour. Res. 48, W07525. https://doi.org/10.1029/2011WR011291.
Huffman, G., Bolvin, D., 2012. TRMM and Other Data Precipitation Data Set Documentation Mesoscale Atmospheric Processes Laboratory. NASA Goddard Space Flight Center and Science Systems and Applications Inc.
Humphrey, V., Gudmundsson, L., Seneviratne, S.I., 2016. Assessing global water storage variability from GRACE: trends, seasonal cycle, subseasonal anomalies and extremes. Surv. Geophys. 37, 357. https://doi.org/10.1007/s10712-016-9367-1.
International Groundwater Resources Assessment Centre, 2004. Graphic Groundwater and Climate Change, International Groundwater Resources Assessment Centre UNESCO, International Hydrological Programme. Division of water sciences. www.graphicnetwork.net.
Jackson, T., Bindlish, R., 2012. Validation of soil moisture and ocean salinity (SMOS) soil moisture over watershed networks in the US. IEEE Trans. Geosci. Remote Sens. 50, 1530–1543.
Jacquette, E., Al Bitar, A., Mialon, A., Kerr, Y., Quesney, A., Cabot, F., et al. 2010. SMOS CATDS level 3 global products over land. In: Neale, C.M.U., Maltese, A. (Eds.), Remote Sensing for Agriculture, Ecosystems, and Hydrology XII. volume 7824 of Proceedings of SPIE-The International Society for Optical Engineering. Conference on Remote Sensing for Agriculture, Ecosystems, and Hydrology XII, Toulouse, France.
Juarez, R.I., Li, W., Fu, R., Fernandes, K., de Oliveira Cardoso, A., 2009. Comparison of precipitation datasets over the tropical South American and African continents. J. Hydrometeor. 10, 289–299. https://doi.org/10.1175/2008JHM1023.1.
Khaki, M., Hoteit, I., Kuhn, M., Awange, J., Forootan, E., van Dijk, A.I.J.M., Schumacher, M., Pattiaratchi, C., 2017a. Assessing sequential data assimilation techniques for integrating GRACE data into a hydrological model. Adv. Water Resour. 107, 301–316. https://doi.org/10.1016/j.advwatres.2017.07.001. ISSN 0309-1708.
Khaki, M., Schumacher, M., Forootan, J., Kuhn, M., Awange, E., van Dijk, A.I.J.M., 2017b. Accounting for spatial correlation errors in the assimilation of GRACE into hydrological models through localization. Adv. Water Resour. https://doi.org/10.1016/j.advwatres.2017.07.024. Available online 1 August 2017, ISSN 0309-1708.
Khaki, M., Ait-El-Fquih, B., Hoteit, I., Forootan, E., Awange, J., Kuhn, M., 2017c. A two-update ensemble Kalman filter for land hydrological data assimilation with an uncertain constraint. J. Hydrol. https://doi.org/10.1016/j.jhydrol.2017.10.032. Available online 25 October 2017, ISSN 0022-1694.
Khaki, M., Forootan, E., Kuhn, M., Awange, J., Papa, F., Shum, C.K., 2018a. A study of Bangladesh's sub-surface water storages using satellite products and data assimilation scheme. Sci. Total Environ. 625, 963–977. https://doi.org/10.1016/j.scitotenv.2017.12.289.
Khaki, M., Forootan, E., Kuhn, M., Awange, J., van Dijk, A.I.J.M., Schumacher, M., Sharifi, M.A., 2018b. Determining water storage depletion within Iran by assimilating GRACE data into the w3RA hydrological model. Adv. Water Resour. 114, 1–18. https://doi.org/10.1016/j.advwatres.2018.02.008.
Khaki, M., Hamilton, F., Forootan, E., Hoteit, I., Awange, J., Kuhn, M., 2018c. Nonparametric data assimilation scheme for land hydrological applications. Water Resour. Res https://doi.org/10.1029/2018WR022854.
Khaki, M., Ait-El-Fquih, B., Hoteit, I., Forootan, E., Awange, J., Kuhn, M., 2018d. Unsupervised ensemble kalman filtering with an uncertain constraint for land hydrological data assimilation. J. Hydrol. 564, 175–190. https://doi.org/10.1016/j.jhydrol.2018.06.080. ISSN 0022-1694.
Khaki, M., Forootan, E., Kuhn, M., Awange, J., Longuevergne, L., Wada, W., 2018e. Efficient basin scale filtering of GRACE satellite products. Remote Sens. Environ. 204, 76–93. https://doi.org/10.1016/j.rse.2017.10.040. ISSN 0034-4257.
Kolassa, J., Reichle, R.H., Liu, Q., Cosh, M., Bosch, D.D., Caldwell, T.G., Colliander, A., Holifield Collins, C., Jackson, T.J., Livingston, S.J., Moghaddam, M., Starks, P.J., 2017. Data assimilation to extract soil moisture information from SMAP observations. Remote Sens. 9, 1179.
Koster, R.D., Suarez, M.J., 1999. A simple framework for examining the interannual variability of land surface moisture fluxes. J. Climate 12, 1911–1917.
Kourgialas, N.N., Karatzas, G.P., 2015. A modeling approach for agricultural water management in citrus orchards: cost-effective irrigation scheduling and agrochemical transport simulation. Environ Monit Assess. 187 (7), 462. https://doi.org/10.1007/s10661-015-4655-7.

Kumar, S., Zaitchik, B., Peters-Lidard, C., Rodell, M., Reichle, R., Li, B., Jasinski, M., Mocko, D., 2016. Assimilation of gridded GRACE terrestrial water storage estimates in the North American land data assimilation system. J. Hydrometeor. 17, 1951–1972. https://doi.org/10.1175/JHM-D-15-0157.1.

Kusche, J., Schmidt, R., Petrovic, S., Rietbroek, R., 2009. Decorrelated GRACE time-variable gravity solutions by GFZ and their validation using a hydrological model. J. Geod. https://doi.org/10.1007/s00190-009-0308-3.

Lahoz, W.A., Geer, A.J., Bekki, S., Bormann, N., Ceccherini, S., Elbern, H., Errera, Q., Eskes, H.J., Fonteyn, D., Jackson, D.R., Khattatov, B., 2007. The assimilation of Envisat data (ASSET) project. Atmos., Chem. Phys. 7, 1773–1796.

Leroux, D.J., Pellarin, T., Vischel, T., Cohard, J.M., Gascon, T., Gibon, F., Mialon, A., Galle, S., Peugeot, C., Seguis, L., 2016. Assimilation of SMOS soil moisture into a distributed hydrological model and impacts on the water cycle variables over the oum catchment in Benin. Hydrol. Earth Syst. Sci. 20, 2827–2840. https://doi.org/10.5194/hess-20-2827-2016.

Li, B., Rodell, M., 2015. Evaluation of a model-based groundwater drought indicator in the conterminous U.S. J. Hydrol. 526, 78–88. https://doi.org/10.1016/j.jhydrol.2014.09.02.

Li, B., Rodell, M., Famiglietti, J.S., 2015. Groundwater variability across temporal and spatial scales in the central and northeastern U.S. J. Hydrol. 525, 769–780. https://doi.org/10.1016/j.jhydrol.2015.04.033.

Li, B., Rodell, M., Zaitchik, B., Reichle, R., Koster, R., 2012. Assimilation of GRACE terrestrial water storage into a land surface model: evaluation and potential value for drought monitoring in western and central Europe. J. Hydrol. 446 447, 103115. https://doi.org/10.1016/j.jhydrol.2012.04.035.

Lorenz, E., 1956. Empirical Orthogonal Function and Statistical Weather Prediction. Technical Report Science Report No 1, Statistical Forecasting Project, MIT, Cambridge.

Magrin, G., Gay Garca, C., Cruz Choque, D., Gimnez, J.C., Moreno, A.R., Nagy, G.J., Nobre, C., Villamizar, A., 2007. Latin America. In: Parry, M.L., Canziani, O.F., Palutikof, J.P., van der Linden, P.J., Hanson, C.E. (Eds.), Climate Change 2007: Impacts, Adaptation and Vulnerability. Contribution ofWorking Group II to the Fourth Assessment Report of the Intergovernmental Panel on Climate Change. Cambridge University Press, Cambridge, UK and NewYork, NY, USA, pp. 581–615.

Magrin, G.O., Marengo, J.A., Boulanger, J.P., Buckeridge, M.S., Castellanos, E., Poveda, G., Scarano, F.R., Vicua, S., 2014. Central and South America. In: Barros, V.R., Field, C.B., Dokken, D.J., Mastrandrea, M.D., Mach, K.J., Bilir, T.E., Chatterjee, M., Ebi, K.L., Estrada, Y.O., Genova, R.C., Girma, B., Kissel, E.S., Levy, A.N., MacCracken, S., Mastrandrea, P.R., White, L.L. (Eds.), Climate Change 2014: Impacts, Adaptation, and Vulnerability. Part B: Regional Aspects. Contribution of Working Group II to the Fifth Assessment Report of the Intergovernmental Panel on Climate Change. Cambridge University Press, Cambridge, United Kingdom and New York, NY, USA, pp. 1499–1566.

Marengo, J.A., 2009. Long-term trends and cycles in the hydrometeorology of the Amazon basin since the late 1920s. Hydrol. Processes 23, 3236–3244.

Mayer-Gürr, T., Zehentner, N., Klinger, B., Kvas, A., 2014. ITSG-grace2014: a new GRACE gravity field release computed in graz. GRACE Science Team Meeting (GSTM), Potsdam am: 29.09.2014.

Morris, B.L., Lawrence, A.R., Chilton, P.J., Adams, B., Calow, R., Klinck, B.A., 2003. Groundwater and Its Susceptibility to Degradation: A Global Assessment of the Problems and Options for Management. Early Warning and Assessment Report Series, RS, 03-3,

Munoz, O., Leyton, I., Nuez, N., et al. 2002. Vegetables collected in the cultivated Andean area of northern Chile: total and inorganic arsenic contents in raw vegetables. J. Agric. Food Chem. 50 (3), 6427.

Niu, G.Y., Yang, Z.L., Mitchell, K.E., Chen, F., Ek, M.B., Barlage, M., Xia, Y., 2011. The community Noah land surface model withmultiparameterization options (noah-MP): 1. Model description and evaluation with local-scale measurements. J. Geophys. Res. 116, D12109. https://doi.org/10.1029/2010JD015139.

Njoku, E.G., et al. 2003. Soil moisture retreival from AMSR-e. IEEE Trans. Geo-science Remote Sens. 41 (2), 215–229.

Oke, P.R., Brassington, G.B., Griffin, D.A., Schiller, A., 2008. The bluelink ocean data assimilation system (BODAS). Ocean Model. 21, 46–70. https://doi.org/10.1016/j.ocemod.2007.11.002.

Ott, E., Hunt, B.R., Szunyogh, I., Zimin, A.V., Kostelich, E.J., Corazza, M., Kalnay, E., Patil, D.J., Yorke, J.A., 2004. A local ensemble Kalman filter for atmospheric data assimilation. Tellus 56A, 415–428.

Pereira, A., Miranda, S., Pacino, M.C., Forsberg, R., 2011. Water storage changes from GRACE data in the La Plata Basin, geodesy for planet earth. Int. Assoc. Geodesy Symposia 136, 613–618. https://doi.org/10.1007/978-3-642-20338-1_75.

Pereira, M.P.S., Justino, F., Malhado, A.C.M., Barbosa, H., Marengo, J., 2014. The influence of oceanic basins on drought and ecosystem dynamics in Northeast Brazil. Environ. Res. Lett. 9 (124013).2014.

Perez-Carrera, A., Cirelli, A.F., 2009. Arsenic and water quality challenges in South America, water and sustainability in arid regions. , pp. 275–293. https://doi.org/10.1007/978-90-481-2776-4_17.

Ramirez, B.H., van der Ploeg, M., Teuling, A.J., Ganzeveld, L., Leemans, R., 2017. Tropical montane cloud forests in the Orinoco River Basin: the role of soil organic layers in water storage and release. Geoderma 298, 14–26. https://doi.org/10.1016/j.geoderma.2017.03.007. 2017. ISSN 0016-7061.

Reager, J.T., Thomas, A.C., Sproles, E.A., Rodell, M., Beaudoing, H.K., Li, B., Famiglietti, J.S., 2015. Assimilation of GRACE terrestrial water storage observations into a land surface model for the assessment of regional flood potential. Remote Sens. 2015 (7), 14663–14679.

Reichle, R.H., 2002. Hydrologic data assimilation with the ensemble Kalman filter. Mon. Wea. Rev 130, 103–114. https://doi.org/10.1175/1520-0493(2002)130<0103:HDAWTE>2.0.CO;2.

Renzullo, L.J., Van Dijk, A.I.J.M., Perraud, J.M., Collins, D., Henderson, B., Jin, H., Smith, A.B., McJannet, D.L., 2014. Continental satellite soil moisture data assimilation improves root-zone moisture analysis for water resources assessment. J. Hydrol. 519, 2747–2762. https://doi.org/10.1016/j.jhydrol.2014.08.008.

Rodell, M., Houser, P., Jambor, U., Gottschalck, J., Mitchell, K., Meng, C., Arsenault, K., Cosgrove, B., Radakovich, J., Bosilovich, M., Entin, J., Walker, J., Lohmann, D., Toll, D., 2004. The global land data assimilation system. Bull. Amer. Meteor. Soc. 85, 381–394. https://doi.org/10.1175/BAMS-85-3-381.

Sanso, B., Guenni, L., 1999. Venezuelan rainfall data analysed by using a Bayesian space-time model. Appl. Stat. 15, 594–612.

Schellekens, J., Dutra, E., Martnez-de la Torre, A., Balsamo, G., van Dijk, A., Sperna Weiland, F., Minvielle, M., Calvet, J.-C., Decharme, B., Eisner, S., Fink, G., Flrke, M., Peenteiner, S., van Beek, R., Polcher, J., Beck, H., Orth, R., Calton, B., Burke, S., Dorigo, W., Weedon, G.P., 2017. A global water resources ensemble of hydrological models: the earth2observe tier-1 dataset. Earth Syst. Sci. Data 9, 389–413. https://doi.org/10.5194/essd-9-389-2017.

Schumacher, M., Kusche, J., Döll, P., 2016. A Systematic Impact Assessment of GRACE Error Correlation on Data Assimilation in Hydrological Models. J. Geod. https://doi.org/10.1007/s00190-016-0892-y.

Schunk, R.W., Scherliess, L., Sojka, J.J., Thompson, D.C., 2004. USU global ionospheric data assimilation models, atmospheric and environmental remote sensing data processing and utilization: an end-to-end system perspective. In: Huang, H.-L.A., Bloom, H.J. (Eds.), Proc. of SPIE. pp. 5548..

Su, C.-H., Ryu, D., Young, R.I., Western, A.W., Wagner, W., 2013. Inter-comparison of microwave satellite soil moisture retrievals over the Murrumbidgee Basin, southeast Australia. Remote Sens. Environ. 134, 1–11.

Sun, T., Ferreira, V., He, X., Andam-Akorful, S., 2016. Water availability of So Francisco River basin based on a Space-Borne geodetic sensor. Water 8, 213. https://doi.org/10.3390/w8050213.

Swenson, S., Chambers, D., Wahr, J., 2008. Estimating geocentervariations from a combination of GRACE and ocean model output. J. Geophys. Res. 113, B08410. https://doi.org/10.1029/2007JB005338.

Swenson, S., Wahr, J., 2002. Methods for inferring regional surface-mass anomalies from gravity recovery and climate experiment (GRACE) measurements of time-variable gravity. J. Geophys. Res. B9 (2193), 107. https://doi.org/10.1029/2001JB000576.

Syed, T.H., Famiglietti, J.S., Chen, J., Rodell, M., Seneviratne, S.I., Viterbo, P., Wilson, C.R., 2005. Total basin discharge for the Amazon and Mississippi River basins from GRACE and a land-atmosphere water balance. Geophys., Res. Lett. 32, L24404. https://doi.org/10.1029/2005GL024851.

Tangdamrongsub, N., Steele-Dunne, S.C., Gunter, B.C., Ditmar, P.G., Weerts, A.H., 2015. Data assimilation of GRACE terrestrial water storage estimates into a regional hydrological model of the Rhine River basin. Hydrol. Earth Syst. Sci. 19, 2079–2100. https://doi.org/10.5194/hess-19-2079-2015.

Tedeschi, R.G., Cavalcanti, I.F., Grimm, A.M., 2013. Influences of two types of ENSO on South American precipitation. Int. J. Climatol. 33, 1382–1400. https://doi.org/10.1002/joc.3519.

Tedeschi, R.G., Collins, M., 2016. The influence of ENSO on South American precipitation during austral summer and autumn in observations and models. Int. J. Climatol. 36, 618–635.

Tian, S., Tregoning, P., Renzullo, L.J., van Dijk, A.I.J.M., Walker, J.P., Pauwels, V.R.N., Allgeyer, S., 2017. Improved water balance component estimates through joint assimilation of GRACE water storage and SMOS soil moisture retrievals. Water Resour. Res. 53. https://doi.org/10.1002/2016WR019641.

Tian, X., Xie, Z., Dai, A., 2008. A land surface soil moisture data assimilation system based on the dual-UKF method and the community land model. J. Geophys. Res. 113, D14127. https://doi.org/10.1029/2007JD009650.

Tippett, M.K., Anderson, J.L., Bishop, C.H., Hamill, T.M., Whitaker, J.S., 2003. Ensemble square root filters. Mon., Weath. Rev. 131, 148–590.

Tourre, Y.M., Jarlan, L., Lacaux, J.P., Rotela, C.H., Lafaye, M., 2008. (2008). Spatio-temporal variability of NDVI-precipitation over southernmost South America: possible linkages between climate signals and epidemics. Environ. Res. Lett. 3, 044008.

Treidel, H., Martin-Bordes, J.L., Gurdak, J.J., 2011. Climate Change Effects on Groundwater Resources: A Global Synthesis of Findings and Recommendations. CRC Press.0203120760, 9780203120767.

Tropical Rainfall Measuring Mission (TRMM)„ 2011. TRMM (TMPA/3b43) rainfall estimate l3 1 month 0.25 degree x 0.25 degree v7, Greenbelt, MD, goddard earth sciences data and information services center (GES DISC), accessed [data access date] https://disc.gsfc.nasa.gov/datacollection/TRMM_3B43_7.html.

van Dijk, A.I.J.M., 2010. The Australian Water Resources Assessment System: Technical Report 3, Landscape Model (Version 0.5) Technical Description. CSIRO: Water for a Healthy Country National Research Flagship,

van Dijk, A.I.J.M., Peña-Arancibia, J.L., Wood, E.F., Sheffield, J., Beck, H.E., 2013. Global analysis of seasonal streamflow predictability using an ensemble prediction system and observations from 6192 small catchments worldwide. Water Resour. Res. 49, 2729–2746. https://doi.org/10.1002/wrcr.20251.

van Dijk, A.I.J.M., Renzullo, L.J., Rodell, M., 2011. Use of gravity recovery and climate experiment terrestrial water storage retrievals to evaluate model estimates by the Australian water resources assessment system. Water Resour. Res. 47, W11524. https://doi.org/10.1029/2011WR010714.

van Dijk, A.I.J.M., Renzullo, L.J., Wada, Y., Tregoning, P., 2014. A global water cycle reanalysis (2003–2012) merging satellite gravimetry and altimetry observations

with a hydrological multi-model ensemble. Hydrol. Earth Syst. Sci. 18, 2955–2973. https://doi.org/10.5194/hess-18-2955-2014.

Villar, P.C., 2016. International cooperation on transboundary aquifers in South America and the Guarani Aquifer case, revista brasileira de Poltica internacional. Rev. bras. polí,t. int 59 (1 Brasília). https://doi.org/10.1590/0034-7329201600107. ISSN 1983-3121.

Vrugt, J.A., ter Braak, C.J.F., Diks, C.G.H., Schoups, G., 2013. Advancing hydrologic data assimilation using particle Markov chain Monte Carlo simulation: theory, concepts and applications. Adv. Water Resour. 51, 457–478. https://doi.org/10.1016/j.advwatres.2012.04.002. Anniversary Issue - 35 Years.

Wahr, J., Molenaar, M., Bryan, F., 1998. Time variability of the earth's gravity field' hydrological and oceanic effects and their possible detection using GRACE. J. Geophys. Res. https://doi.org/10.1029/98JB02844. 103, B12, 30, 205-30.

Whitaker, J.S., Hamill, T.M., 2002. Ensemble data assimilation without perturbed observations. Mon., Wea. Rev. 130, 1913–1924.

Wiese, D.N., 2015. GRACE Monthly Global Water Mass Grids NETCDF RELEASE 5.0. Ver. 5.0 PO.DAAC. CA, USA. https://doi.org/10.5067/TEMSC-OCL05.

Xavier, L., Becker, M., Cazenave, A., Longuevergne, L., Llovel, W., Filho, O.C.R., 2010. Interannual variability in water storage over 2003–2008 in the Amazon Basin from GRACE space gravimetry, in situ river level and precipitation data. Remote Sens. Environ. 114, 1629–1637. https://doi.org/10.1016/J.RSE.2010.02.005.

Yates, D.N., 1997. Climate change impacts on the hydrologic resources of South America: an annual, continental scale assessment. Clim. Res. 9 (1-2), 147–155. December 29.

Yu, Y., Disse, M., Yu, R., Yu, G., Sun, L., Huttner, P., Rumbaur, C., 2015. Large-scale hydrological modeling and decision-making for agricultural water consumption and allocation in the main stem Tarim River, China. Water 7, 2821–2839.

Yue, S., Wang, C., 2004. The Mann-Kendall test modified by effective sample size to detect trend in serially correlated hydrological series. Water Resour. Res. 18, 201. https://doi.org/10.1023/B:WARM.0000043140.61082.60.

Zaitchik, B.F., Rodell, M., Reichle, R.H., 2008. Assimilation of GRACE terrestrial water storage data into a land surface model: results for the Mississippi River Basin. J. Hydrometeorol. 9 (3), 535–548. https://doi.org/10.1175/2007JHM951.1.

Chapter 7

Water balance enforcement

This chapter is covered by the following publications:

- **Khaki, M.**, Ait-El-Fquih, B., Hoteit, I., Forootan, E., Awange, J., Kuhn, M., (2017c). A Two-update Ensemble Kalman Filter for Land Hydrological Data Assimilation with an Uncertain Constraint. Journal of Hydrology, 555:447-462, doi:10.1016/j.jhydrol.2017.10.032.
- **Khaki, M.**, Ait-El-Fquih, B., Hoteit, I., Forootan, E., Awange, J., Kuhn, M., (2018e). Unsupervised Ensemble Kalman Filtering with an Uncertain Constraint for Land Hydrological Data Assimilation. Revised, Journal of Hydrology.

These two papers are proposed to address the knowledge gap (v) outlined in Section 1.4. In order to enhance the estimation of model water storages, one should also involve flux observations and their associated errors in the assimilation procedure (cf. Section 1.3). In the first contribution above, we propose a new filter, so-called weak constrained ensemble Kalman filter (WCEnKF), which involves two Kalman-like update steps; the first updates the model forecast with the observations and the second enforces the water balance through an adjustment of the first update. Note that WCEnKF is also called Modified constrained ensemble Kalman filter (MCEnKF) in this manuscript (e.g., in Figures 4 and 5). The main objective of introducing the new method is to tackle the limitation in existing data assimilation studies, which refers to the inconsistency between hydrological water fluxes, namely precipitation, evaporation, discharge, and water storage changes after updating them with incoming observations. More specifically, contrary to existing methods, which do not include water balance constraint error, the proposed 2-step algorithm incorporates the uncertainty associated with the flux observations into the data assimilation process and optimize the water budget closure. The water budget enforcement in WCEnKF is taken into account using multi-mission remotely sensed observations (for precipitation and evaporation) and ground-based water discharge measurements. The second paper develops the WCEnKF to a more general (unsupervised) framework, in which the covariance associated with the water balance model is

estimated online, along with the model states. Both contributions present the results over eight different basins, i.e., Amazon, Indus, Mississippi, Orange, Danube, St. Lawrence, Murray-Darling, and the Yangtze while using various data for validation. WCEnKF successfully reduces imbalance errors and improves water storage estimates compared to a standard EnKF and open-loop run (or model-free, model run without data assimilation). The state update mechanism in WCEnKF is more general than other existing methods. For the first time, accounting for uncertainties in the balance constraint (or equality constraint) allows avoiding a perfect pseudo-observation (a combination of water fluxes) model scenario, which could help mitigate over-fitting issues. Nevertheless, based on the developed unsupervised WCEnKF (UWCEnKF) in the second paper, the results suggest that the filter can provide even more accurate estimates, e.g., smaller imbalances, through a more flexible scheme for approximating covariance associated to the water balance model. It is worth mentioning that the proposed WCEnKF and UWCEnKF are not used for the data assimilation application cases (Chapter 6) due to the fact that these approaches have not been completely tested and evaluated to be used in the above studies.

Journal of Hydrology 555 (2017) 447–462

Contents lists available at ScienceDirect

Journal of Hydrology

journal homepage: www.elsevier.com/locate/jhydrol

Research papers

A two-update ensemble Kalman filter for land hydrological data assimilation with an uncertain constraint

M. Khaki [a,*], B. Ait-El-Fquih [b], I. Hoteit [b], E. Forootan [c], J. Awange [a], M. Kuhn [a]

[a] Department of Spatial Sciences, Curtin University, Perth, Australia
[b] King Abdullah University of Science and Technology (KAUST), Thuwal, Saudi Arabia
[c] School of Earth and Ocean Sciences, Cardiff University, Cardiff, UK

ARTICLE INFO

Article history:
Received 7 June 2017
Received in revised form 16 October 2017
Accepted 17 October 2017
Available online 25 October 2017
This manuscript was handled by P. Kitanidis, Editor-in-Chief, with the assistance of Niklas Linde, Associate Editor

Keywords:
Constrained data assimilation
Ensemble Kalman filtering
Weak constrained ensemble Kalman filter
Water budget closure
Hydrological modelling

ABSTRACT

Assimilating Gravity Recovery And Climate Experiment (GRACE) data into land hydrological models provides a valuable opportunity to improve the models' forecasts and increases our knowledge of terrestrial water storages (TWS). The assimilation, however, may harm the consistency between hydrological water fluxes, namely precipitation, evaporation, discharge, and water storage changes. To address this issue, we propose a weak constrained ensemble Kalman filter (WCEnKF) that maintains estimated water budgets in balance with other water fluxes. Therefore, in this study, GRACE terrestrial water storages data are assimilated into the World-Wide Water Resources Assessment (W3RA) hydrological model over the Earth's land areas covering 2002–2012. Multi-mission remotely sensed precipitation measurements from the Tropical Rainfall Measuring Mission (TRMM) and evaporation products from the Moderate Resolution Imaging Spectroradiometer (MODIS), as well as ground-based water discharge measurements are applied to close the water balance equation. The proposed WCEnKF contains two update steps; first, it incorporates observations from GRACE to improve model simulations of water storages, and second, uses the additional observations of precipitation, evaporation, and water discharge to establish the water budget closure. These steps are designed to account for error information associated with the included observation sets during the assimilation process. In order to evaluate the assimilation results, in addition to monitoring the water budget closure errors, in situ groundwater measurements over the Mississippi River Basin in the US and the Murray-Darling Basin in Australia are used. Our results indicate approximately 24% improvement in the WCEnKF groundwater estimates over both basins compared to the use of (constraint-free) EnKF. WCEnKF also further reduces imbalance errors by approximately 82.53% (on average) and at the same time increases the correlations between the assimilation solutions and the water fluxes.

1. Introduction

Terrestrial water storage plays an important role in both human life and environment all around the world. Quantifying this major water resource is, therefore, essential and can be done using different tools including ground-based in situ measurements, satellite remote sensing data, and hydrological models. In the last few decades, hydrological models have extensively been used to determine and monitor stored water and fluxes in different forms within landscapes such as ice and snow, glaciers, aquifers, soils, and surface waters (e.g., Chiew et al., 1993; Wooldridge and Kalma, 2001; Döll et al., 2003; Huntington, 2006; van Dijk, 2010). The models have been designed to reflect the behavior of a system of interest while satisfying known physical properties reliably (Smith et al., 2011). However, various sources of uncertainty, due for example, imperfect modeling, data limitations on both temporal and spatial resolutions, errors in forcing fields, as well as empirical model parameters, limit the accuracy of hydrological models (Vrugt et al., 2013; van Dijk et al., 2011; van Dijk et al., 2014). Assimilating accurate observations into models is an effective approach to overcome these limitations (e.g., McLaughlin, 2002; Zaitchik et al., 2008; van Dijk et al., 2014; Gharamti et al., 2016).

Data assimilation is a procedure for incorporating observations of one or more variables (according to their uncertainties) into a numerical (physical) model to increase consistency of model simulations of a certain variable with its changes in the 'real world' (Bertino et al., 2003; Hoteit et al., 2012). Therefore it has been

* Corresponding author.
E-mail address: Mehdi.Khaki@postgrad.curtin.edu.au (M. Khaki).

https://doi.org/10.1016/j.jhydrol.2017.10.032
0022-1694/

widely applied in hydrological studies to improve different water compartments, such as soil moisture (e.g.,Reichle et al., 2002; Brocca et al., 2010; Renzullo et al., 2014), surface water (eg., Alsdorf et al., 2007; Neal et al., 2009; Giustarini et al., 2011, and snow storages (e.g., Liu et al., 2013; Kumar et al., 2015). During past few years, some studies have assessed the capability of Gravity Recovery And Climate Experiment (GRACE) data, available since March 2002, to improve terrestrial water storages (TWS) (e.g., Zaitchik et al., 2008; Eicker et al., 2014; Tangdamrongsub et al., 2015; Schumacher et al., 2016; Tangdamrongsub et al., 2017; Khaki et al., 2017a; Khaki et al., 2017b; Tian et al., 2017) simulated by land (surface) hydrological models.

The water balance equation is applied in land hydrological models to describe the relationships between changes in water storage ($\Delta\mathbf{s}$), evaporation ($\mathbf{e}$), precipitation ($\mathbf{p}$), and discharge ($\mathbf{q}$), i.e., $\Delta\mathbf{s} = \mathbf{p} - \mathbf{e} - \mathbf{q}$ (Sokolov and Chapman, 1974). However, the application of data assimilation may destroy the dynamical balances between water fluxes and water storage changes (Pan and Wood, 2006). In another words, models water storage states are in balance since model structure, e.g., its equations, governs variations in the water state changes due to the incoming and outgoing hydrological water fluxes. An assimilation of water storage states (e.g., GRACE data) does not constraint the assimilated state to be balanced. Eicker et al., 2016 found distinct changes in the linear rates and seasonality of water storage from GRACE and the flux deficit ($\mathbf{p} - \mathbf{e} - \mathbf{q}$) even over large-scale river basins. Therefore, after assimilation, one can expect mismatches between the model estimation of $\Delta\mathbf{s}$ and the flux deficit after each assimilation cycle. This issue must be mitigated to better interpret model derived water storage changes after implementing data assimilation (see, e.g.,Roads et al., 2003; Pan and Wood, 2006; Sahoo et al., 2011).

In order to enhance the estimation of model water storages (e.g., for $\Delta\mathbf{s}$), it is important that the water variables satisfy the water closure equation. One way to do this is to impose a balance constraint based on the water budget equation after each assimilation cycle (Pan et al., 2012). Few assimilation schemes have been proposed in this context. Pan and Wood (2006) developed a constrained ensemble Kalman filter (CEnKF) based on the ensemble Kalman filter (EnKF; Evensen, 1994) to solve the disclosure of the water balance equation after implementing a data assimilation over the southern Great Plains region of the United States. In addition to using CEnKF, Sahoo et al. (2011) and Pan et al. (2012) applied a data merging algorithm to prepare the datasets for data assimilation and to check for imbalance over various major river basins. They merged data from different sources (e.g., in situ observations, remote sensing retrievals, land surface model simulations, and global reanalyses) so that their errors can be used to achieve optimal weights leading to the best estimates for each terrestrial water cycle. These data were then used to resolve water balance errors by applying CEnKF (see also Zhang et al., 2016). In these studies, information about the uncertainties associated with water balance observations, however, have not been incorporated during data assimilation. The strong constraint imposed by assuming observation to be perfect is unrealistic and can cause estimation errors such as over-fitting issues (Tangdamrongsub et al., 2017). This motivates the new filtering technique, which is proposed in this study to involve observation errors in the assimilation procedure.

In this study, a new constrained ensemble Kalman filter, which we refer to as weak constrained ensemble Kalman filter (WCEnKF), is introduced that satisfies the closure of the water balance equation while taking the uncertainties in datasets into the account. WCEnKF is formulated based on the EnKF and imposes the closure constraint as a second update step, where the EnKF analysis members are updated to remain in balance with other variables (hereafter called pseudo-observation, and includes $\mathbf{p}, \mathbf{e}$, and $\mathbf{q}$ through the water balance equation). Water storages are therefore first updated using GRACE observations as in the EnKF in the first step, and the broken water balance is then mitigated using the pseudo-observations in the second EnKF update step. The novelty of the proposed scheme is that it accounts for the uncertainties in the pseudo-observations so that the budget closure is not strongly imposed. Moreover, in contrast to existing schemes, the filter does not seek to redistribute the imbalance between all compartments (i.e., $\Delta s, \mathbf{p}, \mathbf{e}$, and $\mathbf{q}$) and only adjusts the already estimated water storage ($\Delta\mathbf{s}$). WCEnKF treats $\mathbf{p}, \mathbf{e}$, and $\mathbf{q}$ and their uncertainties as a new set of observations, similar to any other observation in a standard EnKF. The imbalance problem requires a particular formulation of the state-space system, for which the process does not only depend on the state at the filtering time but also on the previous time.

The proposed WCEnKF with the dual update steps is used to assimilate GRACE TWS data into the World-Wide Water Resources Assessment (W3RA) hydrological model globally during 2002–2012. In addition to GRACE TWS data, remotely sensed measurements of $\mathbf{p}$ and $\mathbf{e}$ are also used to constrain the water balance in the filter estimates. For this purpose, we use the Tropical Rainfall Measuring Mission (TRMM-3B43; Huffman et al., 2007) precipitation products for $\mathbf{p}$, the Moderate Resolution Imaging Spectroradiometer (MODIS) evaporation data (MOD16; Mu et al., 2007) for $\mathbf{e}$, and the water discharge measurements from various ground stations for $\mathbf{q}$. Although the imbalance constraint is spatially limited to locations, where ground-based discharge data are available, the Kalman-like second update step of WCEnKF spreads the imbalance adjustments to all model grid points. For a better presentation of results, we choose eight globally distributed major basins with a dense network of water discharge measurements and analyze the assimilation solution separately over each basin. Among these basins, the Mississippi River Basin and the Murray-Darling Basin are selected subject to the availability of ground-based data to evaluate the performance of WCEnKF against in situ groundwater measurements.

The remainder of this paper is organized as follows. We first describe the model and data in Section 2. The filtering technique and the data assimilation setup are then described in Section 3. Section 4 presents the assimilation results, analyses the filter estimates and water budget closure (Section 4.3), and evaluates the estimates against in situ data (Section 4.2). Finally, summary and conclusions are provided in Section 5.

2. Model and data

2.1. W3RA Hydrological model

We use a grid distributed biophysical model of W3RA from the Commonwealth Scientific and Industrial Research Organisation (CSIRO). The model is designed to simulate landscape water stored in the vegetation and soil systems (van Dijk, 2010). The $1^\circ \times 1^\circ$ version of W3RA is applied to represent the water balance of the soil, groundwater and surface water stores, in which each cell is modeled independently from its neighbors (van Dijk, 2010; Renzullo et al., 2014). The model parameters include effective soil parameters, water holding capacity and soil evaporation, relating greenness and groundwater recession, and saturated area to catchment characteristics (van Dijk et al., 2013). Forcing datasets consist of the daily meteorological fields of minimum and maximum temperature, downwelling short-wave radiation, and precipitation by Princeton University (Sheffield et al., 2006). The model state is composed of storages of the top, shallow root and deep root soil layers, groundwater storage, and surface water storage. The simulation covers the period from April 2002 to December 2012.

W3RA represents the storage of water in small river channels and consequently surface water storage changes in reservoir and lakes are not simulated by the model. Therefore, it is necessary to remove surface water storages from GRACE TWS data before assimilation even though it has much lesser effects than other water storages such as groundwater and soil moisture. For this purpose, we use the WaterGAP Global Hydrology Model (WGHM; more details on Döll et al., 2003) surface storage estimations. WGHM models the vertical and horizontal water fluxes on a $0.5^\circ \times 0.5^\circ$ grid resolution and describes the major hydrological components, such as snow accumulation, runoff, and the lateral transport of water within the river networks (Forootan et al., 2014). The surface water storages from WGHM are removed from the GRACE TWS before assimilation. Note that after updating the model states using the adjusted GRACE data (first update step in WCEnKF), the removed surface water storages are added to the filtered TWS estimates before applying the water budget closure step (second update step).

2.2. Terrestrial water storage (TWS) data

Monthly TWS derived from GRACE level 2 (L2) gravity field data are used in the first step of the proposed filtering scheme to update the summation of the model derived water storage simulations including top soil, shallow soil, deep soil water, snow, vegetation, and groundwater. GRACE data are provided in terms of the gravity potential Stokes' coefficients, truncated at spherical harmonic degree and order 90, together with their full error information from the ITSG-Grace2016 gravity field model (Mayer-Gurr et al., 2014). Some post-processing steps are applied on the coefficients before converting them into TWSs. Degree 1 and degree 2 (C20) coefficients are replaced by more accurate coefficients that are calculated by Swenson et al. (2008) and the Satellite Laser Ranging solutions (Cheng and Tapley, 2004), respectively. We also apply DDK2 (Kusche et al., 2009) to mitigate colored/correlated noise in the coefficients. The L2 gravity fields are then converted to $1^\circ \times 1^\circ$ TWS fields following Wahr et al. (1998). The mean TWS is taken from the model for the study period and is added to the GRACE TWS change time series to obtain absolute values in accordance with W3RA (Zaitchik et al., 2008). We further exploit the provided full error information of the Stokes' coefficients to construct an observation error covariance matrix for data assimilation. This is done by converting GRACE spherical harmonic error coefficients to error covariances associated with TWS data as suggested by Eicker et al. (2014) and Schumacher et al., 2016. Eicker et al. (2014) showed that applying GRACE TWS data on a $1^\circ \times 1^\circ$ grid resolution results in a rank deficiency problem during data assimilation (see also Khaki et al., 2017b). However, as shown by Khaki et al. (2017b), the application of local analysis (LA) successfully mitigates this problem by spatially limiting the use of ensemble-based covariance information in high-dimensional systems. Therefore, here, we follow Khaki et al. (2017b) and apply LA to cope with rank deficiency problem (see details in Section 3.3).

2.3. Water fluxes

Precipitation data of TRMM-3B43 products (TRMM, 2011; Huffman et al., 2007) is used. This dataset is limited spatially between 50°N and 50°S in latitude, and -180° to $+180^\circ$ in longitude. The data is re-sampled from $0.25^\circ \times 0.25^\circ$ to a monthly $1^\circ \times 1^\circ$ spatial resolution. We also use the relative error available for each gridpoint and different times (Huffman et al., 1997).

We also acquire MOD16 evaporation data from the University of Montana's Numerical Terradynamic Simulation group with eight days temporal resolution and one km spatial resolution (Mu et al., 2011). The gridded data is converted to a monthly temporal scale and $1^\circ \times 1^\circ$ spatial resolution. Following Aires (2014) and Munier et al. (2014), 10 mm uncertainty is considered for the evaporation data.

Different data sources are used to provide water discharge data with a maximum global coverage. In this regard, the largest part of runoff products (1970 globally distributed stations) is acquired from the Global Runoff Data Centre (GRDC). Over Africa, 83 stations are obtained from SIEREM (Systeme d'Informations Environnementales sur les Ressources en Eau et leur Modelisation), an environmental information system for water resources (Boyer et al., 2006). In additions, two dense networks of discharge stations over the United State (3800 stations), Southeast Asia (1700 stations), and Australia (1250 stations) are provided from the United States Geological Survey (USGS), China Hydrology Data Project (Henck et al., 2010; Schmidt et al., 2011), and the Australian Bureau of Meteorology under the Water Regulations (2008). In addition, a number of discharge stations are also obtained from the National River Flow Archive (NRFA), Department of Hydrology and Meteorology of Nepal, the Hydrology and Geochemistry of the Amazon basin (HYBAM) for the Amazon, Orinoco, and Congo basins. Fig. 1 shows the locations of discharge stations distributed globally.

As mentioned, the water budget closure relies on $\mathbf{p}, \mathbf{e}$, and $\mathbf{q}$. Wherever a discharge station is located, it is possible to impose water budget closure adjustment. At each $1^\circ \times 1^\circ$ grid point we use the nearest discharge stations to spatially interpolate the observations $\mathbf{q}$. To this end, an average of data from discharge stations located within 0.5° radius of each grid point is assigned to this grid point. Since no straight information on the data uncertainty is available, two approaches are applied here to specify errors on the data. Sheffield et al. (2009) suggested that the standard errors in the gauge-based data are 5%–10% of the discharge values and Pan et al. (2012) proposed a formula to estimate the discharge error for a basin within a given area A as,

$$\textit{Relative Error}\ (\%) = 5\frac{(A_1 - A)}{(A_1 - A_2)} + 5, \tag{1}$$

where A_1 and A_2 are the areas of Amazon Basin (4.62×10^6 km^2) and Ural Basin (0.19×10^6 km^2), respectively. Here we use Eq. (1) to assign errors to discharge stations located in the major basins of Amazon, Indus, Mississippi, Orange, Danube, St. Lawrence, Murray-Darling, and Yangtze, and 10% of discharge value for any station outside of these areas as suggested by literature (e.g., Pan et al., 2012; Aires, 2014; Munier et al., 2014).

2.4. In situ measurements

In addition to monitoring water budget closure errors using the water fluxes observations, we use in situ groundwater measurements over the Mississippi Basin and Murray-Darling Basin to evaluate the performance of the proposed filter. The distribution of groundwater well stations is presented in Fig. 2. In the Mississippi Basin, independent data are collected from USGS. Additional measurements are provided for the Murray-Darling Basin by the New South Wales Government (NSW) groundwater archive. Monthly well measurements are acquired and time series of groundwater storage anomalies are generated. Generally, a specific yield is required to convert well-water levels to variations in groundwater storage regarding equivalent water heights (Rodell et al., 2007; Zaitchik et al., 2008). This information, however, is not available in our case, so TWS variation from GRACE and Global Land Data Assimilation System (GLDAS) soil moisture are used to calculate the specific yield and scale the observed headwater by modifying the magnitude of groundwater time series (Tregoning et al., 2012; Tangdamrongsub et al., 2015). As Tregoning et al. (2012)

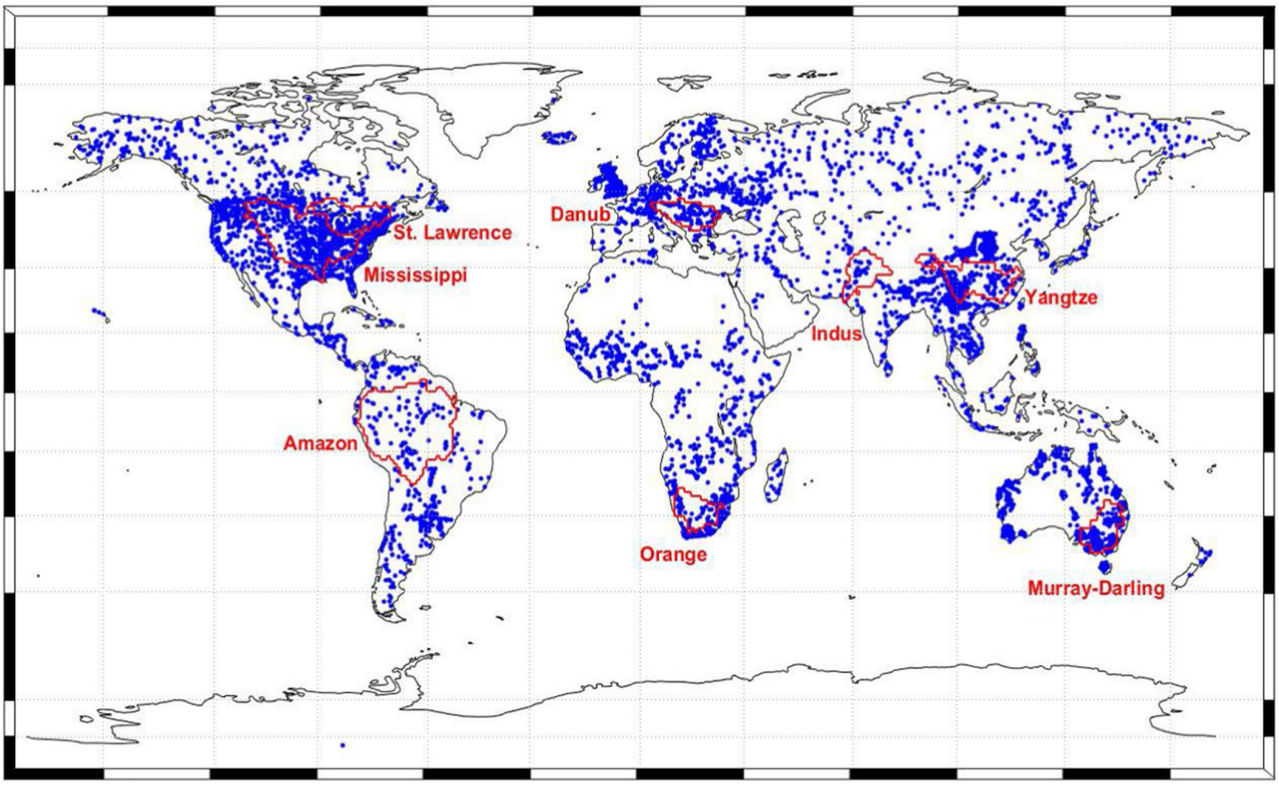

Fig. 1. Distribution of water discharge stations used in this study.

showed, the GW component can be extracted by removing the soil moisture component from GRACE TWS data while other compartments like biomass and surface water variations can be excluded due to their small contribution to regional scale mass variations. The calculated specific yields range between 0.08 and 0.16 over the Murray-Darling Basin, falling within the 0.05–0.2 range suggested by the Australian Bureau of Meteorology (BOM) and Seoane et al. (2013), and range between 0.15 and 0.22 over the Mississippi Basin along with those suggested by Gutentag et al. (1984) (i.e., 0.1–0.3), thereby justifying the application of the method. Using extracted yield factors, one can extract the groundwater components from the measured well-water levels. The scaled groundwater time series are then used to evaluate the data assimilation results over each basin. To this end, we compare groundwater estimates after data assimilation with ground-based groundwater measurements. Details of the datasets used in this study are outlined in Table 1.

3. The weak constrained ensemble Kalman filter (WCEnKF)

3.1. Problem formulation

Let $\{\mathbf{x}_t\}_{t=0}^{T} \in \mathbb{R}^{n_x}$ denote the (unknown) system state process formed by top soil, shallow soil, deep soil water, snow, vegetation, and groundwater. Note that except for groundwater, all the other components are simulated with two hydrological response units (HRU) of tall, e.g., deep-rooted vegetation and short, e.g., shallow-rooted vegetation, which leads to 11 state variables $(5 \times 2 + 1)$ of W3RA at each grid cell (24509 cells in total). Although in general, t refers to model time steps, for the sake of simplicity, we assume that the model time step is equal to the assimilation time step (monthly scale). $\{\mathbf{y}_t\}_{t=0}^{T} \in \mathbb{R}^{n_y}$ represents the GRACE TWS observed process. The state and observed processes are related through a dynamical state-space system of the form,

$$\begin{cases} \mathbf{x}_t = \mathcal{M}_{t-1}(\mathbf{x}_{t-1}) + \boldsymbol{v}_t, \\ \mathbf{y}_t = \mathbf{H}_t\mathbf{x}_t + \mathbf{w}_t, \end{cases} \tag{2}$$

for which the state transition operator, $\mathcal{M}(.)$, is nonlinear. $\mathbf{H}$ is the (observation) design matrix containing 11 ones in each of the 24509 rows, representing the sum of the individual compartments to TWS at each grid cell with all the other elements of the rows being zero (total 269599 columns). The proposed scheme can be easily extended to the case of nonlinear observation operator (i.e., in which $\mathbf{H}_t\mathbf{x}_t$ is replaced by $h_t(\mathbf{x_t})$), as for example discussed in Liu and Xue (2016). The state transition noise process, $\boldsymbol{v} = \{\boldsymbol{v}_t\}_t$, and the observation noise process, $\mathbf{w} = \{\mathbf{w}_t\}_t$, are assumed to be independent, jointly independent, and independent of the initial state, $\mathbf{x}_0$. Furthermore, $\mathbf{x}_0, \boldsymbol{v}_t$, and $\mathbf{w}_t$ are assumed to be Gaussian; $\boldsymbol{v}_t$ and $\mathbf{w}_t$ with zero mean and covariances $\mathbf{Q}_t$ and $\mathbf{R}_t$, respectively.

Data assimilation can destroy the balance between water fluxes. It is therefore essential to incorporate the water balance equation by imposing an equality constraint to restore the balance problem. Changes in monthly mean water storage at two different time steps (e.g., t and $t-1$) should be equal, up to uncertainties in the involved data, to the difference between the monthly mean input ($\mathbf{p}$) and output ($\mathbf{e}$ and $\mathbf{q}$) water storages. This can be formulated as:

$$\mathbf{d}_t = -\mathbf{x}_t + \mathbf{x}_{t-1} + \mathbf{p}_t - \mathbf{e}_t - \mathbf{q}_t + \xi_t, \tag{3}$$

where $\{\xi_t\}_t$ is the noise process accounting for errors associated with the different water fluxes data. Here we assume ξ_t Gaussian white noise with zero mean and covariance $\boldsymbol{\Sigma}_t$, and independent of $\mathbf{x}_0$ and $\{\mathbf{w}_t\}_t$. Defining $\mathbf{z}_t = \mathbf{d}_t - \mathbf{p}_t + \mathbf{e}_t + \mathbf{q}_t$, the constraint Eq. (3) is rewritten as,

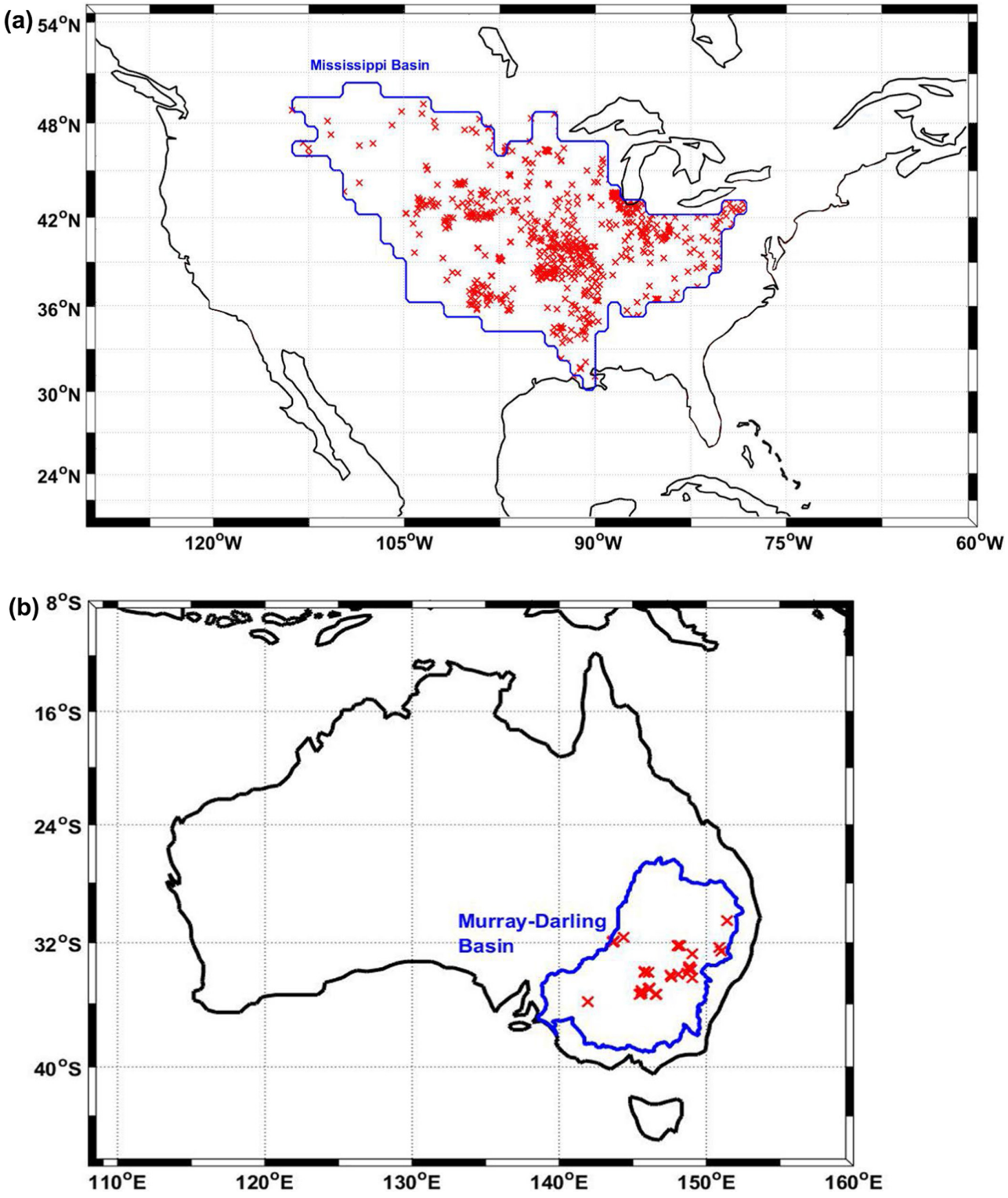

Fig. 2. Locations of groundwater stations within (a) the Mississippi Basin in the US (a) and (b) the Murray-Darling Basin in Australia.

$$\mathbf{z}_t = \mathbf{G}\mathbf{x}_t + \mathbf{L}\mathbf{x}_{t-1} + \xi_t, \tag{4}$$

where $\mathbf{G}$, in general, is the $n_x \times n_x$ (with n_x being the length of x) identity matrix while in this study $\mathbf{G} = \mathbf{H}$ to aggregate different water compartments at each grid point and $\mathbf{L} = -\mathbf{G}$.

In the constrained state-space system Eqs. (2)–(4), we focus on the filtering problem, say, on the estimation, at each time t, of the system state, $\mathbf{x}_t$, conditional on both GRACE TWS observations, $\mathbf{y}_{0:t} \overset{\text{def}}{=} \{\mathbf{y}_0, \mathbf{y}_1, \cdots, \mathbf{y}_t\}$ and "pseudo-observations" $\mathbf{z}_{0:t}$.

Table 1
A summary of the datasets used in this study.

Description	Platform	Data access
Terrestrial water storage (TWS)	GRACE	https://www.tugraz.at/institute/ifg/downloads/gravity-field-models/itsg-grace2014/
Daily accumulated precipitation (**p**)	TRMM-3B42	http://disc2.gesdisc.eosdis.nasa.gov/data/TRMM_L3/TRMM_3B42_Daily.7
MODIS Global Evapotranspiration (**e**)	MOD16	http://www.ntsg.umt.edu/project/mod16
Water discharge (**q**)	GRDC	http://www.bafg.de/GRDC/EN/Home/homepage_node.html
q		http://www.hydrosciences.fr/sierem/consultation/choixaccess.asp?lang=en
q	USGS	https://waterdata.usgs.gov/nwis/sw
q		http://www.bom.gov.au/waterdata/
q	NRFA	http://nrfa.ceh.ac.uk/data/
q		http://www.ore-hybam.org/
q		http://www.hydrology.gov.np/new/bull3/index.php/hydrology/home/main
Hydrological model	W3RA	http://www.wenfo.org/wald/data-software/
Groundwater in situ measurements	USGS	https://water.usgs.gov/ogw/data.html
	NSW	http://waterinfo.nsw.gov.au/pinneena/gw.shtml

Let $\mathbf{r}_t = [\mathbf{y}_t^T, \mathbf{z}_t^T]^T$. As known in the Bayesian estimation theory, the computation of any estimator of $\mathbf{x}_t$ from $\mathbf{r}_{0:t}$ is based on the so-called posterior (filtering or analysis) probability density function (pdf), $p(\mathbf{x}_t|\mathbf{r}_{0:t})$. For instance, the posterior mean (PM) estimator, $\hat{\mathbf{x}}_{t|t}$, which minimizes the mean squared error, is given by

$$\hat{\mathbf{x}}_{t|t} = \mathbb{E}[\mathbf{x}_t|\mathbf{r}_{0:t}], \\ = \int \mathbf{x}_t p(\mathbf{x}_t|\mathbf{r}_{0:t}) d\mathbf{x}_t. \quad (5)$$

The conditional independence property of the system Eqs. (2)–(4) enables for efficient *recursive* computation of this analysis pdf. Indeed, starting at time $t-1$ from $p(\mathbf{x}_{t-1}|\mathbf{r}_{0:t-1})$, one can compute $p(\mathbf{x}_t|\mathbf{r}_{0:t})$ following forecast and update steps as follows:

- *Forecast step.* The state transition pdf, $p(\mathbf{x}_t|\mathbf{x}_{t-1})$, is first used to compute the forecast pdf as (e.g., Ait-El-Fquih et al., 2016),

$$p(\mathbf{x}_t|\mathbf{r}_{0:t-1}) = \int p(\mathbf{x}_t|\mathbf{x}_{t-1}) p(\mathbf{x}_{t-1}|\mathbf{r}_{0:t-1}) d\mathbf{x}_{t-1}. \quad (6)$$

- *Update step with the GRACE TWS data.* Once available, the observation $\mathbf{y}_t$ is first used to update forecast pdf, $p(\mathbf{x}_t|\mathbf{r}_{0:t-1})$ as,

$$p(\mathbf{x}_t|\mathbf{r}_{0:t-1}, \mathbf{y}_t) \propto p(\mathbf{y}_t|\mathbf{x}_t) p(\mathbf{x}_t|\mathbf{r}_{0:t-1}), \quad (7)$$

and

$$p(\mathbf{x}_{t-1}|\mathbf{r}_{0:t-1}, \mathbf{y}_t) \propto p(\mathbf{y}_t|\mathbf{x}_{t-1}) p(\mathbf{x}_{t-1}|\mathbf{r}_{0:t-1}). \quad (8)$$

While the likelihood $p(\mathbf{y}_t|\mathbf{x}_t)$ in the update (7) is given through the observation model, $p(\mathbf{y}_t|\mathbf{x}_{t-1})$ in (8) is not known and needs to be computed beforehand as,

$$p(\mathbf{y}_t|\mathbf{x}_{t-1}) = \int p(\mathbf{y}_t|\mathbf{x}_t) p(\mathbf{x}_t|\mathbf{x}_{t-1}) d\mathbf{x}_t. \quad (9)$$

By ignoring the pseudo-observations, $\mathbf{z}_{0:t-1}$, in Eqs. 7,8, these equations translate as a one-step-ahead (OSA) smoothing process, which computes the OSA smoothing pdf, $p(\mathbf{x}_{t-1}|\mathbf{y}_{0:t})$, from the previous analysis pdf $p(\mathbf{x}_{t-1}|\mathbf{y}_{0:t-1})$ (Ait-El-Fquih and Hoteit, 2016). For simplicity, we refer to pdf $p(\mathbf{x}_{t-1}|\mathbf{r}_{0:t-1}, \mathbf{y}_t)$ as the OSA smoothing pdf (note that the actual OSA smoothing pdfs are $p(\mathbf{x}_{t-1}|\mathbf{r}_{0:t})$, $p(\mathbf{x}_{t-1}|\mathbf{y}_{0:t})$ or $p(\mathbf{x}_{t-1}|\mathbf{z}_{0:t})$).

- *Update step with* $\mathbf{z}_t$. The pdf $p(\mathbf{x}_t|\mathbf{r}_{0:t-1}, \mathbf{y}_t)$ that stems from the update of the forecast pdf with $\mathbf{y}_t$ (Eq. (7)) is in turn updated with $\mathbf{z}_t$ based on the Bayes' rule, leading to the analysis pdf of interest:

$$p(\mathbf{x}_t|\mathbf{r}_{0:t}) \propto p(\mathbf{z}_t|\mathbf{x}_t, \mathbf{y}_t, \mathbf{r}_{0:t-1}) p(\mathbf{x}_t|\mathbf{r}_{0:t-1}, \mathbf{y}_t). \quad (10)$$

The unknown likelihood $p(\mathbf{z}_t|\mathbf{x}_t, \mathbf{y}_t, \mathbf{r}_{0:t-1})$ is computed beforehand as,

$$p(\mathbf{z}_t|\mathbf{x}_t, \mathbf{y}_t, \mathbf{r}_{0:t-1}) \approx \int p(\mathbf{z}_t|\mathbf{x}_t, \mathbf{x}_{t-1}) p(\mathbf{x}_{t-1}|\mathbf{r}_{0:t-1}, \mathbf{y}_t) d\mathbf{x}_{t-1}. \quad (11)$$

3.2. The WCEnKF algorithm

In this section, the WCEnKF algorithm is described in three stages. The definition starts with the forecast step, in which the previous analysis ensemble state is integrated forward with the model to obtain the forecast ensemble. Two analysis (update) steps are then performed. The first updates, following a Kalman filter-like correction, the forecast ensemble based on the GRACE TWS data; the second update uses information of the water budget closure to perform a second Kalman filter-like correction, leading to the analysis ensemble of interest.

From previous section, it is not possible to analytically compute the integrals in Eqs. (5)–(11) because of the nonlinearity of the model $\mathcal{M}(.)$. We therefore derive an EnKF solution (Evensen, 1994; Hoteit et al., 2015) by applying the standard random sampling Properties 1 and 2 listed in Appendix A. Starting at time $t-1$ from an analysis ensemble, $\{\mathbf{x}_{t-1}^{a,(i)}\}_{i=1}^n$, the analysis ensemble at next time (t), $\{\mathbf{x}_t^{a,(i)}\}_{i=1}^n$, can be computed by the following cycles of forecast and update steps.

- *Forecast step.* A forecast ensemble, $\{\mathbf{x}_t^{f,(i)}\}_{i=1}^n$, is first computed by integrating $\{\mathbf{x}_{t-1}^{a,(i)}\}_{i=1}^n$, forward in time with the model:

$$\mathbf{x}_t^{f,(i)} = \mathcal{M}_{t-1}(\mathbf{x}_{t-1}^{a,(i)}) + \boldsymbol{v}^{(i)}, \quad (12)$$

where $\boldsymbol{v}^{(i)}$ is a random sample from the Gaussian $\mathcal{N}(\mathbf{0}, \mathbf{Q}_t)$.
- *Update with GRACE TWS data (first update).* Once a new observation $\mathbf{y}_t$ is available, new ensemble $\{\tilde{\mathbf{x}}_t^{a,(i)}\}_{i=1}^n$ and $\{\tilde{\mathbf{x}}_{t-1}^{s,(i)}\}_{i=1}^n$ are then computed using an EnKF update of the forecast ensemble and the previous analysis ensemble:

$$\mathbf{y}_t^{f,(i)} = \mathbf{H}\mathbf{x}_t^{f,(i)} + \mathbf{w}^{(i)}; \quad \mathbf{w}^{(i)} \sim \mathcal{N}(\mathbf{0}, \mathbf{R}_t), \quad (13)$$

$$\tilde{\mathbf{x}}_t^{a,(i)} = \mathbf{x}_t^{f,(i)} + \mathbf{P}_{\mathbf{x}_t^f}\mathbf{H}^T \underbrace{[\mathbf{H}\mathbf{P}_{\mathbf{x}_t^f}\mathbf{H}^T + \mathbf{R}_t]^{-1}[\mathbf{y}_t - \mathbf{y}_t^{f,(i)}]}_{\boldsymbol{\mu}_t^{(i)}}, \quad (14)$$

$$\tilde{\mathbf{x}}_{t-1}^{s,(i)} = \mathbf{x}_{t-1}^{a,(i)} + \mathbf{P}_{\mathbf{x}_{t-1}^a, \mathbf{x}_t^f}\mathbf{H}^T\boldsymbol{\mu}_t^{(i)}. \quad (15)$$

The covariance matrices $\mathbf{P}_{\mathbf{x}_t^f}$ and $\mathbf{P}_{\mathbf{x}_{t-1}^a, \mathbf{x}_t^f}$, are evaluated beforehand from the previous analysis and forecast ensembles as,

$$\mathbf{P}_{\mathbf{x}_t^f} = (n-1)^{-1}\mathbf{S}_{\mathbf{x}_t^f}\mathbf{S}_{\mathbf{x}_t^f}^T, \quad (16)$$

$$\mathbf{P}_{\mathbf{x}_{t-1}^a, \mathbf{x}_t^f} = (n-1)^{-1}\mathbf{S}_{\mathbf{x}_{t-1}^a}\mathbf{S}_{\mathbf{x}_t^f}^T, \quad (17)$$

where $\mathbf{S}_{\mathbf{x}_{t-1}^a}$ and $\mathbf{S}_{\mathbf{x}_t^f}$ are the perturbation matrices (i.e., matrices with n columns formed by the ensemble members minus the ensemble mean). Eqs. (14) and (15) are EnKF updates of $\mathbf{x}_t^{f,(i)}$ and $\mathbf{x}_{t-1}^{a,(i)}$, respectively. These updates are achieved based on $\mathbf{y}_t$,

with Kalman gains $\mathbf{P}_{\mathbf{x}_t^f}\mathbf{H}^T[\mathbf{H}\mathbf{P}_{\mathbf{x}_t^f}\mathbf{H}^T+\mathbf{R}_t]^{-1}$ (Eq. (14)) and $\mathbf{P}_{\mathbf{x}_{t-1}^a,\mathbf{x}_t^f}\mathbf{H}^T[\mathbf{H}\mathbf{P}_{\mathbf{x}_t^f}\mathbf{H}^T+\mathbf{R}_t]^{-1}$ (Eq. (15)). The $\tilde{\mathbf{x}}_t^{a,(i)}$ is based on $\mathbf{y}_t$ only, and a second update with $\mathbf{z}_t$ is still required. The index '$\sim$' is used for the first update to distinguish it from the second one.

- *Adjustment with the water budget constraint (second update).* The pseudo-observation, $\mathbf{z}_t$, is then used to update $\{\tilde{\mathbf{x}}_t^{a,(i)}\}_{i=1}^n$, again using an EnKF update, leading to the actual state analysis ensemble of interest:

$$\mathbf{z}_t^{f,(i)} = \mathbf{G}\tilde{\mathbf{x}}_t^{a,(i)} + \mathbf{L}\tilde{\mathbf{x}}_{t-1}^{s,(i)} + \boldsymbol{\xi}_t^{(i)}; \quad \boldsymbol{\xi}_t^{(i)} \sim \mathcal{N}(\mathbf{0}, \boldsymbol{\Sigma}_t), \tag{18}$$

$$\mathbf{x}_t^{a,(i)} = \tilde{\mathbf{x}}_t^{a,(i)} + \mathbf{P}_{\tilde{\mathbf{x}}_t^a,\mathbf{z}_t^f}[\mathbf{N}\mathbf{P}_{\boldsymbol{\eta}_t}\mathbf{N}^T + \boldsymbol{\Sigma}_t]^{-1}[\mathbf{z}_t - \mathbf{z}_t^{f,(i)}], \tag{19}$$

with $\mathbf{N} = [\mathbf{G}, \mathbf{L}]$, the cross-covariance $\mathbf{P}_{\tilde{\mathbf{x}}_t^a,\mathbf{z}_t^f}$ is evaluated from the ensembles $\{\tilde{\mathbf{x}}_t^{a,(i)}\}_{i=1}^n$ and $\{\mathbf{z}_t^{f,(i)}\}_{i=1}^n$, as in Eq. (17), and the covariance $\mathbf{P}_{\boldsymbol{\eta}_t}$ is computed from the augmented state ensemble $\{\boldsymbol{\eta}_t^{(i)}\}_{i=1}^n$, where $\boldsymbol{\eta}_t^{(i)} = [(\tilde{\mathbf{x}}_t^{a,(i)})^T, (\tilde{\mathbf{x}}_{t-1}^{s,(i)})^T]^T$, as in Eq. (16). As one can see, Eq. (19) translates an EnKF update of $\tilde{\mathbf{x}}_t^{a,(i)}$, based on the pseudo-observation $\mathbf{z}_t$, where gain is $\mathbf{P}_{\tilde{\mathbf{x}}_t^a,\mathbf{z}_t^f}[\mathbf{N}\mathbf{P}_{\boldsymbol{\eta}_t}\mathbf{N}^T + \boldsymbol{\Sigma}_t]^{-1}$, leading to $\mathbf{x}_t^{a,(i)}$, the state analysis ensemble of interest. The PM Eq. (5) estimate is then approximated by the sample mean of the resulting analysis ensemble. As discussed in the introduction, the pseudo-observations are only available at the discharge observations locations, but the Kalman update Eq. (18) spreads the information to the whole state vectors. A schematic illustration of the filter algorithm is presented in Fig. 3.

Similarly to the standard CEnKF of Pan et al., 2012, the proposed WCEnKF involves one forecast step and two successive update steps. The two filters have the same forecast and first update (with observation $\mathbf{y}_t$) steps, and only differ in their second update (adjustment with pseudo-observation $\mathbf{z}_t$)). The state update mechanism Eqs. (18) and (19) is more general than the one in Pan et al., 2012, as the latter does not involve the OSA smoothing ensemble, $\{\tilde{\mathbf{x}}_{t-1}^{s,(i)}\}_i$ in Eqs. (18) and (19) and assume no noise ($\boldsymbol{\xi}_t^{(i)} = 0$) in Eq. (18) and its covariance $\boldsymbol{\Sigma}_t = 0$ in Eq. (19). As such, CEnKF can be considered as a direct particular case of WCEnKF. As stated above, accounting for uncertainties in the constraint allows avoiding a perfect pseudo-observation model scenario, which should help mitigating for over-fitting issues. The OSA smoothing terms (e.g., $\tilde{\mathbf{x}}_{t-1}^{s,(i)}$ in Eq. (18)) come from the fact that the pseudo-observation, $\mathbf{z}_t$, in the constraint Eq. (4) is not only function of $\mathbf{x}_t$ but also of $\mathbf{x}_{t-1}$.

3.3. Experimental setup

All the water fluxes data (including $\mathbf{p}, \mathbf{e}$, and $\mathbf{q}$) are accumulated to a monthly scale and used in the monthly assimilation processes. The monthly increment (i.e., the difference between the monthly averaged GRACE TWS and simulated TWS) can be added to each day of the current month, which guarantees that the update of the monthly mean is identical to the monthly mean of the daily updates. In practice, the differences between the predictions and the updated states are added as offsets to the state vectors at the last day of each month to generate the ensembles for the next month assimilation step. Given that not enough information are available to accurately estimate the pseudo-observation error covariance Σ, especially for $\mathbf{q}$, to test the sensibility we consider the error values mentioned in Section 2.3 as *reference errors* and test with three different Σ : (1) the *reference errors* values minus 5% of observation values, (2) *reference errors*, and (3) the *reference errors* plus 5% of observation values. We further assume the observation errors to be spatially uncorrelated. This test allows us to analyze the influence of the pseudo-observations on the final results.

To generate an initial ensemble to start the filtering process, we follow Renzullo et al. (2014) and perturb the meteorological forcing fields. To this end, we assume a Gaussian multiplicative error of 30% for precipitation, an additive Gaussian error of 50 W m^{-2} for the shortwave radiation, and a Gaussian additive error of 2 °C for temperature (Jones et al., 2007; Renzullo et al., 2014). The initial ensemble is then computed by sampling the above Gaussian distributions (see details in Renzullo et al., 2014). We, then, integrate the resulting ensemble (with 30 members) forward with the model from January 2000 to April 2002 to generate the initial ensembles at the beginning of the study period. An ensemble of 30 members is selected as it was found large enough to obtain sufficient ensemble spread at reasonable computational cost.

We further apply ensemble inflation and localization to enhance the filters performances (e.g., Anderson et al., 2007). These techniques were proven to be useful in dealing with neglected uncertainties in the system and small ensembles (e.g., Hamill and Snyder, 2002; Bergemann and Reich, 2010). Ensemble inflation with a best case coefficient factor of 1.12 (after testing different values) is applied here to increase the ensemble deviation from the ensemble-mean (Anderson et al., 2007). Local Analysis (LA) (Evensen, 2003) is used to restrict the impact of the measurements in the update step to variables located within a certain distance only (5° as suggested by Khaki et al., 2017b). By spatially limiting the influences of observations over large distances in the sample covariance, LA can help mitigating spatial correlation errors and rank deficiency problem during the assimilation (see Khaki et al., 2017b, for more details). This is particularly useful to account for

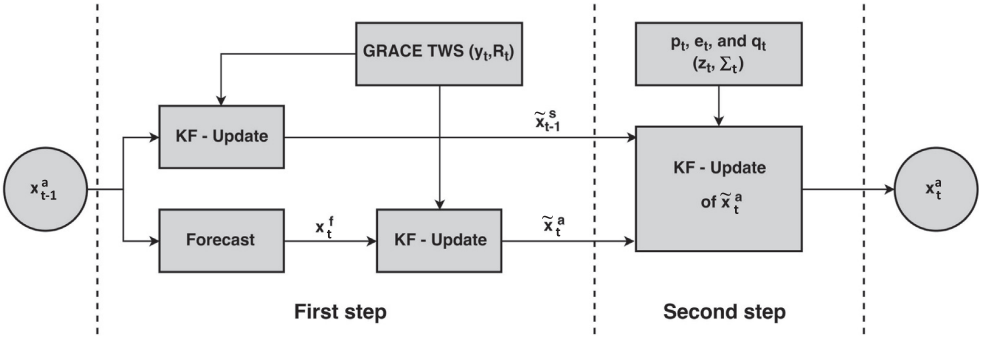

Fig. 3. A schematic illustration of the WCEnKF filter's steps applied for data assimilation in this study.

the spatial correlation errors in satellite products, particularly GRACE (Khaki et al., 2017b; Tangdamrongsub et al., 2017).

4. Results

We first investigate the effects of different scenarios applied for errors associated with the fluxes in Section 4.1. In Section 4.2, we evaluate the performance of WCEnKF against in situ groundwater measurements over the Mississippi River Basin in the US and the Murray-Darling Basin in Australia. To further assess the behavior of the proposed WCEnKF, we compare its results with the standard EnKF for predicting water storages. Then, in Section 4.3, we analyze the assimilation results and the performance of the proposed filter in enforcing the balance between water fluxes, e.g., we assess the behaviour of the filters in dealing with water balance problem.

4.1. Error Sensitivity analysis

We first analyze the effects of the different datasets, i.e., both the GRACE TWS and pseudo-observations on the filter estimates. The incorporation of the pseudo-observations in the second update step of the filter modifies the contribution of GRACE TWS data on the state estimations. As such, the three different covariance error matrices (cf. Section 3.3) of $\mathbf{p}, \mathbf{e}$, and $\mathbf{q}$ would cause that both the GRACE TWS and pseudo-observations contribute differently. For each grid point, we calculate the correlations between the filter estimations of TWS and the water fluxes $\mathbf{p}, \mathbf{e}$, and $\mathbf{q}$ as well as the assimilated GRACE TWS data. The results along with the average imbalance errors (from the water balance equation) are presented in Table 2. It can be seen that applying the first case with minimum error values, as it is expected, leads to a higher correlation between the filter estimates and other water fluxes. The least imbalance error is also achieved in this case. However, in general, increasing the impact of water fluxes in the second step of the filter decreases the correlation between the estimates and GRACE TWS data. This suggests, as we expected, a trade-off between the effects of observations in the first and second step of the filter according to the values of Σ. In the third scenario, for example, applying pseudo-observations with larger errors leads to smaller correlations with the water flux observations and larger correlation to the GRACE TWS data. Note that we also applied a similar test for $\mathbf{p}, \mathbf{e}$, and $\mathbf{q}$ with zero error (such that CEnKF), which resulted in the least imbalance error. Nevertheless, this case leads to larger errors compared to groundwater measurements compared with the three scenarios above. Therefore, hereafter, we only present the results associated with the second scenario (with no additional errors on those that are initially assumed). This case is found to lead to better results when groundwater estimates from each scenario are compared to independent groundwater in situ measurements (details in Section 4.2).

4.2. Assessment against in situ data

The estimated groundwater storage obtained from each filter is compared to the post-processed in situ measurements of groundwater changes (cf. Section 2.4) over the Mississippi Basin and Murray-Darling Basin. To this end, the estimated groundwater storages, as well as model-free run (without data assimilation) are spatially interpolated to the location of the in situ measurements using the nearest neighbour (the closest four grid values). The groundwater misfits (errors) between the in situ measurements and those of the EnKF and WCEnKF are then computed. Figs. 4 and 5 plot the resulting bias, namely, differences between groundwater estimated by the filters and in situ measurements, and STD (of the calculated differences) for the Mississippi Basin and Murray-Darling Basin, respectively.

For both basins, the estimated biases are significantly decreased when the proposed WCEnKF filter is applied. The average estimated bias using WCEnKF is 23.14 mm for the Mississippi Basin and 26.89 mm for the Murray-Darling Basin, indicating an average of 22.10% and 26.38% bias improvements compared to the EnKF. Despite this, we found that the correlation between the filters' estimated groundwater and in situ groundwater time series are large for both basins. An average of 0.76 (at 95% confidence interval) for both basins is achieved, which means that assimilating only GRACE data (as in the EnKF) is good for estimating annual and inter-annual variations, but not enough to accurately recover their amplitudes. The error reduction using WCEnKF is also noticeable in the STD. WCEnKF decreases the uncertainties in the Mississippi Basin and Murray-Darling Basin by 48.87% and 35.19%, respectively.

For every grid point within each basin, we calculate the Root-Mean-Squared Error (RMSE) and also the correlation between in situ measurements and filters results. Note that cross-correlation is applied to account for lag differences between the time series. We further undertake a significance test for the correlation coefficients using t-distribution. The estimated t-value and the distribution at 0.05 significant level are then used to calculate a p-value. The calculated p-values for the correlations in Table 3 lie under 5% indicating coefficients are significant. Table 3 summarizes these results. The Assimilation of the GRACE data using WCEnKF increases the correlation from 0.72 (EnKF) to 0.84 over the Mississippi Basin and from 0.68 to 0.79 for the Murray-Darling Basin. While both filters significantly improve groundwater estimates with respect to model-free run (48.13 on average), the larger RMSE improvements of 15.02% and 16.71% for the Mississippi Basin and the Murray-Darling Basin, respectively, suggest the enhancement gained from the proposed two-updates filter against the one-update filter.

Furthermore, two analyses are undertaken on the forecast steps to investigate which filter is more efficient in keeping observations effects within the system states. Generally, a filter with better forecasts can perform better during an experiment. We calculate average RMSE of groundwater estimates at forecast steps for the Mississippi and Murray-Darling Basins and compare them with those of model-free run (Table 4). It can be seen that both filters reduced RMSE values, while WCEnKF outperforms the EnKF scheme (approximately 12%). We also compute correlations between TWS forecast estimates, both by filters and model-free, and water fluxes (i.e., $\mathbf{p}, \mathbf{e}$, and $\mathbf{q}$). A similar analysis as Table 3 is done to control the significance of correlation coefficients. Average correlations over the basins of Amazon, Indus, Mississippi, Orange,

Table 2
Average correlations and errors between the water storages estimated by WCEnKF and water fluxes observations of $\mathbf{p}, \mathbf{e}$ and $\mathbf{q}$ as well as GRACE TWS data considering three different error values used in the data assimilation process. "Ref" in table refers to the *reference errors* (described in Section 3.3).

Error level	Correlation				Imbalance error (mm)
	p	**e**	**q**	GRACE TWS	
(1) Ref − 5%(observation)	0.78	0.83	0.76	0.77	12.05
(2) Ref + 0%(observation)	0.65	0.72	0.69	0.84	18.31
(3) Ref + 5%(observation)	0.61	0.63	0.58	0.89	37.24

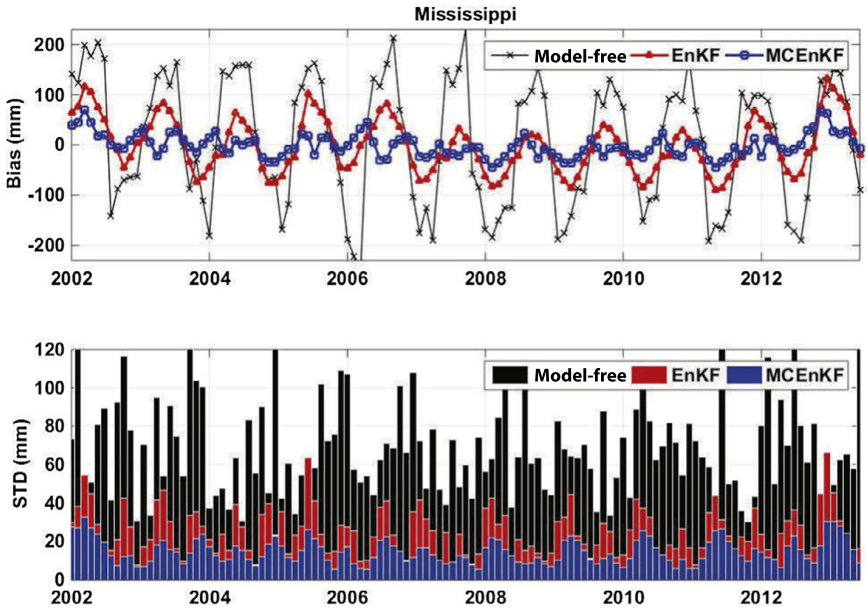

Fig. 4. Average bias and STD of the groundwater results from the EnKF and WCEnKF data assimilation filters over the Mississippi Basin with respect to the in situ groundwater measurements.

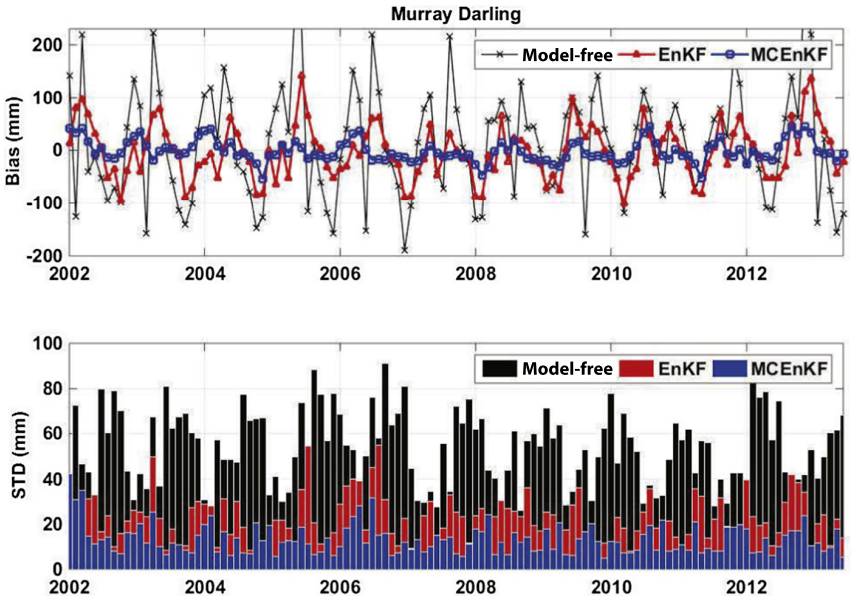

Fig. 5. Average bias and STD of the groundwater results from the EnKF and WCEnKF data assimilation filter over the Murray-Darling Basin with respect to the in situ groundwater measurements.

Table 3
Summary of the evaluation results from each filter and model-free run against the groundwater in situ measurements over the Mississippi Basin and Murray-Darling Basin. For each case the RMSE average and its range (±XX) at the 95% confidence interval is presented.

Method	Mississippi Basin		Murray-Darling Basin	
	RMSE (mm)	Correlation	RMSE (mm)	Correlation
EnKF	56.74 ± 6.12	0.72	41.58 ± 6.48	0.68
Improvement (%) regarding model-free	38.41	36.11	48.96	47.06
WCEnKF	48.22 ± 5.63	0.84	34.63 ± 5.27	0.79
Improvement (%) regarding model-free	47.66	45.23	57.49	54.43
Improvement (%) regarding EnKF	15.02	14.28	16.71	13.92

Table 4
Average RMSE results (with their ranges ±XX at the 95% confidence) by each filter at forecast steps and model-free run compared to the groundwater in situ measurements over the Mississippi Basin and Murray-Darling Basin. Table also contains correlations between TWS estimated by the methods at forecast steps and water fluxes.

Method	RMSE (mm)		Correlation		
	Mississippi Basin	Murray-Darling Basin	**p**	**e**	**q**
Model-free	92.13 ± 12.39	81.46 ± 10.67	0.95	0.86	0.83
EnKF	74.53 ± 8.82	62.71 ± 9.25	0.56	0.53	0.49
WCEnKF	65.48 ± 7.18	47.91 ± 7.95	0.94	0.82	0.85

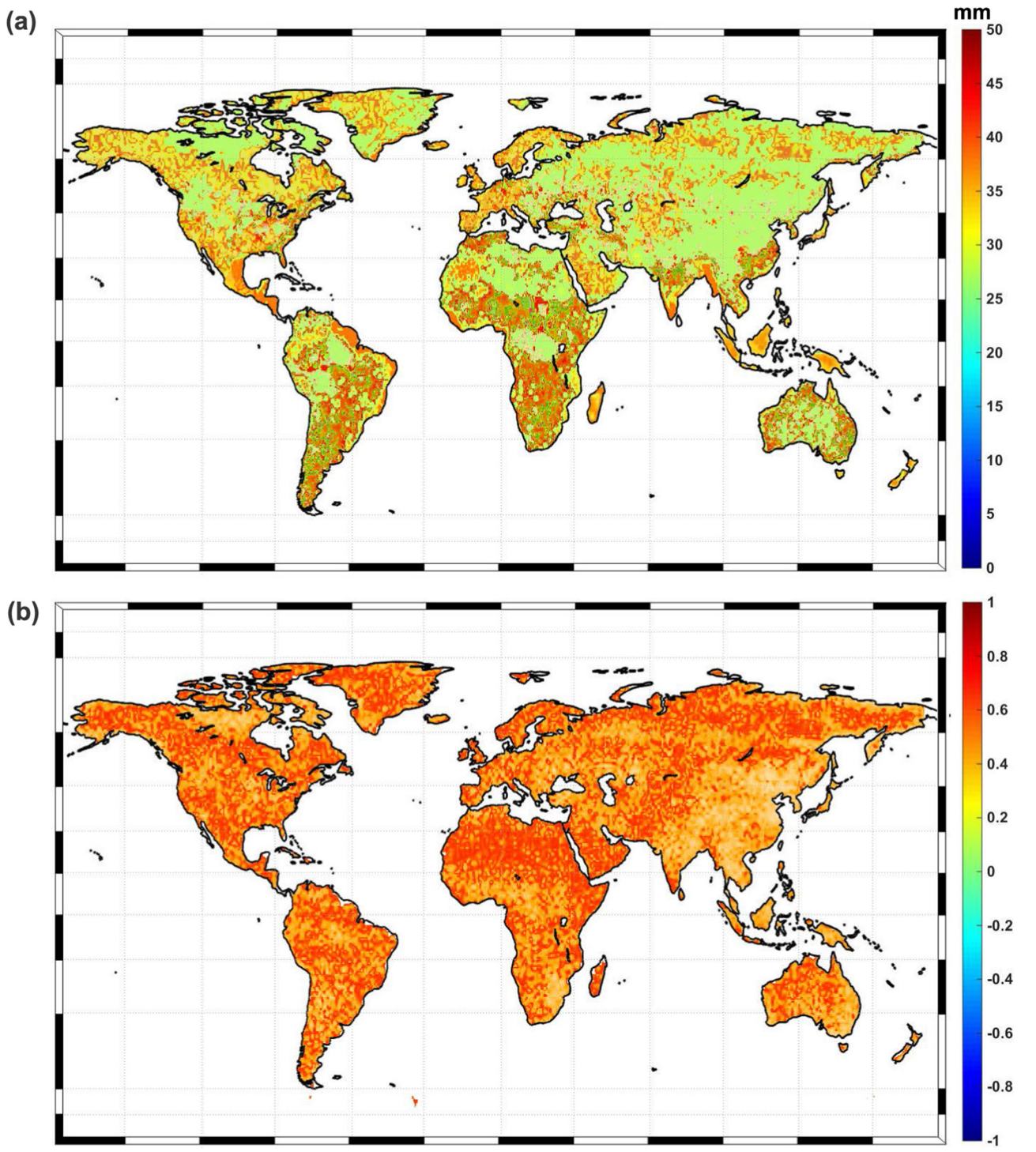

Fig. 6. (a), Temporal average of misfits between the summation of TWS from WCEnKF and the GRACE TWS time series at each grid point, and (b), The correlation between the two TWS time series.

Danube, St. Lawrence, Murray-Darling, and the Yangtze (cf. Fig. 1) are listed in Table 4. Based on the correlation values, it is evident that WCEnKF achieves larger correlations with respect to the EnKF. The proposed filter obtains improved agreement between the assimilation results and the fluxes.

Furthermore, to statistically investigate the difference between average correlation values, ANOVA (analysis of variance; Nelson, 1983; Ullman, 1989) method is applied. The method shows how mean values are different. For every flux correlation, the null hypothesis is that the average correlation for the model-free, EnKF, and WCEnKF are equal. ANOVA tests the above hypothesis at 0.05 significance level. Our experiment indicates that the means are not equal, thus, ANOVA in the second step determines which correlations are different (to the level of significance). After implementing the later step, the EnKF result demonstrates a significantly larger difference from the model-free and WCEnKF. In sum, Table 4 shows that WCEnKF successfully assimilates data sets into the system, which also leads to a better forecast.

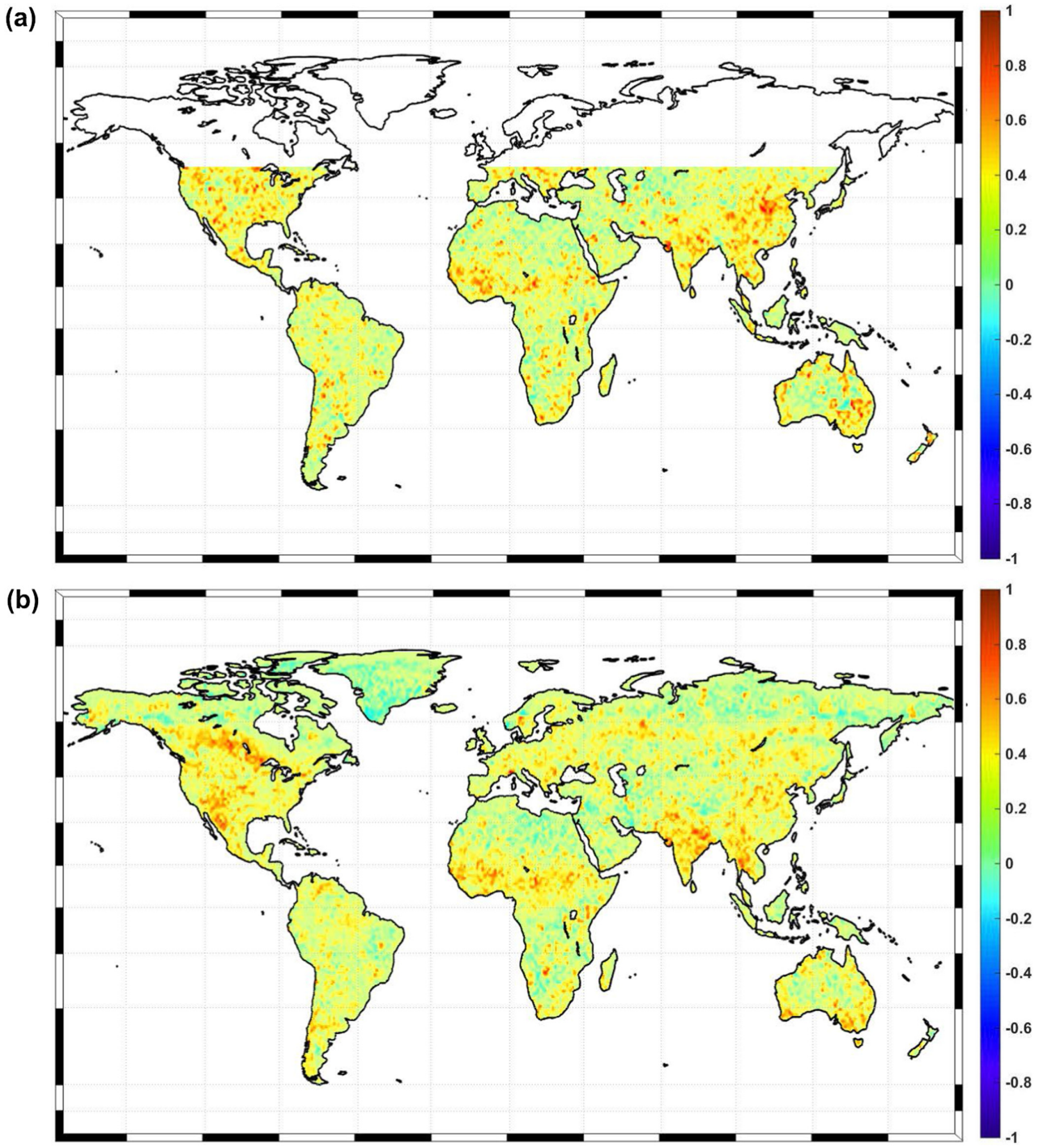

Fig. 7. Correlation between the data assimilation results and **p** (a) and **e** (b) time series at each grid point.

4.3. Water balance enforcement

In the following, we analyze the results of the filter estimates using the second scenario from Section 4.1 in terms of their relationship to the observations and more importantly water budget closure. Fig. 6 shows the results for the comparison between the assimilation results and GRACE TWS data. For each grid point, we calculate the average discrepancy and correlation between the two TWS time series. Results indicate that the error between the model and GRACE data is about 26 mm, which is 69% less than those resulting from the free-run (model runs without assimilation) and 13% higher than data assimilation results using the (one-update) EnKF scheme. This means that the application of the second update step, in some cases, decreases the effects of GRACE data by enforcing the balance between water fluxes. Fig. 6b, in general, suggests a high correlation between the filter estimates and observations. Nevertheless, again, smaller correlations are found in places with a denser discharge stations corresponding to better imbalance control (e.g., central to northern of Asia). Much smaller correlations are observed between GRACE TWS and the model-only results (0.47 on average). Nevertheless, the EnKF provides 11% higher correlation to observations. This is due to the effects of the second update step of the proposed filter.

The above results could be explained by the correlations between the filter estimates and two water fluxes data, i.e., precipitation and evaporation. Indeed, as one can see in Fig. 7, the locations where a high correlation is achieved, are places where the second step of the filter affects more due to the availability of discharge data (cf. Fig. 1). Approximately 33% and 44% larger correlation coefficients for **p** and **e**, respectively, are achieved in the areas where water balance adjustment is used compared with other areas. This illustrates that forcing water balance condition into the assimilation process increases the agreement between model outputs and other water fluxes on the one hand, and may change the effects of the GRACE data on the model on the other hand.

The average imbalance at each grid point is plotted in Fig. 8. The figure clearly demonstrates how the water budget enforcement spatially influences the imbalance between Δs and fluxes. It can be seen that wherever a dense network of water discharge stations exists (cf. Fig. 1), e.g., North America, Southeast Asia, and West Australia, a smaller imbalance between all compartments occurs. For other areas, the imbalance is much larger because the second analysis step of WCEnKF cannot be applied due to the lack of discharge data and the method simply performs as the EnKF. Therefore, this highlights the effect of the second step of WCEnKF in dealing with imbalances. This confirms the previous results that

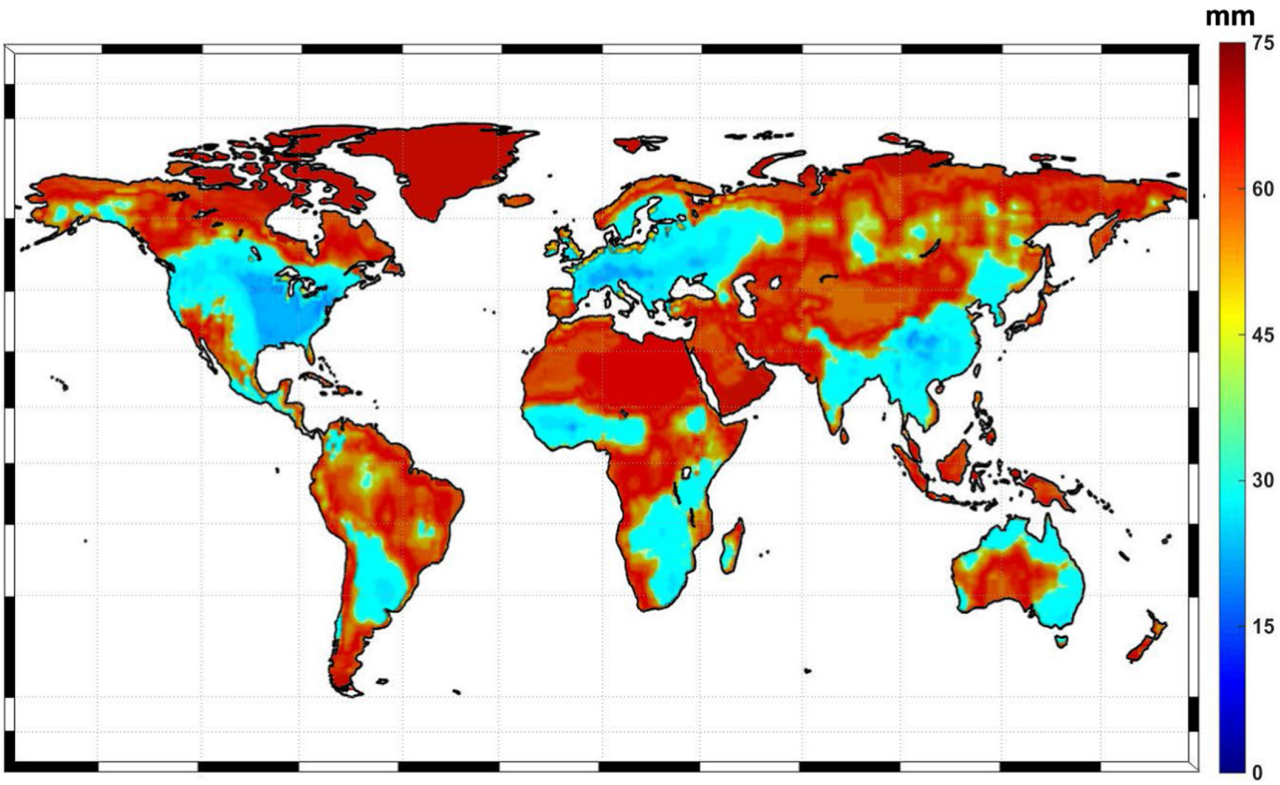

Fig. 8. Temporal average of imbalance errors.

Table 5
Average correlation between the assimilation results (summation of water storages) and the data of **p**, **e** and **q**. The average imbalance errors provided by each filtering method are also indicated.

Method	Correlation			Imbalance error (mm)
	p	**e**	**q**	
EnKF	0.32	0.28	0.24	62.17
WCEnKF	0.65	0.72	0.69	18.31
Improvement (%)	50.76	61.11	65.21	70.55

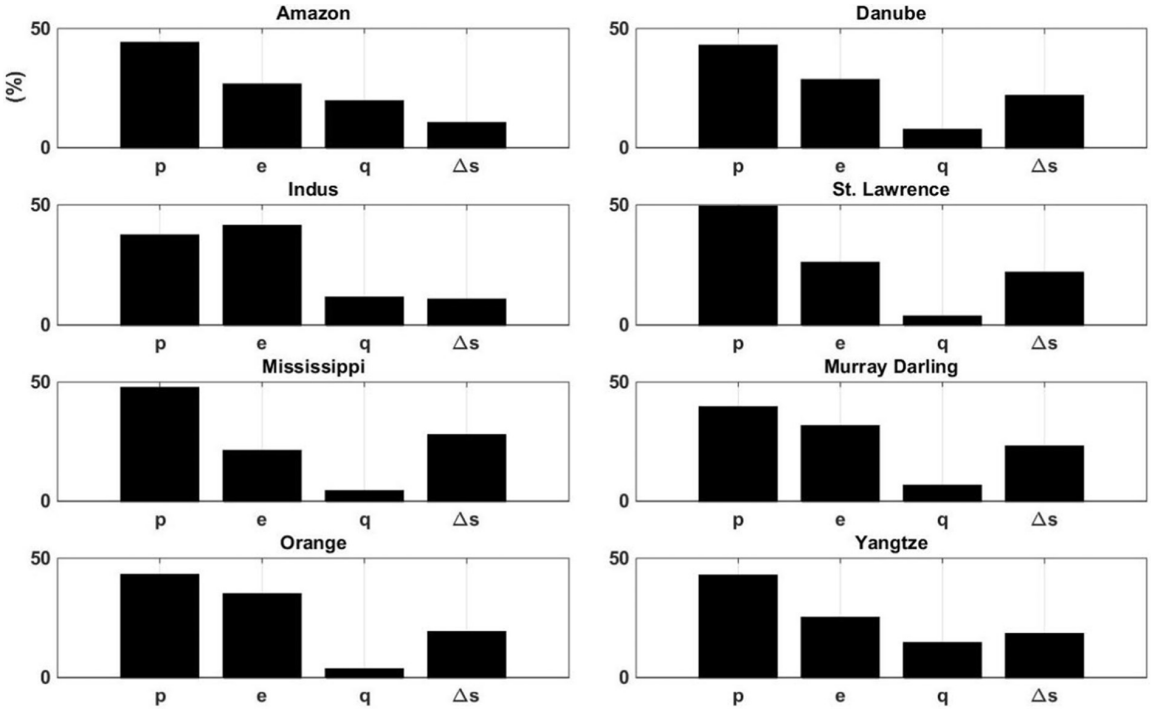

Fig. 9. Contributions of each water flux in water budget closure over different basins.

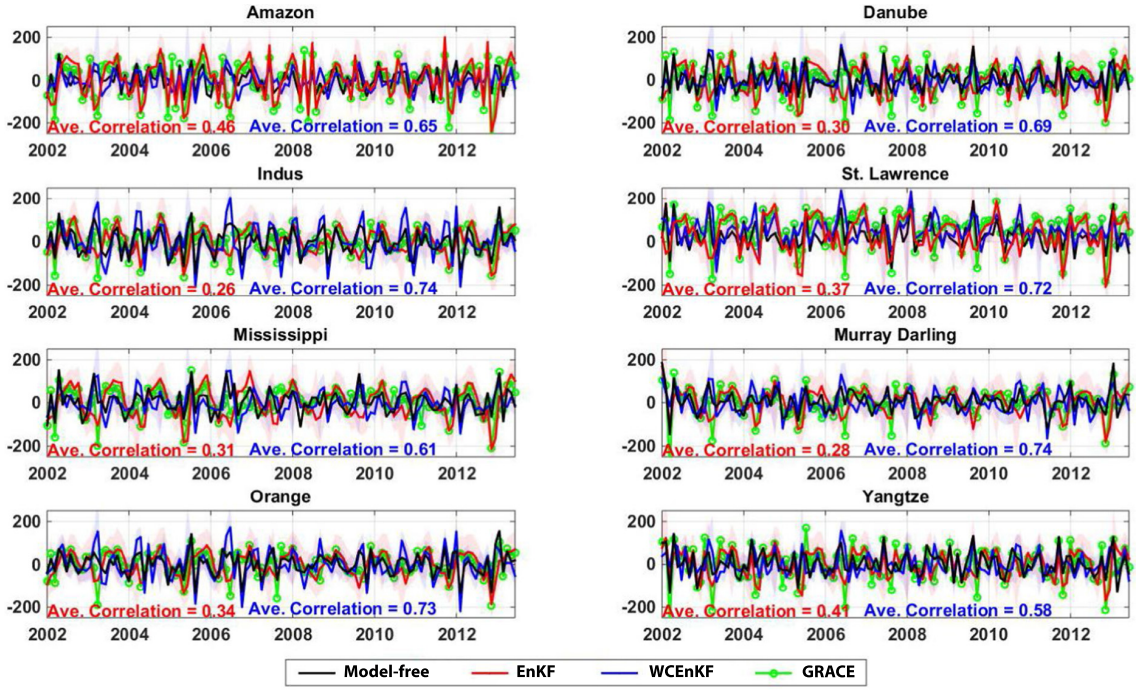

Fig. 10. Spatial average time series of **Δs** from each filter over different basins (units are mm). Shaded areas represent ensemble spreads of water storage change time series. Correlation values of WCEnKF and EnKF are depicted on the figure.

the second update step in WCEnKF increases the agreement between the assimilation outputs and the water fluxes, which results in water imbalance decreases.

Table 5 summarizes the average correlations between the estimated TWS data and water fluxes, **p**, **e** and **q**, and the average estimated imbalance errors as suggested by the EnKF and WCEnKF. Note that we only compare the filters' performances over the points in which discharge data is available. WCEnKF successfully increases the correlation between the results and water variables of **p**, **e** and **q** with average improvements of 33%, 44%, and 45%,

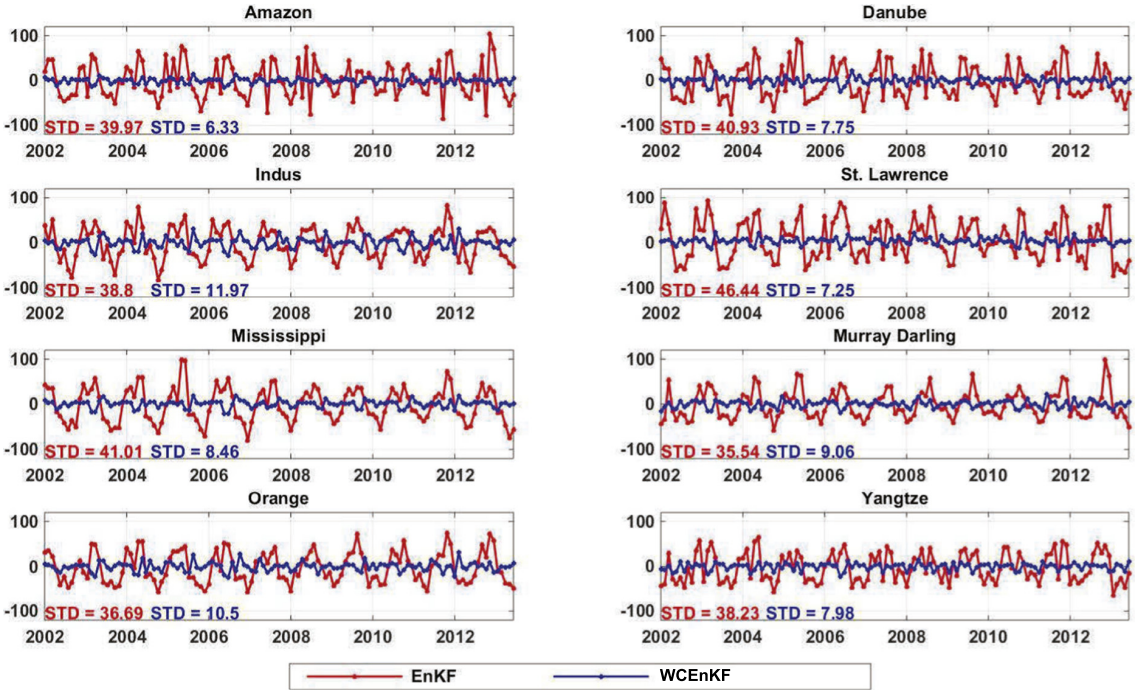

Fig. 11. Average imbalance error time series calculated using the EnKF and WCEnKF filters for each basin (units are mm).

respectively. This leads to a significant imbalance reduction of approximately 82% (suggesting an error of 18.31 mm compared to 62.17 mm for the EnKF).

Next, in order to further investigate the data assimilation results, we focus on the major basins of Amazon, Indus, Mississippi, Orange, Danube, St. Lawrence, Murray-Darling, and the Yangtze (cf. Fig. 1). Due to variability of various water fluxes over different areas, these have different characteristics and behaviors with various contributions through the second update of the filter (Fig. 9). Fig. 9 illustrates the contribution of each water flux in the water budget closure of the basins. This shows how each variable incorporates in the water balance equation differently over each basin. Generally the larger contributions are found for **p** and **e** for all basins. **q** has a larger contribution over the Amazon Basin and relatively small impacts on the Orange Basin and St. Lawrence Basin. The estimated water storage change ($\Delta\mathbf{s}$) effects, however, vary significantly between the basins. It is shown in Fig. 9 that $\Delta\mathbf{s}$ has larger influences over Mississippi, Danube, and Murray-Darling Basins. The share of $\Delta\mathbf{s}$ in each basin is affected by incorporating $\mathbf{p}, \mathbf{e}$ and **q** into the second step of WCEnKF, which is significantly different from the one estimated by the EnKF.

Fig. 10 presents the average $\Delta\mathbf{s}$ as they result from the EnKF and WCEnKF over each basin. It can be seen that the application of water balance adjustment in the filtering process results in a considerable difference between the estimated TWSs. The larger correlations between the two solutions in the Mississippi Basin (0.50) and St. Lawrence Basin (0.47) indicate less influence of the water budget constraint in these basins. However, the weak agreements between the EnKF and WCEnKF results, with about 0.34 correlation on average, suggest a large impact of water balance enforcement on the process. This remarkable difference is expected to have a large effect on imbalance issue for each basin (Fig. 11).

The spatial average time series of imbalance between Δs and fluxes for each basin are shown in Fig. 11 for the EnKF and WCEnKF. In all the cases, the new filter successfully decreases the imbalance in comparison to the EnKF. The EnKF results in larger water balance problem in the Mississippi and Danube basins, while the proposed WCEnKF suggests the best performances over these two basins with average imbalance reductions of 87% and 84%, respectively. We also compute the standard deviation (STD) of each time series (cf. Fig. 11). The large range of calculated STD in the EnKF (10.9 mm) is reduced to 5.64 mm by applying WCEnKF. Furthermore, the proposed filter appropriately improves disagreement between all compartments, both in terms of magnitudes and STDs. Fig. 11 further suggests the importance of implementing the water balance adjustment. The absolute (average) imbalance without using this approach is 67.08 mm, and a large part of it is directly connected to the estimated TWS. The WCEnKF data assimilation decreases this value to approximately 14.45 mm, which leads to both better estimation of TWS and higher agreement with the other water fluxes.

5. Summary and conclusions

GRACE TWS data are assimilated into W3RA covering 2002–2012 to improve model outputs and satisfy the terrestrial water budget balance. For that purpose, we propose a two-update weak constrained EnKF (WCEnKF) scheme that enforces water budget closure using the water fluxes. WCEnKF shows a good performance in integrating GRACE TWS data into the system (first update) and constraining the water balance equation (second update). Larger correlations in terms of groundwater estimates are found between assimilation results using the two-update filter (14.10% average) and ground-based observations, compared with those of the model-free. We also achieve 21.12% (on average) groundwater RMSE reductions using WCEnKF compared with EnKF. The application of the proposed filter shows an ability in imposing the water budget closure constraint as demonstrated by higher correlation of the estimated TWS changes to the $\mathbf{p}, \mathbf{e}$, and **q** (0.33, 0.44, and 0.45, respectively), as well as an imbalance reduction, i.e., from 62.17 mm using the traditional EnKF, to 18.31 mm (82.53% improvement).

There are some key factors that affect the performance of WCEnKF. Most importantly errors associated with pseudo-observations can largely alter the results. It is very difficult to achieve spatio-temporal variations of error characteristics of each water budget component. This study assesses three different error scenarios and investigates their impact on the results. However, the assumptions that are made, especially using a fixed uncertainty, might be inappropriate or sometimes strong since various data sets have performed differently within different areas. Therefore, more investigations are still needed to fully assess the filter's capability in terms of data uncertainties, applying multiple data sets for each variable (e.g., $\mathbf{p}, \mathbf{e}$), and using other types of observations such as soil moisture for data assimilation.

Acknowledgements

We would like to thank Dr. Natthachet Tangdamrongsub for his useful comments, which contributed to the improvement of this study. M. Khaki is grateful for the research grant of Curtin International Postgraduate Research Scholarships (CIPRS)/ORD Scholarship provided by Curtin University (Australia). This work is a TIGeR publication.

Appendix A. Some useful properties of random sampling

Property 1 (Hierarchical sampling; Robert, 2006). Assuming that one can sample from $p(\mathbf{x}_1)$ and $p(\mathbf{x}_2|\mathbf{x}_1)$, then a sample, $\mathbf{x}_2^*$, from $p(\mathbf{x}_2)$ can be generated by drawing $\mathbf{x}_1^*$ from $p(\mathbf{x}_1)$ and then $\mathbf{x}_2^*$ from $p(\mathbf{x}_2|\mathbf{x}_1^*)$.

Property 2 (Conditional sampling; Hoffman and Ribak, 1991). Consider a Gaussian pdf, $p(\mathbf{x}, \mathbf{y})$, with $\mathbf{P}_{xy}$ and $\mathbf{P}_y$ denoting the cross-covariance of $\mathbf{x}$ and $\mathbf{y}$ and the covariance of $\mathbf{y}$, respectively. Then a sample, $\mathbf{x}^*$, from $p(\mathbf{x}|\mathbf{y})$, can be generated as, $\mathbf{x}^* = \widetilde{\mathbf{x}} + \mathbf{P}_{xy}\mathbf{P}_y^{-1}[\mathbf{y} - \widetilde{\mathbf{y}}]$, where $(\widetilde{\mathbf{x}}, \widetilde{\mathbf{y}}) \sim p(\mathbf{x}, \mathbf{y})$.

Appendix B. Derivation of the WCEnKF algorithm

The Eq. (12), which computes the forecast ensemble $\{\mathbf{x}_t^{f,(i)}\}_{i=1}^n$ from the previous analysis one, is obtained by applying Prop. 1 above to the forecast step (6). Regarding the first update step (with $\mathbf{y}_t$), one first applies Prop. 1 on the following formula,

$$p(\mathbf{y}_t|\mathbf{r}_{0:t-1}) = \int \underbrace{p(\mathbf{y}_t|\mathbf{x}_t)}_{\mathcal{N}(\mathbf{H}_t\mathbf{x}_t, \mathbf{R}_t)} p(\mathbf{x}_t|\mathbf{r}_{0:t-1}) d\mathbf{x}_t,$$

to sample the observation forecast ensemble, $\left\{\mathbf{y}_t^{f,(i)}\right\}_{i=1}^n$, as in Eq. (13). Prop. 2 is then used in Eq. (7) to obtain the ensembles $\{\tilde{\mathbf{x}}_t^{a,(i)}\}_{i=1}^n$ (Eq. (14)) and $\{\mathbf{x}_{t-1}^{s,(i)}\}_{i=1}^n$, respectively. For the second update step (with $\mathbf{z}_t$), one first uses Prop. 1 in Eq. (11), with $p(\mathbf{z}_t|\mathbf{x}_t, \mathbf{x}_{t-1}) \overset{(4)}{=} \mathcal{N}(\mathbf{G}\mathbf{x}_t + \mathbf{L}\mathbf{x}_{t-1}, \boldsymbol{\Sigma}_t)$, to obtain the pseudo-observation forecast ensemble $\{\mathbf{z}_t^{f,(i)}\}_{i=1}^n$ (Eq. (18)), then Prop. 2 in Eq. (10) to compute the state analysis ensemble $\{\mathbf{x}_t^{a,(i)}\}_{i=1}^n$ (Eq. (19)).

References

Aires, F., 2014. Combining datasets of satellite retrieved products. Part I: Methodology and water budget closure. J. Hydrometeorol. 15 (4), 16771691.

Ait-El-Fquih, B., El Gharamti, M., Hoteit, I., 2016. A Bayesian consistent dual ensemble Kalman filter for state-parameter estimation in subsurface hydrology. Hydrol. Earth Syst. Sci. 20, 3289–3307. https://doi.org/10.5194/hess-20-3289-2016.

Ait-El-Fquih, B., Hoteit, I., 2016. A variational bayesian multiple particle filtering scheme for large-dimensional systems, in: IEEE Transactions on Signal Processing, vol. 64, no. 20, pp. 5409–5422. https://doi.org/10.1109/TSP.2016.2580524.

Alsdorf, D.E., Rodriguez, E., Lettenmaier, D.P., 2007. Measuring surface water from space. Rev. Geophys. 45, RG2002. https://doi.org/10.1029/2006RG000197.

Anderson, M.C., Norman, J.M., Mecikalski, J.R., Otkin, J.A., Kustas, W.P., 2007. A climatological study of evapotranspiration and moisture stress across the continental United States based on thermal remote sensing: 1. Model formulation. J. Geophys. Res. 112 (D10117). https://doi.org/10.1029/2006JD007506.

Bergemann, K., Reich, S., 2010. A mollified ensemble Kalman filter. Q. J. R. Meteorol. Soc. 136, 16361643. https://doi.org/10.1002/qj.672.

Bertino, L., Evensen G., Wackernagel, H., 2003. Sequential Data Assimilation Techniques in Oceanography, International Statistical Review, vol. 71, No. 2 (Aug., 2003). pp. 223–241.

Boyer, J.F., Dieulin, C., Rouchie, N., Cres, A., Servat, E., Paturel, J.E., Mahe, G., 2006. SIEREM an environmental information system for water resources. 5th World FRIEND Conference, La Havana – Cuba, November 2006 in Climate Variability and Change Hydrological Impacts IAHS 590 Publ. 308. pp. 19–25.

Brocca, L., Melone, F., Moramarco, T., Wagner, W., Naeimi, V., Bartalis, Z., Hasenauer, S., 2010. Improving runoff prediction through the assimilation of the ASCAT soil moisture product. Hydrol. Earth Syst. Sci. 14, 18811893. https://doi.org/10.5194/hess-14-1881-2010.

Cheng, M.K., Tapley, B.D., 2004. Variations in the Earth's oblateness during the past 28 years. J. Geophys. Rese. Solid Earth 109, B09402. https://doi.org/10.1029/2004JB003028.

Chiew, F.H.S., Stewardson, M.J., McMahon, T.A., 1993. Comparison of six rainfall-runoff modelling approaches. J. Hydrol. 147, 136.

Döll, P., Kaspar, F., Lehner, B., 2003. A global hydrological model for deriving water availability indicators: model tuning and validation. J. Hydrol. 270, 105134.

Eicker, A., Schumacher, M., Kusche, J., Dll, P., Mller-Schmied, H., 2014. Calibration/data assimilation approach for integrating GRACE data into the WaterGAP global hydrology model (WGHM) using an ensemble Kalman filter: first results. SurvGeophys 35 (6), 12851309. https://doi.org/10.1007/s10712-014-9309-8.

Eicker, A., Forootan, E., Springer, A., Longuevergne, L., Kusche, J., 2016. Does GRACE see the terrestrial water cycle intensifying? J. Geophys. Res. Atmos. 121, 733745. https://doi.org/10.1002/2015JD023808.

Evensen, G., 1994. Sequential data assimilation with a nonlinear quasi-geostrophic model using Monte Carlo methods to forecast error statistics. J. Geophys. Res. 99, 10143–10162.

Evensen, G., 2003. The ensemble Kalman filter: theoretical formulation and practical implementation. Ocean Dyn. 53, 343367. https://doi.org/10.1007/s10236-003-0036-9.

Forootan, E., Didova, O., Schumacher, M., Kusche, J., Elsaka, B., 2014. Comparisons of atmospheric mass variations derived from ECMWF reanalysis and operational fields, over 2003 to 2011. J. Geodesy 88, 503–514. https://doi.org/10.1007/s00190-014-0696-x.

Gharamti, M.E., Valstar, J., Janssen, G., Marsman, A., Hoteit, I., 2016. On the efficiency of the hybrid and the exact second-order sampling formulations of the EnKF: a reality-inspired 3-D test case for estimating biodegradation rates of chlorinated hydrocarbons at the port of Rotterdam. Hydrol. Earth Syst. Sci. 20 (4561–4583), 2016. https://doi.org/10.5194/hess-20-4561-2016.

Giustarini, L., Matgen, P., Hostache, R., Montanari, M., Plaza, D., Pauwels, V.R.N., De Lannoy, G.J.M., De Keyser, R., Pfister, L., Hoffmann, L., Savenije, H.H.G., 2011. Assimilating SAR-derived water level data into a hydraulic model: a case study. Hydrol. Earth Syst. Sci. 15, 23492365. https://doi.org/10.5194/hess-15-2349-2011.

Gutentag, E.D., Heimes, F.J., Krothe, N.C., Luckey, R.R., Weeks, J.B., 1984. Geohydrology of the High Plains aquifer in parts of Colorado, Kansas, Nebraska, New Mexico, Oklahoma, South Dakota, Texas, and Wyoming, U.S. Geol. Surv. Prof. Pap., 1400-B. 66 pp.

Hamill, T.M., Snyder, C., 2002. Using improved background-error covariances from an ensemble Kalman filter for adaptive observations. Mon. Weather Rev. 130, 15521572. 10.1175/1520-0493(2002) 1301552:UIBECF2.0.CO;2.

Henck, A.H., Montgomery, D.R., Huntington, K.W., Liang, C., 2010. Monsoon control of effective discharge, Yunnan and Tibet. Geology 38, 975–978.

Hoffman, Y., Ribak, E., 1991. Constrained realizations of Gaussian fields – a simple algorithm. Astrophys. J. Part 380, L5–L8. ISSN 0004-637X.

Hoteit, I., Luo, X., Pham, D.T., 2012. Particle Kalman filtering: a nonlinear bayesian framework for ensemble Kalman filters. Mon. Weather Rev. 140 (2), 528–542.

Hoteit, I., Pham, D.T., Gharamti, M.E., Luo, X., 2015. Mitigating observation perturbation sampling errors in the stochastic EnKF. Mon. Weather Rev. 143 (7), 2918–2936.

Huffman, G., Adler, R., Arkin, P., Chang, A., Ferraro, R., Gruber, A., Janowiak, J., McNab, A., Rudolf, B., Schneider, U., 1997. The Global Precipitation Climatology Project (GPCP) combined precipitation dataset. Bull. Amer. Meteor. Soc. 78, 520. https://doi.org/10.1175/1520-0477(1997) 078*0005:TGPCPG*2.0.CO;2.

Huffman, G.J., Adler, R.F., Bolvin, D.T., Gu, G., Nelkin, E.J., Bowman, K.P., Hong, Y., Stocker, E.F., Wolff, D.B., 2007. The TRMM multi-satellite precipitation analysis: quasi- global, multi-year, combined-sensor precipitation estimates at fine scale. J. Hydrometeor. 8 (1), 38–55.

Huntington, T.G., 2006. Evidence for intensification of the global water cycle: review and synthesis. J. Hydrol. 319 (14), 8395. https://doi.org/10.1016/j.jhydrol.2005.07.003.

Jones, D.A., Wang, W., Fawcett, R., Grant, I., 2007. Climate data for the Australian water availability project. In: Australian Water Availability Project Milestone Report. Bur. Met., Australia, 37pp.

Khaki, M., Hoteit, I., Kuhn, M., Awange, J., Forootan, E., van Dijk, A.I.J.M., Schumacher, M., Pattiaratchi, C., 2017a. Assessing sequential data assimilation

techniques for integrating GRACE data into a hydrological model. Adv. Water Resour. 107, 301–316. https://doi.org/10.1016/j.advwatres.2017.07.001. ISSN 0309-1708.
Khaki, M., Schumacher, M., Forootan, J., Kuhn, M., Awange, E., van Dijk, A.I.J.M., 2017b. Accounting for spatial correlation errors in the assimilation of GRACE into hydrological models through localization. Adv. Water Resour. 5. https://doi.org/10.1016/j.advwatres.2017.07.024. Available online 1 August 2017, ISSN 0309-1708.
Kumar, S.V., Peters-Lidard, C.D., Santanello, J.A., Reichle, R.H., Draper, C.S., Koster, R. D., Nearing, G., Jasinski, M.F., 2015. Evaluating the utility of satellite soil moisture retrievals over irrigated areas and the ability of land data assimilation methods to correct for unmodeled processes. Hydrol. Earth Syst. Sci. 19, 4463–4478. https://doi.org/10.5194/hess-19-4463-2015.
Kusche, J., Schmidt, R., Petrovic, S., Rietbroek, R., 2009. Decorrelated GRACE time-variable gravity solutions by GFZ and their validation using a hydrological model. J. Geodesy. https://doi.org/10.1007/s00190-009-0308-3.
Liu, C., Xue, M., 2016. Relationships among four-dimensional hybrid ensemble variational data assimilation algorithms with full and approximate ensemble covariance localization. Mon. Weather Rev. 144, 591606. https://doi.org/10.1175/MWR-D-15-0203.1.
Liu, Y., Peters-Lidard, C.D., Kumar, S., Foster, J.L., Shaw, M., Tian, Y., Fall, G.M., 2013. Assimilating satellitebased snow depth and snow cover products for improving snow predictions in Alaska. Adv. Water Res. 54, 208227. https://doi.org/10.1016/j.advwatres.2013.02.005.
Mayer-Gürr, T., Zehentner, N., Klinger, B., Kvas, A., 2014. ITSG-Grace2014: a new GRACE gravity field release computed in Graz. In: GRACE Science Team Meeting (GSTM), Potsdam am: 29.09.2014.
McLaughlin, D., 2002. An integrate approach to hydrologic data assimilation: interpolation, smoothing, and filtering. Adv. Water Resour. 25, 12751286.
Mu, Q., Heinsch, F.A., Zhao, M., Running, S.W., 2007. Development of a global evapotranspiration algorithm based on MODIS and global meteorology data. Remote Sens. Environ. 111, 519–536. https://doi.org/10.1016/j.rse.2007.04.015.
Mu, Q., Zhao, M., Running, S.W., 2011. Improvements to a MODIS global terrestrial evapotranspiration algorithm. Remote Sens. Environ. 115, 1781–1800.
Munier, S., Aires, F., Schlaffer, S., Prigent, C., Papa, F., et al., 2014. Combining datasets of satellite retrieved products for basin-scale water balance study. Part II: Evaluation on the Mississippi Basin and closure correction model. J. Geophys. Res. 119, 100–116.
Neal, J., Schumann, G., Bates, P., Buytaert, W., Matgen, P., Pappenberger, F., 2009. A data assimilation approach to discharge estimation from space. Hydrol. Process. 23, 36413649.
Nelson, P.R., 1983. A comparison of sample sizes for the analysis of means and the analysis of variance. J. Qual. Technol. 15, 3339.
Pan, M., Wood, E.F., 2006. Data assimilation for estimating the terrestrial water budget using a constrained ensemble Kalman filter. J. Hydrometeorol. 7 (3), 534547.
Pan, M., Sahoo, A.K., Troy, T.J., Vinukollu, R.K., Sheffield, J., Wood, E.F., 2012. Multisource estimation of long-term terrestrial water budget for major global river basins. J. Clim. 25 (9), 31913206.
Reichle, R.H., McLaughlin, D.B., Entekhabi, D., 2002. Hydrologic data assimilation with the ensemble Kalman filter. Mon. Weather Rev. 130, 103114. https://doi.org/10.1175/1520-0493(2002) 130*0103:HDAWTE*2.0.CO;2.
Renzullo, L.J., Van Dijk, A.I.J.M., Perraud, J.M., Collins, D., Henderson, B., Jin, H., Smith, A.B., McJannet, D.L., 2014. Continental satellite soil moisture data assimilation improves root-zone moisture analysis for water resources assessment. J. Hydrol. 519, 27472762. https://doi.org/10.1016/j.jhydrol.2014.08.008.
Roads, J. et al., 2003. GCIP water and energy budget synthesis (WEBS). J. Geophys. Res. 108, 8609. https://doi.org/10.1029/2002JD002583.
Robert, C., 2006. Le choix baysien. Springer-Verlag, Paris. ISSN 978-2-287-25173-3.
Rodell, M., Chen, J., Kato, H., Famiglietti, J.S., Nigro, J., Wilson, C.R., 2007. Estimating groundwater storage changes in the Mississippi River basin (USA) using GRACE. Hydrogeol. J. 15, 159166.
Sahoo, A.K., Pan, M., Troy, T.J., Vinukollu, R.K., Sheffield, J., Wood, E.F., 2011. Reconciling the global terrestrial water budget using satellite remote sensing. Remote Sens. Environ. 115 (8), 1850–1865.
Schmidt, A.H., Montgomery, D.R., Huntington, K.W., Liang, C., 2011. The Question of Communist Land Degradation: New Evidence from Local Erosion and Basin-Wide Sediment Yield in Southwest China and Southeast Tibet, Annals of the Association of American Geographers, First published on: 28 March 2011 (iFirst).
Schumacher, M., Kusche, J., Dll, P., 2016. A systematic impact assessment of GRACE error correlation on data assimilation in hydrological models. J. Geodesy. https://doi.org/10.1007/s00190-016-0892-y.
Seoane, L., Ramillien, G., Frappart, F., Leblanc, M., 2013. Regional GRACE-based estimates of water mass variations over Australia: validation and interpretation. Hydrol. Earth Syst. Sci. 17, 4925–4939. https://doi.org/10.5194/hess-17-4925-2013.
Sheffield, J., Goteti, G., Wood, E.F., 2006. Development of a 50-yearhigh-resolution global dataset of meteorological forcings for land surfacemodeling. J. Clim. 19 (13), 30883111.
Sheffield, J., Ferguson, C.R., Troy, T.J., Wood, E.F., McCabe, M.F., 2009. Closing the terrestrial water budget from satellite remote sensing. Geophys. Res. Lett. 26, L07403. https://doi.org/10.1029/2009GL037338.
Sokolov, A.A., Chapman, T.G., 1974. Methods for Water Balance Computation An International Guide for Research and Practice. The Unesco Press, Paris.
Smith, P.J., Dance, S.L., Nichols, N.K., 2011. A hybrid data assimilation scheme for model parameter estimation: application to morphodynamic modelling. Comput. Fluids 46, 436–441. https://doi.org/10.1016/j.compfluid.2011.01.010. ISSN 0045-7930.
Swenson, S., Chambers, D., Wahr, J., 2008. Estimating geocentervariations from a combination of GRACE and ocean model output. J. Geophys. Res. 113, B08410. https://doi.org/10.1029/2007JB005338.
Tangdamrongsub, N., Steele-Dunne, S.C., Gunter, B.C., Ditmar, P.G., Weerts, A.H., 2015. Data assimilation of GRACE terrestrial water storage estimates into a regional hydrological model of the Rhine River basin. Hydrol. Earth Syst. Sci. 19, 2079–2100. https://doi.org/10.5194/hess-19-2079-2015.
Tangdamrongsub, N., Steele-Dunne, S.C., Gunter, B.C., Ditmar, P.G., Sutanudjaja, E.H., Xie, T., Wang, Z., 2017. Improving estimates of water resources in a semi-arid region by assimilating GRACE data into the PCR-GLOBWB hydrological model. Hydrol. Earth Syst. Sci. 21, 2053–2074.
Tian, S., Tregoning, P., Renzullo, L.J., van Dijk, A.I.J.M., Walker, J.P., Pauwels, V.R.N., Allgeyer, S., 2017. Improved water balance component estimates through joint assimilation of GRACE water storage and SMOS soil moisture retrievals. Water Resour. Res. 53. https://doi.org/10.1002/2016WR019641.
Tregoning, P., McClusky, S., van Dijk, A.I.J.M., Crosbie, R.S., Pea-Arancibia, J.L., 2012. Assessment of GRACE Satellites for Groundwater Estimation in Australia. National Water Commission, Canberra, p. 82.
Tropical Rainfall Measuring Mission (TRMM), 2011. TRMM (TMPA/3B43) Rainfall Estimate L3 1 month 0.25 degree x 0.25 degree V7, Greenbelt, MD, Goddard Earth Sciences Data and Information Services Center (GES DISC), Accessed [Data Access Date] < https://disc.gsfc.nasa.gov/datacollection/TRMM3B437.html>.
Ullman, N.R., 1989. The Analysis of Means (ANOM) for signal and noise. J. Qual. Technol. 21, 111127.
van Dijk, A.I.J.M., 2010. The Australian Water Resources Assessment System: Technical Report 3, Landscape model (version 0.5) Technical Description, CSIRO: Water for a Healthy Country National Research Flagship.
van Dijk, A.I.J.M., Renzullo, L.J., Rodell, M., 2011. Use of Gravity Recovery and Climate Experiment terrestrial water storage retrievals to evaluate model estimates by the Australian water resources assessment system. Water Resour. Res. 47, W11524. https://doi.org/10.1029/2011WR010714.
van Dijk, A.I.J.M., Pea-Arancibia, J.L., Wood, E.F., Sheffield, J., Beck, H.E., 2013. Global analysis of seasonal streamflow predictability using an ensemble prediction system and observations from 6192 small catchments worldwide. Water Resour. Res. 49, 27292746. https://doi.org/10.1002/wrcr.20251.
van Dijk, A.I.J.M., Renzullo, L.J., Wada, Y., Tregoning, P., 2014. A global water cycle reanalysis (20032012) merging satellite gravimetry and altimetry observations with a hydrological multi-model ensemble. Hydrol. Earth Syst. Sci. 18, 29552973. https://doi.org/10.5194/hess-18-2955-2014.
Vrugt, J.A., ter Braak, C.J.F., Diks, C.G.H., Schoups, G., 2013. Advancing hydrologic data assimilation using particle Markov chain Monte Carlo simulation: theory, concepts and applications. Advances in Water Resources, Anniversary Issue – 35 Years, 51, 457–478, doi: 10.1016/j.advwatres.2012.04.002.
Wahr, J.M., Molenaar, M., Bryan, F., 1998. Time variability of the Earth's gravity field: hydrological and oceanic effects and their possible detection using GRACE. J. Geophys. Res. 108 (B12), 3020530229. https://doi.org/10.1029/98JB02844.
Wooldridge, S.A., Kalma, J.D., 2001. Regional-scale hydrological modelling using multiple-parameter landscape zones and a quasi-distributed water balance model. Hydrol. Earth Syst. Sci. 5, 59–74.
Zaitchik, B.F., Rodell, M., Reichle, R.H., 2008. Assimilation of GRACE terrestrial water storage data into a land surface model: results for the Mississippi River Basin. J. Hydrometeorol. 9 (3), 535548. https://doi.org/10.1175/2007JHM951.1.
Zhang, Y., Pan, M., Wood, E.F., 2016. On creating global gridded terrestrial water budget estimates from satellite remote sensing. Surveys Geophys. 37 (2), 249268.

Journal of Hydrology 564 (2018) 175–190

Contents lists available at ScienceDirect

Journal of Hydrology

journal homepage: www.elsevier.com/locate/jhydrol

Research papers

Unsupervised ensemble Kalman filtering with an uncertain constraint for land hydrological data assimilation

M. Khaki[a,b,*], B. Ait-El-Fquih[c], I. Hoteit[c], E. Forootan[d], J. Awange[a], M. Kuhn[a]

[a] School of Earth and Planetary Sciences, Discipline of Spatial Sciences, Curtin University, Perth, Australia
[b] School of Engineering, University of Newcastle, Callaghan, New South Wales, Australia
[c] King Abdullah University of Science and Technology (KAUST), Thuwal, Saudi Arabia
[d] School of Earth and Ocean Sciences, Cardiff University, Cardiff, UK

ARTICLE INFO

This manuscript was handled by G. Syme, Editor-in-Chief, with the assistance of Behzad Ataie-Ashtiani, Associate Editor

Keywords:
Constrained data assimilation
Ensemble Kalman Filter (EnKF)
Unsupervised Weak Constrained Ensemble Kalman Filter (UWCEnKF)
Water budget closure
Hydrological modeling

ABSTRACT

The standard ensemble data assimilation schemes often violate the dynamical balances of hydrological models, in particular, the fundamental water balance equation, which relates water storage and water flux changes. The present study aims at extending the recently introduced Weak Constrained Ensemble Kalman Filter (WCEnKF) to a more general framework, namely unsupervised WCEnKF (UWCEnKF), in which the covariance of the water balance model is no longer known, thus requiring its estimation along with the model state variables. This extension is introduced because WCEnKF was found to be strongly sensitive to the (manual) choice of this covariance. The proposed UWCEnKF, on the other hand, provides a more general unsupervised framework that does not impose any (manual, thus heuristic) value of this covariance, but suggests an estimation of it, from the observations, along with the state. The new approach is tested based on numerical experiments of assimilating Terrestrial Water Storage (TWS) from Gravity Recovery and Climate Experiment (GRACE) and remotely sensed soil moisture data into a hydrological model. The experiments are conducted over different river basins, comparing WCEnKF, UWCEnKF, and the standard EnKF. In this setup, the UWCEnKF constrains the system state variables with TWS changes, precipitation, evaporation, and discharge data to balance the summation of water storage simulations. In-situ groundwater and soil moisture measurements are used to validate the results of the UWCEnKF and to evaluate its performances against the EnKF. Our numerical results clearly suggest that the proposed framework provides more accurate estimates of groundwater storage changes and soil moisture than WCEnKF and EnKF over the different studied basins.

1. Introduction

Hydrological models play important roles in environmental studies and are crucial for hydrological applications. Due to a variety of factors, such as model structural errors, data deficiency, and uncertainty in inputs and parameters, the outputs of these models can be far from perfect. Data assimilation techniques offer a framework to improve the models simulations by constraining their outputs to the observations. However, the application of assimilation schemes could introduce an imbalance between water fluxes, namely precipitation $\mathbf{p}$, evaporation $\mathbf{e}$, discharge $\mathbf{q}$, and changes in water storage, $\Delta\mathbf{s}$, through the water balance equation $\Delta\mathbf{s} = \mathbf{p}-\mathbf{e}-\mathbf{q}$. The water balance equation is applied in land hydrological models to describe the relationships between these fluxes (Sokolov and Chapman, 1974). The model structure governs variations in the water state changes due to the incoming and outgoing hydrological water fluxes. Data assimilation of any water storages, e.g., soil moisture and/or terrestrial water storage (TWS), breaks the existing balance because the assimilated state does not satisfy the water balance property (Khaki et al., 2017).

Existing data assimilation methodologies under water budget enforcement rely on a "perfect observations" assumption in the closure constraint (e.g., Pan and Wood, 2006; Sahoo et al., 2011; Pan et al., 2012). For example, Pan and Wood (2006) proposed a constrained ensemble Kalman filter (CEnKF) that imposes regional water balance constraint to improve the filtering results. The CEnKF involves two successive EnKF-like updates. The first update uses the observations to update the state forecast, following an EnKF-like step, while the second update imposes the balance constraint via another EnKF-like correction, yet with a different form. Other studies have applied data merging algorithms along with the CEnKF (see, e.g., Sahoo et al., 2011; Pan et al., 2012; Zhang et al., 2016) to provide the flux datasets from various resources for water balance control. Although these improved datasets

* Corresponding author at: Department of Spatial Sciences, Curtin University, Perth, Australia.
E-mail address: Mehdi.Khaki@postgrad.curtin.edu.au (M. Khaki).

https://doi.org/10.1016/j.jhydrol.2018.06.080

Available online 05 July 2018

have resulted in better state estimates over different river basins by incorporating more accurate information about the constraints, the assumption of perfect observations is still problematic. This assumption leads to a strong constraint, which is unrealistic and may cause various issues. Simon and Chia (2002) suggested that even though it does not present any theoretical problems, the assumption can result in a singular covariance matrix, which in practice increases the possibility of numerical issues. Furthermore, by neglecting errors associated with flux observations, one can expect more estimation errors because of the strong water budget enforcement, which could also lead to over-fitting issues (Tangdamrongsub et al., 2017).

In a recent study, Khaki et al. (2017) proposed a new two-update ensemble Kalman-based scheme, a Weak Constrained Ensemble Kalman Filter (WCEnKF), that involves uncertainties in the water budget balance enforcement equation. Unlike previous studies (e.g., Pan and Wood, 2006; Sahoo et al., 2011; Pan et al., 2012; Khaki et al., 2017), water balance uncertainty is added to the equality constraint formulation, which allows for a more realistic water balance control during filtering. This has been framed in a supervised framework, i.e., by assigning approximate error covariance to the water balance observations before filtering, which may not allow for an optimal estimation of corrections (in the second step of the filter) to be applied to results from the first step of the filter. The present study aims to extend the work of Khaki et al. (2017) to the case where the covariance associated with flux observations is unknown, proposing an unsupervised framework to estimate it along with the hydrology state variable. The proposed Unsupervised WCEnKF (UWCEnKF) introduces an iterative scheme in the second update step of the WCEnKF.

In order to assess the performance of the UWCEnKF, numerical experiments are carried out to assimilate the Gravity Recovery And Climate Experiment (GRACE) derived terrestrial water storage (TWS), as well as soil moisture products from the Advanced Microwave Scanning Radiometer-Earth Observing System (AMSR-E) and Soil Moisture and Ocean Salinity (SMOS) into a hydrological model. Assimilating GRACE TWS data has been performed in a number of previous studies to constrain the mass balance of hydrological models over different river basins (e.g., Zaitchik et al., 2008; van Dijk et al., 2014; Eicker et al., 2014; Reager et al., 2015; Schumacher et al., 2016; Khaki et al., 2018; Khaki et al., 2018). Several studies already demonstrated a great capability of AMSR-E and SMOS datasets to constrain model estimates through data assimilation (e.g., De Jeu et al., 2008; Renzullo et al., 2014; Leroux et al., 2016; Tian et al., 2017). It has also been shown that simultaneous assimilation of the different datasets generally leads to better results in terms of state estimates (e.g., Zhang et al., 2014; Renzullo et al., 2014; Han et al., 2015; Tian et al., 2017; Lievens et al., 2017) as compared to individual assimilation of the different datasets. This motivates the current study to simultaneously assimilate GRACE TWS and soil moisture observations from AMSR-E and SMOS. We also apply the standard EnKF to compare its results with the proposed UWCEnKF filter. This enables to evaluate the relevance of the proposed approach for enforcing the water budget closure.

We further consider multiple observations of the water components in the water budget equation. This is done to achieve the best estimates of **p** and **e** over different basins (see Fig. 1). Multi-mission products for precipitation and evaporation are used in the data merging approach of Sahoo et al. (2011) to derive a single data set for each observation type (i.e., **p** and **e**). The approach estimates uniform datasets independently for each basin. The merged data, as well as the water discharge measurements from various ground stations, are then applied to constrain the water balance equation in the UWCEnKF's second update. This experiment is undertaken over eight globally distributed basins; Amazon, Indus, Mississippi, Orange, Danube, St. Lawrence, Murray-Darling, and the Yangtze, to better explore the capability of the proposed filter.

The remainder of the paper is organized as follows. We first describe the data and model in Section 2. The UWCEnKF algorithm and experiments set up are described in Sections 3 and 4, respectively. We illustrate and discuss the experiments results in Section 5 and conclude the study in Section 6.

2. Model and data

2.1. Hydrological model

Vertical water compartments of the globally distributed World-Wide Water Resources Assessment system (W3RA) model, developed in 2008 by the Commonwealth Scientific and Industrial Research Organisation (CSIRO; Australia), are used to simulate water storages. W3RA is a one-dimensional system that simulates landscape water stored in the vegetation and soil systems (van Dijk, 2010). Here, we use the 1°×1° version of the model to represent the water balance of the soil, groundwater and surface water storage, in which each cell is modeled independently from its neighbors (van Dijk, 2010). Groundwater dynamics in the model includes recharge from deep drainage, capillary rise (estimated with a linear diffusion equation), evaporation from groundwater saturated areas, and discharge. The model assumes that redistribution between grid cells can be ignored. Groundwater and river water dynamics are simulated at grid cell level and hence parameters are equal across the grid cell. Meteorological data sets of minimum and maximum temperature, downwelling short-wave radiation, and precipitation products provided by Princeton University (http://hydrology.princeton.edu) are used to force the W3RA model between 2003 and 2013. The model state is composed of the top, shallow and deep root soil water, snow, vegetation, groundwater, and surface water storage.

2.2. Assimilated observations

Observations are assimilated in two steps. The first step assimilates GRACE TWS and satellite soil moisture observations, which are used to update the forecast state, while the second step enforces the water balance constraints, based on water flux observations.

2.2.1. Data used in the first update

GRACE level 2 (L2) gravity field data provided by the ITSG-Grace2016 (Mayer-Gürr et al., 2014) is used to compute monthly TWS after applying a few standard corrections. These include replacing degree 1 (C10, C11, S11) and degree 2 (C20) coefficients by more accurate coefficients from Swenson et al. (2008) and the Satellite Laser Ranging solutions (Cheng and Tapley, 2004), respectively. The gravity fields are then converted to 3°×3° TWS fields (Wahr et al., 1998). Khaki et al. (2017) showed that implementing GRACE TWS with this spatial resolution exploits better impacts of GRACE TWS mainly because of larger correlation errors in the higher spatial resolution fields, which can be problematic during assimilation (see also Eicker et al., 2014; Schumacher et al., 2016). Colored/correlated noise and leakage errors are reduced using the Kernel Fourier Integration (KeFIn) filter, as proposed by Khaki et al. (2018). The KeFIn filter works through a two-step post-processing algorithm: in the first step it mitigates the measurement noise and the aliasing of unmodeled high-frequency mass variations, and in the second step it decreases the leakage errors. Note that, here, rather using model outputs, fixed signal to noise ratio is applied during the KeFIn filtering (see Khaki et al., 2018, for details). The application of the KeFIn filter was shown in Khaki et al. (2018) to outperform a number of existing GRACE filtering techniques, e.g., land-grid-scaling method applied in Mass Concentration blocks (Mascons) products justifying its use in the current study.

Furthermore, soil moisture products from the Advanced Microwave Scanning Radiometer for EOS (AMSR-E) and ESA's Soil Moisture Ocean Salinity (SMOS) Earth Explorer mission are used to update soil storage variations. AMSR-E measures surface brightness temperature that corresponds to surface soil moisture content of 2 cm depth (Njoku, 2003).

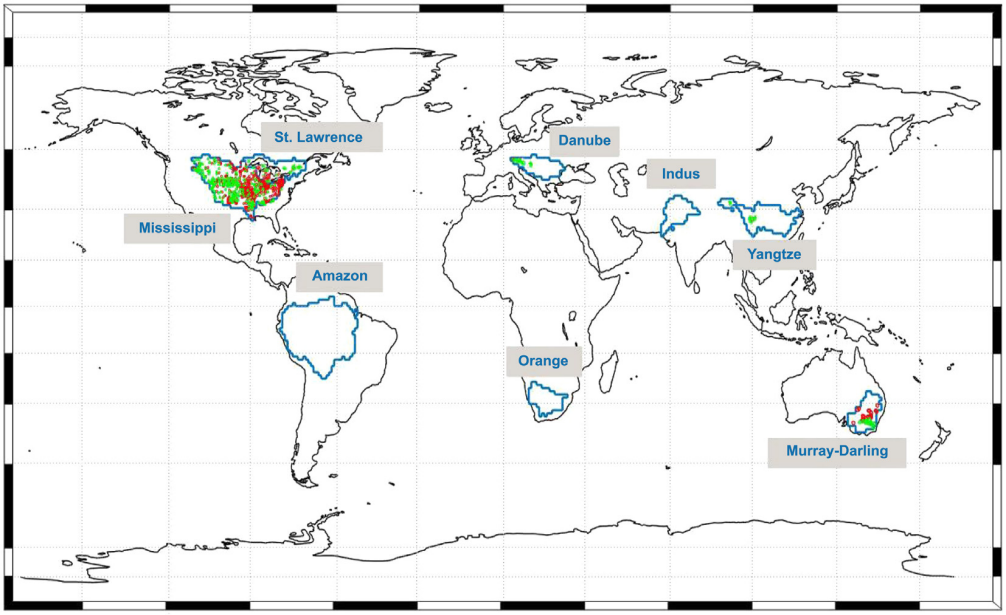

Fig. 1. The location of study basins. The figure also contains the distribution of in situ groundwater (red) and soil moisture (green) gauge stations. (For interpretation of the references to colour in this figure legend, the reader is referred to the web version of this article.)

SMOS, on the other hand, measures microwave emissions from Earth's surface at about 5 cm depth. Here we use descending passes (see, e.g., De Jeu and Owe, 2003) of gridded Level-3 land surface product AMSR-E (Njoku, 2004) between 2003 and 2011, and Level 3 CATDS (Centre Aval de Traitement des Donnees SMOS) on ascending passes (see, e.g., Draper et al., 2009) for the period of 2011 to 2013. These passes are selected due to their higher agreement with in situ measurements (see also Jackson and Bindlish, 2012; Su et al., 2013). Both data products are rescaled to a monthly 1°×1° scale for the present study. Cumulative distribution function (CDF) matching (Reichle and Koster, 2004; Drusch et al., 2005) is applied to rescale the observations and remove the bias between the model simulations and observations. These measurements are mainly used to constrain the model variability, and not its absolute values. CDF matching relies on the assumption that the difference between observed soil moisture and that of the model is stationary and guarantees that the statistical distribution of both time series is the same (Draper et al., 2009; Renzullo et al., 2014).

2.2.2. Data used in the second update

Multiple data sets are used for flux net observations. Details of these products are outlined in Table 1. For precipitation, we use the Tropical Rainfall Measuring Mission (TRMM-3B43; Huffman et al., 2007), NOAA CPC Morphing Technique (CMORPH; Joyce et al., 2004), the Global Precipitation Climatology Project (GPCP) Version 2.3 (Adler et al., 2003), Global Precipitation Climatology Centre (GPCC; Schneider et al., 2008), and CPC unified gauge dataset (Chen et al., 2002). TRMM-3B43, CMORPH, and GPCP are used to generate the merged precipitation for data assimilation, while GPCC and CPC are applied for uncertainty analysis (cf. Section 4.1). Evaporation data are collected from MODIS Global Evapotranspiration Project (MOD16; Mu et al., 2007), Global Land Evaporation Amsterdam Model (GLEAM; Miralles et al., 2011), ERA-interim (Simmons et al., 2007), and Variable Infiltration Capacity (VIC) land surface model (Liang et al., 1994). Similar to precipitation, an uncertainty analysis is undertaken for evaporation with respect to ERA-interim and VIC products. All of these products are rescaled into a monthly 1°×1° spatial resolution. Various data sources are considered for discharge (see Table 1) to achieve the maximum amount of coverage within the basins of Amazon, Indus, Mississippi, Orange, Danube, St. Lawrence, Murray-Darling, and Yangtze (Fig. 1).

2.3. In-situ measurements

Monthly in situ groundwater and soil moisture measurements are used to validate the results. The groundwater stations are located in the Mississippi, St. Lawrence, and Murray-Darling basins. Specific yield values provided by the literature (e.g., Gutentag et al., 1984; Strassberg et al., 2007; Seoane et al., 2013; Khaki et al., 2017) are used to convert well measurements into groundwater storage anomalies. We further use in situ soil moisture measurements over the Mississippi, St. Lawrence, Danube, Yangtze, and Murray-Darling basins to assess the estimated soil moisture. These data are collected from the International Soil Moisture Network (ISMN) and the moisture-monitoring network. It is worth mentioning that the temporal averages from the in situ time series are removed before using them to validate the assimilation results. The distribution of both groundwater and soil moisture in situ products are displayed in Fig. 1. Details of the datasets are outlined in Table 1.

3. Methodology

3.1. Problem formulation

Our discrete-time state-space system is represented as,

$$\begin{cases} \mathbf{x}_t &= \mathscr{M}_{t-1}(\mathbf{x}_{t-1}) + \nu_t, \\ \mathbf{y}_t &= \mathbf{H}_t\mathbf{x}_t + \mathbf{w}_t, \end{cases} \tag{1}$$

where $\mathbf{x}_t \in \mathbb{R}^{n_x}$ and $\mathbf{y}_t \in \mathbb{R}^{n_y}$ stand for the system state and the observation at time t and of sizes n_x and n_y, respectively. In system (1), $\mathscr{M}_{t-1}(.)$ is a nonlinear operator integrating the system state from time $t-1$ to t, and $\mathbf{H}_t$ is the observational (design) operator at time t, which is linear in our application. Note, however, that the proposed scheme can be easily extended to the nonlinear case (Liu and Xue, 2016). The model process noise, $\nu = \{\nu_t\}_{t=0}^{T}$, and the observation process noise, $\mathbf{w} = \{\mathbf{w}_t\}_{t=0}^{T}$, are assumed to be independent in time, jointly independent, and independent of the initial state, shown by $\mathbf{x}_0$. Furthermore, ν_t and $\mathbf{w}_t$ are assumed to be Gaussian with zero means and covariances $\mathbf{Q}_t$ and $\mathbf{R}_t$, respectively. The model time step, t, is considered to be equal to the assimilation time step. More details about the

Table 1
A summary of the datasets used in this study.

Product	Platform	Reference
Terrestrial water storage (TWS)	GRACE	Mayer-Gürr et al. (2014)
Soil moisture	AMSR-E	Njoku (2004)
Soil moisture	SMOS	Draper et al. (2009)
Precipitation (**p**)	TRMM-3B42	Huffman et al. (2007)
Precipitation (**p**)	CMORPH	Joyce et al. (2004)
Precipitation (**p**)	GPCP	Adler et al. (2003)
Precipitation (**p**)	GPCC	Schneider et al. (2008)
Precipitation (**p**)	CPC	Chen et al. (2002)
Evapotranspiration (**e**)	MOD16	Mu et al. (2007)
Evapotranspiration (**e**)	GLEAM	Miralles et al. (2011)
Evapotranspiration (**e**)	ERA-interim	Simmons et al. (2007)
Evapotranspiration (**e**)	VIC	Liang et al. (1994)
Water discharge (**q**)	GRDC	http://www.bafg.de/GRDC/EN/Home/homepage_node.html
Water discharge (**q**)		http://www.hydrosciences.fr/sierem/consultation/choixaccess.asp?lang=en
Water discharge (**q**)	USGS	https://waterdata.usgs.gov/nwis/sw
Water discharge (**q**)		http://www.bom.gov.au/waterdata/
Water discharge (**q**)	NRFA	http://nrfa.ceh.ac.uk/data/
Water discharge (**q**)		http://www.ore-hybam.org/
Water discharge (**q**)		http://www.hydrology.gov.np/new/bull3/index.php/hydrology/home/main
Hydrological model	W3RA	http://www.wenfo.org/wald/data-software/
Groundwater in situ measurements	NSW	http://waterinfo.nsw.gov.au/pinneena/gw.shtml
Groundwater in situ measurements	USGS	https://water.usgs.gov/ogw/data.html
Soil moisture in situ measurements	OzNet	Smith et al. (2012)
Soil moisture in situ measurements	ISMN	https://ismn.geo.tuwien.ac.at/

state-space formulation (i.e., about the structures of $\mathbf{x}_t$, $\mathbf{y}_t$, $\mathcal{M}_t$ and $\mathbf{H}_t$) of our application can be found in Khaki et al. (2017).

The ensemble Kalman filter update step does not constrain the water fluxes and this likely distorts their balance ($\Delta\mathbf{s} = \mathbf{p}-\mathbf{e}-\mathbf{q}$). This was enforced by Khaki et al. (2017), up to a weak constraint:

$$\mathbf{d}_t = -\mathbf{x}_t + \mathbf{x}_{t-1} + \mathbf{p}_t-\mathbf{e}_t-\mathbf{q}_t + \boldsymbol{\xi}_t, \tag{2}$$

accounting for the uncertainty in the different water fluxes data through a noise term $\boldsymbol{\xi}_t$, which we assume here to be Gaussian with zero mean and covariance, $\boldsymbol{\Sigma}$, and independent of $\boldsymbol{\xi}_{t'\neq t}$, $\{\nu_t\}_{t=0}^T$, $\{\mathbf{w}_t\}_{t=0}^T$ and $\mathbf{x}_0$. Considering Eq. (2), one can see that changes in the water storage at two successive time steps is equal to the difference between precipitation and summation of evaporation and discharge up to uncertainties in the involved data. The constraint in Eq. (2) can be rewritten as another observation equation in the state-space formulation, Eq. (3), which also involves the state at the previous time,

$$\mathbf{z}_t = \mathbf{G}\mathbf{x}_t + \mathbf{L}\mathbf{x}_{t-1} + \boldsymbol{\xi}_t, \tag{3}$$

where $\mathbf{z}_t \overset{\text{def}}{=} \mathbf{d}_t-\mathbf{p}_t + \mathbf{e}_t + \mathbf{q}_t$ plays the role of a "pseudo-observation", $\mathbf{L}$ is an $n_z \times n_x$ identity matrix, and $\mathbf{G} = -\mathbf{L}$ (here, $n_z = n_x$). Define $\mathbf{r}_t = [\mathbf{y}_t^T, \mathbf{z}_t^T]^T$ and $\mathbf{r}_{0:t} = \{\mathbf{r}_0, \mathbf{r}_1, \cdots, \mathbf{r}_t\}$. In the state-space system (1)–(3), a generic filtering algorithm has been recently introduced by Khaki et al. (2017), recursively computing the analysis pdf of the state $\mathbf{x}_t$ from the history of the augmented observations, $\mathbf{r}_{0:t}$, $p(\mathbf{x}_t|\mathbf{r}_{0:t})$. The computation of $p(\mathbf{x}_t|\mathbf{r}_{0:t})$ from $p(\mathbf{x}_{t-1}|\mathbf{r}_{0:t-1})$ proceeds in a succession of a forecast step and two Bayesian update steps. The forecast step consists of moving from $p(\mathbf{x}_{t-1}|\mathbf{r}_{0:t-1})$ to the forecast pdf, $p(\mathbf{x}_t|\mathbf{r}_{0:t-1})$, based on the state transition pdf $p(\mathbf{x}_t|\mathbf{x}_{t-1})$ (which is described by the state model). The resulting forecast pdf is then updated, based on the likelihood of the observations, $p(\mathbf{y}_t|\mathbf{x}_t)$ (which is represented by the observation model), resulting in an unconstrained analysis pdf[1], $p(\mathbf{x}_t|\mathbf{r}_{0:t-1}, \mathbf{y}_t)$. The latter is, in turn, updated in the second Bayesian step, based on the likelihood of the pseudo-observation, $p(\mathbf{z}_t|\mathbf{x}_{t-1,t})$ (which is represented by the constraint Eq. (3)), leading to the desirable analysis pdf at the current time t, $p(\mathbf{x}_t|\mathbf{r}_{0:t})$. Details about these steps can be found in (Khaki et al., 2017).

In a supervised framework, where the parameters of the constrained state-space system (including $\boldsymbol{\Sigma}$) are known, the above generic algorithm was implemented by Khaki et al. (2017) through Monte Carlo approximation of the posterior mean (PM) estimate of the state and its covariance, which led to the ensemble Kalman-type WCEnKF. Khaki et al. (2017) noticed that the WCEnKF is sensitive to the choice of $\boldsymbol{\Sigma}$, which can strongly affect the filter behaviors. Here, we design a more general unsupervised framework in which $\boldsymbol{\Sigma}$ is an unknown diagonal covariance matrix, which thereby needs to be estimated concurrently with the state.

3.2. The Unsupervised Weak Constrained Ensemble Kalman Filter (UWCEnKF)

3.2.1. The generic algorithm

The UWCEnKF shares the same forecast and first update steps as the WCEnKF, but computes the posterior distribution of both state and pseudo-observation noise covariance in the second update step, instead of only that of the state. In a Bayesian framework, this consists in viewing the covariance, $\boldsymbol{\Sigma}$, as another random variable with a given prior pdf; the goal is then to compute its posterior pdf jointly with the state[2], $p(\mathbf{x}_{t-1}, \mathbf{x}_t, \boldsymbol{\Sigma}|\mathbf{r}_{0:t})$. However, the statistical dependencies between the states, $\mathbf{x}_{t-1:t}$, and the covariance, $\boldsymbol{\Sigma}$, makes its computation quite tricky. One way to overcome this difficulty is to resort to the variational Bayesian (VB) approach and approximate $p(\mathbf{x}_{t-1}, \mathbf{x}_t, \boldsymbol{\Sigma}|\mathbf{r}_{0:t})$ with a separable pdf $q(\mathbf{x}_{t-1}, \mathbf{x}_t, \boldsymbol{\Sigma}|\mathbf{r}_{0:t}) = q(\mathbf{x}_{t-1}, \mathbf{x}_t|\mathbf{r}_{0:t})q(\boldsymbol{\Sigma}|\mathbf{r}_{0:t})$, under the Kullback–Leibler divergence (KLD) minimization criteria (Jaakkola and Jordan, 2000; Smidl and Quinn, 2008; Ait-El-Fquih and Hoteit, 2015; Ait-El-Fquih and Hoteit, 2016). This reads,

$$\begin{aligned} q(\mathbf{x}_{t-1}, \mathbf{x}_t, \boldsymbol{\Sigma}|\mathbf{r}_{0:t}) &= \underset{\phi(\mathbf{x}_{t-1},\mathbf{x}_t,\boldsymbol{\Sigma}|\mathbf{r}_{0:t})}{\operatorname{argmin}} \mathrm{KLD}(\phi(\mathbf{x}_{t-1}, \mathbf{x}_t, \boldsymbol{\Sigma}|\mathbf{r}_{0:t})||p(\mathbf{x}_{t-1}, \mathbf{x}_t, \boldsymbol{\Sigma}|\mathbf{r}_{0:t})), \\ &= \underset{\phi(\mathbf{x}_{t-1},\mathbf{x}_t,\boldsymbol{\Sigma}|\mathbf{r}_{0:t})}{\operatorname{argmin}} \mathbb{E}_{\phi(\mathbf{x}_{t-1},\mathbf{x}_t,\boldsymbol{\Sigma}|\mathbf{r}_{0:t})}\left[\ln\left(\frac{\phi(\mathbf{x}_{t-1},\mathbf{x}_t,\boldsymbol{\Sigma}\mid\mathbf{r}_{0:t})}{p(\mathbf{x}_{t-1},\mathbf{x}_t,\boldsymbol{\Sigma}\mid\mathbf{r}_{0:t})}\right)\right], \end{aligned} \tag{4}$$

[1] The term *unconstrained* comes from the fact that these pdfs are not based on the pseudo-observation, $\mathbf{z}_t$, that "represents" the equality constraint.

[2] For the sake of clarity, the inclusion of both $\mathbf{x}_t$ and $\mathbf{x}_{t-1}$ in the joint posterior pdf of interest is due to the fact that both these states appear in the pseudo-observation model Eq. (3), which necessitates estimating both of them.

where $\mathbb{E}_{\phi(u)}[f(u)]$ denotes the expected value of $f(u)$ with respect to (w.r.t.) the pdf $\phi(u)$. The solution of Eq. (4) can be obtained from (the proof can be found for instance in Smidl and Quinn (2006), pages 28–31):

$$q(\mathbf{x}_{t-1}, \mathbf{x}_t|\mathbf{r}_{0:t}) \propto \exp(\mathbb{E}_{q(\boldsymbol{\Sigma}|\mathbf{r}_{0:t})}[\ln(p(\mathbf{x}_{t-1}, \mathbf{x}_t, \boldsymbol{\Sigma}, \mathbf{r}_{0:t}))]), \tag{5}$$

$$q(\boldsymbol{\Sigma}|\mathbf{r}_{0:t}) \propto \exp(\mathbb{E}_{q(\mathbf{x}_{t-1}, \mathbf{x}_t|\mathbf{r}_{0:t})}[\ln(p(\mathbf{x}_{t-1}, \mathbf{x}_t, \boldsymbol{\Sigma}, \mathbf{r}_{0:t}))]). \tag{6}$$

According to Eqs. (5) and (6), the independence that is inserted between the marginal posteriors, $q(\mathbf{x}_{t-1}, \mathbf{x}_t|\mathbf{r}_{0:t})$ and $q(\boldsymbol{\Sigma}|\mathbf{r}_{0:t})$, is partially compensated by the fact that each of these pdfs remains dependent on the expected value of $\ln(p(\mathbf{x}_{t-1}, \mathbf{x}_t, \boldsymbol{\Sigma}, \mathbf{r}_{0:t}))$ w.r.t. the other. However, this property of "cyclic" dependence between $q(\mathbf{x}_{t-1}, \mathbf{x}_t|\mathbf{r}_{0:t})$ and $q(\boldsymbol{\Sigma}|\mathbf{r}_{0:t})$ makes it impossible to exactly evaluate these pdfs, or any of their statistics, such as for instance their means, which are taken as the PM estimates of the states and the covariance, $\boldsymbol{\Sigma}$, respectively. A standard approximation is to proceed with cyclic iterations between (5) and (6), evaluating one pdf after the other, until convergence is reached (Smidl and Quinn, 2008; Sato, 2001; Massoud et al., 2018). Based on the factorization,

$$p(\mathbf{x}_{t-1}, \mathbf{x}_t, \boldsymbol{\Sigma}, \mathbf{r}_{0:t}) \propto p(\mathbf{z}_t|\mathbf{x}_{t-1}, \mathbf{x}_t, \boldsymbol{\Sigma})p(\mathbf{x}_{t-1}, \mathbf{x}_t|\mathbf{r}_{0:t-1}, \mathbf{y}_t)q(\boldsymbol{\Sigma}|\mathbf{r}_{0:t-1}), \tag{7}$$

which stems from the conditional independence properties of the state-space system 1,2,refEq4, the iterative form of Eqs. (5) and (6) becomes,

$$q^{(\ell)}(\mathbf{x}_{t-1}, \mathbf{x}_t|\mathbf{r}_{0:t}) \propto \exp(\mathbb{E}_{q^{(\ell-1)}(\boldsymbol{\Sigma}|\mathbf{r}_{0:t})}[\ln(p^{(\ell-1)}(\mathbf{z}_t|\mathbf{x}_{t-1}, \mathbf{x}_t, \boldsymbol{\Sigma}))])p(\mathbf{x}_{t-1}, \mathbf{x}_t|\mathbf{r}_{0:t-1}, \mathbf{y}_t), \tag{8}$$

$$q^{(\ell)}(\boldsymbol{\Sigma}|\mathbf{r}_{0:t}) \propto \exp(\mathbb{E}_{q^{(\ell)}(\mathbf{x}_{t-1}, \mathbf{x}_t|\mathbf{r}_{0:t})}[\ln(p^{(\ell-1)}(\mathbf{z}_t|\mathbf{x}_{t-1}, \mathbf{x}_t, \boldsymbol{\Sigma}))])q(\boldsymbol{\Sigma}|\mathbf{r}_{0:t-1}), \tag{9}$$

where $p^{(\ell)}(.)$ and $q^{(\ell)}(.)$ respectively denote the pdfs $p(.)$ and $q(.)$ at iteration ℓ. As can be seen below (cf. Section 3.2.2), iterating over the pdfs Eqs. (8) and (9) amounts in practice to iterate over their (approximate) parameters, thereby leading to an unsupervised ensemble-based filtering scheme, which iterates in its second step over the PM estimates of the states and the pseudo-observation noise covariance.

3.2.2. Practical implementation

For the sake of simplicity, we first focus on the case of a homogeneous noise with a covariance matrix,

$$\boldsymbol{\Sigma} = \lambda \times \mathbb{I}_{n_z}, \tag{10}$$

where λ is the variance value and $\mathbb{I}_{n_z}$ denotes the $n_z \times n_z$ identity matrix. The more general inhomogeneous case will be discussed later. The prior probability distribution $p(\lambda)$ is chosen as an inverse-Gamma distribution (as a natural choice for variances), with shape and scale parameters $\hat{\alpha}_0$ and $\hat{\beta}_0$, respectively (Smidl and Quinn, 2006). In the case of non-informative priors, one could take $\hat{\alpha}_0 = \hat{\beta}_0$ relatively small. At each iteration $(\ell-1) \rightarrow (\ell)$, inserting in Eqs. (8) and (9) the Gaussian pdf,

$$p^{(\ell-1)}(\mathbf{z}_t|\mathbf{x}_{t-1}, \mathbf{x}_t, \boldsymbol{\Sigma}) = \mathcal{N}_{\mathbf{z}_t}(\mathbf{G}\mathbf{x}_t + \mathbf{L}\mathbf{x}_{t-1}, \boldsymbol{\Sigma}^{(\ell-1)}),$$

one obtains a posterior $q^{(\ell)}(\lambda|\mathbf{r}_{0:t})$ that is also an inverse-Gamma distribution with parameters, $\hat{\alpha}_t$ and $\hat{\beta}_t^{(\ell)}$, given in Eqs. 17,18 below. Likewise, $q^{(\ell)}(\mathbf{x}_{t-1}, \mathbf{x}_t|\mathbf{r}_{0:r})$ is Gaussian with an ensemble representation given in Eqs. (14)–(16).

3.2.2.1. The UWCEnKF. Starting at time $t-1$ from an analysis ensemble, $\{\mathbf{x}_{t-1}^{a,(i)}\}_{i=1}^m$, and shape and scale parameters $(\hat{\alpha}_{t-1}, \hat{\beta}_{t-1})$ of the inverse-Gamma posterior pdf $p(\lambda|\mathbf{r}_{0:t-1})$, these at the next time t can be computed following a succession of a forecast and two update steps. The forecast step, which computes the forecast ensemble, $\{\mathbf{x}_t^{f,(i)}\}_{i=1}^m$, and the first update step (with $\mathbf{y}_t$), which computes the unconstrained analysis and smoothing ensembles, $\{\widetilde{\mathbf{x}}_t^{a,(i)}\}_{i=1}^m$ and $\{\widetilde{\mathbf{x}}_{t-1}^{s,(i)}\}_{i=1}^m$, are identical to those in Khaki et al. (2017), namely,

$$\mathbf{x}_t^{f,(i)} = \mathscr{M}_{t-1}(\mathbf{x}_{t-1}^{a,(i)}) + \nu^{(i)}, \tag{11}$$

$$\widetilde{\mathbf{x}}_t^{a,(i)} = \mathbf{x}_t^{f,(i)} + \mathbf{P}_{\mathbf{x}_t^f}\mathbf{H}^T \underbrace{\left[\mathbf{H}\mathbf{P}_{\mathbf{x}_t^f}\mathbf{H}^T + \mathbf{R}_t\right]^{-1}[\mathbf{y}_t + \epsilon^{(i)} - \mathbf{H}\mathbf{x}_t^{f,(i)}]}_{\mu_t^{(i)}}, \tag{12}$$

$$\widetilde{\mathbf{x}}_{t-1}^{s,(i)} = \mathbf{x}_{t-1}^{a,(i)} + \mathbf{P}_{\mathbf{x}_{t-1}^a, \mathbf{x}_t^f}\mathbf{H}^T \times \mu_t^{(i)}, \tag{13}$$

where $\mathbf{P}_{\mathbf{x}_t^f}$ is the sample forecast error covariance and $\mathbf{P}_{\mathbf{x}_{t-1}^a, \mathbf{x}_t^f}$ represents the sample cross-covariance between the previous analysis and current forecast errors, $\nu^{(i)} \sim \mathcal{N}(\mathbf{0}, \mathbf{Q}_t)$, and $\epsilon^{(i)} \sim \mathcal{N}(\mathbf{0}, \mathbf{R}_t)$.

As for the second update step (with $\mathbf{z}_t$), which applies the adjustment to enforce the water budget balance constraint, it involves iterations to compute Eqs. (8) and (9). Let $\hat{\alpha}_t = \hat{\alpha}_{t-1} + \frac{n_z}{2}$, the iteration begins with the initialization $\hat{\lambda}_t^{(0)} = \frac{\hat{\beta}_{t-1}}{\hat{\alpha}_t}$ and correspondingly $\hat{\boldsymbol{\Sigma}}_t^{(0)} = \hat{\lambda}_t^{(0)} \times \mathbb{I}_{n_z}$. For $\ell = 0 \cdots L$, the state members are first updated as,

$$\mathbf{z}_t^{f,(i,\ell)} = \mathbf{G}\widetilde{\mathbf{x}}_t^{a,(i)} + \mathbf{L}\widetilde{\mathbf{x}}_{t-1}^{s,(i)} + \boldsymbol{\xi}_t^{(i,\ell)}; \quad \boldsymbol{\xi}_t^{(i,\ell)} \sim \mathcal{N}(\mathbf{0}, \hat{\boldsymbol{\Sigma}}_t^{(\ell)}), \quad i = 1, \cdots, m, \tag{14}$$

$$\mathbf{x}_t^{a,(i,\ell)} = \widetilde{\mathbf{x}}_t^{a,(i)} + \mathbf{P}_{\widetilde{\mathbf{x}}_t^a, \mathbf{z}_t^{f,\ell}} \underbrace{\left[\mathbf{M}\mathbf{P}_{\boldsymbol{\eta}_t}\mathbf{M}^T + \hat{\boldsymbol{\Sigma}}_t^{(\ell)}\right]^{-1}[\mathbf{z}_t - \mathbf{z}_t^{f,(i,\ell)}]}_{\nu_t^{(i,\ell)}}, \quad i = 1, \cdots, m, \tag{15}$$

$$\mathbf{x}_{t-1}^{s,(i,\ell)} = \widetilde{\mathbf{x}}_{t-1}^{s,(i)} + \mathbf{P}_{\widetilde{\mathbf{x}}_{t-1}^s, \mathbf{z}_t^{f,\ell}} \times \nu_t^{(i,\ell)}, \quad i = 1, \cdots, m, \tag{16}$$

where $\mathbf{M} \overset{\text{def}}{=} [\mathbf{G}, \mathbf{L}]$; $\mathbf{P}_{\widetilde{\mathbf{x}}_t^a, \mathbf{z}_t^{f,\ell}}$ and $\mathbf{P}_{\widetilde{\mathbf{x}}_{t-1}^s, \mathbf{z}_t^{f,\ell}}$ are the sample cross-covariances computed using the ensembles $\{\widetilde{\mathbf{x}}_t^{a,(i)}\}_{i=1}^m$, $\{\widetilde{\mathbf{x}}_{t-1}^{s,(i)}\}_{i=1}^m$ and $\{\mathbf{z}_t^{f,(i,\ell)}\}_{i=1}^m$; and $\mathbf{P}_{\boldsymbol{\eta}_t}$ is the sample covariance of the ensemble $\{\boldsymbol{\eta}_t^{(i)}\}_{i=1}^m$ with $\boldsymbol{\eta}_t^{(i)} \overset{\text{def}}{=} [(\widetilde{\mathbf{x}}_t^{a,(i)})^T, (\widetilde{\mathbf{x}}_{t-1}^{s,(i)})^T]^T$. Based on the resulting ensembles, the observation noise variance is then updated as,

$$\hat{\beta}_t^{(\ell+1)} = \hat{\beta}_{t-1} + \frac{1}{2}[||\mathbf{z}_t - \mathbf{G}\hat{\mathbf{x}}_t^{a,(\ell)} - \mathbf{L}\hat{\mathbf{x}}_{t-1}^{s,(\ell)}||^2 + \text{Trace}(\mathbf{M}\mathbf{P}_{\gamma_t^\ell}\mathbf{M}^T)], \tag{17}$$

$$\hat{\lambda}_t^{(\ell+1)} = \hat{\beta}_t^{(\ell+1)}/\hat{\alpha}_t, \tag{18}$$

$$\hat{\boldsymbol{\Sigma}}_t^{(\ell+1)} = \hat{\lambda}_t^{(\ell+1)} \times \mathbb{I}_{n_z}, \tag{19}$$

where $\hat{\mathbf{x}}_t^{a,(\ell)}$ and $\hat{\mathbf{x}}_{t-1}^{s,(\ell)}$ are the (empirical) means of the ensembles $\{\mathbf{x}_t^{a,(i,\ell)}\}_{i=1}^m$ and $\{\mathbf{x}_{t-1}^{s,(i,\ell)}\}_{i=1}^m$, respectively; and $\mathbf{P}_{\gamma_t^\ell}$ is the sample covariance of the ensemble $\{\boldsymbol{\gamma}_t^{(i,\ell)}\}_{i=1}^m$ with $\boldsymbol{\gamma}_t^{(i,\ell)} \overset{\text{def}}{=} [(\mathbf{x}_t^{a,(i,\ell)})^T, (\mathbf{x}_{t-1}^{s,(i,\ell)})^T]^T$. The $\hat{\boldsymbol{\Sigma}}_t^{(L)}$ and $\{\mathbf{x}_t^{a,(i,L)}\}_{i=1}^m$ are then considered as the analysis covariance and state estimates, respectively, that will be used in the next assimilation cycle. In our numerical experiments, only few iterations (less than 10) were needed to reach convergence based on the variance estimate. Note that instead of pre-setting the number of iterations, L, on may use an alternative stopping criteria based, for instance, on the relative squared error norm (RSEN) of the estimated state and/or variance(s), or the evidence lower bound (ELB), defined as (Blei et al., 2017),

$$\mathscr{E}_1 = \mathbb{E}_{q(\xi_t, \boldsymbol{\Sigma}|\mathbf{r}_{0:t})}[\ln(p(\mathbf{v}_t, \boldsymbol{\Sigma}, \mathbf{r}_t|\mathbf{r}_{0:t-1}))] - \mathbb{E}_{q(\xi_t, \boldsymbol{\Sigma}|\mathbf{r}_{0:t})}[\ln(q(\mathbf{v}_t, \boldsymbol{\Sigma}|\mathbf{r}_{0:t}))], \tag{20}$$

with $\mathbf{v}_t = [\mathbf{x}_t^T, \mathbf{x}_{t-1}]^T$. Note that it is not possible to use the KLD as this requires the knowledge of the target pdf, $p(\mathbf{v}_t, \boldsymbol{\Sigma}|\mathbf{r}_{0:t})$, which, indeed, is not known. Furthermore, minimizing the KLD amounts to maximizing the ELB (Blei et al., 2017). However, a problem occurs in practice with ELB (20) in case of large dimensional systems (i.e., when $n_x > m$). In such a case, the covariance $\mathbf{P}_{\gamma_t}$, whose inverse is involved in the expression of the (assumed Gaussian) pdf, $q(\mathbf{v}_t|\mathbf{r}_{0:t})$, is a low-rank matrix, and thus not invertible. To overcome this limitation, we propose to remove the variable, $\mathbf{v}_t$, from the ELB, by rather using pdfs that are conditional on this variable (i.e., for which $\mathbf{v}_t$ is a fixed known value). Since the iterations' process occurs in the second update step (i.e., which uses $\mathbf{z}_t$), we assign to $\mathbf{v}_t$ the mean $\hat{\boldsymbol{\eta}}_t$ of $\{\boldsymbol{\eta}_t^{(i)}\}_{i=1}^m$, which, indeed, is an approximation of $\mathbb{E}_{q(\xi_t|\mathbf{r}_{0:t-1}, \mathbf{y}_t)}[\mathbf{v}_t]$ (i.e., the unconstrained analysis mean of $\mathbf{v}_t$). The resulting ELB reads,

$$\mathscr{E}_2 = \mathbb{E}_{q(\boldsymbol{\Sigma}|\mathbf{r}_{0:t})}[\ln(p(\boldsymbol{\Sigma}, \mathbf{r}_t|\mathbf{r}_{0:t-1}, \hat{\boldsymbol{\eta}}_t))] - \mathbb{E}_{q(\boldsymbol{\Sigma}|\mathbf{r}_{0:t})}[\ln(q(\boldsymbol{\Sigma}|\mathbf{r}_{0:t}))],$$
$$\approx \text{cte} + \mathbb{E}_{q(\boldsymbol{\Sigma}|\mathbf{r}_{0:t})}[\ln(p(\mathbf{z}_t|\boldsymbol{\Sigma}, \hat{\boldsymbol{\eta}}_t))] + \mathbb{E}_{q(\boldsymbol{\Sigma}|\mathbf{r}_{0:t})}[\ln(q(\boldsymbol{\Sigma}|\mathbf{r}_{0:t-1}))]$$
$$- \mathbb{E}_{q(\boldsymbol{\Sigma}|\mathbf{r}_{0:t})}[\ln(q(\boldsymbol{\Sigma}|\mathbf{r}_{0:t}))], \tag{21}$$

where the term "cte" encompasses all the terms that do not depend on Σ. This suggests that the convergence of the proposed scheme can be monitored based either on the change in $\mathscr{E}_2$ only, the change in RSEN of the state only, the change in $\mathscr{E}_2$ and RSEN of the state, or, as stated above, the change in RSEN of both state and $\boldsymbol{\Sigma}$. Finally, based on the Gaussian expression of $p(\mathbf{z}_t|\boldsymbol{\Sigma}, \hat{\boldsymbol{\eta}}_t)$ and the inverse-Gamma expression of $q(\boldsymbol{\Sigma}|\mathbf{r}_{0:t-1})$ and $q(\boldsymbol{\Sigma}|\mathbf{r}_{0:t})$, one readily shows that Eq. (21) at iteration $(\ell) \rightarrow (\ell + 1)$ is given as,

$$\mathscr{E}_2^{(\ell)} \approx \text{cte} + \frac{\hat{\alpha}_t}{\hat{\beta}_t^{(\ell+1)}}[\hat{\beta}_t^{(\ell+1)} - \hat{\beta}_{t-1} - \|\mathbf{z}_t - \mathbf{M}\hat{\boldsymbol{\eta}}_t\|^2/2] - \ln(\hat{\beta}_t^{(\ell+1)}), \tag{22}$$

where cte gathers the terms that do not vary with iterations (i.e., independent of (ℓ)).

The adaptation of the algorithm above to the case of an inhomogeneous noise with a covariance is straightforward,

$$\boldsymbol{\Sigma} = \text{diag}(\lambda^1, \cdots, \lambda^{n_z}), \tag{23}$$

where diag($\mathbf{v}$) denotes a diagonal matrix with diagonal $\mathbf{v}$. More specifically, Eqs. (11)–(16) that compute the state ensembles are kept unchanged, and only those related to the noise variance will be updated (i.e., Eqs. (17)–(19) for each λ^j). Each variance $\lambda^j, \quad j = 1, \cdots, n_z$, is estimated separately from the others, $\lambda^k, \quad k \neq j$, by a direct application of Eqs. (17)–(19), which, correspond to the $n_z \times 1$ vectorial model (3), on the scalar (marginal) model,

$$\mathbf{z}_{t,j} = \mathbf{G}(j, :)\mathbf{x}_t + \mathbf{L}(j, :)\mathbf{x}_{t-1} + \boldsymbol{\xi}_{t,j}, \tag{24}$$

where $\mathbf{z}_{t,j}$ and $\boldsymbol{\xi}_{t,j}$ respectively denote the j^{th} component of $\mathbf{z}_t$ and $\boldsymbol{\xi}_t$ (i.e., $\boldsymbol{\xi}_{t,j} \sim \mathcal{N}(\mathbf{0}, \lambda^j)$), and $\mathbf{G}(j, :)$ and $\mathbf{L}(j, :)$ are the j^{th} rows of $\mathbf{G}$ and $\mathbf{L}$, respectively. A schematic illustration of this algorithm is presented in Fig. 2.

4. Experimental setup

4.1. Data merging

A single product for each water flux term of precipitation ($\mathbf{p}$) and evaporation ($\mathbf{e}$) is required to close the water balance in the second update step of UWCEnKF. One can use only one data product for each flux components, e.g., only TRMM-3B43 for $\mathbf{p}$ for the filtering process. However, this may introduce errors because various products are subject to a different rate of uncertainty over different areas. Alternatively, the different data products for each component can be merged into a unique $\mathbf{p}$ and $\mathbf{e}$ to better represent the water balance over the globally distributed basins (Sahoo et al., 2011). Here, we merge various datasets of precipitation and evaporation prior to data assimilation. To this end, we follow Sahoo et al. (2011) and merge the data considering their relative error levels w.r.t. non-satellite products. This combination is done in a way that satellite-based products are merged to be used in data assimilation while other products are only applied for the merging objective. For $\mathbf{p}$, the average of GPCC and CPC unified gauge over each basin is assumed as the truth and is used to estimate the error level of each satellite-based product, i.e, TRMM-3B43, CMORPH, and GPCP. A similar strategy is applied for evaporation, where ERA-interim and VIC products are used to quantify the error level associated with the data of MOD16 and GLEAM outputs that are based on satellite products (Miralles et al., 2011). It is worth mentioning that a more robust merging process can be achieved by involving ground-based measurements as a reference rather than ERA-interim and VIC. Obtaining and analyzing such an enhanced evaporation dataset from in situ stations over all tested basins is however very difficult and is out of the scope of this study. Therefore, we use these model outputs to merge satellite-based datasets into a single $\mathbf{e}$. Once the references are calculated, we use a multiplicative error model to estimate the offset, scale parameter, and

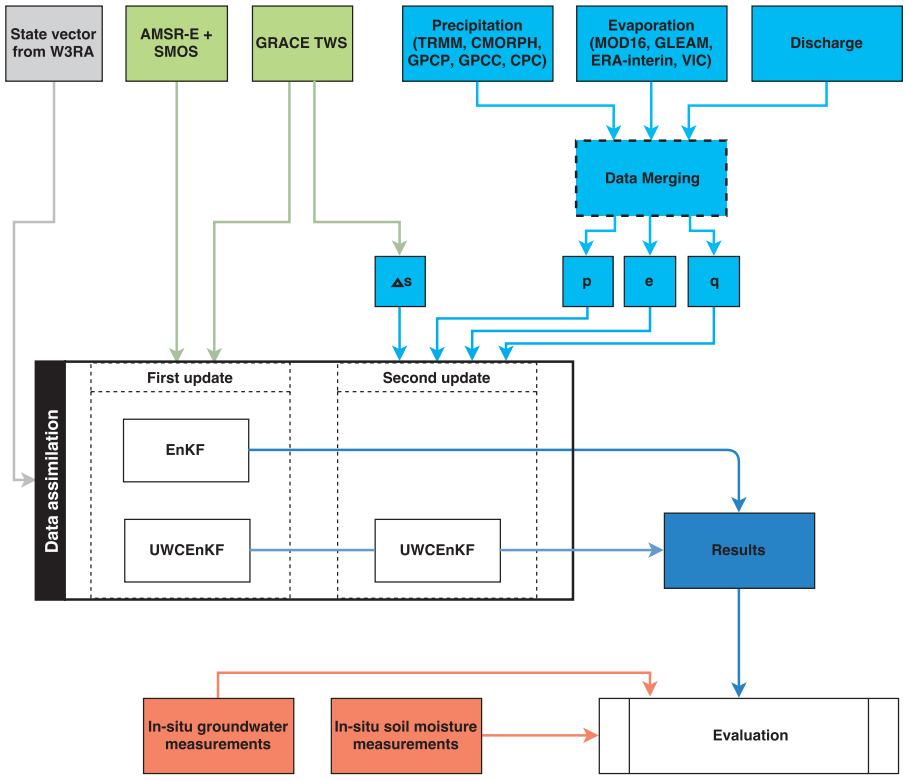

Fig. 2. A schematic illustration of the UWCEnKF steps applied for data assimilation, as well as data merging process.

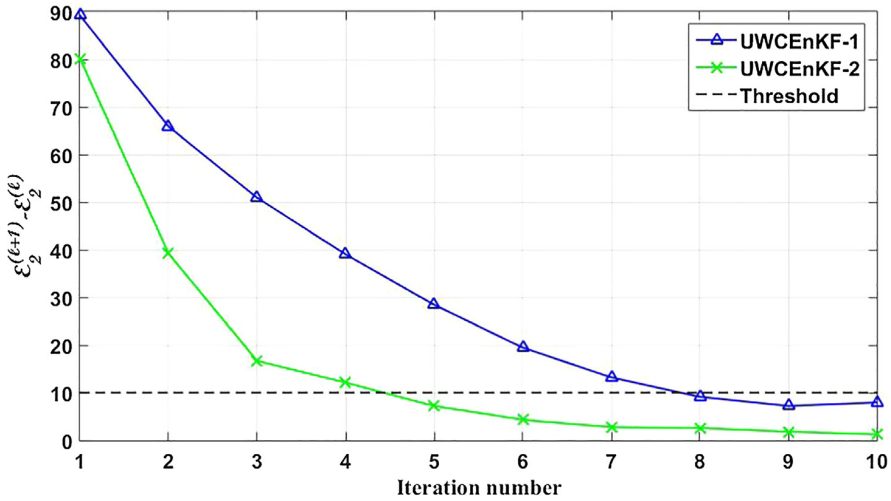

Fig. 3. Average $\mathscr{E}_2^{(\ell+1)}-\mathscr{E}_2^{(\ell)}$ estimates (unit is mm) from UWCEnKF-1 and UWCEnKF-2 filters during assimilation in each iteration (for $\ell = 0\cdots10$). The threshold value (10 mm) is chosen arbitrary based on a trial and error procedure.

error variance for each data product. These variances are then used to compute the observations weights as,

$$w_i = \frac{1}{\sigma_i^2} \Big/ \sum_{k=1}^{n_p} \frac{1}{\sigma_k^2}. \tag{25}$$

For each data product (i), using the error variances of that specific product σ_i^2 and all products (σ_k^2) in the same data type (with the total number of n_p), weight w_i can be calculated. Eq. (25) is applied for both precipitation and evaporation to provide merged data with reduced error (Luo et al., 2007; Sahoo et al., 2011). Note that the above approach is applied only to merge the various data products and to obtain uniform precipitation and evaporation datasets prior to assimilation. The estimated errors (e.g., σ_i^2 in Eq. (25)) are used only for this objective and are not related to the water flux error covariance calculation in the filtering procedure (cf. Section 3.2).

4.2. Data assimilation

To start the assimilation process, the initial ensemble is generated by perturbing the forcing fields. To this end, we use Monte Carlo sampling to perturb the precipitation, shortwave radiation, and temperature field considering a Gaussian multiplicative error of 30% for precipitation, an additive Gaussian error of 50 Wm^{-2} for the shortwave radiation, and a Gaussian additive error of 2 °C for temperature (Jones et al., 2007). The system state includes top soil, shallow soil, deep soil water, snow, vegetation, surface, and groundwater storages. Except for groundwater and surface storage, all the other components are simulated with two hydrological response units (HRU) of tall, e.g., deep-rooted vegetation and short, e.g., shallow-rooted vegetation. This leads to a state vector of dimension $(2 \times 5 + 1 + 1) \times 1695$ (corresponding to 1695 grid points over all basins).

All observations, including GRACE TWS, satellite soil moisture data, and water fluxes are assimilated monthly. The monthly increment is then be added to each day of the current month, which guarantees that the update of the monthly mean is identical to the monthly mean of the daily updates. Here, the differences between the predictions and the updated state variables are added as offsets to the state variables at the last day of each month to generate the ensembles for the next month assimilation step (see Eicker et al., 2014 for more details). The observation operator aggregates different water storages at each grid point to update with GRACE TWS and scales the top-layer soil storage by the field capacity value to provide a relative wetness for updating with the soil moisture products of AMSR-E and SMOS (Renzullo et al., 2014).

In addition, observation error covariances for the first update step are required. Full error information about the Stokes' coefficients are used to construct the TWS error covariance matrix. This is done by converting GRACE spherical harmonic error coefficients to TWS error covariances following Khaki et al. (2017). Since such an information is not available for soil moisture products, we assume their error covariances to be uncorrelated with standard deviations of 0.04 $m^3\,m^{-3}$ for SMOS (as suggested by Leroux et al. (2016)) and 0.05 $m^3\,m^{-3}$ for AMSR-E (as suggested by De Jeu et al. (2008)). We further apply two common auxiliary techniques of ensemble variance inflation and covariance localization to mitigate for the ensemble spread collapse and rank deficiency (Anderson, 2001; Houtekamer and Mitchell, 2001). These include an ensemble inflation with a coefficient factor of 1.12 and Local Analysis (LA) with a localization length scale of 5° (see Khaki et al., 2017, for more details).

5. Results

The results are discussed in three parts. UWCEnKF implementation is first presented and discussed in Section 5.1.1. The validation of the proposed approach against in situ groundwater and soil moisture measurements is then presented in Section 5.2. The relevance of the second update step in UWCEnKF and its overall effects on the assimilation system performance is finally analyzed in Section 5.3. UWCEnKF estimates are also compared with the results of WCEnKF and EnKF. UWCEnKF is tested with both constant (*Structure in Eq. (10)*, indicated by UWCEnKF-1) and spatially varying (*Structure in Eq. (23)*, indicated by UWCEnKF-2) error variances for the water balance equation. While UWCEnKF-1 assigns a fixed error variance to water fluxes at all points, different values for individual points are calculated by UWCEnKF-2.

5.1. Implementation results

5.1.1. Iteration impacts

We first study the sensitivity of UWCEnKF-1, and UWCEnKF-2 to the iteration procedure. As mentioned, in contrast with WCEnKF, which assumes that these uncertainties are known, UWCEnKF estimates the error covariance through an iteration process. To show how this iteration works, we compare the convergence of UWCEnKF-1 and UWCEnKF-2, based on Eq. (22), in Fig. 3. The average evolutions of $\mathscr{E}_2^{(\ell+1)}-\mathscr{E}_2^{(\ell)}$ (the difference between Eq. (22) in each two successive iterations) from both filters for $\ell = 0\cdots10$ are shown in this figure. After

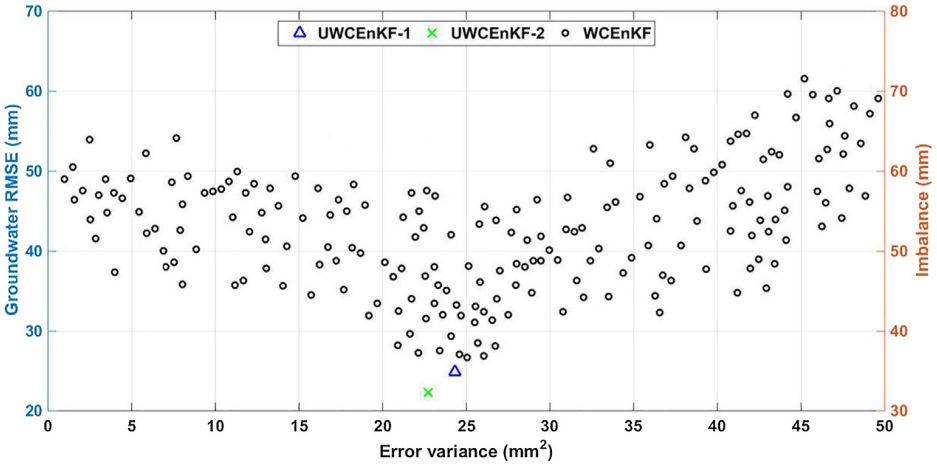

Fig. 4. Average groundwater RMSE and imbalance for various implementations of the WCEnKF filter using different error variance assumed (circles) considering different error variance. UWCEnKF-1 and UWCEnKF-2 results are indicated by triangle and cross, respectively.

few iterations, generally less than 8, both UWCEnKF-1 and UWCEnKF-2 converge. Faster convergence and lower differences $\mathscr{E}_2^{(\ell+1)}-\mathscr{E}_2^{(\ell)}$ are also generally achieved by UWCEnKF-2 compared to UWCEnKF-1. It can be seen that after 5 iterations, UWCEnKF-2 decreases to a value below the selected arbitrary threshold of $\mathscr{E}_2^{(\ell+1)}-\mathscr{E}_2^{(\ell)} = 10mm$. This is due to the fact that UWCEnKF-2 enables more degree of freedom in the optimization process by using different error variance for each grid point as compared to UWCEnKF-1, which tries to fit a single value for the entire domain.

In order to demonstrate the relevance of the UWCEnKF, we compare its results against those of the WCEnKF with various preselected values of error variances. The sensitivity of the WCEnKF to the choice of $\boldsymbol{\Sigma}$ can be seen in Figs. 4. The various implementations of the WCEnKF result in different performances in terms of imbalance and the Root-Mean-Squared Error (RMSE), which is calculated based on the assimilation results and groundwater in situ measurements over the Murray-Darling Basin. The estimated groundwater time series from the WCEnKF and UWCEnKF are spatially interpolated to the nearest gauge stations. The difference between in situ and filtered time series are then used to calculate the RMSE.

Each circle in Figs. 4 refers to the average results of an independent implementation of WCEnKF. It can be seen that the results of this filter largely vary depending on the selection of the error variance. Overall, lower imbalance and RMSE are obtained by assuming 20–30 mm^2. UWCEnKF-1 and UWCEnKF-2, on the other hand, achieve better results, shown by the triangle and cross, respectively, in a single implementation. The optimization algorithms used in UWCEnKF cause this independence of the error variance choice. It can also be seen that WCEnKF can achieve comparable results to that of UWCEnKF-1 in few cases. UWCEnKF-2, however, generally leads to the minimum RMSE and imbalance.

5.1.2. Spatial and temporal balance error variance

The performance of the proposed UWCEnKF in estimating water balance error variance and their effects on the imbalance between water fluxes are discussed in this section and is further compared with WCEnKF results. Both spatial and temporal variabilities are examined. Fig. 5 shows the temporally averaged error variances assigned to the observations for WCEnKF, as well as those estimated by UWCEnKF-1 and UWCEnKF-2 over the Amazon Basin. It can be seen that UWCEnKF-1 and UWCEnKF-2 estimate different errors at each iteration. The error variance maps in WCEnKF, on the other hand, is fixed to what has been assigned prior to data assimilation. After eight iterations, it is observed that the error estimated by UWCEnKF-1 is closer to the average of UWCEnKF-2 results (34.70 mm^2), i.e., 41.19 mm^2 for UWCEnKF-1 and, in comparison to 68.74 mm^2 for WCEnKF. This indicates that both UWCEnKF-1 and UWCEnKF-2 result in uncertainties with close magnitude for water balances and the implemented algorithms allow for such an adjustment during iteration steps. Furthermore, Fig. 5 depicts the spatial variability characteristics of error variances estimated by UWCEnKF-2. This property allows for more flexibility for error adjustment in UWCEnKF-2. These flexibilities in the UWCEnKF filtering method, as illustrated in Fig. 6, result in a smaller imbalance.

The better performances of UWCEnKF-1 and UWCEnKF-2 compared to WCEnKF in minimizing imbalance errors are clear in Fig. 6, where each map shows the estimated imbalance corresponding to Fig. 5 setups. Fig. 6 shows that the iteration algorithm effectively reduces imbalance errors, even after only few iterations (e.g., four). In addition, it can be seen that the applied algorithm in UWCEnKF provides the opportunity for error variances to be adjusted with no supervision as in WCEnKF. UWCEnKF-2, with more flexibility for such adjustment than UWCEnKF-1 (cf. Fig. 5), leads to the smaller imbalance, that is ~6 mm (absolute average of all values) against ~13 mm (on average) for UWCEnKF-1. This larger improvement for UWCEnKF-2 results is achieved by estimating different error variance values over each grid point, and correspondingly applying different rate of adjustments (based on the estimated water balance uncertainty) from the equality constraint to the points.

An example of the above mentioned spatially varying error variance in UWCEnKF-2 can be seen in Fig. 7. Fig. 7a depicts the average imbalance over Murray-Darling basin after jointly assimilating GRACE TWS and satellite soil moisture in the first analysis step of UWCEnKF. It is worth mentioning that we find larger impacts of GRACE TWS data (approximately 7.5 times for all the basins) on the imbalance between fluxes compared to the satellite soil moisture products, which could be explained by the fact that contrary to the soil moisture assimilation, GRACE data influences all compartments. The temporally averaged estimated variances are displayed in Fig. 7b. It can be seen that both estimated maps exhibit similar spatial patterns in some areas. One can also see in Fig. 7b that, in general, a larger variance is estimated over the areas with larger imbalance. Fig. 7c shows the average applied increments in the second analysis step of UWCEnKF-2 to account for the above imbalances. It is clear that larger increments are applied over the areas with larger imbalances, e.g., the north, southeast, and southwest parts of the basin. The areas such as the central parts, which display smaller imbalance in Fig. 7a, are also assigned smaller increments as shown in Fig. 7c.

Similar flexibilities for error variance estimation in UWCEnKF can

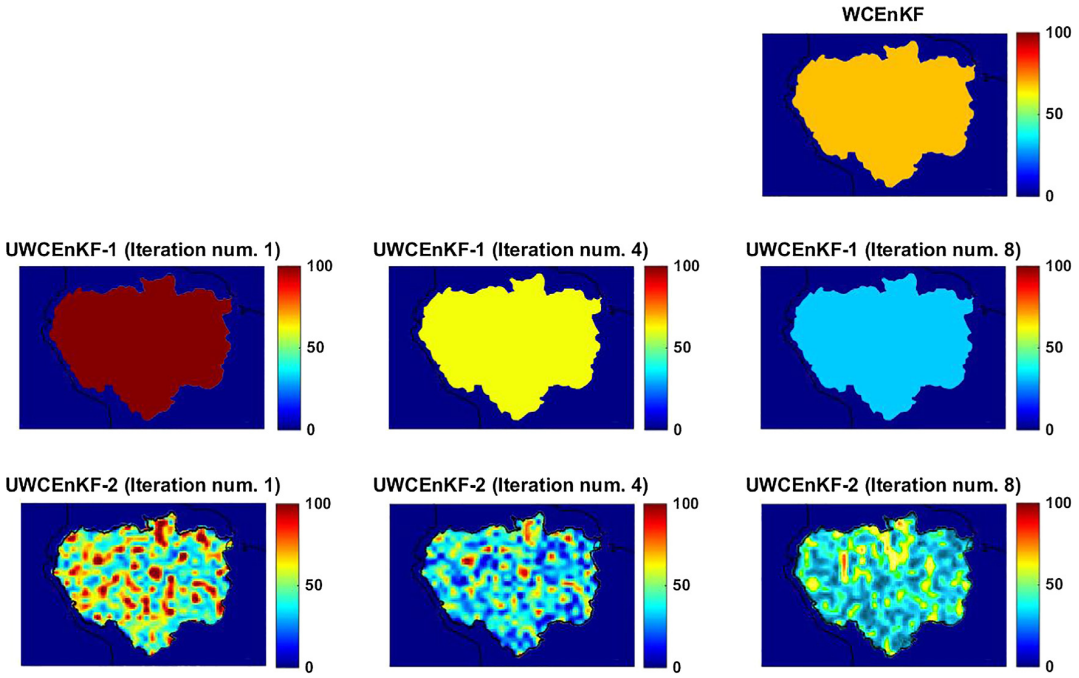

Fig. 5. Spatial variability of error variances estimated by WCEnKF, UWCEnKF-1, and UWCEnKF-2. The corresponding results for different iterations are also demonstrated for WCEnKF-1 and UWCEnKF-2.

also be seen from the temporal variabilities of error variances as demonstrated in Fig. 8. The water balance error variances at each assimilation step are estimated from UWCEnKF-1 for the entire Orange Basin and from UWCEnKF-2 for each grid point (green shaded area) of the basin. The figure also plots that of UWCEnKF-2 derived spatially averaged values, as well as errors used in WCEnKF. Again, it is clear from Fig. 8 that UWCEnKF-1 and UWCEnKF-2 allow for larger variations in error estimations than WCEnKF. It can also be seen that errors at each point can vary independently in UWCEnKF-2, which results in a better uncertainty adjustment. This can help for optimal imbalance minimization in the filter.

Both spatial and temporal variabilities of error variances are summarized in Fig. 9 over all basins, which shows variation ranges of water balance covariance in time (vertical lines) and space (horizontal lines)

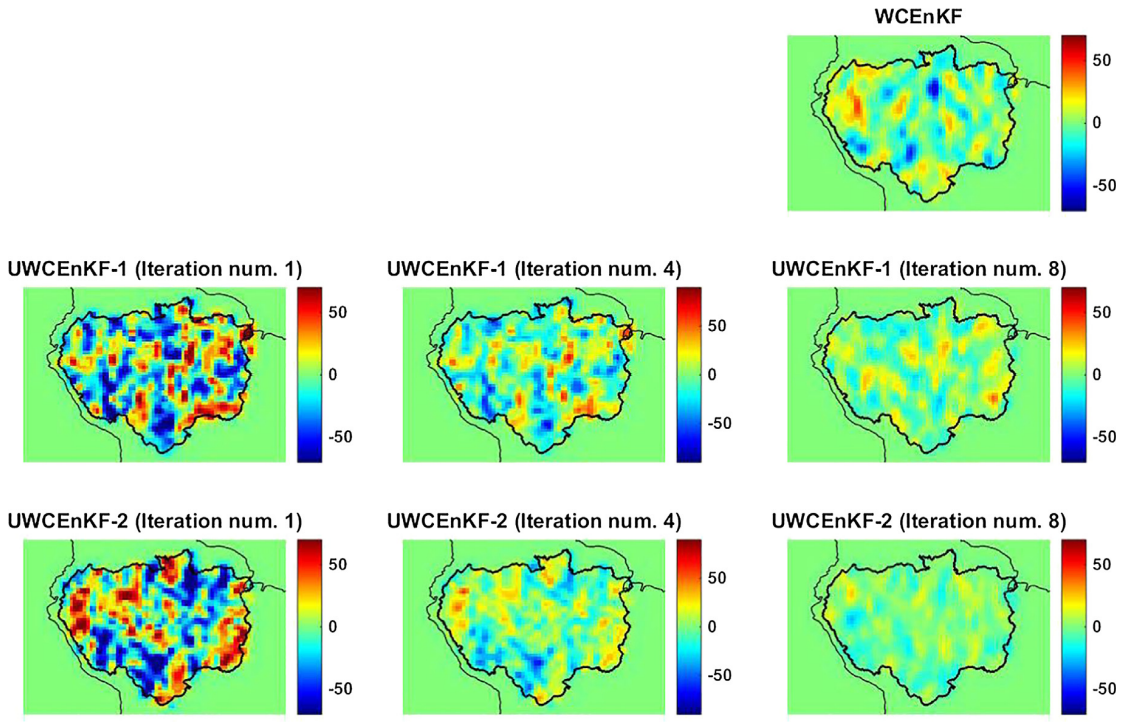

Fig. 6. Spatial variability of imbalances from WCEnKF, UWCEnKF-1, and UWCEnKF-2 corresponding to the errors presented in Fig. 5.

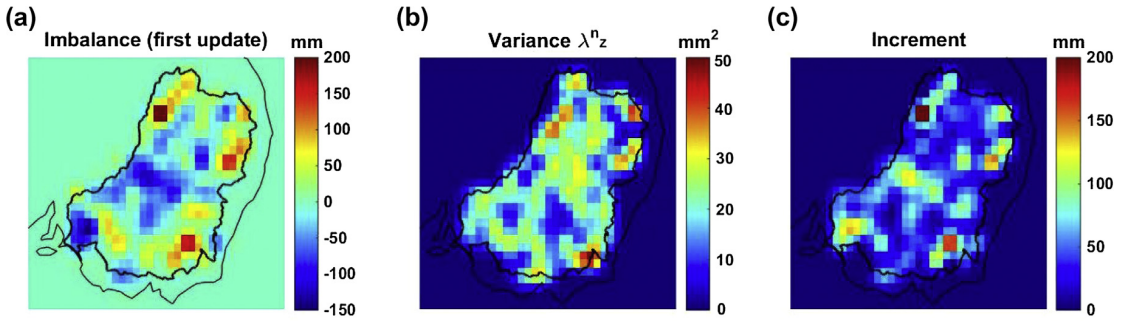

Fig. 7. Temporarily averaged maps of imbalances from UWCEnKF-2's first update (a), estimated error variance (b), and increments applied in the second analysis step of UWCEnKF-2 (c).

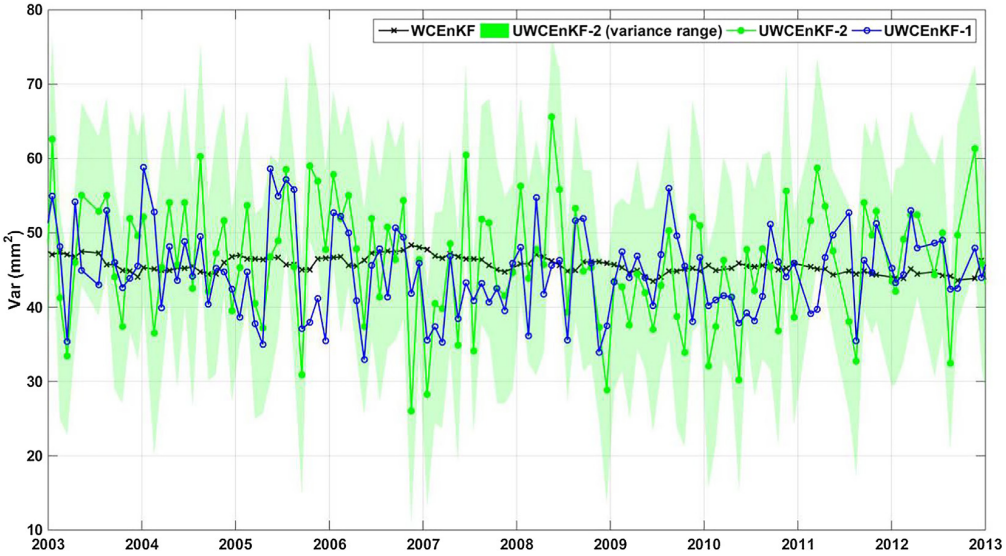

Fig. 8. Average water balance variances estimated by UWCEnKF-1 and UWCEnKF-2. The plots also contains the assigned variance values for WCEnKF implementation.

for WCEnKF, UWCEnKF-1, and UWCEnKF-2. In contrast to WCEnKF and UWCEnKF-1, spatial variabilities can be observed in UWCEnKF-2 results. As discussed, this helps for a better error adjustment during the filtering process. In terms of temporal variations, both UWCEnKF-1 and UWCEnKF-2 perform comparably well representing a larger range of changes than WCEnKF over all basins. The unsupervised error estimation algorithm in UWCEnKF enables to estimate an "optimal" water balance error calculation, which as it will be shown in Section 5.3 (cf.

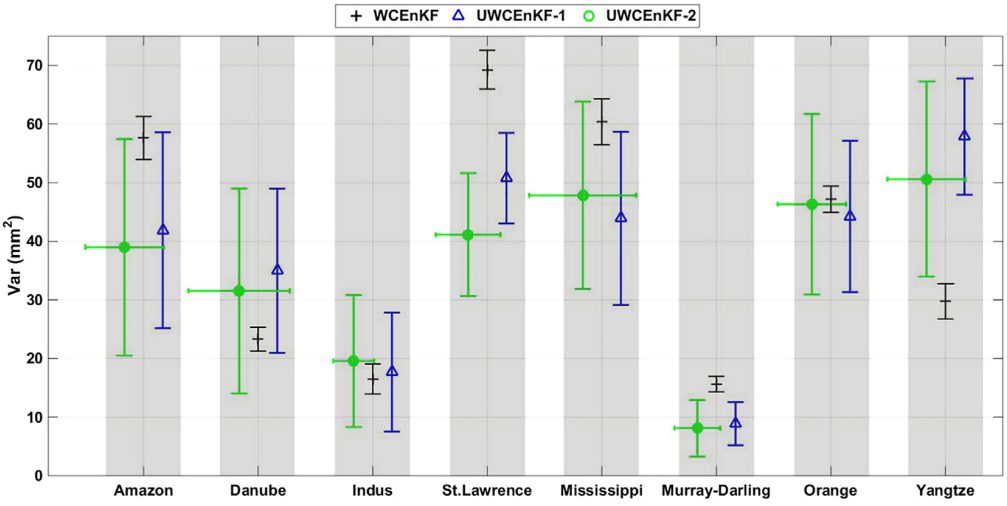

Fig. 9. Variation ranges of water balance covariance in time (vertical lines) and space (horizontal lines) for WCEnKF, UWCEnKF-1, and UWCEnKF-2.

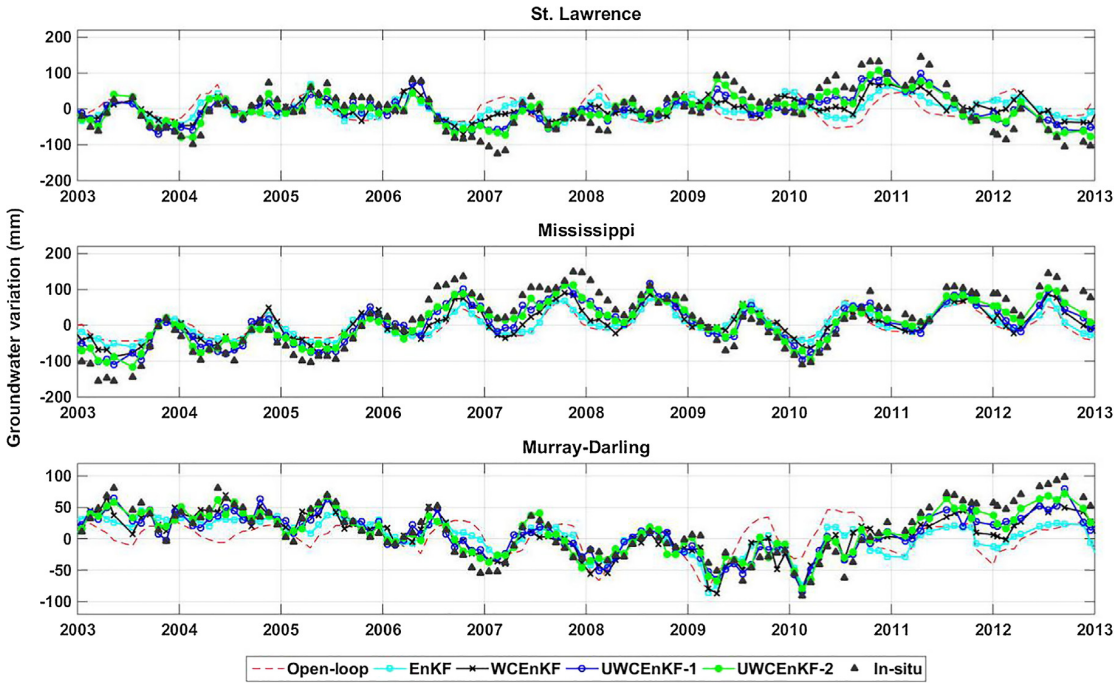

Fig. 10. Average groundwater variation time series by the open-loop run, EnKF, WCEnKF, UWCEnKF-1, and UWCEnKF-2 over St. Lawrence, Mississippi, and Murray-Darling basins.

Fig. 15) leads to smaller imbalance errors. In cases where assigned error to WCEnKF is close to what is calculated by UWCEnKF, e.g., Indus Basin, the final achieved imbalance from the filters are also close. In other cases with larger differences between assigned and estimated errors, there are larger discrepancies in imbalances.

5.2. Validations with in situ measurements

The performances of the EnKF and UWCEnKF are compared with in situ measurements. UWCEnKF was tested with both constant (UWCEnKF-1) and spatially varying (UWCEnKF-2) error variances for the water balance equation. Fig. 10 shows the average groundwater time series over the Mississippi, Murray-Darling and the St. Lawrence basins, estimated by the open-loop run (without assimilation), EnKF, WCEnKF, UWCEnKF-1, and UWCEnKF-2. Remarkable improvement can be seen from the different filters compared to the open-loop time series. In this regard, WCEnKF and UWCEnKF generally perform better than EnKF. This is more evident when a considerable trend exists in the time series, e.g., within the Murray-Darling basin after 2009 and St. Lawrence between 2010 and 2012. It can also be seen that UWCEnKF groundwater time series in most of the times better match to those of in situs. A clear example of this can be found in Murray-Darling basin 2011–2013. Furthermore, comparing UWCEnKF-1 and UWCEnKF-2, better agreements between in situ and estimated groundwater changes are achieved for UWCEnKF-2 over all three basins, particularly in the Mississippi basin.

To better monitor how UWCEnKF improves the groundwater estimates, their results are compared with in situ measurements and against those of EnKF. RMSE and standard deviation (STD) are calculated for groundwater error time series, i.e., the difference between in situ and filtered groundwater time series, at the location of each in situ station. Figs. 11 and 12 display the results over the Murray-Darling and Mississippi basins, respectively.

One can see that the filters successfully reduce RMSE and STD w.r.t. the open-loop run. This indicates the relevance of assimilation for decreasing state estimate errors. The groundwater estimate improvements are different for each filter. UWCEnKF-1 and UWCEnKF-2 suggest more (18% on average) error reduction than EnKF. Overall, more pronounced error reductions are achieved over the Mississippi basins, which could be attributed to larger model errors within the basin. Slightly better performances (~4%) in terms of groundwater error reduction are obtained with UWCEnKF-2 compared to UWCEnKF-1. We also compute the correlations (at 0.05 significance level) between the filtered and in situ groundwater time series. Similarly, larger correlations result from the filter estimates compared to the open-loop run, namely, 14% from EnKF, 26% for UWCEnKF-1, and 29% for UWCEnKF-2. The correlation results also confirm that UWCEnKF provides better estimates of the groundwater time series.

In-situ soil moisture measurements are also used to assess the assimilation impact on soil storage. To this end, similar to groundwater assessment, filtered soil moisture time series at the stations' locations are compared with their in situ counterpoints at different layers. Fig. 13 shows root-zone soil moisture variation time series as estimated by the various filters, as well as in situ measurements over the Mississippi, Murray-Darling, St. Lawrence, Danube, and the Yangtze basins. It can be seen that all filters decrease the misfits between estimated and measured soil moisture variations. In some cases, however, UWCEnKF, and to a lesser degree WCEnKF, performs better, e.g., Mississippi (2009), Murray-Darling (2004 and 2008), and Danube (2006). There are also various occasions during which the WCEnKF and UWCEnKF-1 results are very close, such as St. Lawrence 2010–2012 and Yangtze 2005–2006. This can be explained by the fact that both methods use a single error variance value for water balance uncertainties, so whenever a good approximation is used to assign this value prior to data assimilation in WCEnKF, close to what is estimated in UWCEnKF-1, the corresponding state estimates seen to be also close. UWCEnKF-2, on the other hand, performs relatively better, being more successful in matching soil moisture estimates to the in situ soil moisture variations.

The correlation results between the monthly soil moisture estimates for all filters w.r.t. the monthly in situ measurements are presented in Table 2. Note that different soil moisture estimates of various soil layers are compared to soil moisture measurements at corresponding layers

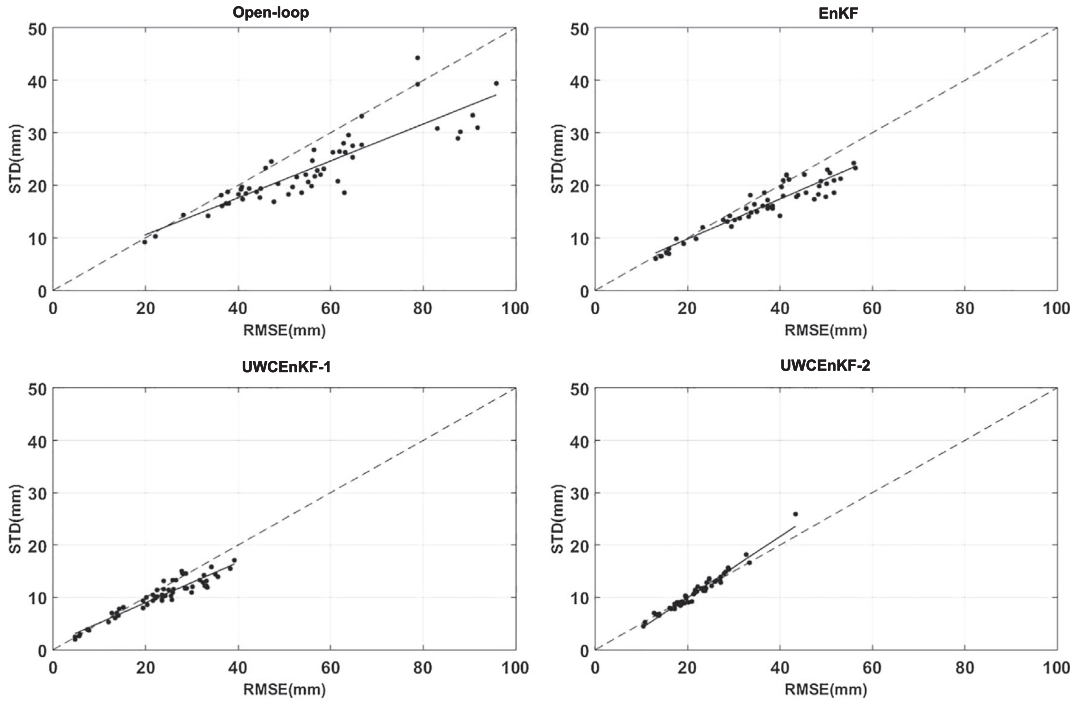

Fig. 11. Average RMSE and STD of the groundwater results from the EnKF, UWCEnKF-1, and UWCEnKF-2 filters over the Murray-Darling basin regarding the in situ groundwater measurements.

and their average are reported in the table. For instance, the model top layer is compared with 0–8 cm measurements over the Murray-Darling basin and 0–10 cm over Mississippi basin, summations of the model top, shallow, and a small portion of deep-root soil layers are tested against 0–30 cm and 0–50 cm measurements over the Murray-Darling and Mississippi basins, respectively, and summations of the model's soil layers are compared to 0–90 cm (for Murray-Darling) and 0–100 cm (for Mississippi) soil measurements. Due to a difference between the soil moisture estimates (i.e., column water storage measured in mm) and the in situ measurements (i.e., volumetric soil moisture), only a correlation analysis is conducted. Additionally, in order to statistically assess the results, a significance test for the correlation coefficients is applied

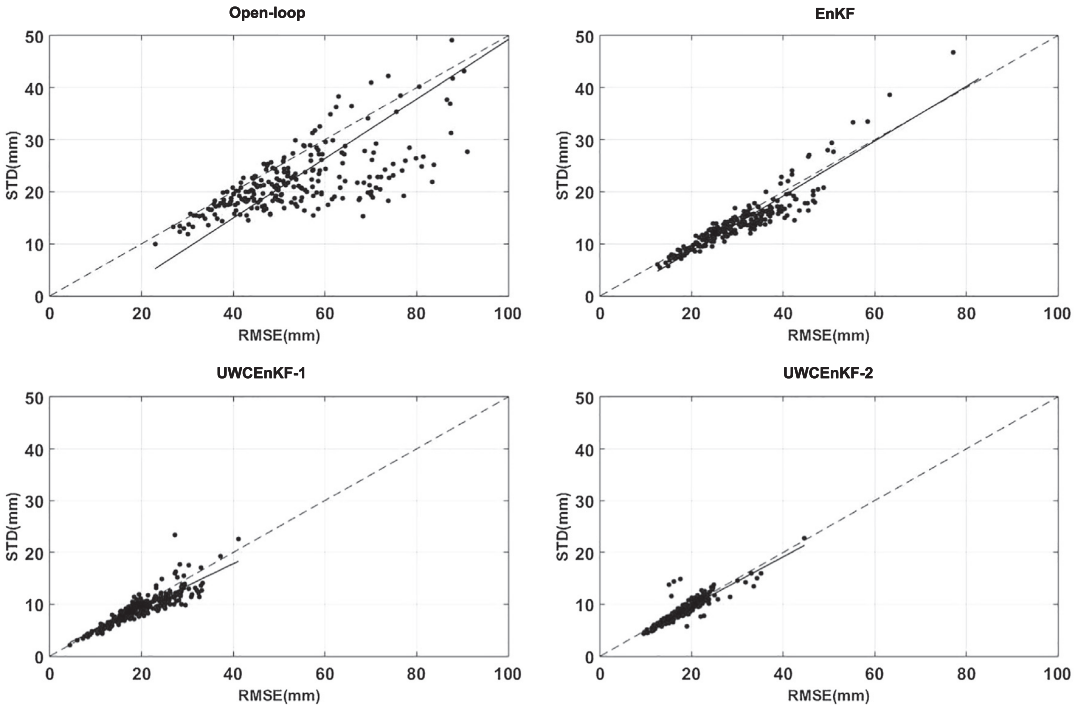

Fig. 12. Average RMSE and STD of the groundwater results from the EnKF, UWCEnKF-1, and UWCEnKF-2 filters over the Mississippi basin regarding the in situ groundwater measurements.

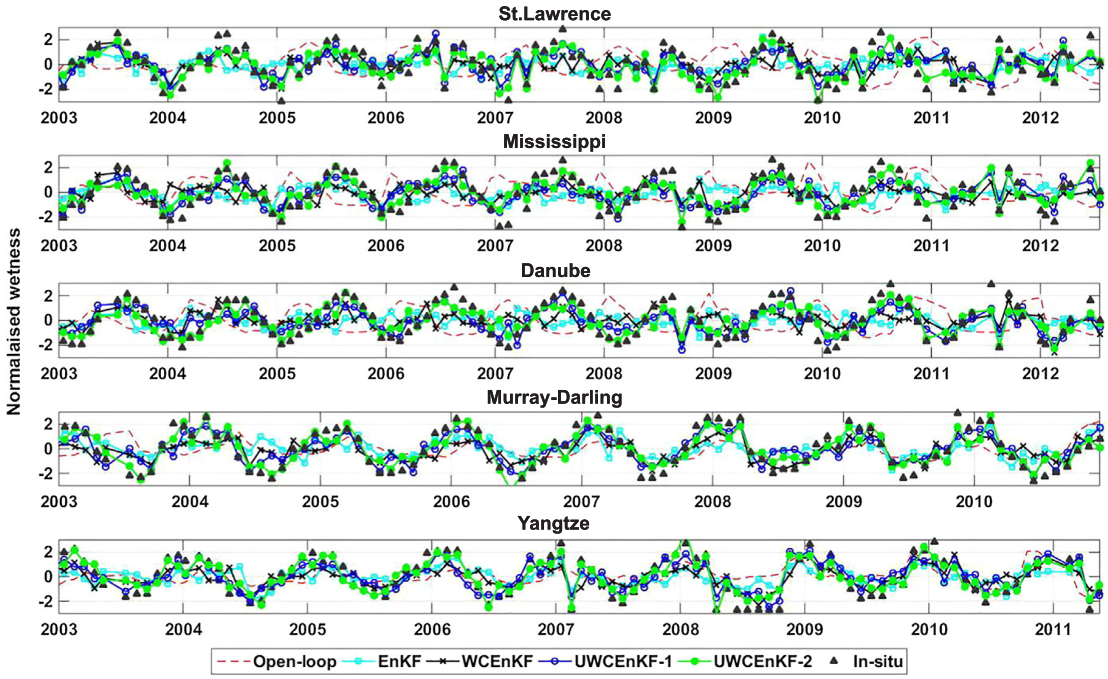

Fig. 13. Average soil moisture variation time series by the open-loop run, EnKF, WCEnKF, UWCEnKF-1, and UWCEnKF-2 over St. Lawrence, Mississippi, Danube, Yangtze, and Murray-Darling basins.

based on the t-distribution. The estimated t-value and the distribution at 0.05 significant level are used to calculate the p-value, which is assumed to be significant if it lies under 5%.

The results indicate that assimilation significantly improves soil storages regardless of the applied filter. All the filters have positive effects on soil moisture estimates. UWCEnKF performs better than both WCEnKF and EnKF with respectively 6% and 11% higher correlations with the in situ measurements. It can also be seen that in some cases, e.g., Mississippi basin, the filters generally perform comparably, especially WCEnKF and UWCEnKF-1. This indicates that WCEnKF is capable of improving soil moisture estimates as UWCEnKF subject to using an accurate water balance uncertainty because this is the only difference between the two approaches. The largest improvement with an average 20.28% for all basins is achieved by UWCEnKF-2, better than UWCEnKF-1 (17.75% on average) and noticeably larger than EnKF (7.85%).

We further examine the assimilation results against independent discharge data over different basins. It is worth mentioning that these discharge datasets are not assimilated. The average correlations between the estimated water discharge time series and those from the in situ data over each basin are presented in Table 3. Improvements are achieved for all assimilation experiments w.r.t. the open-loop run. The EnKF increases the correlation by 4% (on average), while UWCEnKF-1 and UWCEnKF-2 increase the correlation by approximately 23% and 24%, respectively. Again, UWCEnKF provides better results than EnKF over all basins. The largest correlation values are obtained for the Murray-Darling and Amazon basins, while the largest correlation improvements are achieved over the Orange, Amazon, and the Yangtze basins.

Table 3
Average correlations between the filtered water discharge and independent observations over different basins.

Basin	Open-loop	EnKF	UWCEnKF-1	UWCEnKF-2
Amazon	73.62	78.04	95.26	96.58
Danube	76.13	76.28	90.77	90.60
Indus	77.08	74.71	84.48	85.37
St. Lawrence	68.55	80.65	87.41	89.17
Mississippi	71.91	73.78	94.29	93.32
Murray-Darling	79.36	83.12	96.31	96.89
Orange	69.47	71.82	93.42	94.05
Yangtze	71.15	75.49	92.69	93.91

5.3. Impact of the equality constraint

To further investigate the relevance of the second analysis step of UWCEnKF, we calculate correlations between the filters estimates and assimilated observations at the forecast and analysis steps for all basins.

Table 2
Average correlations between in situ and soil moisture estimates from various methods. Improvements in the assimilation results are calculated as *[(assimilation - open-loop run)/open-loop run] × 100(%)*.

Basin	Open-loop	EnKF	WCEnKF	UWCEnKF-1	UWCEnKF-2
Danube	0.67	0.74	0.79	0.81	0.82
St. Lawrence	0.69	0.72	0.76	0.84	0.87
Mississippi	0.72	0.81	0.85	0.86	0.88
Murray-Darling	0.76	0.83	0.86	0.89	0.91
Yangtze	0.73	0.75	0.78	0.80	0.81
Improvements (%)	–	7.85	13.22	17.75	20.28

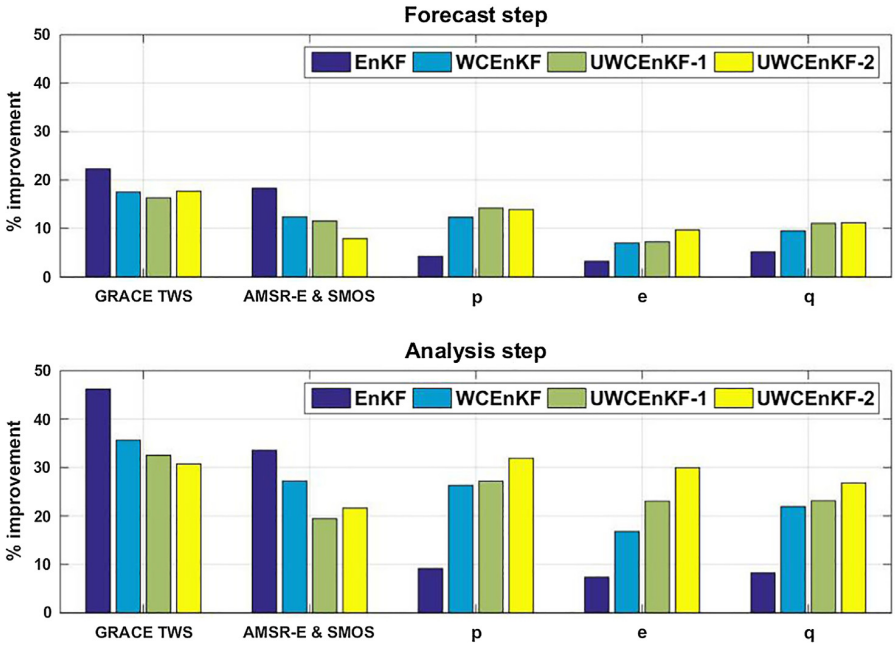

Fig. 14. Average correlation improvements of filtered TWS time series to GRACE TWS, **p**, **e**, and discharge **q** with respect to open-loop run in forecast and analysis steps. For AMSR-E + SMOS correlation, filtered top soil storage estimates are used.

The average correlations improvements w.r.t. the open-loop run are plotted in Fig. 14. As expected, larger correlations are obtained in the analysis step. In general, applying EnKF results in larger correlations between the estimates and assimilated observations (e.g., GRACE TWS and AMSR-E + SMOS) because during the EnKF assimilation the full magnitude of the update is applied to the variables regardless of the water balance. However, the WCEnKF and UWCEnKF take into account the water balance in a second update, which leads to the most improvements regarding **p**, **e**, and **q**. This is due to the fact that the first update in the WCEnKF and UWCEnKF corrects the state variables with the observations, and the second update corrects the water balance. This suggests that water budget constraint slightly degrades the effects of observations in the (second) update step in both WCEnKF and UWCEnKF filters, which is generally due to the observation overfitting problem, when no constraint is applied (e.g., standard EnKF) in data assimilation (see also Tangdamrongsub et al., 2017; Khaki et al., 2017). Furthermore, there is a degree of disagreement between TWS changes and other flux observations (e.g., precipitation, evaporation, and discharge), which could be attributed to different sources of uncertainties in the observations (see, e.g., Aires, 2014; Munier et al., 2015). The water budget constraint applied to data assimilation (i.e., the second update of UWCEnKF) accounts for this effect by further correcting the estimated states from the first update step based on GRACE TWS. The second step partly removes the artifacts from data assimilation of GRACE in the first step. It can clearly be seen that UWCEnKF provides higher correlations to the flux observations than WCEnKF. This improvement is more pronounced by using UWCEnKF-2. UWCEnKF's both variants remarkably increase the correlations between TWS estimates and water fluxes compared to EnKF. Overall, a better performance is observed for UWCEnKF-2 in comparison to UWCEnKF-1.

The results of water budget closure resulting from each filter for every basin are shown in Fig. 15. UWCEnKF-1 and UWCEnKF-2 clearly reduce water budget imbalances for all basins compared to WCEnKF and especially EnKF. It can also be seen that UWCEnKF-2 better enforces the balance between water components after assimilation. The absolute imbalance from UWCEnKF-2 is 15.28 mm, 8.26% smaller than UWCEnKF-1, 17.84% smaller than WCEnKF, and 36.47% smaller than EnKF. Note that these average values are computed for all basins. The imbalance reductions can also be seen from the reported STD values for each time series in Fig. 15. In all basins, the largest STD results from the EnKF and the least from the UWCEnKF-2. In some cases such as Indus, and to a lesser degree Amazon, WCEnKF performs comparably to UWCEnKF-1. UWCEnKF-2, on the other hand, achieves the largest water budget imbalance reduction, in terms of amplitude and STD, which confirms the results of Fig. 14, as well as the validation results against in situ measurements.

6. Conclusions

This study introduced an Unsupervised Weak Constrained Ensemble Kalman Filter (UWCEnKF) to mitigate for water budget imbalance while accounting for uncertainties in the inputs of the water balance components. UWCEnKF is an extension of the previously proposed Weak Constrained Ensemble Kalman Filter (WCEnKF) to a more general (unsupervised) framework, in which the covariance associated with the water balance model is estimated along with the system state. Numerical experiments were carried out to assess the performance of the UWCEnKF against WCEnKF, as well as the standard Ensemble Kalman Filter (EnKF). The filters' results examinations against available in situ measurements indicated that UWCEnKF performs best in terms of groundwater error reduction and soil moisture estimate improvements. In general, UWCEnKF reduced groundwater errors (w.r.t. groundwater in situ measurements) by 18% (on average), and 11% (on average) more than EnKF and WCEnKF, respectively. UWCEnKF-2 also achieved 4% (on average) smaller groundwater RMSE than UWCEnKF-1. Furthermore, UWCEnKF increased the correlation values between soil moisture estimates and those of the in situ measurements by 6% more than WCEnKF and 12% more than EnKF. Again, UWCEnKF-2 performed better than UWCEnKF-1 with larger soil moisture correlations w.r.t. the in situ soil moisture measurements, i.e., 20.28% against 17.75%. UWCEnKF also achieved larger correlations to independent discharge datasets, e.g., respectively 6% and 11% larger correlations with the in situ measurements than WCEnKF and EnKF. The experiments results also suggested that the UWCEnKF using spatially varying error variances for the water balance equation provides better groundwater and soil moisture estimates than applying a constant error

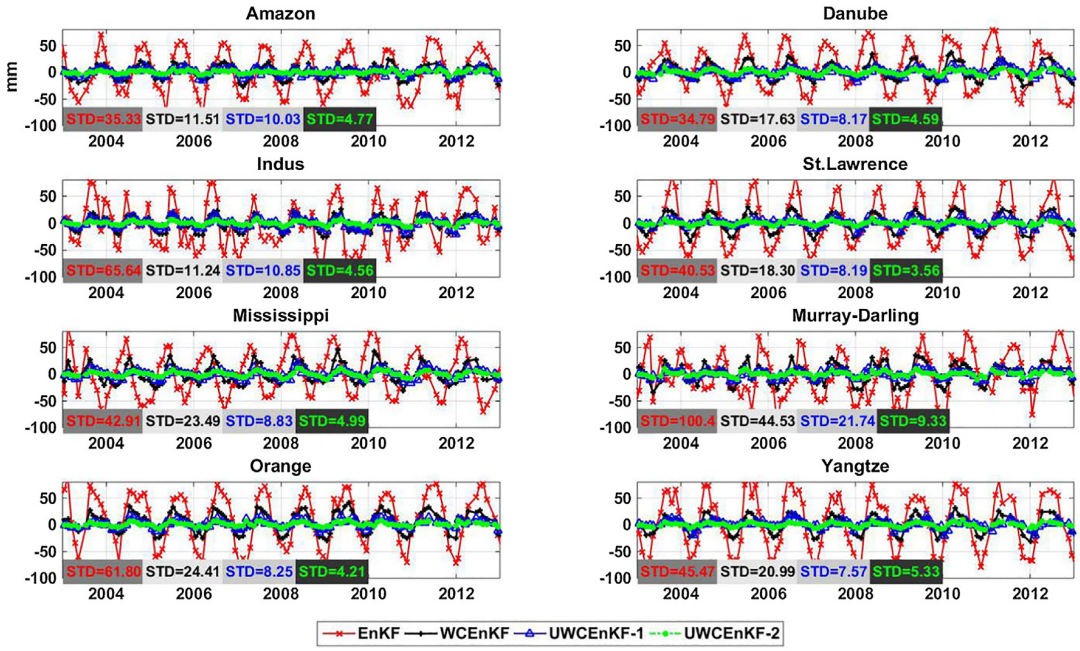

Fig. 15. Average water budget imbalance time series calculated using EnKF, WCEnKF, and UWCEnKF variants for each basin (units are mm).

variance. A similar performance was also obtained for the water budget imbalance reduction, where the prior variant better mitigated the imbalance problem than the latter case.

Overall, UWCEnKF achieved maximum correlations with the flux observations, both during the forecast and analysis steps. The largest imbalance reduction was also obtained using UWCEnKF. More specifically, the absolute imbalance for UWCEnKF-2 is 15.28 mm, 8.26% smaller than UWCEnKF-1, 17.84% smaller than WCEnKF, and 36.47% smaller than EnKF. These results demonstrate the relevance of the new proposed unsupervised scheme, which is straightforward to implement and computationally not intensive. Future work will consider extending the proposed framework to jointly estimate the model biases with the state and the observation error variance.

Acknowledgement

M. Khaki is grateful for the research grant of Curtin International Postgraduate Research Scholarships (CIPRS)/ORD Scholarship provided by Curtin University (Australia). This work is a TIGeR publication.

References

Adler, R.F., Susskind, J., Huffman, G.J., Bolvin, D., Nelkin, E., Chang, A., et al., 2003. Global precipitation climatology project V2.1 monthly 2.5 deg global 1979-present (satellite only and gauge adjusted) 2003: the version-2 global precipitation climatology project (GPCP) monthly precipitation analysis (1979-present). J. Hydrometeorol. 4, 1147–1167.

Ait-El-Fquih, B., Hoteit, I., 2015. Fast Kalman-like Filtering in large-dimensional linear and Gaussian state-space models. IEEE Trans. Signal Process. 63, 5853–5867.

Ait-El-Fquih, B., Hoteit, I., 2016. A variational Bayesian multiple particle filtering scheme for large-dimensional systems. IEEE Trans. Signal Process. 64, 5409–5422.

Anderson, J., 2001. An ensemble adjustment Kalman filter for data assimilation. Mon. Weather Rev. 129, 2884–2903. https://doi.org/10.1175/1520-0493(2001)1292884:AEAKFF2.0.CO;2.

Aires, F., 2014. Combining datasets of satellite retrieved products. Part I: Methodology and water budget closure. J. Hydrometeorol. 15 (4), 1677–1691.

Blei, David M., Kucukelbir, Alp, McAuliffe, Jon D., 2017. Variational inference: a review for statisticians. J. Am. Stat. Assoc. 112 (518), 859–877. https://doi.org/10.1080/01621459.2017.1285773.

Chen, M., Xie, P., Janowiak, J.E., Arkin, P.A., 2002. Global land precipitation: a 50-yr monthly analysis based on gauge observations. J. Hydrometeorol. 3, 249–266.

Cheng, M.K., Tapley, B.D., 2004. Variations in the Earth's oblateness during the past 28 years. J. Geophys. Res. Solid Earth 109, B09402. https://doi.org/10.1029/2004JB003028.

De Jeu, R.A.M., Owe, M., 2003. Further validation of a new methodology for surface moisture and vegetation optical depth retrieval. Int. J. Remote Sens. 24, 4559–4578. https://doi.org/10.1080/0143116031000095934.

De Jeu, R.A.M., Wagner, W., Holmes, T.R.H., Dolman, A.J., van de Giesen, N.C., Friesen, J., 2008. Global soil moisture patterns observed by space borne microwave radiometers and scatterometers. Surv. Geophys. 29 (4–5), 399–420. https://doi.org/10.1007/s10712-008-9044-0.

Draper, C.S., Mahfouf, J.-F., Walker, J.P., 2009. An EKF assimilation of AMSR-E soil moisture into the ISBA land surface scheme. J. Geophys. Res. 114, D20104. https://doi.org/10.1029/2008JD011650.

Drusch, M., Wood, E.F., Gao, H., 2005. Observation operators for the direct assimilation of TRMM microwave imager retrieved soil moisture. Geophys. Res. Lett. 32, L15403.

Eicker, A., Schumacher, M., Kusche, J., Döll, P., Müller-Schmied, H., 2014. Calibration/data assimilation approach for integrating GRACE data into the WaterGAP global hydrology model (WGHM) using an ensemble Kalman filter: first results. SurvGeophys 35 (6), 1285–1309. https://doi.org/10.1007/s10712-014-9309-8.

Gutentag, E.D., Heimes, F.J., Krothe, N.C., Luckey, R.R., Weeks, J.B., 1984. Geohydrology of the High Plains aquifer in parts of Colorado, Kansas, Nebraska, New Mexico, Oklahoma, South Dakota, Texas, and Wyoming, U.S. Geol. Surv. Prof. Pap., 1400-B, 66 pp.

Han, R., Tian, X.J., Fu, Y., Cai, Z.N., 2015. Real-data assimilation experiment with a joint data assimilation system: assimilating carbon dioxide mole fraction measurements from the Greenhouse gases Observing Satellite. Atmos. Oceanic Sci. Lett. 9 (2), 107–113. https://doi.org/10.1080/16742834.2016.1133070.

Houtekamer, P.L., Mitchell, H.L., 2001. A sequential ensemble Kalman filter for atmospheric data assimilation. Mon. Weather Rev. 129 (1), 123–137.

Huffman, G.J., Adler, R.F., Bolvin, D.T., Gu, G., Nelkin, E.J., Bowman, K.P., Hong, Y., Stocker, E.F., Wolff, D.B., 2007. The TRMM multi-satellite precipitation analysis: quasi- global, multi-year, combined-sensor precipitation estimates at fine scale. J. Hydrometeor. 8 (1), 38–55.

Jaakkola, T.S., Jordan, M.I., 2000. Bayesian parameter estimation via variational methods. Stat. Comput. 10, 25–37.

Jackson, T., Bindlish, R., 2012. Validation of Soil Moisture And Ocean Salinity (SMOS) soil moisture over watershed networks in the US. IEEE Trans. Geosci. Remote Sens. 50, 1530–1543.

Jones, D.A., Wang, W., Fawcett, R., Grant, I., 2007. Climate data for the Australian water availability project. In: Australian Water Availability Project Milestone Report. Bur. Met., Australia, 37pp.

Joyce, R.J., Janowiak, J.E., Arkin, P.A., Xie, P.P., 2004. CMORPH: a method that produces global precipitation estimates from passive microwave and infrared data at high spatial and temporal resolution. J. Hydrometeorol. 5, 487–503.

Khaki, M., Ait-El-Fquih, B., Hoteit, I., Forootan, E., Awange, J., Kuhn, M., 2017. A two-update ensemble Kalman filter for land hydrological data assimilation with an uncertain constraint. J. Hydrol. 555, 447–462. https://doi.org/10.1016/j.jhydrol.2017.10.032. ISSN 0022-1694.

Khaki, M., Schumacher, M., Forootan, J., Kuhn, M., Awange, E., van Dijk, A.I.J.M., 2017. Accounting for spatial correlation errors in the assimilation of GRACE into Hydrological Models through localization. Adv. Water Resour. 108, 99–112. https://

doi.org/10.1016/j.advwatres.2017.07.024. ISSN 0309-1708.
Khaki, M., Hoteit, I., Kuhn, M., Awange, J., Forootan, E., van Dijk, A.I.J.M., Schumacher, M., Pattiaratchi, C., 2017. Assessing sequential data assimilation techniques for integrating GRACE data into a hydrological model. Advances in Water Resources 107, 301–316. https://doi.org/10.1016/j.advwatres.2017.07.001. ISSN 0309-1708.
Khaki, M., Forootan, E., Kuhn, M., Awange, J., Papa, F., Shum, C.K., 2018. A study of Bangladesh's Sub-surface water storages using satellite products and data assimilation scheme. Sci. Total Environ. 625, 963–977. https://doi.org/10.1016/j.scitotenv.2017.12.289.
Khaki, M., Forootan, E., Kuhn, M., Awange, J., van Dijk, A.I.J.M., Schumacher, M., Sharifi, M.A., 2018. Determining water storage depletion within Iran by assimilating GRACE data into the W3RA hydrological model. Adv. Water Resour. 114, 1–18. https://doi.org/10.1016/j.advwatres.2018.02.008.
Khaki, M., Forootan, E., Kuhn, M., Awange, J., Longuevergne, L., Wada, W., 2018. Efficient basin scale filtering of GRACE satellite products. Remote Sensing of Environment 204, 76–93. https://doi.org/10.1016/j.rse.2017.10.040. ISSN 0034-4257.
Leroux, D.J., Pellarin, T., Vischel, T., Cohard, J.-M., Gascon, T., Gibon, F., Mialon, A., Galle, S., Peugeot, C., Seguis, L., 2016. Assimilation of SMOS soil moisture into a distributed hydrological model and impacts on the water cycle variables over the Ouémé catchment in Benin. Hydrol. Earth Syst. Sci. 20, 2827–2840. https://doi.org/10.5194/hess-20-2827-2016.
Liang, X., Lettenmiar, D.P., Wood, E.F., Burges, S.J., 1994. A simple hydrologically based model of land-surface water and energy fluxes for general-circulation models. J. Geophys. Res. 99, 14415–14428. https://doi.org/10.1029/94JD00483.
Lievens, H., Reichle, R.H., Liu, Q., De Lannoy, G.J.M., Dunbar, R.S., Kim, S.B., Das, N.N., Cosh, M., Walker, J.P., Wagner, W., 2017. Joint Sentinel-1 and SMAP data assimilation to improve soil moisture estimates. Geophys. Res. Lett. 44, 6145–6153. https://doi.org/10.1002/2017GL073904.
Liu, C., Xue, M., 2016. Relationships among four-dimensional hybrid ensemble-variational data assimilation algorithms with full and approximate ensemble covariance localization. Mon. Weather Rev. 144, 591–606. https://doi.org/10.1175/MWR-D-15-0203.1.
Luo, L., Wood, E.F., Pan, M., 2007. Bayesian merging of multiple climate model forecasts for seasonal hydrological predictions. J. Geophys. Res. 112, D10102. https://doi.org/10.1029/2006JD007655.
Massoud, E.C., Huisman, J., Benincà, E., Dietze, M.C., Bouten, W., Vrugt, J.A., Adler, F., 2018. Probing the limits of predictability: data assimilation of chaotic dynamics in complex food webs. Ecol. Lett. 21, 93–103. https://doi.org/10.1111/ele.12876.
Mayer-Gürr, T., Zehentner, N., Klinger, B., Kvas, A., 2014. ITSG-Grace2014: a new GRACE gravity field release computed in Graz. In: GRACE Science Team Meeting (GSTM), Potsdam am: 29.09.2014.
Miralles, D.G., Holmes, T.R.H., de Jeu, R.A.M., Gash, J.H., Meesters, A.G.C.A., Dolman, A.J., 2011. Global land-surface evaporation estimated from satellite-based observations. Hydrol. Earth Syst. Sci. 15, 453–469.
Mu, Q., Heinsch, F.A., Zhao, M., Running, S.W., 2007. Development of a global evapotranspiration algorithm based on MODIS and global meteorology data. Remote Sens. Environ. 111, 519–536. https://doi.org/10.1016/j.rse.2007.04.015.
Munier, S., Aires, F., Schlaffer, S., Prigent, C., Papa, F., 2014. Combining datasets of satellite retrieved products for basin-scale water balance study. Part II: Evaluation on the Mississippi Basin and closure correction model. J. Geophys. Res.: Atmos. Am. Geophys. Union 119, 100–116.
Njoku, E.G., et al., 2003. Soil moisture retreival from AMSR-e. IEEE Trans. Geosci. Remote Sens. 41 (2), 215–229.
Njoku, E.G., 2004. AMSR-E/Aqua Daily L3 Surface Soil Moisture, Interpretive Parameters, QC EASE-Grids. Version 2. [indicate subset used]. Boulder, Colorado USA: NASA National Snow and Ice Data Center Distributed Active Archive Center. doi:https://doi.org/10.5067/AMSR-E/AELAND3.002.
Pan, M., Wood, E.F., 2006. Data assimilation for estimating the terrestrial water budget using a constrained ensemble Kalman filter. J. Hydrometeorol. 7 (3), 534–547.
Pan, M., Sahoo, A.K., Troy, T.J., Vinukollu, R.K., Sheffield, J., Wood, E.F., 2012. Multisource estimation of long-term terrestrial water budget for major global river basins. J. Clim. 25 (9), 3191–3206.
Reager, J.T., Thomas, A.C., Sproles, E.A., Rodell, M., Beaudoing, H.K., Li, B., Famiglietti, J.S., 2015. Assimilation of GRACE terrestrial water storage observations into a land surface model for the assessment of regional flood potential. Remote Sens. 7 (11), 14663–14679. https://doi.org/10.3390/rs71114663.
Reichle, R.H., Koster, R.D., 2004. Bias reduction in short records of satellite soil moisture. Geophys. Res. Lett. 31, L19501. https://doi.org/10.1029/2004GL020938.
Renzullo, L.J., Van Dijk, A.I.J.M., Perraud, J.M., Collins, D., Henderson, B., Jin, H., Smith, A.B., McJannet, D.L., 2014. Continental satellite soil moisture data assimilation improves root-zone moisture analysis for water resources assessment. J. Hydrol. 519, 2747–2762. https://doi.org/10.1016/j.jhydrol.2014.08.008.
Sahoo, A.K., Pan, M., Troy, T.J., Vinukollu, R.K., Sheffield, J., Wood, E.F., 2011. Reconciling the global terrestrial water budget using satellite remote sensing. Remote Sens. Environ. 115 (8), 1850–1865.
Sato, M., 2001. Online model selection based on the variational Bayes. Neural Comput. 13, 1649–1681.
Schneider, U., Fuchs, T., Meyer-Christoffer, A., Rudolf, B., 2008. In: G.P.C. Centre (Ed.), Internet Publication.
Seoane, L., Ramillien, G., Frappart, F., Leblanc, M., 2013. Regional GRACE-based estimates of water mass variations over Australia: validation and interpretation. Hydrol. Earth Syst. Sci. 17, 4925–4939. https://doi.org/10.5194/hess-17-4925-2013.
Schumacher, M., Kusche, J., Döll, P., 2016. A systematic impact assessment of GRACE error correlation on data assimilation in hydrological models. J. Geodesy. https://doi.org/10.1007/s00190-016-0892-y.
Simmons, A.J., Uppala, S., Dee, D., Kobayashi, S., 2007. ERA-interim: New ECMWF reanalysis products from 1989 onwards, ECMWF Newsletter No. 110 – Winter 2006/07.
Simon, D., Chia, T.L., 2002. Kalman filtering with state equality constraints. IEEE Trans. Aerosp. Electron. Syst. 38, 128–136.
Smidl, V., Quinn, A., 2006. The Variational Bayes Method in Signal Processing. Springer.
Smidl, V., Quinn, A., 2008. Variational bayesian filtering. IEEE Trans. Signal Process. 56, 5020–5030.
Smith, A.B., Walker, J.P., Western, A.W., Young, R.I., Ellett, K.M., Pipunic, R.C., Richter, H., 2012. The Murrumbidgee soil moisture monitoring network data set. Water Resour. Res. 48 (7), 1–6. https://doi.org/10.1029/2012WR011976.
Sokolov, A.A., Chapman, T.G., 1974. Methods for Water Balance Computation An International Guide for Research and Practice. The Unesco Press, Paris.
Strassberg, G., Scanlon, B.R., Rodell, M., 2007. Comparison of seasonal terrestrial water storage variations from GRACE with groundwater-level measurements from the High Plains Aquifer (USA). Geophys. Res. Lett. 34, L14402. https://doi.org/10.1029/2007GL030139.
Su, C.-H., Ryu, D., Young, R.I., Western, A.W., Wagner, W., 2013. Inter-comparison of microwave satellite soil moisture retrievals over the Murrumbidgee Basin, southeast Australia. Remote Sens. Environ. 134, 1–11.
Swenson, S., Chambers, D., Wahr, J., 2008. Estimating geocenter variations from a combination of GRACE and ocean model output. J. Geophys. Res. 113, B08410. https://doi.org/10.1029/2007JB005338.
Tangdamrongsub, N., Steele-Dunne, S.C., Gunter, B.C., Ditmar, P.G., Sutanudjaja, E.H., Xie, T., Wang, Z., 2017. Improving estimates of water resources in a semi-arid region by assimilating GRACE data into the PCR-GLOBWB hydrological model. Hydrol. Earth Syst. Sci. 21, 2053–2074.
Tian, S., Tregoning, P., Renzullo, L.J., van Dijk, A.I.J.M., Walker, J.P., Pauwels, V.R.N., Allgeyer, S., 2017. Improved water balance component estimates through joint assimilation of GRACE water storage and SMOS soil moisture retrievals. Water Resour. Res. 53. https://doi.org/10.1002/2016WR019641.
van Dijk, A.I.J.M., 2010. The Australian Water Resources Assessment System: Technical Report 3, Landscape model (version 0.5) Technical Description, CSIRO: Water for a Healthy Country National Research Flagship.
van Dijk, A.I.J.M., Renzullo, L.J., Wada, Y., Tregoning, P., 2014. A global water cycle reanalysis (2003–2012) merging satellite gravimetry and altimetry observations with a hydrological multi-model ensemble. Hydrol. Earth Syst. Sci. 18, 2955–2973. https://doi.org/10.5194/hess-18-2955-2014.
Wahr, J.M., Molenaar, M., Bryan, F., 1998. Time variability of the Earth's gravity field: hydrological and oceanic effects and their possible detection using GRACE. J. Geophys. Res. 108 (B12), 30205–30229. https://doi.org/10.1029/98JB02844.
Zaitchik, B.F., Rodell, M., Reichle, R.H., 2008. Assimilation of GRACE terrestrial water storage data into a land surface model: results for the Mississippi River Basin. J. Hydrometeorol. 9 (3), 535–548. https://doi.org/10.1175/2007JHM951.1.
Zhang, J., Campbell, J.R., Hyer, E.J., Reid, J.S., Westphal, D.L., Johnson, R.S., 2014. Evaluating the impact of multisensor data assimilation on a global aerosol particle transport model. J. Geophys. Res. Atmos. 119, 4674–4689. https://doi.org/10.1002/2013JD020975.
Zhang, Y., Pan, M., Wood, E.F., 2016. On creating global gridded terrestrial water budget estimates from satellite remote sensing. Surv. Geophys. 37 (2), 249–268.

Chapter 8

Summary and conclusion

This thesis investigated the application of the Gravity Recovery And Climate Experiment (GRACE) terrestrial water storage (TWS) for improving land hydrological model performances from various perspectives. Special considerations were given to address the limitations in existing methods by proposing new techniques. These include introducing new GRACE data filtering, examining various data assimilation filtering methods for assimilating GRACE TWS data, developing tuning techniques to use the full potential of GRACE observations for constraining system states, and proposing a new assimilation filter for both updating water storage states and enforcing the model dynamical balances, i.e., the fundamental water balance equation, on their estimates. The following summarizes the main outcomes of the thesis, which, to the best of the author knowledge, are new scientific contributions.

- The accuracy of GRACE TWS estimation is very important for hydrological data assimilation, thus, a powerful post-processing filtering method must be applied to improve the data product prior to the assimilation process. To this end, a new two-step filtering method, Kernel Fourier Integration (KeFIn) was proposed. The filter, first, reduces the GRACE measurement noise and aliasing of unmodelled high-frequency mass variations, and second, uses an anisotropic kernel to isolate the interfered signals to account for leakage problems. Evaluation of the proposed KeFIn filter against common techniques using different datasets suggested that the new filter successfully removes striping and reduces leakage errors. The KeFIn filtering method mitigated existing problems with other leakage filtering methods, e.g., dependence to an auxiliary model and over smoothing. The results within the 43 globally distributed river basins showed that the KeFIn filter (i) tackles the amplitude damping caused by smoothing, and (ii) increases flexibility towards a variety of basins (shapes and sizes of basins as well as the magnitude of TWS). We found that the proposed KeFIn filter reduces the leakage errors over most of the basins with an area less than 1 million km^2, thus, we concluded it is well-suited for leakage error reduction over small basins. This is

mainly due to the point that the filter is capable of recovery more signals, which typically are smoothed out by applying other existing methods. The KeFIn filter contrary to most of the existing methods does not require additional auxiliary data, e.g., hydrological models for scale factor methods, which makes it easier to be used by the GRACE community. More importantly, the proposed filter can simultaneously address both GRACE error types of aliasing and leakage, which is more efficient than applying a different filter for each error source. Despite its promising performance, the method may not be able to reduce all possible artificial features appearing in the two steps of the post-processing algorithm. In particular, more investigations are required to optimize parameters that are used within the filter. Nevertheless, the proposed filter can largely improve the GRACE data assimilation efficiency by providing more accurate GRACE-derived TWS for integrating into the hydrological models (objective (i), Section 1.4).

- After improving GRACE TWS estimates, a specific strategy is required to effectively merge them into the models by considering their spatial and temporal characteristics (cf. objective (ii), Section 1.4). For this purpose, tuning techniques were applied to maximize the effect of GRACE observation by using its full error information. This is particularly important considering that previous studies mostly neglect the impact of GRACE error covariance matrix and existing correlation between grid points that can lead to inaccurate estimates. In other words, by assuming an uncorrelated constant error value, an important part of observations have not being used during data assimilation. In this thesis, however, this problem was addressed by introducing the local analysis (LA) technique. The performance of LA was assessed in accounting for the existing correlation in GRACE data and improving its effect on model states. LA was applied to solve the mathematical problem of using correlated data for assimilation especially when the observation spatial resolution is high (e.g., 1° gridded TWS). Existing studies either assume that the observations are uncorrelated or apply them on basin scale to prevent the rank deficiency problem. The results showed that implementing LA, with the 5° localization halfwidth length, successfully reduces data assimilation errors compared to other cases with no tuning technique applied. This improvement is larger for the cases with smaller grid sizes along with higher error correlations. LA addressed the rank deficiency problem in using the full information from the error covariance matrix for a higher spatial resolution of GRACE TWS data (e.g., 1°). This, to the best of the author's knowledge, for the first time, allowed us to be able to apply GRACE TWS along with its associated error covariance at finer spatial resolutions (e.g., 1° and 2° against basin scale) for the hydrological data assimilation.

- Furthermore, the impacts of the GRACE TWS different spatial and temporal resolutions were investigated during assimilation. The observations were assimilated for a 5-day and

monthly temporal scale and for different grid resolutions (1° to 5° and a basin scale) to achieve the best case scenario while using LA tuning approach. Even though LA improved the assimilation results using GRACE TWS data for all of the above cases, the best performance was found with the application of GRACE data in assimilation with 3° spatial resolution at 5-day temporal scale. These findings can be helpful for any GRACE data assimilation experiment, however, further assessment needs to be undertaken to examine other potential methods like the inflation of the observation error variances and circulant approximation. Moreover, the impact of vertical localization on distribution GRACE TWS corrections between different water compartments is also important, which should be investigated in future studies.

- In addition to GRACE data post-processing and an assimilation tuning technique, a robust data assimilation framework requires an appropriate filtering method. Various data assimilation techniques from the common sequential methods were tested to investigate their capabilities in assimilating GRACE TWS into the hydrological model (cf. objective (iii), Section 1.4). Different aspects of these filtering techniques, e.g., state estimate improvement, forecasting, uncertainties quantification, and stability during the process were examined. The filters were selected from the two most commonly applied algorithms, ensemble Kalman filter (stochastic and deterministic), and Particle Filter. The effects of the filtering methods on the ensembles spread and the estimation error covariance matrices were investigated. The filter state estimates were further evaluated against in-situ groundwater measurements and in-situ soil moisture data. The most promising results were obtained from the Square Root Analysis (SQRA) and Ensemble Square-Root Filter (EnSRF), demonstrating significantly better performance than the other implemented filters. These two filters, along with standard Ensemble Kalman Filter (EnKF) also showed a good ability to sample representative ensembles. Furthermore, monitoring the impacts of the applied filters on the ensembles spread and the estimation error covariance matrices showed that the best results belong to SQRA, EnSRF, and EnKF. SQRA and EnSRF perform better in reducing error covariance after each assimilation step. In a statistical sense, EnSRF and SQRA filters provided the least Root-Mean-Squared Errors (RMSE) and maximum correlations for both groundwater level and soil moisture in-situ measurements. In contrast, the Deterministic EnKF (DEnKF) was the least successful in the experiment and suggested a larger error in the state estimates. In the case of the Particle filter, the Systematic Resampling technique was found to be more robust. Even though that it is tried to cover a wide range of data assimilation filters in this thesis, more investigations are still required to various aspects of filters in different hydrological applications with various types of assimilation observations, as well as to explore other filters such as newly developed particle filters and smoothing filters.

- Using the best case scenarios above, e.g., in terms of GRACE TWS noise filtering, tuning technique, GRACE spatial and temporal resolutions, and assimilation filtering technique, the application of GRACE data assimilation for improving hydrological model estimates was explored over different domains as mentioned in thesis objective (iv) (cf. Section 1.4). The performance of GRACE data assimilation was investigated over different areas, e.g., Bangladesh, Iran, and various basins in South America. Various assessments were undertaken and demonstrate the capability of data assimilation for improving model simulations over these areas. Significant improvements were obtained in water storage estimates after data assimilation compared to open-loop runs (model run without data assimilation), e.g., in terms of trends and multi-year variations, especially for groundwater storage. The data assimilation approach allows for separating GRACE TWS into different water compartments based on the physical processes implemented in the model equations. This allowed us to individually analyze various water storage compartments from hydrological models, which were improved using GRACE TWS through data assimilation. Based on the various validations applied to the results, the new information of groundwater and soil moisture are more reliable, which can be used for water management and agriculture objectives. As a result, considerable groundwater depletions were found over Iran and Bangladesh after correcting these storage values using GRACE products while such negative trends do not exist in the open-loop run results. An average -8.9 mm/year water storages decline was observed during 2002 to 2012 with a larger rate since 2005 suggesting that Iran is becoming considerably dryer. A significant decline in groundwater storage ($\sim$32% reduction between 2003 and 2013) was found over Bangladesh by the assimilation results. In the absence of any considerable decrease in precipitation over the region, the remarkable groundwater reduction can be referred to human impacts. In South America, more soil moisture and groundwater anomalies were found over central, northern and western parts. Moreover, negative trends are found for groundwater over some parts of South America. These application studies demonstrated that GRACE data assimilation can successfully introduces missing trends and corrects the amplitude and phase of seasonal changes in water storage simulated by models. These effects are usually difficult to be captured by models due to extreme climate-induced and anthropogenic impacts, which can be retrieved using data assimilation. The approach was found to be effective for studying water storage changes over the regions with no regional model and limited ground-based measurements, e.g., in developing countries.

- Aside from data assimilation tuning and filtering techniques, the impacts of observations on the consistency between hydrological water fluxes, namely precipitation, evaporation, discharge, and water storage changes within the model should also be taken into account. The application of data assimilation can destroy the dynamical balances between water fluxes and water storage changes. In order to enhance the estimation of model water storages, one

should also involve flux observations and their associated errors in the assimilation procedure. A new constrained ensemble Kalman filter was introduced that satisfies the closure of the water balance equation after integrating water storage observations while taking the uncertainties in datasets into account. The new two-update weak constrained EnKF (WCEnKF) scheme showed a good performance in integrating GRACE TWS data into the system (first update) and constraining the water balance equation (second update). Larger correlations in terms of groundwater estimates were found between assimilation results using the two-update filter and ground-based observations, compared with those of the standard EnKF, as well as open-loop run. A similar performance was achieved from the evaluation of results against in-situ groundwater measurements. From the application of the second step of WCEnKF, smaller imbalances between estimated water storage changes and other fluxes, i.e., precipitation, evaporation, and discharge were obtained within eight different basins around the world contrary to the standard EnKF data assimilation filter. WCEnKF successfully addressed the thesis objective (v) (cf. Section 1.4) by minimizing the imbalance between water fluxes after GRACE data assimilation. Additional improvements were acquired using the proposed extension to WCEnKF, Unsupervised WCEnKF (UWCEnKF), which contrary to WCEnKF assumes that uncertainty associated with water budget balance enforcement is unknown. UWCEnKF shows a larger flexibility to covariance associated to the water balance model, which allows for slightly better estimates compared to WCEnKF. In addition to smaller imbalance error, both WCEnKF and UWCEnKF obtained higher correlation values to flux observations. This indicate that the second analysis applied in these filters further improve model estimates with respect to climatic indicators. The superiority of constrained filters against EnKF implied that assimilation of observation in the traditional way can introduce artifacts to state estimates, which reduced by applying the new filters. Moreover, UWCEnKF and to a lesser degree WCEnKF overcame the overfitting problem in existing data assimilation methods in hydrological application, which is related to applying unrealistic corrections in analysis steps due to inaccurate model and observation errors and correspondingly assigning inaccurate weights. Despite these advantages, future extensions to WCEnKF and UWCEnKF are needed to account for non-climatic impacts. Such effects, e.g., irrigation and water use, are only reflected in GRACE TWS and water discharge observations and this fact should be considered while applying the water balance equation in the second step of the proposed filters.

Bibliography

Adams, R.M., Peck, D.E., (2008). Effects of Climate Change on Drought Frequency: Impacts and Mitigation Opportunities, Chapter 7 in Mountains, Valleys, and Flood Plains: Managing Water Resources in a Time of Climate Change. A. Dinar and A. Garrido, eds. Routledge Publishing.

Adler, R.F., Susskind, J., Huffman, G.J., Bolvin, D., Nelkin, E., Chang, A., et al., (2003). Global precipitation climatology project V2.1 monthly 2.5 deg global 1979–present (satellite only and gauge adjusted) 2003: The version-2 global precipitation climatology project (GPCP) monthly precipitation analysis (1979–present). Journal of Hydrometeorology, 4, 1147-1167.

Alazzy, A.A., Lü, H., Chen, R., Ali, A.B., Zhu, Y., Su, J., (2017). Evaluation of Satellite Precipitation Products and Their Potential Influence on Hydrological Modeling over the Ganzi River Basin of the Tibetan Plateau. Advances in Meteorology, Volume 2017, Article ID 3695285, 23 pages, doi:10.1155/2017/3695285.

Arulampalam, M.S., Maskell, S., Gordon, N., Clapp, T., (2002). A tutorial on particle filters for online nonlinear/non-Gaussian Baysian tracking, IEEE Transactions on Signal Processing, 50(2):174–188.

Awange, J.L., Gebremichael, M., Forootan, E., Wakbulcho, G., Anyah, R., Ferreira, V.G., Alemayehu, T., (2014a). Characterization of Ethiopian mega hydrogeological regimes using GRACE, TRMM and GLDAS datasets. Advances in Water Resources, 74:64-78, doi:10.1016/j.advwatres.2014.07.012.

Awange, J.L., Forootan, E., Kuhn, M., Kusche, J., Heck, B., (2014b). Water storage changes and climate variability within the Nile Basin between 2002 and 2011. Advances in Water Resources, 73:1–15, doi:10.1016/j.advwatres.2014.06.010.

Batten, G.D., (1998). Plant analysis using near infrared reflectance spectroscopy: The potential and the limitations. Australian Journal of Experimental Agriculture, 38(7):697–706.

Baur, O., Kuhn, M., Featherstone, W. E., (2009). GRACE-derived ice-mass variations over Greenland by accounting for leakage effects. Journal of Geophysical Research, 114, B06407, doi:10.1029/2008JB006239.

Beck, H.E., van Dijk, A.I.J.M., de Roo, A., Miralles, D.G., McVicar, T.R., Schellekens, J., Bruijnzeel, L.A., (2016). Global-scale regionalization of hydrologic model parameters, Water Resour. Res., 52, 3599–3622, doi:10.1002/2015WR018247.

Becker, M., Lovel, W., Cazenave, A., Güntner, A., Crétaux, J.F., (2010). Recent Hydrological Behavior of the East African Great Lakes Region Inferred from GRACE, Satellite Altimetry and Rainfall Observations. Comptes Rendus Geoscience, 342(3):223-233, doi:10.1016/j.crte.2009.12.010.

Benada, J.R., (1997). PODAAC Merged GDR (TOPEX/POSEIDON) Generation B User's Handbook, Version 2.0. JPL D-11007. Pasadena: Jet Propulsion Laboratory, California Institute of Technology.

Bennett, A.F., (2002); Inverse Modeling of the Ocean and Atmosphere, Cambridge University Press, New York, ISBN:0-521-81373-5, 234 pp.

Berger, H., Forsythe, M., (2004). Satellite wind superobbing. Met Office Forecasting Research Technical Report, 451, Doc ID :NWPSAF-MO-VS-016.

Berry, P.A.M., Garlick, J.D., Freeman, J.A., Mathers, E.L., (2005). Global Inland Water Monitoring from Multi-Mission Altimetery. Geophysical Research Letter, 32:L16401, doi:10.1029/2005GL022814.

Bertino, L., Evensen G., Wackernagel, H., (2003). Sequential Data Assimilation Techniques in Oceanography. International Statistical Review, 71(2):223-241, doi:10.1111/j.1751-5823.2003.tb00194.x.

Birkett, C.M., (1995). The Contribution of TOPEX/POSEIDON to the Global Monitoring of Climatically Sensitive Lakes. Journal of Geophysical Research 25: 179–25.

Birkett, C.M., Mertes, L.A.K., Dunne, T., Costa, M.H., Jasinski, M.J., (2002). Surface Water Dynamics in the Amazon Basin: Application of Satellite Radar Altimetry. Journal of Geophysical Research, 107(D20):LBA 26-1–LBA 26-21, doi:10.1029/2001JD000609.

Bishop, C. H., Etherton, B., Majumdar, S. J., (2001). Adaptive sampling with the ensemble transform Kalman filter, Part I: theoretical aspects. Mon. Wea. Rev. 129, 420–436.

Bousserez, N., Henze, D.K., (2016). Optimal and scalable methods to approximate the solutions of large-scale Bayesian problems: Theory and application to atmospheric inversions and data assimilation. Physics, Data Analysis, Statistics and Probability [physics.data-an], arXiv:1609.06431.

Boyer, J.F., Dieulin, C., Rouchie, N., Cres, A., Servat, E., Paturel, J.E.,Mahe, G., (2006). SIEREM an environmental information system for water resources. 5th World FRIEND Conference, La Havana - Cuba, November 2006 in Climate Variability and Change – Hydrological Impacts IAHS Publ. 308, p19-25.

Brocca, L., Melone, F., Moramarco, T., Wagner, W., Naeimi, V., Bartalis, Z., Hasenauer, S., (2010). Improving runoff prediction through the assimilation of the ASCAT soil moisture product. Hydrology and Earth System Sciences, 14:1881–1893, doi:10.5194/hess-14-1881-2010.

Carrasco-Benavides, M., Ortega-Farías, S., Lagos, L.O., Lagos, L.O., Kleissl, J., Morales L. Poblete-Echeverría, C., Allen, R.G., (2012). Crop coefficients and actual evapotranspiration of a drip-irrigated Merlot vineyard using multispectral satellite images. Irrigation Science, 30(6):485–497, doi:10.1007/s00271-012-0379-4.

Caselles, V., Sobrino, J.A., Coll, C., (1992). On the use of satellite thermal data for determining evapotranspiration in partially vegetated areas. International Journal of Remote Sensing, 13:2669–2682, doi:10.1080/01431169208904071.

Chang, B., Kruger, U., Kustra, R., Zhang, J., (2013). Canonical Correlation Analysis based on Hilbert-Schmidt Independence Criterion and Centered Kernel Target Alignment, Volume 28: Proceedings of The 30th International Conference on Machine Learning, 2, 28, 316-324, http://jmlr.csail.mit.edu/proceedings/papers/v28/chang13.pdf.

Chen, M., Xie, P., Janowiak, J.E., Arkin, P.A., (2002). Global land precipitation: A 50-yr monthly analysis based on gauge observations. Journal of Hydrometeorology, 3, 249-266.

Chen, J.L., Wilson, C.R., Famiglietti, J.S., Rodell, M., (2007). Attenuation effect on seasonal basin-scale water storage changes from GRACE time-variable gravity. Journal of Geodesy, 81(4):237–245, doi:10.1007/s00190-006-0104-2.

Chen, J.L., Wilson, C.R., Tapley, B.D., Yang, Z.L., Niu, G.Y., (2009). 2005 drought event in the Amazon River basin as measured by GRACE and estimated by climate models. Journal of Geophysical Research, 114, B05404, doi:10.1029/2008JB006056.

Chiew, F.H.S., Stewardson, M.J., McMahon, T.A., (1993). Comparison of six rainfall-runoff modelling approaches. Journal of Hydrology, 147:1-36, doi:10.1016/0022-1694(93)90073-I.

Chenoweth, J., Hadjikakou, M., Zoumides, C., (2014). Quantifying the human impact on water resources: a critical review of the water footprint concept, Hydrology and Earth System Sciences, 18:2325-2342, doi:10.5194/hess-18-2325-2014.

Christiansen, L., Krogh, P.E., Bauer-Gottwein, P., Andersen, O.B., Leiriäo, S., Binning, P.J., Rosbjerg, D., (2007). Local to regional hydrological model calibration for the Okavango River Basin from In-situ and space borne gravity observations. Proceedings of 2nd Space for Hydrology Workshop, Geneva, Switzerland, 12-14.

Coumou, D., Rahmstorf, S., (2012). A decade of weather extremes. Nature Climate Change, 2(7):1–6, doi:10.1038/nclimate1452.

Courtier, P., Thépaut, J.N., Hollingsworth, A., (1994). A strategy for operational implementation of 4DVAR, using an incremental approach. Quarterly Journal of the Royal Meteorological Society, 120:1367-1387, doi:10.1002/qj.49712051912.

Dando, M.L., Thorpe, A.J., Eyre, J.R., (2007). The optimal density of atmospheric sounder observations in the Met Office NWP system. Quarterly Journal of the Royal Meteorological Society, 133:1933–1943, doi:10.1002/qj.175.

De Jeu, R.A.M., Owe, M., (2003). Further validation of a new methodology for surface moisture and vegetation optical depth retrieval. Int J Remote Sens, 24:4559–4578, doi:10.1080/0143116031000095934.

De Lannoy, G., Pauwels, V.R.N., Houser, P.R., Verhoest, N.E.C., Gish, T., (2007). Representativeness of point soil moisture observations, upscaling and assimilation. IUGG General Assembly, Perugia Italy, Session HS2004, July 2-13.

Devi, G.K., Ganasri, B.P., Dwarakish, G.S., (2015). A Review on Hydrological Models. Aquatic Procedia, 4:1001-1007, doi:10.1016/j.aqpro.2015.02.126.

Dobslaw, H., Bergmann-Wolf, I., Forootan, E., Dahle, C., Mayer-Guerr, T., Kusche, J., Flechtner, F., (2016). Modeling of present-day atmosphere and ocean non-tidal de-aliasing errors for future gravity mission simulations. Journal of Geodesy, 90(5):423-436, doi:10.1007/s00190-015-0884-3.

Döll, P., Kaspar, F., Lehner, B., (2003). A global hydrological model for deriving water availability indicators: model tuning and validation. Journal of Hydrology, 270:105–134, doi:10.1016/S0022-1694(02)00283-4.

Draper, C.S., Mahfouf, J.-F., Walker, J.P., (2009). An EKF assimilation of AMSR-E soil moisture into the ISBA land surface scheme, J. Geophys. Res., 114, D20104, doi:10.1029/2008JD011650.

Drusch, M., Wood, E.F., Gao, H., (2005). Observation operators for the direct assimilation of TRMM microwave imager retrieved soil moisture. Geophysical Research Letters, 32, L15403.

Eicker, A., Schumacher, M., Kusche, J., Döll, P., Müller-Schmied, H., (2014). Calibration/data assimilation approach for integrating GRACE data into the WaterGAP global hydrology model (WGHM) using an ensemble Kalman filter: first results. Surveys in Geophysics, 35(6):1285–1309, doi:10.1007/s10712-014-9309-8.

Eicker, A., Forootan, E., Springer, A., Longuevergne, L., Kusche J., (2016). Does GRACE see the terrestrial water cycle "intensifying"? Journal of Geophysical Research: Atmospheres, 121:733–745, doi:10.1002/2015JD023808.

Enenkel, M., Reimer, C., Dorigo, W., Wagner, W., Pfeil, I., Parinussa, R., and De Jeu, R., (2016). Combining satellite observations to develop a global soil moisture product for near-real-time applications, Hydrology and Earth System Sciences, 20:4191-4208, doi:/10.5194/hess-20-4191-2016.

Evensen, G., (1994). Sequential data assimilation with a nonlinear quasi-geostrophic model using Monte Carlo methods to forecast error statistics, Journal of Geophysical Research: Oceans, 99(C5):10143–10162, doi:10.1029/94JC00572.

Evensen, G., (2003). The ensemble Kalman filter: Theoretical formulation and practical inplementation, Ocean Dynamics, 53, 343–367, http://dx.doi.org/10.1007/s10236-003-0036-9.

Evensen, G., (2004). Sampling strategies and square root analysis schemes for the EnKF. Ocean Dyn. 54(6), 539-560.

Evensen, G., (2009). Data assimilation. The Ensemble Kalman Filter. Springer, Berlin Heidelberg, 2. edition, ISBN 978-3-642-03711-5.

Famiglietti, J.S., Ryu, D., Berg, A.A., Rodell, M., Jackson, T.J., (2008). Field observations of soil moisture variability across scales, Water Resour. Res., 44, W01423, doi:10.1029/2006WR005804.

Forootan, E., Didova, O., Kusche, J., Löcher, A., (2013). Comparisons of atmospheric data and reduction methods for the analysis of satellite gravimetry observations. Journal of Geophysical Research: Solid Earth, 118(5):2382–2396, doi:10.1002/jgrb.50160.

Forootan, E., Rietbroek, R., Kusche, J., Sharifi, M. A., Awange, J., Schmidt, M., Omondi, P., Famiglietti, J., (2014a). Separation of large scale water storage patterns over Iran using GRACE, altimetry and hydrological data. Remote Sensing of Environment, 140:580-595, doi:10.1016/j.rse.2013.09.025.

Forootan, E., Didova, O., Schumacher, M., Kusche, J., Elsaka, B., (2014b). Comparisons of atmospheric mass variations derived from ECMWF reanalysis and operational fields, over 2003 to 2011. Journal of Geodesy, 88:503-514, doi:10.1007/s00190-014-0696-x.

Frappart, F., Ramillien, G., Leblanc, M., Tweed, S.O., Bonnet, M-P., Maisongrande, P., (2011). An independent Component Analysis approach for filtering continental hydrology in the GRACE gravity data. Remote Sensing of Environment, 115(1):187-204, doi:10.1016/j.rse.2010.08.017.

Frappart, F., Ramillien, G., Seoane, L., (2016). Monitoring Water Mass Redistributions on Land and Polar Ice Sheets using the GRACE Gravimetry from Space Mission. In Baghdadi N., Zribi M. (Eds.). Land Surface Remote Sensing in Continental Hydrology, 255-279, doi:10.1016/B978-1-78548-104-8.50008-5.

Geruo, A, Wahr, j., Zhong, S., (2013). Computations of the viscoelastic response of a 3-D compressible Earth to surface loading: an application to Glacial Isostatic Adjustment in Antarctica and Canada. Geophys J Int; 192 (2): 557-572, doi:10.1093/gji/ggs030.

Getirana, A., Kumar, S., Girotto, M., Rodell, M., (2017). Rivers and floodplains as key components of global terrestrial water storage variability. Geophysical Research Letters, 44, doi:10.1002/2017GL074684.

Gharamti, M.E., Valstar, J., Janssen, G., Marsman, A., Hoteit, I., (2016). On the efficiency of the hybrid and the exact second-order sampling formulations of the EnKF: a reality-inspired 3-D test case for estimating biodegradation rates of chlorinated hydrocarbons at the port of Rotterdam. Hydrology and Earth System Sciences, 20:4561-4583, doi:10.5194/hess-20-4561-2016.

Girotto, M., De Lannoy, G.J., Reichle, R.H., Rodell, M., (2016). Assimilation of gridded terrestrial water storage observations from GRACE into a land surface model. Water Resources Research, 52(5):4164-4183, doi:10.1002/2015WR018417.

Girotto, M., De Lannoy, G.J., Reichle, R.H., Rodell, M., Draper, C., Bhanja, S.N., Mukherjee, A., (2017). Benefits and Pitfalls of GRACE Data Assimilation: a Case Study of Terrestrial Water Storage Depletion in India. Geophysical Research Letters, 44(9):4107–4115, doi:10.1002/2017GL072994.

Giustarini, L., Matgen, P., Hostache, R., Montanari, M., Plaza, D., Pauwels, V.R.N., De Lannoy, G.J.M., De Keyser, R., Pfister, L., Hoffmann, L., Savenije, H.H.G., (2011). Assimilating SAR-derived water level data into a hydraulic model: a case study. Hydrology and Earth System Sciences, 15:2349–2365, doi:10.5194/hess-15-2349-2011.

Glenn, E.P., Huete, A.R., Nagler, P.L., Hirschboeck, K.K., Brown, P., (2007). Integrating remote sensing and ground methods to estimate evapotranspiration. Critical Reviews in Plant Sciences, 26:139–168, doi:10.1080/07352680701402503.

Gutentag, E.D., Heimes, F.J., Krothe, N.C., Luckey, R.R., Weeks, J.B., (1984). Geohydrology of the High Plains aquifer in parts of Colorado, Kansas, Nebraska, New Mexico, Oklahoma, South Dakota, Texas, and Wyoming, U.S. Geol. Surv. Prof. Pap., 1400-B, 66 pp.

Han, S.C., Shum, C.K., Jekeli, C., Kuo, C.Y., Wilson, C.R., Seo, K.W., (2005). Non-isotropic filtering of GRACE temporal gravity for geophysical signal enhancement. Geophysical Journal International, 16:18-25, doi:10.1111/j.1365-246X.2005.02756.x.

Harris, I.C., (2008). Climatic Research Unit (CRU) time-series datasets of variations in climate with variations in other phenomena. NCAS British Atmospheric Data Centre, date of citation, University of East Anglia Climatic Research Unit; Jones, P.D., http://catalogue.ceda.ac.uk/uuid/3f8944800cc48e1cbc29a5ee12d8542d.

Henck, A.H., Montgomery, D.R., Huntington, K.W., Liang, C., (2010). Monsoon control of effective discharge, Yunnan and Tibet, Geology, v. 38, p. 975-978.

Hichri, S., Benzarti, F., Amiri, H., (2012). Robust Noise Filtering in Image Sequences. International Journal of Computer Applications, 50(18):0975–8887, doi:10.5120/7871-1156.

Hoteit, I., Pham, D.T., Blum, J., (2002). A simplified reducedorder kalman filtering and application to altimetric data assimilation in tropical Pacific. Journal of Marine Systems, 36:101–127, doi:10.1016/S0924-7963(02)00129-X.

Hoteit, I., Triantafyllou, G., Petihakis G., (2005). Efficient data assimilation into a complex, 3-D physical-biogeochemical model using partially-local Kalman filters. Annales Geophysicae, European Geosciences Union, 23(10):3171-3185.

Hoteit, I., Pham, D.T., Triantafyllou, G., Korres, G., (2008). A new approximate solution of the optimal nonlinear filter for data assimilation in meteorology and oceanography. Monthly Weather Review, 136:317-334, doi:10.1175/2007MWR1927.1.

Hoteit, I., Luo, X., Pham, D.T., (2012). Particle Kalman Filtering: A Nonlinear Bayesian Framework for Ensemble Kalman Filters. Monthly Weather Review, 140(2):528-542, doi:10.1175/2011MWR3640.1.

Hoteit, I., Pham, D.T., Gharamti, M. E., Luo, X., (2015). Mitigating Observation Perturbation Sampling Errors in the Stochastic EnKF, Monthly Weather Review, 143(7):2918-2936, doi:10.1175/MWR-D-14-00088.1.

Houborg, R., Rodell, M., Li, B., Reichle, R.H., Zaitchik, B.F., (2012). Drought indicators based on model-assimilated Gravity Recovery and Climate Experiment (GRACE) terrestrial water storage observations. Water Resources Research, 48:W07525, doi:10.1029/2011WR011291.

Huang, S., Kumar, R., Flörke, M., Yang T., Hundecha, Y., Kraft, P., Gao, C., Gelfan, A., Liersch, S., Lobanova, A., Strauch, M., Ogtrop, F.V., Reinhardt, J., Haberlandt, U., Krysanova, V., (2016). Evaluation of an ensemble of regional hydrological models in 12 large-scale river basins worldwide. Climatic Change, 141(3):381–397, doi:10.1007/s10584-016-1841-8.

Huffman, G.J., Adler, R.F., Bolvin, D.T., Gu, G., Nelkin, E.J., Bowman, K.P., Hong, Y., Stocker, E.F., Wolff, D.B., (2007). The TRMM Multi-satellite Precipitation Analysis: Quasi- Global, Multi-Year, Combined-Sensor Precipitation Estimates at Fine Scale. J. Hydrometeor., 8(1), 38-55.

Huntington, T.G., (2006). Evidence for intensification of the global water cycle: Review and synthesis. Journal of Hydrology,319(1–4):83–95, doi:10.1016/j.jhydrol.2005.07.003.

Hwang, C.W., Kao, Y.H., (2010). A Preliminary Analysis of Lake Level and Water Storage Changes over Lakes Baikal and Balkhash from Satellite Altimetry and Gravimetry. Terrestrial. Atmospheric and Oceanic Sciences, 22:97–108, doi:10.3319/TAO.2010.05.19.01(TibXS).

Irmak, A., Kamble, B., (2009). Evapotranspiration data assimilation with genetic algorithms and SWAP model for on-demand irrigation. Irrigation Science, 28(1):101–112, doi:10.1007/s00271-009-0193-9.

Jackson, T., Bindlish, R., (2012). Validation of Soil Moisture And Ocean Salinity (SMOS) soil moisture over watershed networks in the US, IEEE Trans. Geosci. Remote Sens., 50, 1530–1543.

Jazwinski, A.H., (1970). Stochastic Processes and Filtering Theory. Academic Press, 64:376 pp, ISBN:9780080960906.

Jekeli, C., (1981). Alternative methods to smooth the Earth's gravity field. Technical report 327, Department of Geodesy and Science and Surveying, Ohio State University.

Joyce, R.J., Janowiak, J.E., Arkin, P.A., Xie, P.P., (2004). CMORPH: A method that produces global precipitation estimates from passive microwave and infrared data at high spatial and temporal resolution. Journal of Hydrometeorology, 5, 487-503.

Jung, M., Reichstein, M., Ciais, P., Seneviratne, S.I., Sheffield, J., Goulden, M.L., et al. (2010), Recent decline in the global land evapotranspiration trend due to limited moisture supply, Nature, 467(7318):951–954, doi:10.1038/nature09396.

Kalnay, E., (2003). Atmospheric modelling, data assimilation and predictability. Cambridge University Press, ISBN:9780521796293.

Kang, S., Su, X., Tong, L., Shi, P., Yang, X., Abe, Y., Du, T., Shen, Q., Zhang, J., (2004). The impacts of human activities on the water–land environment of the Shiyang River basin, an arid region in northwest China. Hydrological Sciences Journal, 49(3):413-427, doi:10.1623/hysj.49.3.413.54347.

Khaki, M., Forootan, E., Sharifi, M.A., (2014). Satellite radar altimetry waveform retracking over the Caspian Sea. International Journal of Remote Sensing, 35(17):6329–6356, doi:10.1080/01431161.2014.951741.

Khaki, M., Forootan, E., Sharifi, M.A., Awange, J., Kuhn, M., (2015). Improved gravity anomaly fields from retracked multimission satellite radar altimetry observations over the Persian Gulf and the Caspian Sea. Geophysical Journal International, 202(3):1522-1534, doi:10.1093/gji/ggv240.

Khaki, M., Schumacher, M., J., Forootan, Kuhn, M., Awange, E., van Dijk, A.I.J.M., (2017a). Accounting for Spatial Correlation Errors in the Assimilation of GRACE into Hydrological Models through localization. Advances in Water Resources, 108:99-112, doi:10.1016/j.advwatres.2017.07.024.

Khaki, M., Hoteit, I., Kuhn, M., Awange, J., Forootan, E., van Dijk, A.I.J.M., Schumacher, M., Pattiaratchi, C., (2017b). Assessing sequential data assimilation techniques for integrating GRACE data into a hydrological model. Advances in Water Resources, 107:301-316, doi:10.1016/j.advwatres.2017.07.001.

Khaki, M., Ait-El-Fquih, B., Hoteit, I., Forootan, E., Awange, J., Kuhn, M., (2017c). A Two-update Ensemble Kalman Filter for Land Hydrological Data Assimilation with an Uncertain Constraint. Journal of Hydrology, 555:447-462, doi:10.1016/j.jhydrol.2017.10.032.

Khaki, M., Forootan, E., Kuhn, M., Awange, J., Longuevergne, L., Wada, Y., (2018a). Efficient Basin Scale Filtering of GRACE Satellite Products. Remote Sensing of Environment, 204:76-93, doi:10.1016/j.rse.2017.10.040.

Khaki, M., Forootan, E., Kuhn, M., Awange, J., Papa, F., Shum, C.K., (2018b). A Study of Bangladesh's Sub-surface Water Storages Using Satellite Products and Data Assimilation Scheme. Science of The Total Environment, 625:963-977, doi:10.1016/j.scitotenv.2017.12.289.

Khaki, M., Forootan, E., Kuhn, M., Awange, J., van Dijk, A.I.J.M., Schumacher, M., Sharifi, M.A., (2018c). Determining Water Storage Depletion within Iran by Assimilating GRACE data into the W3RA Hydrological Model. Advances in Water Resources, 114:1-18, doi:10.1016/j.advwatres.2018.02.008.

Khaki, M., Awange, J. (2018d). The Application of Remotely Sensed Products to Enhance Model-derived Water Storage Changes over South America. Science of The Total Environment, 647:1557-1572, doi:10.1016/j.scitotenv.2018.08.079.

Khaki, M., Ait-El-Fquih, B., Hoteit, I., Forootan, E., Awange, J., Kuhn, M., (2018e). Unsupervised Ensemble Kalman Filtering with an Uncertain Constraint for Land Hydrological Data Assimilation. Journal of Hydrology, 564:175-190, doi:10.1016/j.jhydrol.2018.06.080.

Khaki, M., Hamilton, F., Forootan, E., Hoteit, I., Awange, J., Kuhn, M., (2018). Non-parametric Data Integration scheme for Land Hydrological Applications. Water Resources Research, 54:4946–4964, doi:10.1029/2018WR022854.

Kidd, C., Levizzani, V., (2011), Status of satellite precipitation retrievals. Hydrology and Earth System Sciences, 15:1109-1116, doi:10.5194/hess-15-1109-2011.

Klees, R., Revtova, E. A., Gunter, B. C., Ditmar, P., Oudman, E., Winsemius, H. C., (2008). The design of an optimal filter for monthly GRACE gravity models. Geophysical Journal International, 175(2):417-432, doi:10.1111/j.1365-246X.2008.03922.x.

Koch, K.R., (2007). Introduction to Bayesian Statistics (2nd), Springer, ISBN:978-3-540-72726-2, doi:10.1007/978-3-540-72726-2.

Komma, J., Bloschl, G., Reszler, C., (2008). Soil moisture updating by ensemble Kalman filtering in real-time flood forecasting. Journal of Hydrology, 357(3–4):228–242, doi:10.1016/j.jhydrol.2008.05.020.

Kumar, S.V., Peters-Lidard, C.D., Mocko, D., Reichle, R.H., Liu, Y., Arsenault, K.R., Xia, Y., Ek, M., Riggs, G., Livneh, B., Cosh, M., (2014). Assimilation of remotely sensed soil moisture and snow depth retrievals for drought estimation. Journal of Hydrometeorology, 15:2446-2469, doi:10.1175/JHM-D-13-0132.1.

Kumar, S.V., Peters-Lidard, C.D., Santanello, J.A., Reichle, R.H., Draper, C.S., Koster, R.D., Nearing, G., Jasinski, M.F., (2015). Evaluating the utility of satellite soil moisture retrievals over irrigated areas and the ability of land data assimilation methods to correct for unmodeled processes. Hydrology and Earth System Sciences, 19:4463-4478, doi:10.5194/hess-19-4463-2015.

Kumar, S., Zaitchik, B., Peters-Lidard, C., Rodell, M., Reichle, R., Li, B., Jasinski, M., Mocko, D., (2016). Assimilation of Gridded GRACE Terrestrial Water Storage Estimates in the North American Land Data Assimilation System. Journal of Hydrometeorology, 17:1951–1972, doi:10.1175/JHM-D-15-0157.1.

Kusche, J., (2007). AApproximate decorrelation and non-isotropic smoothing of time-variable GRACE-type gravity field models. Journal of Geodesy, 81:733–749, doi:10.1007/s00190-007-0143-3.

Kusche, J., Klemann, V., Bosch, W., (2012). Mass distribution and mass transport in the Earth system. Journal of Geodynamics, 59-60:1-8, doi:10.1016/j.jog.2012.03.003.

Kusche, J., Eicker, A., Forootan, E., Springer, A., Longuevergne L., (2016). Mapping probabilities of extreme continental water storage changes from space gravimetry. Geophysical Research Letters, 43:8026-8034, doi:10.1002/2016GL069538.

Kustas, W.P., Norman, J.M., (1996). Use of remote sensing for evapotranspiration monitoring over land surfaces. Hydrological Sciences Journal, 41(4):495–516, doi:10.1080/02626669609491522.

Lahoz, W.A., Geer, A.J., Bekki, S., Bormann, N., Ceccherini, S., Elbern, H., Errera, Q., Eskes, H.J., Fonteyn, D., Jackson, D.R., Khattatov, B., (2007). The Assimilation of Envisat data (ASSET) project, Atmos. Chem. Phys., 7:1773-1796, doi:10.5194/acp-7-1773-2007.

Landerer, F. W., Swenson, S. C., (2012). Accuracy of scaled GRACE terrestrial water storage estimates. Water Resources Research, 48(4):W04531, doi:10.1029/2011WR011453.

Lee, H., Shum, C.K., Yi, Y., Ibaraki, M., Kim, J.W., Braun, A., Kuo, C.Y., Lu, Z., (2009). Louisiana Wetland Water Level Monitoring Using Retracked TOPEX/POSEIDON Altimetry. Marine Geodesy, 32:284–302, doi:10.1080/01490410903094767.

Lee, H., Seo, D.-J., Koren, V., (2011). Assimilation of streamflow and in situ soil moisture data into operational distributed hydrologic models: Effects of uncertainties in the data and initial model soil moisture states, Advances in Water Resources, 34(12):1597–1615, doi:10.1016/j.advwatres.2011.08.012.

Li, B., Rodell, M., Zaitchik, B.F., Reichle, R.H., Koster, R.D., van Dam, T.M., (2012). Assimilation of GRACE terrestrial water storage into a land surface model: Evaluation and potential value for drought monitoring in western and central Europe. Journal of Hydrology, 446–447:103-115, doi:10.1016/j.jhydrol.2012.04.035.

Li, Y., Ryu, D., Western, A.W., Wang, Q.J., (2015). Assimilation of stream discharge for flood forecasting: Updating a semidistributed model with an integrated data assimilation scheme, Water Resources Research, 51:3238–3258, doi:10.1002/2014WR016667.

Liang, X., Lettenmiar, D.P.,Wood, E.F., Burges, S.J., (1994). A simple hydrologically based model of land–surfacewater and energy fluxes for general-circulationmodels. Journal of Geophysical Research, 99, 14,415-14,428, doi:10.1029/94JD00483.

Liechti, C.T., Matos, J.P., Boillat, J.-L., Schleiss, A.J., (2012). Comparison and evaluation of satellite derived precipitation products for hydrological modeling of the Zambezi River Basin. Hydrology and Earth System Sciences, 16:489-500, doi:10.5194/hess-16-489-2012.

Liou, Y.-A., Kar, S.K., (2014). Evapotranspiration Estimation with Remote Sensing and Various Surface Energy Balance Algorithms—A Review. Energies, 7:2821-2849, doi:10.3390/en7052821.

Liu, Z.Q., Rabier., F., (2003). The potential of high-density observations for numerical weather prediction: A study with simulated observations. Quarterly Journal of the Royal Meteorological Society, 129:3013–3035, doi:10.1256/qj.02.170.

Long, D., Yang, Y., Wada, Y., Hong, Y., Liang, W., Chen, Y., Yong, B., Hou, A., Wei, J., Chen, L., (2015). Deriving scaling factors using a global hydrological model to restore GRACE total water storage changes for China's Yangtze River Basin. Remote Sensing of Environment, 168:177-193, doi:10.1016/j.rse.2015.07.003.

Longuevergne, L., Scanlon, B. R., Wilson, C. R., (2010). GRACE Hydrological estimates for small basins: Evaluating processing approaches on the High Plains Aquifer, USA. Water Resources Research, 46(11):W11517, doi:10.1029/2009WR008564.

Longuevergne, L., Wilson, C.R., Scanlon, B.R., Crétaux, J.F., (2013). GRACE water storage estimates for the Middle East and other regions with significant reservoir and lake storage. Hydrology and Earth System Sciences, 17:4817–4830, doi:10.5194/hess-17-4817-2013.

Lorenz, E., (1956). Empirical orthogonal function and statistical weather prediction. Technical Report Science Report No 1, Statistical Forecasting Project. MIT, Cambridge.

Mayer-Gürr, T., Zehentner, N., Klinger, B., Kvas, A., (2014). ITSG-Grace2014: a new GRACE gravity field release computed in Graz. - in: GRACE Science Team Meeting (GSTM). Potsdam am: 29.09.2014.

McLaughlin, D., (2002). An integrate approach to hydrologic data assimilation: Interpolation, smoothing, and filtering, Advances in Water Resources, 25:1275–1286, doi:10.1016/S0309-1708(02)00055-6.

McMillan, H.K., Hreinsson, E.Ö., Clark, M.P., Singh, S.K., Zammit, C., Uddstrom, M.J., (2013). Operational hydrological data assimilation with the recursive ensemble Kalman filter. Hydrology and Earth System Sciences, 17(1):21–38, doi:10.5194/hess-17-21-2013.

Miralles, D.G., Holmes, T.R.H., de Jeu, R.A.M., Gash, J.H., Meesters, A.G.C.A., Dolman, A.J., (2011). Global land-surface evaporation estimated from satellite-based observations, Hydrology and Earth System Sciences, 15, 453–469.

Mohammadi-Ghaleni, M., Ebrahimi, K., (2011). Assessing impact of irrigation and drainage network on surface and groundwater resources — Case study: Saveh Plain, Iran. ICID 21st International Congress on Irrigation and Drainage, 15–23 October 2011, Tehran, Iran.

Moradkhani, H., Hsu, K.L., Gupta, H., Sorooshian, S., (2005). Uncertainty assessment of hydrologic model states and parameters: Sequential data assimilation using the particle filter. Water Resources Research, 41:W05012, doi:10.1029/2004WR003604.

Moradkhani, H., Sorooshian, S., (2008). General review of rainfall-runoff modeling: model calibration, data assimilation, and uncertainty analysis. Hydrological modeling and the water cycle. 291 page, ISBN 978-3-540-77842-4.

Moradkhani, H., DeChant, C.M., Sorooshian, S., (2012). Evolution of ensemble data assimilation for uncertainty quantification using the particle filter-Markov chain Monte Carlo method. Water Resources Research, 48:W12520, doi:10.1029/2012WR012144.

Mu, Q., Heinsch, F.A., Zhao, M., Running, S.W., (2007). Development of a global evapotranspiration algorithm based on MODIS and global meteorology data. Remote Sensing of Environment 111, 519-536, doi:10.1016/j.rse.2007.04.015.

Müller Schmied, H., S. Eisner, D. Franz, M. Wattenbach, F. Portmann, M. Flörke, Döll, P., (2014). Sensitivity of simulated global-scale freshwater fluxes and storages to input data, hydrological model structure, human water use and calibration, Hydrol. Earth. Syst. Sci., 18, 3511–3538, doi:10.5194/hess-18-3511-2014.

Munier, S., Aires, F., Schlaffer, S., Prigent, C., Papa, F., Maisongrande, P., et al., (2014). Combining datasets of satellite retrieved products for basin-scale water balance study. Part II: Evaluation on the Mississippi Basin and closure correction model. Journal of Geophysical Research: Atmospheres, American Geophysical Union, 119:100-116, doi10.1002/2014JD021953.

Najmaddin, P.M., Whelan, M.J., Balzter, H., (2017). Application of Satellite-Based Precipitation Estimates to Rainfall-Runoff Modelling in a Data-Scarce Semi-Arid Catchment. Climate, 5(2):32-32, doi:10.3390/cli5020032.

Neal, J., Schumann, G., Bates, P., Buytaert, W., Matgen, P., Pappenberger, F., (2009). A data assimilation approach to discharge esti- mation from space. Hydrological Processes, 23:3641–3649, doi:10.1002/hyp.7518.

Orlowsky, B., Seneviratne, S.I., (2014). On the spatial representativeness of temporal dynamics at European weather stations, Int. J. Climatol., 34(10), 3154–3160, doi:10.1002/joc.3903.

Pan, M., Wood, E.F., (2006). Data assimilation for estimating the terrestrial water budget using a constrained ensemble Kalman filter. Journal of Hydrometeorology, 7(3):534–547, doi:10.1175/JHM495.1.

Pan, M., Sahoo, A.K., Troy, T.J., Vinukollu, R.K., Sheffield, J., Wood, E.F., (2012). Multisource Estimation of Long-Term Terrestrial Water Budget for Major Global River Basins. Journal of Climate, 25(9):3191–3206, doi:10.1175/JCLI-D-11-00300.1.

Papa, F., Frappart, F., Malbeteau, Y., Shamsudduha, M., Vuruputur, V., et al. (2015). Satellite-derived surface and sub-surface water storage in the Ganges–Brahmaputra River Basin, Journal of Hydrology: Regional Studies, Volume 4, Part A, Pages 15-35, ISSN 2214-5818, doi:10.1016/j.ejrh.2015.03.004.

Peng, J., Niesel, J., Loew, A., Zhang, S., Wang, J., (2015). Evaluation of Satellite and Reanalysis Soil Moisture Products over Southwest China Using Ground-Based Measurements. Remote Sensing, 7(11):15729-15747, doi:10.3390/rs71115729.

Piao, S., Ciais, P., Huang., Y., Shen, Z., Peng, S., Li, J., et al., (2010). The impacts of climate change on water resources and agriculture in China. Nature, 467:43–51, doi:10.1038/nature0936.

Pipunic, C., Walker, P., Western, A., (2008). Assimilation of remotely sensed data for improved latent and sensible heat flux prediction: A comparative synthetic study. Remote Sensing of Environment, 112(4):1295–1305, doi:10.1016/j.rse.2007.02.038.

Prashar, A., Jones, H.G., (2016). Assessing drought responses using thermal infrared imaging. Methods in Molecular Biology, 1398:209-19, doi:10.1007/978-1-4939-3356-3_17.

Qureshi, A.S., Ahmad, Z.U., Krupnik, T.J., (2015). Moving from resource development to resource management: problems prospects and policy recommendations for sustainable groundwater management in Bangladesh. Water Resources Management, 29(12):4269–4283, doi:10.1007/s11269-015-1059-y.

Ray, R.L., Fares, A., He, Y., Temimi, M., (2017). Evaluation and Inter-Comparison of Satellite Soil Moisture Products Using In Situ Observations over Texas, U.S.. Water, 9(6):372, doi:10.3390/w9060372.

Reager, J.T., Thomas, A.C., Sproles, E.A., Rodell, M., Beaudoing, H.K., Li, B., Famiglietti, J.S., (2015). Assimilation of GRACE Terrestrial Water Storage Observations into a Land Surface Model for the Assessment of Regional Flood Potential. Remote Sensing, 7(11):14663-14679, doi:10.3390/rs71114663.

Renzullo, L.J., Van Dijk, A.I.J.M., Perraud, J.M., Collins, D., Henderson, B., Jin, H., Smith, A.B., McJannet, D.L., (2014). Continental satellite soil moisture data assimilation improves root-zone moisture analysis for water resources assessment. Journal of Hydrology, 519:2747–2762, doi:10.1016/j.jhydrol.2014.08.008.

Reichle, R. H., McLaughlin, D. B., Entekhabi, D., (2002). Hydrologic Data Assimilation with the Ensemble Kalman Filter. Monthly Weather Review, 130:103–114, doi:10.1175/1520-0493(2002)130¡0103:HDAWTE¿2.0.CO;2.

Reichle, R.H., Koster, R.D., (2004). Bias reduction in short records of satellite soil moisture, Geophys. Res. Lett., 31, L19501, doi:10.1029/2004GL020938.

Reichle, R.H., Kumar, S.V., Mahanama, S.P.P., Koster, R.D., Liu, Q., (2010). Assimilation of satellite-derived skin temperature observations into land surface models. Journal of Hydrometeorology, 11:1103-1122, doi:10.1175/2010JHM1262.1.

Reichle, R.H., De Lannoy, G.J., Forman, B.A., Draper, C.S., Liu, Q., (2013). Connecting satellite observations with water cycle variables through land data assimilation: Examples using the NASA GEOS-5 LDAS. Earth's Hydrological Cycle, 35(3):577–606, doi:10.1007/978-94-017-8789-5_6.

Robert, C., Blayo, E., Verron, J., (2006). Comparison of reduced-order, sequential and variational data assimilation methods in the tropical Pacific Ocean. Ocean Dynamics, 56:624, doi:10.1007/s10236-006-0079-9.

Rodell, M., Houser, P., Jambor, U., Gottschalck, J., Mitchell, K., Meng, C., Arsenault, K., Cosgrove, B., Radakovich, J., Bosilovich, M., Entin, J., Walker, J., Lohmann, D., Toll, D., (2004). The Global Land Data Assimilation System. Bulletin of the American Meteorological Society, 85:381–394, doi:10.1175/BAMS-85-3-381.

Sahoo, A.K., Pan, M., Troy, T.J., Vinukollu, R.K., Sheffield, J., Wood, E.F., (2011). Reconciling the global terrestrial water budget using satellite remote sensing. Remote Sensing of Environment, 115(8):1850-1865, doi:10.1016/j.rse.2011.03.009.

Sakov, P., Oke, P.R., (2008). A deterministic formulation of the ensemble Kalman filter: an alternative to ensemble square root filters, Tellus 60A, 361–371.

Schellekens, J., Dutra, E., Martínez-de la Torre, A., Balsamo, G., van Dijk, A., Sperna Weiland, F., Minvielle, M., Calvet, J.-C., Decharme, B., Eisner, S., Fink, G., Flörke, M., Peßenteiner, S., van Beek, R., Polcher, J., Beck, H., Orth, R., Calton, B., Burke, S., Dorigo, W., and Weedon, G. P., (2017). A global water resources ensemble of hydrological models: the eartH2Observe Tier-1 dataset, Earth Syst. Sci. Data, 9, 389-413, doi:10.5194/essd-9-389-2017.

Schmidt, A.H., Montgomery, D.R., Huntington, K.W., Liang, C., (2011). The Question of Communist Land Degradation: New Evidence from Local Erosion and Basin-Wide Sediment Yield in Southwest China and Southeast Tibet, Annals of the Association of American Geographers,, First published on: 28 March 2011 (iFirst).

Schneider, U., Fuchs, T., Meyer-Christoffer, A., Rudolf, B., (2008). In G. P. C. Centre (Ed.), Internet publication.

Schumacher, M., Kusche, J., Döll, P., (2016). A systematic impact assessment of GRACE error correlation on data assimilation in hydrological models. Journal of Geodesy, 90(6):537–559, doi:10.1007/s00190-016-0892-y.

Schumacher, M., Forootan, E., van Dijk, A.I.J.M., Müller Schmied, H., Crosbie, R.S., Kusche, J., Döll, P., (2018). Improving drought simulations within the Murray-Darling Basin by combined calibration/assimilation of GRACE data into the WaterGAP Global Hydrology Model. Remote Sensing of Environment, 204:212-228, doi:10.1016/j.rse.2017.10.029.

Schunk, R.W., Scherliess, L., Sojka, J.J., Thompson, D.C., (2004). USU global ionospheric data assimilation models, Atmospheric and Environmental Remote Sensing Data Processing and Utilization: an End-to-End System Perspective. Proceedings of SPIE, 5548:327-336, doi:10.1117/12.562448.

Schuurmans, J.M., Troch, P.A., Veldhuizen, A., Bastiaanssen, W.G.M, Bierkensd, M.F.P., (2003). Assimilation of remotely sensed latent heat flux in a distributed hydrological model. Advances in Water Resources, 26(2):151–159, doi:10.1016/S0309-1708(02)00089-1.

Seo, D.J., Koren, V., Cajina, N., (2003). Real-time variational assimilation of hydrologic and hydrometeorological data into operational hydrologic forecasting. Journal of Hydrometeorology, 4:627–641, doi:10.1175/1525-7541(2003)004¡0627:RVAOHA¿2.0.CO;2.

Seo, K.W., Wilson, C.R., (2005). Simulated estimation of hydrological loads from GRACE. Journal of Geodesy, 78:442-456, doi:10.1007/s00190-004-0410-5.

Seoane, L., Ramillien, G., Frappart, F., Leblanc, M., (2013). Regional GRACE-based estimates of water mass variations over Australia: validation and interpretation, Hydrol. Earth Syst. Sci., 17, 4925-4939, doi:10.5194/hess-17-4925-2013.

Simmons, A. J., Uppala, S., Dee, D., Kobayashi, S., (2007). ERA-interim: New ECMWF reanalysis products from 1989 onwards, ECMWF Newsletter No. 110 — Winter 2006/07.

Sokolov, A.A., Chapman, T.G., (1974). Methods for Water Balance Computation An International Guide for Research and Practice, The Unesco Press, Paris.

Stewart, L.M., Dance, S.L., Nichols, N.K., (2008). Correlated observation errors in data assimilation. International Journal for Numerical Methods in Fluids, 56:1521–1527, doi:10.1002/fld.1636.

Stone, J.V., (2004). Independent component analysis: a tutorial introduction. MIT Press, London.

Strassberg, G., Scanlon, B.R., Rodell, M., (2007). Comparison of seasonal terrestrial water storage variations from GRACE with groundwater-level measurements from the High Plains Aquifer (USA), Geophys. Res. Lett., 34, L14402, doi:10.1029/2007GL030139.

Su, C.-H., Ryu, D., Young, R.I., Western, A.W., Wagner, W., (2013). Inter-comparison of microwave satellite soil moisture retrievals over the Murrumbidgee Basin, southeast Australia. Remote Sensing of Environment, 134, 1–11.

Subramanian, A.C., Hoteit, I., Cornuelle, B., Miller, A.J., Song, H., (2012). Linear versus Nonlinear Filtering with Scale-Selective Corrections for Balanced Dynamics in a Simple Atmospheric Model. Atmospheric Sciences, 69(11):3405-3419, doi:10.1175/JAS-D-11-0332.1.

Sun, Y.A., Morris, A., Mohanty, S., (2009). Comparison of deterministic ensemble Kalman filters for assimilating hydrogeological data. Advances in Water Resources, 32(2):280-292, doi:10.1016/j.advwatres.2008.11.006.

Swenson, S., Wahr, J., (2002). Methods for inferring regional surface-mass anomalies from Gravity Recovery and Climate Experiment (GRACE) measurements of time-variable gravity. Journal of Geophysical research, 107(B9):2193, doi:10.1029/2001JB000576.

Swenson, S., Wahr, J., (2006). Post-processing removal of correlated errors in GRACE data. Geophysical Research Letters, 33:L08402, doi:10.1029/2005GL025285.

Swenson, S., Chambers, D., Wahr, J., (2008). Estimating geocentervariations from a combination of GRACE and ocean model output. Journal of Geophysical research, 113, B08410, doi:10.1029/2007JB005338.

Talagrand, O., Courtier, P., (1987). Variational Assimilation of Meteorological Observations With the Adjoint Vorticity Equation. I: Theory. Quarterly Journal of the Royal Meteorological Society, 113:1311–1328, doi:10.1002/qj.49711347812.

Tangdamrongsub, N., Steele-Dunne, S.C., Gunter, B.C., Ditmar, P.G., Weerts, A.H., (2015). Data assimilation of GRACE terrestrial water storage estimates into a regional hydrological model of the Rhine River basin. Hydrology and Earth System Sciences, 19:2079-2100, doi:10.5194/hess-19-2079-2015.

Tangdamrongsub, N., Steele-Dunne, S.C., Gunter, B.C., Ditmar, P.G., Sutanudjaja, E.H., Xie, T, Wang, Z., (2017). Improving estimates of water resources in a semi-arid region by assimilating GRACE data into the PCR-GLOBWB hydrological model. Hydrology and Earth System Sciences, 21:2053-2074, doi:10.5194/hess-21-2053-2017.

Tapley, B.D., Bettadpur, S., Watkins, M., Reigber, C., (2004). The gravity recovery and climate experiment: mission overview and early results. Geophys Res Lett 31:L09607, http://dx.doi.org/10.1029/2004GL019920.

Thomas, A.C., Reager, J.T., Famiglietti, J.S., Rodell, M., (2014). A GRACE-based water storage deficit approach for hydrological drought characterization. Geophysical Research Letters, 41:1537–1545, doi:10.1002/2014GL059323.

Tian, S., Tregoning, P., Renzullo, L.J., van Dijk, A.I.J.M., Walker, J.P., Pauwels, V.R.N., Allgeyer, S., (2017). Improved water balance component estimates through joint assimilation of GRACE water storage and SMOS soil moisture retrievals. Water Resources Research, 53(3):1820–1840, doi:10.1002/2016WR019641.

Tregoning, P., McClusky, S., van Dijk, A.I.J.M., Crosbie, R.S., Peña-Arancibia, J.L., (2012). Assessment of GRACE Satellites for Groundwater Estimation in Australia. National Water Commission, Canberra, 82 pp.

Tsonis, A.A., Triantafyllou, G.N., Georgakakos, K.P., (1996). Hydrological applications of satellite data: 1. Rainfall estimation. Journal of Geophysical Research: Atmospheres, 101(D21):26517–26525, doi:10.1029/96JD01654.

Usowicz, B., Marczewski, W., Usowicz, J., Lukowski, M., Lipiec, J., (2014). Comparison of Surface Soil Moisture from SMOS Satellite and Ground Measurements. International Agrophysics, 28(3):359-369, doi:10.2478/intag-2014-0026.

Valdés-Pineda, R., Demaría, E.M.C., Valdés, J.B., Wi, S., Serrat-Capdevilla, A., (2016). Bias correction of daily satellite-based rainfall estimates for hydrologic forecasting in the Upper Zambezi, Africa. Hydrology and Earth System Sciences Discussion, doi:10.5194/hess-2016-473, 2016.

Van Camp, M., Radfar, M., Martens, K., Walraevens, K., (2012). Analysis of the groundwater resource decline in an intramountain aquifer system in Central Iran. Geologica Belgica, 15(3):176-180, https://popups.uliege.be:443/1374-8505/index.php?id=3644.

van Dijk, A.I.J.M., (2010a). The Australian Water Resources Assessment System: Technical Report 3, Landscape model (version 0.5) Technical Description. CSIRO: Water for a Healthy Country National Research Flagship.

van Dijk, A.I.J.M., (2010b.) AWRA Technical Report 3. Landscape Model (version 0.5), Technical Description, Canberra.

van Dijk, A.I.J.M., Renzullo, L.J., Rodell, M., (2011). Use of Gravity Recovery and Climate Experiment terrestrial water storage retrievals to evaluate model estimates by the Australian water resources assessment system. Water Resources Research, 47:W11524, doi:10.1029/2011WR010714.

van Dijk, A.I.J.M., Peña-Arancibia, J.L., Wood, E.F., Sheffield, J., Beck, H.E., (2013). Global analysis of seasonal streamflow predictability using an ensemble prediction system and observations from 6192 small catchments worldwide, Water Resources Research, 49:2729–2746, doi:10.1002/wrcr.20251.

van Dijk, A.I.J.M., Renzullo, L.J., Wada, Y., Tregoning, P., (2014). A global water cycle reanalysis (2003–2012) merging satellite gravimetry and altimetry observations with a hydrological multi-model ensemble. Hydrology and Earth System Sciences, 18:2955–2973, doi:10.5194/hess-18-2955-2014.

van Leeuwen, P.J., Evensen, G., (1996). Data assimilation and inverse methods in terms of a probabilistic formulation. Monthly Weather Review, 124:2898–2913, doi:10.1175/1520-0493(1996)124¡2898:DAAIMI¿2.0.CO;2.

Voss, K.A., Famiglietti, J.S., Lo, M.-H., de Linage, C., Rodell, M., Swenson, S.C., (2013). Groundwater depletion in the Middle East from GRACE with implications for transboundary water management in the Tigris–Euphrates–Western Iran region. Water Resources Research, 49(2):904–914, doi:10.1002/wrcr.20078.

Vrugt, J.A., Diks, C.G., Gupta, H.V., Bouten, W., Verstraten, J.M., (2005). Improved treatment of uncertainty in hydrologic modeling: Combining the strengths of global optimization and data assimilation. Water Resources Research, 41:W01017, doi:10.1029/2004WR003059.

Vrugt, J.A., Gupta, H.V., Nuallain, B.O., (2006). Real-time data assimilation for operational ensemble streamflow forecasting. Journal of Hydrometeorology, 7(3):548–565, doi:10.1175/JHM504.1.

Vrugt, J.A., ter Braak, C.J.F., Diks, C.G.H., Schoups, G., (2013). Advancing hydrologic data assimilation using particle Markov chain Monte Carlo simulation: theory, concepts and applications, Advances in Water Resources, 51:457-478, doi:10.1016/j.advwatres.2012.04.002.

Wahr, J., Molenaar, M., Bryan, F., (1998). Time variability of the Earth's gravity field' Hydrological and oceanic effects and their possible detection using GRACE. Journal of Geophysical research, 103, B12, 30, 205-30, 229, doi:10.1029/98JB02844.

Wang, J., Xu, K., Zhou, K., Lin, S., Hu, S., Guo, B., (2006). Spherical harmonics scaling. Visual Comput, 22: 713. doi:10.1007/s00371-006-0057-8.

Watkins, M.M., Wiese, D.N., Yuan, D.-N., Boening, C., Landerer, F.W., (2015). Improved methods for observing Earth's time variable mass distribution with GRACE using spherical cap mascons. Journal of Geophysical Research: Solid Earth, 120(4):2648–2671, doi:10.1002/2014JB011547.

Weerts, A.H., El Serafy, G.Y.H., (2006). Particle filtering and ensemble Kalman filtering for state updating with hydrological conceptual rainfall-runoff models. Water Resources Research, 42:W09403, doi:10.1029/2005WR004093.

Whitaker, J.S., Hamill, T.M., (2002). Ensemble data assimilation without perturbed observations. Monthly Weather Review, 130:1913–1924, doi:10.1175/1520-0493(2002)130¡1913:EDAWPO¿2.0.CO;2.

Wiese, D.N., (2015). GRACE monthly global water mass grids NETCDF RELEASE 5.0. Ver. 5.0. PO.DAAC, CA, USA. Dataset accessed [YYYY-MM-DD] at doi:10.5067/TEMSC-OCL05.

Wood, E.F., Su, H., McCabe, M., Su, B., (2003). Estimating Evaporation from Satellite Remote Sensing. In Proceedings of the 2003 IEEE International Geoscience and Remote Sensing Symposium (IGARSS'03), Toulouse, France, 21–25 July 2003, 2:1163–1165, doi:10.1109/IGARSS.2003.1294045.

Wooldridge, S.A., Kalma, J.D., (2001). Regional-scale hydrological modelling using multiple-parameter landscape zones and a quasi-distributed water balance model. Hydrological Earth System Sciences, 5:59-74.

Wouters, B., Schrama, E.J.O., (2007). Improved accuracy of GRACE gravity solutions through empirical orthogonal function filtering of spherical harmonics. Geophysical Research Letters, 34:L23711, doi:10.1029/2007GL032098.

Wouters, B., Bonin, J.A., Chambers, D.P., Riva, R.E. M., Sasgen, I., Wahr, J., (2014). GRACE, time-varying gravity, Earth system dynamics and climate change. Reports on Progress in Physics, 77(11):116801, doi:10.1088/0034-4885/77/11/116801.

Xue, J., Su, B., (2017). Significant Remote Sensing Vegetation Indices: A Review of Developments and Applications. Journal of Sensors, vol. 2017, Article ID 1353691, 17 pages, doi:10.1155/2017/1353691

Yao, C., Luo, Z., Wang, H., Li, Q., Zhou, H., (2016). GRACE-Derived Terrestrial Water Storage Changes in the Inter-Basin Region and Its Possible Influencing Factors: A Case Study of the Sichuan Basin. China. Remote Sensing, 8(6):444, doi:10.3390/rs8060444.

Yeh, P. J. F., Swenson, S. C., Famiglietti, J. S., Rodell, M., (2006). Remote sensing of ground water storage changes in Illinois using the Gravity Recovery and Climate Experiment (GRACE). Water Resources Research, 42:W12203, doi:10.1029/2006WR005374.

Zaitchik, B.F., Rodell, M., Reichle, R.H., (2008). Assimilation of GRACE terrestrial water storage data into a land surface model: results for the Mississippi River Basin. Journal of Hydrometeorology, 9(3):535–548, doi:10.1175/2007JHM951.1.

Zhang, Z. Z., Chao, B. F., Lu, Y., Hsu, H. T., (2009). An effective filtering for GRACE time-variable gravity: Fan filter. Geophysical Research Letters, 36:L17311, doi:10.1029/2009GL039459.

Zhang, Y., Bocquet, M., Mallet, V., Seigneur, C., Baklanov, A., (2012). Real-time air quality forecasting, Part I: History, techniques, and current status. Atmospheric Environment, 60:632-655, doi:10.1016/j.atmosenv.2012.06.031.

Zhang, Y., Pan, M., Wood, E.F., (2016). On Creating Global Gridded Terrestrial Water Budget Estimates from Satellite Remote Sensing. Surveys in Geophysics, 37(2):249–268, doi:10.1007/s10712-015-9354-y.

Appendix A. Copyright permission statements

I certify that I collected permission from the copyright owners to use my own publications in which the copyright is held by another party (e.g. publishers, co-author). The obtained permissions for individual publishers are enclosed below.

Mehdi Khaki

Title: Efficient basin scale filtering of GRACE satellite products

Author: M. Khaki,E. Forootan,M. Kuhn,J. Awange,L. Longuevergne,Y. Wada

Publication: Remote Sensing of Environment

Publisher: Elsevier

Date: January 2018

Title: Accounting for spatial correlation errors in the assimilation of GRACE into hydrological models through localization

Author: M. Khaki,M. Schumacher,E. Forootan,M. Kuhn,J.L. Awange,A.I.J.M. van Dijk

Publication: Advances in Water Resources

Publisher: Elsevier

Date: October 2017

Title: Assessing sequential data assimilation techniques for integrating GRACE data into a hydrological model

Author: M. Khaki,I. Hoteit,M. Kuhn,J. Awange,E. Forootan,A.I.J.M. van Dijk,M. Schumacher,C. Pattiaratchi

Publication: Advances in Water Resources

Publisher: Elsevier

Date: September 2017

Title: A study of Bangladesh's sub-surface water storages using satellite products and data assimilation scheme

Author: M. Khaki,E. Forootan,M. Kuhn,J. Awange,F. Papa,C.K. Shum

Publication: Science of The Total Environment

Publisher: Elsevier

Date: 1 June 2018

Title: A two-update ensemble Kalman filter for land hydrological data assimilation with an uncertain constraint

Author: M. Khaki,B. Ait-El-Fquih,I. Hoteit,E. Forootan,J. Awange,M. Kuhn

Publication: Journal of Hydrology

Publisher: Elsevier

Date: December 2017

Appendix B. Statements of contribution by others

The thesis compromises six published and two under-review papers in peer-reviewed journals. In all of the contributions, I have been the first-author. In the following, the author and co-authors' contributions for these papers are described and signed.

To Whom It May Concern,

I, Mehdi Khaki, planned the studies, designed the analytical and numerical experiments, processed the data using my own software, interpreted the numerical results, and wrote the manuscripts. Co-authors provided their technical comments as to improve the manuscripts for submission. I worked with the co-authors to introduce novel data assimilation algorithms (in papers 7 and 8). All the above holds for the following publications:

1. **Khaki, M.**, Forootan, E., Kuhn, M., Awange, J., Longuevergne, L., Wada, Y., (2018a). Efficient Basin Scale Filtering of GRACE Satellite Products. Remote Sensing of Environment, 204:76-93, doi:10.1016/j.rse.2017.10.040.

2. **Khaki, M.**, Schumacher, M., J., Forootan, Kuhn, M., Awange, E., van Dijk, A.I.J.M., (2017a). Accounting for Spatial Correlation Errors in the Assimilation of GRACE into Hydrological Models through localization. Advances in Water Resources, 108:99-112, doi:10.1016/j.advwatres.2017.07.024.

3. **Khaki, M.**, Hoteit, I., Kuhn, M., Awange, J., Forootan, E., van Dijk, A.I.J.M., Schumacher, M., Pattiaratchi, C., (2017b). Assessing sequential data assimilation techniques for integrating GRACE data into a hydrological model. Advances in Water Resources, 107:301-316, doi:10.1016/j.advwatres.2017.07.001.

4. **Khaki, M.**, Forootan, E., Kuhn, M., Awange, J., Papa, F., Shum, C.K., (2018b). A Study of Bangladesh's Sub-surface Water Storages Using Satellite Products and Data Assimilation Scheme. Science of The Total Environment, 625:963-977, doi:10.1016/j.scitotenv.2017.12.289.

5. **Khaki, M.**, Forootan, E., Kuhn, M., Awange, J., van Dijk, A.I.J.M., Schumacher, M., Sharifi, M.A., (2018c). Determining Water Storage Depletion within Iran by Assimilating GRACE data into the W3RA Hydrological Model. Advances in Water Resources, 114:1-18, doi:10.1016/j.advwatres.2018.02.008.

6. **Khaki, M.**, Awange, J. (2018d). The Application of Remotely Sensed Products to Enhance Model-derived Water Storage Changes over South America. Revised and resubmitted to Science of The Total Environment.

7. **Khaki, M.**, Ait-El-Fquih, B., Hoteit, I., Forootan, E., Awange, J., Kuhn, M., (2017c). A Two-update Ensemble Kalman Filter for Land Hydrological Data Assimilation with an Uncertain Constraint. Journal of Hydrology, 555:447-462, doi:10.1016/j.jhydrol.2017.10.032.

8. **Khaki, M.**, Ait-El-Fquih, B., Hoteit, I., Forootan, E., Awange, J., Kuhn, M., (2018e). Unsupervised Ensemble Kalman Filtering with an Uncertain Constraint for Land Hydrological Data Assimilation. Revised and resubmitted to Journal of Hydrology.

Mehdi Khaki _____

I, as a Co-Author, endorse that this level of contributions by the candidate indicated above is appropriate.

Ehsan Forootan _____

Joseph L. Awange _____

Michael Kuhn _____

Ibrahim Hoteit _____

Boujemaa Ait-El-Fquih _____

Albert I.J.M. van Dijk _____

Maike Schumacher _____

Charitha Pattiaratchi _____

Fabrice Papa _____

C.K. Shum _____

Laurent Longuevergne _____

Ali Sharifi _____

Yoshihide Wada _____